SYMPOSIUM SUR LES MÉCANISMES DE RÉACTION NUCLÉAIRE ET LES PHÉNOMÈNES DE POLARISATION

SYMPOSIUM ON NUCLEAR REACTION MECHANISMS AND POLARIZATION PHENOMENA

1969

COMPTE RENDU DU SYMPOSIUM

PROCEEDINGS OF THE SYMPOSIUM

Comité local d'organisation

Local Organizing Committee

B. CUJEC

Q. HO KIM

R. J. SLOBODRIAN

LES PRESSES DE L'UNIVERSITÉ LAVAL

Bibliothèque Nationale du Québec

SYMPOSIUM SUR LES MÉCANISMES DE RÉACTION NUCLÉAIRE ET LES PHÉNOMÈNES DE POLARISATION

SYMPOSIUM ON NUCLEAR REACTION MECHANISMS AND POLARIZATION PHENOMENA

SYMPOSIUM SUR LES MÉCANISMES DE RÉACTION NUCLÉAIRE ET LES PHÉNOMÈNES DE POLARISATION

SYMPOSIUM ON NUCLEAR REACTION MECHANISMS AND POLARIZATION PHENOMENA

SYMPOSIUM SUR LES MÉCANISMES DE RÉACTION NUCLÉAIRE ET LES PHÉNOMÈNES DE POLARISATION

SYMPOSIUM ON NUCLEAR REACTION MECHANISMS AND POLARIZATION PHENOMENA

1969

COMPTE RENDU DU SYMPOSIUM

PROCEEDINGS OF THE SYMPOSIUM

Comité local d'organisation

Local Organizing Committee

B. CUJEC

Q. HO KIM

R. J. SLOBODRIAN

LES PRESSES DE L'UNIVERSITÉ LAVAL

Québec, 1970

DÉPÔT LÉGAL (QUÉBEC) DEUXIÈME TRIMESTRE 1970

QC
794
$9

© 1970

LES PRESSES DE
L'UNIVERSITÉ LAVAL

TOUS DROITS RÉSERVÉS
IMPRIMÉ AU CANADA

D'7001174

Photo des participants au Symposium

FOREWORD

A Symposium on Nuclear Reaction Mechanisms and Polarization Phenomena was held at Laval University, September 1 and 2, 1969. The discussions centered around some chosen topics but were otherwise informal.

This volume contains the texts of papers presented at the Symposium as submitted by their authors, to whom we would like to express our particular gratitude. Discussions and comments, always lively and informative, were recorded on magnetic tape, but are not reproduced here in order not to betray the informal character of the meeting. To all participants we wish to express our great appreciation.

PRÉFACE

Un symposium sur les Mécanismes de Réaction Nucléaires et Phénomènes de Polarisation fut tenu à l'Université Laval les ler et 2 septembre 1969. Les discussions étaient centrées autour de sujets choisis; le format adopté était autrement libre avec un minimum de formalités.

Ce volume contient les textes des travaux présentés au Symposium tels que soumis par leurs auteurs. À eux tous nous exprimons notre profonde gratitude. Les discussions spontanées, toujours vivantes et informatives, et dont nous possédons un enregistrement complet, ne sont cependant pas reproduites ici pour ne pas trahir le caractère intime de la réunion. À tous les participants nous exprimons notre grande appréciation.

ACKNOWLEDGEMENTS

To the many people who have contributed to the organization of this Symposium we wish to express our gratitude. To Professors Larkin Kerwin and Fernand Bonenfant we are indebted for their continued and generous support. Our colleagues and students of the Nuclear Physics Laboratory assumed enthousiastically the many chores related to the Symposium. The efficient technical help of Monsieur G. Parent was widely appreciated. Madame P. Bourget, by the competence and patience she brought to the secretarial work, proved to be our most precious collaborator.

The publication of this volume is financed by the National Research Council of Canada. To the officers of this organism, and in particular to Dr H. Williamson, we wish to express our great appreciation.

REMERCIEMENTS

L'organisation de cette conférence n'aurait pas été possible sans l'assistance désintéressée d'un grand nombre de personnes auxquelles nous tenons à exprimer ici notre reconnaissance. Aux professeurs Larkin Kerwin et Fernand Bonenfant nous sommes redevables pour leur généreux et constant appui. De nos collègues et de nos étudiants du Laboratoire de Physique Nucléaire nous avons reçu des encouragements précieux et une aide enthousiaste. Le travail technique vraiment efficace de Monsieur G. Parent a considérablement facilité notre tâche. Par sa compétence et sa patience, Madame P. Bourget, la secrétaire du comité d'organisation, s'est prouvée une collaboratrice inestimable.

La publication de ce volume est financée par le Conseil National de Recherches du Canada. Que les responsables de cet organisme , et en particulier le Dr H. Williamson, reçoivent ici nos sincères remerciements pour leur générosité.

TABLE DES MATIERES

Préface	VI-VII
Remerciements	VIII-IX
Photo du groupe	V
Programme	XIII-XIV

Séance 1	1
Séance 2	73
Séance 3	285
Séance 4	421

Index des auteurs et des participants	499

TABLE OF CONTENTS

Foreword	VI-VII
Acknowledgements	VIII-IX
Group photographe	V
Program	XIII-XIV

Session 1	1
Session 2	73
Session 3	285
Session 4	421

List of Contributors and Participants	499

INAUGURATION, sous la présidence de Monsieur le vice-recteur Professeur LARKIN KERWIN et Monsieur le directeur du département de Physique, Professeur FERNAND BONENFANT.

DISCOURS DE BIENVENUE par M. LARKIN KERWIN

Conférenciers invités

1. RÉSONNANCES

A.K. KERMAN (Massachussets Institute of Technology)
Nuclear Reaction Theory

S. FALLIEROS (Brown University)
Theory of Analog Resonances

W. HAEBERLI (The University of Wisconsin)
Polarization Effects in the Study of
Analog States

R.H. DAVIS (Florida State University)
Scattering of Alpha Particles by ^{40}Ca

1. RESONANCES

2. RÉACTIONS DIRECTES

D.A. BROMLEY (Yale University)
Quasi-Molecular Phenomena in Nuclear Physics

N.K. GLENDENNING (University of California)
The Role of Inelastic Process in
Nucleon Transfer Reactions

J. RAYNAL (Centre d'Etudes Nucléaires de Saclay)
Couplage LS dans les descriptions macroscopiques et microscopiques des réactions nucléaires.

P.E. HODGSON (Oxford University)
Macroscopic to Microscopic: Recent Work on the
Optical model.

R. SCHAEFFER (Centre d'Etudes Nucléaires de Saclay)
La DWBA antisymétrisée et l'étude des fonctions d'onde microscopiques.

2. DIRECT REACTIONS

3. RÉACTIONS AVEC PROJECTILES POLARISÉS

3. REACTIONS WITH POLARIZED PROJECTILES

P. HUBER (Universität Basel)
Reactions with Polarized Deuterons on Light Nuclei

P. CATILLON
(Centre d'Etudes Nucléaires de Saclay)
Effets liés au spin dans la diffusion de protons et les réactions (p-d)

P.W. KEATON (Los Alamos Scientific Laboratory)
Work with Polarized Tritons at Los Alamos

S. ROMAN (University of Birmingham)
Study of Stripping Reactions Induced by 12 MeV Vector Polarized Deuterons

4. RÉACTIONS AUX ÉNERGIES MOYENNES

4. REACTIONS AT INTERMEDIATE ENERGIES

N. MARTY (Faculté des Sciences de Paris et Orsay)
Réactions nucléaires à moyenne énergie

E.T. BOSCHITZ (National Aeronautics and Space Administration)
The Interaction of Intermediate Energy Protons with Light Nuclei.

L. ROSEN presented by P.W. KEATON (Los Alamos Scientific Laboratory
The Status of the Los Alamos Meson Factory.

SEANCE
SESSION 1

PRESIDENT CHAIRMAN

D. A. BROMLEY

THEORY OF ANALOG RESONANCES

S. Fallieros †

Brown University

We will start this discussion with a simple quantum mechanical model that illustrates some interesting features of analog states and then proceed with a more systematic description of the theory. The model is well known, it is discussed e.g. in the book of Condon and Shortley. It consists of a set of quantum levels ψ_r eigenstates of an unperturbed Hamiltonian H_o, and an additional state ψ_A also an eigenstate of H_o, i.e.

$$H_o \psi_r = E_r \psi_r$$
$$H_o \psi_A = E_A \psi_A \qquad (1)$$

We let this state A couple with the states r and denote by M_r the corresponding matrix element. The new spectrum that results from this coupling is given by the equations

---

† Supported in part by the U.S. Atomic Energy Commission.

$$H\psi = E\psi$$

$$\psi = c_A \psi_A + \sum_r c_r \psi_r \tag{2}$$

or alternatively by

$$(E - E_r)\, c_r = M_r c_r$$
$$(E - E_A)\, c_A = \sum_r M_r c_r \,. \tag{3}$$

The new eigenvalues can be obtained from the familiar graphical representation of the equations

$$E - E_A = \sum_r \frac{M_r^2}{E - E_r} \tag{4}$$

while the average behavior of $|c_A|^2$ which measures the participation of ψ_A in the states ψ is given by

$$\overline{|c_A|^2} = \frac{D}{\pi} \frac{W}{(E - E_A)^2 + W^2} \,. \tag{5}$$

In this expression D represents the average level spacing and

$$W = \pi \frac{\overline{|M_r|^2}}{D} \tag{6}$$

characterizes the spreading of the state A in the new spectrum. We consider now a physical property Q and let q_A and q_r denote the corresponding

value of this property in the states A and r respectively. We then find

$$Q = q_A c_A + \sum_r q_r c_r$$

and

$$|Q|^2 = \left| q_A + q \frac{E - E_A}{M} \right|^2 |\overline{c_A}|^2 \quad . \qquad (7)$$

In this expression the indices r in q_r and M_r have been dropped. Let us consider first the case where $q = 0$ but $q_A \neq 0$. The energy dependence of $|Q|^2$ is then given by the expression in eq. 5 and we say that the state ψ_A acts as a doorway state as far as the property Q is concerned. In general however when $q \neq 0$ we expect that interference effects will appear between the contributions of the states A and r. This is illustrated by the expression in eq. 7 which indicates the asymmetric energy distribution that results from this interference.

The qualitative relevance of these considerations to the discussion of observed features of analog resonances should be clear. The wave function ψ_A obviously represents the analog state, i.e. the state obtained from a certain parent by a rotation in isospin space while ψ_r corresponds to the compound-nucleus background that surrounds it. The coexistence of the two is what is observed experimentally with interference effects generally expected and accounting e.g. for the asymmetric distribution of the particle-emission widths around the analog resonance peak.

We now proceed with a more systematic discussion of the scattering amplitude describing an analog resonance reaction.[1] The approach will be essentially the same as before. We consider the complete scattering amplitude for a transition from an initial state $|i\rangle$ to a final state $|f\rangle$ i.e.

$$\langle f | T(E) | i \rangle$$

$$= \langle f | H' + H' \frac{1}{E^+ - H} H' | i \rangle \tag{8}$$

and separate it into a term describing the reaction in the absence of the analog and a term containing the effect due to the analog state. This separation is easily performed with the help of the projection operators

$$\Lambda_A = |A\rangle\langle A| \tag{9}$$

and

$$\bar{\Lambda} = 1 - \Lambda_A .$$

If we now introduce a Hamiltonian $\bar{H}$ by $\bar{H} = \bar{\Lambda} H \bar{\Lambda}$ and a transition operator t(E) that has the analog state $|A\rangle$ projected out of all intermediate stages we can write the reaction amplitude in the absence of the state $|A\rangle$ in the form

$$\langle f | t(E) | i \rangle$$

$$= \langle f | H' + H' \frac{\bar{\Lambda}}{E^+ - \bar{H}} H' | i \rangle . \tag{10}$$

In addition to connecting the channels $|i\rangle$, $|f\rangle$ etc. the operator t(E) has matrix elements coupling these states to $|A\rangle$ as well as diagonal matrix elements $t_{AA}(E)$. If we define

$$t_{Ai}(E) = M_{Ai}(E)$$

and (11)

$$t_{AA}(E) = \Sigma(E)$$

we can write the complete expression for T_{fi} in the form

$$T_{fi} = t_{fi} + M_{fA} \frac{1}{E - E_A - \Sigma(E)} M_{Ai} \qquad (12)$$

where E_A is the analog-state energy i.e. $\langle A|H|A\rangle$ and the amplitudes M_{Ai} etc. are symmetric by time-reversal invariance. Unitarity implies the following restrictions:

$$\sum_f |T_{fi}|^2 = -\,\mathrm{Im}\, T_{ii}$$

$$\sum_f |t_{fi}|^2 = -\,\mathrm{Im}\, t_{ii}$$

$$\sum_f |M_{Af}|^2 = -\,\mathrm{Im}\, \Sigma(E) \,. \qquad (13)$$

We can also introduce the S-matrix and a corresponding matrix U by

$$S = 1 - 2iT$$

$$U = 1 - 2it \tag{14}$$

The relations in eq. 13 above are clearly consequences of the unitarity of the operators S and U. In the case of U this condition is written in the form

$$t - t^{\dagger} = -2i\, t^{\dagger} \bar{\Lambda}\, t$$

or

$$t\bar{\Lambda} = t^{\dagger}\bar{\Lambda}\, U\bar{\Lambda} \tag{15}$$

While the first expression is simply a restatement of the second and third relations in eq. 13, the second gives the additional condition

$$M_{Ai} = \sum_{f} M^{*}_{Af}\, U_{fi} \tag{16}$$

restricting the phases of the off-diagonal matrix elements t_{Ai}. In the case where only pure elastic scattering is possible we can drop the various indices and write in an obvious notation

$$M(E) = U(E)\, M^{*}(E) \tag{17}$$

and

$$S(E) = U(E) - 2i \frac{M^2(E)}{E - E_A - \Sigma(E)}$$

$$= U(E) \left[1 - 2i \frac{|M(E)|^2}{E - E_A - \Sigma(E)} \right]$$

$$= U(E) \frac{E - E_A - \Sigma^*(E)}{E - E_A - \Sigma(E)} \qquad (18)$$

The self-energy function $\Sigma(E)$ can in this case be written in the form

$$\Sigma(E) = \frac{1}{\pi} \int dE' \frac{|M(E')|^2}{E^+ - E'} \qquad (19)$$

which can be easily generalized to include the many-channel case if the appropriate channel indices are introduced.

In the above expressions we have written the complete transition amplitude as a sum of a background term and a resonant term which since $Im\,\Sigma(E) \neq 0$ seems to have a simple Breit-Wigner form. The simplicity of these relations is however somewhat misleading since all the matrix elements appearing in e.g., eq. 12 are in general strongly energy dependent. These fluctuations on the other hand disappear when the average is taken. We will define the average amplitudes by the standard expressions[2] of the form

$$\langle T(E)\rangle = \int dE' \; \frac{I/\pi}{(E-E')^2 + I^2} \; T(E')$$

$$= T(E + iI) \tag{20}$$

while the average cross-section is essentially given by

$$\langle |T(E)|^2 \rangle$$

$$= |\langle T(E)\rangle|^2 + \langle |T_f(E)|^2 \rangle \; . \tag{21}$$

In this expression we have introduced the fluctuation amplitude

$$T_f(E) = T(E) - \langle T(E)\rangle \tag{22}$$

which describes e.g. the compound elastic scattering. (We are restricting our discussion to the one-channel case in order to keep the notation simple. Generalization to the cases with many open channels is straightforward.) The unitarity condition remains essentially unchanged i.e.

$$\langle |T(E)|^2 \rangle = -\,\mathrm{Im}\,\langle T(E)\rangle$$

and the average scattering amplitude becomes

$$\langle T(E) \rangle = t(E+iI) + \frac{M^2(E+iI)}{E - E_A - \Sigma(E)}$$

$$= \langle t(E) \rangle + \frac{\langle M(E) \rangle^2}{E - E_A - \Sigma(E)} \quad . \tag{23}$$

The second term in this equation does now have a Breit-Wigner form since only the average values of $M(E)$ and $\Sigma(E)$ appear. We have omitted a term iI in the denominator assuming that it is much smaller than the imaginary part of Σ. We now introduce the quantities Γ_p and Γ by

$$\Gamma_p = 2 \, |\langle M \rangle|^2$$

$$\Gamma = -2 \, \mathrm{Im} \langle \Sigma(E) \rangle \tag{24}$$

to represent the widths appearing in the numerator and the denominator of eq. 23. (Phase space factors are hidden in the matrix elements and do not appear explicitly.) From eq. 19 we find immediately

$$\Gamma = -\frac{2}{\pi} \mathrm{Im} \int dE' \, \frac{|M(E')|^2}{E + iI - E'}$$

$$= 2 \langle |M(E)|^2 \rangle \quad . \tag{25}$$

This result makes clear the difference between the widths Γ_p and Γ. While

the first is given by the square of the average of the matrix element connecting the analog state with the particle continuum the second is the average of the absolute square of this quantity. The two differ exactly because of the presence of the rapid fluctuations in $M(E)$ mentioned above. More explicitly we can introduce the fluctuating term $M_f(E)$ in analogy with eq. 22.

$$M_f(E) = M(E) - \langle M(E) \rangle \tag{26}$$

and obtain

$$\Gamma = 2\,|\langle M(E) \rangle|^2 + 2\,\langle |M_f(E)|^2 \rangle$$

$$= \Gamma_p + \Gamma_f \tag{27}$$

with the fluctuation width Γ_f defined by this equation. Clearly Γ_f is a positive quantity and represents the total spreading of the analog resonance among the states that surround it. One can interpret Γ_p and Γ_f as representing respectively prompt and delayed particle emission from the analog state.

The last quantity of interest in eq. 23 is the phase of the average matrix element $\langle M \rangle$. It is clear from eq. 17 that the phase of $M(E)$ is equal to that of $U(E)$, the matrix that describes the scattering in the absence of the analog. This is no longer true however when the average is taken since

$$\langle M(E) \rangle = \langle U(E)\, M^{*}(E) \rangle$$

$$\neq \langle U(E) \rangle \langle M^{*}(E) \rangle$$

i.e. the average of the product $U(E)M^{*}(E)$ is not the same as the product of the average values at least as long as U is not a smoothly varying function of the energy. In addition to producing the spreading width Γ_f the fluctuations will therefore introduce a phase difference between $\langle M \rangle$ and $\langle U \rangle$. If we separate as before the S-matrix $U(E)$ into its average and fluctuating parts

$$U(E) = \langle U(E) \rangle + U_f(E) \tag{28}$$

and define δ and η by

$$\langle U(E) \rangle = e^{2i\delta} e^{-2\eta} \tag{29}$$

we can write

$$\langle M(E) \rangle = \langle U(E) \rangle \langle M(E) \rangle^{*} + \langle U_f(E)\, M_f^{*}(E) \rangle$$

$$= e^{2i(\delta+\phi)} \langle M(E) \rangle^{*} \tag{30}$$

where the last line defines the phase difference ϕ of $\langle M \rangle$ and $\langle U \rangle$. Again it is clear that ϕ vanishes when $U_f = 0$ i.e., when no fluctuations are present. We can also easily establish that when $U_f = 0$ we also have $M_f = 0$ i.e., there is no spreading width Γ_f. In this case obviously $\eta = 0$ and the overall transmission coefficient $1-|\langle S \rangle|^2$ also vanishes.

From eq. 30 we can obtain a useful relation restricting the values of the physical parameters of the problem. If we take the absolute square of

$$\langle M(E) \rangle \left[1 - e^{-2\eta} e^{-2i\phi} \right] = \langle U_f(E) M_f^*(E) \rangle$$

and remember the definitions of eqs. 24, 27 and 29 we obtain

$$\begin{aligned} \Gamma_p \left[1 + e^{-4\eta} - 2 e^{-2\eta} \cos 2\phi \right] &= 2 \left| \langle U_f M_f^* \rangle \right|^2 \\ &\leq \left[1 - e^{-4\eta} \right] \Gamma_f \end{aligned}$$

where Schwarz's inequality was applied in the last line. This relation was first obtained by Kerman and De Toledo Piza.[3] We can obtain a number of interesting results by imposing the requirement that the above inequality reduces to an equality. For this to happen we must have

$$M_f(E) = \alpha U_f(E) \tag{31}$$

where α is a complex number independent of energy. We will not discuss the derivations in detail but simply state some results that follow from eq. 31. If we introduce the quantities Δ and E_0 by

$$\Delta = -2 \, \mathrm{Im} \, \alpha \langle M(E) \rangle$$

$$E_0 + \Delta = E_A + R_e \Sigma(E+i\Gamma) \tag{32}$$

we find that the transmission coefficient takes the simple form

$$1 - |\langle S \rangle|^2 = \frac{(E-E_0)^2}{(E-E_0-\Delta)^2 + \Gamma^2/4} \left(1 - e^{-4\eta}\right) \tag{33}$$

and vanishes for a particular energy E_0. This follows from the coherence between the emission and scattering amplitude implied by eq. 31 which causes a completely destructive interference between the background and resonance terms in $\langle S \rangle$. Under these assumptions we also find

$$\frac{\Gamma_p \Gamma_f}{\Delta^2 + \Gamma^2/4} = 1 - e^{-4\eta} \tag{34}$$

and

$$\sin 2\phi = -\frac{2\Delta}{\Gamma} \sinh 2\eta \tag{35}$$

which agrees at least in the limit of small η with the expression for the phase ϕ first written down by Robson.[4] A more complete study of these

and other related results will be presented elsewhere.

We will close this discussion with a brief description of the effect of the analog state on the proton strength function. The fine-structure widths will be those appearing in the K-matrix expansion

$$K(E) = \sum_r \frac{\Gamma_r/2}{E - E_r}$$

with

$$S(E) = \frac{1 - i\,K(E)}{1 + i\,K(E)} \,. \tag{36}$$

As before, phase-space factors are not shown explicitely. If D is the level spacing, the average value of Γ_r/D is given by

$$-\,\mathrm{Im}\,K(E + iI) = I \sum_r \frac{\Gamma_r/2}{(E - E_r)^2 + I^2}$$

$$= \frac{\pi}{2} \left\langle \frac{\Gamma_r}{D} \right\rangle \,. \tag{37}$$

The complete K-matrix is now expressed as a sum of a term $\kappa(E)$ describing the situation in the absence of the analog and a term containing the analog

$$K(E) = \kappa(E) + \frac{m^2(E)}{E - E_A - \Sigma_0(E)} \tag{38}$$

where all the quantities are now real. They are related to the matrix elements appearing in the S-matrix by

$$U(E) = \frac{1 - i\kappa(E)}{1 + i\kappa(E)}$$

$$M(E) = \frac{m(E)}{1 + i\kappa(E)}$$

and

$$\Sigma_0(E) = \Sigma(E) + i \frac{m^2(E)}{1 + i\kappa(E)} \quad . \tag{39}$$

A straightforward calculation now gives

$$\mathrm{Im}\, K(E+iI) = \mathrm{Im}\, \kappa(E+iI) \left| \frac{E - E_A - \langle \Sigma \rangle}{E - E_A - \langle \Sigma_0 \rangle} \right|^2 \frac{1 - |\langle S \rangle|^2}{1 - |\langle U \rangle|^2} \tag{40}$$

In the limit where eq. 33 is valid this finally becomes

$$\left\langle \frac{\Gamma_c}{D} \right\rangle = \left\langle \frac{\Gamma_c}{D} \right\rangle_0 \frac{(E - E_0)^2}{|E - E_A - \Sigma_0(E)|^2} \tag{41}$$

where $\langle \Gamma_c / D \rangle_0$ was introduced to denote the proton strength function in the absence of the analog. The disappearance of the fine structure at the energy E_0 is noticed again. We find however that the real and imagniary parts of $\Sigma_0(E+iI)$ are not identical to the quantities appearing in the denominator of eq. 33. Neither the position of the peak nor the width of the energy distribution of the strength function are therefore identical to those of the transmission coefficient.

The asymmetric energy distributions of the strength function and the transmission coefficient and the conditions under which these quantities vanish at a certain point in the spectrum have been discussed by several authors.[5,6,7] In this discussion we have attempted to summarize in a rather general way these conditions. The common functional dependence on the energy, of the fluctuations of the decay and the scattering amplitudes was found to be the appropriate requirement.

Acknowledgments

Most of the work presented in this report was done in collaboration with Professor G. E. Brown.

Discussions with Professor A. Kerman are greatfully acknowledged.

References

1. G. E. Brown and S. Fallieros, to be published.

2. G. E. Brown, Rev. Mod. Phys. 31 (1959) 893.

3. A. F. R. de Toledo Piza and A. K. Kerman, Annals of Physics 43, (1967) 363; 48 (1968) 173.

4. D. Robson, Phys. Rev. 137B (1965) 535.

5. W. M. MacDonald and A. Mekjian, Phys. Rev. 160, (1967) 730; Phys. Rev. Lett. 18 (1967) 706; Nucl. Phys. A121 (1968) 385.

6. C. Mahaux and H. A. Weidenmüller, Nucl. Phys. A91 (1967) 241; A94 (1967) 1; A97 (1967) 378, "Shell-Model Approach to Nuclear Reactions, John Wiley and Sons Inc., New York (1969).

7. S. Fallieros and R. A. Ferrell, Phys. Rev. 154 (1967) 921.

The Scattering of Alpha Particles by ^{40}Ca*

R. H. Davis

Department of Physics, Florida State University, Tallahassee, Florida

Abstract: A complex potential model description of the scattering of alpha particles by ^{40}Ca in the bombarding energy range 5 to 18 MeV is discussed. Phase equivalent potentials which best represent the angular distributions at high energies are presented and a possible means of choosing one of them is considered. Between 5 and 10 MeV bombarding energy, the introduction of a compound elastic scattering term is found to be essential. This analysis requires energy averaging of the data. The complex potential model has been further extended by making the imaginary part ℓ-dependent in order to obtain satisfactory fits to energy averaged angular distributions. The variation of the parameters throughout the entire energy range is obtained and the significance of the statistical parameters is reviewed.

I. INTRODUCTION

This paper is a report on several recent studies of the elastic scattering of alpha particles by ^{40}Ca. The data between 5 and 12 MeV bombarding energy are those obtained by John et al.[1] while those between 12 and 18 MeV have been reported by Robinson et al.[2] This paper further draws upon the work of A. E. Bisson, J. P. Aldridge, and K. A. Eberhard.

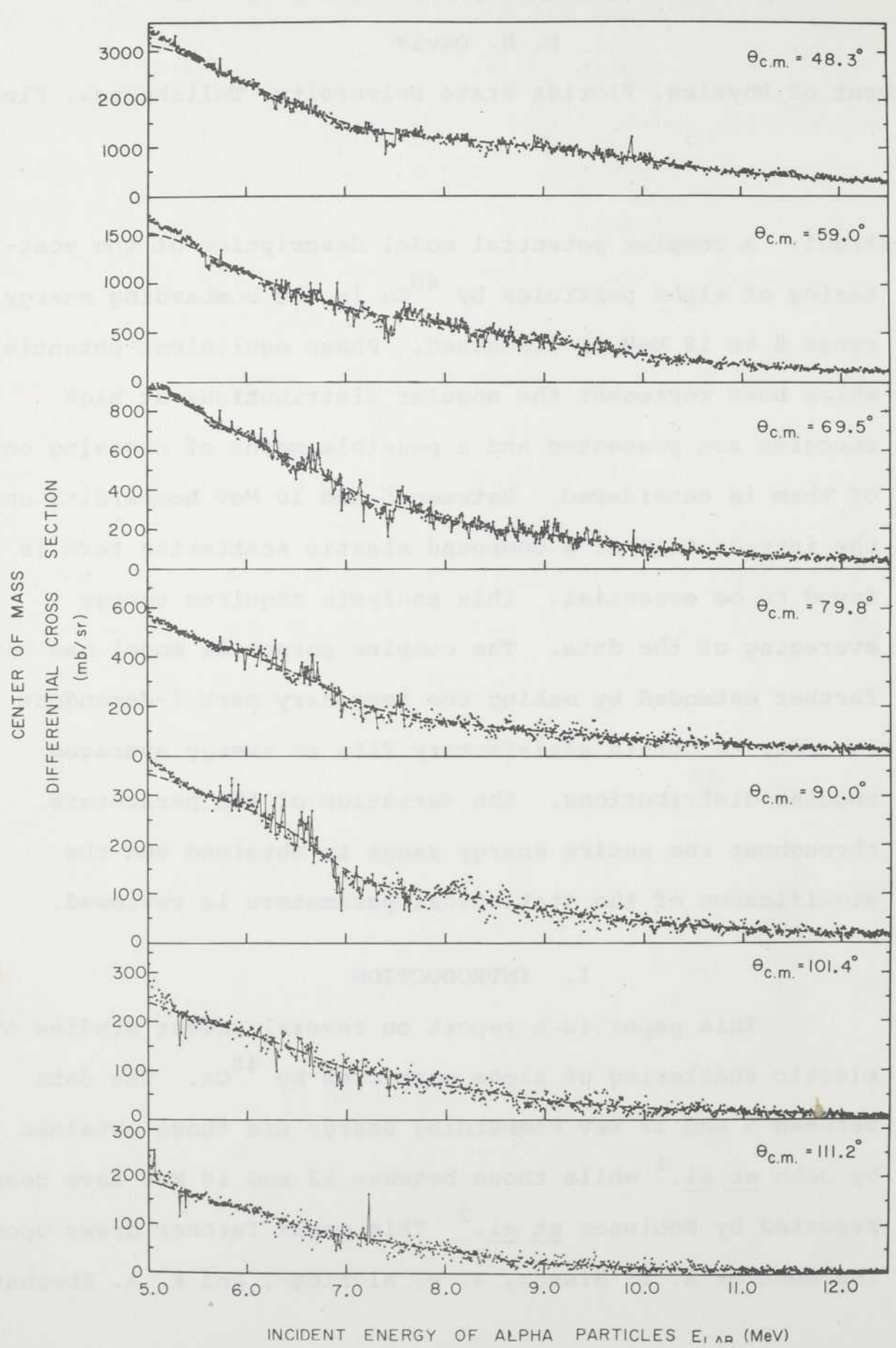

Fig. 1. Excitation curves for $^{40}Ca(\alpha,\alpha)^{40}Ca$ at forward and middle angles, 5.0 to 12.5 MeV.

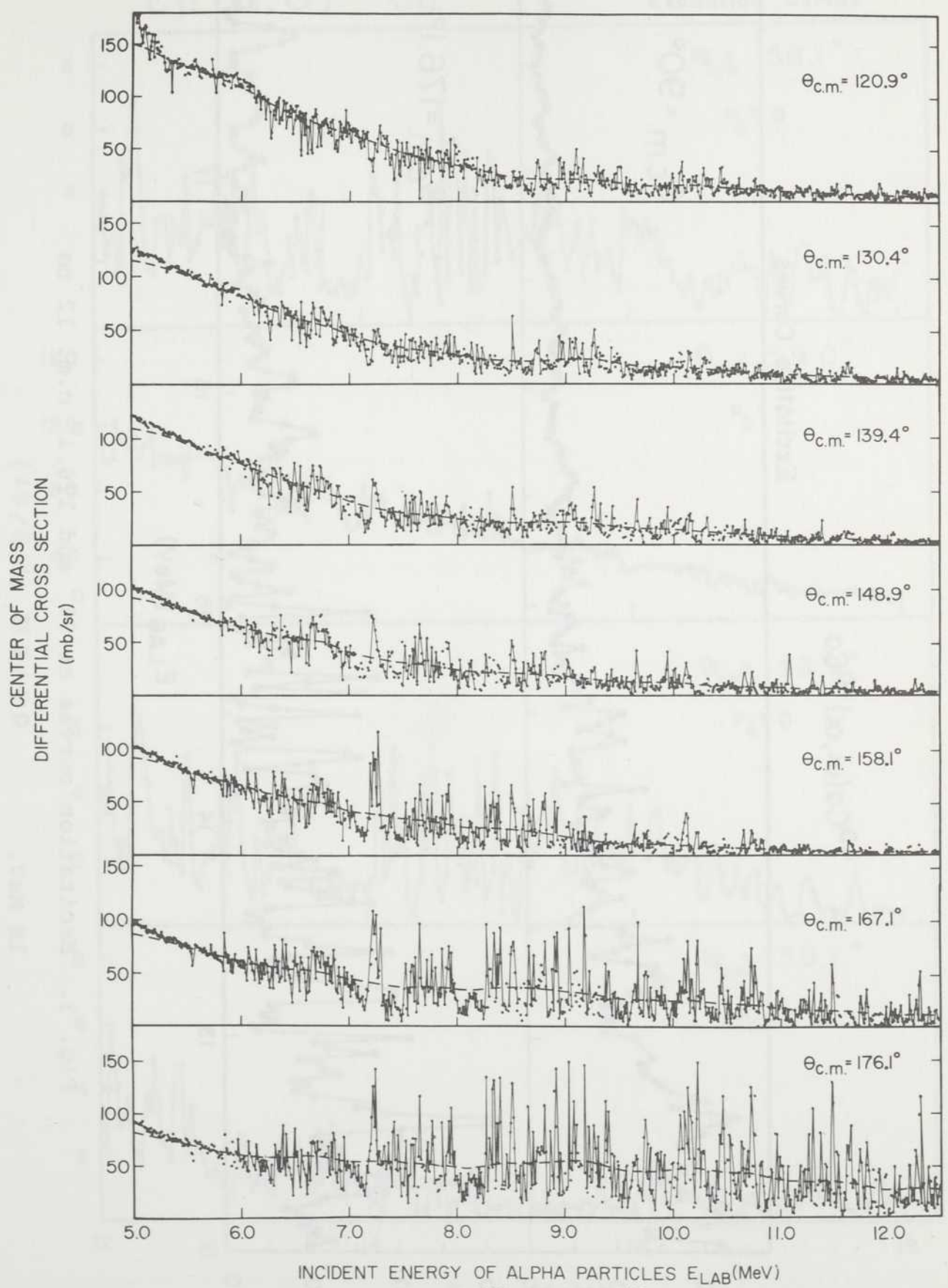

Fig. 2. Excitation curves for $^{40}Ca(\alpha,\alpha)^{40}Ca$ at backward angles, 5.0 to 12.5 MeV.

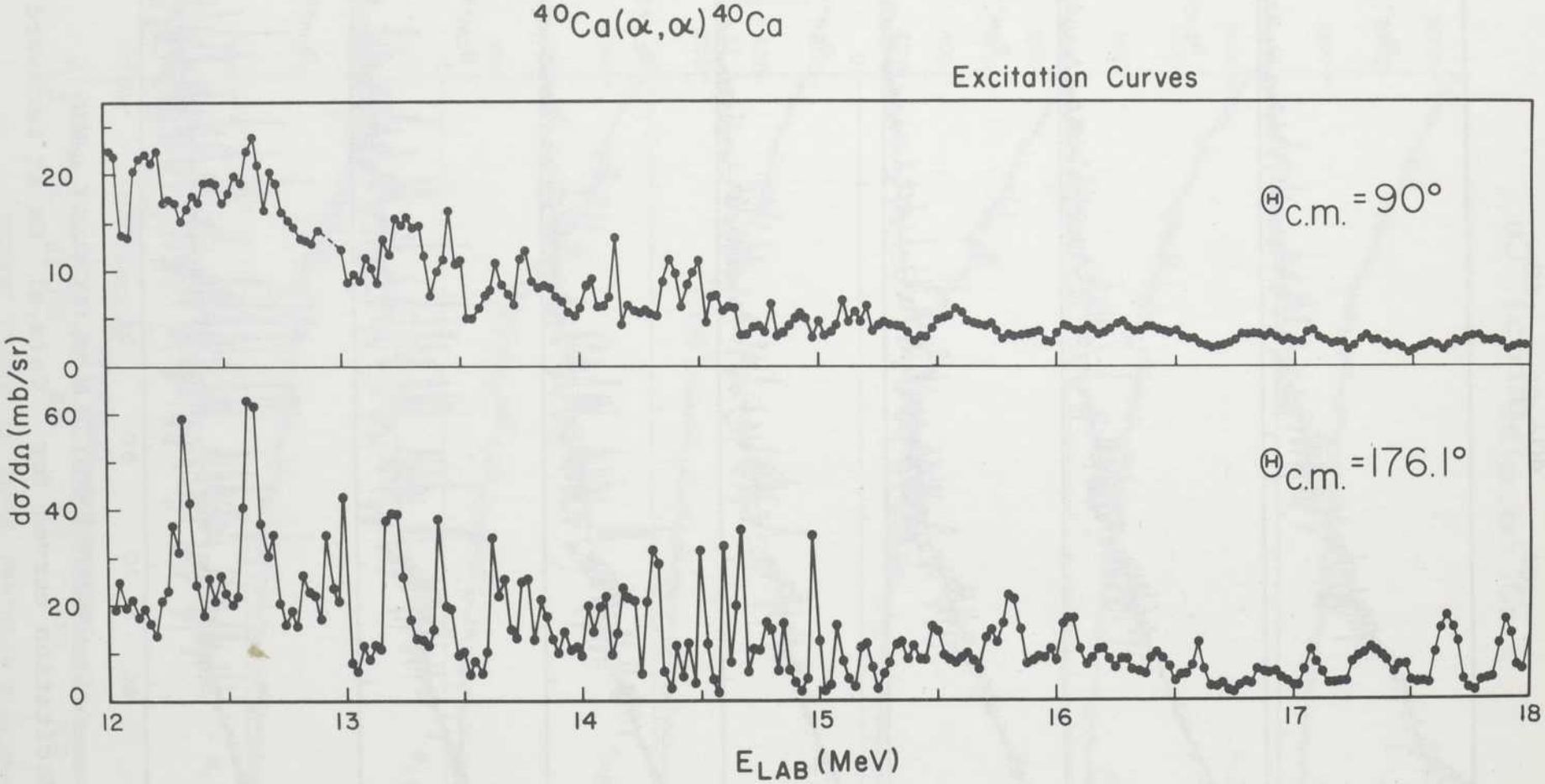

Fig. 3. Excitation curves at 90° and 176.1° c.m. 12 to 18 MeV.

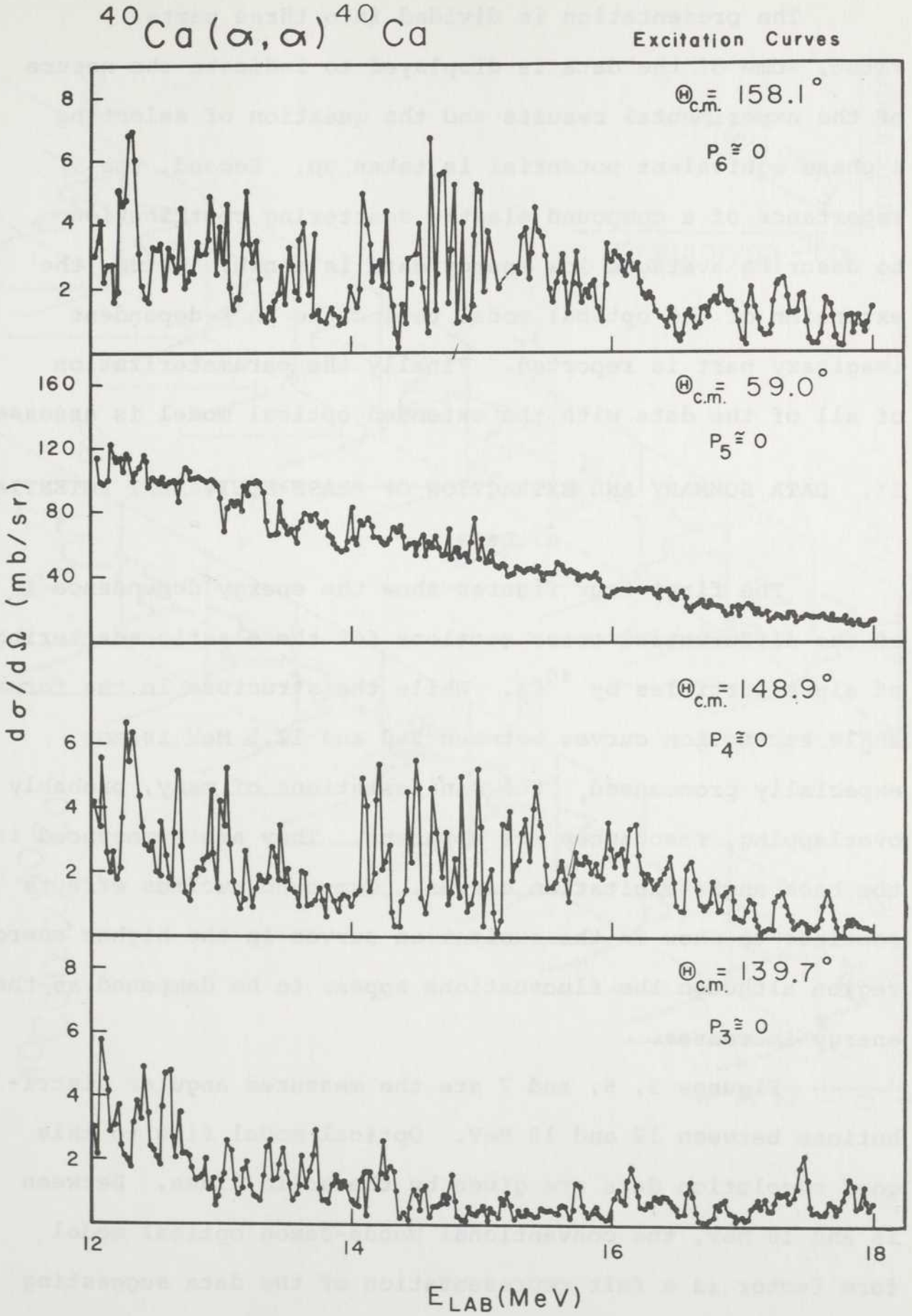

Fig. 4. Excitation curves at backward angles 12 to 18 MeV.

The presentation is divided into three parts. First, some of the data is displayed to indicate the nature of the experimental results and the question of selecting a phase equivalent potential is taken up. Second, the importance of a compound elastic scattering contribution to describe averaged low energy data is shown. Third, the extension of the optical model to include an ℓ-dependent imaginary part is reported. Finally the parameterization of all of the data with the extended optical model is assessed.

II. DATA SUMMARY AND EXTRACTION OF PHASE EQUIVALENT POTENTIALS

A. Data

The first four figures show the energy dependence of the differential cross sections for the elastic scattering of alpha particles by ^{40}Ca. While the structure in the forward angle excitation curves between 5.0 and 12.5 MeV is not expecially pronounced, the manifestations of many, probably overlapping, resonances are apparent. They are pronounced in the back angle excitation curves. Compound nucleus effects continue to show in the excitation curves in the higher energy region although the fluctuations appear to be dampened as the energy increases.

Figures 5, 6, and 7 are the measured angular distributions between 12 and 18 MeV. Optical model fits to this good resolution data are given by the solid lines. Between 16 and 18 MeV, the conventional Woods-Saxon optical model form factor is a fair representation of the data suggesting

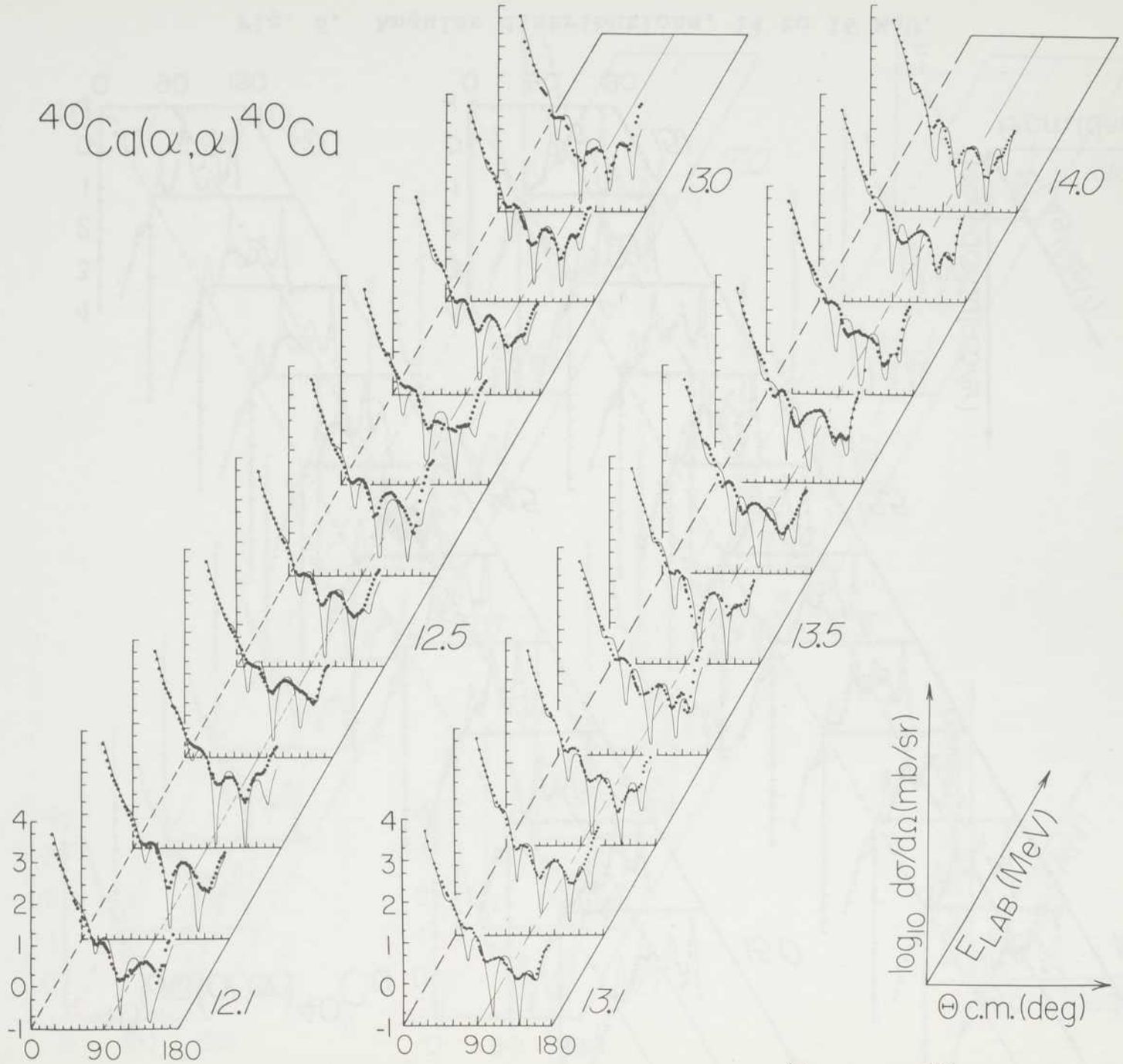

Fig. 5. Angular distributions for $^{40}Ca(\alpha,\alpha)^{40}Ca$ 12 to 14 MeV

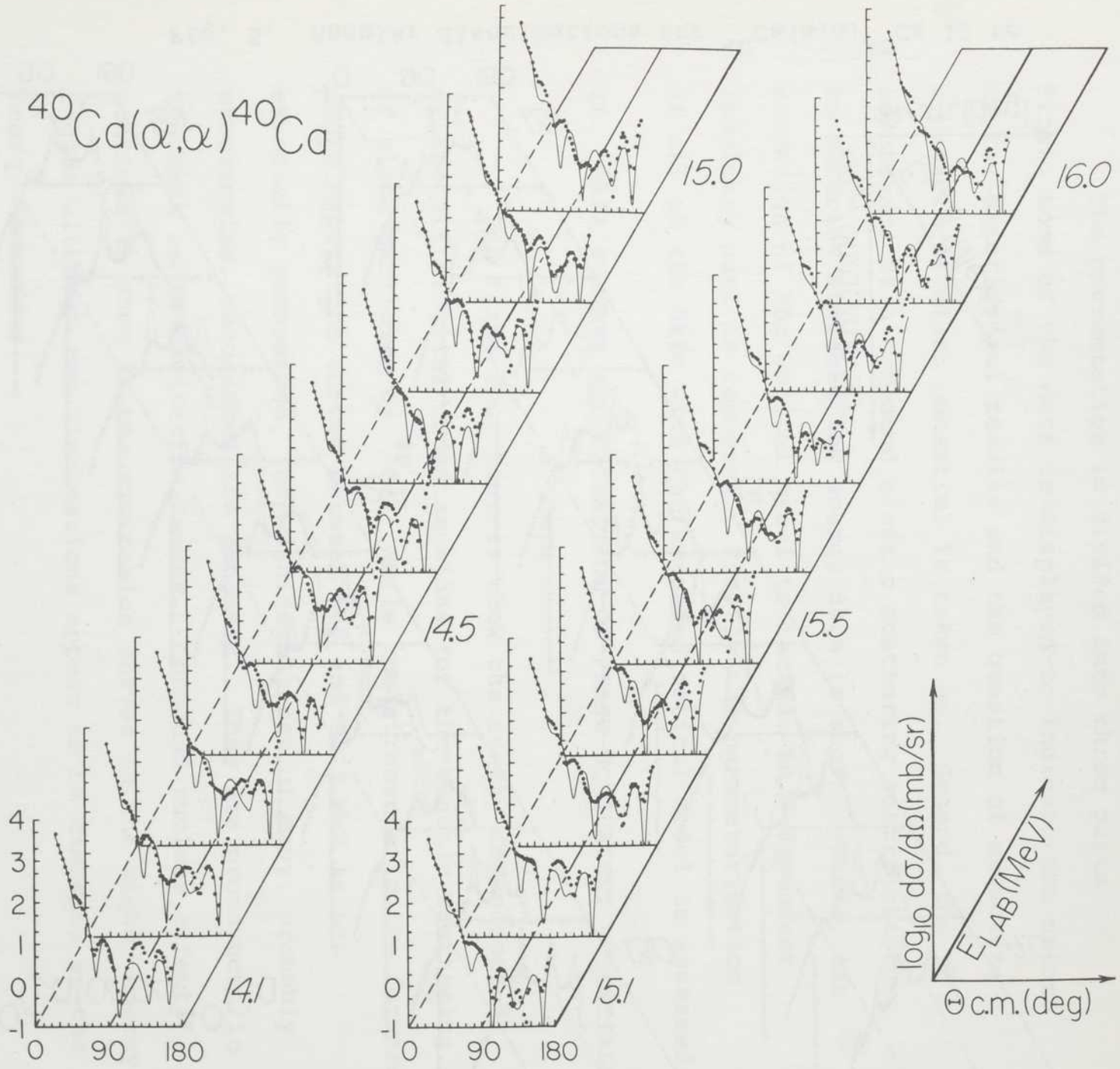

Fig. 6. Angular distributions, 14 to 16 MeV.

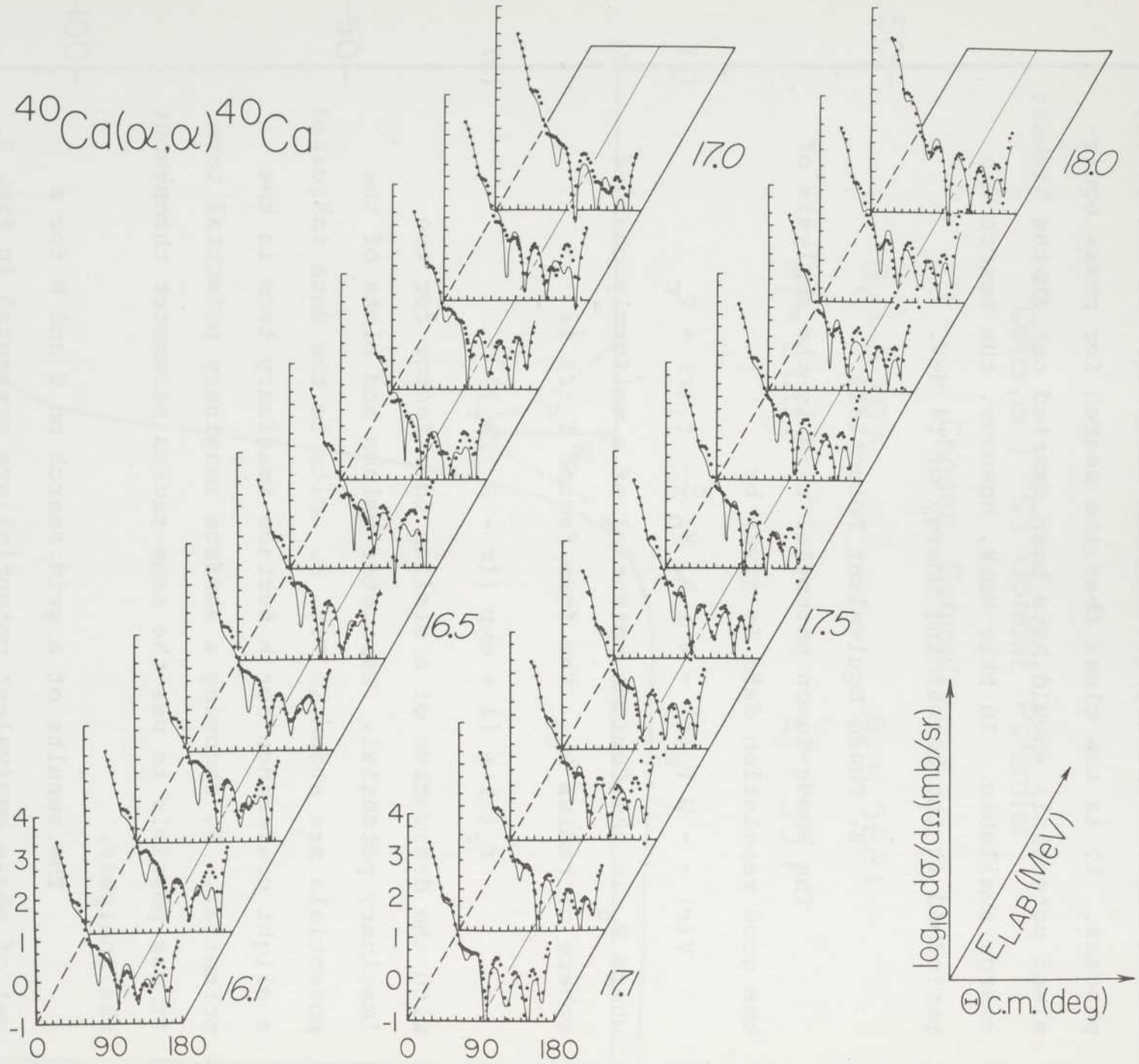

Fig. 7. Angular distributions, 16 to 18 MeV.

that a direct scattering mechanism dominates the scattering process. It is now clear that the search for phase equivalent potentials should have been carried out at the highest energy available. In this work, however, the search was performed at the bombarding energy of 14 MeV.

B. Phase Equivalent Potentials

The Woods-Saxon potential used in the analysis of the good resolution data is given by

$$V(r) = - U f_m(r) - 4 i A_i W_D \frac{d}{dr} f_i(r) + V_c \qquad (1)$$

where V_c is the Coulomb potential of a uniformly charged sphere of radius R_c. The form factor $f_r(r)$ is

$$f_r(r) = \{1 + \exp [(r - R_r)/A_r]\}^{-1} \qquad (2)$$

with the derivative of a similar form factor for the imaginary potential. Parameter values and plots of the potentials are shown in Fig. 8. Fits to the data indicated a slight preference for a surface imaginary term in the potential. By choosing a surface imaginary potential term it was possible to use the same radius parameter throughout the analysis.

The results of a grid search on U and W for a set of phase equivalent potential are presented in Fig. 9. Contours of a fitting parameter $\mathcal{J}^2$ are plotted against the coordinates U and W. The quantity $\mathcal{J}^2$ is the usual χ^2 function divided by the Rutherford scattering cross section in order to force a better fit to the back angle scattering data. The x symbols shown on the plot are the minima for the χ^2 function.

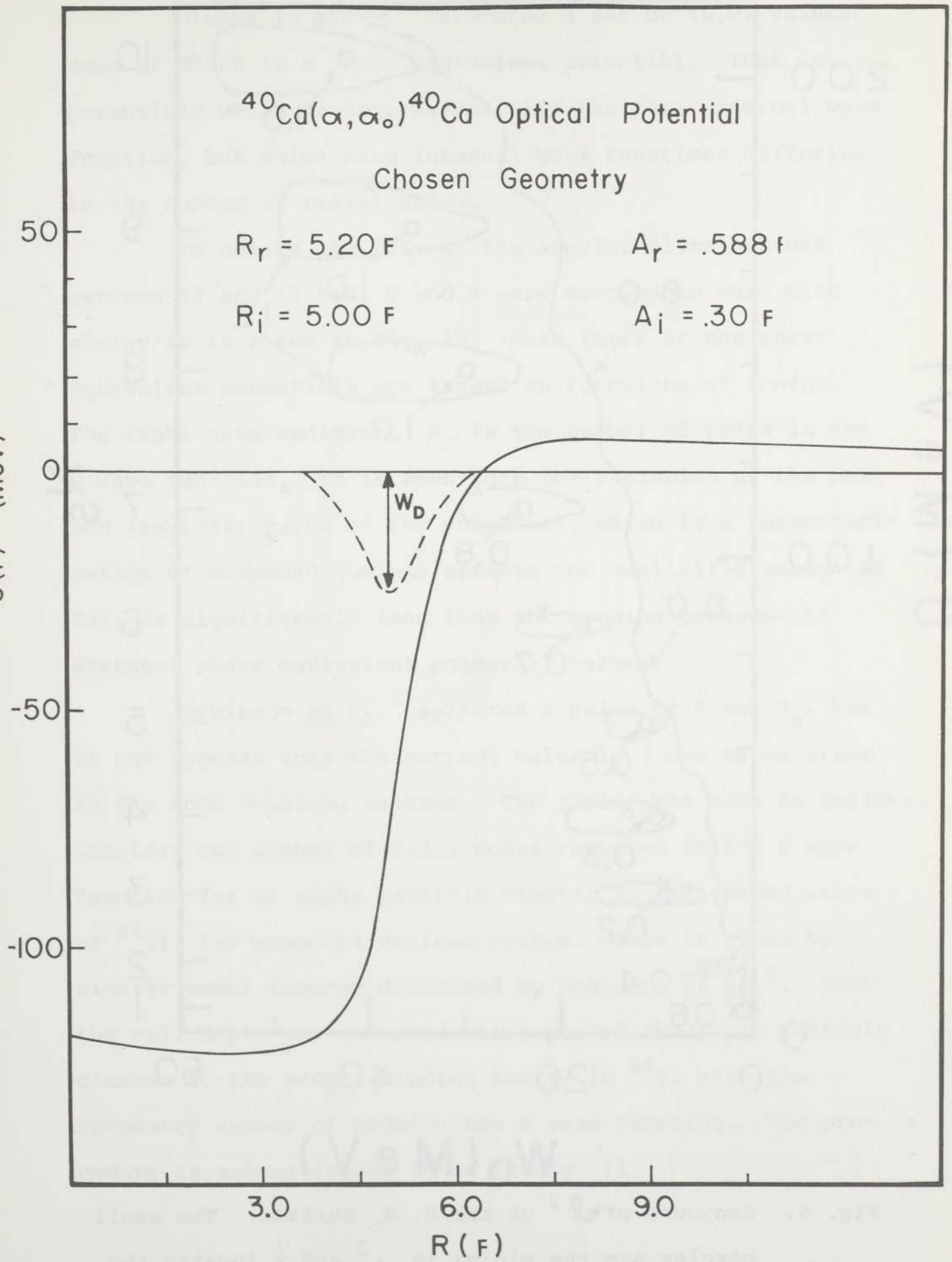

Fig. 8. Optical model potential.

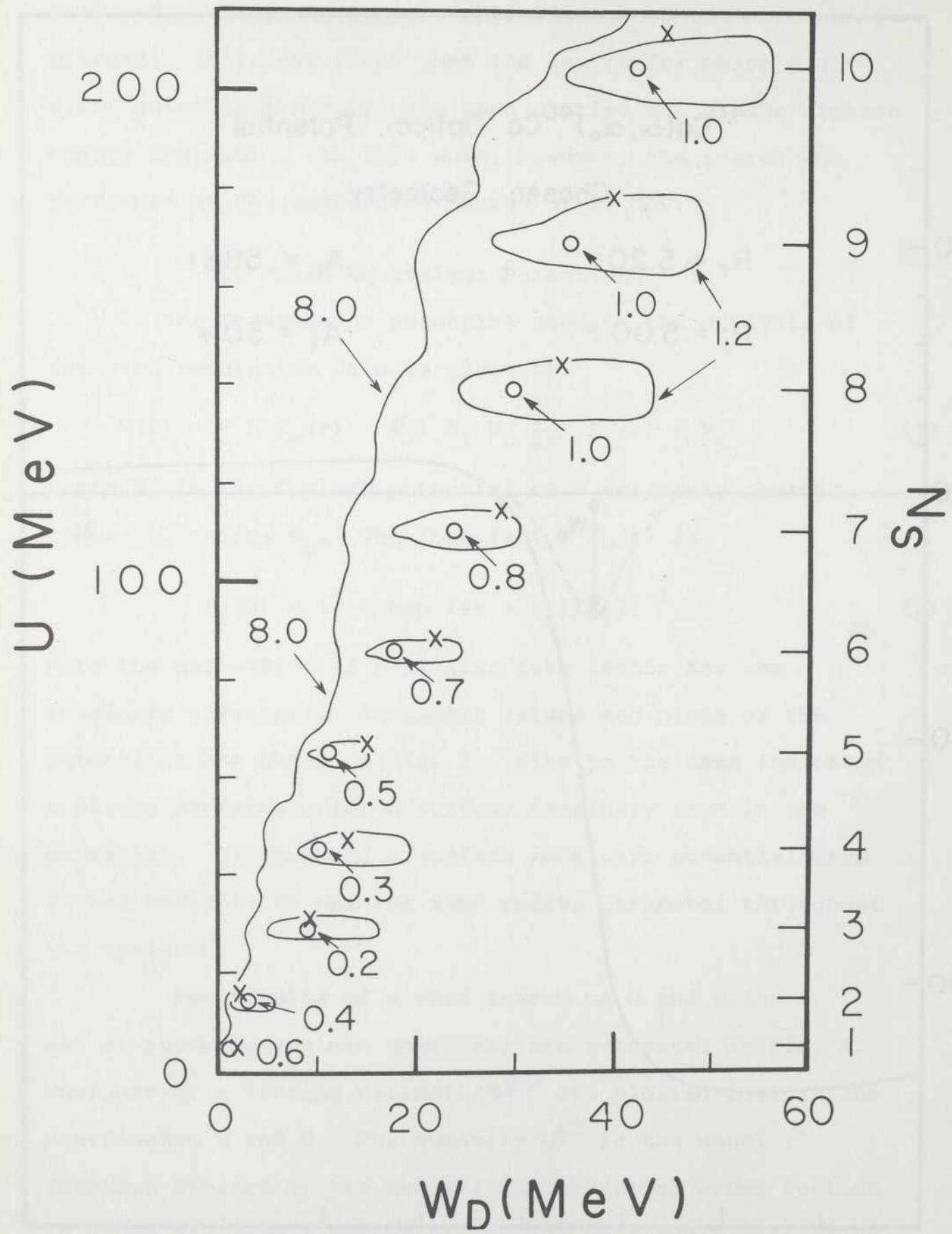

Fig. 9. Contours of χ^2 on the U, W_o surface. The small circles are the minima in χ^2 and $\underline{x}$ locates the minima in χ^2. The label N_s is the number of nodes in the S wave function.

Minima in the χ^2 determine a set of (U,W) values each of which is a phase equivalent potential. That is, potentials which produce essentially the same external wave function, but which have internal wave functions differing in the number of radial nodes.

To obtain the fits to the angular distributions between 12 and 18 MeV, U and W were allowed to vary with energy as is shown in Fig. 10. Here three of the phase equivalent potentials are traced as functions of energy. The right hand ordinate, N_s, is the number of nodes in the S wave function. It is seen that the variation of the real and imaginary parts of the potential, which is a parameterization of compound nucleus effects not explicitly accounted for, is significantly less than the spacing between the averaged phase equivalent potential values.

Robinson et al.[2] selected a value of 8 for N_s, but it now appears that the correct value is 7 due to an error in the node counting routine. The choice was made as follows. Consider the number of radial nodes required in the S wave function for an alpha particle cluster in the ground state of ^{44}Ti, the compound nucleus system. This is given by cluster model theorem discussed by Robinson et al.[2]. Next the well depth was computed which placed the alpha particle cluster at the proper binding energy in ^{44}Ti with the necessary number of nodes in the S wave function. The procedure is schematically shown in Fig. 11.

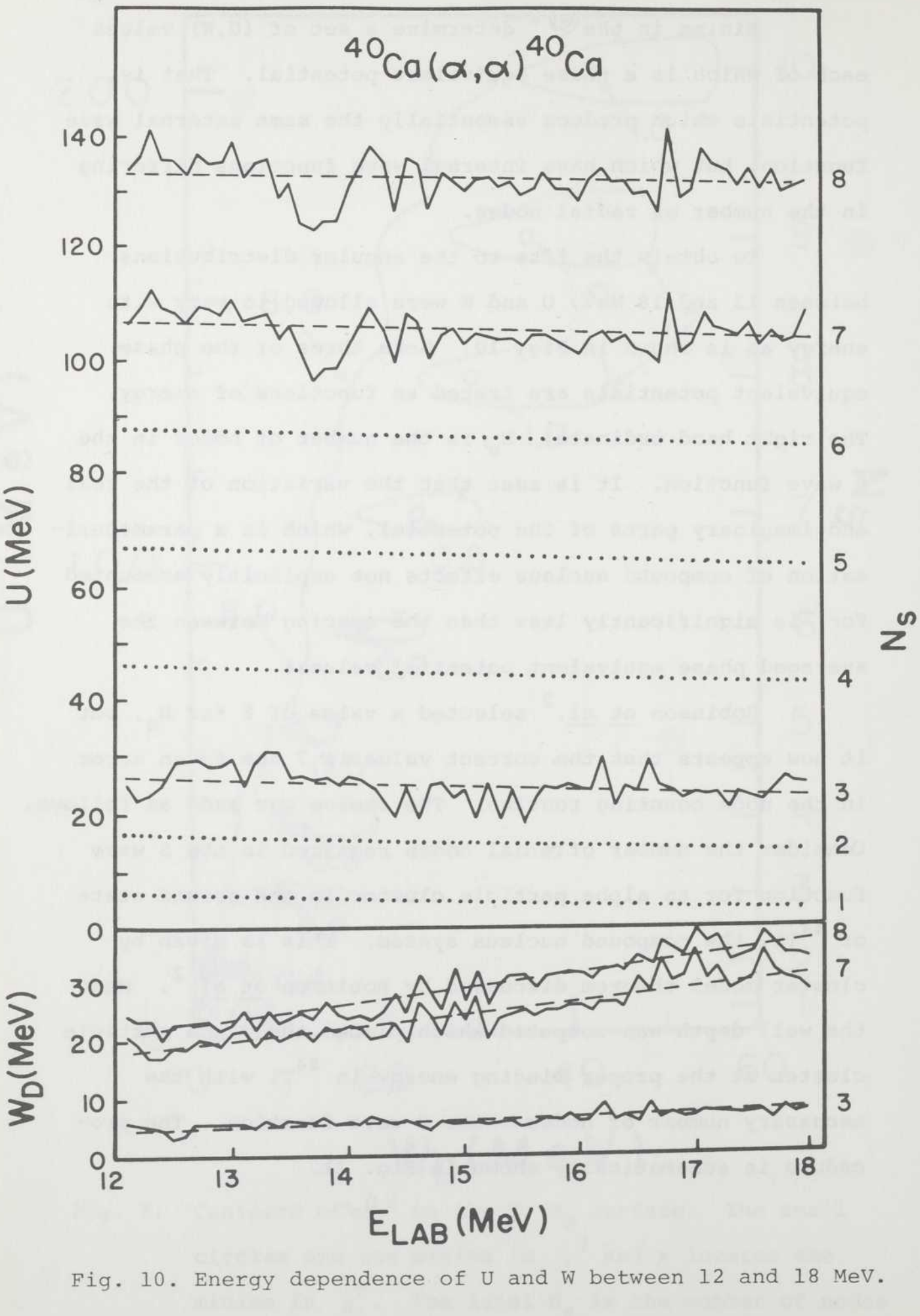

Fig. 10. Energy dependence of U and W between 12 and 18 MeV.

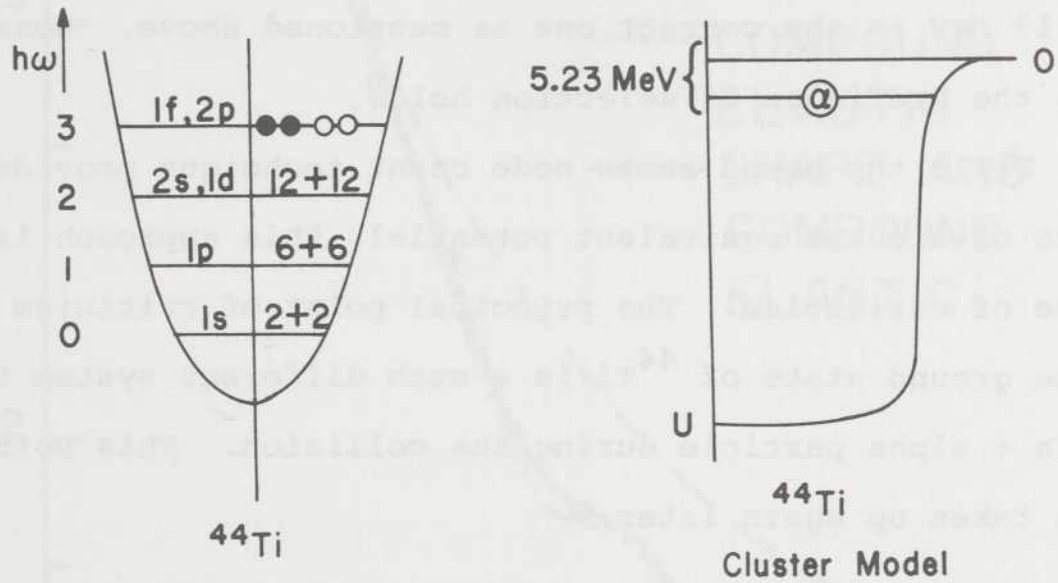

Fig. 11. Diagram of the bound state calculation technique for selecting one of the phase equivalent potentials.

The well depth obtained from the bound state calculation is in surprisingly good agreement with one of the phase equivalent real well depths (within several percent) Robinson et al.[2] selected a value of 136 MeV which agrees well with the 132 MeV phase equivalent potential well depth. A more recent calculation shows that the $N_s = 7$ value of about 713 MeV is the correct one as mentioned above. Nonetheless the precision of selection holds.

While the bound state node count technique provided a choice of a phase equivalent potential, this approach is not free of ciriticism. The principal point of criticism is that the ground state of ^{44}Ti is a much different system than the ^{40}Ca + alpha particle during the collision. This point will be taken up again later.

III. COMPOUND ELASTIC SCATTERING CONTRIBUTION

Equipped with one of the phase equivalent potentials as discussed in the previous section, analysis of the data between 5.0 and 12.5 MeV was undertaken. It was immediately clear that an optical model analysis with a Woods-Saxon form factor did not produce satisfactory fits to the good resolution data. The nature of the discrepancy is shown in Fig. 12 where the curve labeled shape elastic is that generated by the Woods-Saxon form factor. Computed yields at back angles were generally too low. Searches for parameter sets which would remove this discrepancy were unsuccessful.

(dσ/dΩ)c.m.(mb/sr)

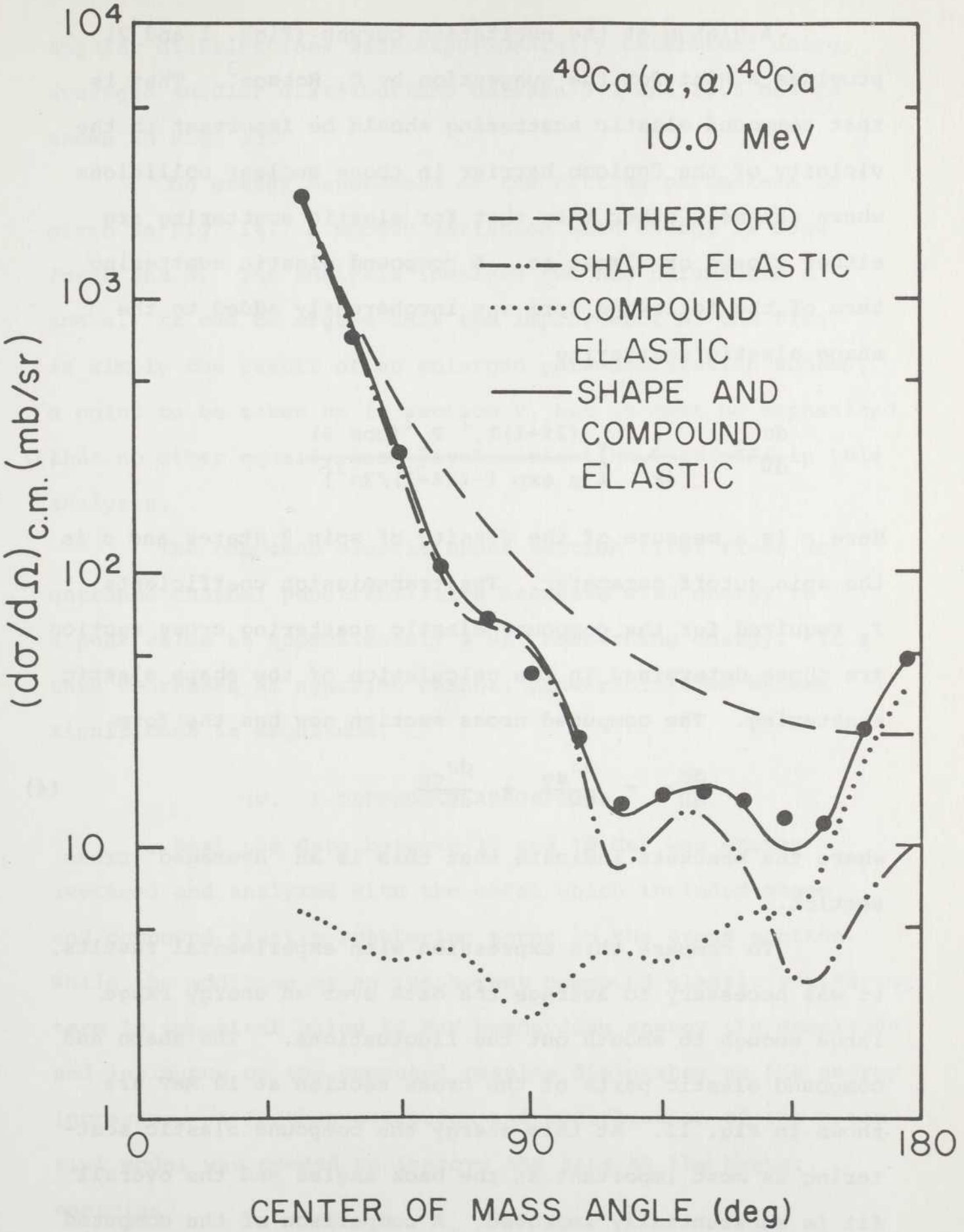

Fig. 12. Fit to 10.0 MeV data with shape and compound elastic scattering model.

A glance at the excitation curves (Figs. 1 and 2) provides a hint for the suggestion by D. Robson[3]. That is that compound elastic scattering should be important in the vicinity of the Coulomb barrier in those nuclear collisions where channels other than that for elastic scattering are either closed or almost so. A compound elastic scattering term of the following form was incoherently added to the shape elastic scattering

$$\frac{d\sigma_{ce}}{d\Omega} = \frac{1}{4k^2} \sum_{\ell} \frac{(2\ell+1)T_\ell^{\,2}\, P_\ell^{\,2}(\cos\theta)}{\rho \exp\left[-\ell(\ell+1)/2\sigma^2\right]} \qquad (3)$$

Here ρ is a measure of the density of spin 0 states and σ is the spin cutoff parameter. The transmission coefficients T_ℓ required for the compound elastic scattering cross section are those determined in the calculation of the shape elastic scattering. The computed cross section now has the form

$$\left\langle \frac{d\sigma}{d\Omega} \right\rangle = \frac{d\sigma_{se}}{d\Omega} + \frac{d\sigma_{ce}}{d\Omega} \qquad (4)$$

where the brackets indicate that this is an "averaged" cross section.

To compare this expression with experimental results, it was necessary to average the data over an energy range large enough to smooth out the fluctuations.[1] The shape and compound elastic parts of the cross section at 10 MeV are shown in Fig. 12. At this energy the compound elastic scattering is most important at the back angles and the overall fit is substantially improved. A comparison of the computed

angular distributions with experimentally determined energy averaged angular distributions between 5.5 and 12.5 MeV is shown in Fig. 13.

The energy dependence of the fitting parameters is given in Fig. 14. A smooth variation with energy is seen for U and W. The analysis involves two new parameters ρ and σ. It can be argued that the improvement of the fits is simply the result of an enlarged parameterization scheme, a point to be taken up in section V, but it must be emphasized that no other equally good parameterization was found in this analysis.

The compound elastic cross section first rises as entrance channel penetrabilities increase with energy to a peak value at approximately 9 MeV bombarding energy. It then decreases as reaction channel penetrabilities become significant in magnitude.

IV. ℓ-DEPENDENT ABSORPTION

Next the data between 12 and 18 MeV was energy averaged and analyzed with the model which included shape and compound elastic scattering terms in the cross section. While the addition of an incoherent compound elastic scattering term is important below 12 MeV bombarding energy its magnitude and influence on the computed results diminishes as the energy increases. A further extension and modification of the potential model was needed to improve the fits at the higher energies.

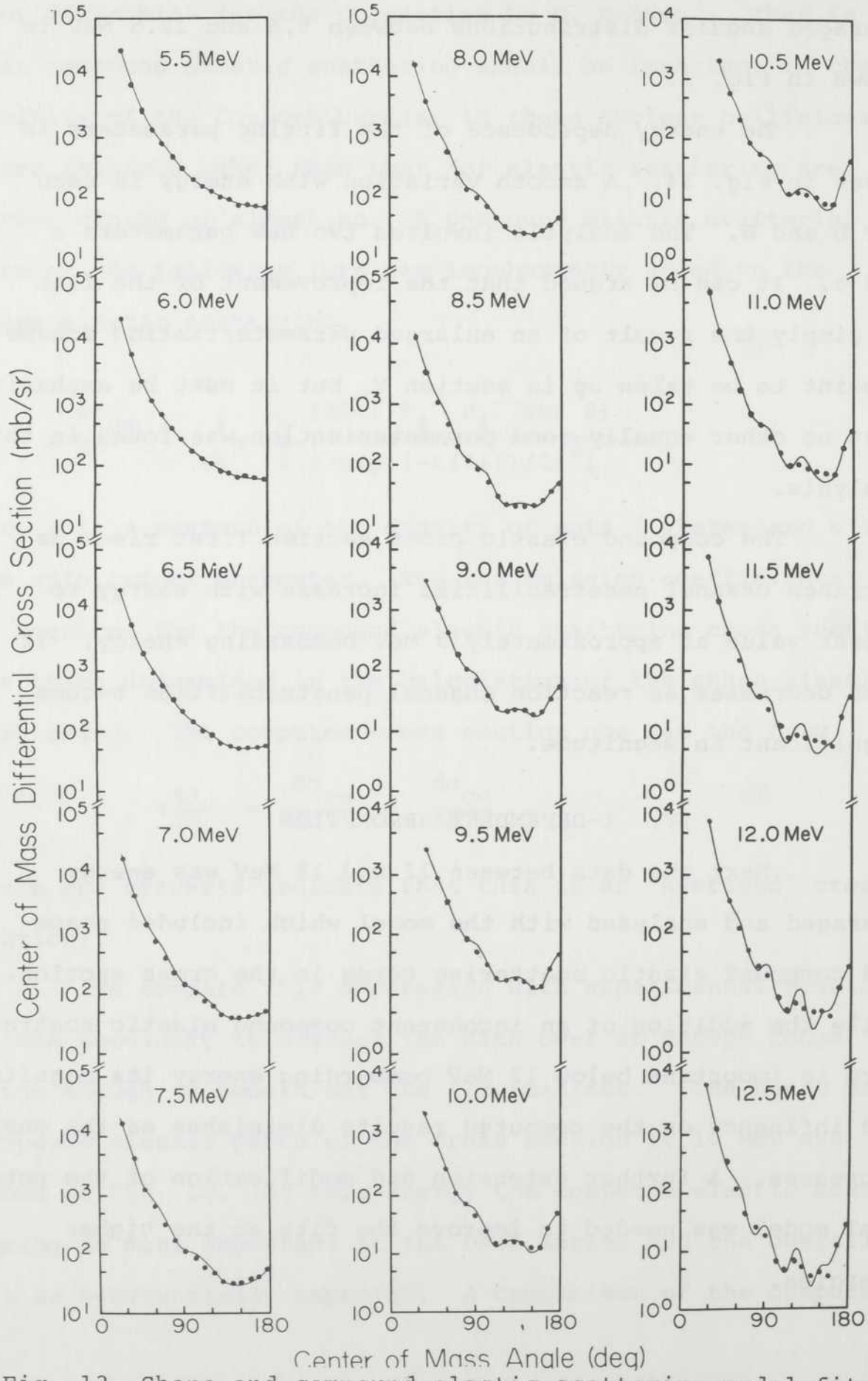

Fig. 13. Shape and compound elastic scattering model fits to data, 5.5 to 12.5 MeV.

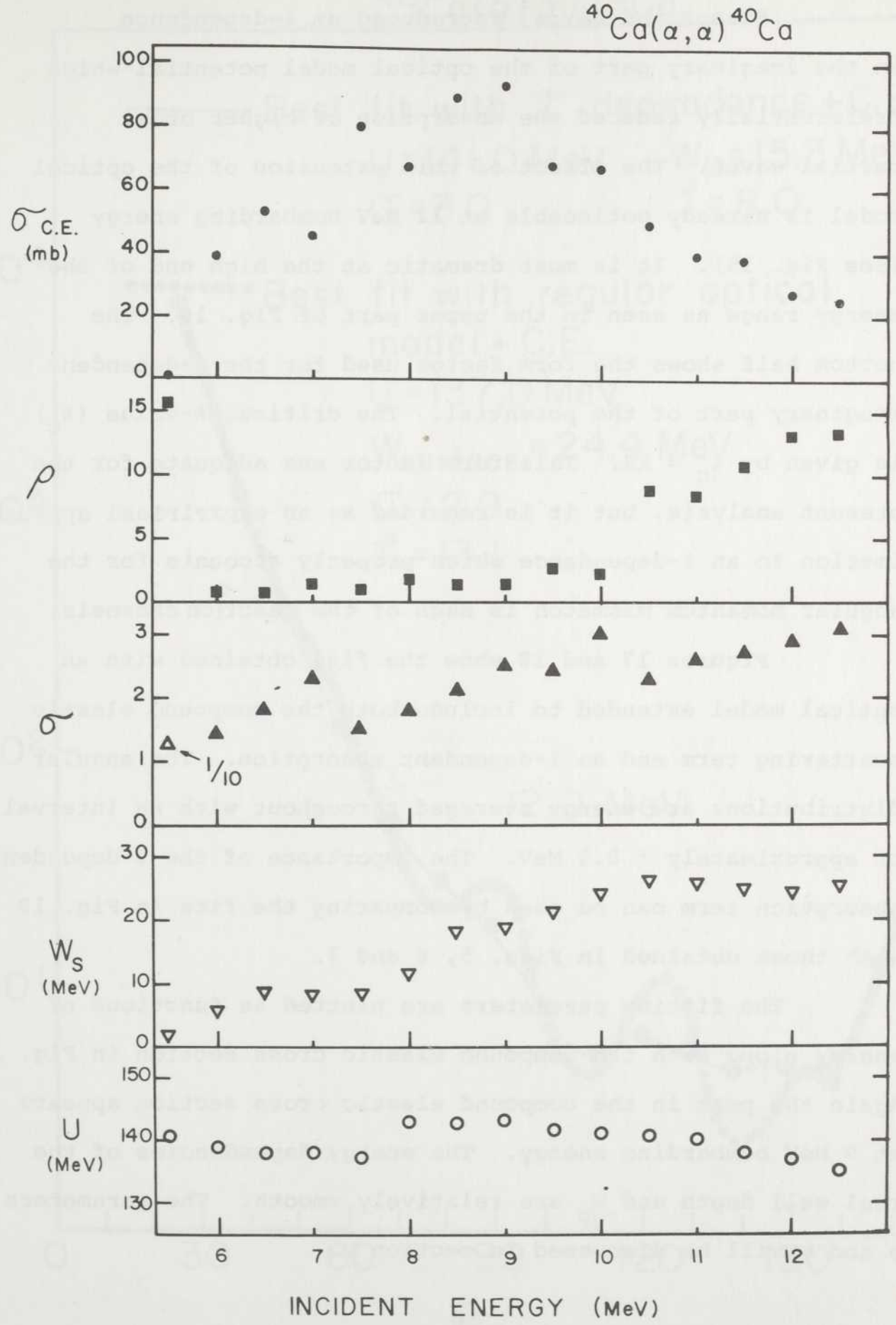

Fig. 14. Energy dependence of parameters, 5.5 to 12.5 MeV.

Bisson and Davis[4] introduced an ℓ-dependence in the imaginary part of the optical model potential which preferentially reduced the absorption of higher order partial waves. The effect of this extension of the optical model is already noticeable at 12 MeV bombarding energy (See Fig. 15). It is most dramatic at the high end of the energy range as seen in the upper part of Fig. 16. The bottom half shows the form factor used for the ℓ-dependent imaginary part of the potential. The critical ℓ-value (ℓ_c) is given by $\ell_c = kR$. This form factor was adequate for the present analysis, but it is regarded as an empiririical approximation to an ℓ-dependence which properly accounts for the angular momentum mismatch in each of the reaction channels.

Figures 17 and 18 show the fits obtained with an optical model extended to include both the compound elastic scattering term and an ℓ-dependent absorption. The angular distributions are energy averaged throughout with an interval of approximately $\pm$ 0.5 MeV. The importance of the ℓ-dependent absorption term can be seen by comparing the fits in Fig. 18 with those obtained in Figs. 5, 6 and 7.

The fitting parameters are plotted as functions of energy along with the compound elastic cross section in Fig. 19. Again the peak in the compound elastic cross section appears at 9 MeV bombarding energy. The energy dependencies of the real well depth and W_p are relatively smooth. The parameters ρ and σ will be discussed in section V.

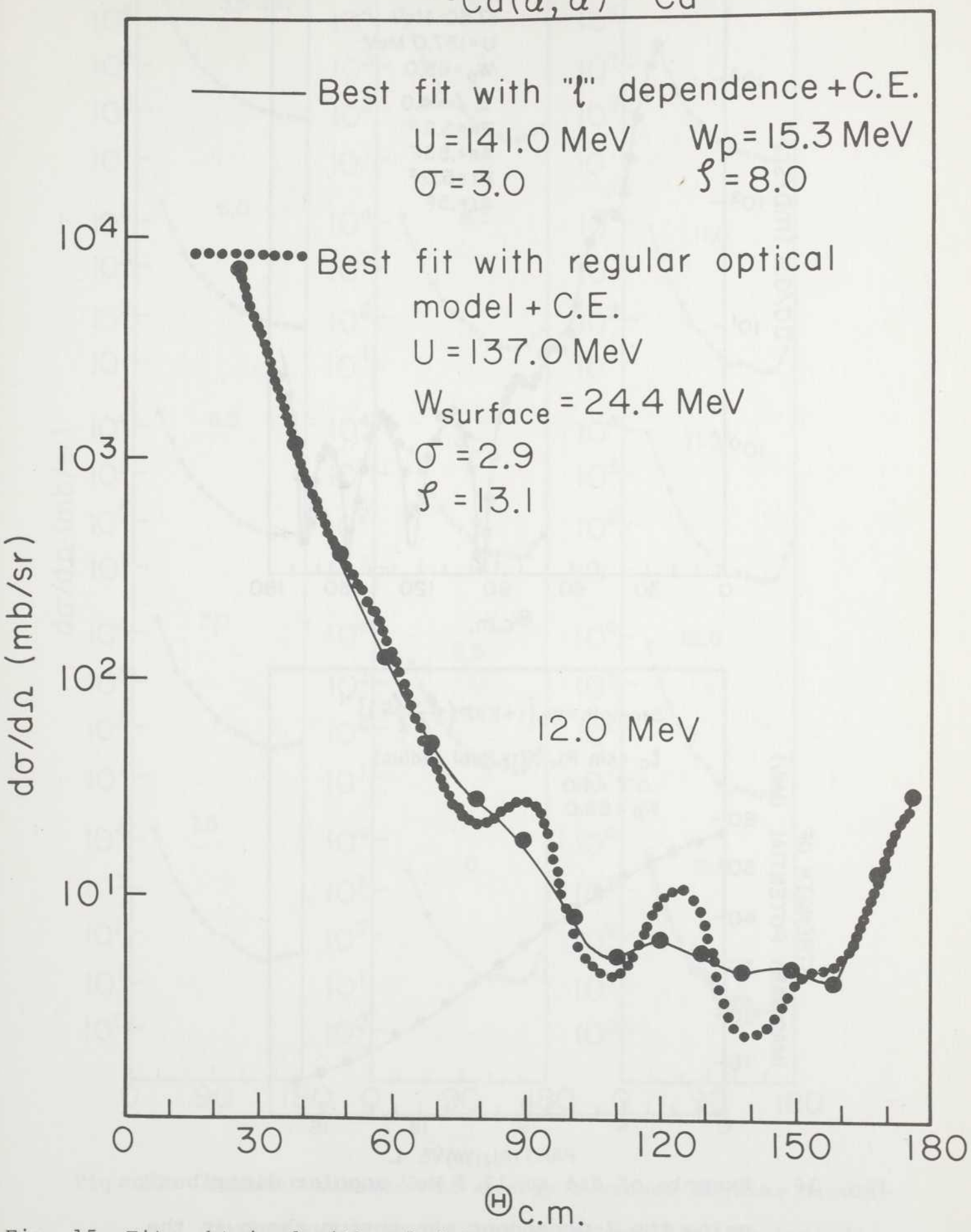

Fig. 15. Fits obtained with and without ℓ-dependent absorption at 12.0 MeV.

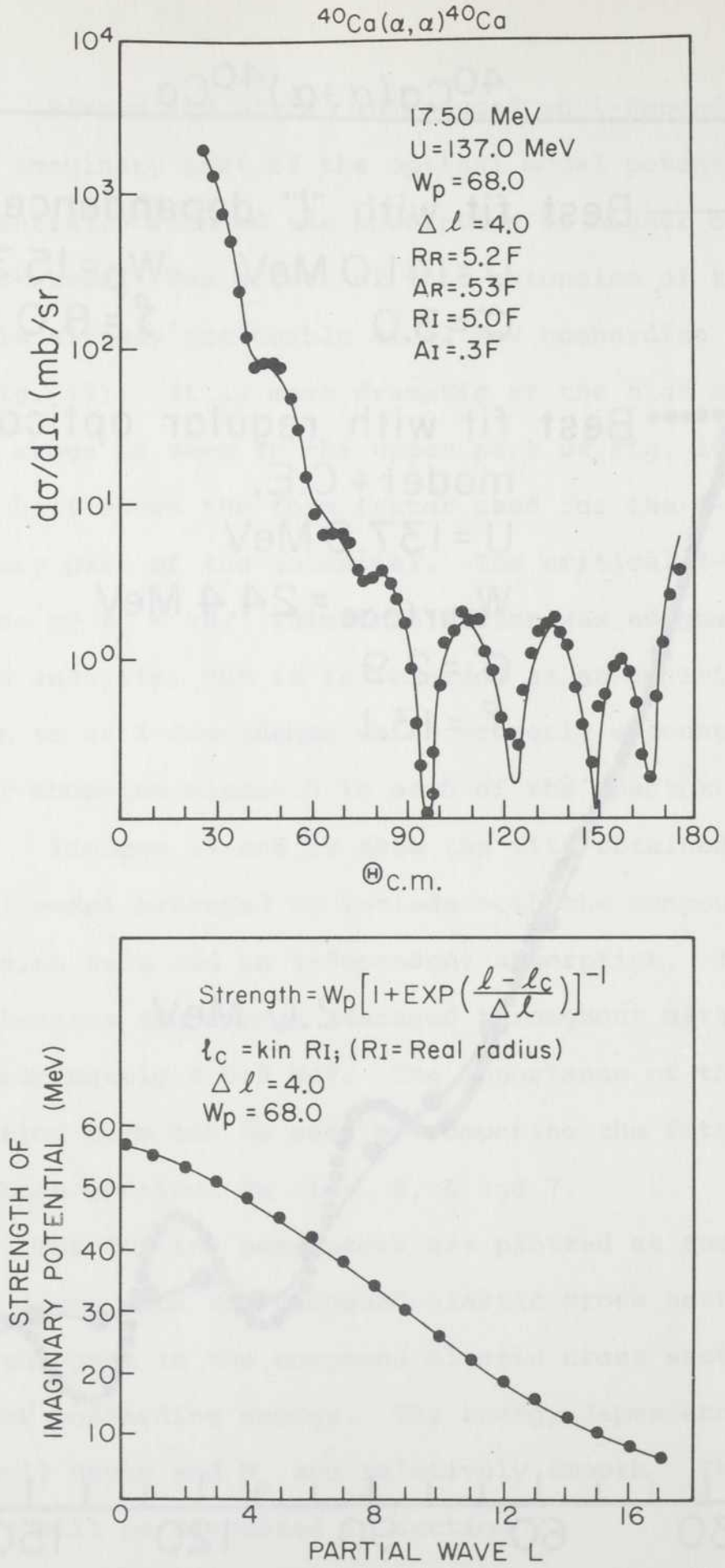

Fig. 16. Example of fit to 17.5 MeV angular distribution using the ℓ-dependent absorption shown in the lower part. This form factor for the ℓ-dependence was used throughout this analysis.

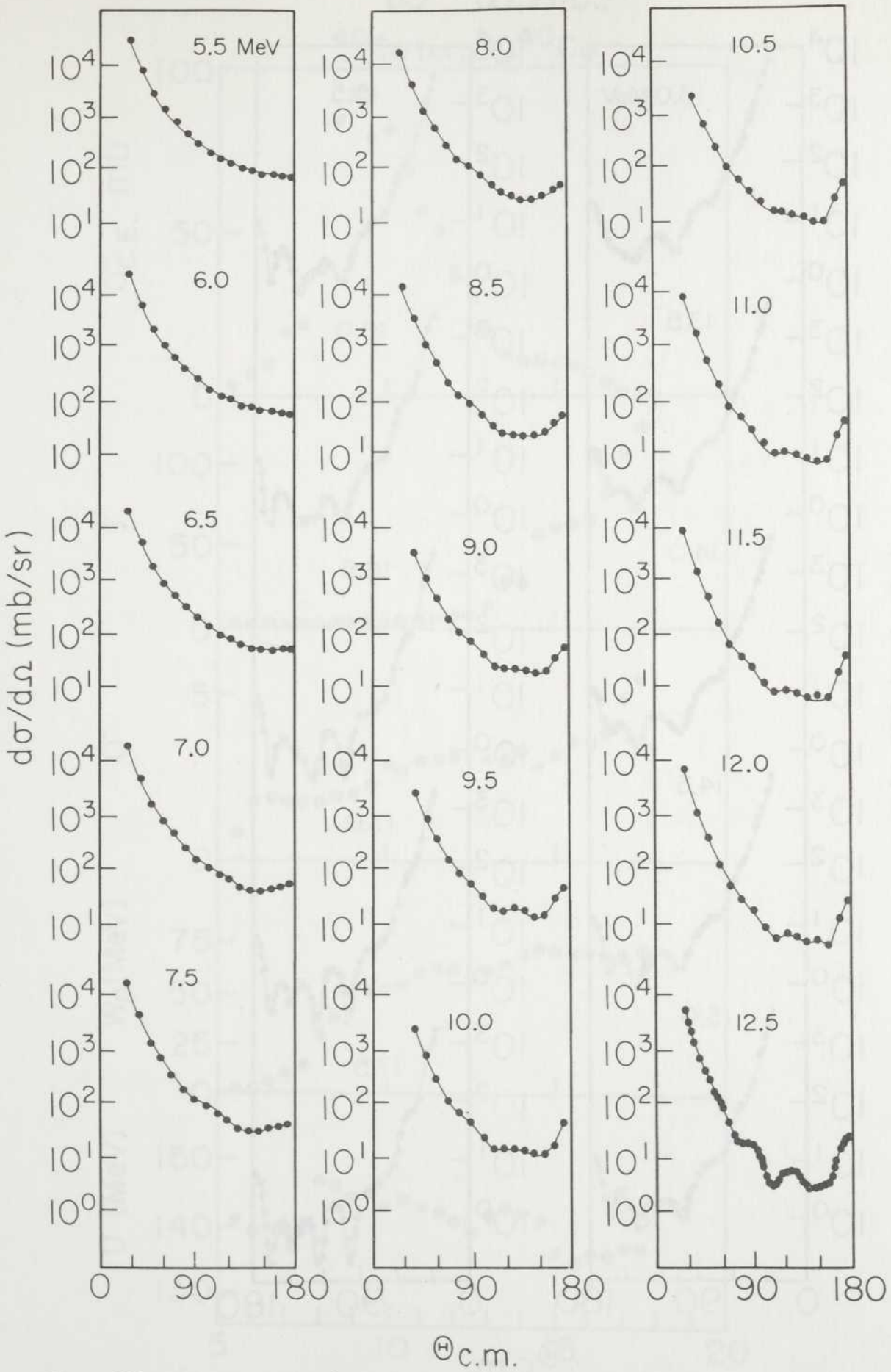

Fig. 17. Parameterization of energy averaged angular distributions with an optical model modified to include compound elastic scattering and an ℓ-dependent imaginary part, 5.5 to 12.5 MeV.

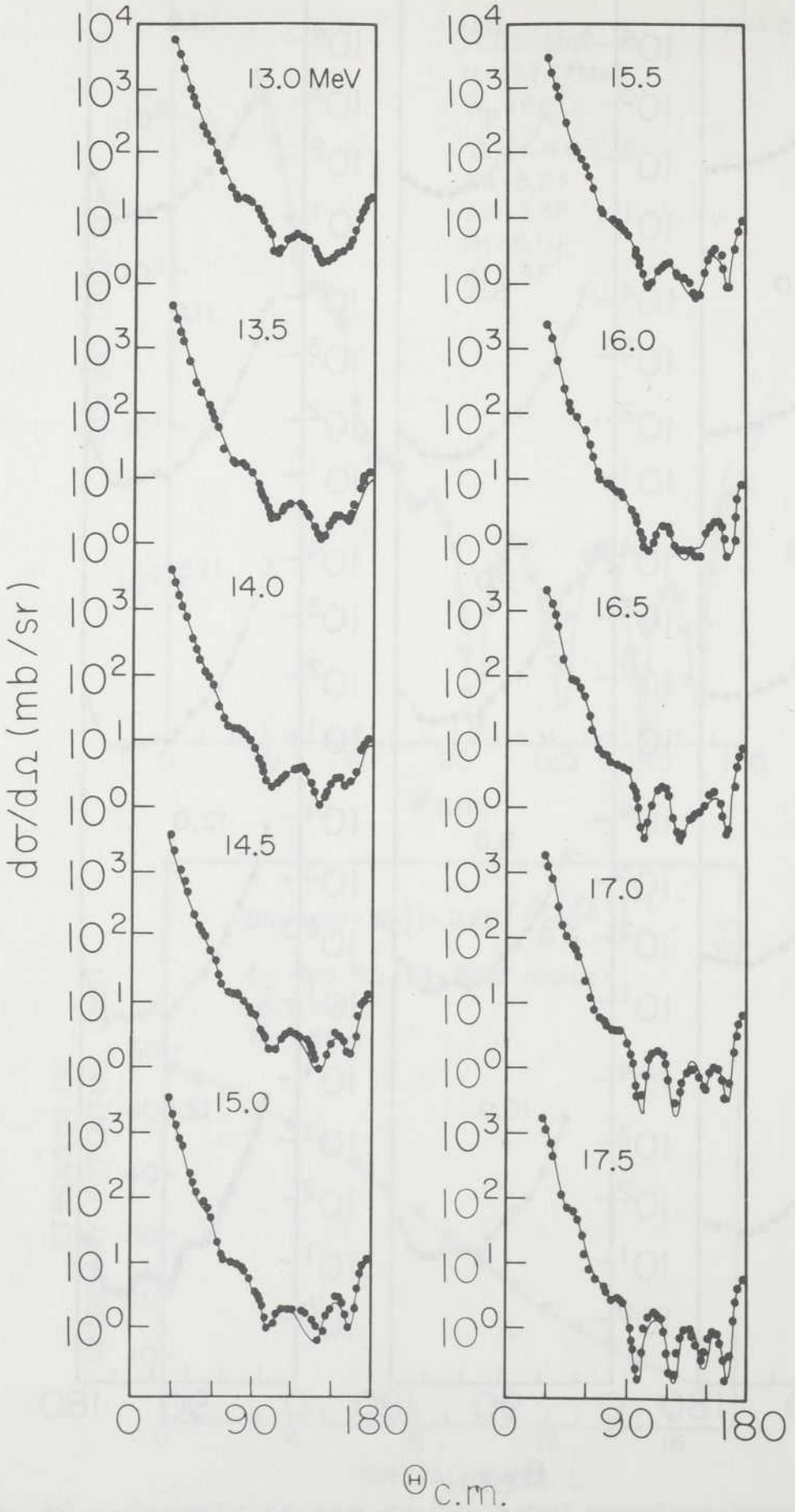

Fig. 18. Parameterization of energy averaged angular distributions with an optical model modified to include compound elastic scattering and an ℓ-dependent imaginary part, 13.0 to 17.5 MeV.

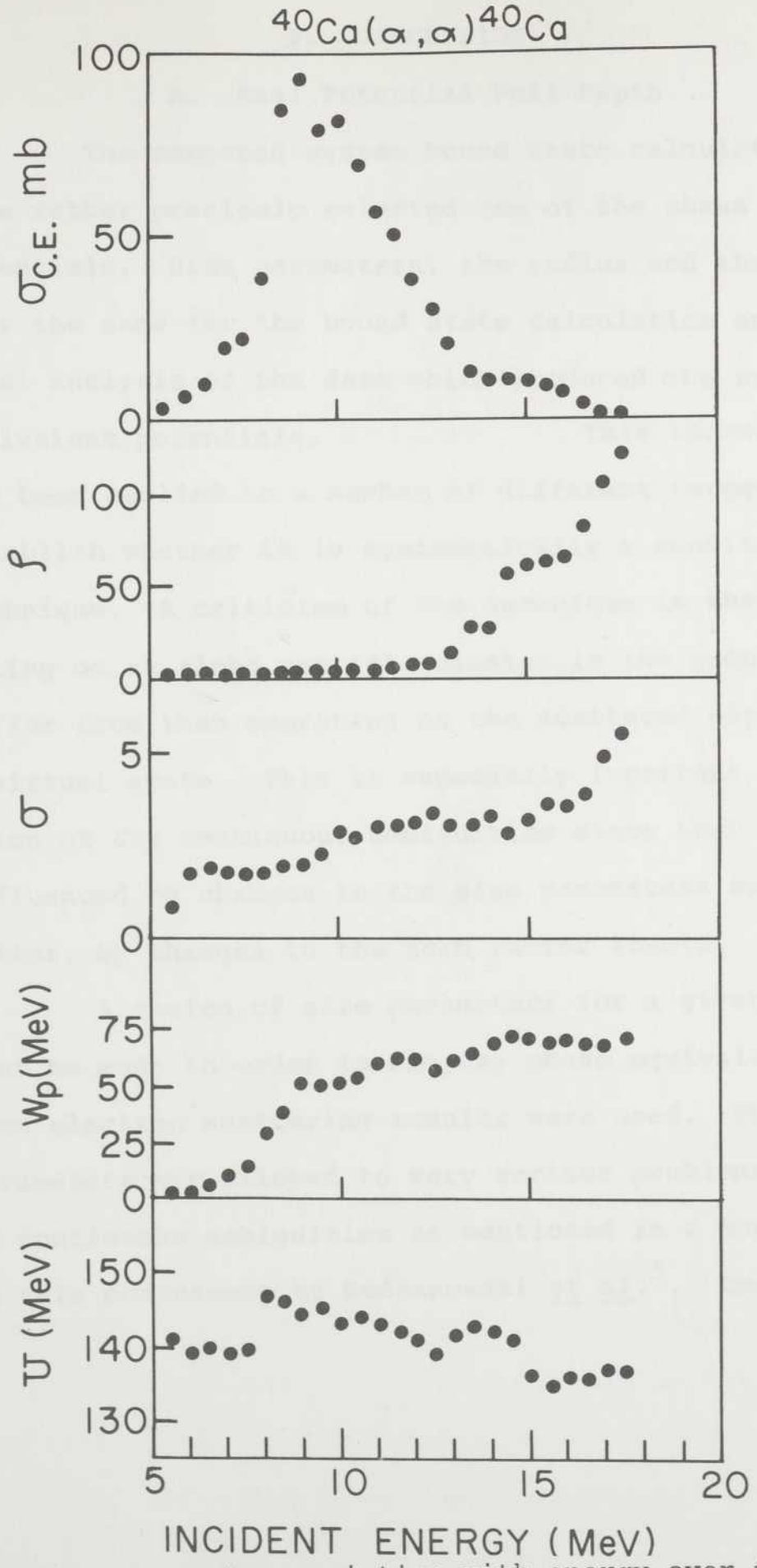

Fig. 19. Parameter variation with energy over the bombarding energy range 5 to 18 MeV.

V. DISCUSSION

A. Real Potential Well Depth

The compound system bound state calculation discussed here rather precisely selected one of the phase equivalent potentials. Size parameters, the radius and the diffuseness were the same for the bound state calculation and the optical model analysis of the data which produced the set of phase equivalent potentials. This technique has not yet been applied to a number of different target nuclei to establish whether it is systematically a sensitive selection technique. A criticism of the technique is that the potential acting on an alpha particle cluster in the ground state may differ from that operating on the scattered alpha particle in a virtual state. This is especially important in the consideration of the continuous ambiguities since they are strongly influenced by changes in the size parameters and, for that matter, by changes in the form factor itself.

A choice of size parameters for a given form factor must be made in order to display phase equivalent potentials. Here electron scattering results were used. When the size parameters are allowed to vary serious problems arise because of continuous ambiguities as mentioned in a contribution to this conference by Budzanowski et al.[5]. Conversely, a

determination of the real well depth by microscopic calculations involving nucleon-alpha or nucleon-nucleon interactions makes alpha particle scattering a sensitive tool for the study of the structure of the nuclear surface. This point is made by Jackson[6] in a contribution to this symposium.

Before the question of a proper potential for alpha particle scattering is closed it appears essential to better establish the systematics of the continuous ambiguities involving the size parameters and the well depth consistent with the requirements of microscopic calculations for the well depth. An ultimate test will be the application of such potentials to reaction data and the phenomena of radioactive alpha particles decay. Real well depths over a range 20 to 200 MeV have been used in different analyses of both elastic scattering and reactions induced by alpha particles. One point of semantic confusion is the question of the potential for the aggregate of four nucleons in contrast with the potential for alpha particle the nucleons of which already exist in a potential describing the alpha particle.

B. Significance of Compound Elastic Scattering Parameters

The results of an investigation into the significance of the adjustable parameters in the compound elastic cross section have been reported by Bisson et al.[7] and by Eberhard et al.[8] The relevant relation between σ and τ is

$$\tau = \sigma^2 \frac{h^2}{T} (1 + W_{Res})^{-1} \qquad (5)$$

where τ is a moment of inertia, T is the nuclear temperature, and W_{Res} is a correction term which depends on the mass A_ν of the particle ν by which the compound nucleus decays and on the mass A_{Res} of the corresponding residual nucleus,

$$W_{Res} \cong \frac{5}{2} \left(\frac{A_\nu}{A_{Res}}\right) \qquad (6)$$

The experimentally determined values for the ratio of the moment of inertia to that for a rigid sphere are plotted in Fig. 20. The error bars show the variation in the point due to a 10% variation in the data. Above 11 MeV the experimental values are exactly those for a rigid body and below they decrease smoothly with decreasing energy down to 8 MeV. Below 8 MeV they increase again but here the analysis is no longer valid so that no significance can be attached to this behaviour. The solid line represents a calculation by Vonach et. al.[9] based on the super-conductor model. The agreement, where comparison can be made, is quite good.

In Fig. 21 the experimental values of ρ are compared with a plot of the function

$$\rho = \frac{1}{4} \left(2\pi \frac{\Gamma_o}{D_o}\right) \qquad (7)$$

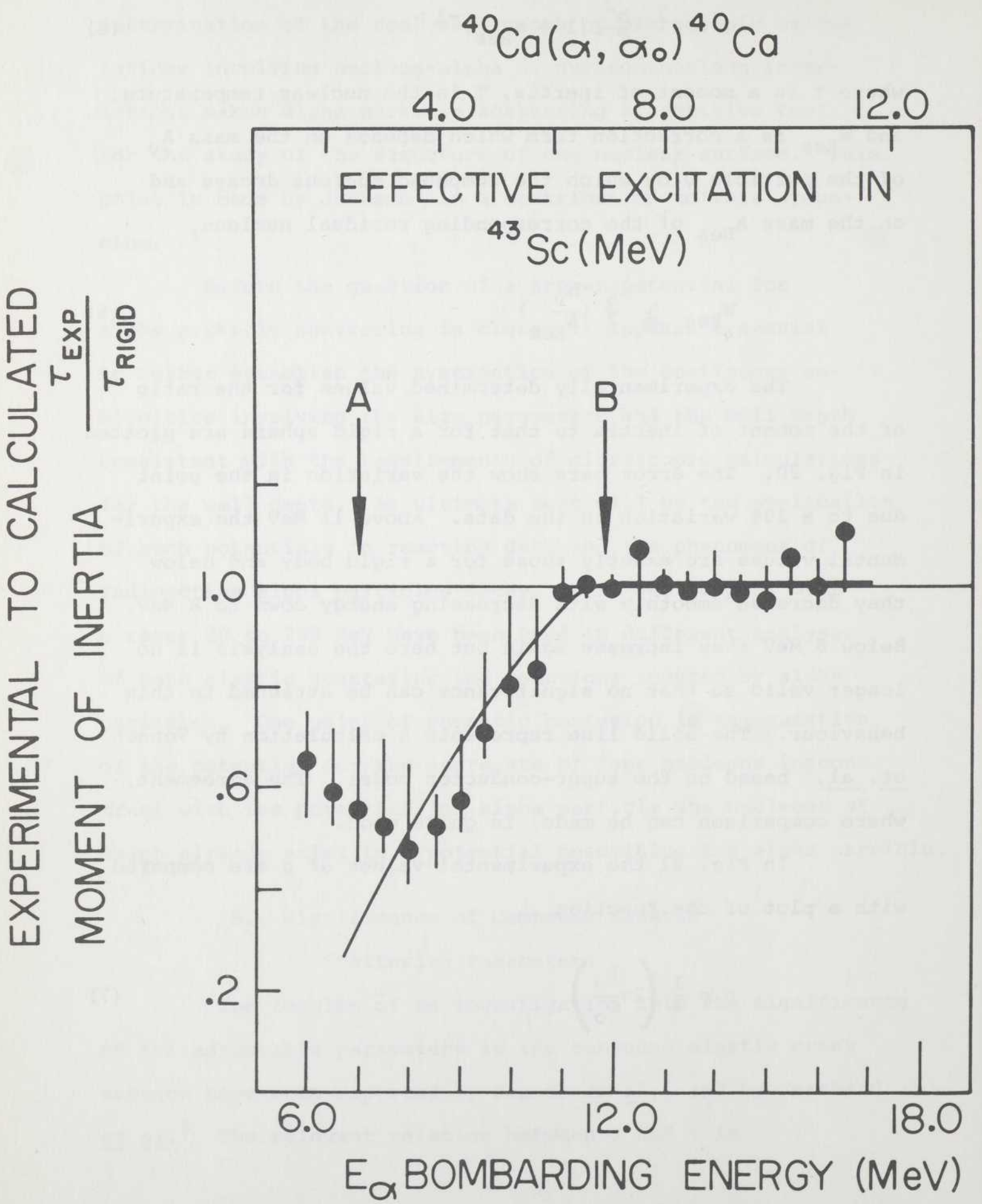

Fig. 20. Ratio of the experimentally determined moment of inertia to the rigid body value as a function of bombarding energy.

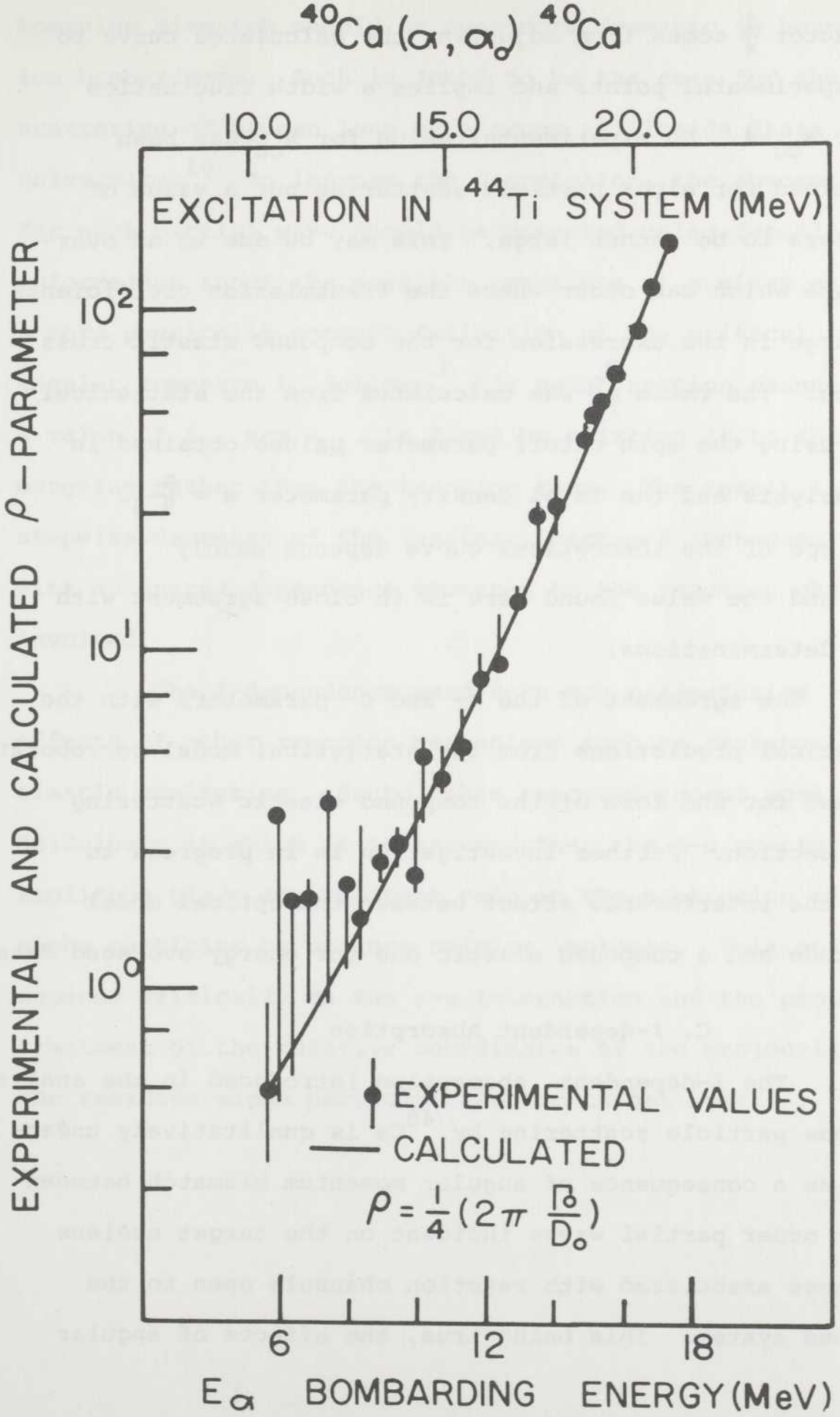

Fig. 21. Comparison of ρ values found in this analysis with calculated values.

the factor $\frac{1}{4}$ comes from adjusting the calculated curve to the experimental points and implies a width fluctuation factor $W_{cc}=4$. No experimental value for W_{cc} has been determined for alpha particle scattering but a value of 4 appears to be rather large. This may be due to an over-estimate which can occur where the transmission coefficients are large in the expression for the compound elastic cross section. The ratio $\frac{D_o}{\Gamma_o}$ was calculated from the statistical model using the spin cutoff parameter values obtained in the analysis and the level density parameter $a = \frac{A}{9.5}$. The slope of the theoretical curve depends mainly on a, and the value found here is in close agreement with other determinations.

The agreement of the σ- and ρ- parameters with the theoretical predictions from the statistical model corroborates the need for and form of the compound elastic scattering cross section. Further investigation is in progress to study the interference effect between the optical model amplitude and a compound elastic one for energy averaged data.

C. ℓ-dependent Absorption

The ℓ-dependent absorption introduced in the analysis of alpha particle scattering by ^{40}Ca is qualitatively understood as a consequence of angular momentum mismatch between higher order partial waves incident on the target nucleus and those associated with reaction channels open to the compound system. This being true, the effects of angular

momentum mismatch should be even more dramatic in heavy ion bombardment. Such is found to be the case for the scattering of oxygen ions by a group at Florida State University.[10] To improve the description, the absorption for each partial wave should be computed using detailed information about the possible reactions at a given energy. A more physically correct definition of the critical angular momentum ℓ_c follows.[3] For each reaction channel a value of ℓ_c, say ℓ_{ci}, is fixed by relating it to the outgoing rather than the incoming flux. The result is a stepwise decrease of the imaginary part as ℓ increases with an energy dependence governed by the reaction channels involved.

The ℓ-dependence used here may parameterize the effects of other reaction mechanisms such as exchange elastic scattering. Santo[11] has reported recent work at Heidelberg in which it is assumed that the α-α scattering amplitude plays an important role in the scattering of alpha particles by various calcium isotopes. This analysis depends critically on the α-α interaction and the proper treatment of the relative coordinates of the projectile, the resident alpha particle, and the target core.

REFERENCES

*Research supported in part by the Air Force Office of Scientific Research; Office of Aerospace Research, U. S. Air Force, under Grant No. AFOSR-69-1674, and the National Science Foundation (Grant NSF-GJ-367).

1. Joseph John, C. P. Robinson, J. P. Aldridge and R. H. Davis, Phys. Rev. 177, 1755 (1969).
2. C. P. Robinson, J. P. Aldridge, J. John and R. H. Davis, Phys. Rev. 171, 1241 (1968).
3. D. Robson, private communication.
4. A. E. Bisson and R. H. Davis, Phys. Rev. Letters 22, 542 (1969).
5. A. Budzanowski, K. Grotowshi, L. Jarlzyk, B. Kazys, K. Olkiewicz, and A. Strzalkowski, Symposium on Nuclear Reaction Mechanisms and Polarization Phenomena, Laval University, Quebec (1969).
6. D. F. Jackson, Symposium on Nuclear Reaction Mechanisms and Polarization Phenomena, Laval University, Quebec (1969).
7. A. E. Bisson, K. A. Eberhard, and R. H. Davis (submitted to Phys. Rev.)
8. K. A. Eberhard, A. E. Bisson and R. H. Davis, International Conference on Nuclear Reactions Induced by Heavy Ions, Heidelberg (1969).
9. H. K. Vonach, R. Vandenbosch, and I. R. Huizenga Nuclear Physics 60, 70 (1964).

10. R. A. Chatwin, J. S. Eck, A. Richter, and D. Robson, International Conference on Nuclear Reactions Induced by Heavy Ions, Heidelberg (1969).

11. G. Gaul, H. Lüdecke, R. Santo, H. Schmeing, N. C. Schmeing, and R. Stock, International Conference on Clustering Phenomena in Nuclei, Ruhr University, Bochum (1969).

SCHEMATIC TREATMENT OF RESONANCES IN A POTENTIAL USING WEINBERG'S QUASI-PARTICLES.

R.Huby. Dept. of Theoretical Physics, The Chadwick Lab., Univ. of Liverpool, U.K.

In treating nuclear reactions which involve resonance levels, it is desirable to have simple but good, schematic formulae for both the scattering amplitude and the wave-function around resonance. While most resonances are many-body phenomena, an important basic case is potential resonance for a partial wave of non-zero l-value, which may be needed for incorporation in more complicated problems. A method which offers peculiar advantages, partic ularly as regards the wave-function, is the decomposition of the equations by means of Weinberg's quasi-particles (Weinberg Phys. Rev. 131 (1963) 440). A resonance is then associated with a discrete (though not square-integrable) quasi-particle wave-function $\psi_0(E,\underset{\sim}{r})$, which is an eigenfunction of the Lippmann-Schwinger kernel $I = (E+i\varepsilon-H_0)^{-1}V$. The resonance process means a transition into this state from the free wave and out again. (This original method of Weinberg's is denoted the T-matrix scheme, in contrast to an alternative K-matrix scheme which is also developed as permitting more accurate approximation.) One defines a separable potential $V_0 = [V|\psi_0\rangle\langle\psi_0^*|V]\langle\psi_0^*|V|\psi_0\rangle^{-1}$, and then the residual potential $V'=V-V_0$ is treated as a perturbation. This leads to formulae for the scattering amplitude and wave-function, expressed in terms of $\psi_0(E,\underset{\sim}{r})$, the eigenvalue $\alpha(E)$ of I, and the scattering due to V' alone, the latter being expanded in powers of V' (quasi-Born series). The scattering amplitude contains a term proportional to $[1-\alpha(E)]^{-1}$, and so a pole occurs at complex E for which $\alpha(E)=1$. However, it is possible to describe a resonance without ever going to complex energy at all. The resonance energy E_0 is defined by $\mathrm{Re}\,\alpha(E_0)=1$, and a linear expansion in E is made about this point. The resulting T-matrix element on the energy shell is

$$T_\ell(E) = T'_\ell(E) + \frac{1}{2\pi}\frac{\Gamma}{E-E_0+\frac{1}{2}i\Gamma},$$

where $T'_\ell(E)$ is the background contribution due to V', and Γ has a simple formula in terms of $\psi_0(E_0)$, the latter being suitably normalised. The scattering wave-function may be written

$$\psi(E,\underset{\sim}{r}) = \chi(E,\underset{\sim}{r}) + \sqrt{\frac{\Gamma}{2\pi}}\,\frac{\psi_0(E,\underset{\sim}{r})}{E-E_0+\frac{1}{2}i\Gamma} + (\text{background terms due to } V'),$$

where $\chi(E,\underset{\sim}{r})$ is the energy-normalised free wave. These formulae exhibit typical Breit-Wigner behaviour, and the term $\psi_0(E,\underset{\sim}{r})$ in the wave-function is identified with the resonance level. The function $\psi_0(E,\underset{\sim}{r})$ looks nearly-bound inside the potential, but it tunnels smoothly through the barrier and has the proper outgoing tail at large distances. These features are considered valuable in making the wave-function apt for further applications. All the quantities appearing admit of numerical calculation. One advantage is the avoidance of any joining radius. The connection between a resonance and an eigenfunction of the Lippmann-Schwinger kernel has been seen by previous authors (e.g. Meetz, J.Math.Phys. 3 (1962) 690; Herzenberg & Mandl Phys. Lett. 6 (1963) 288).

THREE-BODY MODEL OF Li^6 AND DEUTERON-ALPHA SCATTERING

Paul E. Shanley
Department of Physics
University of Notre Dame
Notre Dame, Indiana 46556

The properties of Li^6 and deuteron-alpha scattering have been studied in an exact three-particle model in which the neutron, proton and alpha particle interact through separable two-body forces. The alpha particle has been assumed to be structureless and Coulomb effects neglected. As a basis of the low-energy nucleon-alpha interaction, a three-term separable potential has been fit to low energy neutron-alpha scattering in the partial waves $s_{1/2}$, $p_{3/2}$ and $p_{1/2}$. The three-body formalism of Amado was generalized to allow spin-dependent two-body interactions in an arbitrary partial wave and numerical solution of the resulting three-body equations gives the binding energies of the T=0 and T=1 states in Li^6 as well as the phase shifts, angular distributions, and deuteron polarization in d-α scattering, and also the total cross section for $d + \alpha \rightarrow n + p + \alpha$ up to 30 MeV. Given the assumptions of the model, the agreement of the calculated quantities with experiment is quite good. Some discussion of the results with respect to phenomenological optical model fits to deuteron-nucleus scattering will also be given.

$^{11}B(p, \alpha)2\alpha$: exemple de réaction séquentielle composée-composée

Gisèle Goulard - Université Laval, Québec, Canada

L'étude porte sur une réaction du type $A + B \rightarrow C^* \rightarrow D + G^* \rightarrow D + E + F$. Les noyaux C* et G* sont supposés avoir un temps de vie suffisamment long pour être considérés comme des noyaux composés. Pour le noyau G*, les énergies de résonance sont E_λ et les largeurs Γ_λ. Dans le cas du noyau C*, la largeur réduite γ^2 dans la voie de sortie, est définie pour un état G* assimilé à un état d'énergie donnée. On utilise alors le formalisme de la matrice R [1], pour expliciter l'amplitude de diffusion dans le système de coordonnées où le noyau C* est au repos. Pour la réaction $^{11}B(p, \alpha)2\alpha$, comme il y a trois particules identiques dans l'état final, il faut symétriser l'amplitude de diffusion. Mais dans une réaction séquentielle, ceci est relié à l'ordre d'émission des particules et les différents termes de l'amplitude n'existent que si les conditions de cinématique le permettent.

Une application numérique est donnée pour des protons incidents de 2 MeV. A cette énergie, un niveau de ^{12}C existe avec une énergie de résonance de 17.77 MeV [2]. Dans la formule développée de la section efficace, deux sortes de termes interviennent, des termes carrés (ΣA) et des termes d'interférence (ΣB). Les contributions venant de chacun de ces termes sont représentées dans les figures 1 et 2 et la section efficace différentielle dans le système du laboratoire (σ_L) par la courbe de la fig. 3. On constate que les termes (ΣB) sont aussi importants que les termes (ΣA) et que les valeurs négatives obtenues dans les termes d'interférence produisent une diminution de la largeur du pic central dans σ_L. Cet amincissement est tout à fait en accord avec les résultats expérimentaux [3] [4].

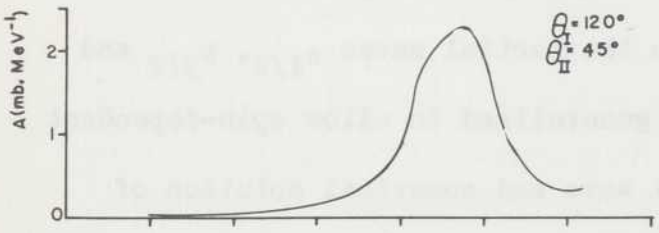

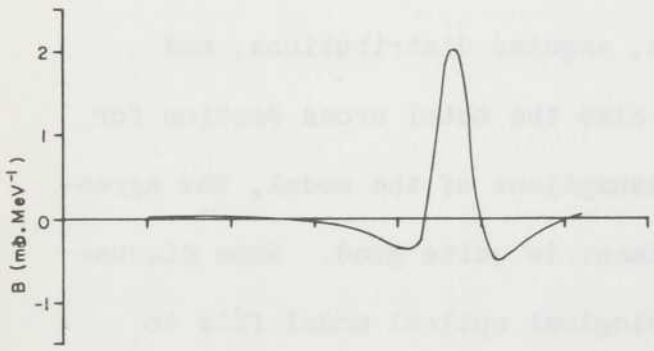

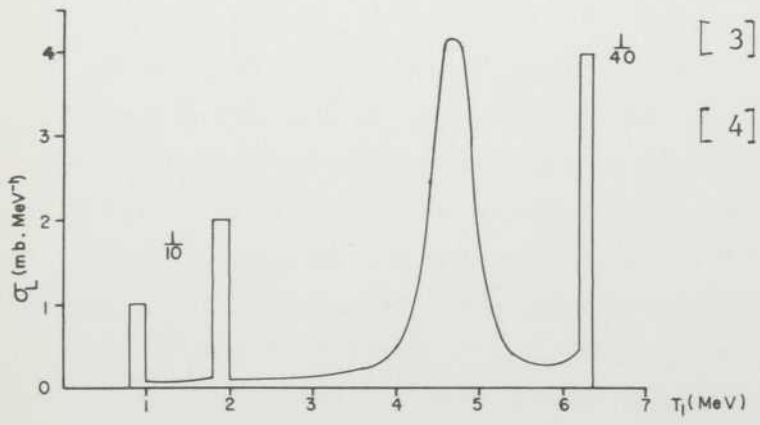

[1] A.M. Lane, R.G. Thomas, Rev. Mod. Phys. 30 (1958) 334.

[2] R.E. Segel et al., Phys. Rev. B139 (1965) 818.

[3] J.D. Bronson et al., Nucl. Phys. 68 (1965) 241.

[4] J.L. Québert, L. Marquez, Nucl. Phys. A126 (1969) 646.

ANALYSIS OF INELASTIC SCATTERING VIA ANALOGUE RESONANCES

S. RAMAVATARAM

Département de Physique

Université Laval, Québec.

The Robson R-matrix theory of Analogue resonances[1] which has been very successful in explaining elastic scattering data has been extended by Lane and Robson[2] to the discussion of inelastic scattering following analogue resonance excitation. Formulae which take into account multi-channel effects have been derived for the various width parameters associated with the analogue resonances.

The theory takes advantage of the rather simple configurational structure of the analogue state wave function and makes use of the Bloch[3] boundary condition operator to go from the bound state $|\lambda>$ (representing the analogue in zeroth order) defined as:

$$|\lambda> \;=\; T_{-}|\psi>$$

where $|\psi>$ represents the (neutron + target) system to the physically acceptable resonance state $|g_{\lambda}>$ which describes a continuum proton in the field of the target nucleus. The total width Γ, the partial widths Γ_c and the spreading width

(arising from mixing of the analogue state with neighboring $T_<$ states) which characterise the resonance may be defined in terms of $|\lambda\rangle$ or $|g_\lambda\rangle$. The definitions in terms of the former are useful in obtaining theoretical estimates of the parameters Γ and Γ_c. The definition of Γ in terms of $|g_\lambda\rangle$ may then be used to determine the spreading width W_o that is directly related to the experimentally observed quantity.

Although the general treatment allows for inclusion of the residual Coulomb effects over all space the Robson assumption that "external mixing" is the dominant effect considerably simplifies the procedure to be followed in the theoretical estimates. Further simplifications that facilitate the calculations follow from the assumption that the reduced width amplitudes from the background states contributing to various exit channels have random signs. Under these assumptions we obtain:

$$\Gamma = \sum_c 2P_c\gamma_{\lambda c}^2 + 2\sum_c \gamma_{\lambda c}^2 \left[(\Delta S_c^2 - P_c^2)\, \mathrm{Im}R^o_{cc} + 2\Delta S_c P_c \mathrm{Re}R^o_{cc}\right]$$

$$\Gamma_c = 2P_c\left|\gamma_{\lambda c} + \gamma_{\lambda c}\,(\Delta S_c + iP_c)R^o_{cc}\right|^2$$

and $$W_o = \Gamma - \sum_c \Gamma_c .$$

In the above, ΔS_c and P_c arise from boundary condition considerations and R^o_{cc} is an R-function representing background contributions. In the sum on c, all channels having non-zero overlaps with zeroth-order analogue state $|\lambda>$ must be included.

In the following the results of an investigation of the validity of these theoretical ideas are presented for the ^{207}Pb(p,p') reaction. This reaction has several interesting aspects. The wave function representing the 0^+ state in ^{208}Bi consists of various proton-particle, neutron-hole configurations in which consistent with Pauli principle one of the excess neutrons in the orbits $n\ell j = 3p_{\frac{1}{2}}$ to $1h_{9/2}$ would be converted to a proton. Thus there are several inelastic channels which have non-zero overlaps with the analogue state $|\lambda>$ allowing for the possibility of examining the multichannel effects. The experimental data[4,5] apart from providing estimates of the individual Γ_c and Γ for direct comparison with theory shows the interesting feature that the sum of the partial width is considerably less than the observed total width suggesting a relatively large W_o.

The parameters of the theory were obtained for realistic potentials. Consistent with the assumption that internal mixing is negligible the depth of the real potential was assumed to be that required for the bound state problem defining

the state $|\lambda>$. The R-function R^{o}_{cc} is evaluated using the R-matrix relation[6]

$$R^{o}_{cc} = \frac{1}{f_c(E)-B_c}$$

where B_c is the Kapur-Peierls[7] boundary condition and $f_c(E)$ is the logarithmic derivative of the solution to the Schrodinger equation appropriate to the channel under consideration. The radial dependence of the various theoretical parameters was investigated. It was observed that not only can radii be found to fit W_o (90 KeV) and Γ(220 KeV) separately but that it is possible to obtain reasonable agreement with experiment for both parameters with the same value for the radius (9.3F) defining the surface. A comparison of the observed partial resonance width Γ_c with theoretical values estimated for the best fit radius (9.3F) is given in table. It is worth noting that theory predicts $\Gamma_{p_{\frac{1}{2}}}/\Gamma_{p_{3/2}}$ to be <1 while the (p,p') data suggests that the ratio is >1. However recent improved estimates[(8)] obtained in the reaction ^{207}Pb(p,np') indicate that this ratio is of the order of 0.87 which is in better qualitative agreement with the theoretical estimates.

Channel (J^π)	Γ_c^{exp} (KeV) ref 5)	Γ_c^{th} (KeV)
$\frac{1}{2}^-$	61 ± 15	32
$\frac{5}{2}^-$	17 ± 4	25
$\frac{3}{2}^-$	50 ± 11	47
$\frac{13}{2}^+$	---	--
$\frac{7}{2}^-$	---	6
$\frac{9}{2}^-$	---	--

REFERENCES

1. D. Robson, Phys. Rev. 137 (1965) 535

2. D. Robson and A.M. Lane Phys. Rev. 161 (1967) 982

3. C. Bloch, Nucl. Phys. 4 (1957) 503.

4. B.L. Anderson et al. Phys. Lett. 22 (1966) 657

5. G.H. Lenz and G.M. Temmer, Nucl. Phys. A112(1968)625

6. A.M. Lane and R.G.Thomas, Revs. Mod. Phys. 30 (1950)257

7. P.L. Kapur and R.E.Peierls, Proc. Roy. Soc. (London)A166(1938)277

8. G.J. Igo et al. Phys. Rev. Lett. 22 (1969) 724.

REACTIONS $^{40}Ca(\alpha,p)^{43}Sc$ AND $^{50}Cr(\alpha,p)^{53}Mn$ BELOW 11 MeV.

B. Čujec, C.A. Bouchard, R. Lamontagne, D. Vitoux.

Université Laval - QUEBEC, Canada.

The cross sections have been measured at several angles, varying the incident energy in 30 keV intervals between 8.5 and 11 MeV for the reaction $^{40}Ca(\alpha,p)^{43}Sc$, and between 7.0 and 9.5 MeV for the reaction $^{50}Cr(\alpha,p)^{53}Mn$. For $^{40}Ca(\alpha,p)^{43}Sc$, the measurements between 9.1 and 9.5 MeV were performed also in 7 keV intervals. The excitation functions show pronounced fluctuations. Some intermediate structure resonances ($\Gamma \approx 100$ keV) also are present. The angular distributions for cross sections, averaged over 0.6 MeV, are essentially isotropic. The total cross section values are presented in Table. They agree, according to rough estimates, with the compound nucleus picture. The 7 keV data have been analysed by Ericson's method. The analysis gives the coherence width at $\sim$ 13.7 MeV excitation energy in ^{44}Ti, $\Gamma = 12.4 \pm 0.4$ keV.

Table. Total Cross Sections (mb); $\Delta E = 0.6$ MeV

	$^{40}Ca(\alpha,p)^{43}Sc$			$^{40}Ca(\alpha,\alpha)$.	$^{50}Cr(\alpha,p)^{53}Mn$	
Eα-Lab \ Ex, J_f^π	0, $7/2^-$	0.145, $3/2^+$	0.475, $3/2^-$	Compound Elastic 1)	0, $7/2^-$	0.383, $5/2^-$
7.6				80	2.5	3.0
8.2				62	4.9	5.7
8.8	29.2	24.9	15.8	88	6.0	6.7
9.4	41.2	22.8	16.4	64	(5.3)	(7.5)
10.0	38.5	21.3	15.1	64		
10.6	29.3	16.2	15.0	47		

1) J. John, C.P. Robinson, J.P. Aldridge, R.M. Davis, Phys. Rev., 177, 1755 (1969).

MECANISME DE REACTION POUR $^{12}C(h,p)^{14}N$

F. HAAS, B. HEUSCH, A. GALLMANN & D.A. BROMLEY*
Institut de Recherches Nucléaires - STRASBOURG - France

Une étude détaillée des distributions angulaires des protons et des corrélations angulaires p-γ, mesurées dans la géométrie colinéaire de Litherland et Ferguson, a été réalisée pour la réaction $^{12}C(h,p)^{14}N$ à des énergies de bombardement comprises entre 4.5 et 11 MeV. Le mécanisme de réaction est complexe et se compose à la fois des interactions directes et par noyau composé. Une structure résonnante prononcée ainsi que la population sélective des sous-états magnétiques ont été mises en évidence. Ces phénomènes peuvent être expliqués par des résonnances quasi-géantes, dans la région d'excitation comprise entre 17 et 23 MeV du noyau composé ^{15}O, décrites par le couplage de protons isolés au coeur excité du noyau résiduel. Une dépendance systématique de la population des sous-états magnétiques $/m/=1$ du niveau à 7.03 MeV de ^{14}N et de la remontée à l'arrière des distributions angulaires correspondantes a été observée. L'explication suggérée est basée sur l'hypothèse d'un mécanisme de stripping par particules lourdes favorisée par la forme oblate du noyau ^{12}C.

Des mesures sont en cours actuellement dans notre laboratoire pour déterminer si les effets observés s'étendent à d'autres niveaux excités ou si accidentellement nous avons mis en évidence un cas particulièrement favorable.

-:-:-:-:-:-

* Adresse permanente : Wright Nuclear Structure Laboratory,
Yale University, NEW HAVEN, Connecticut.

SEANCE
SESSION 2

PRESIDENT CHAIRMAN

P. HUBER

COUPLAGE $\vec{L}.\vec{S}$ DANS LES DESCRIPTIONS MACROSCOPIQUES ET MICROSCOPIQUES DE LA DIFFUSION INELASTIQUE DE PROTONS.

par

Jacques RAYNAL

Centre d'Etudes Nucléaires de Saclay, France.

I- INTRODUCTION

Le couplage $\vec{L}.\vec{S}$ a été introduit dans le modèle optique pour décrire la polarisation dans la diffusion élastique de particules de spin non nul. Sa nécessité s'est faite sentir avant que des mesures précises de polarisation n'aient été effectuées. On a commencé par utiliser un potentiel $\vec{L}.\vec{S}$ dont le facteur de forme se déduit du facteur de forme du potentiel central en analogie avec les formules obtenues en éliminant les petites composantes de l'équation de Dirac. L'intensité de ce potentiel était fixée phénoménologiquement; elle est de signe opposé et beaucoup plus grande que celle prédite par l'équation de Dirac. Plus tard, des mesures plus précises de polarisation ont conduit à utiliser pour le potentiel $\vec{L}.\vec{S}$ un rayon et une largeur de surface plus faibles que les paramètres correspondants du potentiel central réel.

Simultanément, le même potentiel $\vec{L}.\vec{S}$ a été utilisé dans l'étude des réactions nucléaires directes, soit en équations couplées, soit en DWBA. Il intervient dans la description de l'onde des particules incidente et sortante. Ainsi, dans le modèle rotationnel, où les différents états de

la cible sont décrits par un potentiel optique déformé, on a d'abord utilisé les potentiels imaginaire et $\vec{L}.\vec{S}$ seulement comme couplages diagonaux: seul le potentiel central réel était déformé. Par la suite, on a déformé aussi le potentiel imaginaire pour rendre mieux compte des sections efficaces de diffusion inélastique. Avec l'apparition de mesures précises de polarisation et d'asymétrie dans les diffusions inélastiques, on a pensé à déformer aussi le potentiel $\vec{L}.\vec{S}$. Les premiers calculs utilisèrent l'expression que l'on rencontre dans le modèle optique le plus simple, en la rendant hermitique Cette méthode n'est pas valable car:

- l'expression obtenue n'est pas vectorielle;
- au point de vue macroscopique, elle rompt l'analogie avec l'élimination des petites composantes de l'équation de Dirac;
- au point de vue microscopique, elle est très différente d'une interaction $\vec{L}.\vec{S}$ nucléon-nucléon.

Shérif et Blair[1] ont proposé de garder l'analogie avec l'équation de Dirac. L'expression qu'ils utilisent est plus compliquée que la précédente. Cependant, on peut obtenir une forme relativement simple qui permet d'en discuter les effets et de l'utiliser dans des calculs de voies couplées. Les résultats très encourageants obtenus en DWBA[1-2-3] s'obtiennent aussi en équation couplées; on retrouve aussi que le potentiel $\vec{L}.\vec{S}$ doit souvent être plus déformé que le potentiel central.

D'autre part, le formalisme de l'hélicité permet[4] d'écrire une interaction $\vec{L}.\vec{S}$ nucléon-nucléon sous forme d'un développement multipolaire relativement maniable. Comme on admet que l'interaction $\vec{L}.\vec{S}$ nucléon-nucléon a une portée plus faible que l'interaction scalaire, il est logique de considérer sa portée comme nulle. A cette limite, l'interaction $\vec{L}.\vec{S}$ n'existe que dans l'état relatif $L = 1$; comme elle impose $S = 1$, il s'ensuit $T = 1$. Cette interaction est donc deux fois plus importante entre deux protons qu'entre un proton et un neutron, ce qui peut expliquer que le potentiel $\vec{L}.\vec{S}$ doive être plus ou moins déformé suivant la nature des nucléons excités dans la cible. Si, dans l'expression obtenue à la limite de la portée nulle, on néglige tout ce qui n'a pas d'équivalent macroscopique et si on rend le reste hermitique, on obtient une expression très proche de celle de la description macroscopique.

Dans ce qui suit, nous considérons uniquement la diffusion de particules de spin $\frac{1}{2}$. En général, les formules ne sont pas valables pour des particules de spin plus grand.

II - DESCRIPTION MACROSCOPIQUE

Nous entendons par description macroscopique une description du noyau cible dans laquelle les orbites des nucléons qui le composent n'interviennent pas. La cible est connue sous la forme d'une densité de masse $\rho(\vec{r})$.

A) CALCUL DES AMPLITUDES DE DIFFUSION

Pour simplifier, considérons un noyau d'état initial 0^+ et d'état final 2^+, décrit par le modèle rotationnel. Le noyau cible est représenté par un potentiel $V(\vec{r}, \hat{r}')$, dont le rayon dépend de la direction considérée. Ce potentiel peut se développer en multipoles:

$$V(\vec{r},\hat{r}') = \sum_{\lambda} v_{\lambda}(r)\, Y_{\lambda}^{\mu}(\hat{r}) Y_{\lambda}^{\mu *}(\hat{r}') \qquad (1)$$

où $\vec{r}'$ est la direction de l'axe de symétrie intrinsèque du noyau.

Pour une onde partielle incidente l_i, j_i fixée, le spin total du système $J = j_i$ et sa parité $\pi = (-)^{l_i}$ sont fixés.

Si J est assez grand, à J et π correspondent cinq ondes sortantes possibles l_f, j_f. On obtient ainsi un système de six équations différentielles couplées, de la forme:

$$y_i'' + \sum_j V_{ij} y_j = E\, y_i \qquad (2)$$

avec

$$V_{ij} = \sum_\lambda G_{ij}^\lambda\, v_\lambda(r) \qquad (3)$$

où G_{ij}^λ est un certain coefficient géométrique. Les valeurs de λ qui interviennent dans la somme (3) sont limitées par les relations triangulaires entre les spins de la cible des voies i et j. Le système d'équations (2) peut être résolu tel quel pour obtenir les amplitudes de diffusion S_{ij}, ou seulement au premier ordre de l'interaction $v_2(r)$ dans un calcul de DWBA.

Nous nous proposons d'écrire le potentiel $\vec{L}.\vec{S}$ déformé sous une forme analogue à l'expression (3) en faisant intervenir exactement le même coefficient géométrique que pour le potentiel central.

B) EXPRESSION DU COUPLAGE $\vec{L}.\vec{S}$ DEFORME

L'opérateur $\vec{L}.\vec{S}$ appliqué à une onde partielle l_i, j_i a une valeur propre l_i si $j_i = l_i + \frac{1}{2}$ et $(-l_i-1)$ si $j_i = l_i - \frac{1}{2}$. Nous noterons cette valeur propre par γ_i. Les premiers essais de couplage $\vec{L}.\vec{S}$ déformé utilisaient:

$$G_{if}^{\lambda} \left[\frac{1}{r} \frac{d}{dr} v_{\lambda}(r)\right] \frac{\gamma_i + \gamma_f}{2} \qquad (4)$$

Nous désirons obtenir une expression analogue en partant de:

$$\vec{\nabla} V_{\lambda}(r) Y_{\lambda}^{v}(\hat{r}) \wedge \frac{\vec{\nabla}}{i} \vec{\sigma} \qquad (5)$$

ce qui peut se faire par les manipulations élémentaires qui sont résumées dans l'Appendice A. On obtient ainsi l'expression:

$$G_{if}^{\lambda} \{ \frac{1}{r} \frac{d}{dr} V_{\lambda}(r)\gamma_i + \frac{1}{r}(\gamma_i - \gamma_f)V_{\lambda}(r) \frac{d}{dr} + \frac{1}{2r^2} V_{\lambda}(r) [\lambda(\lambda + 1)-(\gamma_f - \gamma_i)(\gamma_f - \gamma_i \pm 1)]\} \qquad (6)$$

Le signe + est obtenu si on utilise des fonctions d'onde radiales normalisées comme des $j_\ell(r)$; le signe - correspond à des fonctions d'onde radiales multipliées par r, de comportement sinusoïdal à l'infini.

Les expressions (4) et (6) ont des comportements très différents. Si les moments angulaires sont grands, de l'ordre de L, le terme (4) est important si $j_i - l_i = j_f - l_f$ et croit linéairement avec L. Par contre, le terme (6) est grand si $j_i - l_i \neq j_f - l_f$ et croit quadratiquement avec L. Cependant, il faut aussi tenir compte du comportement du coefficient géométrique G_{if} qui est essentiellement

$$\sqrt{(2j_i+1)(2j_f+1)} \begin{pmatrix} j_f & \lambda & j_i \\ -\frac{1}{2} & 0 & \frac{1}{2} \end{pmatrix}$$

A la limite des grands moments angulaires, il est plus important si $j_i - l_i = j_f - l_f$ que dans le cas contraire et le rapport tend vers L.

En résumé, lorsque le moment angulaire croit, le couplage $\vec{L}.\vec{S}$ déformé est favorisé par rapport au potentiel central, dans un rapport de l'ordre du moment angulaire, et cela pour les formes (4) et (6). Cependant, la forme (4) est importante seulement si $j_i - l_i = j_f - l_f$ et la forme (6)

seulement dans le cas contraire. Le potentiel central est important quand la forme (6) ne l'est pas et vice-versa.

Le comportement de l'expression (6) est typiquement vectoriel. En effet, la différence $(\gamma_i - \gamma_f)$ se retrouve dans le rapport de la géométrie correspondant à un transfert de spin à celle correspondant à une interaction scalaire:

$$\begin{Bmatrix} l_i & l_f & J \\ \frac{1}{2} & \frac{1}{2} & 1 \\ j_i & j_f & J \end{Bmatrix} = \frac{\gamma_i - \gamma_f}{\sqrt{3J(\ +1)}} \quad \begin{Bmatrix} l_i & l_f & J \\ \frac{1}{2} & \frac{1}{2} & 0 \\ j_i & j_f & J \end{Bmatrix}$$

En première approximation, ce terme a un effet sur l'asymétrie ou la polarisation et aucun sur la section efficace. Au contraire, l'expression (4) n'a pas ce caractère; dans une certaine mesure, on peut la considérer comme une modification du couplage $\vec{L}.\vec{S}$ dans les voies initiale et finale.

Le couplage $\vec{L}.\vec{S}$ déformé sera d'autant plus important que l'énergie est élevée. Dans ce cas, les expressions (4) et (6) donnent des résultats nettement différents pour l'asymétrie dans la diffusion inélastique. C'est le cas de

Mg^{24} à 50 Mev[5] pour lequel il y a même des effets sur la section efficace de diffusion inélastique; ces effets sont les mêmes pour les deux expressions. A plus basse énergie, les effets du potentiel $\vec{L}.\vec{S}$ déformé sont moins importants et sont noyés dans ceux du couplage $\vec{L}.\vec{S}$ purement optique.

L'équation (6) contient un terme dérivatif. Ce terme disparaît pour les potentiels diagonaux:

$$V_{ii} = \sum_{\lambda} G^{\lambda}_{ii} \{\frac{1}{r}\frac{d}{dr} V_{\lambda}(r)\ \gamma_i + \frac{V_{\lambda}(r)}{r^2}\ \lambda(\lambda+1)\} \qquad (7)$$

De plus, pour $\lambda = 0$, on retrouve le couplage $\vec{L}.\vec{S}$ habituel.

E) ECIS

Le couplage $\vec{L}.\vec{S}$ déformé a été introduit dans un programme d'équations couplées utilisant la méthode des itérations séquentielles[6]. Le terme dérivatif compliquerait beaucoup les programmes d'équations couplées normaux car leur méthode numérique est basée sur l'absence de dérivées premières dans le système d'équations (2). La méthode d'itérations séquentielles consiste à écrire le système sous la forme:

$$y_1'' + (V_{11}-E)y_1 = - \sum_{j\neq 1} V_{1j}y_j \qquad (8)$$

$$y_i'' + (V_{ii}-E)y_i = - \sum_{j\neq i} V_{ij}y_j \qquad (9)$$

et à chercher une solution qui soit purement sortante pour $i\neq 1$. L'équation (8) correspond à l'état initial et l'équation (9) à l'état final. Le point de départ du processus d'itération est $y_i^{(0)}$, solution normalisée de l'équation sans second membre pour $i=1$, et $y_i^{(0)} = 0$ pour $i\neq 1$. Les équations de l'itération sont

$$y_1^{(n)''} + (V_{11}-E)y_1^{(n)} = - \sum_{j=1} V_{ij}y_j^{(n-1)} \qquad (10)$$

$$y_i^{(n)''} + (V_{ii}-E)y_i^{(n)} = - \sum_{j<i} V_{ij}y_j^{(n)} - \sum_{j>i} V_{ij}y_j^{(n-1)} \qquad (11)$$

Il faut obtenir la solution particulière de l'équation (10) qui correspond à un multipole d'onde plane plus une onde sortante et pour les équations (11) la solution particulière qui soit purement sortante. Pour cela, il faut connaître la solution des équations sans second membre. Le même calcul pourrait se faire en utilisant la fonction de Green formée avec deux solutions particulièresdes équations sans second membre.

Cette méthode nécessite plus de place que les méthodes habituelles de résolution d'équations couplées. Elle est plus rapide car le temps nécessaire croit comme le carré du nombre d'équations couplées et non comme le cube. Pour un calcul (0^+, 2^+), elle est deux fois plus rapide.

Les figures 1, 2 et 3 montrent des résultats obtenus dans le modèle vibrationnel pour Ni^{60} à 16,5 Mev. Dans le modèle vibrationnel, il n'y a pas de couplage entre les différentes équations correspondant à l'état 2^+: la première approximation de l'ECIS est strictement identique à la DWBA. Les figures 1 et 2 montrent les résultats des approximations successives dans un calcul 0^+, 2^+. La figure 3 montre que, dès la première approximation, on obtient d'excellents résultats pour un état à deux phonons[7].

Cette méthode serait particulièrement adaptée pour résoudre des équations couplées intégro-différentielles. Ici il suffit d'ajouter les termes dérivatifs au second membre.

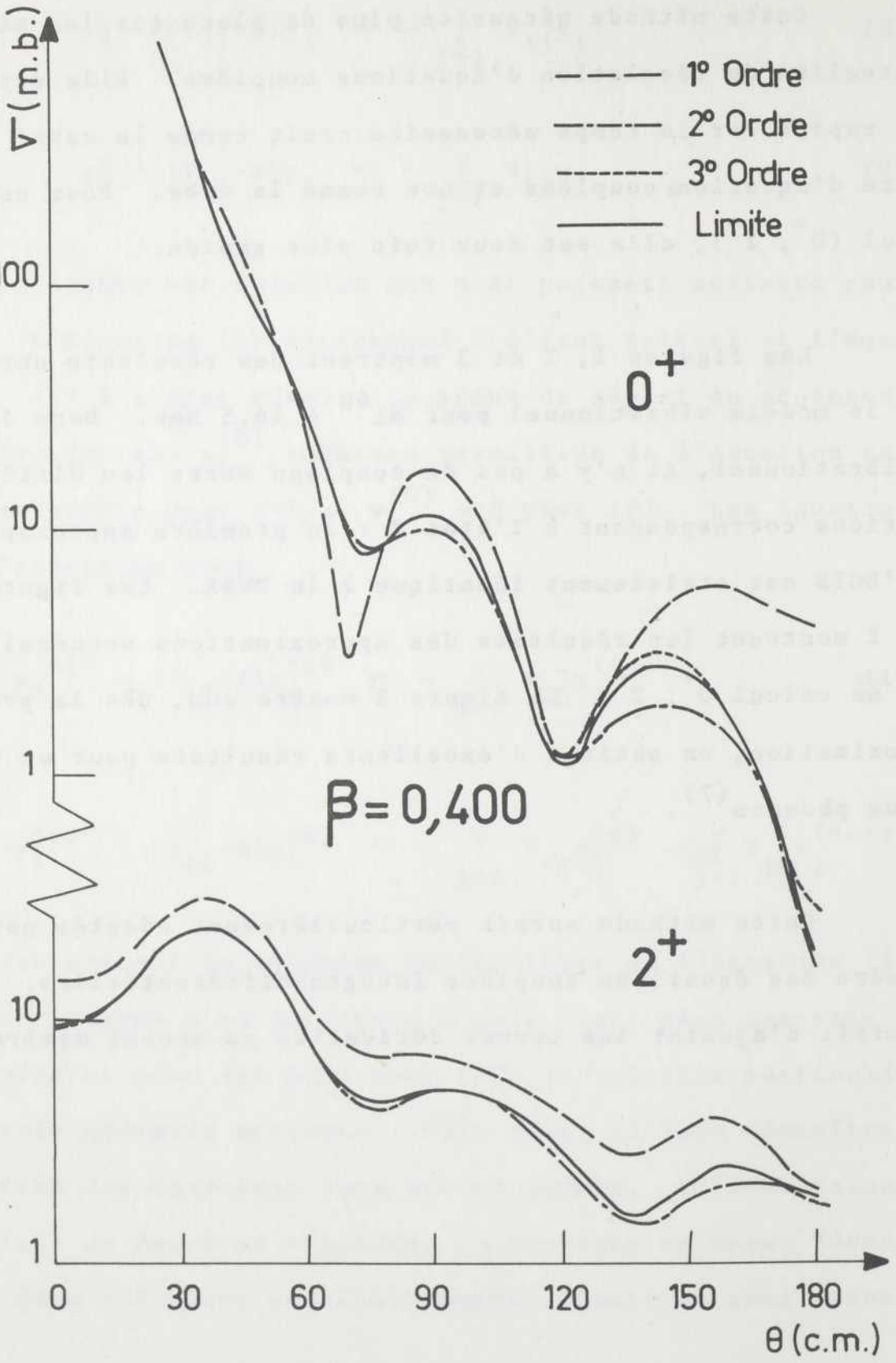
1° Ordre
2° Ordre
3° Ordre
Limite
σ (m.b.)
100
10
1
0+
β = 0,400
2+
10
1
0
30
60
90
120
150
180
θ (c.m.)

Figure 1

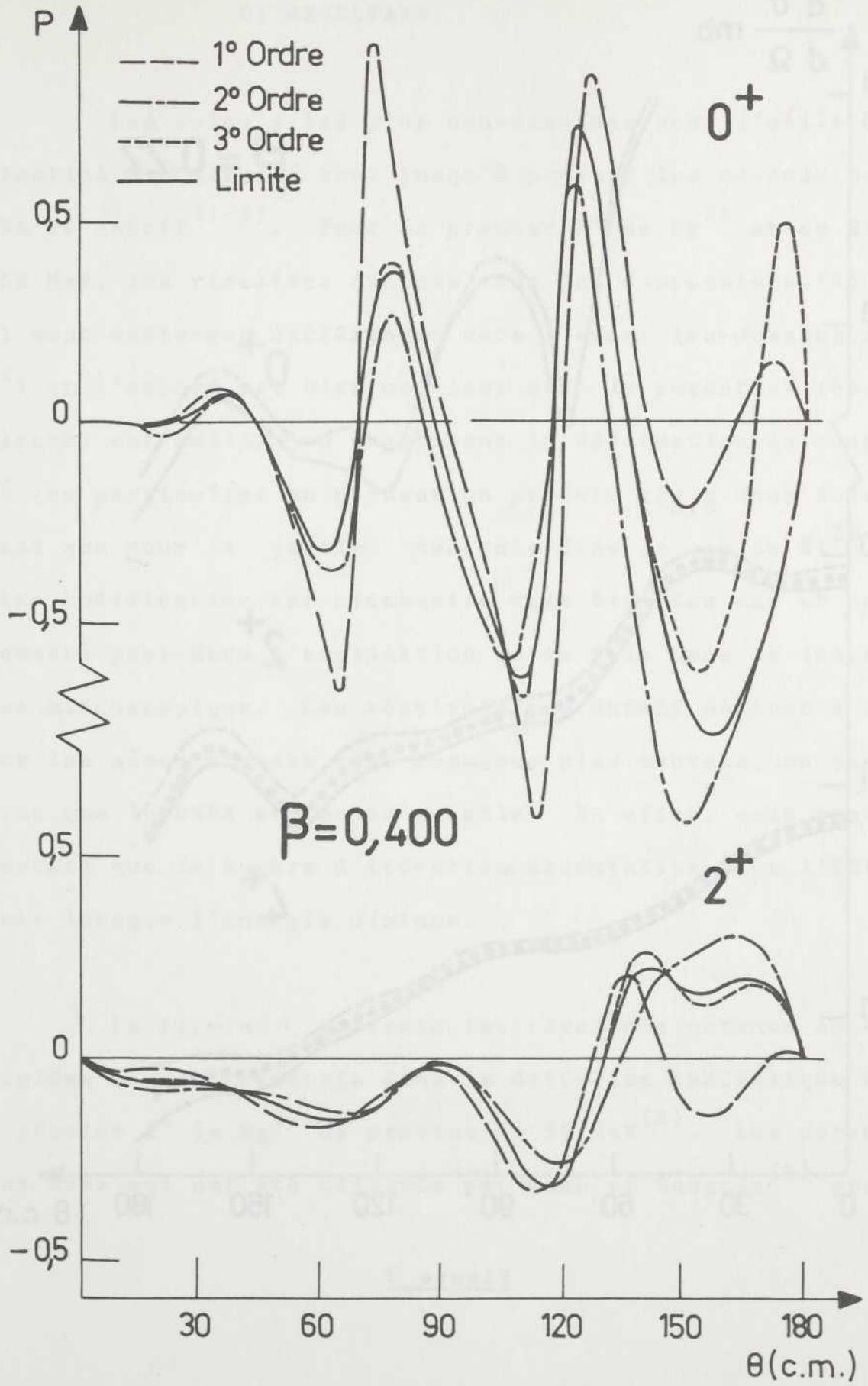
P
1° Ordre
2° Ordre
3° Ordre
Limite
0,5
0
-0,5
0+
β=0,400
0,5
0
-0,5
2+
30
60
90
120
150
180
θ(c.m.)

Figure 2

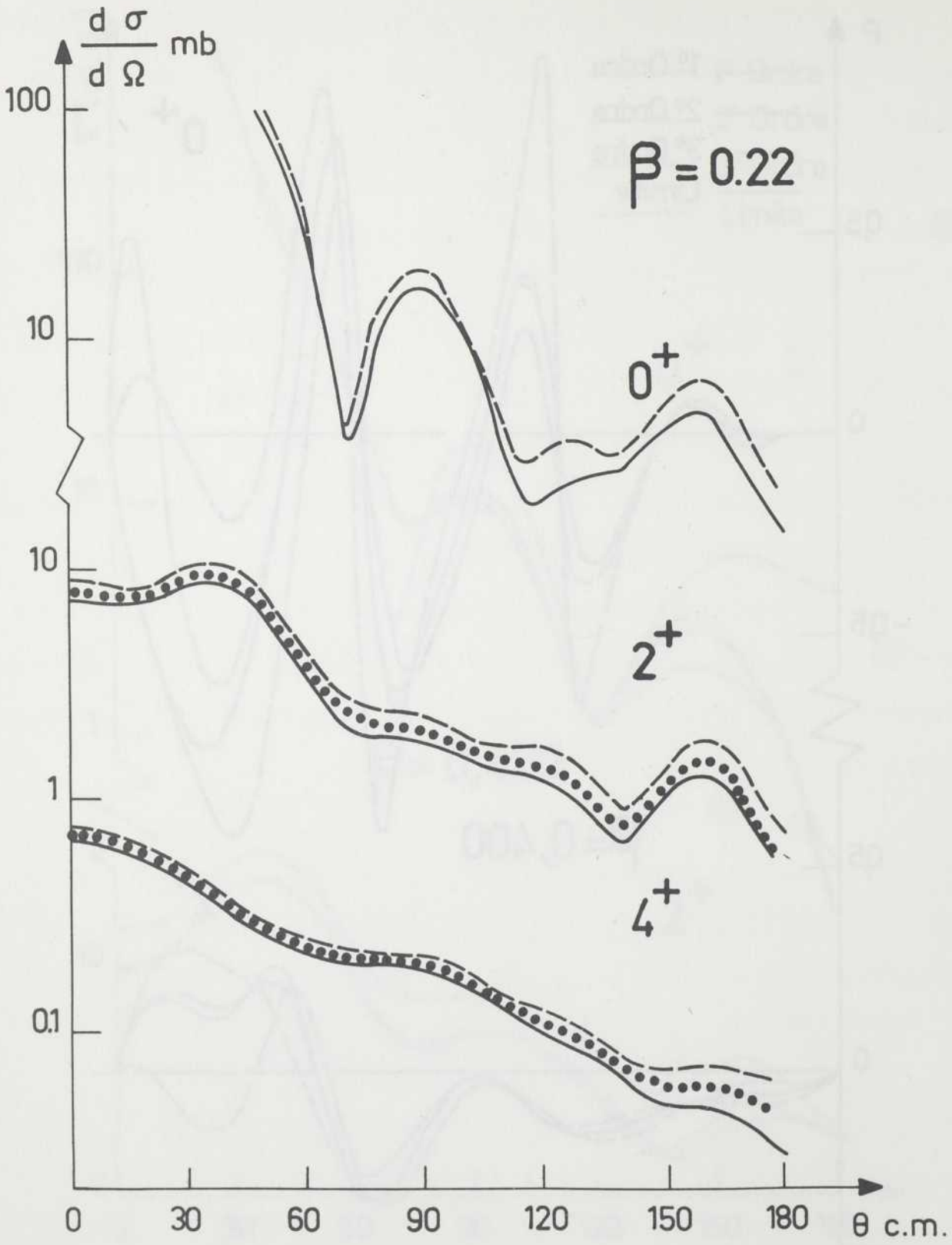

Figure 3

D) RESULTATS

Les calculs les plus convaincants pour l'utilité du potentiel $\vec{L}.\vec{S}$ déformé sont jusqu'à présent les calculs de DWBA de Shérif[1-3]. Pour le premier 2^+ de Mg^{24} et de Si^{28} à 50 MeV, les résultats obtenus avec les expressions (4) et (6) sont nettement différentes vers l'avant (au-dessous de 80^o) et l'accord est bien meilleur avec le potentiel (6). L'accord est amélioré en augmentant la déformation du couplage $\vec{L}.\vec{S}$ (en particulier en prenant un produit $r\beta_{\vec{L}.\vec{S}}$ deux fois plus grand que pour la partie centrale dans le cas de Si^{28}). Cette modification est nécessaire dans bien des cas et on trouvera peut-être l'explication de ce fait dans la description microscopique. Les résultats que Shérif obtient à 20 MeV pour les mêmes niveaux sont beaucoup plus mauvais, en partie parce que la DWBA est moins valable. En effet, nous avons constaté que le nombre d'itérations nécessaires dans l'ECIS croit lorsque l'énergie diminue.

La figure 4 présente les résultats obtenus en équations couplées pour l'asymétrie dans la diffusion inélastique sur le premier 2^+ de Mg^{24} de protons de 50 MeV[8]. Les potentiels sont ceux qui ont été utilisés par Rush et Ganguly[5] pour

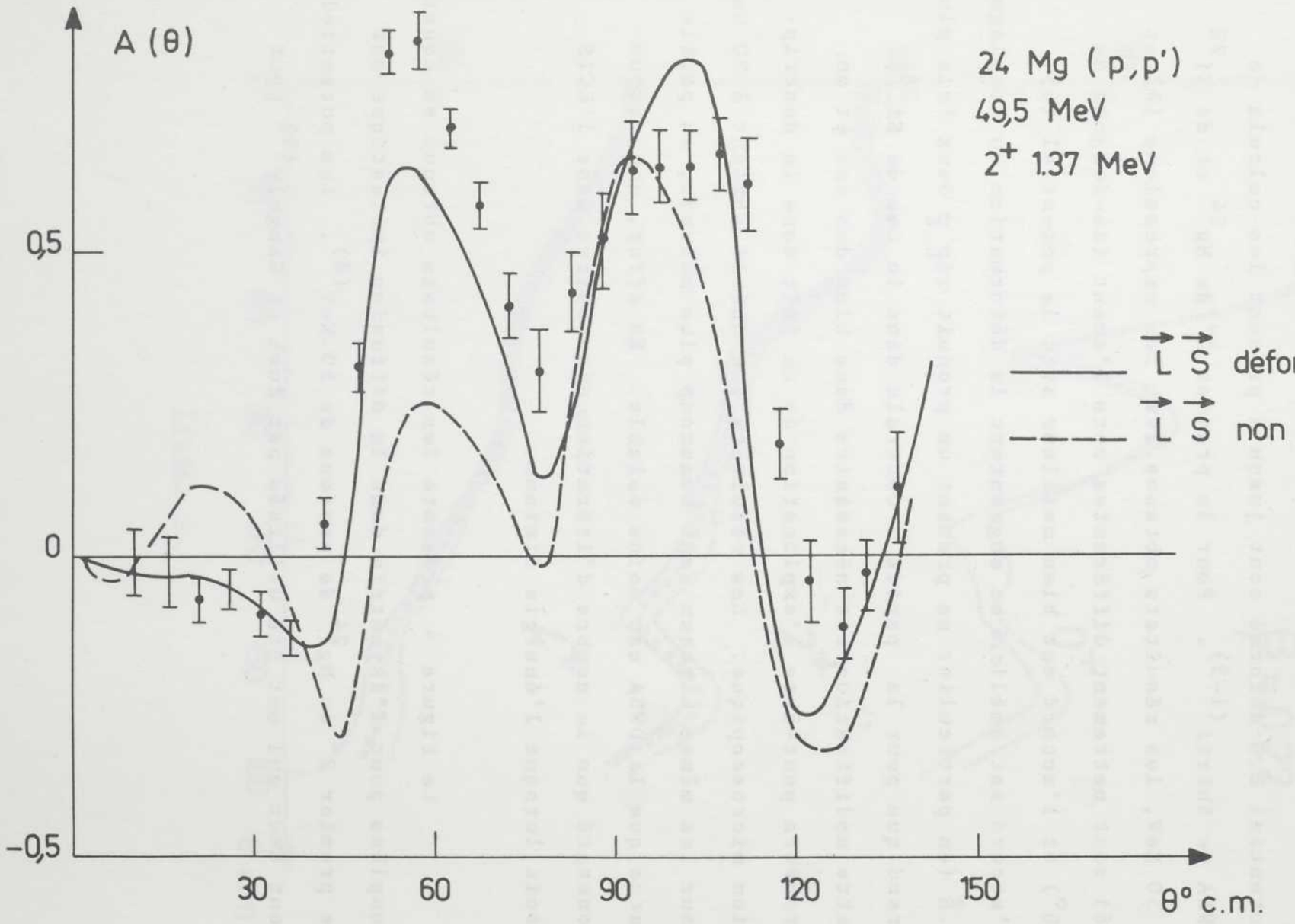
A (θ)
0,5
0
-0,5
30
60
90
120
150
θ° c.m.
24 Mg (p,p')
49,5 MeV
2+ 1.37 MeV
L S déformé
L S non déformé

Figure 4

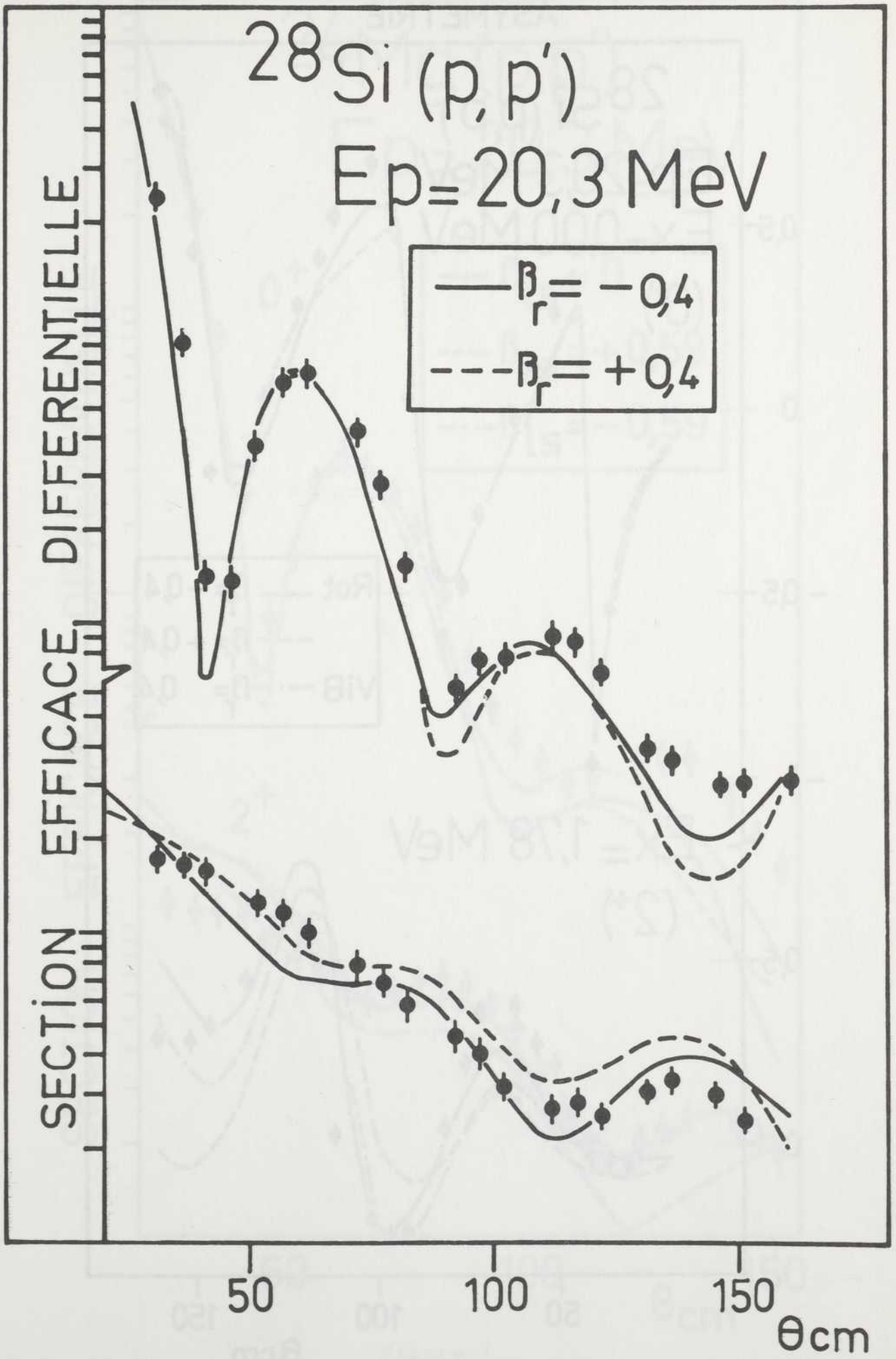
^{28}Si (p, p')
Ep= 20,3 MeV
—— β_r = −0,4
--- β_r = +0,4
SECTION EFFICACE DIFFERENTIELLE
50
100
150
θcm

Figure 5

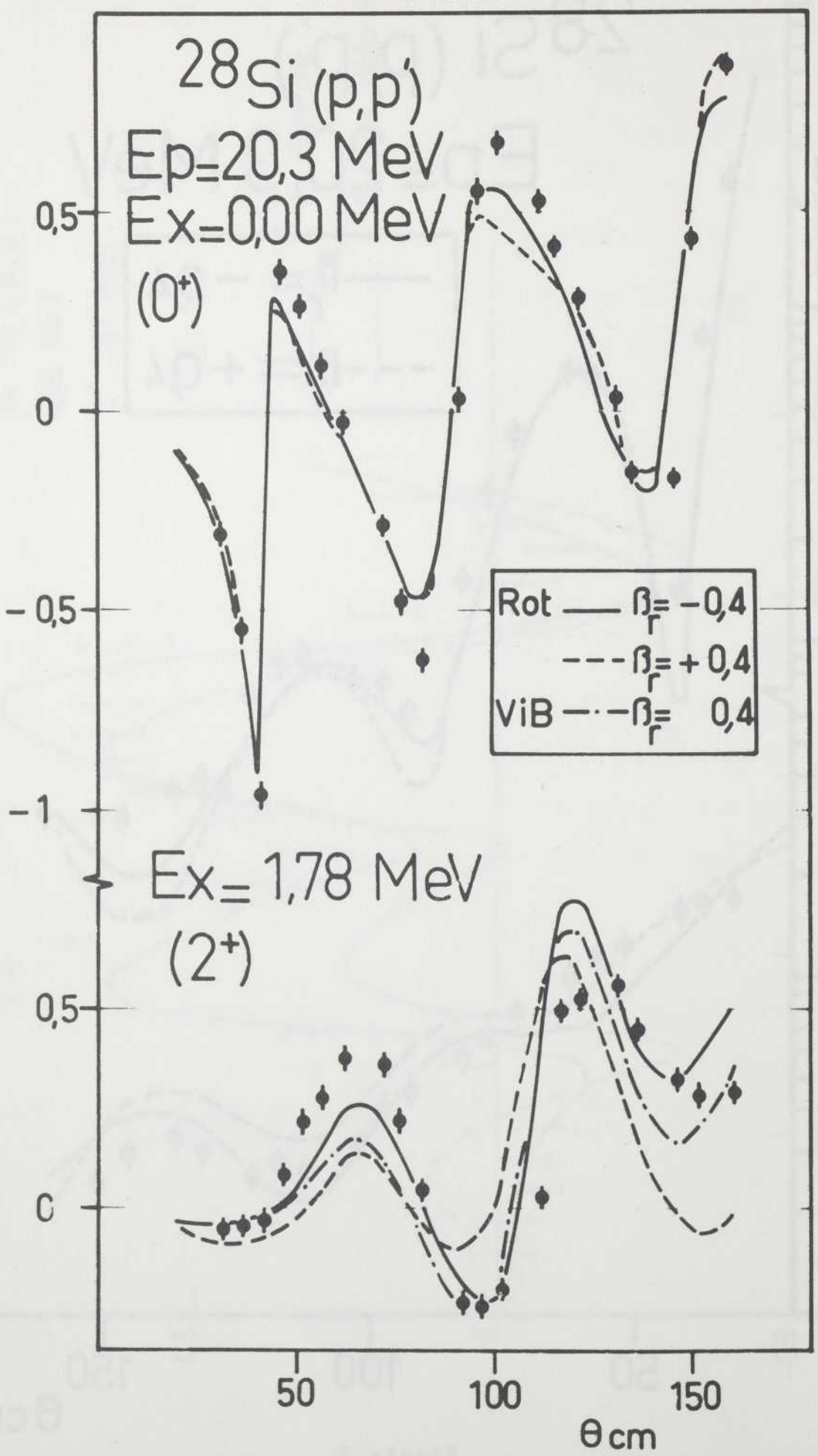
ASYMÉTRIE
28Si (p,p')
Ep=20,3 MeV
Ex=0,00 MeV
(0+)
Rot —— βr= −0,4
--- βr= +0,4
ViB —·— βr= 0,4
Ex= 1,78 MeV
(2+)
0,5
0
−0,5
−1
0,5
0
50
100
150
θ cm

Figure 6

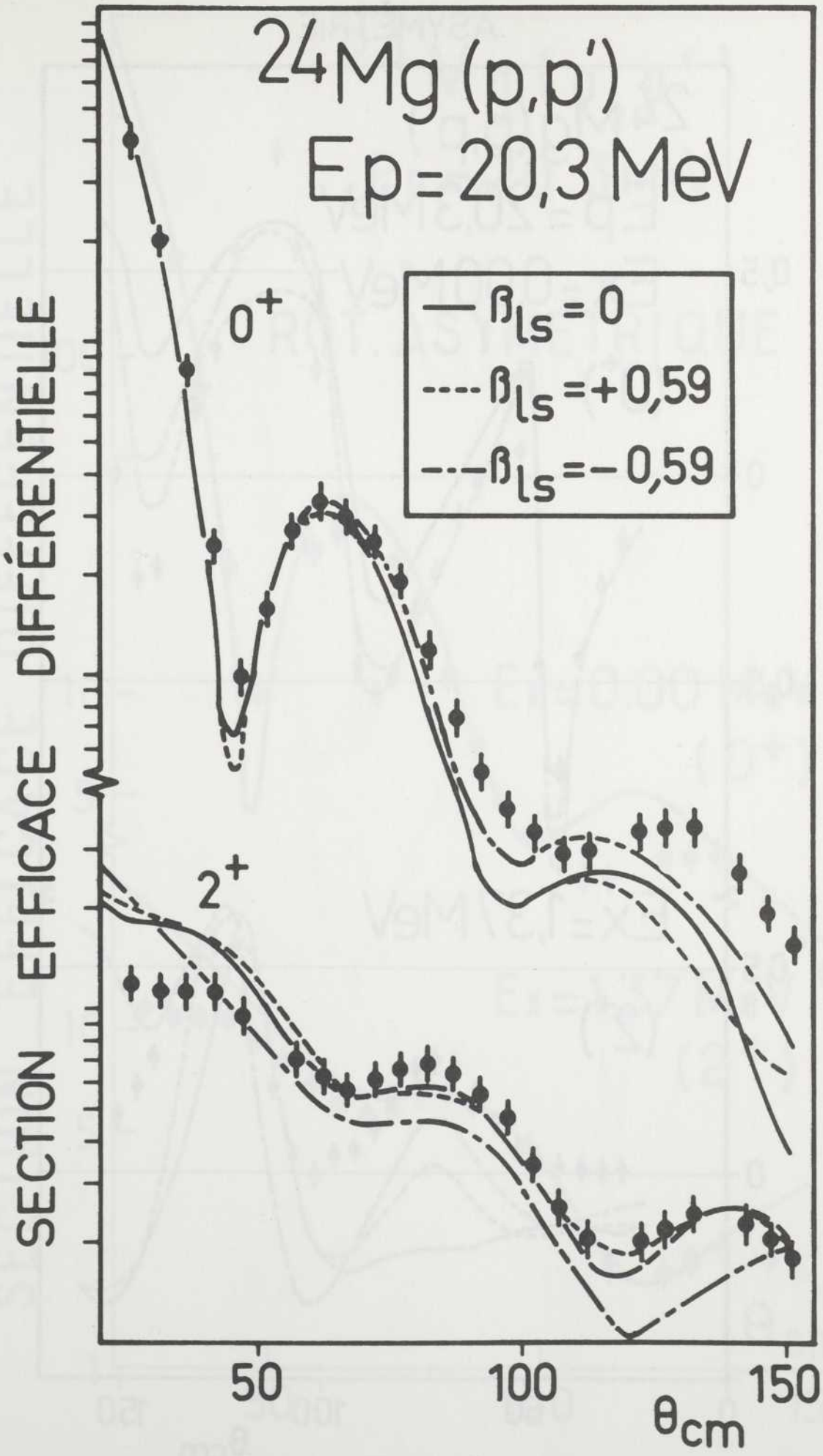
24Mg (p,p')
Ep = 20,3 MeV
0+
2+
— ßls = 0
---- ßls = +0,59
---- ßls = −0,59
SECTION EFFICACE DIFFÉRENTIELLE
50
100
150
θcm

Figure 7

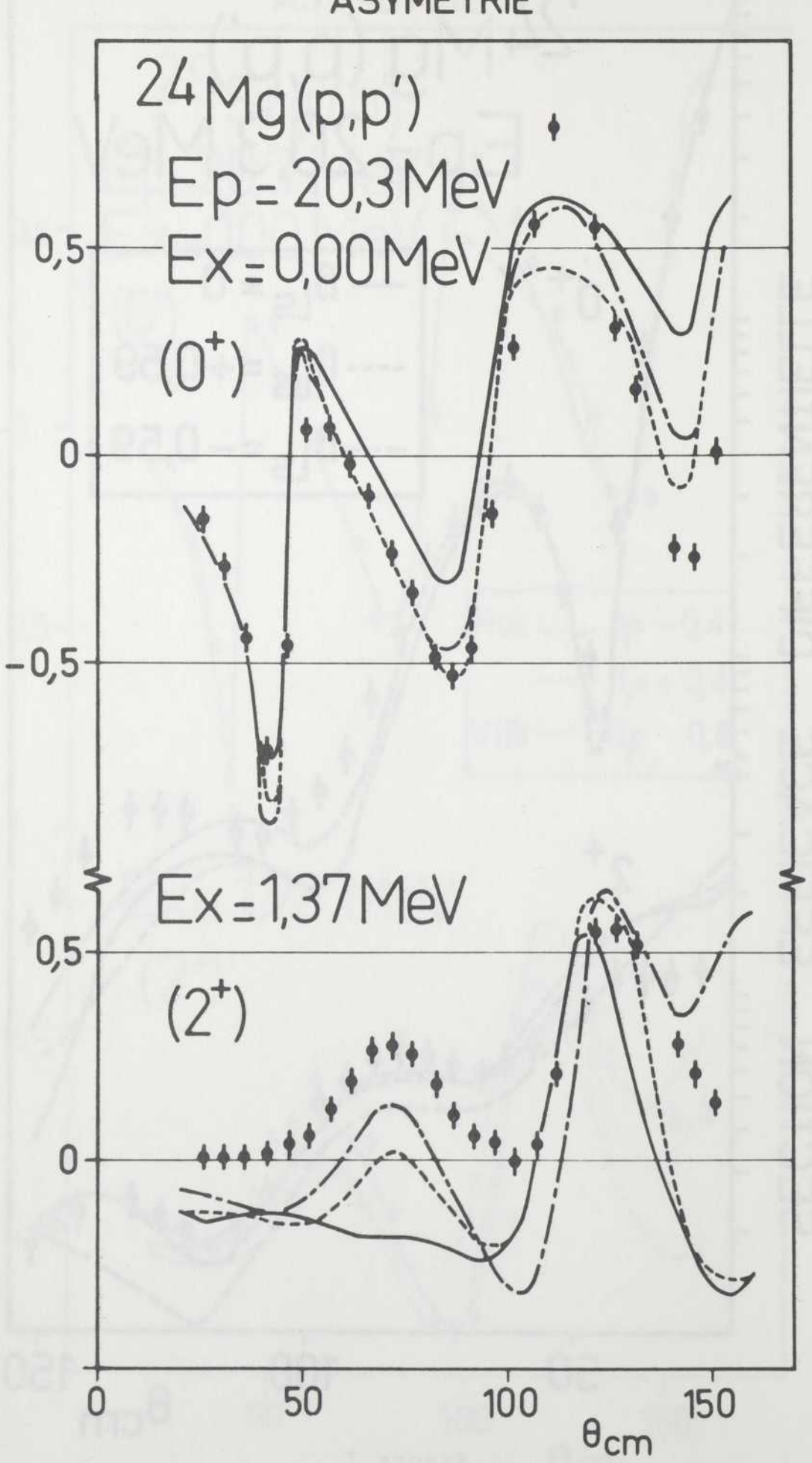
ASYMÉTRIE
24Mg(p,p')
Ep = 20,3 MeV
Ex = 0,00 MeV
(0+)
0,5
0
-0,5
Ex = 1,37 MeV
(2+)
0,5
0
0
50
100
150
θcm

Figure 8

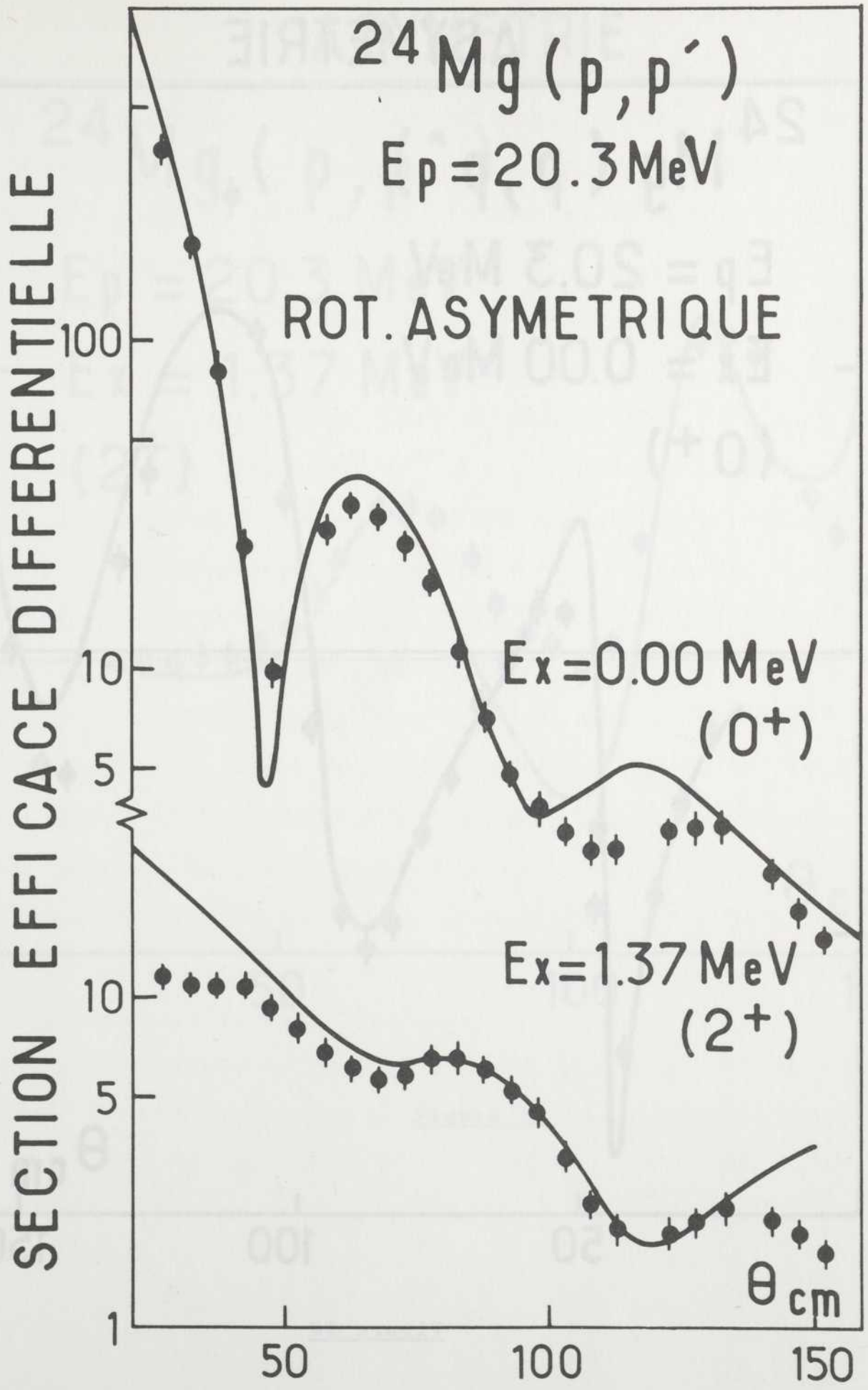
^{24}Mg(p,p')
Ep=20.3MeV
ROT. ASYMETRIQUE
Ex=0.00 MeV
(0+)
Ex=1.37 MeV
(2+)
θ cm
SECTION EFFICACE DIFFERENTIELLE
100
10
5
10
5
1
50
100
150

Figure 9

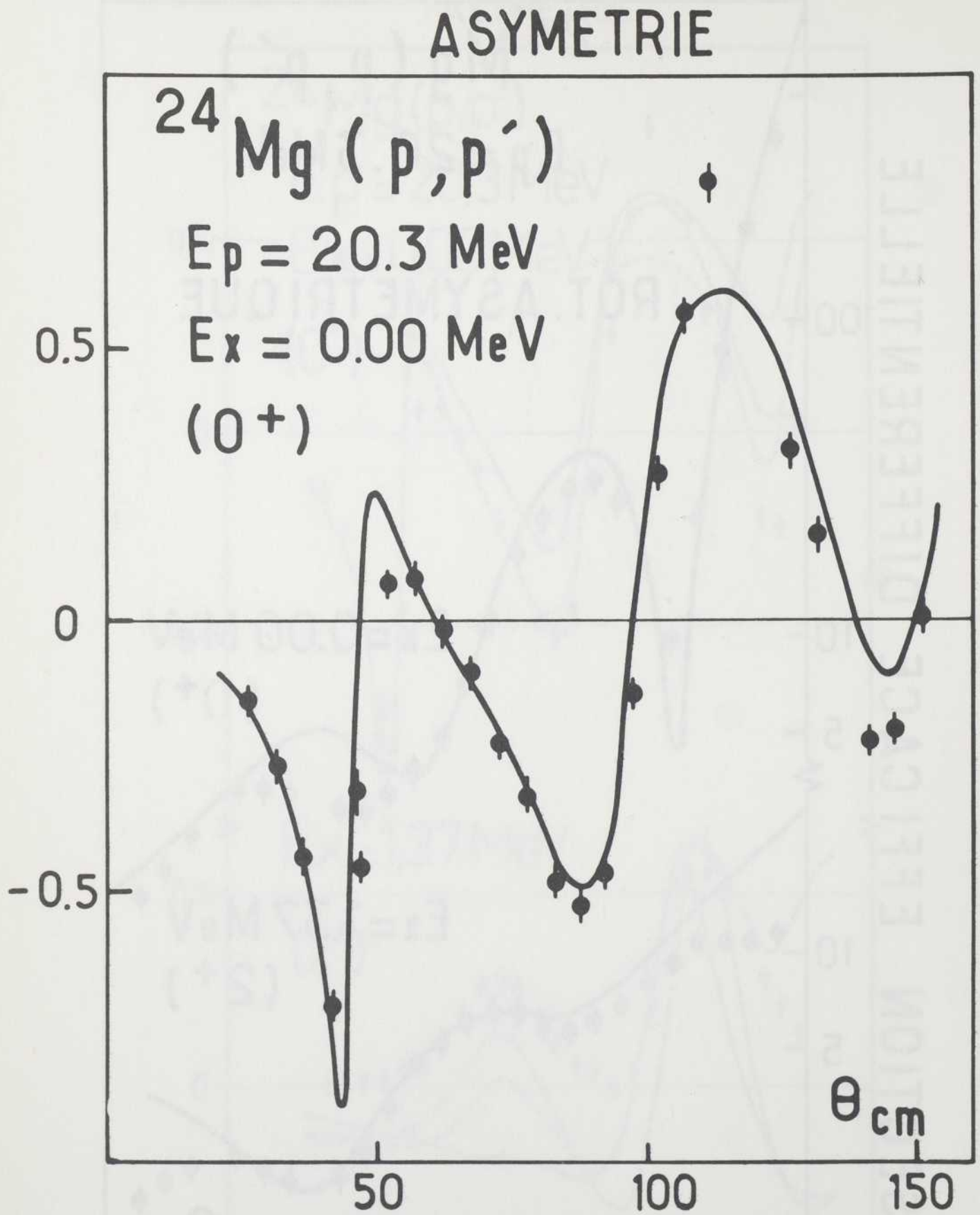

Figure 10

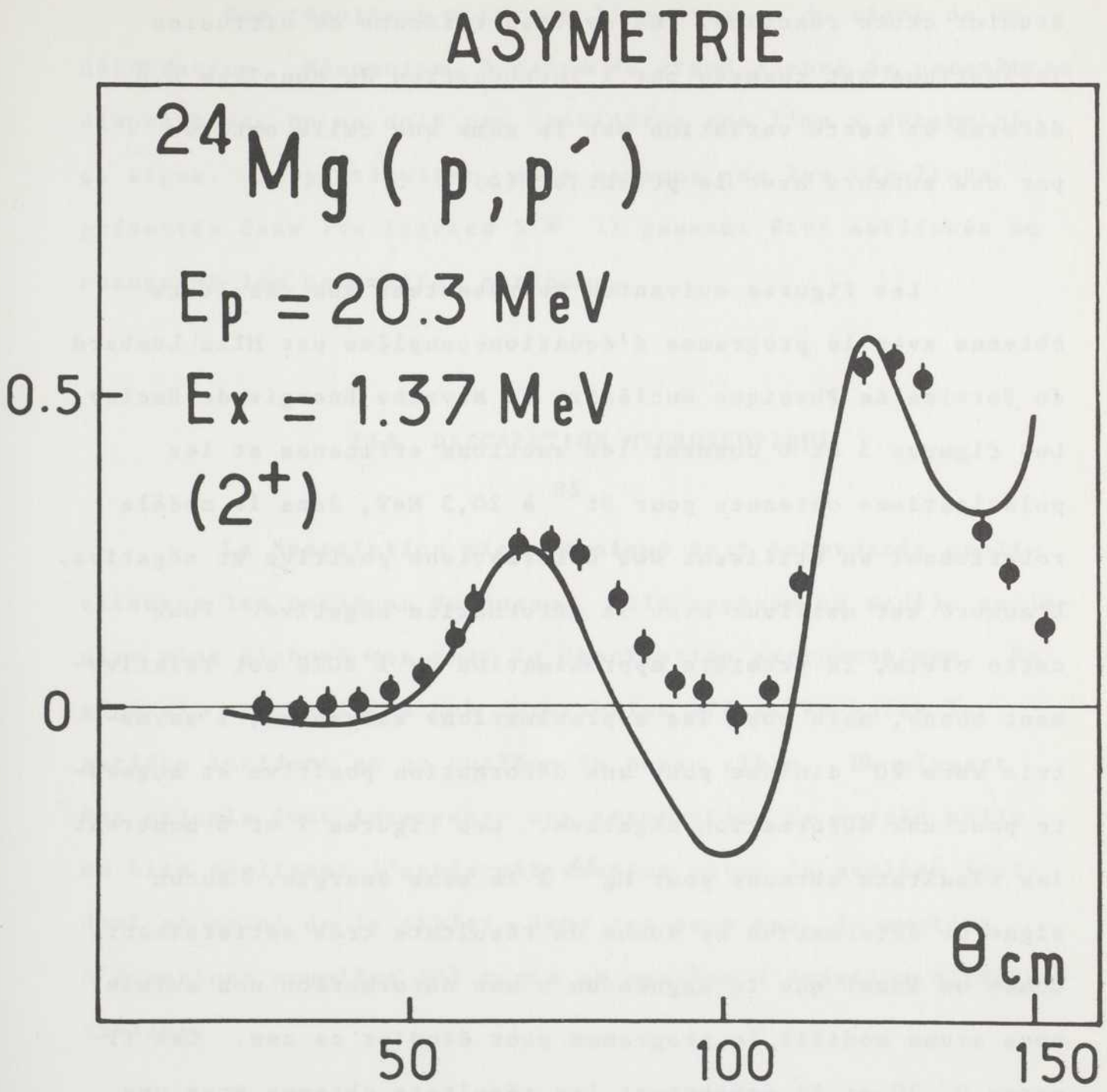

Figure 11

étudier cette réaction. La section efficace de diffusion inélastique est changée par l'introduction du couplage $\vec{L}.\vec{S}$ déformé et cette variation est la même que celle obtenue par ces auteurs avec le potentiel (4).

Les figures suivantes représentent des résultats obtenus avec le programme d'équationscouplées par Mlle Lombard du Service de Physique Nucléaire de Moyenne Energie de Saclay. Les figures 5 et 6 donnent les sections efficaces et les polarisations obtenues pour Si^{28} à 20,3 MeV, dans le modèle rotationnel en utilisant des déformations positive et négative. L'accord est meilleur avec la déformation négative. Pour cette cible, la première approximation de l'ECIS est relativement bonne, mais pour les approximations suivantes, l'asymétrie vers 70^{o} diminue pour une déformation positive et augmente pour une déformation négative. Les figures 7 et 8 montrent les résultats obtenus pour Mg^{24} à la même énergie. Aucun signe de déformation ne donne de résultats très satisfaisant. Comme on admet que le magnésium a une déformation non axiale, nous avons modifié le programme pour étudier ce cas. Les figures 9, 10 et 11 présentent les résultats obtenus avec une déformation intermédiaire entre allongé et aplati ($\gamma = 30^{o}$) et un état 2^{+} décrit par un mélange de bandes de 55^{o}.

Ces résultats montrent l'importance du signe de la déformation. Néanmoins, à cause du grand nombre de paramètres disponibles, on ne doit pas considérer que l'on a déterminé ce signe. En particulier, nous pensons que les résultats présentés dans les figures 5 à 11 peuvent être améliorés en changeant les paramètres optiques.

III DESCRIPTION MICROSCOPIQUE

La description microscopique fait intervenir explicitement les nucléons du noyau. Elle suppose un modèle nucléaire plus élaboré que pour la description macroscopique. En général, on considère une interaction effective entre le nucléon incident et un nucléon du noyau cible. La plupart des calculs font intervenir une interaction de portée nulle ou bien négligent l'antisymétrisation entre le nucléon incident et celui de la cible: dans ces deux cas, le système d'équations couplées (2) reste un système d'équations différentielles.

Nous devons d'abord présenter le formalisme de l'hélicité[4] pour le développement multipolaire d'une interaction; ce formalisme a été utilisé pour cette étude du couplage $\vec{L}.\vec{S}$ nucléon-nucléon.

A) FORMALISME DE L'HELICITE

Pour calculer un élément de matrice particule-trou d'une interaction de portée finie $< j_1' j_1^{-1}; J\ M|V_{12}|j_2 j_2'^{-1}; J\ M>$ on peut projeter les spins sur les rayons vecteurs: sur $\vec{r}_1$ pour les états j_1 et j_1' et sur $\vec{r}_2$ pour les états j_2 et j_2'. A tout opérateur V_{12} correspondent des multipoles d'hélicité $a^J(1,2)$, $b^J(1,2)$ et $c^J(1,2)$ pour les éléments de matrice de parité naturelle et $d^J(1,2)$, $e^J(1,2)$ et $f^J(1,2)$ pour les états de parité non naturelle.

En intégrant sur la variable r_2 et en sommant sur les spins correspondants, on obtient deux facteurs de forme. Dans le cas d'une parité naturelle, ce sont:

$$A^J(r_1) = \mathcal{G}^J_{j_2 j_2'} \int [a^J(1,2) + \alpha^J_{j_2 j_2'}\ b^J(2,1)] \phi_{j_2}(r_2) \phi_{j_2'}(r_2) r_2^2 dr_2 \qquad (12)$$

$$B^J(r_1) = \mathcal{G}^J_{j_2 j_2'} \int [b^J(1,2) + \alpha^J_{j_2 j_2'} c^J(1,2)]\ \phi_{j_2}(r_2) \phi_{j_2'}(r_2) r_2^2\ dr_2 \qquad (13)$$

avec

$$\mathcal{G}^J_{jj'} = (-)^{j+\frac{1}{2}} \sqrt{\frac{(2j+1)(2j'+1)}{2J+1}} \begin{pmatrix} j' & J & j \\ -\frac{1}{2} & 0 & \frac{1}{2} \end{pmatrix} \qquad (14)$$

et

$$\alpha^{J}_{jj'} = \frac{\gamma - \gamma'}{\sqrt{J(J+1)}} \qquad (15)$$

Dans le cas d'une parité non naturelle, on obtient des formules analogues avec d, e, f au lieu de a, b et c, mais:

$$\alpha^{J}_{jj'} = \frac{\gamma+\gamma' + 2}{\sqrt{J(J+1)}} \qquad (16)$$

A partir de ces facteurs de forme, on obtient l'élément de matrice particule-trou par:

$$\langle j_1' j_1^{-1};\ JM|V_{12}|j_2 j_2'^{-1};\ JM\rangle = (-)^{j_1'-j_1}\ \mathcal{G}^{J}_{j_1 j_1'} \qquad (17)$$

$$\int \left[A^{J}(r_1) + \alpha^{J}_{j_1 j_1'} B^{J}(r_1)\right]\ \phi_{j_1}(r_1)\phi_{j_1'}(r_1) r_1^2 dr_1$$

Dans l'étude de réactions directes, si on n'antisymétrise pas le nucléon incident avec celui de la cible, les potentiels de couplage s'expriment avec les facteurs de forme A(r) et B(r) et les mêmes coefficients géométriques qui apparaissent dans la formule (17).

Dans le cas d'une interaction centrale, ne dépendant pas des spins, et telle que:

$$V(r_1-r_2) = \sum_J (2J+1)\, V_J(r_1,r_2)\, P_J(\cos \widehat{r_1 r_2}) \quad (18)$$

les multipoles d'hélicité sont:

$$a^J(1,2) = (2J+1)\, V_J$$

$$b^J = c^J = d^J = e^J = f^J = 0 \quad (19)$$

Pour une interaction $\vec{\sigma}_1 \cdot \vec{\sigma}_2$ ce sont:

$$a^J = b^J = 0$$

$$c^J = -(2J+1)\, V_J$$

$$f^J = J\, V_{J-1} + (J+1)\, V_{J+1} \quad (20)$$

$$e^J = \sqrt{J(J+1)}(V_{J-1} - V_{J+1})$$

$$f^J = (J+1)V_{J-1} + J\, V_{J+1}$$

Une interaction $\vec{L}.\vec{S}$ nucléon-nucléon de portée finie a des multipoles d'hélicité moins simples; ils sont donnés dans l'Appendice B.

B) CALCUL SANS ANTISYMETRISATION

La plupart des calculs de réaction nucléaire avec une description microscopique de la cible utilisent soit une portée finie en négligeant l'antisymétrisation du nucléon incident avec les nucléons de la cible, soit une interaction de portée nulle. Bien que le couplage $\vec{L}.\vec{S}$ puisse être utilisé avec une portée finie et en antisymétrisant complètement, cela n'a pas été fait jusqu'ici. Avec R. Shaeffer, nous avons commencé à étudier ce problème.

Le simple examen des formules de l'Appendice B permet de voir comment le facteur de forme dépend des valeurs propres γ_i et γ_f. Pour l'excitation d'un état de parité naturelle, on obtient:

$$A(r) + B(r)(\gamma_i-\gamma_f) + A_1(r)(\gamma_i-\gamma_f)^2 + A_2(r)(\gamma_i-\gamma_f)(\gamma_i+\gamma_f+2)$$
$$+ B_1(r)(\gamma_i+\gamma_f+2) + \{\mathcal{A}(r) + \mathcal{B}(r)(\gamma_i-\gamma_f)\}\frac{d}{dr} \qquad (21)$$

et pour l'excitation d'un état de parité non naturelle:

$$A(r) + B(r)(\gamma_i+\gamma_f+2) + A_1(r)(\gamma_i+\gamma_f+2)^2 \qquad (22)$$

Dans les deux cas, les facteurs de forme $A(r)$, $A_1(r)$, ... ont une structure si complexe que nous ne pouvons pas mettre en évidence des relations entre eux.

Pour l'excitation d'un état de parité naturelle, le facteur de forme contient un terme dérivatif, tout comme le facteur de forme collectif. A la limite des grands moments angulaires, le facteur de forme microscopique a la même structure que le facteur de forme collectif.

Pour l'excitation d'un état de parité non naturelle, le facteur de forme ne contient pas de terme dérivatif. On obtient une contribution importante si $j_i - l_i = j_f - l_f$; cependant le coefficient géométrique $\mathcal{G}$ est plus faible dans ce cas que si $j_i - l_i \neq j_f - l_f$. Comme dans le modèle collectif, le potentiel $\vec{L}.\vec{S}$ devient de plus en plus important par rapport au potentiel central lorsque le moment angulaire augmente et leur rapport croit linéairement, malgré l'aspect quadratique de l'expression.

C) PORTEE NULLE

En général, on obtient la limite de portée nulle des multipoles d'hélicité en remplaçant les V_J par $\delta(r_1 - r_2)/r_1^2$. Si on fait cette opération pour le couplage $\vec{L}.\vec{S}$ (ou pour le

potentiel tenseur) on obtient zéro. Nous devons donc calculer le terme suivant. La première contribution non nulle vient de $\delta''(\vec{r}_1-\vec{r}_2)$ dont il faut connaître le développement multipolaire. Pour obtenir un résultat général, considérons un potentiel quelconque de portée μ, $V(|\vec{r}_1-\vec{r}_2|/\mu)$. Ses multipoles V_L sont reliés entre eux. En posant:

$$W(q,\mu) = \int e^{i\vec{q}.r} V(r/\mu) d^3r \quad , \tag{23}$$

on obtient

$$V_L(r_1,r_2,\mu) = \frac{1}{(2\pi)^3} \int_o^\infty q^2 \, W(q) j_L(qr_1) j_L(qr_2) dq \tag{24}$$

La fonction W dépend de la portée de la façon suivante:

$$W(q,\mu) = \mu^3 \, W'(q\mu) \tag{25}$$

où $W'(q\mu)$ est la transformée de V pour une portée unité. W'est une fonction paire de q. Nous pouvons poser:

$$W'(q) = \sum_n c_n (-q^2)^n \tag{26}$$

et obtenir le développement des multipoles en fonction de la portée:

$$V_L(r_1,r_2,\mu) = \left(\frac{\mu}{2\pi}\right)^3 \sum_n c_n(-\mu^2)^n \int q^{2(1+n)} j_L(qr_1) j_2(qr_2) dq$$

$$= \left(\frac{\mu}{2\pi}\right)^3 \sum_n c_n(-\mu^2)^n V_L^n(r_1,r_2) \qquad (27)$$

En utilisant l'équation des $j_L(r)$, on obtient une relation de récurrence entre les $V_L^n(r_1,r_2)$

$$V_L^n(r_1,r_2) = -\left[\frac{1}{r_1}\frac{d^2}{dr_1^2} r_1 - \frac{L(L+1)}{r_1^2}\right] V_L^{n-1}(r_1,r_2) \qquad (28)$$

qui permet de tout exprimer en fonction de $V_L^o(r_1,r_2)$ en faisant agir les opérateurs de dérivation sur la fonction de r_1 présente dans la définition de l'élément de matrice. On obtient ainsi:

$$V_L^n(r_1,r_2) = \frac{(-)^n}{r_1^2}\delta(r_1-r_2)\left\{r_1\frac{d^2}{dr_1^2}\frac{1}{r_1} - \frac{L(L+1)}{r_1^2}\right\}^n \qquad (29)$$

En faisant ce calcul sur le développement multipolaire de l'interaction $\vec{L}.\vec{S}$, on obtient:

$$G^\lambda \left\{ [\lambda(\lambda+1)(\alpha_1^2+\alpha_2^2-2)-1]\frac{V_\lambda(r)}{r^2} \right. \qquad (30)$$

$$+\left[1-(-)^{\ell_1+\ell_1'+\lambda}\alpha_1\alpha_2\right]\left[-(\gamma_1+\gamma_1'+1)\frac{V_\lambda(r)}{r^2} + (\gamma_2+\gamma_2'-\gamma_1-\gamma_1')\frac{1}{r}\frac{d}{dr}\{V_\lambda(r)\}\right]$$

$$\left.+\left[1+(-)^{\ell_1+\ell_1'+\lambda}\right]\left[(\gamma_1+\gamma_2'+1)\frac{V_\lambda(r)}{r^2} + (\gamma_2-\gamma_2'-\gamma_1+\gamma_1')\left(\frac{V_\lambda(r)}{r}\frac{d}{dr} + \frac{1}{r}\varphi_2\frac{d}{dr}(\varphi_2')\right)\right]\right\}$$

avec les coefficients α donnés par les formules (15) ou (16) suivant la parité de l'excitation. Pour un élément de matrice particule-trou: $<(j_1' j_1^{-1})\lambda|V|(j_2 j_2'^{-1})\lambda>$, le coefficient géométrique est

$$G^{\lambda} = (-)^{j_2'-j_1} \sqrt{(2j_1+1)(2j_1'+1)(2j_2+1)(2j_2'+1)} \begin{matrix} j_2' & \lambda & j_2 \\ -\frac{1}{2} & 0 & \frac{1}{2} \end{matrix} \quad \begin{matrix} j_1' & \lambda & j_1 \\ -\frac{1}{2} & 0 & \frac{1}{2} \end{matrix} \tag{31}$$

Dans la formule (30), nous avons exprimé la contribution nucléaire sous la forme la plus proche possible de la description macroscopique: $V_\lambda(r)$ est le produit des fonctions d'onde de la particule et du trou qui décrivent l'excitation de la cible. A titre de comparaison, une interaction $(a+b\ \vec{\sigma}_1\vec{\sigma}_2)\delta(r_1-r_2)$ donnerait pour une excitation de parité naturelle:

$$G^{\lambda}\ \{\ a-b\ \alpha_1\alpha_2\}\ \ V_\lambda(r) \tag{32}$$

et pour une excitation de parité non naturelle:

$$G^{\lambda}\ \{\ b(1+\alpha_1\alpha_2)\}\ V_\lambda(r) \tag{33}$$

Si l'état excité est très collectif, beaucoup de nucléons contribuent et on peut supposer que les termes contenant

γ_2 et γ_2' s'annulent en moyenne ainsi que le facteur de forme $\frac{1}{r}\ \phi_2\ \frac{d}{dr}\ (\phi_2')$. Pour un niveau de parité naturelle, on obtient ainsi:

$$G\left\{\frac{V_\lambda(r)}{r^2}\left[(\gamma_f-\gamma_i)(\gamma_f-\gamma_i-1)\ -\ 2\lambda(\lambda+1)\right]-\frac{2V_\lambda(r)}{r}\ (\gamma_i-\gamma_f)\ \frac{d}{dr}\right.$$

$$\left.-\ \frac{2}{r}(\gamma_i+\gamma_f)\ \frac{d}{dr}\left[V_\lambda(r)\right]\right\} \qquad (34)$$

Cette expression n'est pas hermitique. Si on la rend hermitique, on a:

$$G\left\{\frac{V_\lambda(r)}{r^2}\left[\ (\gamma_f-\gamma_i)(\gamma_f-\gamma_i-1)\ -\ 2\lambda(\lambda+1)\right]\right.$$

$$\left.-\ \frac{2}{r}(\gamma_i-\gamma_f)\ \ \frac{V_\lambda}{r}\ \frac{d}{dr}\ -\ \frac{2}{r}\ \gamma_i\ \ \frac{d}{dr}\ \left[V_\lambda(r)\right]\right\} \qquad (35)$$

qui est proportionnelle à l'expression obtenue dans le modèle macroscopique, à un facteur 2 devant $\lambda(\lambda + 1)$ près.

Dans les mêmes conditions, on obtient pour l'excitation d'un niveau de parité non naturelle:

$$G \left\{ \frac{V_\lambda}{r^2} \left[(\gamma_i+\gamma_f+2)(\gamma_i+\gamma_f+1) - 2\lambda(\lambda+1) \right] \right.$$
$$\left. - (\gamma_i+\gamma_f) \frac{1}{r} \frac{d}{dr} \left[V_\lambda(r) \right] \right\} \qquad (36)$$

qui est parfaitement hermitique.

Cette interaction $\vec{L}.\vec{S}$ n'existe que pour un moment angulaire relatif L=1, qui est la plus petite valeur pour le moment angulaire pour laquelle elle puisse contribuer. Comme elle n'existe que si S=1, elle s'annule pour T=0. Cela peut se vérifier sur l'expression complète: l'intégrale directe est égale à l'intégrale d'échange. Par conséquent, elle est deux fois plus intense entre deux protons qu'entre un proton et un neutron.

L'utilisation d'un potentiel $\vec{L}.\vec{S}$ de portée nulle est parfaitement justifiée. Par exemple, Hamada et Johnston[9] utilisent un potentiel $\vec{L}.\vec{S}$ de portée moitié de celle du potentiel central; de plus, leur couplage $\vec{L}.\vec{S}$ est plus faible pour T=0 que pour T=1, ce qui est un autre argument en faveur de l'utilisation des formules de portée nulle.

D) RESULTATS

Nous n'avons encore aucun résultat avec un modèle microscopique. Nous espérons en obtenir avec le programme de DWBA de Schaeffer, en utilisant un couplage $\vec{L}.\vec{S}$, soit de portée finie, soit de portée nulle.

IV CONCLUSION

La description microscopique permet de comprendre que la déformation du couplage $\vec{L}.\vec{S}$ soit plus importante pour certaines cibles que pour d'autres. Expérimentalement, les asymétries dans la diffusion inélastique sont plus grandes si la cible a des couches fermées ou un excès de protons (Zn^{90}, Mo^{92}) que si elle a un excès de neutrons (Zn^{92}). La différence que l'on obtient dans la description microscopique est soulignée par un effet en sens inverse pour le potentiel central. La description microscopique apporte donc une explication qualitative aux variations de la déformation du couplage $\vec{L}.\vec{S}$ que la description macroscopique ne pouvait que constater.

REFERENCES

1. H. Sherif et J.S. Blair, Phys. Let. 26B(1968)489.
2. H. Sherif et R. de Swiniarski, Phys. Lett. 28B(1968)96
3. H. Sherif, Nucl. Phys. A131 (1969) 532
4. J. Raynal, Nucl. Phys. A97 (1967) 572
5. A.A. Rush et N.K.Ganguly, Nucl. Phys. A117 (1968)101
6. J. Raynal, Equations couplées et DWBA, Aussois, 1968
7. J. Raynal, Communication à la Conférence de Dubna (1968)
8. J. Raynal, Communication à la Conférence de Montréal(1969)
9. T. Hamada et I.D. Johnston, Nucl. Phys. 34(1962) 382.

LEGENDES DES FIGURES

Figure 1. Sections efficaces de diffusion élastique et inélastique sur le premier 2^+ de Ni^{60} à 16,5 Mev, dans le modèle vibrationnel avec une déformation de 0,400. Les paramètres du modèle optique utilisés sont: 49,15Mev, 1,25 fermi et 0,65 fermi pour le potentiel central réel; 11,30 Mev, 1,25 fermi et 0,47 fermi pour le potentiel imaginaire de surface; 5,4 Mev, 1,12 fermi et 0,47 fermi pour le potentiel $\vec{L}.\vec{S}$. Tous les potentiels sont déformés, le potentiel $\vec{L}.\vec{S}$ avec la forme (4).

Figure 2. Polarisation de la diffusion élastique et asymétrie de la diffusion inélastique correspondant à la figure 1.

Figure 3. Diffusion de protons de 18,6 Mev sur le Ni^{58} dans le modèle vibrationnel. L'état 2^+ est décrit par un phonon et l'état 4^+ par deux phonons. La courbe continue présente les résultats des équations couplées, la courbe en tirets la première approximation de l'ECIS. La courbe en pointillés a été obtenue en résolvant en équations couplées les niveaux 0^+ et 2^+ et en calculant le 4^+ au premier ordre.

Figure 4. Asymétrie dans la diffusion inélastique sur le premier 2^+ de Mg^{24} à 49,5 Mev. Les paramètres sont ceux utilisés en équation couplées par Rush et Ganguly[5].

Figure 5. Section efficace de diffusion élastique et inélastique sur le premier 2^+ de Si^{28} à 20,3 Mev (expérience de Saclay). Les courbes en continu et en tirets correspondent respectivement à une déformation négative et une déformation positive dans le modèle rotationnel.

Figure 6. Asymétries correspondant au même calcul que pour la figure 5. La courbe en traits mixtes pour l'asymétrie dans la diffusion inélastique correspond au modèle vibrationnel.

Figure 7. Section efficace de diffusion élastique et inélastique sur le premier 2^+ de Mg^{24} à 20,3 MeV (expériences de Saclay), dans le modèle rotationnel. Le calcul a été fait avec un produit βr constant et correspond à $\beta = \pm 0{,}49$ pour le potentiel central.

Figure 8. Asymétries correspondant au même calcul que pour la figure 7.

Figure 9. Section efficace élastique et inélastique sur le premier 2^+ de Mg^{24} à 20,3 MeV dans le modèle rotationnel asymétrique ($\beta = 0{,}49; \gamma = 30^\circ$). La courbe correspond à un mélange de bandes de 55°.

Figure 10. Polarisation dans la diffusion élastique correspondant au même calcul que pour la figure 9.

Figure 11. Asymétrie dans la diffusion inélastique correspondant au même calcul que pour la figure 9.

APPENDICE A

Nous désirons calculer

$$\frac{1}{i}\left[\vec{\nabla}\{V_\lambda(r)\ Y_\lambda^\nu(\theta,\varphi)\} \wedge \vec{\nabla}\right].\vec{\sigma}$$

Formulaire :

$$\vec{\nabla} = \frac{\vec{r}}{r}\frac{d}{dr} - i\frac{1}{r^2}\ \vec{r}\wedge\vec{L} \qquad (A\text{-}1)$$

$$i\ \vec{\sigma}(\vec{A}\wedge\vec{B}) = (\vec{\sigma}.\vec{A}).(\vec{\sigma}.\vec{B}) - (\vec{A}.\vec{B}) \qquad (A\text{-}2)$$

$$(\vec{A}\wedge\vec{B}).(\vec{C}\wedge\vec{D}) = (\vec{A}.\vec{C})(\vec{B}.\vec{D}) - (\vec{B}.\vec{C})(\vec{A}.\vec{D}) \qquad (A\text{-}3)$$

$$\vec{\sigma},\vec{\nabla} = \frac{(\vec{\sigma}.\vec{r})}{r}\left\{\frac{d}{dr} - \frac{1}{r}(\vec{\sigma}.\vec{L})\right\} \qquad (A\text{-}4)$$

En utilisant la formule (A-1), on obtient

$$- \left[\vec{\sigma}.\vec{\nabla}\{V_\lambda(r)\ Y_\lambda^\nu(\theta,\varphi)\} \right] . \left[\vec{\sigma}.\vec{\nabla} \right] + \left[\vec{\nabla}\{V_\lambda(r)\ Y_\lambda^\nu(\theta,\varphi)\}.\vec{\nabla} \right]$$

En remarquant que $(\vec{\sigma}.\vec{r})$ anticommute avec $(\vec{\sigma}.\vec{L})$:

$$- \frac{(\vec{\sigma}.\vec{r})^2}{r^2} \left[\left\{ \frac{d}{dr} + \frac{1}{r}(\vec{\sigma}.\vec{L}) \right\} \left\{ V_\lambda(r)\ Y_\lambda^\nu(\theta,\varphi) \right\} \right] \left[\frac{d}{dr} - \frac{1}{r}(\vec{\sigma}.\vec{L}) \right]$$

$$+ \frac{d}{dr}\{V_\lambda(r)\}\ Y_\lambda^\nu(\theta,\varphi)\ \frac{d}{dr} + \frac{V_\lambda(r)}{r^2} \left[\vec{r} \wedge \vec{L}\ \{Y_\lambda^\nu(\theta,\varphi)\} \right] . \frac{1}{r^2} [\vec{r} \wedge \vec{L}]$$

Les termes ayant deux dérivations s'éliminent. Il reste

$$\frac{1}{r}\frac{d}{dr}\{V_\lambda(r)\}\ Y_\lambda^\nu(\theta,\varphi)(\vec{\sigma}.\vec{L}) - \frac{V_\lambda(r)}{r}\ \{\vec{\sigma}.\vec{L}(Y_\lambda^\nu)\}\frac{d}{dr}$$

$$+ \frac{V_\lambda(r)}{r^2} \left[\vec{\sigma}.\vec{L}\ \{Y_\lambda^\nu(\theta,\varphi)\} \right] (\vec{\sigma}.\vec{L}) - \frac{V_\lambda(r)}{r^2} \left[\vec{L}\ \{Y_\lambda^\nu(\theta,\varphi)\}.\vec{L} \right]$$

En utilisant

$$\vec{L}\,\{Y_\lambda^\nu(\theta,\varphi)\}.\vec{L} = \frac{1}{2}\left[\vec{L}^2\, Y_\lambda^\nu(\theta,\varphi) - \vec{L}^2\{Y_\lambda^\nu(\theta,\varphi)\} - Y_\lambda^\nu(\theta,\varphi)\,\vec{L}^2\right]$$

$$\vec{L}^2 = (\vec{\sigma}.\vec{L})^2 + (\vec{\sigma}.\vec{L})$$

on peut exprimer tous les opérateurs avec $(\vec{\sigma}.\vec{L})$. En appelant γ_i et γ_f les valeurs propres de $(\vec{\sigma}.\vec{L})$ pour l'onde particlle initiale et finale, on obtient

$$\frac{1}{i}\left[\vec{\nabla}\{V_\lambda(r)\; Y_\lambda^\nu(\theta,\varphi)\}\wedge\vec{\nabla}\right].\vec{\sigma} =$$

$$= Y_\lambda^\nu(\theta,\varphi)\left[\frac{1}{r}\frac{d}{dr}\{V_\lambda(r)\}\gamma_i + \frac{V_\lambda}{2r^2}\{\lambda(\lambda+1) - (\gamma_f-\gamma_i)(\gamma_f-\gamma_i\pm 1)\}\right.$$
$$\left. + \frac{V_\lambda}{r}(\gamma_i-\gamma_f)\frac{d}{dr}\right]$$

(avec un signe - si la fonction radiale est multipliée par r suivant l'usage).

APPENDICE B

Pour l'interaction $\vec{L}.\vec{S}$ relative:

$$V(|\vec{r}_1-\vec{r}_2|)\ \{\vec{L}_1 + \vec{L}_2 + i\ \vec{r}_1\Lambda\vec{r}_2\ (\frac{1}{r_2}\frac{d}{dr_2} - \frac{1}{r_1}\frac{d}{dr_1})$$

$$+ \frac{1}{r_2^2}\vec{r}_1\Lambda\ (\vec{r}_2\ \Lambda\vec{L}_2) + \frac{1}{r_1^2}\ \vec{r}_2\Lambda\ (\vec{r}_1\Lambda\vec{L}_1)\}\ \ (\vec{\sigma}_1 + \vec{\sigma}_2)$$

les multipoles invariants par renversement du temps sont:

$$a^J(1,2) = -2(2J+1)\ V_J - \tfrac{1}{2}(\frac{r_1}{r_2} + \frac{r_2}{r_1})\ \Big\{J(J-1)\ V_{J-1} - (J+1)(J+2)$$

$$V_{J+1}\Big\} + \tfrac{1}{2}J(J+1)\Big\{\frac{r_1}{r_2}\left(\alpha^J_{j_2j_2'}\right)^2 + \frac{r_2}{r_1}\left(\alpha^J_{j_1j_1'}\right)^2\Big\}(V_{J-1}-V_{J+1})$$

$$c^J(1,2) = (2j+1)\ V_J - \tfrac{1}{2}(\frac{r_1}{r_2} + \frac{r_2}{r_1})\ \Big\{\ (J+1)\ V_{J-1} + J\ V_{J+1}\Big\}$$

$$d^J(1,2) = -\tfrac{1}{2}J(J+1)\ \Big\{\ 2 - \left(\alpha^J_{j_1j_1'}\right)^2 - \left(\alpha^J_{j_2j_2'}\right)^2\Big\}\ (V_{J-1} - V_{J+1})$$

$$e^J(1,2) = -\tfrac{1}{2}\sqrt{J(J+1)}\ \Big[\Big\{\ (J+2)\ V_{J-1} - (2J+1)\ \frac{r_2}{r_1}\ V_J + (J-1)\ V_{J+1}\Big\}$$

$$-\left(\alpha^J_{j_1j_1'}\right)^2\ \Big\{(J+1)V_{J-1} - (2J+1)\frac{r_2}{r_1}\ V_J + J\ V_{J+1}\Big\}\Big]$$

$$f^J(1,2) = -(J+1)\ V_{J-1} - J\ V_{J+1} + \tfrac{1}{2}(2J+1)\left(\frac{r_1}{r_2} + \frac{r_2}{r_1}\right) V_J$$

Le multipole b est la somme de deux parties:

1°) un terme dérivatif:

$$b_1^J(1,2) = \tfrac{1}{2}\sqrt{J(J+1)}\ \Big[(V_{J-1} - V_{J+1})\ \Delta_{12}\ \left(r_2 \frac{d}{dr_1} - r_1 \frac{d}{dr_2}\right)$$

$$+\left(r_2 \frac{d}{dr_1} - r_1 \frac{d}{dr_2}\right)\ \Delta_{12}\ (V_{J-1} - V_{J+1})\Big]$$

où $\Delta_{12} = r_1^2 r_2^2$ ou $=1$ suivant la définition des fonctions d'onde. Ce terme peut s'écrire avec seulement la dérivée de la fonction d'onde à droite, sous la forme suivante:

$$b_1^J(1,2) = \sqrt{J(J+1)}\ \Big[(V_{J-1} - V_{J+1})\ \Delta_{12}\left(r_2 \frac{d}{dr_1} - r_1 \frac{d}{dr_2}\right)$$

$$+ \tfrac{1}{2}\left(\frac{r_2}{r_1} - \frac{r_1}{r_2}\right)\left(c_1 V_{J-1} + c_2 V_{J+1}\right)\Big]$$

où $c_1 = J+1$ et $c_2 = J$ si $\Delta_{12} = r_1^2 r_2^2$ et $c_1 = J-1$ et $c_2 = J+2$ si $\Delta_{12} = 1$.

2°) un terme impair dans la permutation de j_1 et j_2 avec j_1' et j_2':

$$b_2^J(1,2) = \frac{(j_1+\frac{1}{2})^2 - (j_1'+\frac{1}{2})^2}{2\sqrt{J(J+1)}} \left[-(2J+1)\, V_J + \frac{r_2}{r_1} \{ (J+1)\, V_{J-1} \right.$$

$$\left. +J\, V_{J+1} \} \right] + \frac{(j_2+\frac{1}{2}) - (-)^{j_2+j_2'+J} (j_2'+\frac{1}{2})}{2\alpha^J_{j_2 j_2'}}$$

$$\left[(2J+1)V_J - \frac{r_1}{r_2} \{ J\, V_{J-1} + (J+1)\, V_{J+1} \} \right]$$

Si $j_2 = j_2'$ et J pair, la deuxième partie de $b_2^J(1,2)$ devient infinie car le coefficient $\alpha^J_{j_2 j_2'}$ est nul; cependant, en calculant le facteur de forme à un corps, $b^J(1,2)$ est multiplié par $\alpha^J_{j_2 j_2'}$ et la contribution reste finie.

Je remercie R. Schaeffer qui m'a aidé à vérifier ces formules, et à trouver une erreur dans celles publiées à la référence 4.

MACROSCOPIC TO MICROSCOPIC

Recent work on the Optical Model

P. E. Hodgson

Nuclear Physics Laboratory, Oxford.

Introduction

1. Elastic Scattering

    1.1 The Phenomenological Optical Potential

    1.2 Microscopic Calculation of the Optical Potential

    1.3 Nuclear Charge and Matter Distributions

    1.4 Resonances in Elastic Scattering

2. Inelastic Scattering and Charge Exchange Reactions

    2.1 Macroscopic Inelastic Scattering

    2.2 Microscopic Inelastic Scattering

    2.3 Charge Exchange Reactions

3. Nucleon Transfer Reactions

4. Isobaric Analogue State Reactions

    4.1 Elastic and Quasi-elastic Scattering

    4.2 Quasi-inelastic Scattering

    4.3 Microscopic Analysis of Isobaric Analogue Resonances

5. Total Cross-Sections

6. Discussion

References.

INTRODUCTION

There are two basic ways of approaching the solution of a nuclear reaction or nuclear structure problem. The first correlates the experimental data by phenomenological relations whose general form is established by simple considerations. The second starts with the phenomenological nucleon-nucleon interaction and calculates from this the characteristics of the phenomena under investigation. A few years ago these two approaches remained almost entirely distinct. The phenomenological approach suffered from many ambiguities in the forms of the interactions proposed and these could only be removed by rather ad hoc assumptions. It was thus difficult to distinguish the real and arbitrary elements in this phenomenological work. The calculations based on the nucleon-nucleon interaction tended to run into severe computational difficulties which generated much obscure fromalism from which it was rare for anything intelligible to experimentalists to emerge.

Quite recently these two approaches have begun to link up in a most instructive way. This has come about partly because more accurate data has reduced the ambiguities in the phenomenological analyses and shown up some of their deficiencies and partly because more tractable ways of carrying out the basic calculations from the nucleon-nucleon interactions have been developed. All this work has of course been made possible by

advances in high speed electronic computation. This unification of the two approaches is the subject of this lecture. It will be considered with reference to work on elastic scattering, inelastic scattering, nucleon transfer reactions and isobaric analogue state reactions. Much of it is concerned with a detailed understanding of differential and total cross-sections but this work is an essential preliminary to any detailed study of the polarizations and hence its relevance to the present conference. Indeed, it is only work along these lines that has established the general character of the reactions to the extent that is necessary before the polarisations can be properly understood. Polarisation data will certainly be of crucial importance in testing the limits of validity of the new calculations.

1. E L A S T I C S C A T T E R I N G

1.1 The phenomenological optical potential

During the last decade many analyses of differential cross-sections and polarisations have been made using the optical model. On the whole it has been found possible to account for these data with potentials whose parameters show little variation through the periodic table and a small linear energy dependence. Current work is directed partly to the problem of investigating the presence of small terms in the optical potential, and partly to the more accurate study of the terms already known.

One of the smaller terms in the optical potential is that depending on the spins of the incident nucleon and target nucleus. This spin-spin term may be written

$$V_{ss}(r) = -V_{ss} f(r) \, \underset{\sim}{I} \cdot \underset{\sim}{\sigma} / I \qquad (1.1.1)$$

where I is the nuclear spin.

Several experiments have recently been made to investigate this term. Batty and Tschalär (1969) have measured the depolarisation parameter for the scattering of 50 MeV. protons by B^{10}, Al^{27}, Si, Co^{59}, Ni, $In^{113,115}$, and Bi^{209}. This was done at the first minimum in the differential elastic scattering cross-section since calculations by Stamp (1967) showed that

the effects of the spin-spin term are likely to be most prominent at these angles. All their results are consistent with a depolarisation parameter D = 1, and thus provide no evidence for the presence of a spin-spin term.

The spin-spin term may also be investigated by measuring the cross-section for the elastic scattering of nucleons by oriented deformed nuclei. Fisher et al (1967) measured the scattering of 8 and 15 MeV. neutrons by Ho^{165} and the analysis of their data using the coupled-channels rotational model provided no evidence for the presence of a spin-spin term, and set the limits -340 KeV. < V_{ss} < 540 KeV. on its strength. Measurements of the transmission of 7.9 MeV polarised neutrons through oriented Co^{59} nuclei enabled Kobayashi et al (1968) to set the limits $V_{ss} = +1.7 \pm 3.8$ MeV.

More attention has been devoted to the isospin term in the optical potential, since this can in principle be found by an accurate analysis of differential elastic cross-sections for the scattering of nucleons by a range of nuclei. Some recent measurements of Perey and Perey (1968) have forced a re-examination of the whole question of the isospin dependence of the optical potential and this has caused a revision of our knowledge not only of the isospin term but of the central term as well.

The isospin term in the optical potential (Lane, 1962) is usually written in the form $U_1 \underline{t}.\underline{T}/4A$, where $\underline{t}$ and $\underline{T}$

are the isospin vectors of the incident particle and the target nucleus respectively, U_1 is the isospin potential and the atomic weight A is introduced for later convenience. The corresponding potentials for protons and neutrons are

$$\mu_p = \mu_0 + \mu_1 \frac{N-Z}{A}$$

$$\mu_n = \mu_0 - \mu_1 \frac{N-Z}{A} \qquad (1.1.2)$$

where U_0 is the isospin independent part of the potential.
If the potentials are energy-dependent the corresponding expressions are

$$\mu_p = \mu_0 - \beta E + (1-\beta)\mu_1 \frac{N-Z}{A} + \epsilon\, Z/A^{1/3}$$

$$\mu_n = \mu_0 - \beta E - (1-\beta)\mu_1 \frac{N-Z}{A} \qquad (1.1.3)$$

A detailed optical model analysis of the differential cross-section for the elastic scattering of 9-22 MeV protons by a range of nuclei Perey (1963) gave the expression

$$\mu_p = 53.3 - 0.55E + 27\frac{N-Z}{A} + 0.4\, Z/A^{1/3} \qquad (1.1.4)$$

for the depth of the real potential with Saxon-Woods form and fixed form factor parameters $r_o = 1.25$ and $a = 0.65$. The term $0.4Z/A^{1/3}$ arises from the energy dependence of the nuclear

potential in the presence of the Coulomb field. The corresponding expression for the neutron potential would be similar to (1.1.4) but with this last term omitted and the sign of the isospin term reversed. The neutron data are, however, not sufficiently accurate for this to be established.

Many subsequent investigations have confirmed the expression (1.1.4) and in particular it was found possible to confirm independently the presence of the last two terms even though they vary in a similar way with atomic number. This is possible by comparing the results obtained from analyses of scattering by isotopic sequencies with those found from a range of nuclei across the periodic table (Satchler, 1967; Hodgson, 1967).

The isospin term in the nucleon optical potential is also responsible for quasi-elastic (p,n) reactions proceeding to the analogue state of the target. The best analysis of data on these reactions leads to an average value of $U_1 = 29.5$ MeV for the isospin potential (Schwarcz, 1966). This is consistent with the value $U_1 = 34 \pm 5$ MeV obtained from proton scattering when allowance is made for the effect of coupling to the low-lying collective states (Perey, 1963).

It was always recognised that it is a matter of convenience to put all the isospin dependence into the real potential depth in (1.1.2) since there might well be an isospin dependence in the other parameters as well. Within certain limits, however, the optical model analysis determines only Ur_o^2 so the isospin

dependence can be included in either parameter witout difficulty. The form factor is also assumed to be the same for all the terms in (1.1.2) even though the analysis of the (p,n) quasi-elastic cross-sections indicates that it is more probably surface-peaked (Satchler Drisko and Bassel, 1964). This approximation is possible because the isospin term is small and the addition of a small surface-peaked term is equivalent to a change in the radius which in turn is equivalent to a change in the potential depth.

Recent work by Perey and Perey (1968) on the differential cross-sections and polarisations of 11 MeV protons elastically scattered by a range of nuclei with $50 \leqslant A \leqslant 70$ has shown that the dependance of the real potential depth on the nucleus symmetry parameter $\alpha = (N-Z)/A$ is more complicated than that indicated by (1.1.4). They find a different dependence for nuclei of different isospin, as shown in fig.1.1.1 and point out that this may be interpreted as a dependence on the atomic weight A. Greenless, Pyle and Tang (1968) have shown that such a dependence may be obtained simply by assuming that the volume of the optical potential is proportional to A. (see eqn. 1.2.7). This gives the expression

$$\mathcal{U} = \frac{500}{8.87\left(1 + 2.52A^{-2/3}\right)} \qquad (1.1.5)$$

for a real Saxon-Woods potential with $r_u = 1.285$, $a_n = 0.65$ and the constant is adjusted to fit the data. If these potentials are plotted as a function of the symmetry parameter,

fig. 1.1.2 shows that this formula gives, for the nuclei studied by Perey, a strong dependence on the symmetry parameter even though the potential has no explicit symmetry dependence. Such a potential would be unable to cause (p,n) quasi-elastic reactions. The behaviour previously attributed to the isospin potential is thus shown to have a purely geometric origin.

It is interesting to see if the isospin dependence known to be present from (p,n) reactions can be combined with (1.1.5) to give a phenomenological expression that accurately represents the experimental data. The expression obtained by adding the last two terms of (1.1.4) to (1.1.5) and adjusting the coefficient of the first term to optimise the fit to the data, viz.

$$V = \frac{106.75A}{R^3(1+\pi^2a^2/R^2)} + 24\alpha + \frac{0.517T(1-\alpha)}{\alpha R} \qquad (1.1.6)$$

is compared with the data of Perey et al in fig. 1.1.3, (dashed line) and it is apparent that the fit is qualitative only. If the expression (1.1.6) is solved for R it is found that the values obtained depend only on A, and as shown in fig. (1.1.3) this dependence may be represented by the expression

$$R' = 1.204A^{1/3} + 0.304 \qquad (1.1.7)$$

where the prime is introduced as a reminder that R' is no longer a nuclear radius. The dependence of V on T and α given by these

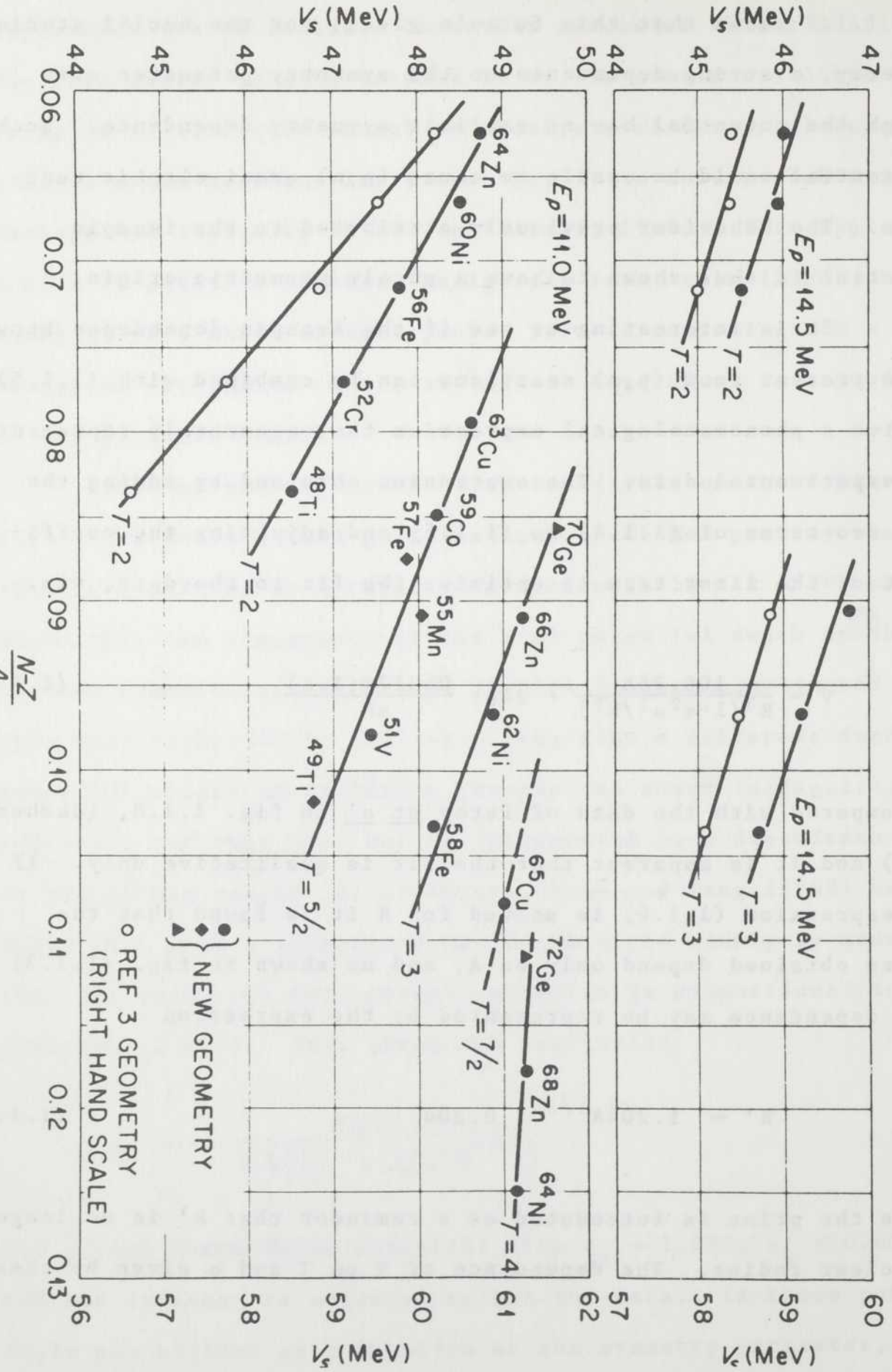

Fig. 1.1.1 Real potential depths as a function of the symmetry parameter (N-Z)/A for 11 MeV protons scattered by a range of nuclei. (Perey and Perey, 1968).

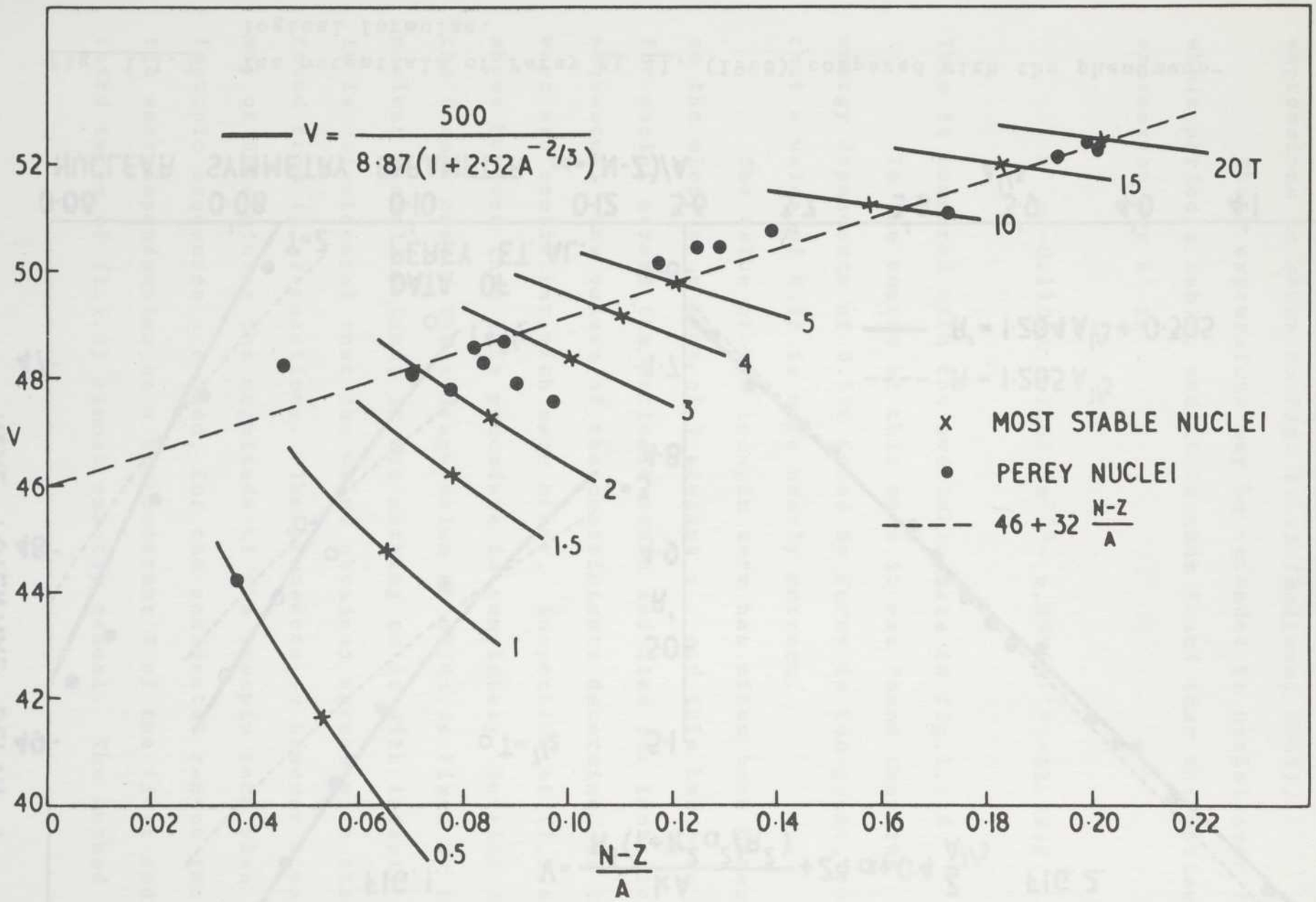

Fig.1.1.2 Variation of real potential depth with symmetry parameter obtained by assuming that volume of the optical potential is proportional to A. This is compared with the points corresponding to the nuclei studied by Perey and Perey.

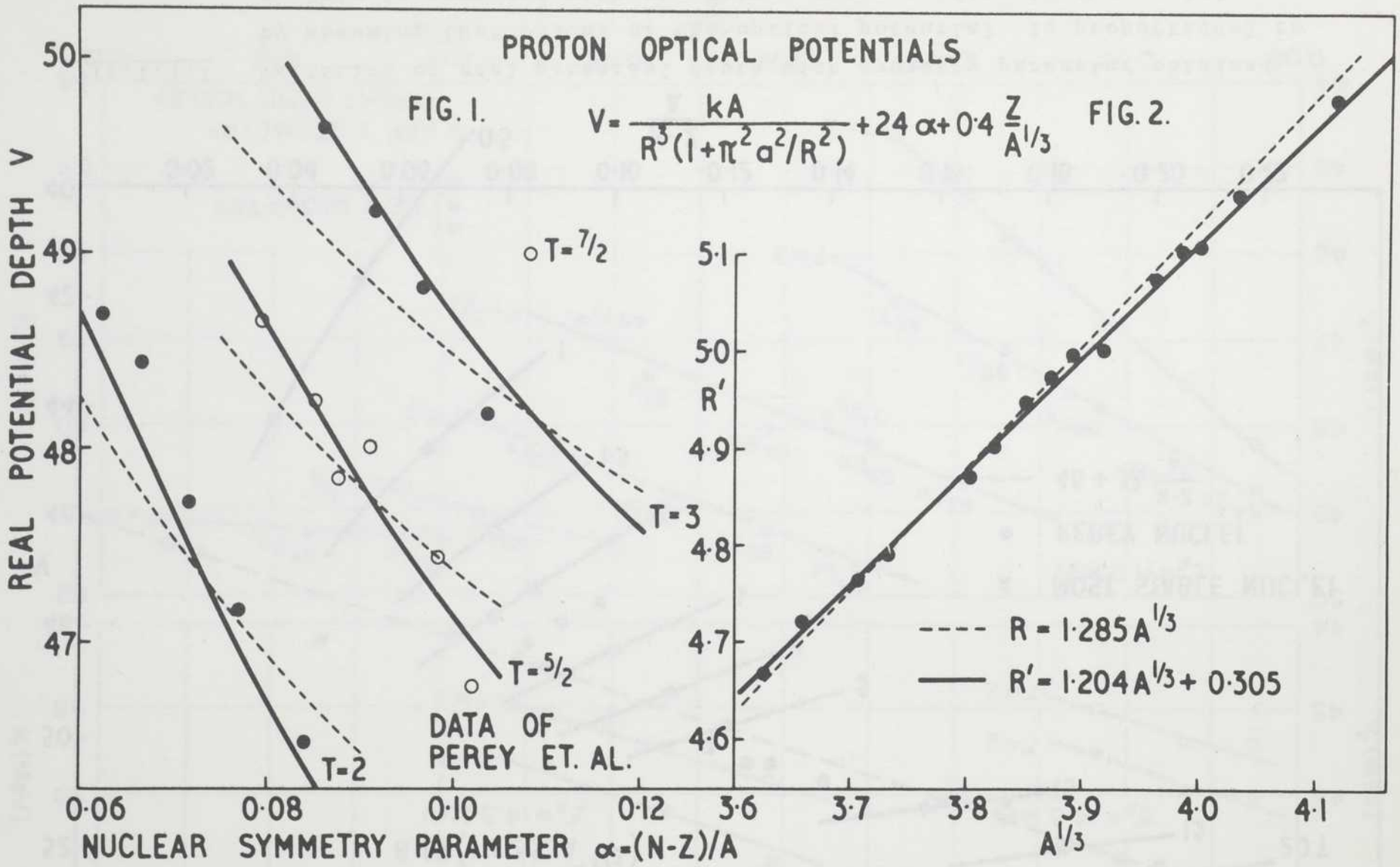

Fig. 1.1.3 The potentials of Perey et al, (1968) compared with the phenomenological formulae.

expressions is shown in fig. 1.1.3 (Hodgson, 1969).

These expressions may be extended to nuclei over the whole periodic table, and it is then found that the optimum expression for R' is

$$R' = -0.1104A + 1.6118A^{2/3} - 6.2991A^{1/3} + 11.5932 \qquad (1.1.8)$$

This is compared with the available data in fig.1.1.4.

In the course of this work it was found that the energy dependence of 0.55E found by Perey is too great, and that a value of 0.2E is more nearly correct.

The value of the isospin term has often been determined as the slope of a plot of V against α , and this has been done for nuclei across the periodic table and also for isotopic sequences. The values of the coefficients determined in these ways are consistent with each other. Inspection of (1.1.6) shows however that this procedure is completely invalid in the former case. The average value of $dV/d\alpha$ is fixed by the nuclear stability line; it has nothing to do with isospin and it is coincidental that the value obtained agrees with that found from (p,n) reactions. The procedure is however a valid way of determining the magnitude of the isospin term when isotopic sequences are used, for the accidental reason that the weak dependancies on α for constant T of the first and third terms of (1.1.6) almost exactly cancel. The method is

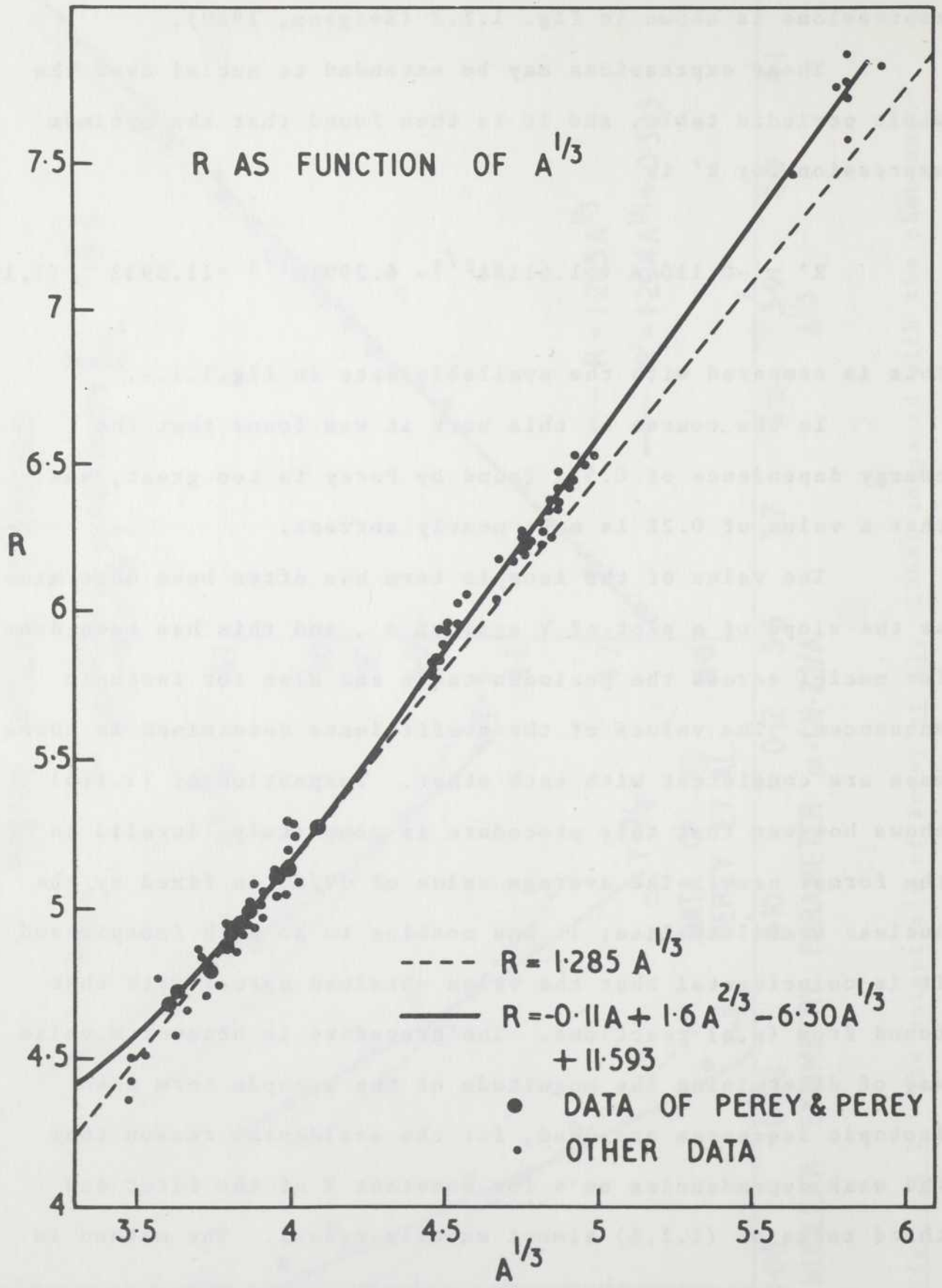
R AS FUNCTION OF A^1/3
7·5
7
6·5
R
6
5·5
5
4·5
4
3·5
4
4·5
5
5·5
6
A^1/3
---- R = 1·285 A^1/3
—— R = -0·11A + 1·6A^2/3 - 6·30A^1/3 + 11·593
● DATA OF PEREY & PEREY
• OTHER DATA

Fig. 1.1.4

however subject to uncertainties due to non-systematic structure differences between members of the isotopic sequence .

It is thus somewhat more difficult to determine the isospin term in the optical potential from analyses of proton elastic scattering than has hitherto been believed. This suggests the desirability of further accurate determinations from (p,n) reactions and from the comparison of proton and neutron elastic scattering data.

Existing neutron data are not sufficiently accurate to show isospin effects, but they are almost certainly present. The difficulty of determining the isospin potential from the proton elastic scattering data alone shows the importance of accurate neutron elastic scattering measurements.

The isospin term in the optical potential depends quite critically on the relative extent of the proton and neutron density distributions, so it is quite possible that it varies from nucleus to nucleus in a way that cannot easily be represented by a term in the nucleon-nucleus optical potential. This is suggested by analyses of (p,n) cross-sections (Satchler et al, 1964; Schwarez, 1966; Thrulow, 1968; Batty et al, 1968) showing that some data are better fitted with a surface and some with a volume isospin potential, although a surface form is usually preferred. Microscopic calculations of the isospin

term confirm this conclusion (Batty et al, 1968, 1969). Elastic scattering is not so sensitive as (p,n) reactions to the detailed form of the isospin potential, so it is possible for the isospin potentials to vary from nucleus to nucleus and yet have equivalent volume potentials that still shows the systematic behaviour indicated by the analyses summarised in this section.

1.2 Microscopic Calculation of the Optical Potential

It is usual to establish the overall form of the nucleon-nucleus optical potential by rather general arguments, making use of the saturation property of nuclear forces and their exponential fall-off at large distances. This indicates that the real part of the optical potential is uniform in the nuclear interior, falls rapidly in the region of the nuclear surface and thereafter goes exponentially to zero. This is conveniently represented by a function of the Saxon-Woods form. Approximate values of the parameters may be found by semi-classical arguments and these may be improved by detailed comparison with the experimental data. This procedure is necessary because the purely phenomenological approach cannot fix the form of the potential without ambiguity, while the potentials derived from fundamental considerations are insufficiently accurate.

This approach is now proving inadequate in several respects. Thus it is not clear to what extent the potential is non-local or what is its symmetry dependence and the radial form of the imaginary part of the potential as a function of energy still remains largely unknown. It is thus desirable to improve the methods of calculating the optical potential and if possible to derive it from the nucleon-nucleon interaction.

Many attempts have been made to calculate the nucleon-nucleus potential from many-body theory. The earlier calculations (Watson 1958; Brueckner *et al*, 1961; Frahn and Lemmer, 1967; Feshbach, 1958; Lemmer *et al*, 1959) did not take sufficient account of the identity of the incident particle and the target nucleons. This may be done using Green's functions and some calculations have been made in this way (Giai *et al*, 1966; Vinh Mau, 1969). They have not yet been carried to the stage when detailed comparisons with experiment can be made.

These calculations are attempts to determine the most general form of the optical potential valid at all energies. It is simpler to try to calculate the potential at one energy and this may be done using the expression for the optical potential derived by Kerman, McManus and Thaler, (1959)

$$V(r) = A \int t(|r - r'|)\, \rho(r')\, dr' \qquad (1.2.1)$$

where $t(|\underline{r}-\underline{r}'|)$ is the spin-isospin average of the real part of the nucleon-nucleon effective interaction and $\rho(r')$ the nuclear

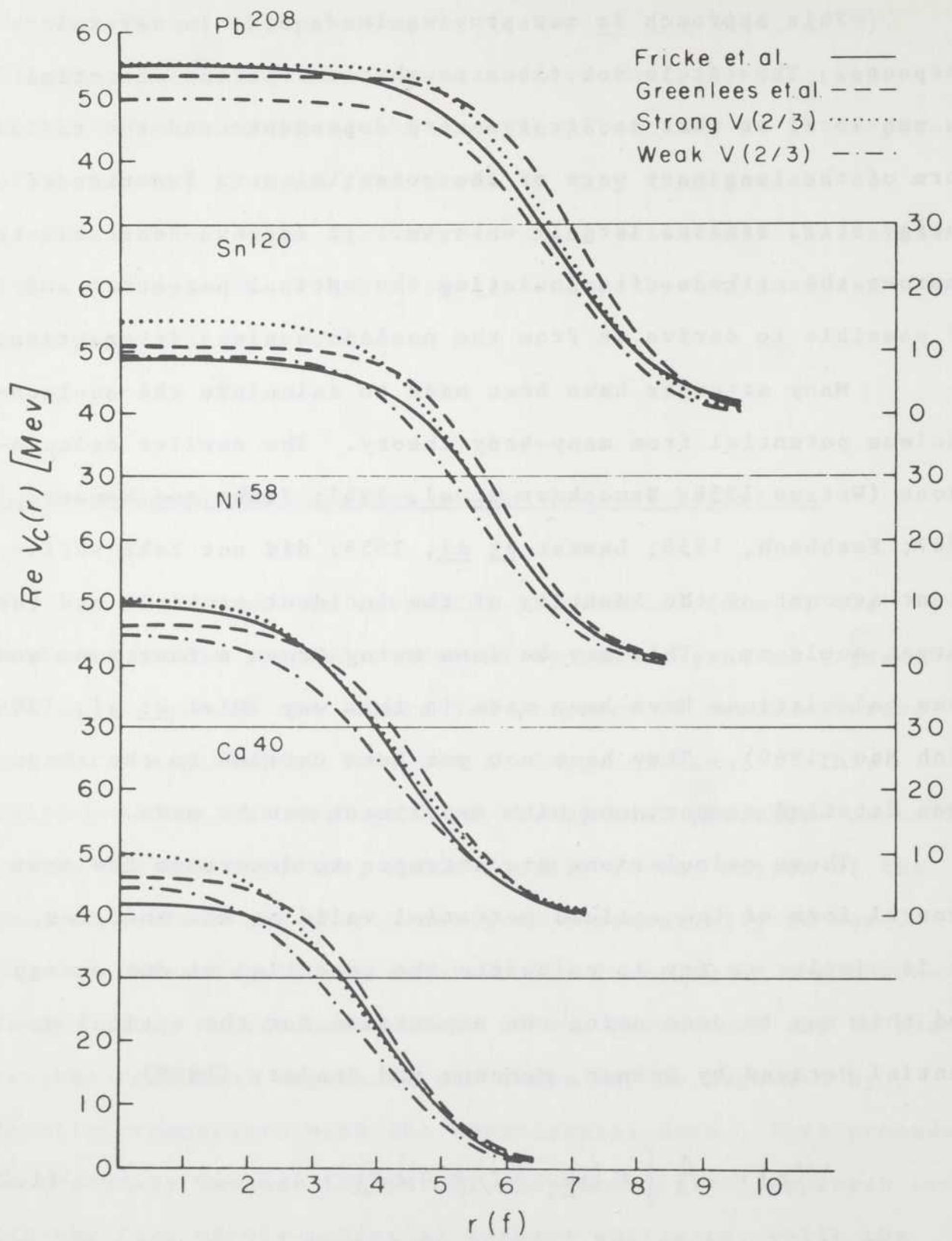

Fig. 1.2.1

Real part of the central potential (Slanina and McManus, 1968).

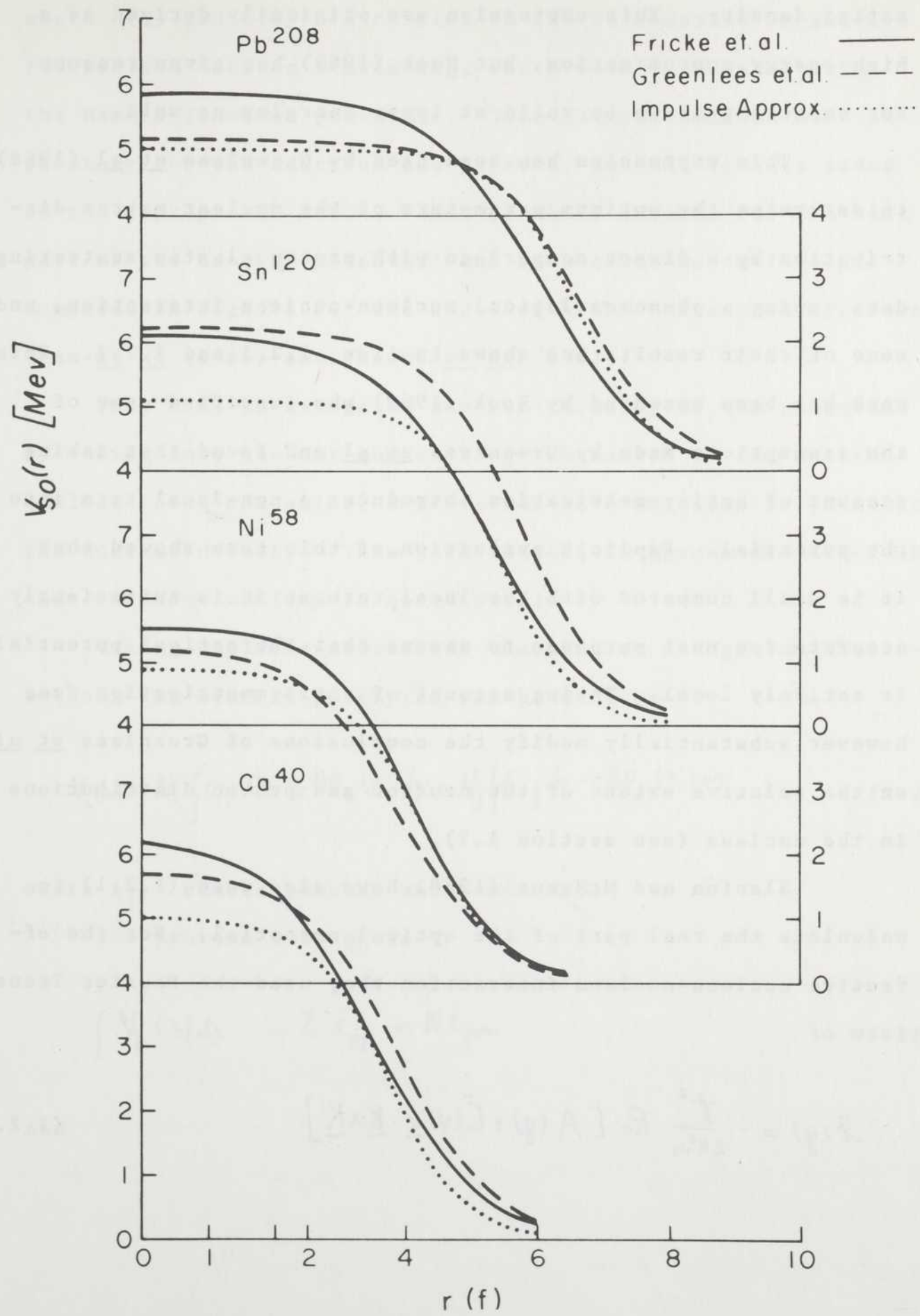

Fig. 1.2.2

Real part of the spin-orbit potential (Slanina and McManus, 1968)

matter density. This expression was originally derived as a high-energy approximation, but Rook (1969) has given reasons for expecting it to be valid at lower energies as well.

This expression has been used by Greenlees et al (1968) to determine the optimum parameters of the nuclear matter distribution by a direct comparison with proton elastic scattering data, using a phenomenological nucleon-nucleon interaction, and some of their results are shown in figs, 1.2.1 and 1.2.2. This work has been extended by Rook (1969) who justified some of the assumptions made by Greenlees et al and found that taking account of antisymmetrisation introduces a non-local term into the potential. Explicit evaluation of this term showed that it is small compared with the local term so it is sufficiently accurate for most purposes to assume that the optical potential is entirely local. Taking account of antisymmetrisation does however substantially modify the conclusions of Greenlees et al on the relative extent of the neutron and proton distributions in the nucleus (see section 1.3).

Slanina and McManus (1968) have also used (1.2.1) to calculate the real part of the optical potential. For the effective nucleon-nucleon interaction they used the Fourier Transform of

$$\bar{t}(q) = -\frac{\hbar^2}{2\pi^2 m} Re\left[A(q) + \tilde{C}(q)\, \underset{\sim}{\sigma} \cdot \underset{\sim}{K} \times \underset{\sim}{K'}\right] \qquad (1.2.2)$$

where A(q) and $\tilde{C}(q)$ are related to the Wolfenstein parameters for nucleon-nucleon scattering, which were calculated from the Hameda-Johnston potential. This calculation was made separately for the neutrons and protons, and the results added in the appropriate ratio. Some of their results for the real part of the central potential and spin-orbit potentials are compared in figs. 1.2.1 and 1.2.2 with the potentials of Greenlees et al (1966) and Fricke et al (1967).

They also investigated the non-locality of the potential by taking into account the exchange character of the nucleon-nucleon force and using Hartree-Fock wavefunctions to calculate the nuclear density. This work showed, in agreement with Rook, that the non-locality is quite small.

Taking explicit account of the neutron and proton distributions the central potential can be written

$$V_i(\underline{r}) = N_i \int t_{ii}(|\underline{r}-\underline{r}'|)\rho_i(\underline{r}')d\underline{r}' + N_j \int t_{ij}(|\underline{r}-\underline{r}'|)\rho_j(\underline{r}')d\underline{r}' \qquad (1.2.3)$$

where $i_j j$ denote protons and neutrons.

For protons this gives

$$\int V_p(\underline{r})d\underline{r} = Z\bar{t}_{pp} + N\bar{t}_{pn} \qquad (1.2.4)$$

and

$$\langle r^2_{op,p}\rangle = \frac{Z\bar{t}_{pp}\left(\langle x^2_{pp}\rangle + \langle r^2_p\rangle\right) + N\bar{t}_{pn}\left(\langle x^2_{pn}\rangle + \langle r^2_n\rangle\right)}{Z\bar{t}_{pp} + N\bar{t}_{pn}} \qquad (1.2.5)$$

where $\langle x^2\rangle$ and $\langle r^2\rangle$ denote the mean square radii of the corresponding t ($\underline{r}$-$\underline{r}'$) and nucleon density destributions respectively.

If we put $\langle r^2_p\rangle = \langle r^2_n\rangle = \langle r^2_m\rangle$ and $\langle x^2_{pp}\rangle = \langle x^2_{pn}\rangle = \langle x^2\rangle$ then

$$\langle r^2_{pp}\rangle = \langle x^2\rangle + \langle r^2_m\rangle \qquad (1.2.6)$$

This expression is used in the next section.

Also,

$$\int V_p(\underline{r})d\underline{r} = A\bar{t} \qquad (1.2.7)$$

which leads to the expression (1.1.5) used in the last section. It is also interesting to see if there is any evidence for a dependence of the integrated potential on the nuclear symmetry term $\alpha = (N-Z)/A$. Since (1.2.4) may be rewritten

$$\int V_p(\underline{r})d\underline{r} = \frac{A}{2}(\bar{t}_{pn} + t_{pp}) + \tfrac{1}{2}(N-Z)(\bar{t}_{pn} - t_{pp}), \qquad (1.2.8)$$

such a dependence is to be expected if $\bar{t}_{pn} \neq \bar{t}_{pp}$.

The isospin part of the optical potential has been calculated from (1.2.1) by Batty et al, (1969), and used to evaluate the density distribution of the excess neutrons and the cross-sections for (p,n) reactions to the isobaric analogue state. A more detailed calculation has been made by Zimanyi and Gyarmati (1968) who expand the total wavefunction into a series of terms representing the bound and free particles, and hence obtain a set of coupled equations, similar to the Lane equations, for the wavefunctions of the neutrons and protons. Solution of these equations with simple forms for the interaction potentials gives the isospin part of the optical potential and shows, in agreement with Greenlees et al, that it changes from a surface-peaked form for medium weight nuclei like Ca^{48} and Fe^{54} to a volume form for heavy nuclei like Sn and Pb.

Microscopic calculations have also been made of the elastic scattering of alpha-particles by nuclei, using an optical potential defined by

$$V_\alpha(r) = \int \ell m \, (\underline{t}) \, V_{eff} \, (|\underline{r} - \underline{R}|) \, d\underline{t}$$

where $V_{eff}(|\underline{r}-\underline{R}|)$ is an effective alpha-nucleon interaction whose parameters are adjusted to fit the data. Calculations by Jackson and Kembhavi (1969) and by Morgan and Jackson (1969) showed that a satisfactory fit may be obtained to the differential cross-section for the elastic scattering of 42 MeV alpha-particles by Ca^{42} using a gaussian form for the effective iteraction. This interaction may then be used to calculate the inelastic scattering

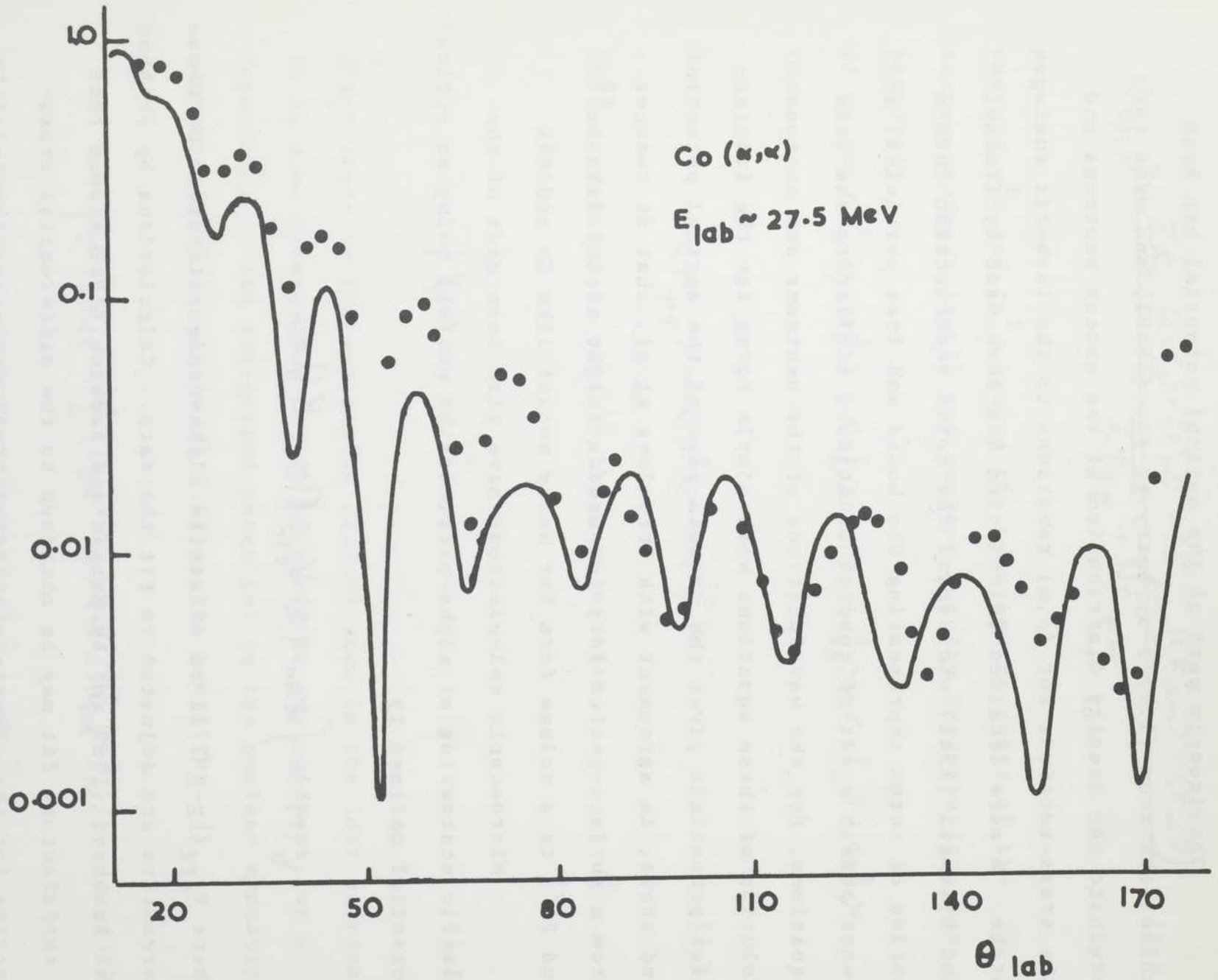

Fig.1.2.3 Differential cross-section for the elastic scattering of 27.5 MeV alpha-particles by Cobalt compared with microscopic model calculations. (Budzanowski et al, 1969).

as well (see section 2.2).

The reformulated optical model of Greenlees et al (1968) has been applied by Budzanowski et al (1969) to analyse data on the elastic scattering of 27.5 MeV alpha-particles by Ca^{40} and Co^{59}. They derived the alpha-nucleon potential by folding a Yukawa nucleon-nucleon potential with the matter distribution of the alpha-particle and then used this potential in the Greenlees formalism to obtain the real part of the alpha-nucleus potential. A phenomenological potential of the Saxon-Woods form was used for the imaginary part and the preliminary fits shown in Fig. 1.2.3 are quite comparable in quality to those obtained with the optical model.

It is much more difficult to calculate the imaginary part of the optical potential since this takes account of all the non-elastic processes. Many attempts have been made but only qualitative success has been achieved.

1.3 Nuclear Charge and Matter Distributions

The work described in the previous section together with other investigations enables the mean square radius and to some extent the shape of the distributions of protons and neutrons in the nucleus to be determined.

If the optical potential V(r) is for simplicity expressed as the folding of the matter distribution $\rho(\underline{r})$ and the nucleon-nucleon interaction $v(|\underline{r}-\underline{r}'|)$ is used instead of $t(|\underline{r} - \underline{r}'|)$

$$V(r) = \int \rho(\underline{r}')\, v(|\underline{r} - \underline{r}'|)\, d\underline{r}' \qquad (1.3.1)$$

it follows that the corresponding mean square radii are related by

$$\langle r_{op}^2 \rangle = \langle r_m^2 \rangle + \langle x^2 \rangle \qquad (1.3.2)$$

Greenlees et al (1968) took a Fermi distribution for the nuclear matter

$$\rho(r) = \frac{1}{1 + \exp\left(\frac{r - r_m}{a_m}\right)} \qquad (1.3.3)$$

and varied r_m and a_m to optimise the fit to the data using (1.3.1) and a Yukawa form with the appropriate exchange mixture for $v(\underline{r} - \underline{r}')$. They found that $\langle r_m^2 \rangle$ is insensitive to the particular values of r_m and a_m over quite a wide range provided the combination is such that the experimental data is correctly fitted. The mean square radius is thus more accurately determined by the analysis than the individual values of r_m and a_m.

It is known from electron scattering that the charge distribution in nuclei may be quite accurately represented by the expression

$$\rho_{ch}(r) = \frac{1}{1 + \exp\left(\frac{r - R_e}{a_c}\right)} \qquad (1.3.4)$$

where the parameters $R_c = (1.106 + 1.05 \times 10^{-4} A) A^{1/3}$ and $a_c = 0.502f$ (Hafstadter, 1963; Collard et al, 1967; Van Niftrik, 1969), Bethe and Elton, 1968). The mean square radius proton distribution is then given by

$$\langle r_p^2 \rangle = \langle r_{ch}^2 \rangle - 0.6 \qquad (1.3.5)$$

making allowance for the finite side of the proton.

From the nuclear matter and proton distributions determined in this way the neutron distribution may be found by subtraction, taking account of the numbers of protons and neutrons in the nucleus concerned. The results for six nuclei form Ni^{58} to Pb^{208} consistently indicated that the neutron root mean square radius exceeds the proton root mean square radius differ by about 0.7 f:

$$\delta \equiv \langle r_n^2 \rangle^{1/2} - \langle r_p^2 \rangle = 0.1 \qquad (1.3.6)$$

and comparison with (1.3.2) led to the value (Greenlees et al, 1968)

$$\langle r_m^2 \rangle = 2.25 \pm 0.6 \qquad (1.3.7)$$

which is consistant with other determinations.

A similar analysis may be applied to deuteron optical potentials. In this case the mean square radius is given by

$$\langle r^2_{op} \rangle_\alpha = \langle r^2_m \rangle + \langle r^2_n \rangle + \langle r^2_\alpha \rangle \qquad (1.3.8)$$

where the last term is the mean square radius of the deuteron. Subtraction of the valuesof the mean square radii of the optical potentials describing deuteron and proton scattering gives (Rook, 1968)

$$\langle r^2_\alpha \rangle = 1.31 \qquad (1.3.9)$$

which is much smaller than the experimental value of 4.45. The difference may probably be accounted for by the neglect of the spatial polarisation of the deuteron.

Luetzelschwab and Hafele (1969) have applied a similar analysis to their data on the elastic scattering of 35 MeV helions by a range of nuclei. They find that

$$\langle r^2_p \rangle - \langle r^2_e \rangle \approx 1 + 0.21 A^{1/3}$$

which they interpret as due to the neutron distribution extending further beyond the proton distribution as A increases.

An analysis by Holmquist and Wiedling (1968) of the elastic scattering of neutrons by a range of nuclei using a method similar to that of Greenlees et al gave a value $\delta \sim 0.5$f.

Further evidence on the distribution of protons and neutrons in the nucleus can be obtained from studies of pion production, from pion and kaon capture, from the energies of single-particle and analogue states, from Hartree-Fock calculations and from the liquid drop model.

The Margolis model for pion production in the interaction of fast protons with nuclei has been extended by Hirt (1969) to include a possible difference between the neutron and proton rms radii, and applying this model to the experimental data for Pb gives a value $\delta \approx 0.6$f.

The work on pion capture indicates that the proton and neutron distributions have similar radii, though it is desirable that the experimental measurements be repeated to a higher accuracy. (Auerbach et al, 1968).

The analysis of kaon capture by nuclei (Burhop 1967, Davis et al, 1967) indicates that neutrons are more likely to be found than protons in the outer fringe of the matter distribution. Calculations indicate that the capture is most likely to occur in the region where the density is less that about 10% of the central density, so this result may still be consistent with the mean square radii of the neutron and proton distributions being nearly the same. More recent work (Bugg et al, 1969) has however thrown some doubt on this evidence for a neutron halo in heavy nuclei.

Rost (1968) has shown that the energies of most of the single-particle and single-hole states in the nuclei obtained by adding or removing a neutron from Pb^{208} are quite accurately given by neutron and proton potentials having the Saxon-Woods form and somewhat different parameters. These potentials can be used to generate the neutron and proton distributions in Pb^{208} and it is found that the neutron distribution has a root mean square radius exceeding that of the proton distribution by about 0.7f. The proton charge distribution gives an excellent fit to the differential cross-sections for the elastic scattering of 175-250 MeV electrons by Pb^{208} (Elton, 1968), but the potentials give spectroscopic factors in disagreement with those obtained from direct reactions (Parkinson et al, 1969; Dost et al, 1967). This work is, however, subject to some uncertainty due to the effect of the rearrangement energy and other corrections to the single particle energies, which were not taken into account to the calculations.

Thus about a year ago several independent investigations by different methods indicated that the neutron RMS radius exceeded the proton RMS radius by about 0.5-0.7f a considerable difference that was at variance with previous work (Elton, 1961, 1967; Schrack et al, 1962). However, over the last year several additional analyses have shown that higher order terms in several cases reduce this difference to more acceptable values, and other work has confirmed the lower figure.

Thus the work of Rook (1968) showed that a substential portion of the difference between the neutron and proton root mean square radii disappears when the requirements of antisymmetrisation are taken into account. Thus we have

$$\langle r_m^2 \rangle \simeq \langle r_p^2 \rangle \simeq \langle r_n^2 \rangle \qquad (1.3.10)$$

The mean radius of the nucleon-nucleon interaction may then be written using (1.3.2) and (1.3.5)

$$\langle r_v^2 \rangle = \langle r_{op}^2 \rangle - \langle r_{ch}^2 \rangle + 0.6 \qquad (1.3.11)$$

where all the quantities on the right are well determined. The results of a number of accurate optical model analyses were studied by Rook, who found that $\langle r_v^2 \rangle$ determined in this way shows no systematic variation across the periodic table, which indicates the consistency of the analysis, although the near equality of $\langle r_{op}^2 \rangle$ and $\langle r_{ch}^2 \rangle$ gives rise to large fluctuations. The mean value is

$$\langle r_v^2 \rangle = 5.42 \qquad (1.3.12)$$

which is substantially larger than the value found by Greenlees et al.

Greenlees (1969) has recently repeated his calculations allowing different density distributions for the neutrons and protons and taking higher order terms into account. The

new calculations no longer indicate a unique value for $\langle r_v^2 \rangle$ so he takes $\langle r_v^2 \rangle = 4.27$ from optimum nucleon-nucleon potentials He finds that the value of δ is about zero for Ni^{58}, Ni^{60} and Co^{59} and about 0.15f for Sn^{120} and Pb^{208}, with an uncertainty of 0.1f.

The density-dependent Kallio-Kolltveit potential has been used by Freidman (1969) to calculate both the matter distribution and the optical potential. He found that a correction must be made to the value of the RMS matter radius of Greenlees et al,

$$\langle r_m^2 \rangle = \langle r_m^2 \rangle_{GPT} - \frac{6}{5} R_m \propto a m \qquad (1.1.13)$$

where α' is defined in terms of the parameters of the Kallio-Kolltveit potential. This leads to the expression

$$\langle r_m^2 \rangle = \frac{1+\alpha' S}{1+\frac{5}{3}\alpha' S} \langle r_{GPT}^2 \rangle - \langle r_{NN}^2 \rangle \qquad (1.1.14)$$

where S is a known function of R_m and a_m. The effect of these corrections is to reduce the value of δ from 0.7f to about 0.1-0.2f for medium and heavy nuclei.

Vautherin and Veneroni (1969) have made a Hartree-Fock calculation for Pb^{208} using the Brink-Boeker interaction.

Their values for the proton radii agree well with the electron scattering values, and the difference between the neutron and proton RMS was found to be $\delta = 0.2\text{-}0.3$f for different versions of the interaction. Earlier Hartree-Fock calculations by Tarbutton and Davies (1968) gave a negligible value for δ. Blin-Stoyle (1969) has found that effects of nuclear radii on second-forbidden correction to super allowed β decay rates require $\delta \sim -0.2$f for lighter nuclei.

A detailed calculation of the neutron and proton density distributions has been made by Myers (1968) using the liquid drop model and some of his results are shown in fig. 1.3.1. According to this model $\delta \simeq 0.1\text{-}0.2$f depended on A. A calculation by Rook (1969) based on the semi-empirical mass formula is consistent with this result.

Meldner (1968) has calculated the neutron and proton densities from a realistic single particle Hamiltonian adjusted to fit a wide range of experimental data, and he finds that $\delta \sim 0.1$.

A calculation by Nolan et al (1968) has shown that the neutron and proton density distributions can also be investigated using the energies of isobaric analogue states. This is possible because the analogue of the grand state of a nucleus is formed by changing a neutron into a proton and the energy required to do this depends on the spatial extension of their

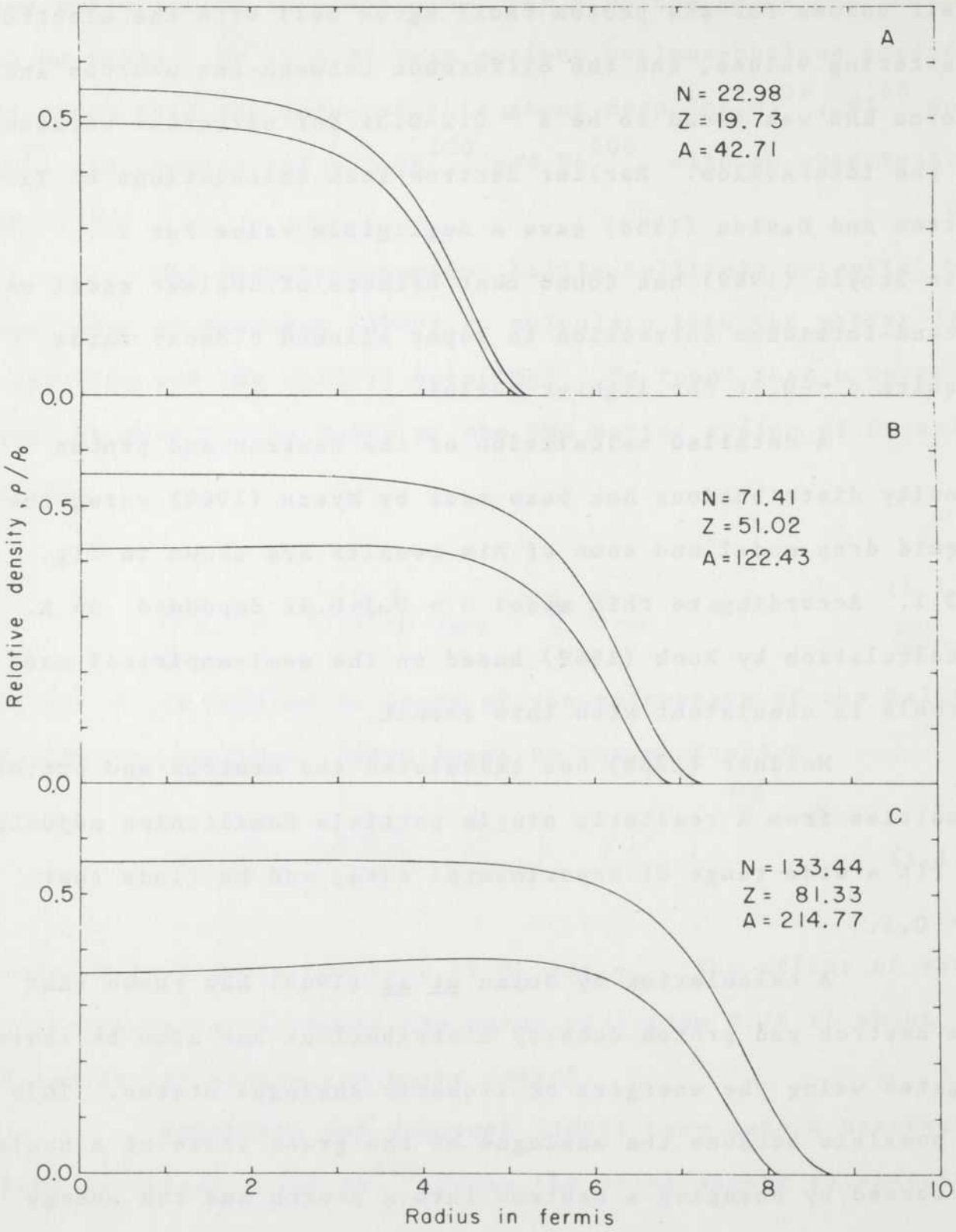

Fig.1.3.1 Neutron and proton densities (with Coulomb and Coulomb-exchange energies included) as a function of the radial distance for three cases representative of stable nuclei. The number of particles these distributions correspond to is shown (Myers, 1968).

respective wavefunctions. The first calculations indicated that the neutron root mean square radius exceeds the proton root mean square radius by about 0.07 ± 0.03 f. but later more accurate work using Saxon-Woods wavefunctions indicates that the half-density radius of the neutron distribution is less than that of the proton distribution. A value of 0.2f for this difference is obtained by Bethe and Siemens (1968) from a similar calculation using the Thomas-Fermi model. Recent calculations by Auerbach et al (1969) taking into account corrections to the Coulomb displacement energies give a value of less than 0.1f.

The results of all these determinations of the difference between the neutron and proton RMS radii are summarized in Table 1.3.1.

A detailed analysis of mesonic x-ray data led Barret et al (1965) to suggest that nuclei have a proton halo, namely that a small fraction of the charge (~10%) extends to large distances (~8f). An analysis by van Niftrik (1969) showed that while such haloes are not excluded by elastic scattering data, there is no evidence that they are present (van Niftrik et al 1969).

The relative extension of the neutrons and protons in the nuclear surface is the result of a delicate balance between opposing tendencies. The protons repel each other electrostatically, tending to push them out beyond the neutrons. Most

TABLE 1.3.1

Results of determinations of the difference between the RMS radii of nuclear neutron and proton distributions.

Reference	Method	$\langle r_n^2 \rangle^{\frac{1}{2}} - \langle r_p^2 \rangle^{\frac{1}{2}}$
Elton, 1961	Neutron elastic scattering	0.1 - 0.2
Schrack et al, 1962	Neutral pion Photoproduction	0 ± 0.2
Greenlees et al, 1968	Reformulated optical model	0.7
Holmqvist & Wiedling, 1968	Neutron elastic scattering	0.5
Auerbach et al, 1968	Pion capture	0
Rost, 1968	Single particle bound states	0.7
Rook, 1968	Reformulated optical model corrected for antisymmetrisation	0.2
Nolen et al, 1968	Isobaric analogue state energies	0.07 ± 0.03
Bethe and Siemens, 1968	Isobaric analogue state energies	0.2
Cavanagh, 1968	Single particle bound states in Sn	0.3
Vautherin & Veneroni,1968	Hartree Fock	0.2 - 0.3
Freidman, 1969	Nucleon-nucleon interaction	0.1 - 0.2
Myers, 1968	Liquid drop	0.2
Meldner, 1968	Single particle bound states	0.1
Auerbach et al, 1969	Isobaric analogue state energies	<0.1
Greenlees et al, 1969	Corrected reformulated optical model	0 - 0.15

nuclei, however, have more neutrons than protons and the excess neutrons are in the higher orbits so this tends to give an excess of neutrons in the surface region. The proton-neutron interaction is stronger than the neutron-neutron or proton-proton interactions and this strongly opposes any tendency for the protons and neutrons to separate (Wilets, 1958). The net result of this is that the proton and neutron distributions are very similar and their root mean square radii are unlikely to differ by more than 0.1-0.2f. This does not exclude the possibility that the distributions differ appreciably in the outer fringe region, where the nuclear density is less than a tenth of its maximum value. There is also some evidence that the density distribution is more diffuse than the proton density distribution in the region of the nuclear surface (Bethe, 1968; Donnely, 1968).

1.4 Resonances in Elastic Scattering

The differential cross-sections for the elastic scattering of nucleons by nuclei frequently show resonance behaviour when the energy corresponds to that of a state in the compound nucleus. Such resonances are particularly prominent at low energies on light nuclei, for then they are well separated from each other and most, if not all, of the reaction channels are energetically closed.

These resonances may be analysed in several ways, depending on the extent to which account is taken of the underlying nuclear structure. The simplest method is to parameterise the background by, for example, the hard-sphere phase shifts, and then superpose the resonances by adding Breit-Wigner amplitudes whose parameters are adjusted to fit the data. The next level of sophistication is to use the optical model to describe the background and then it is found that the resonances that have a single-particle character are given automatically, and so do not have to be represented by Breit-Wigner amplitudes. If the coupling of the elastic channel to one or more inelastic channels is also included, and the appropriate coupled equations of the extended optical model are solved, then more complicated resonances are automatically generated. Finally, the whole calculations can be made in a microscopic manner, starting from the nucleon-nucleon interaction. Proceeding in this way, more and more resonances can be shown to be consequences of the postulated interactions, leaving only those of very complicated structure to be described by the Breit-Wigner formulae.

The positions of the unbound single particle states in a potential may be found by calculating the scattering phase shifts as a function of energy and seeing which of them

display a resonance behaviour. A calculation of this type has been made by Schiffer (1963) for the $d_{\frac{5}{2}}$ resonance at 1.75 MeV in the elastic scattering of protons by carbon. The parameters of the potential are adjusted to give the observed resonance energy, and then its width is given automatically. The ratio of the experimental to the calculated width gives immediately the single-particle strength of the nuclear state. In the work of Schiffer, $\Gamma_{expt} = 61$ KeV and $\Gamma_{calc} = 56$ Kev showing that it is essentially a pure single-particle state. This method of determining the purity of single-particle states is preferable to that using barrier penetrability factors that are not accurately known.

The inelastic channels most strongly coupled to the elastic channel are frequently those corresponding to a collective nuclear excitation. When the energy of the incident particle is that of a single-particle state plus a collective excitation a resonance occurs. If the single-particle state is bound, a virtual excitation can take place, providing the energy of the collective excitation is greater than the incident energy. The effects on the scattering cross-sections due to this process can be calculated by the coupled-channels formalism.

An example of this process is provided by the elastic scattering of neutrons by C^{12}. An optical model calculation gives the single-particle $d_{\frac{3}{2}}$ level at 3.67 MeV but additional resonances are observed at 2.08 and 2.95 MeV. These levels

may be understood as the coupling of the 2^+ collective excitation of the C^{12} nucleus at 4.43 MeV with the single-particle $2s_{\frac{1}{2}}$ state at 3.09 MeV in C^{13}.

The calculation of the neutron scattering taking this coupling into account proceeds in the same way as that described by Buck (1963) for proton elastic and inelastic scattering except that the inelastic channel is closed and so the corresponding wavefunction has the appropriate exponentially decaying form outside the nucleus.

Several calculations have been made of the low-energy scattering of nucleons by carbon in this way (Okai and Tamura, 1962; Lovacs, 1966; Reynolds et al, 1968; Pisent and Sarius, 1967; Barnard, 1967). Recently, a full coupled-channels calculation assuming an oblate rotational target has been made by Pascolini et al, 1969). Their results for the elastic scattering of protons by carbon are given in fig. 1.4.1 and Table 1.4.1, and the corresponding neutron results without further adjustment of parameters in fig. 1.4.2 and Table 1.4.2. The overall agreement indicates the essential correctness of the model, though there are several discrepancies that require further investigation. The optimum value of the deformation parameter was 0.4, a value that is in accord with Coulomb excitation and mean life measurements (Stelson and McGowan, 1963; Stelson and Grodzins, 1965). This high value indicates a strong coupling situation, so that it

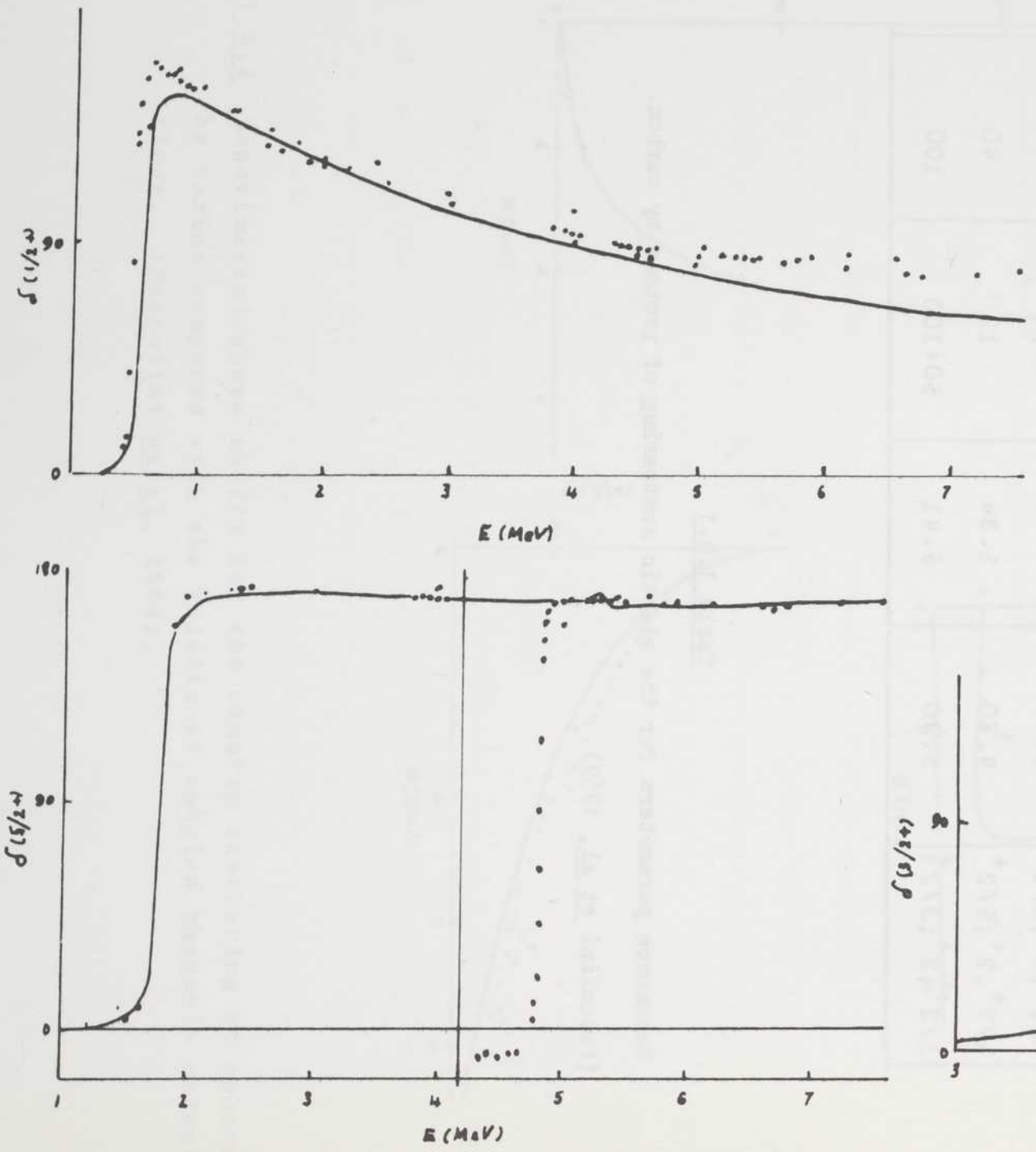

Fig. 1.4.1

Experimental phase shifts for the elastic scattering of protons by carbon compared with the results of coupled-channels calculations.
(Pascolini et al, 1969)

Resonance parameters in the p-^{12}C scattering process

Dominant Configuration (i,I;J)	Resonance Energy in the Laboratory Frame (MeV)		Γ (keV)	
	Experimental	Calculated	Experimental	Calculated
$1/2^+,0^+;1/2^+$	0.46	0.54	32	87
$5/2^+,0^+;5/2^+$	1.70	1.76	61	76
$3/2^+,0^+;3/2^+$	6.70	6.70	1720	2300
$1/2^+,2^+;5/2^+$	4.80	5.34	12	40
$1/2^+,2^+;3/2^+$	5.30	5.41	50÷100	100

Table 1.4.1

Resonance parameters for the elastic scattering of protons by carbon.

(Pascolini et al, 1969)

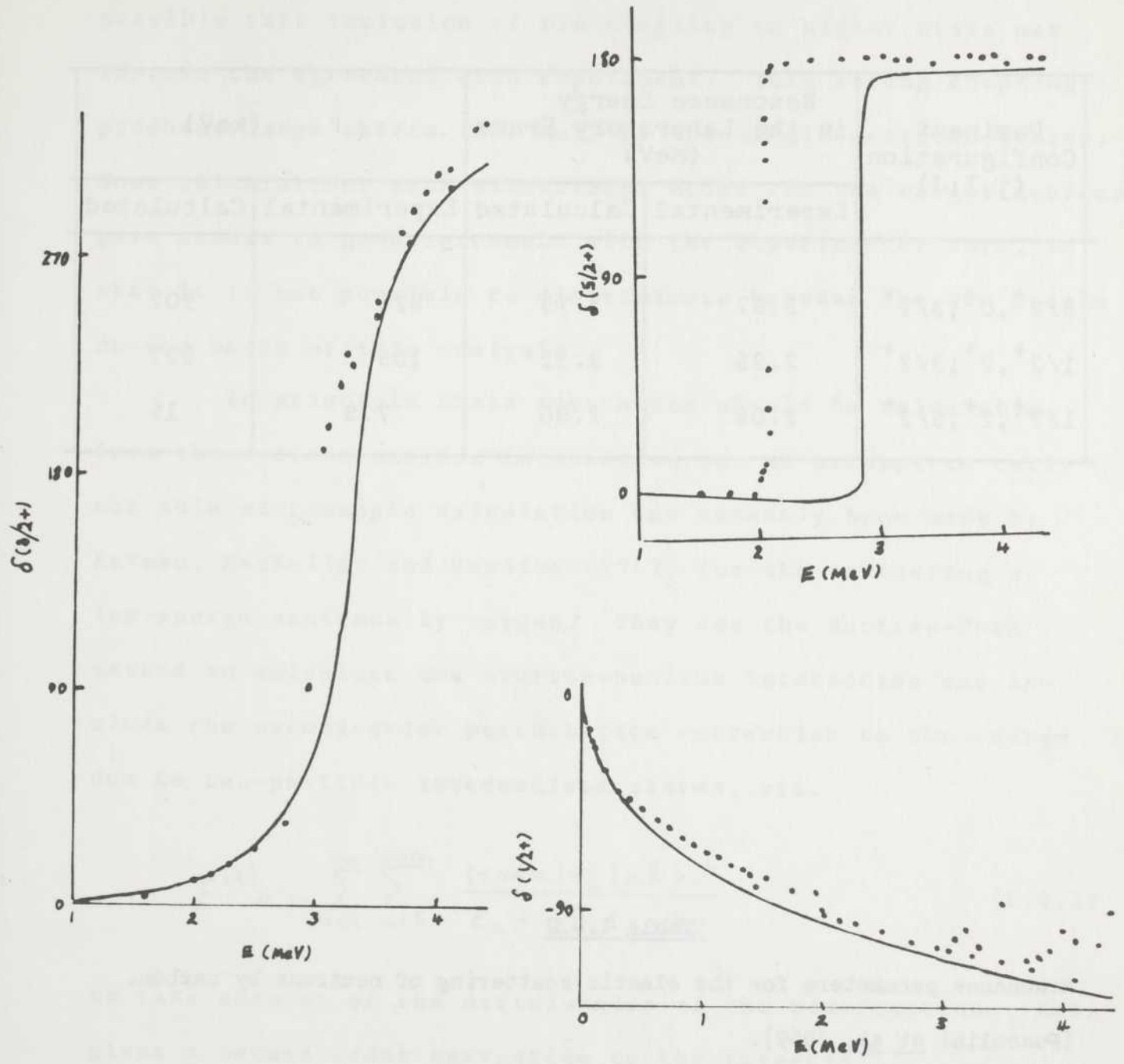

Fig. 1.4.2 Experimental phase shifts for the elastic scattering of neutrons by carbon compared with the results of coupled channels calculations. (Pascolini et al, 1969).

Resonance parameters in the n-^{12}C scattering process

Dominant Configuration (j,I;J)	Resonance Energy in the Laboratory Frame (MeV)		Γ (keV)	
	Experimental	Calculated	Experimental	Calculated
$3/2^+,0^+;3/2^+$	3.67	3.75	926	907
$1/2^+,2^+;3/2^+$	2.95	3.12	105	527
$1/2^+,2^+;5/2^+$	2.08	2.90	7.9	15

Table 1.4.2

Resonance parameters for the elastic scattering of neutrons by carbon. (Pascolini et al, 1969).

is necessary to use the coupled-channels formalism. It is possible that inclusion of the coupling to higher state may improve the agreement with experiment. This strong coupling produces large shifts (1-3 MeV) of the single-particle states. Some calculations with vibrational model for the target nucleus gave almost as good agreement with the experimental data, so that it is not possible to discriminate between the two models on the basis of this analysis.

In principle these resonances should be calculable from the nucleon-nucleon interaction and an attempt to carry out this microscopic calculation has recently been made by Kerman, MacKellar and Reading (1969) for the scattering of low-energy neutrons by oxygen. They use the Hartree-Fock method to calculate the neutron-nucleus interaction and include the second-order perturbation correction to the energy due to two-particle intermediate states, viz.

$$E^{(2)} = -\sum_{m<n}^{occ}\sum_{a<b}^{unocc} \frac{|\langle mn|v_A|ab\rangle|^2}{\varepsilon_a+\varepsilon_b-\varepsilon_m-\varepsilon_n} \qquad (1.4.1)$$

to take account of the deficiencies of the wavefunction. This gives a second order correction to the potential

$$\langle\gamma|V^{(2)}|\gamma'\rangle = -\sum_{m}^{occ}\sum_{a<b}^{unocc} \frac{\langle\gamma_m|v_A|ab\rangle\langle ab|v_A|\gamma'_m\rangle}{\varepsilon_a+\varepsilon_b-\varepsilon_m-\varepsilon_{\gamma'}} \qquad (1.4.2)$$

The nucleons were antisymmetrised, and this gives rise to the non-locality in the potential.

The resulting Schrodinger equation was solved to give the phase shifts as a function of energy. Several successful prescriptions for the nucleon-nucleon potential were used, and the results are compared in figs. 1.4.3 and 1.4.4 with the phase-shifts found from the measured cross-sections. It is notable that the calculated curves show quite a wide spread, and that they bracket the experimental values. This indicates the essential consistency of the analysis, and if the accuracy of the calculations could be improved it might provide a way of distinguishing between the nucleon-nucleon potentials.

Resonances in elastic scattering due to the excitation of isobaric analogue states are discussed in section 4.1.

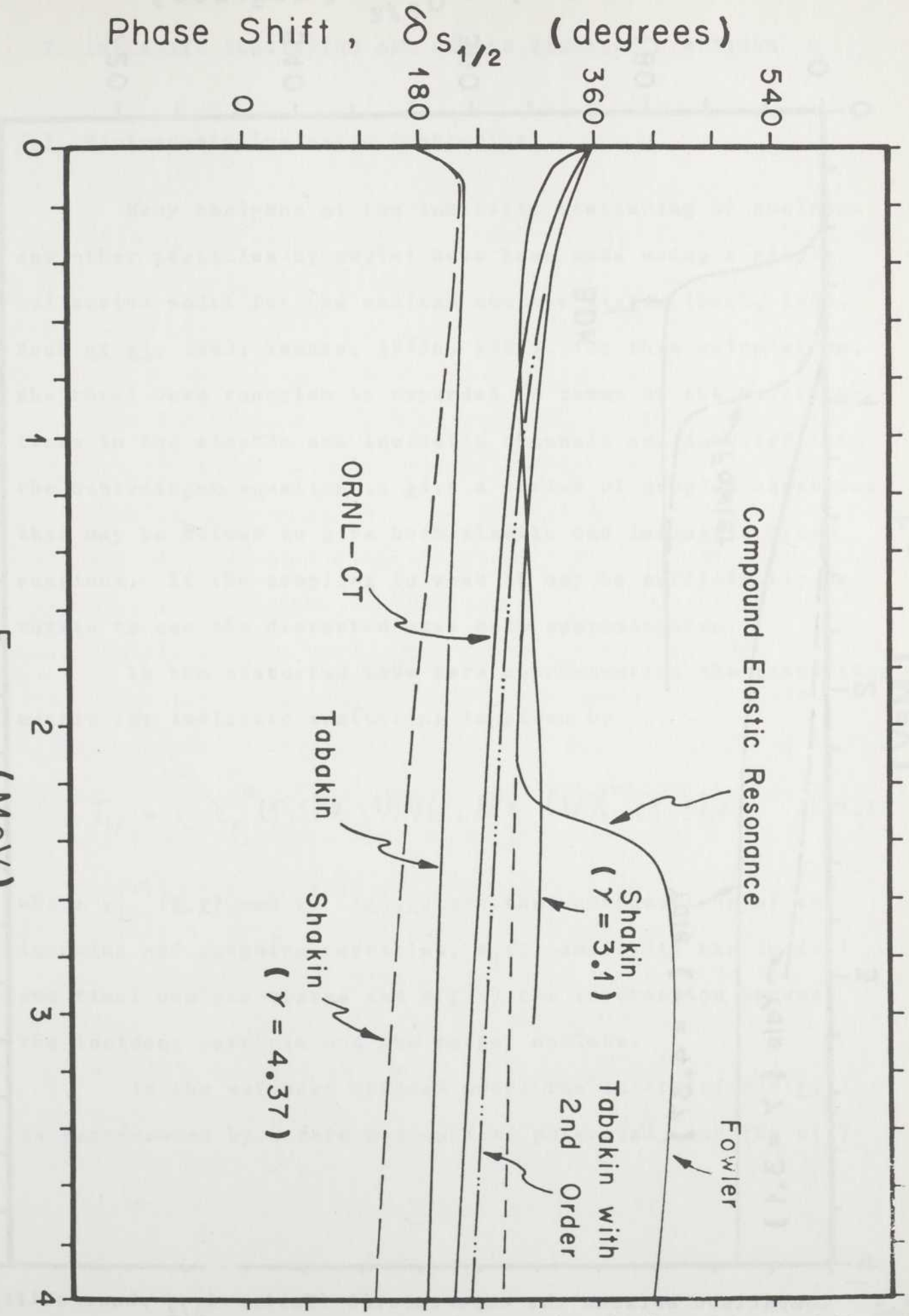

Fig.1.4.3 Comparison between the experimental (Fowler) $s_{\frac{1}{2}}$ phase-shifts for the elastic scattering of neutrons by oxygen and those calculated from a Hartree-Fock potential using various nucleon-nucleon potentials (Kerman et al, 1969).

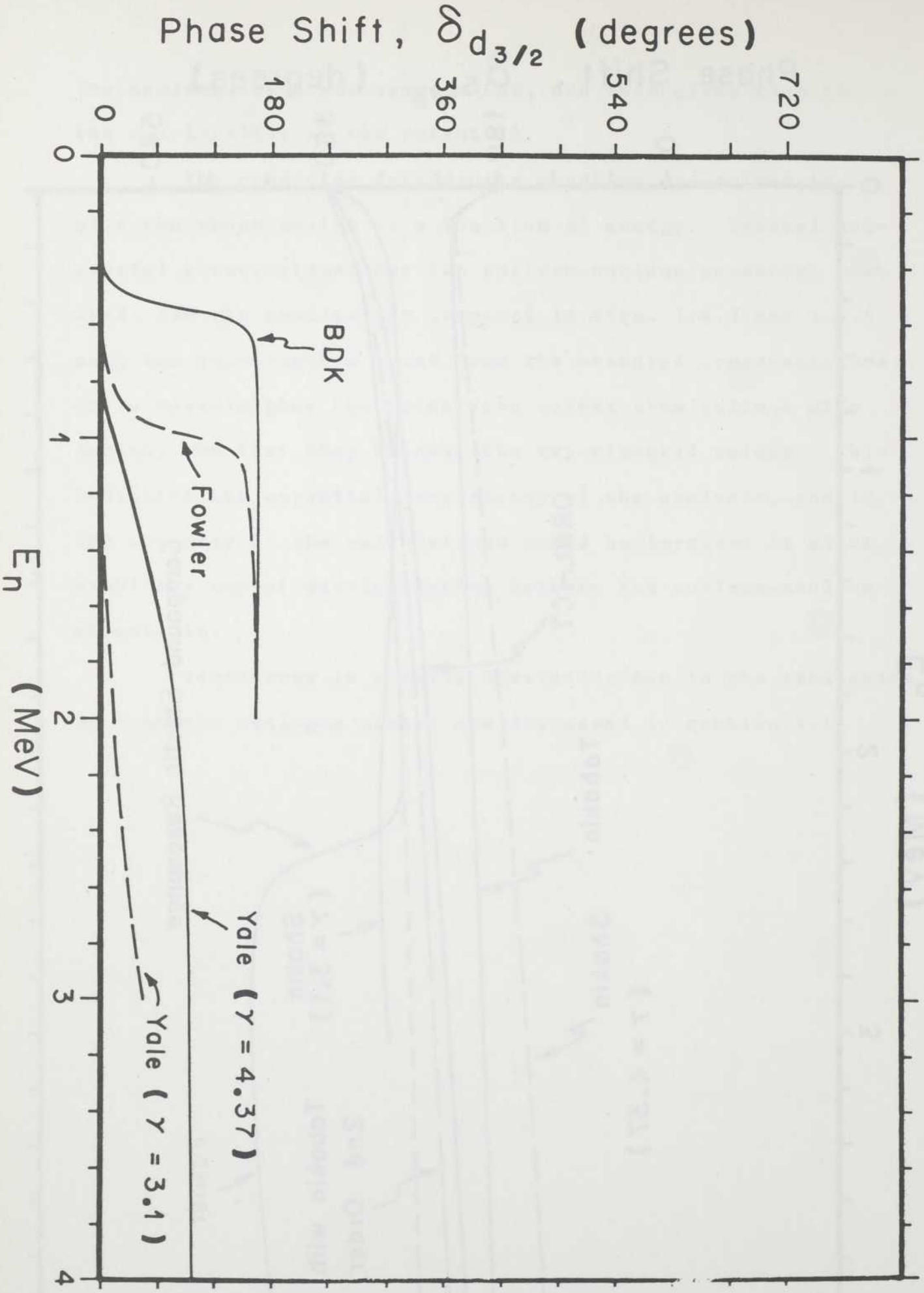

Fig. 1.4.4 Comparison between the experimental (Fowler $d_{3/2}$ phase shifts for the elastic scattering of neutrons by oxygen and those calculated from a Hartree-Fock potential using various nucleon-nucleon potentials. (Kerman et al, 1969).

2. INELASTIC SCATTERING AND CHARGE EXCHANGE REACTIONS

2.1 Macroscopic Inelastic Scattering

Many analyses of the inelastic scattering of nucleons and other particles by nuclei have been made using a simple collective model for the excited nuclear states (Buck, 1963, Buck et al, 1963; Tamura, 1965a, 1967). In this calculation, the total wave function is expanded in terms of the wavefunctions in the elastic and inelastic channels and inserted into the Schrodinger equation to give a series of coupled equations that may be solved to give both elastic and inelastic cross sections. If the coupling is weak it may be sufficiently accurate to use the distorted wave Born approximation.

In the distorted wave Born approximation the transition matrix for inelastic scattering is given by

$$T_{if} = \langle \chi_f^{(-)}(\underline{K}', \underline{r}) \phi_f(\xi) | V(\underline{r}, \xi) | \phi_i(\xi) \chi_i^{(+)}(\underline{K}, \underline{r}) \rangle \qquad (2.1.1)$$

where $\chi_i^{(+)}(\underline{K},\underline{r})$ and $\chi_f^{(-)}(\underline{K}',\underline{r})$ are the wavefunctions of the incoming and outgoing particles, $\phi_i(\xi)$ and $\phi_f(\xi)$ the initial and final nuclear states and $V(\underline{r},\xi)$ the interaction between the incident particle and the target nucleus.

In the extended optical model the interaction $V(\underline{r},\xi)$ is represented by a deformed optical potential, and the $\phi(\xi)$

are collective wavefunctions. Thus for the rotational model

$$V(\underline{r},\xi) = V(r-R_o) - \beta R_o Y_2^o(\theta,\phi)\frac{dV}{dr} \qquad (2.1.2)$$

and for the vibrational model

$$V(\underline{r},\xi) = V(r-R_o) - \sum_m \alpha_m Y_2^m(\theta,\phi) R_o \frac{dV}{dr} \qquad (2.1.3)$$

Higher order terms may be included in both these expansions, and this allows the excitation of higher states to be calculated. Since V(r) is diagonal in the nuclear wavefunctions the effective potential responsible for the inelastic excitation is due to the second and higher terms.

Several recent studies have shown that to obtain the best overall agreement with experimental data it is necessary to deform the imaginary and spin-orbit terms in the optical potential as well as the real central term. Some examples of the fits to the experimental data that can be obtained by this method are shown in fig. 2.1.1. (Tjin a Djie *et al*, 1968).

In some cases, however, it has not been found possible to obtain an adequate fit to the data, indicating that the model is proving inadequate. Thus the analysis of the inelastic scattering of 11 MeV protons by ^{62}Ni and ^{64}Ni leading to the excitation of the triplet of vibrational states (Dickens *et al*, 1963) required different values of the deformation parameter for each state, which destroys the simplicity of the model.

Similar discrepancies have been found in other reactions (Tamura 1968; McGowan et al, 1965; Kolasinski et al, 1969; Sherif, 1969).

In the case of nucleon and deuteron scattering the coupling between the different channels is usually quite weak so that providing the excitation is a single-step process; it is usually adequate to use the DWBA theory instead of solving the coupled equations. In other cases, particularly for alpha-particle scattering, it is sometimes found that the coupling is so strong that the optimum fit cannot be found by the usual iterative technique of coupling the channels one by one (Tamura, 1965b; Budzanowski et al, 1968). It is then necessary to iterate many parameters at once, which is very time-consuming and also subject to the uncertainty concerning the effect of the channels not explicitly considered. A further difficulty concerning the analysis of inelastic alpha-particle scattering is that in many cases it seems that the best fits are obtained with the shallower optical potentials, although the deeper ones seem to be more plausible on theoretical grounds. This is illustrated in figs. 2.1.2-2.1.4. At higher energies, however, the coupling is weaker and the analysis gives consistent results (Morgan and Jackson, 1969).

Some analyses of proton inelastic scattering have shown that it is difficult to fit the polarisations asymmetries and spin-flip probabilities with the simple collective model (Glashausser et al, 1967; Fricke et al, 1967, Fulling and Satchler, 1968). Marked improvement is obtained by taking into account the more accurate form of the spin-orbit potential (Sherif and Blair, 1968, Rook, 1968; Sherif, 1969; Kolasinski et al, 1969 but some discrepancies still remain.

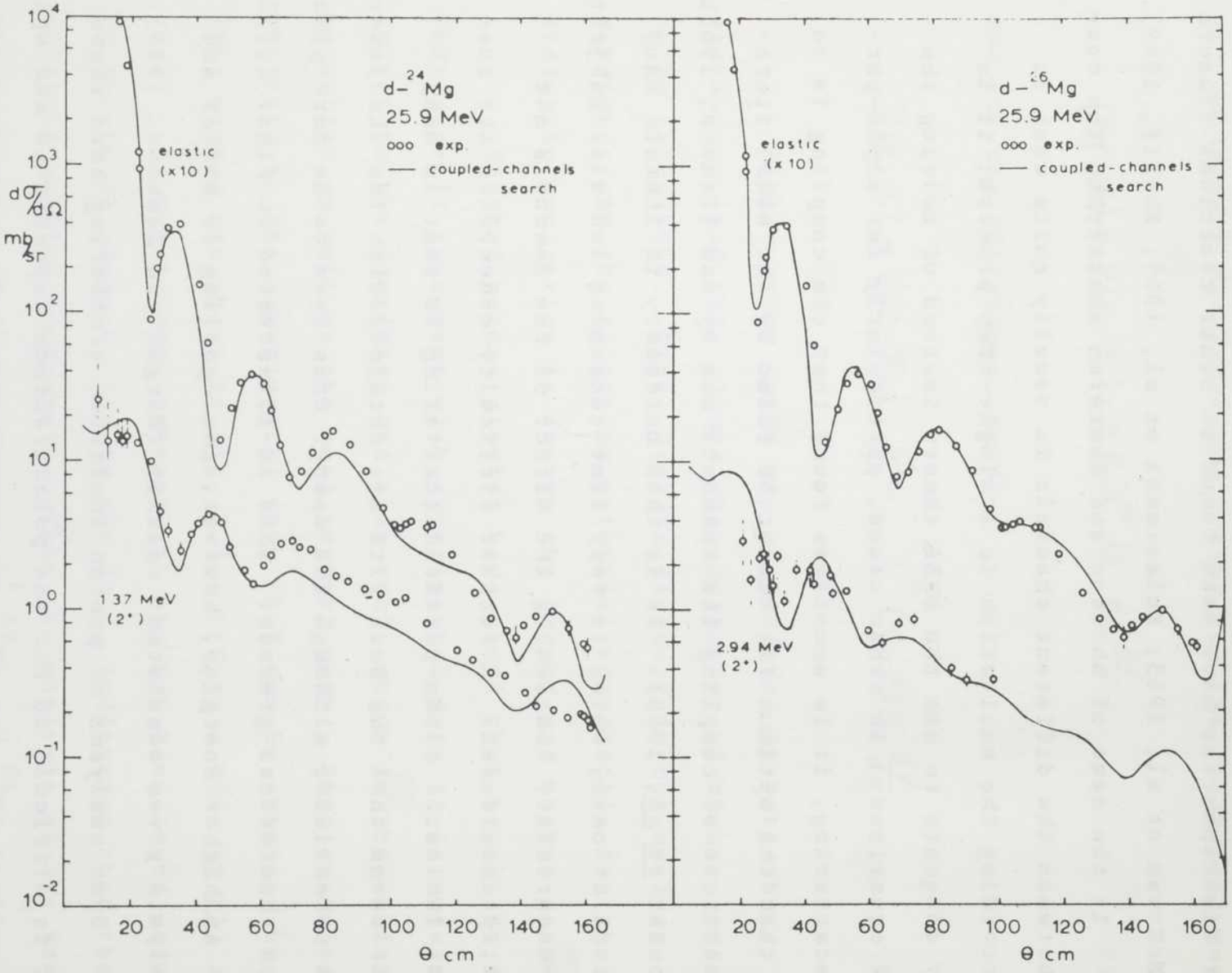

Fig.2.1.1 Coupled-channels analysis with complex coupling for ^{24}Mg and ^{26}Mg. The elastic scattering cross sections have been raised by a factor 10 (Tjin a Djie, 1968).

by a factor 10 (Tjin a Djie, 1968).

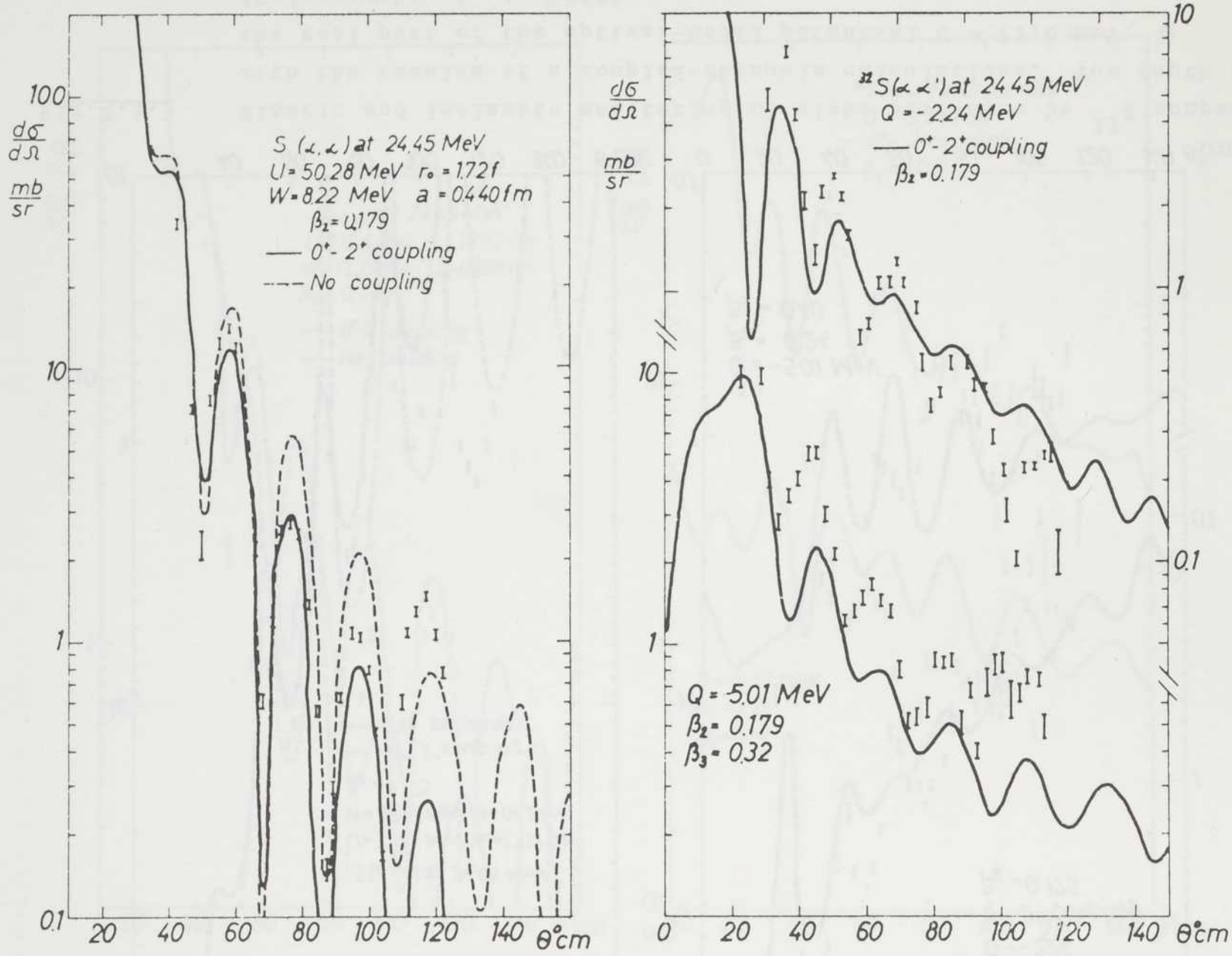

Fig. 2.1.2 Elastic and inelastic scattering of alpha particles by ^{32}S compared with the results of a coupled-channels calculations. The depth of the real part of the optical-model potential U = 50.3 MeV. (Budzanowski et al, 1968.

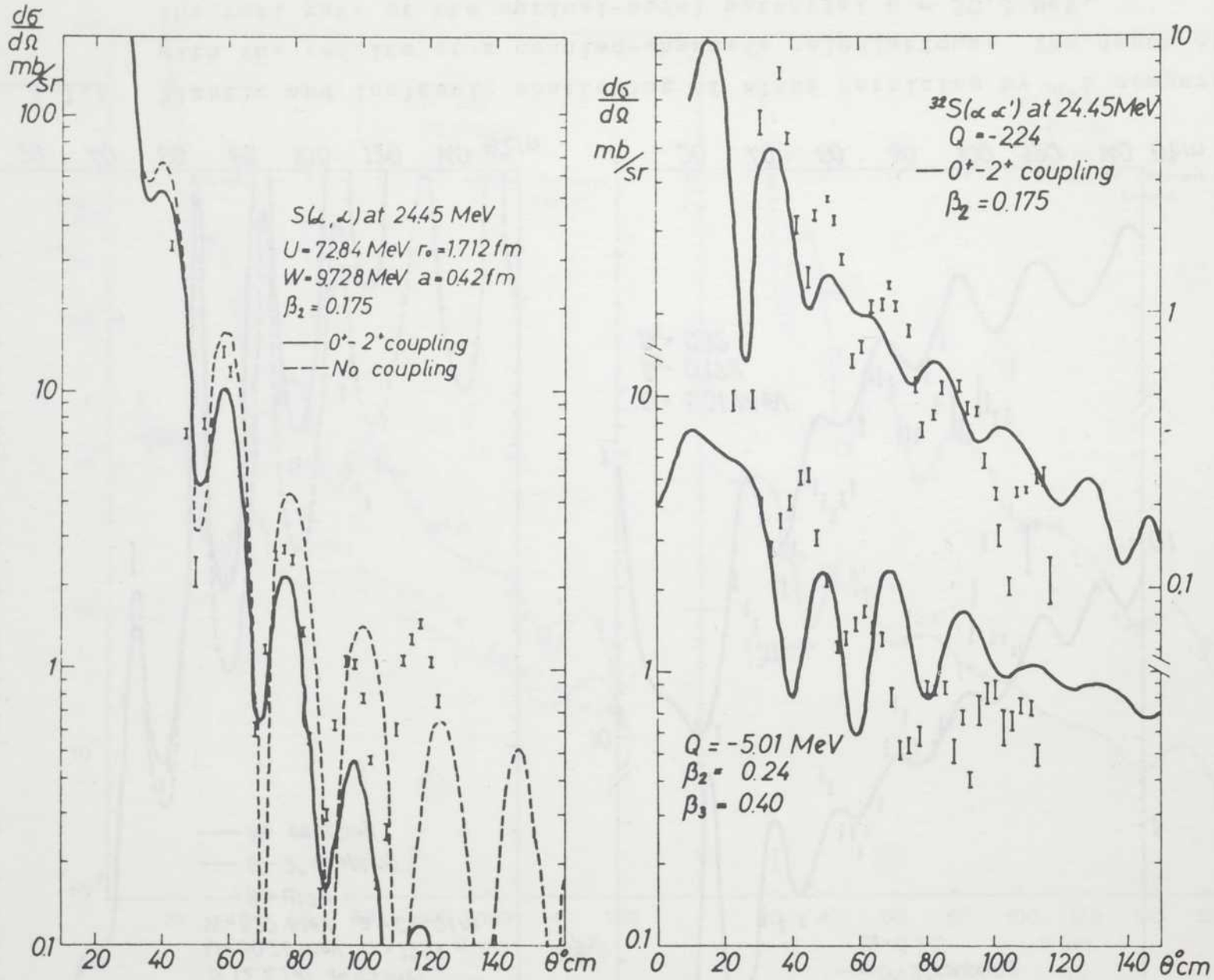

Fig.2.1.3 Elastic and inelastic scattering of alpha particles by ^{32}S compared with the results of a coupled-channels calculations. The depth of the real part of the optical-model potential U = 72.8 MeV. (Budzanowski et al, 1968)

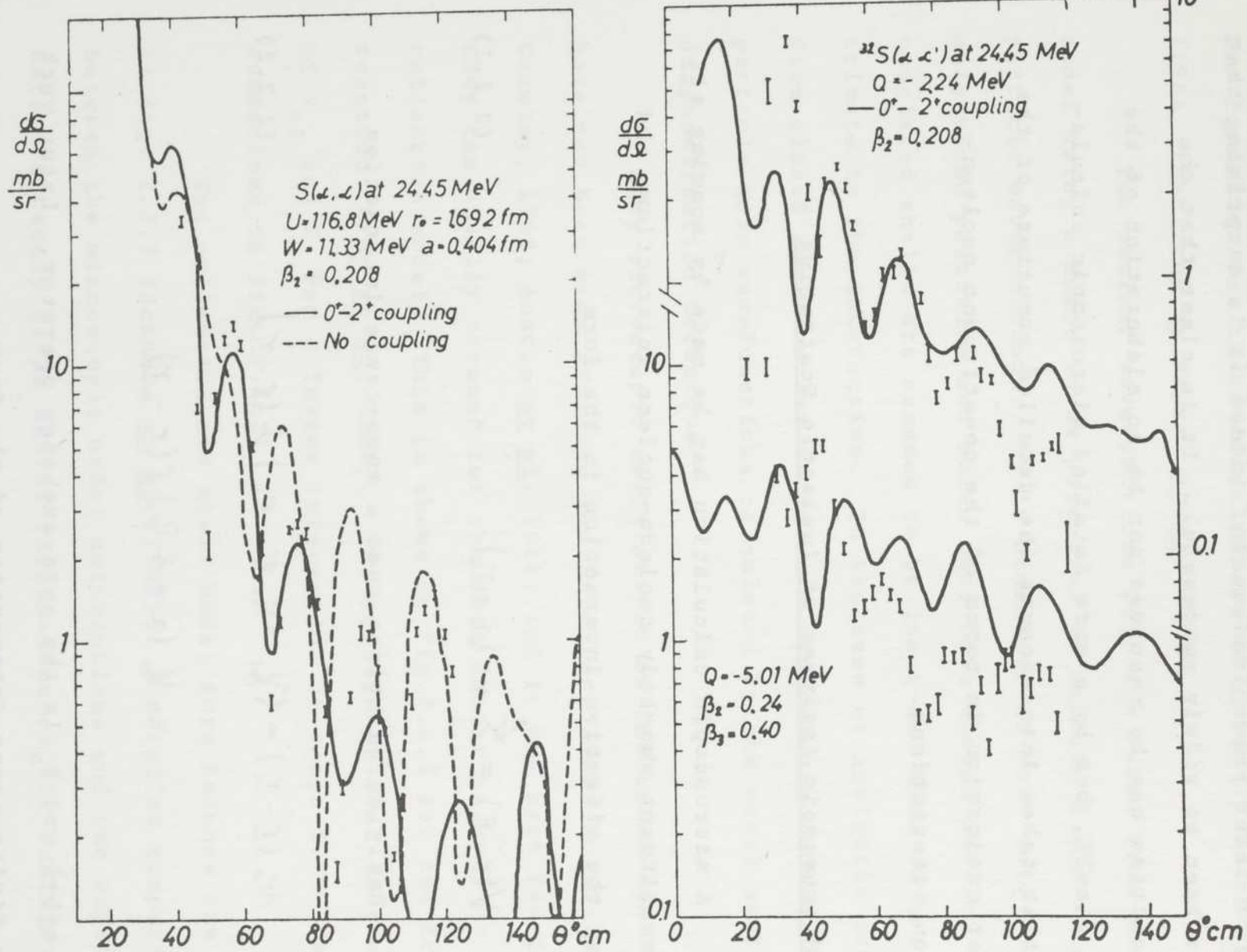

Fig. 2.1.4 Elastic and inelastic scattering of alpha particles by ^{32}S compared with the results of a coupled-channels calculations. The depth of the real part of the optical-model potential U 116.8 MeV. (Budzanowski et al, 1968).

It is not unexpected that so simple a model should sooner or later prove inadequate; indeed it is surprising that it has been so widely successful. It is clear that the difficulties can be resolved not by an elaboration of the model itself, but by a more detailed microscopic calculation that takes into account the detailed structure of the nuclear excitation in terms of the constituent nucleon-nucleon interactions.

2.2 Microscopic Analyses of Inelastic Scattering

A microscopic calculation may be made by summing all the constituant two-body nucleon-nucleon interactions and writing the effective interaction in the form

$$V(\underline{r},\xi) = \sum_{i=1}^{A} v(\underline{r}-\underline{r}_i) \qquad (2.2.1)$$

Early calculations used a zero-range interaction

$$v_o(\underline{r}-\underline{r}_i) = (V_{01} + V_{11}\,\underline{\sigma}\cdot\underline{\sigma}_i)\,\delta(\underline{r}-\underline{r}_i) \qquad (2.2.2)$$

$$\equiv V_o(a + b P_\sigma)\,\delta(\underline{r}-\underline{r}_i)$$

where a+b=1 and P_σ is the spin-exchange operator. Later work used a finite-range interaction of the form

$$v_f(\underline{r}-\underline{r}_i) = \frac{\exp(-\alpha|\underline{r}-\underline{r}_i|)}{\alpha|\underline{r}-\underline{r}_i|}\,(W + B P_\sigma - H P_t - M P_\sigma P_t) \qquad (2.2.3)$$

always including the electrostatic interaction where appropriate. The formalism for these calculations is given by Satchler (1964, 1966) and by Bassel et al, (1962).

The nuclear wavefunctions $\phi(\xi)$ are found from the shell model using a Saxon-Woods potential to calculate the single-particle wavefunctions. It is necessary to take into account only those particles and holes away from closed shells; the completed shells are assumed to be inert and thus do not contribute to the interaction. In the case of inelastic scattering from closed shell nuclei it is more appropriate to use the particle-hole wavefunctions calculated by the usual matrix diagonalisation technique.

Many microscopic calculations of inelastic scattering have now been made (Fulling and Satchler, 1968; Austin and Crawley, 1968; Austin et al, 1968) and it has been found that they can usually account for the data almost as well as the collective model. This is shown in fig.2.2.1 for the $Zr^{90}(p,p')$ reaction (Gray et al, 1966). The results of some determinations of V_{ol} and V_u for a Yukawa interaction of range 1.4f are summarised in fig. 2.2.2.

The collective and shell model form factors are compared in fig. 2.2.3 (Johnson et al, 1966). A detailed comparison between the microscopic model calculations and the experimental data frequently gives useful information on the configuration of the state concerned.

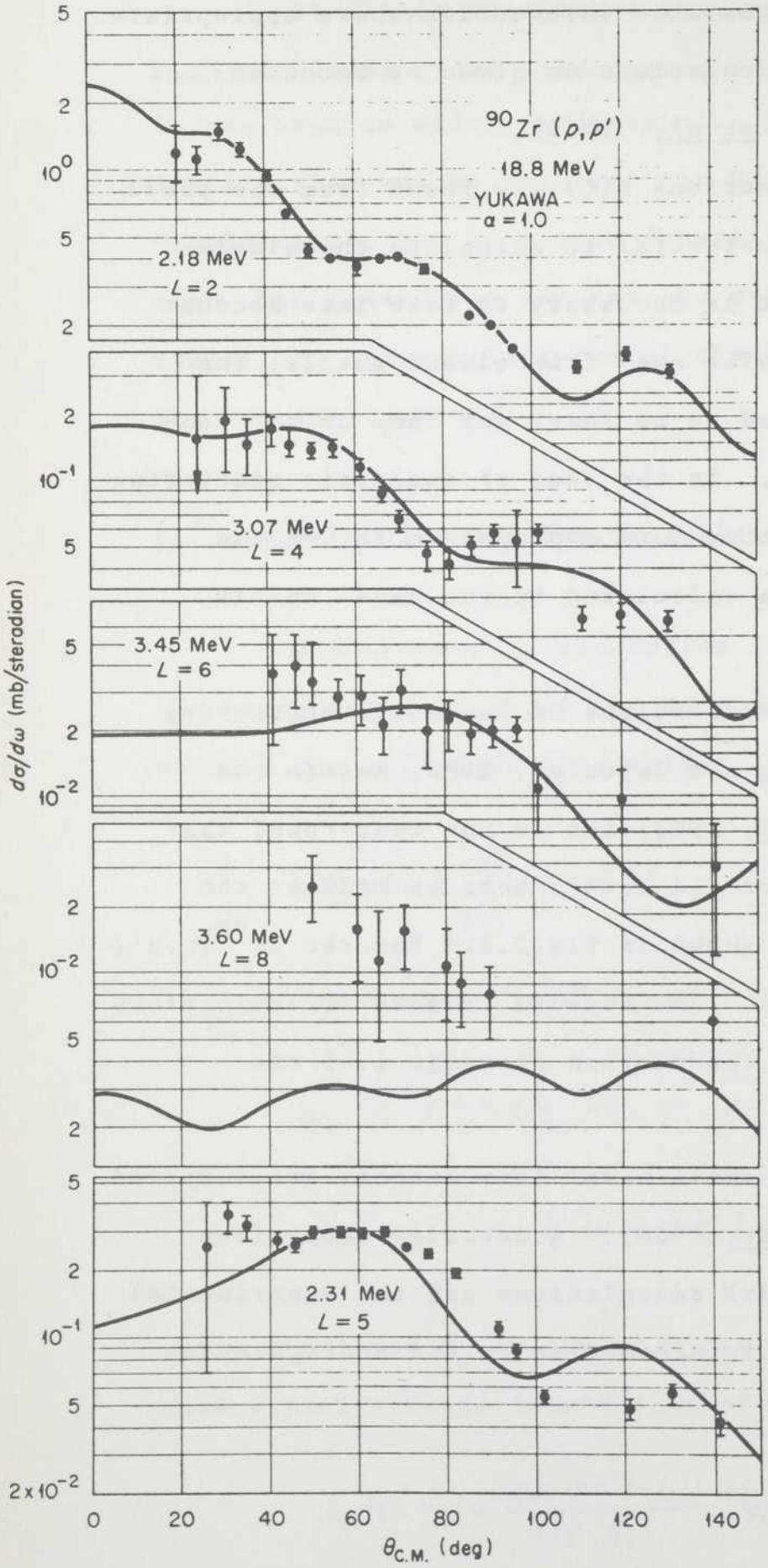

Fig.2.2.1

Differential cross-sections for the Zr^{90}(p,p') reaction compared with microscopic calculations of the excitation of the states of the $g^2_{9/2}$ configuration and the 5^- state of the $g_{9/2}$ configuration according to the shell model. (Gray et al, 1966).

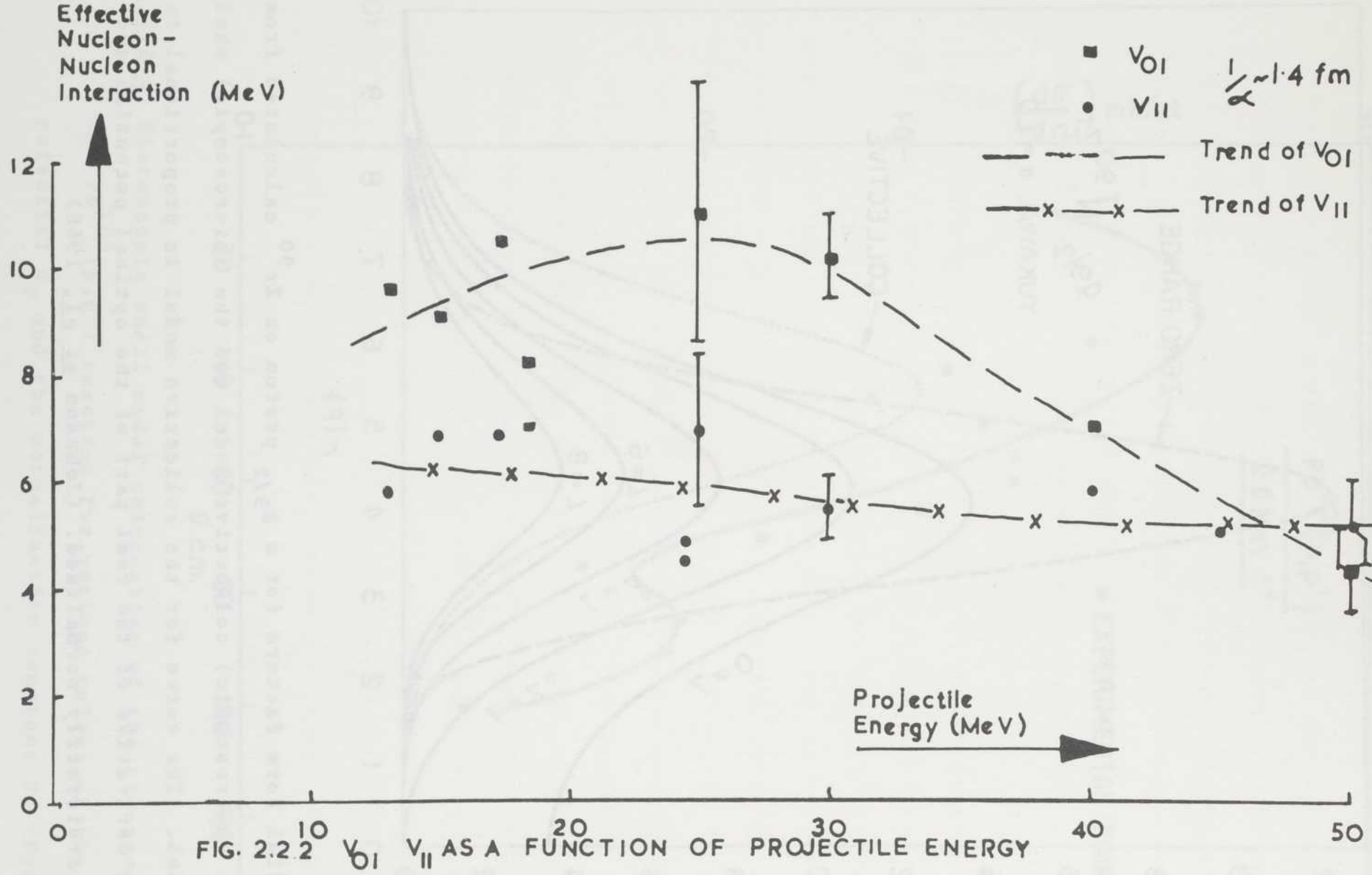

FIG. 2.22 V_{01} V_{11} AS A FUNCTION OF PROJECTILE ENERGY

Values of the effective interaction potentials as a function of energy obtained from microscopic analyses of inelastic scattering and charge-exchange reactions.

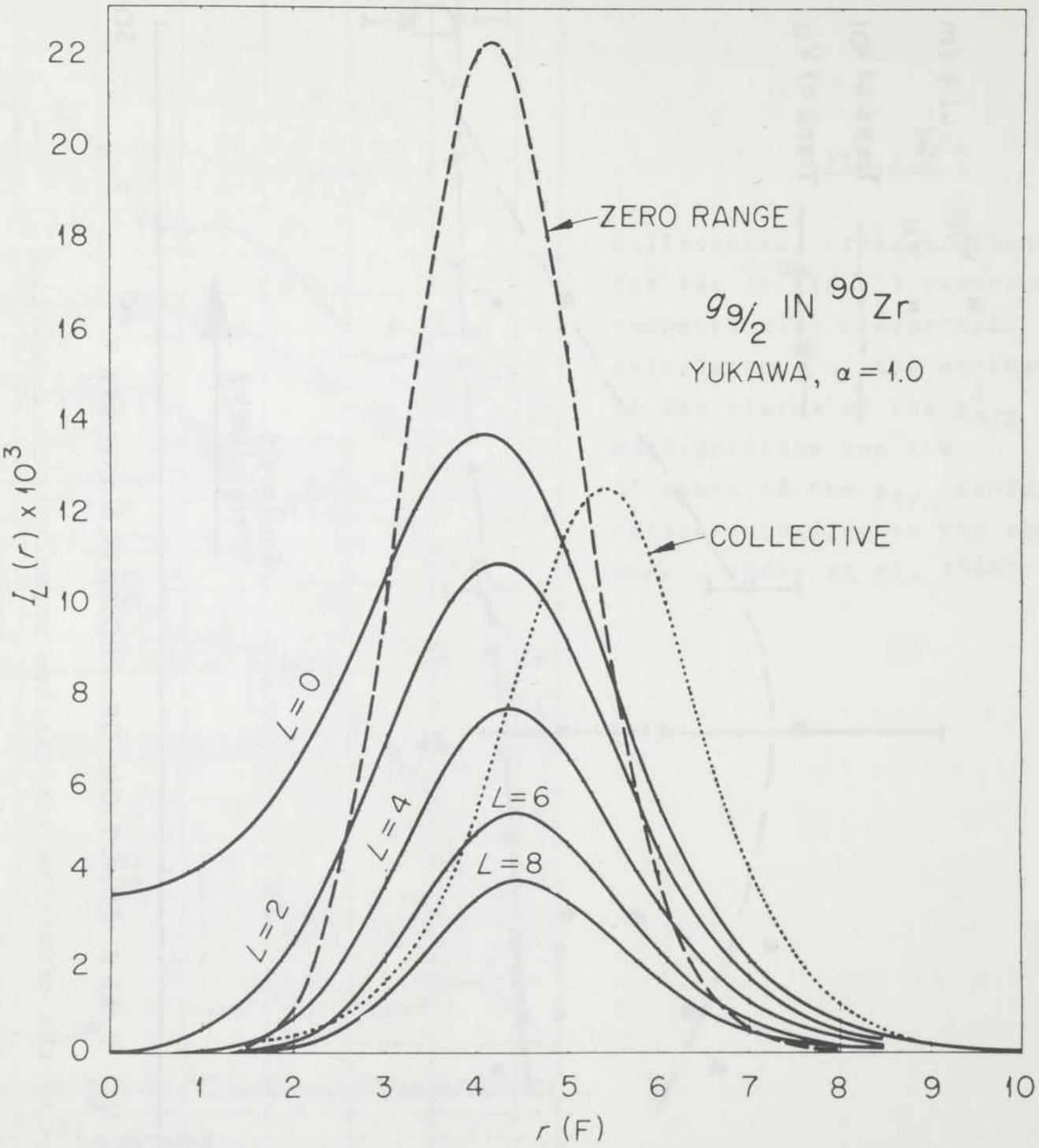

Fig.2.2.3 Radial form factors for a $g_{9/2}$ proton on Zr^{90} calculated from the (macroscopic) collective model and the (microscopic) shell model. The curve for the collective model is proportional to the derivative of the real part of the optical potential and is arbitrarily normalised. (Johnson et al, 1966)

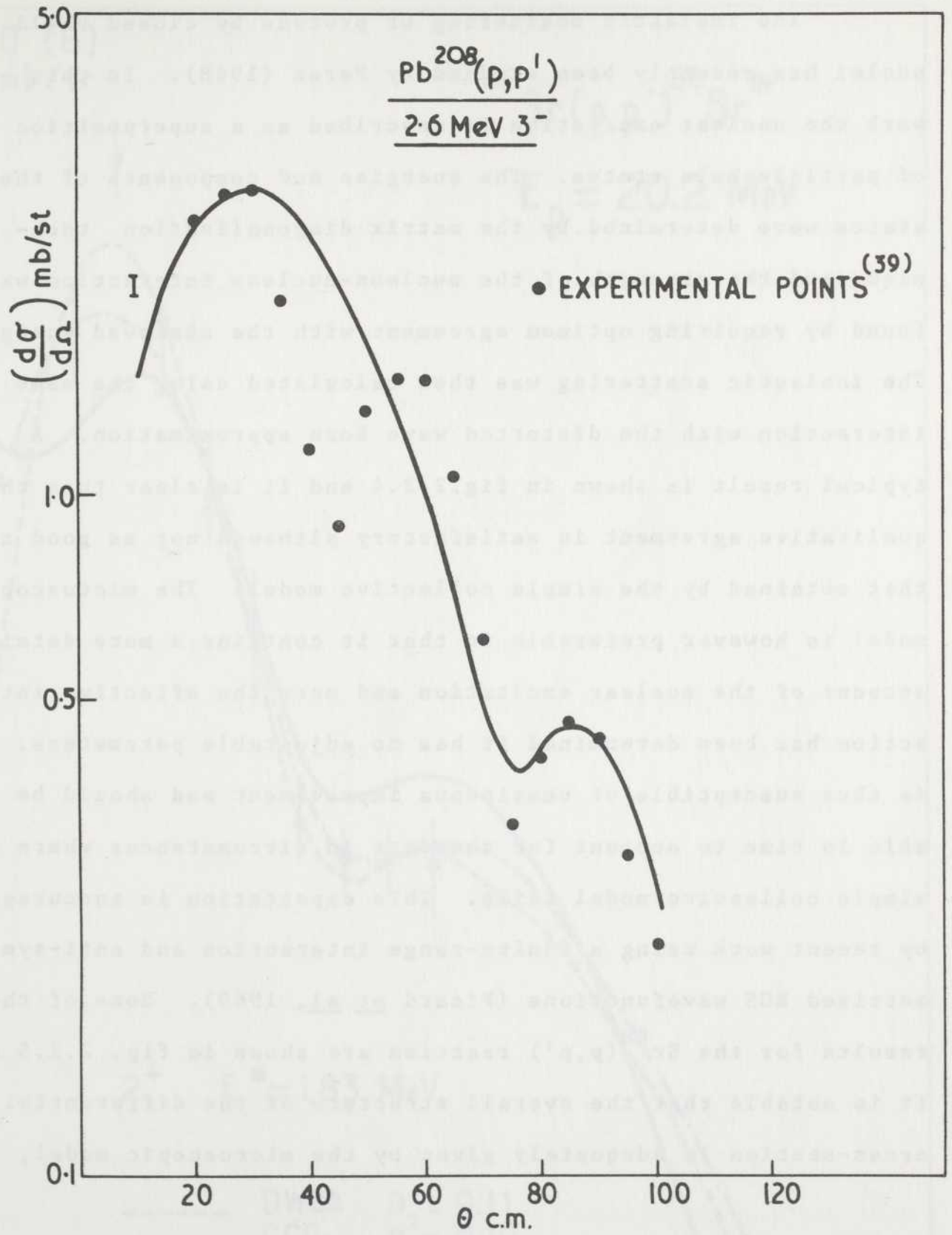

Fig.2.2.4 Microscopic shell model calculation of the cross-section of the $Pb^{208}(p,p')$ reaction for various values of the optical potential V_N and the normalisation constant N. (Perez, 1968).

The inelastic scattering of protons by closed shell nuclei has recently been studied by Perez (1968). In this work the nuclear excitation is described as a superposition of particle-hole states. The energies and components of the states were determined by the matrix diagonalisation technique and the strength of the nucleon-nucleon interaction was found by requiring optimum agreement with the observed energies. The inelastic scattering was then calculated using the same interaction with the distorted wave Born approximation. A typical result is shown in fig.2.2.4 and it is clear that the qualitative agreement is satisfactory although not as good as that obtained by the simple collective model. The microscopic model is however preferable in that it contains a more detailed account of the nuclear excitation and once the effective interaction has been determined it has no adjustable parameters. It is thus susceptible of continuous improvement and should be able in time to account for the data in circumstances where the simple collective model fails. This expectation is encouraged by recent work using a finite-range interaction and anti-symmetrised BCS wavefunctions (Picard et al, 1969). Some of their results for the $Sr^{88}(p,p')$ reaction are shown in fig. 2.2.5 and it is notable that the overall structure of the differential cross-section is adequately given by the microscopic model,

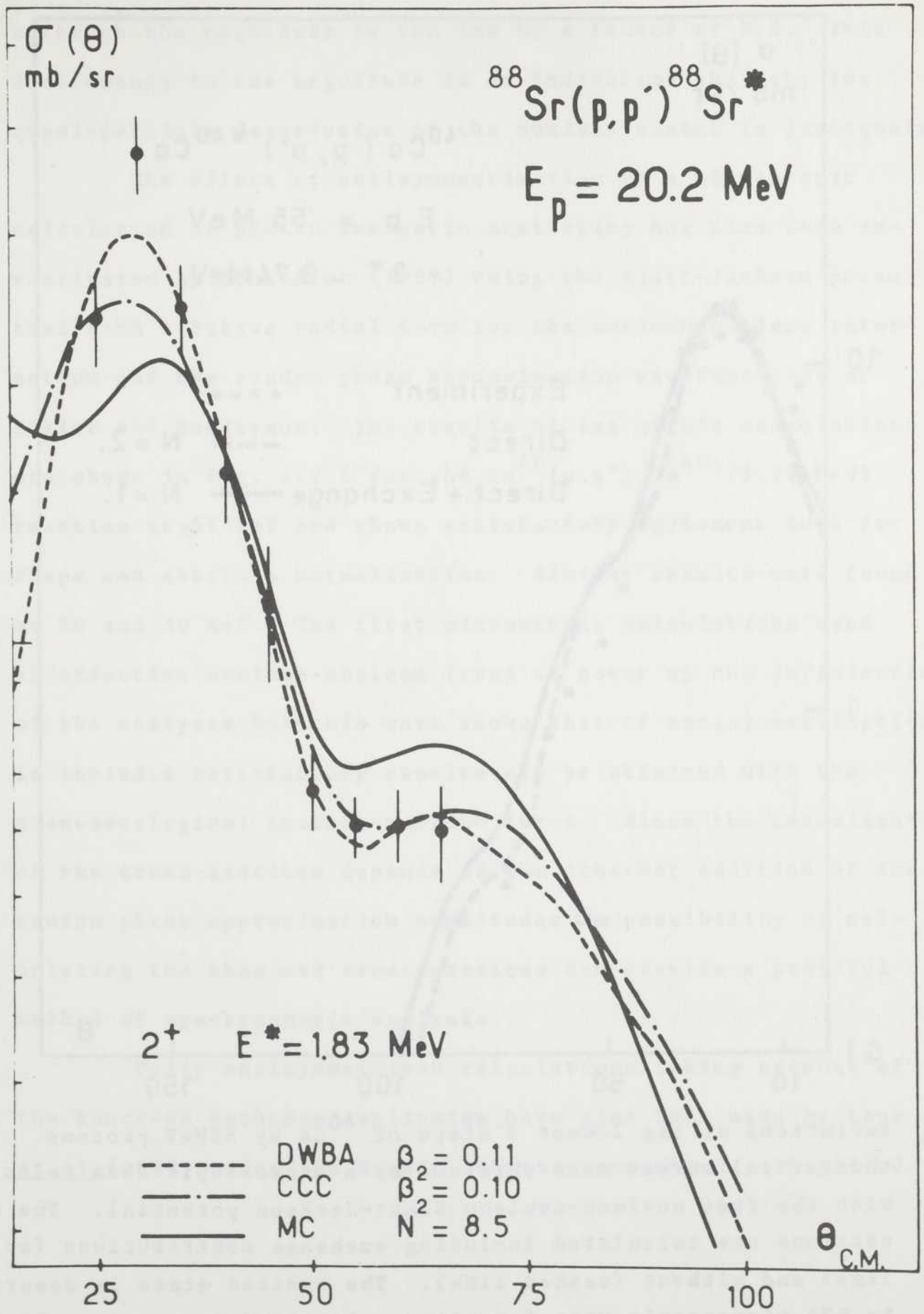

Fig. 2.2.5

Experimental data for the reaction Sr^{88}(p,p') compared with distorted wave and coupled-channels collective calculations and with a microscopic calculation (Picard et al, 1969)

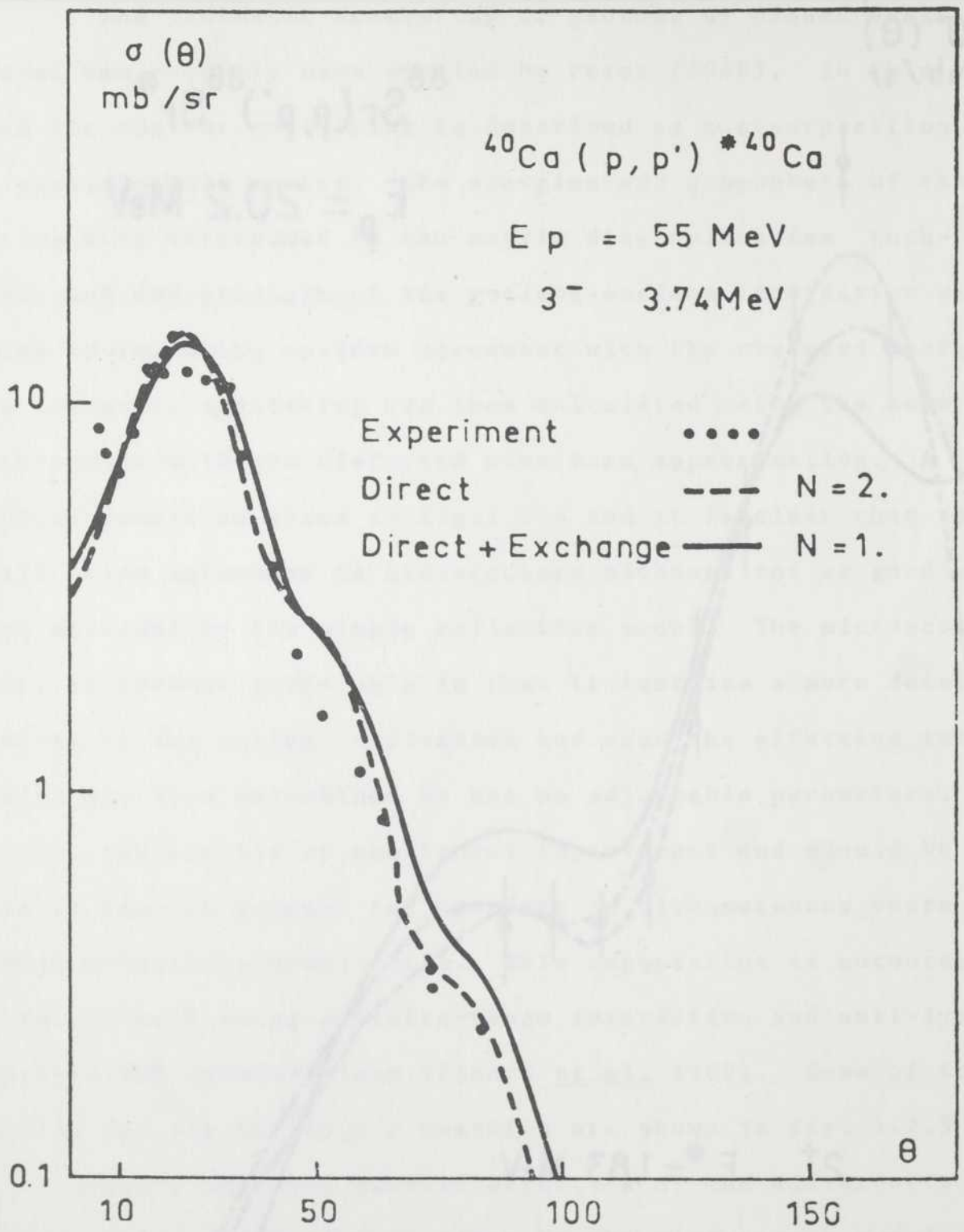

Fig.2.2.6 Excitations of the lowest 3^- state of ^{40}Ca by 55MeV protons. The theoretical curves were obtained by a microscopic DWBA calculation with the free nucleon-nucleon Blatt-Jackson potential. The cross sections are calculated including exchange contributions (solid line) and without (dashed line). The excited state is described by RPA microscopic wave functions. In order to compare the angular distributions, the theoretical cross sections are multiplied by the indicated (N) normalization factors (Schaeffer, 1969).

although the magnitude is too low by a factor of 8.5. This discrepancy in the magnitude is an indication that the two quasi-particle description of the nuclear states is inadequate.

The effect of antisymmetrisation on a microscopic calculation of proton inelastic scattering has also been investigated by Schaeffer (1969) using the Blatt-Jackson potential with a Yukawa radial form for the nucleon-nucleon interaction and the random phase approximation wavefunctions of Gillet and Sanderson. The results of one of his calculations are shown in fig. 2.2.6 for the $Ca^{40}(p,p')\ Ca^{40}$ (3.74 MeV) reaction at 55 MeV and shows satisfactory agreement both for shape and absolute normalisation. Similar results were found at 20 and 30 MeV. The first microscopic calculations used an effective nucleon-nucleon force to cover up the deficiencies of the analysis but this work shows that if antisymmetrisation is included satisfactory results can be obtained with the phenomenological nucleon-nucleon force. Since the normalisation of the cross-sections depends on the coherent addition of the random phase approximation amplitudes the possibility of calculating the absolute cross-sections can provide a powerful method of spectroscopic analysis.

Fully antisymmetrised calculations taking account of the knock-on exchange amplitudes have also been made by Love et al (1969) using the Hamada-Johnston potential. They find

this to be very important, especially for higher L-values, and also that core polarisation effects cannot be neglected (Petrovich et al, 1969; Glashausser et al, 1968; Love and Satchler, 1967).

The next development in the theory of inelastic scattering is to use the microscopic description of the interaction in the coupled-channels formalism; this is necessary if the coupling is strong or if the amplitude being calculated is the sum of two or more interfering processes. The first calculations of this type were made by Glendenning (1966) and by Glendenning et al (1966).

A recent calculation (Faessler et al,1966) has been made of the inelastic scattering of 17.8 MeV protons by the Ni isotopes, using the wave functions calculated by Plastino et al (1966) with the surface delta interaction and also with those obtained with the finite range interaction of Arvieu et al (1964). The results (some of which are shown in fig. 2.2.7) indicate that both the vibrational model and the two-quasiparticle method are inadequate for treating the nuclear states involved in the transition, and that a more detailed calculation taking account of the mixing between the two-quasiparticle and the two-photon configurations is required. It is notable that the polarisations calculated from the two different wavefunctions differ much more than the corresponding differential cross-sections, so that polarisation measurements would provide a much more searching test of the adequacy of the theory.

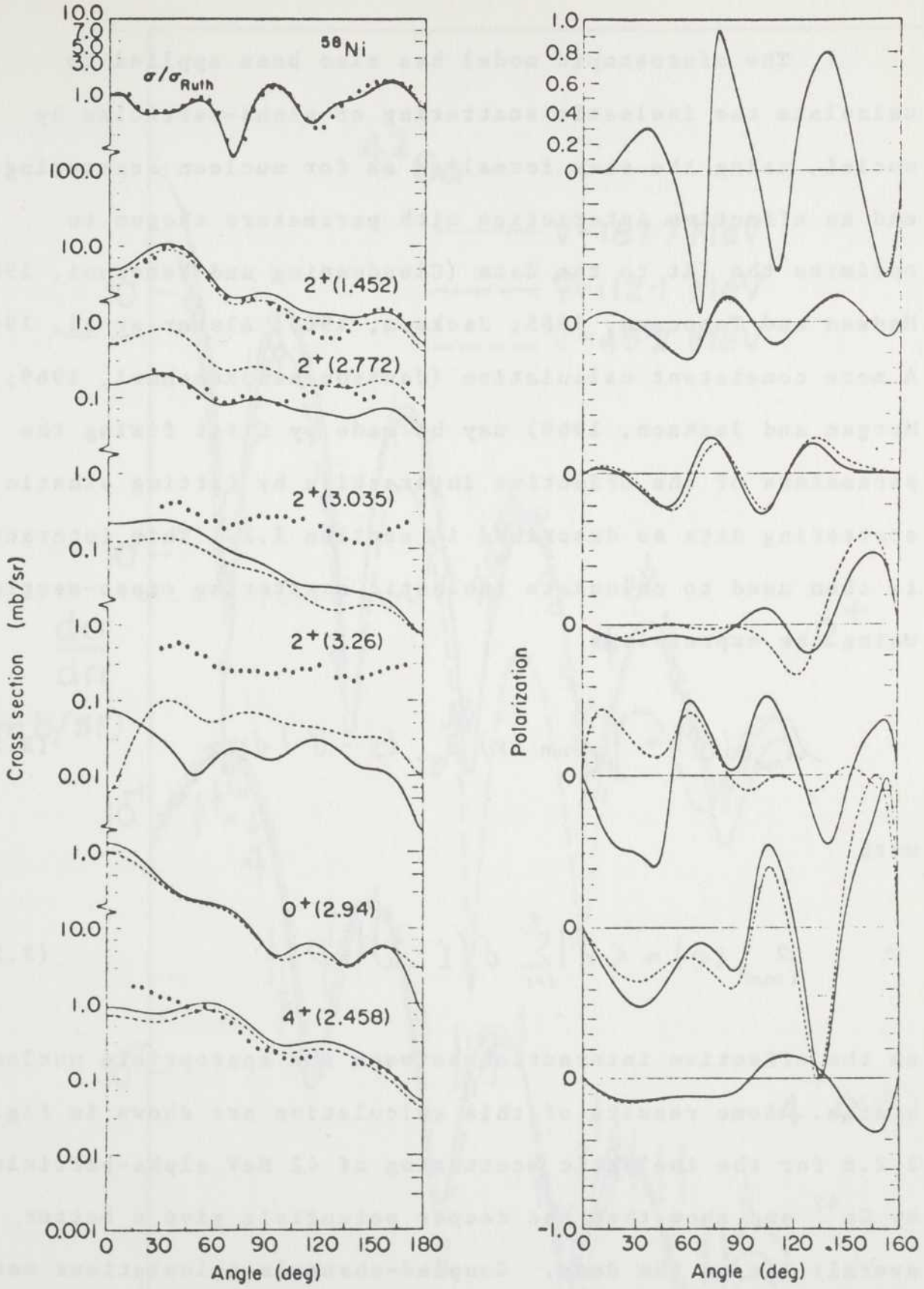

Fig.2.2.7 Differential cross-sections and polarisations for 17.8 MeV protons elastically and inelastically scattered from Ni^{58} calculated with a coupled-channels microscopic model using wavefunctions calculated with a surface delta interaction (solid lines) and with finite range interaction (dotted lines) (Faessler et al, 1966).

The microscopic model has also been applied to calculate the inelastic scattering of alpha-particles by nuclei, using the same formalism as for nucleon scattering, and an effective interaction with parameters chosen to optimise the fit to the data (Glendenning and Veneroni, 1965; Madsen and Tobocman, 1965; Jackson, 1965; Alster et al, 1966). A more consistant calculation (Jackson and Kemehari, 1969; Morgan and Jackson, 1969) may be made by first fixing the parameters of the effective interaction by fitting elastic scattering data as described in section 1.2. This interaction is then used to calculate inelastic scattering cross-sections, using the expressions

$$\mathcal{U}_{nn'}(\underline{R}) = \int \rho_{nn'}(r)\, V_{egg}(\underline{r} - \underline{R})\, d\underline{r} \qquad (2.2.4)$$

with

$$\rho_{nn'}(\underline{r}) = \langle n' | \sum_{i=1}^{A} \delta(\underline{r} - \underline{r}_i) | n \rangle \qquad (2.2.5)$$

as the effective interaction between the appropriate nuclear states. Some results of this calculation are shown in fig. 2.2.8 for the inelastic scattering of 42 MeV alpha-particles by Ca^{42} and show that the deeper potentials give a better overall fit to the data. Coupled-channels calculations were also made with this microscopic model and gave almost the same result as the distorted wave theory.

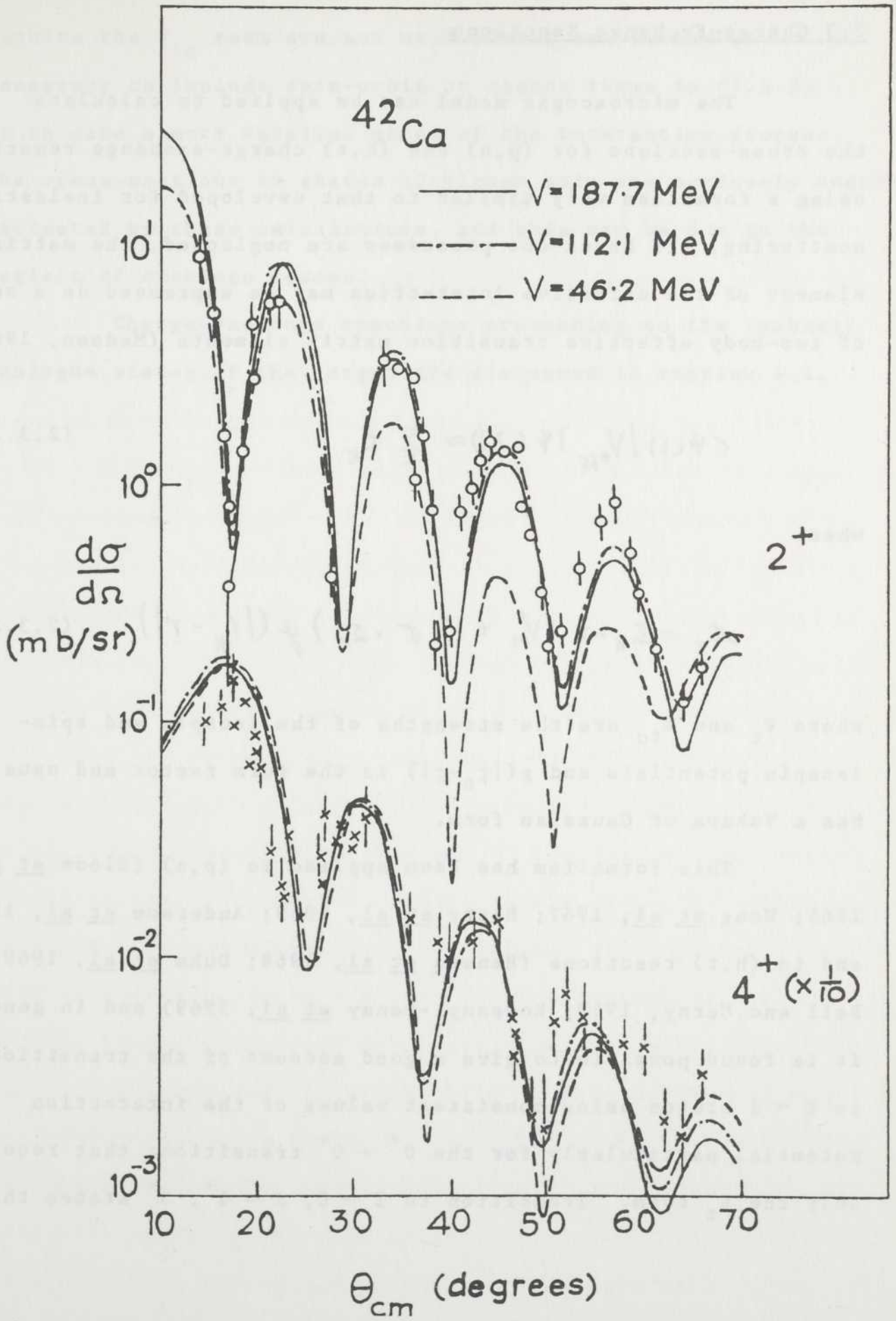

Fig.2.2.8 Differential cross-section for the inelastic scattering of 42 MeV alpha-particles by Ca^{42} compared with distorted wave microscopic potentials of different depths. (Morgan and Jackson, 1969).

2.3 Charge-Exchange Reactions

The microscopic model can be applied to calculate the cross-sections for (p,n) and (h,t) charge-exchange reactions, using a formalism very similar to that developed for inelastic scattering. If knock-out processes are neglected, the matrix element of the effective interaction may be expressed as a sum of two-body effective transition matrix elements (Madsen, 1966)

$$\langle \psi(1) | V_{eff} | \psi(2) \rangle \approx \sum_K t_K \qquad (2.3.1)$$

where

$$t_K = \underline{\tau}_K \cdot \tau \, (V_{01} + V_{11} \, \underline{\sigma} \cdot \underline{\sigma}_K) \, g(|\underline{r}_K - \underline{r}|) \qquad (2.3.2)$$

where V_t and $V_{t\sigma}$ are the strengths of the isospin and spin-isospin potentials and $g(|\underline{r}_t - \underline{r}|)$ is the form factor and usually has a Yukawa or Gaussian form.

This formalism has been applied to (p,n) (Bloom *et al*, 1965; Wong *et al*, 1967; Batty *et al*, 1969; Anderson *et al*, 1969) and to (h,t) reactions (Hansen *et al*, 1968; Duhm *et al*, 1969; Ball and Cerny, 1969; Kossanyi-Denay *et al*, 1969) and in general it is found possible to give a good account of the transitions to $T = 1$ states using consistent values of the interaction potential particularly for the $0^+ \rightarrow 0^+$ transitions that require only the V_t term. Transition to $T = 0$, $J = 1^+$, 3^+ states that

require the $V_{t\sigma}$ term are not well fitted and it may be necessary to include spin-orbit or tensor terms in (2.3.2) or to make a more detailed model of the interaction process. The cross-sections to states of higher spin are seriously underestimated by these calculations, and this may be due to the neglect of exchange forces.

Charge-exchange reactions proceeding to the isobaric analogue states of the target are discussed in section 4.1.

3. NUCLEON TRANSFER REACTIONS

Over the last few years, the DWBA has been extensively used to analyse the cross-sections for the (d,p) and other direct one-nucleon transfer reactions. This often makes possible the determination of the spin and parity of the final state and the spectroscopic factor of the transition. One of the most remarkable features of the differential cross-sections of these reactions is the systematic differences that are frequently found between those corresponding to $j = \ell + \frac{1}{2}$ and $j = \ell - \frac{1}{2}$ transitions; these are the j-dependent effects (Lee and Schiffer 1964). In many cases these differences are so systematic that they can be used with some confidence to determine the j-value of the final state. Unfortunately, however, many attempts to reproduce these effects by the DWBA were not successful (Lee and Schiffer, 1964, Glashausser and Rickey, 1967). A possible solution of this difficulty has been found by Robson (1968), who showed that if the radius of the spin-orbit part of the deuteron potential is taken to be rather less than that of the real potential, the j-dependent effects are reproduced quite well by the DWBA calculation. Such a difference between the radii of the central and spin orbit potentials has already been found for proton elastic scattering. The calculations of Robson were made for the $Ca^{40}(d,p)Ca^{41}$ reaction at 9 MeV and the $Fe^{54}(d,p)Fe^{55}$ reaction at 10 MeV and it would be interesting to see if the j-dependent effects observed for many other reactions are also reproduced. Johnson and Santos (1967) have shown

that taking into account the d-state of the internal wavefunction of the deuteron in the DWBA calculation also produces j-dependent effects on the differential cross-sections similar to those observed. The magnitude of this correction depends strongly on the angular momentum of the transferred particle and is large when $l_n = 3$. The relative contributions of these two processes to the j-dependent effect is not yet clear and it would be interesting to study the magnitudes of their contributions to the same reactions.

The distorted wave theory can also be used to calculate the polarisations of the emitted protons but on the whole the fits to the experimental data are disappointing. The polarisations could in principle be used to distinguish between $j = l + \frac{1}{2}$ and $j = l - \frac{1}{2}$ transitions but in practice it is easier to do this from the differential cross-sections. It is likely that the polarisations in (d,p) and other one-nucleon transfer reactions will only be fully understood when account is taken of the spatial polarisation of the deuteron and possibly also of the effect of other channels in the reaction.

Santos (1969) has recently studied the effect of taking the D-state of the deuteron into account in distorted wave calculations of the differential cross-sections and polarisations in stripping reactions. The results of some of his calculations are shown in figs 3.1 and 3.2 and it is notable that the fit to the differential cross sections is often markedly

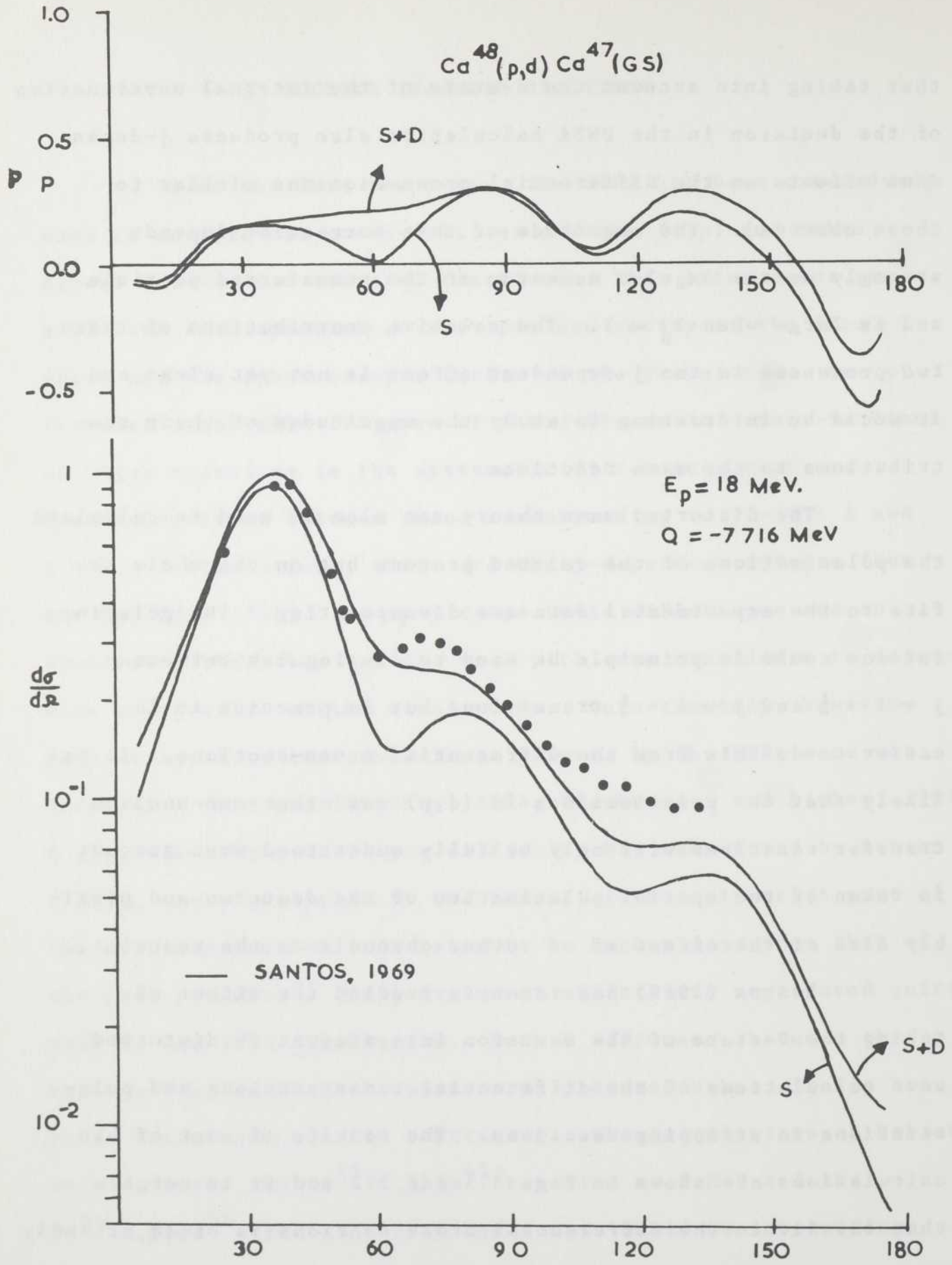

Fig.3.1 Differential cross-section for the $Ca^{48}(p,d)Ca^{47}$ (GS) reaction at 18 MeV compared with distorted wave calculation with and without the inclusion of the D-state of the deuterons. The corresponding calculated polarisations are also shown. (Santos, 1969).

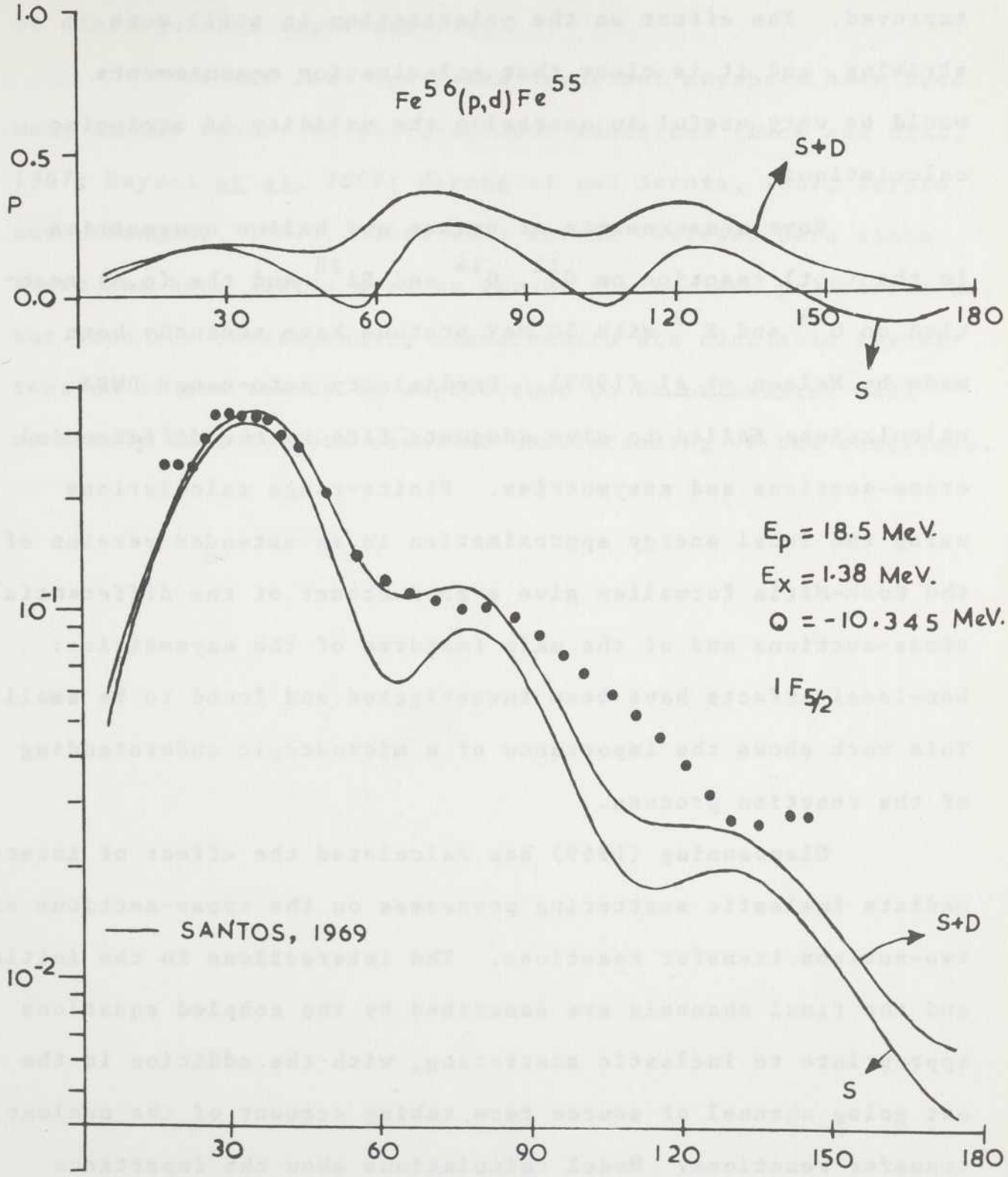

Fig. 3.2

Differential cross-section for the $Fe^{56}(p,d)Fe^{55}$ (1.38 MeV state) at 18.5 MeV compared with distorted wave calculations with and without the inclusion of the D-state of the deuterons The corresponding calculated polarisations are also shown. (Santos, 1969).

improved. The effect on the polarisation is still more striking, and it is clear that polarisation measurements would be very useful in assessing the validity of stripping calculations.

Some measurements of triton and helion assymetries in the (p,t) reaction on C^{12}, O^{16} and Si^{28} and the (p,h) reaction on O^{16} and F^{19} with 50 MeV protons have recently been made by Nelson et al (1969). Preliminary zero-range DWBA calculations failed to give adequate fits to the differential cross-sections and assymetries. Finite-range calculations using the local energy approximation in an extended version of the Rook-Mitia formalism give a good account of the differential cross-sections and of the main features of the asymmetries. Non-local effects have been investigated and found to be small. This work shows the importance of a microscopic understanding of the reaction process.

Glendenning (1969) has calculated the effect of intermediate inelastic scattering processes on the cross-sections of two-nucleon transfer reactions. The interactions in the initial and the final channels are described by the coupled equations appropriate to inelastic scattering, with the addition in the out going channel of source term taking account of the nuclear transfer reactions. Model calculations show the importance of these inelastic processes and yield the unexpected result that the polarisations for the higher order processes are the same as those for the first-order processes, so that they cannot

be distinguished experimentally.

Over the last few years important advances have been made in the theory of photo-nuclear reactions (Buck and Hill, 1967; Raynal et al, 1967; Marangoni and Saruis, 1967; Saruis and Marangoni, 1967). This will not be reviewed here since there has been little work so far on the nucleon polarisations, but when the corresponding measurements are available the extension of the theory to enable them to be calculated will certainly lead to more detailed understanding of the reactions.

4. ISOBARIC ANALOGUE STATE REACTIONS

4.1 Elastic and Quasi-elastic Scattering

Inclusion of an isospin term in the optical potential couples together the neutron and proton channels, and the Lane equations for the corresponding wavefunctions may be solved to give the cross-sections for elastic scattering and for quasi-elastic scattering to the isobaric analogue state of the target nucleus. The coupled equations may be solved exactly by numerical integration or by the Green's function formalism (Hufner and Shakin, 1969; Bondorf and Bund, 1969) but the isospin coupling term is so small that the distorted wave Born approximation is usually sufficiently accurate. Several calculations of this type have been made for (p,n) scattering (Satchler *et al*, 1964; Schwarcz, 1966; Thurlow, 1968; Batty *et al*, 1969) and the analysis of the experimental data has provided information on the isospin term in the optical potential. A similar analysis may be made of quasi-elastic (h,t) reactions (Wesolowski *et al*, 1968; Kunz *et al*, 1969). If the isospin term is assumed to be real and its strength is obtained from elastic scattering analyses, there are no adjustable parameters in this calculation. It is then often found that the shapes but not the magnitudes of the observed resonances and angular distributions are correctly given. The correct magnitude may be obtained by allowing the isospin term to become complex, but this introduces at least

one adjustable parameter, since the imaginary part of the isospin term cannot be determined from elastic scattering data.

The Lane equations give a macroscopic semi-phenomenological account of quasi-elastic scattering. The formalism for the corresponding microscopic analyses have been given by Robson (1965) Mahaux and Weidenmuller (1967) and de Toledo Pisa and Kerman (1966), and their results for the resonance positions and widths may be related to the macroscopic quantities using the Green's function formalism (Hufner and Shakin, 1969).

Charge-exchange reactions to the isobaric analogue state may also be analysed by the microscopic formalism described in section 2.3 (Satchler, 1967; Wesolowski et al, 1968). Some calculations by Batty et al, (1968) showed that the data for (p,n) reactions at 30 MeV can be fitted with a Yukawa form of radius 0.8 fm for $g(\underline{r}_i - \underline{r})$ and a strength adjusted to fit the data. The effective interaction is probably complex but taking account of this would introduce another adjustable parameter.

At lower energies, when the (p,n) channel is closed, the excitation function for elastic scattering shows resonances at energies such that the incident channel is coupled by the isospin interaction to a bound analogue eigenstate in the compound nucleus. Providing these are pure single particle states, the Lane equations with appropriate potentials give these

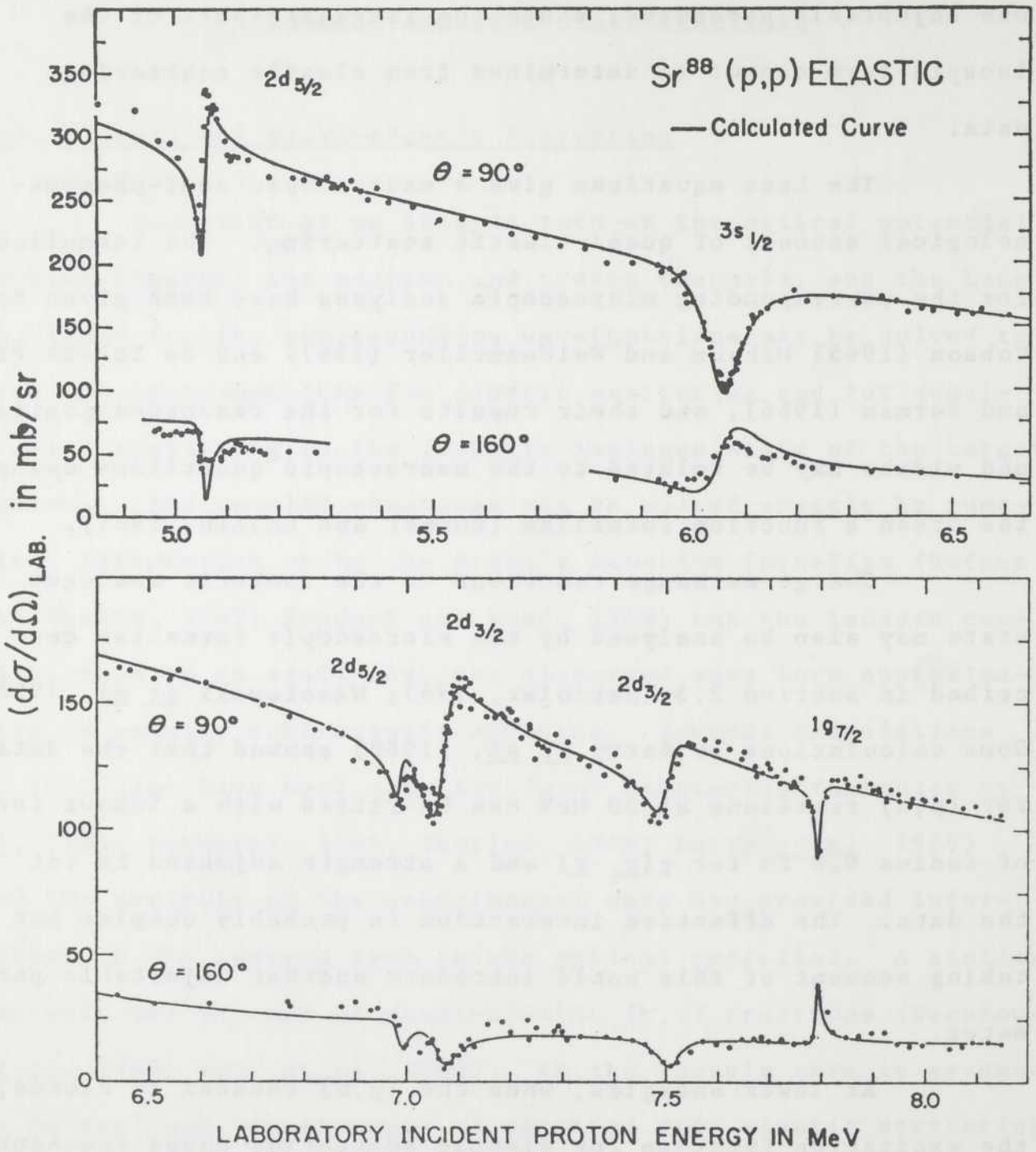

Fig.4.1.1 Differential cross-sections for the elastic scattering of protons by Sr^{88} at 90^{o} and 160^{o} compared with calculations using the non-local coupled Lane equations. (Bartels et al, 1969)

resonances automatically, and several analyses have been made in this way (Auerbach et al, 1966; Bondorf et al, 1966; Tamura, 1966). These analyses yield the spectroscopic factor for the compound state and values obtained compare favourably with those obtained from stripping reactions. (Harney, 1968).

This formalism has been extended Bartels et al, (1969) to account for reactions in which the single particle analogue resonances are split into several fragments, and some of their results for the Sr^{88}(p,p) reaction are shown in fig. 4.1. Microscopic analyses of these reactions are considered in section 4.3.

4.2 Quasi-inelastic Scattering

Quasi-inelastic scattering reactions proceeding to excited states of the nucleus that is the analogue of the target may be considered to take place in two steps, the collective excitation of the target nucleus and the transition to the analogue state. These can take place in either order, and in each case the reaction leaves as residual nucleus the analogue of the target in one of its excited states. The cross-sections for these reactions may be calculated either by the distorted wave theory (Satchler et al, 1964) or by introducing both the isospin and the collective excitation terms into the optical potential, thus giving for each partial wave a set of up to eight coupled equations for the corresponding scattered wave-functions. A macroscopic calculation of quasi-inelastic

scattering has been made by Kunz et al, (1969) for the (h,t) reaction on the Ni isotopes using the distorted wave equivalents to these equations. They found that in order to fit the data they had to use a large charge-exchange deformation parameter, in desagreement with the results obtained at lower energies. A microscopic calculation, however, using a finite range Yukawa interaction gave a consistent description of quasi-elastic and quasi-inelastic scattering. The relative contribution of the f and p configurations to the neutron excess were also calculated by the microscopic model and were consistent with shell model estimates. Microscopic calculations of the (h,t) reaction have also been made by Wesolowoski et al (1968), who were able to obtain satisfactory agreement to the experimental data for the Ti^{48} (h,t) reaction to the analogue of the 2^+ state of Ti^{48} at 0.99 MeV.

4.3 Microscopic Analysis of Isobaric Analogue Resonances

Elastic and inelastic scattering cross-sections frequently show characteristic resonances when the incident energy is such that the compound nucleus is excited to an energy corresponding to that of the ground or low-lying state of the analogue nucleus. These resonances may be analysed by superposing

background and resonant amplitudes and hence their parameters may be determined. A more fundamental approach is to use the coupled-channels formalism to describe the wavefunctions in the elastic and inelastic channels, so that the resonances appear automatically from the solution of the appropriate wave equations, provided the correct potentials are used. Such a calculation was first attempted by Tamura (1966), in a case where the nuclear excitation could be described by the collective model. This work, however, took account of only one of the states produced by the application of the T-operator to the ground state of the analogue nucleus, and is thus valid to the extent that the other states give a small contribution. It is thus interesting to seek a reaction in which the complete number of states is not too large, and to analyse it by the coupled channels formalism taking all the corresponding channels into account.

A suitable case is the elastic and inelastic scattering of protons by Pb^{207}, illustrated in fig.4.3.1. The state of Bi^{208} that is the analogue of the ground state of Pb^{208} may be written as the coherent sum of all possible proton-particle neutron-hole states in Bi^{208}, so that

$$T^- \left[\; \right]^{0^+} = \sum_i \left(\frac{2J_i + 1}{2T_0} \right)^{1/2} \left[\times \; \right]^{0^+} \qquad (4.3.1)$$

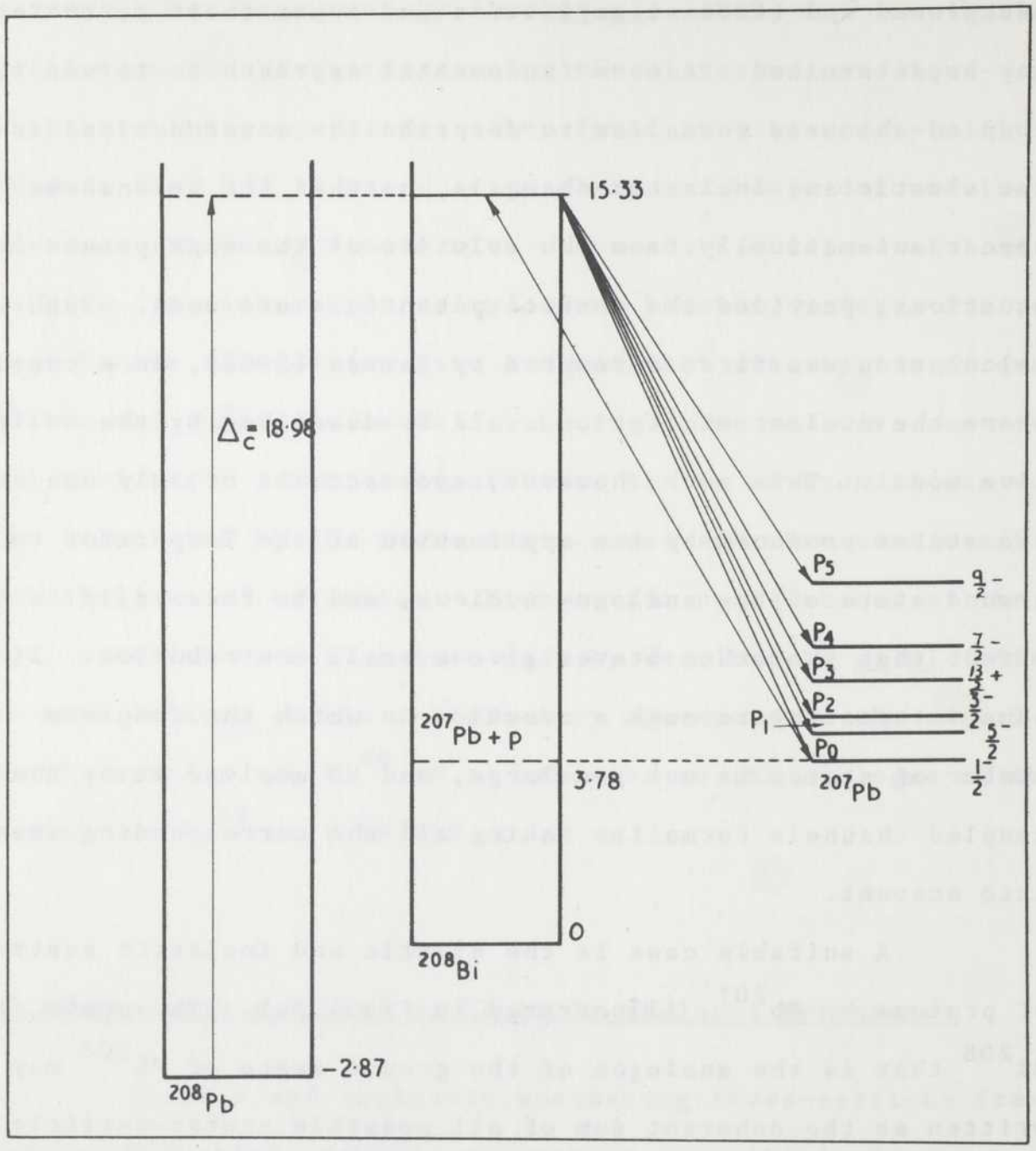

Fig. 4.3.1

Energy level diagram for the Pb^{207}(p,p') analogue state reaction.

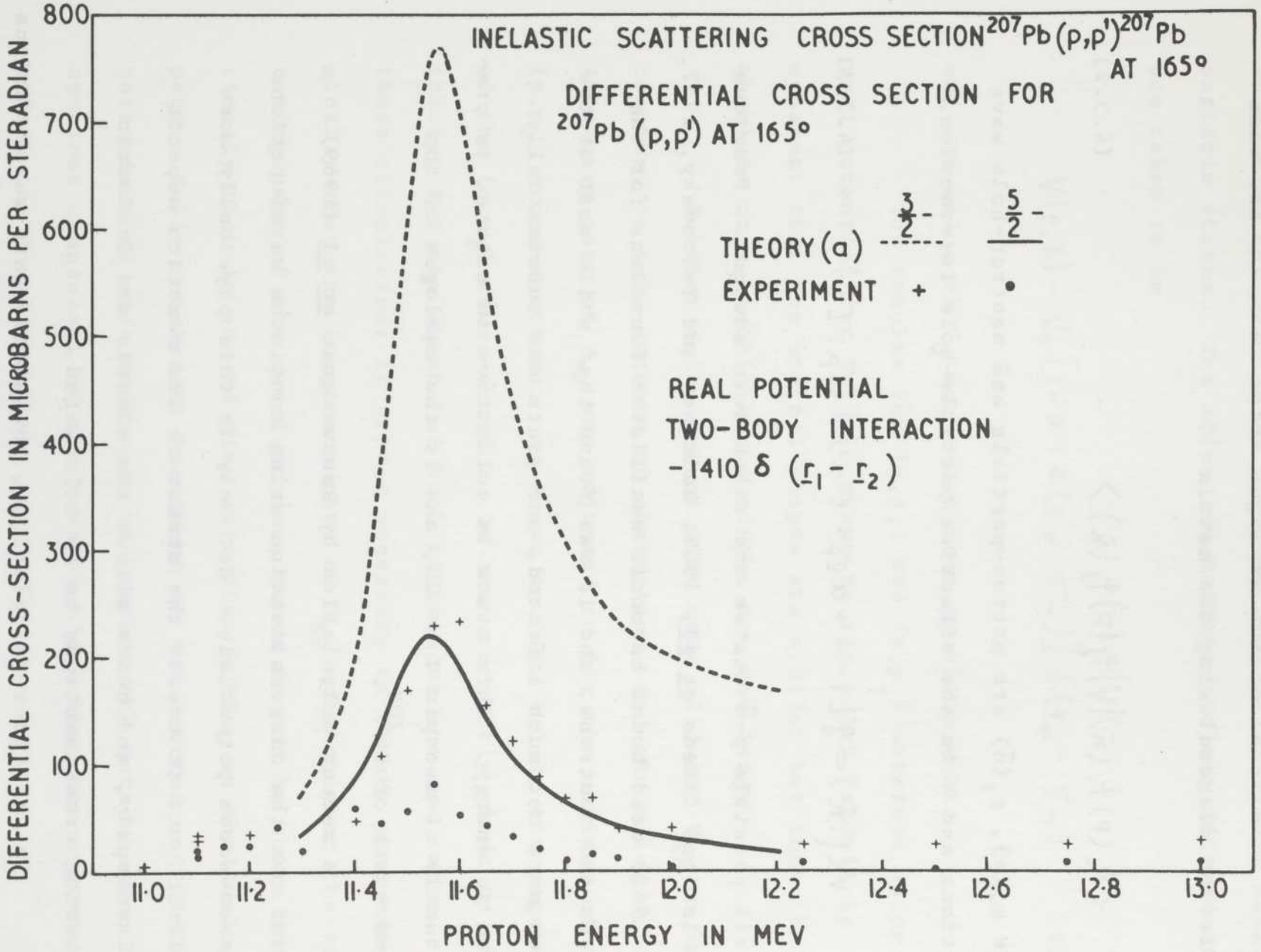

Fig.4.3.2 Experimental data for the $Pb^{207}(p,p')$ reactions compared with coupled channels calculations with a real two-body potential (Ramavataram *et al*, 1969).

This model of the analogue state in Bi^{208} has been studied by diagonalising the matrix

$$\langle \psi_i(p)\psi_i(\bar{n})|V|\psi_j(p)\psi_j(\bar{n})\rangle \qquad (4.3.2)$$

where $\psi_i(p)$, $\psi_i(\bar{n})$ are proton-particle and neutron-hole wave functions and V is the effective particle-hole interaction.

$$V(p,\bar{n}) = g[1-\alpha+\alpha\,\underline{\sigma}_p\cdot\underline{\sigma}_{\bar{n}}]\,\delta(\underline{r}_p-\underline{r}_{\bar{n}}) \qquad (4.3.3)$$

and all possible p-$\bar{n}$ states are taken into account. Previous calculations (Ikeda et al, 1962; Balashov and Yadrovsky, 1967, Kuo, 1968) used bound harmonic oscillator functions for the protons and neutrons, and it was found that while most of the states were not much affected, one state was substantially raised in energy. This state is collective in nature, is predominantly of isospin $T_> = 22$, and is the analogue of the ground state of Pb^{208}.

A recent calculation by Ramavataram et al (1969) carried out the diagonalisation using continuum wavefunctions in Saxon-Woods potentials. Not only is this physically more realistic, but it treats the structure and reaction aspects simultaneously, and hence allows the elastic and inelastic scattering cross-sections to be calculated.

In the first calculations, the bound state wavefunctions were generated by Saxon-Woods potentials with depths adjusted

to give an optimum fit to the positions of the known single particle states. The effective nucleon-nucleon interaction was taken to be

$$V(p,\tilde{n}) = V_0 \left[1 - \alpha + \alpha(\underline{\sigma}_p \cdot \underline{\sigma}_n)\right] \delta(\underline{r}_p - \underline{r}_n) \qquad (4.3.4)$$

and the value of V_0 was taken from previous work.

The results for (p,p_1) and (p,p_2) obtained using a real potential for V_{HF} are known in fig.4.3.2, and it is apparent that the overall shapes are similar but that the absolute cross-sections and widths are too large.

Further calculations were made allowing V_{HF} to be complex, to take account of absorption, and the value of the imaginary part of V_{HF} was adjusted to fit the maximum of the (p,p_1) cross-sections. As shown in fig. 4.3.3, the magnitude of the (p,p_2) cross-section is then correctly given by the theory, but the widths of both resonances are too large. In these calculations it proved necessary to ensure phenomenologically that the imaginary part of V_{HF} acts only on the scattering part of the wavefunction, since it can be shown analytically that it should give zero when acting on the analogue part. Fully consistent treatment of the neutron and proton potentials is also necessary to prevent the introduction of spurious components of the wavefunctions that can appreciably affect the final results.

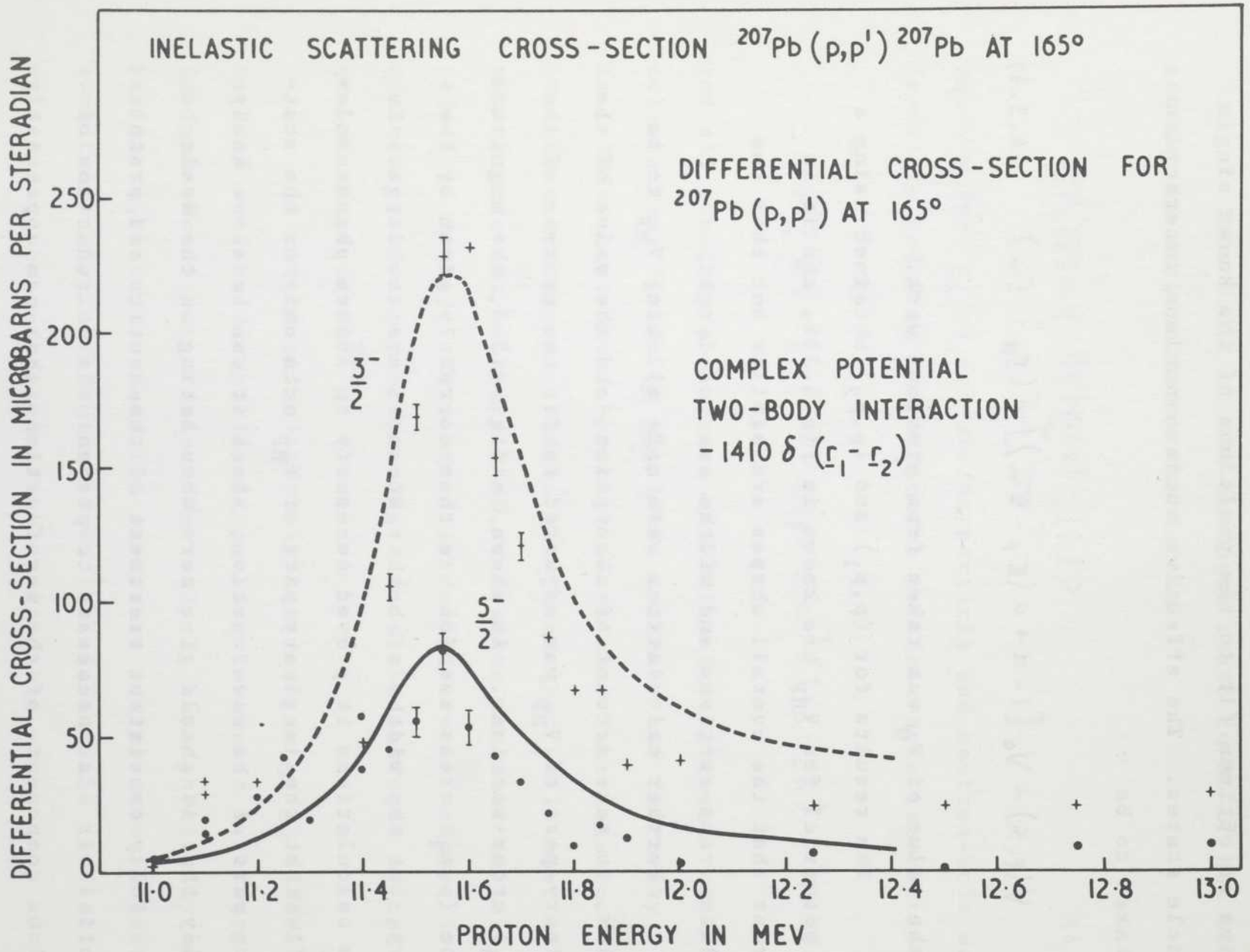

Fig.4.3.3 Experimental data for the $Pb^{207}(p,p')$ reactions compared with coupled channels calculations with a complex two-body potential (Ramavataram *et al*, 1969).

5. TOTAL CROSS SECTIONS

The total cross-section for the interaction of neutrons with nuclei can be calculated from the appropriate optical potential, and in general the values obtained agree well with the energy-averaged experimental data. This illustrated in fig. 5.1 for the total cross section for neutrons on iron compared with calculations using the local equivalent of the Perey-Buck non-local potential.

When examined with high energy resolutions, these cross-sections show gross-structure due to the resonances in the compound nucleus, and Lipperheide (1969) has parameterised these by writing the potential in the form

$$\tilde{V}_E(\underline{r},\underline{r}') = V(r) + \sum_{i=1}^{N} \frac{\tilde{v}_i(r)\,\tilde{v}_i(r')}{E - E_i + \frac{1}{2}iW_i} \qquad (5.1)$$

where V(r) is the usual optical potential and the second term takes account of the gross-structure resonances. The summation runs over all the resonances, and E_i is the energy of the i^{th} resonance and W_i its width. The functions v(r) are represented for ease of computation by square wells. Providing the resonances do not overlap the corresponding scattering amplitude has the form

$$f = f_0 + \sum_i \frac{\Gamma_i^{\uparrow}(E)}{E - (E_i + \Delta) + \frac{1}{2}i\left(W + \Gamma_i^{\uparrow}(E)\right)} \qquad (5.2)$$

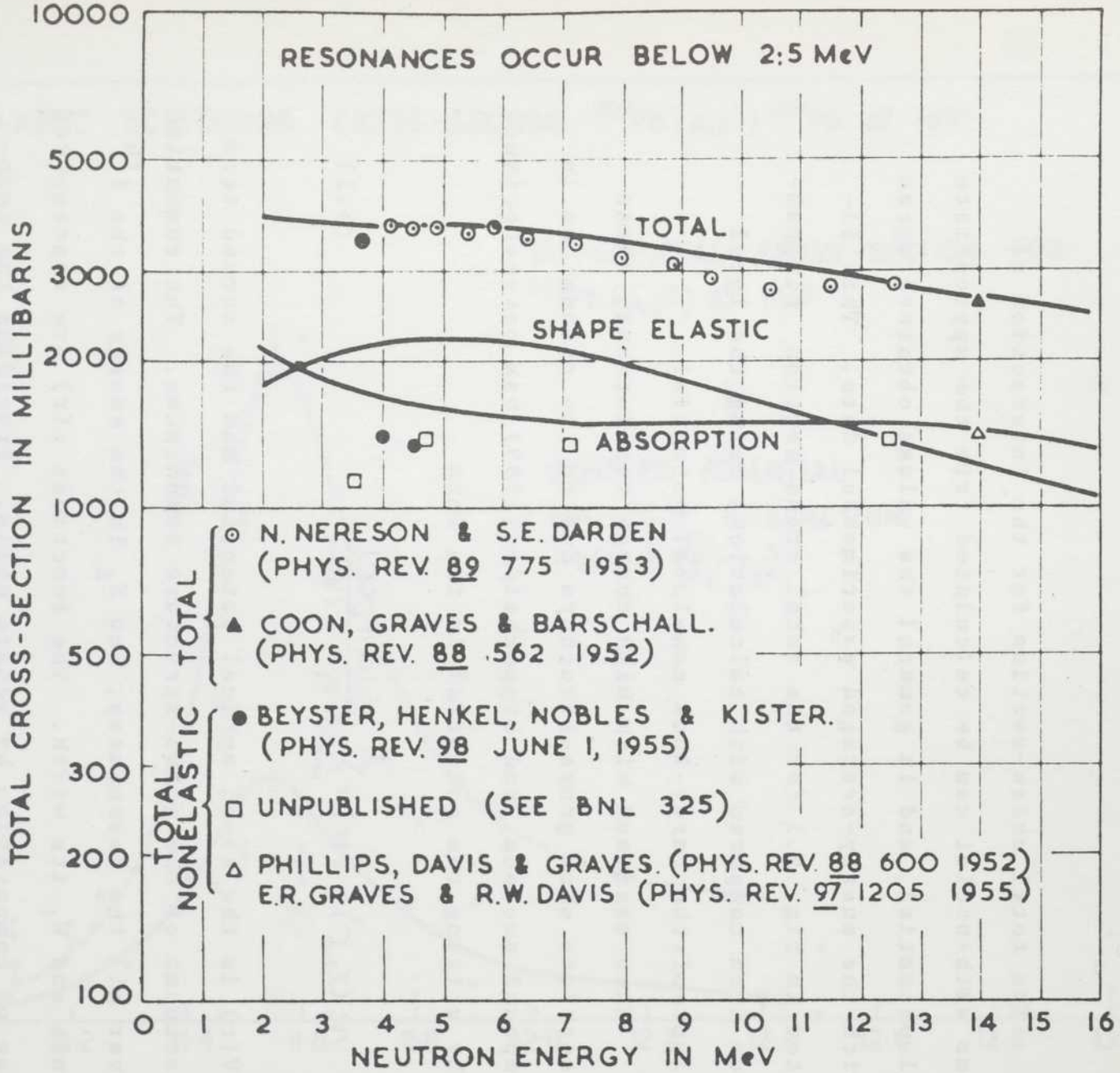

Fig.5.1

Total cross-sections for neutrons on iron, compared with calculations using the local equivalent of the Perey-Buck potential. (Wilmore and Hodgson, 1964).

where Δ is the level shift and the escape width

$$\Gamma_i^{\uparrow}(E) = \int \nu(r)\, \psi_E^{(o)}(r)\, dr \qquad (5.3)$$

and $\psi_E^{(o)}(r)$ is the elastic scattering wavefunction.

The observed resonances are interpreted as intermediate or gross-structure resonances corresponding to doorway states in the nuclear excitation process. Lipperheide fitted the most prominent resonances and hence obtained the parameters of the intermediate states.

A microscopic understanding of the work may be obtained using the wave equation for the elastic scattering wavefunction in the Feshbach formalism

$$\left[E - H_{OPT} - \sum_m \langle \phi_o | PHQ | \phi_m \rangle \frac{1}{E-\varepsilon_m} \langle \phi_m | QHP | \phi_o \rangle\right] U_o(r_c) = 0 \qquad (5.4)$$

where $\phi_o(r_1 \ldots r_A)$ and $\phi_m(r_o \ldots r_A)$ are bound state wavefunctions for negative energy states and in the continuum respectively, P the operator projecting the elastic channel out of the total wavefunction, and $U_o(r_o)$ the scattering wavefunction. This expression contains all the resonances so it is necessary to average over the fine structure in order to obtain an expression containing the gross-structure resonances. This may be done by weighting with a Lorentzian of width W and integrating

over energy, thus introducing an additional term $\frac{1}{2}iW$ in the denomination of (5.4). Making the identification

$$v(r) = \langle \phi_0 | PHQ | \phi_m \rangle \tag{5.5}$$

gives exactly the form (5.1) for the interaction potential.

Hay (1969) has recently made a microscopic calculation of the gross-structure resonances by diagonalising the 2p1h matrix with an effective zero-range interaction and Saxon-Woods wavefunctions. This gives the energies of the resonances and their widths are obtained from the expression

$$\Gamma_m^{\uparrow} = \frac{2k}{E} \gamma_m^2 \tag{5.6}$$

where

$$\gamma_m = \langle \phi_m | QHP | \phi_0 \mu_0 \rangle \tag{5.7}$$

His results for the escape widths of $\frac{1}{2}^+$ states in Ca^{41} are shown in fig. 5.2. A comparison with the experimental data shows that many more states are observed, and that they have smaller widths, indicating that the states are fragmented and mixed by coupling to 3p2h and higher configurations. However, as shown in fig. 5.3, the calculated and experimental strength

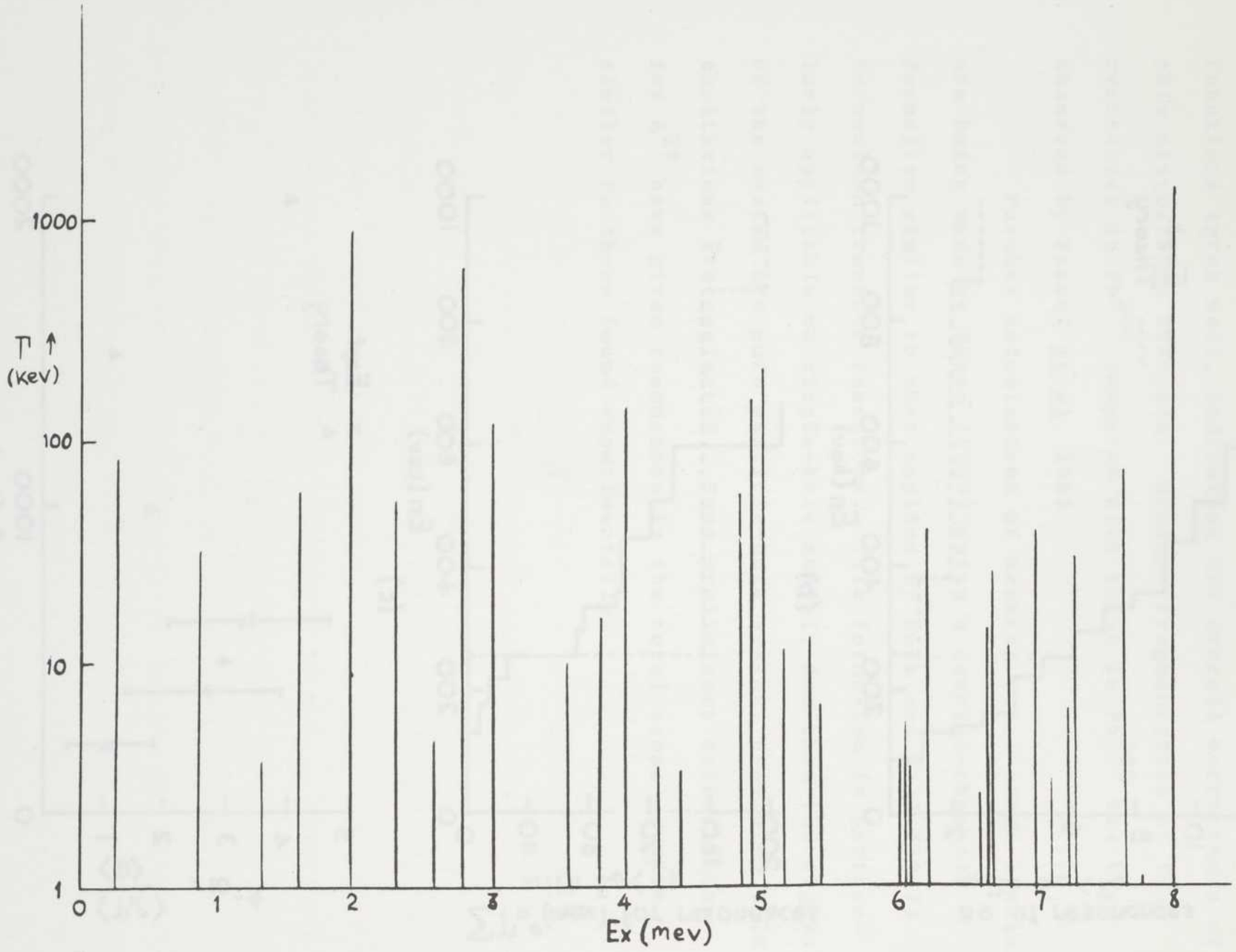

Fig.5.2

Espace widths of $\frac{1}{2}^+$ states in Ca^{41}. (Hay, 1969).

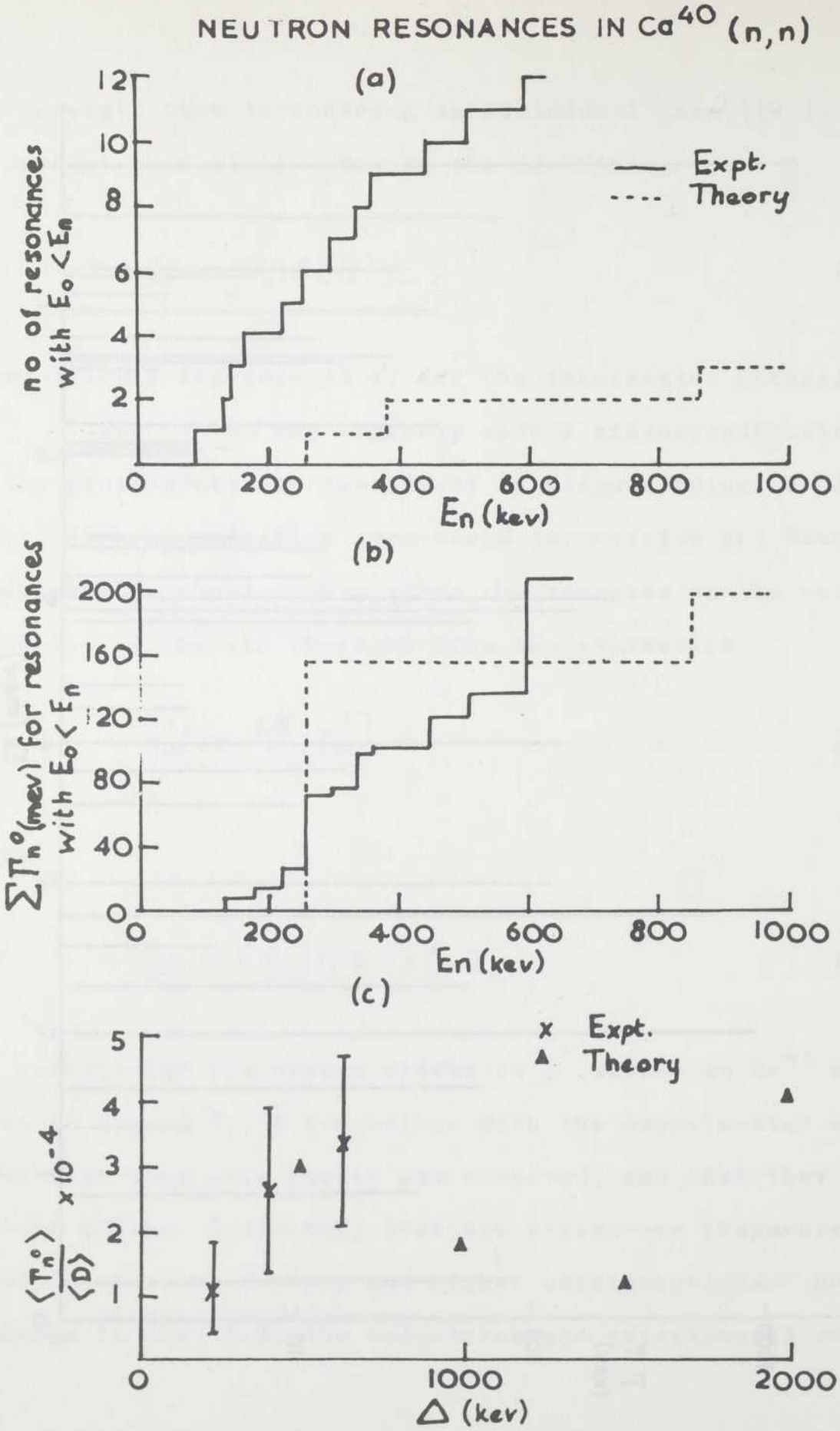

Fig.5.3 Neutron resonances in Ca^{40}. Cumulative plots of the numbers (a) and strengths (b) of the resonances and of the strength function, for the experimental data and for the calculations of Hay (1969).

functions agree well, indicating the overall correctness of this microscopic analysis. Similar fragmentation of the resonances in Pb^{206} compared with those in Pb^{208} has been observed by Farrel et al, 1965.

Further calculations of neutron total cross-sections are being made by Edens (1969) using a coupled-channels formalism similar to that applied by Buck and Hill (1967) to nucleon transfer reactions. This formalism is particularly applicable to single-hole nuclei, for then the eigenstates of the system are pure particle-hole states, providing 2p2h excitations are neglected. Some preliminary calculations for K^{39} have given resonances in the total cross-section similar to those found experimentally.

6. DISCUSSION

The work summarised in this review shows that over the last few years there has been an impressive development in the detailed microscopic understanding of many nuclear reactions in terms of the basic nucleon-nucleon interactions. To a great extent this has either justified the phenomenological formulae or rendered them superfluous.

It is perhaps an appropriate moment to consider the direction this work is likely to take in the future and what is likely to be learnt from it. In the first place it can confidently be predicted that there will be further extensive microscopic calculations of the differential cross-sections of a wide range of nuclear reactions that will show increasingly good agreement with the experimental data and may even impose useful constraints on the parameters of the nucleon-nucleon interaction. Polarisation measurements will be increasingly important and as they will certainly prove more difficult to fit than the differential cross-sections and they will stimulate further detailed developments of the theory.

The distinction between nuclear reaction and nuclear structure calculations is now becoming blurred and it is increasingly usual for the calculation to be made as a whole and then the measure of agreement to the data is a confirmation of both the reaction and the structure theories.

It may be useful to use reactions that enable nuclei far from the stable valley to studied, in particular the multi-nucleon transfer reactions. These are likely to be increasingly important in nuclear reaction studies. Higher order processes are of interest for the development of nuclear reaction theory, and these can be most easily studied in reactions where simpler processes are forbidden.

Particularly extensive microscopic calculations have been made of inelastic scattering, and further advances are likely to be made in the form of the effective interaction and in the ways used to overcome the difficulties associated with the hard core. It is also a powerful tool for studying nuclear wavefunctions and is giving useful information on the extent to which higher excitations, including particularly core polarisations, must be taken into account. It is however important to ask whether this information cannot be obtained more easily in other ways, for example by measurements of gamma transition rates. This is certainly easier when the transitions are strong, and the calculations are generally simpler. In other cases the transition may be too weak and it is easier to use inelastic scattering. Thus to some extent the two processes are complementary.

The developments of the last few years have made it possible to calculate the main features of most elastic and simple inelastic and one-nucleon transfer reactions by micro-

scopic calculations starting from the nucleon-nucleon interaction. The corresponding polarisations can be calculated with less confidence, and further detailed developments of nuclear reaction and nuclear structure theories will increasingly depend on the availability of accurate polarisation data with which that predictions can be compared.

I thank all who contributed to this review by discussion and by sending preprints of their work, in particular Dr J.R. Rook, Dr D.Wilmore, Mr W.D. Hay, Mr D.J. Edens, Dr J. Reading, Dr A. Budzanowski and Professor G.W. Greenlees.

REFERENCES

Alster, J., Shreve, D.C., and Peterson, R.J., Phys. Rev. 144, 999, 1966.

Anderson, J.D., Bloom, S.D., Wong, C., Hornyak, W.F., and Madsen, V.A., Phys. Rev. 177, 1416, 1969.

Arvieu, R., Salusti, E., and Veneroni, M. Phys. Lett. 8, 334, 1964

Auerbach, E.H., Dover, C.B., Kerman, A.K., Lemmer, R.H., and Schwarcz, E.H., Phys. Rev. Lett. 17, 1184, 1966.

Auerbach, E.H., Quereshi, H.M., and Sternheim, M.M., Phys. Rev. Lett. 21, 162, 1968.

Auerbach, N., Hügner, J., Kerman, A.K., and Shakin, C.M. preprint 1969.

Austin, S.M,, and Crawley, G.M., Phys. Lett. 27B, 570, 1968.

Austin, S.M., Locard, P.J., Benenson, W. and Crawley, G.M., Phys. Rev. 176, 1227, 1968.

Balashov, V.V., and Yadrovisky, E.L., Phys. Lett. 25B, 67, 1967.

Ball, G.C., and Cerny, J., Phys. Rev. 177, 1466, 1969

Barnard, A.C.L., Phys. Rev. 155, 1135, 1967

Barrat, R.C., Brodsky, S.J., Erickson, G.W. and Goldhaber, M.H., Phys. Rev. 166, 1589, 1968.

Bartels, E.C., Cosman, E.R., Kerman, A.K., and Spencer, J.E., Phys. Rev. 179, 995, 1969.

Bassel, R.H., Satchler, G.R., Drisko, R.M., and Rost, E., Phys. Rev. 128, 2693, 1962.

Batty, C.J., Benner, B.E., Freidman, E., Tschalar, C., Williams, L.E., Clough, A.S., and Hunt, J.B., Nucl. Phys. A116, 643, 1968; A120, 297, 1969.

Batty, C.J., Freidman, E., and Greenlees, G.W., Nucl. Phys. A127, 368, 1969.

Batty, C.J., Tschalar, C., Symposium on Nuclear Reactions Mechanisms and Polarisation Phenomena (Laval) 1969.

Bethe, H.A., Phys. Rev. 167, 879, 1968.

Bethe, H.A., and Elton, L.R.B., Phys. Rev. Lett. 20, 745, 1968.

Bethe, H.A., and Siemens, P.J., Phys. Lett. 27B, 549, 1968.

Blin-Stoyle, R.J., Phys. Letters, 29B, 12, 1969.

Bloom, S.D., Anderson, J.D., Hornyak, W.F., and Wong, C., Phys. Rev. Lett. 15, 264, 1965.

Bondorf, J.P., and Bund, G.W.,

Bondorf, J.P., Jagare, S., and Lutken, H., Phys. Lett. 21, 185, 1966.

Brueckner, K.A., Lockett, A.M., and Rotenberg, M., Phys. Rev. 121, 255, 1961.

Buck, B., Phys. Rev., 130, 712, 1963.

Buck, B., and Hill, A.D., Nuc. Phys. A95, 271, 1967.

Buck, B., Stamp, A.P., and Hodgson, P.E., Phil. Mag. 8, 1805, 1963.

Budzanowski, A., Dudek, A., Grotowski, K., Strzalkowski, A., Quebec Conference Paper, 1969.

Budzanowski, A., Hill, A.D., and Hodgson, P.E., Nuc. Phys. A117, 509, 1968.

Budzanowski, A., Grotowski, K., Strzalkowski, A., Private Communication, 1969.

Bugg, W.M., Condo, G.T., Cohn, H.O., and Hill, A.D., Nuc. Phys. A124, 212, 1969.

Burhop, E.H.S., Nuc. Phys. B1, 438, 1967.

Collard, H.R., Elton, L.R.B., and Hofstadter, R., Landolt-Bornstein tables, new series group 1. Vol. 2, Ed. K.H. Hellw (Springer Verlog, 1967).

Davis, D.H., Lovell, S.P., Csejthey-Barth, M., Sacton, J., Schorochoff, G., and O'Reilly, M., Nuc. Phys. B1, 434, 1967.

De Toledo Piza, A.F.R., Kerman, A.K., Fallieros, S., and Venter, R.H., Nuc. Phys. 89, 369, 1966.

Dickens, J.K., Perey, F.G., Silva, R.J., and Tamura, T., Phys. Lett. 6, 53, 1963.

Donnely, I. J., Phys. Letters, 28B, 161, 1968.

Dost, M., Hering, W.R., and Smith, W.R., Nuclear Phys. A93, 357, 1967.

Duhm, H.H., Detraz, C., and Finlay, R., Proceedings of the Second International Conference on Nuclear Isospin (Asilomar, 1969).

Edens, D.J., Private communication 1969.

Elton, L.R.B., Nuc. Phys. 23, 681, 1961.

Elton, L.R.B., Phys. Rev. 158, 970, 1967.

Elton, L.R.B., Proceedings of the symposium in the use of Nimrod for nuclear structure physics, RHEL/R166, 1968.

Faessler, A., Glendenning, N.K., and Plastino, A., UCRL-16976, 1966.

Farrell, J.A., Kyker, G.C., Bilpuch, E., and Newson, W., Phys. Lett. 17, 286, 1965.

Feshbach, H., Annals of Physics 5, 357, 1958.

Fisher, T.R., Safrata, R.S., Shelley, E.G., McCarthy, J., Austin, S.M., and Barret, R.C., Phys. Rev. 157, 1149, 1967.

Frahn, W.E., and Lemmer, R.H., Nuovo Cimento 5, 1567, 1967.

Freidman, E., (Preprint, 1969).

Fulling, S.A., and Satchler, G.R., Nuc. Phys. A111, 81, 1968.

Giai, N.V., Sawicki, J., and Vinh Mau, N., Phys. Rev. 141, 913, 1966.

Gillet, V., and Sanderson, E., Nuc. Phys. 54, 472, 1964.

Glashausser, C., Harvey, B.G., Hendrie, B.L., Mahoney, J., McClatchie, E.A., and Saudinos, J., Phys. Rev. Lett. 21, 918, 1968.

Glaushausser, C., and Rickey, M.E., Phys. Rev. 154, 1033, 1967.

Glaushausser, C., De Swiniarski, R., Thirion, J., and Hill, A. D., Phys. Rev. 164, 1437, 1967.

Glendenning, N.K., Phys. Lett.21, 549, 1966; UCRL Report 18104, 1968; Montreal Conference, 1969.

Glendenning, N.K., Harvey, B.G., Hendrie, D.L., Jarvis, O.N., and Mahoney, J., Proceedings of the International Conference on Nuclear Structure (Gatlinberg) 25, 1966.

Glendenning, N.K., and Veneroni, M., Phys. Lett. 14, 228, 1965.

Gray, W.S., Kenefick, R.A., Kraushaar, J.J., and Satchler, G.R., Phys. Rev. 142, 735, 1966.

Greenlees, G.W., Pyle, G.J., and Tang, Y.C., Phys. Rev. 171, 1115, 1968.

Greenlees, G.W., Pyle, G.J., and Tang, Y.C., Phys. Lett. 26B, 658, 1968.

Greenlees, G.W., Private communication, 1969.

Harney, H.L., Nuc. Phys. A119, 591, 1968.

Hauser, L.F., Stelts, M.L., Vidol, J.G., Wesolowski, J.J., and Madsen, B.A., Phys. Rev. 174, 1155, 1968.

Hay, W.D., Thesis (Oxford) 1969.

Hayakawa, S.I., Kraushaar, J.J., Kunz, P.D., and Rost, E. Phys. Lett. 29B, 327, 1969.

Hirt, W., Nuc. Phys. B9, 447, 1969.

Hodgson, P.E., Canad. J. Phys. 45, 449, 1967; Nuc. Phys. A103, 127, 1967.

Hofstadter, R., Nuclear and Nuclear Structure (Benjamin) 1963.

Holmquist, B., and Wiedling, T., Phys. Lett. 27B, 411, 1968.

Hufner, J., and Shakin, C.M.,

Ikeda, K., Fuju, S., and Fujita, F.I., Phys. Lett. 2, 169, 1962.

Jackson, D. F., Phys. Lett. 14, 118, 1969.

Jackson, D.F., and Kembhavi, V.K., (Preprint) 1969.

Johnson, M.B., Owen, L.W., and Satchler, G.R., Phys. Rev. 142, 748, 1966.

Johnson, R.C., and Santos, F.D., Phys. Rev. Lett. 19, 364, 1967.

Kerman, A.K., and McKellar, A.D., and Reading, J.F., (Private communication) 1969.

Kerman, A.K., McManus, H., and Thaller, R.M., Ann. of Phys. 8, 551, 1959.

Kobayashi, S., Nagamine, K., Uchida, A., Karoti, K., Imaizumi M., and Mikuni, A., Prog. Theor. Phys. (Japan) 40, 1451, 1968.

Kossanyi-Demay, P., Roussel, P., Faraggi, H., and Schaeffer, R., Preprint, 1969.

Kunz, P.D., Rost, E., Johnson, R.R., and Hayakawa, S.I., Colorado, Preprint COO-535-592.

Kuo, T.T.S., Nuc. Phys. A122, 325, 1968.

Lane, A.M., Nuc. Phys. 35, 676, 1962.

Lee, L.L., and Schiffer, J.P., Phys. Rev. Lett., 12, 108, 1964; Phys. Rev. 136, B405, 1964.

Lemmer, R.H., Maris, Th. A., and Tang, Y.C., Nuc. Phys. 12, 618, 1959.

Lipperheide, R., Private communication 1969.

Love, W.G., Owen, L.W., Drisko, R.M., Satchler, G.R., Stafford, R., Philpott, R.J., and Pinkston, W.T., Phys. Lett. 29B, 478, 1969.

Love, W.G., and Satchler, G.R., Nucl. Phys. A101, 424, 1967.

Lovacs, I., Nuclear Physics 81, 353, 1966.

Luetzelschwab, J.W., and Hafele, J.C., Phys. Rev. 180, 1023, 1969.

Madsen, V.A., Nuc. Phys. 80, 177, 1966.

Madsen, V.A., and Tobocoman, W., Phys. Rev. 139, B864, 1965.

Mahaux, C., and Weidnmüller, H.A., Nuc. Phys. 89, 33, 1967.

Marangoni, M., and Sarius, A.M., Phys. Lett. 24B, 218, 1967.

Meldner, H., Phys. Rev. 178, 1815, 1968.
Morgan, C.G., and Jackson, D.F. (Preprint) 1969.
Myers, W.D., University of California Radiation Laboratory Report, No.18214, 1968.

Nelson, J.M.; Chant, N.S., and Fisher, P.S. (Private communication, 1969.

Nolan, J.A., Schiffer, J.P., and Williams, M., Phys. Lett. 27B, 1, 1968.

Oaki, S., and Tamura, T., Nuc. Phys. 31, 185, 1962.

Parkinson, W.C., Hendrie, D.L., Duhm, H.H., Mahoney, J. Sandinos, J., and Satchler, G.R., Phys. Rev. 178, 1976, 1969.

Pascolini, A., Pisent, G., and Zardi, F., (Preprint) 1969.

Perey, F.G., Phys. Rev. 131, 745, 1963.

Perey, F.G., and Perey, C.M., Phys. Lett. 26B, 123, 1968.

Perey, F.G., Perey, C.M., Dickens, J.K., and Silva, R.J., Phys. Rev. 175, 1460, 1968.

Perez, S.M., Thesis (Oxford) 1968

Petrovich, F., McManus, H., Madson, V.A., and Atkinson, J. Phys. Rev. Lett. 22, 895, 1969.

Picard, J., Beer, O., El Behay, A., Lopato, P., Teren, Y., Vallois, G., and Schaeffer, R., Nuc. Phys. A128, 481, 1969.

Pisent, G., and Sarius, A.M., Nuc. Phys. A91, 561, 1967.

Planstino, A., Faessler, A., and Moszkowski, S.A., Bull, Ann. Phys. Soc. 11, 320, 1966.

Ramavataram, S., Wilmore, D., and Edens, D.J., Montreal Conference Paper, 1969.

Raynal, J., Melkanoff, M.A., and Sawada, T., Nuc. Phys. A101, 369, 1967.

Reynolds, J.T., Slavik, C.J., Lubitz, C.R., and Francis, N.C., Phys. Rev. 176, 1213, 1968.

Robson, D., Phys. Rev., 137, B535, 1965.

Robson, B.A., PHys. Lett. 26B, 501, 1968.

Rook, J.R., 1968 (Unpublished lectures); Phys. Lett. 29B 86, 1969, and private communication.

Rost, E. Phys. Lett. 26B, 184, 1968.

Santos, F.D., Private communication 1969.

Sarius, A.M. and Marangoni, M., Nuc. Phys. A132, 433, 1969.

Satchler, G.R., Nuc. Phys. 55, 1, 1964; Ibid 77, 481, 1966.

Satchler, G.R., Nuc. Phys. A91, 75, 1967; Ibid A92, 273, 1967.

Satchler, G.R., Drisko, R.M., and Bassel, R.H., Phys. Rev. 136 B637, 1964.

Schaeffer, R., Nuc. Phys. A132, 186, 1969.

Schiffer, J.P., Nuc. Phys. 46, 246, 1963.

Schrack, R.A., Leiss, J.E., and Penner, S., Phys. Rev. 127 1772, 1962.

Schwarcz, E.H., Phys. Rev. 149, 752, 1966.

Sherif, H., Nuc. Phys. A131, 532, 1969.

Sherif, H., and Blair, J.S., Phys. Lett. 26B,489, 1968.

Stamp, A.P., Phys. Rev. 153, 1052, 1967.

Stelson, P.H., and McGowan, F.K., Ann. Rev. Nuc. Sci. 13, 163, 1963.

Stelson, P.H., and Grodzin, L., Nuclear Data A1, 21, 1965.

Tamura, T., Rev. Mod. Phys. 37, 679, 1965a; Nuc. Phys. 73 241, 1965b.

Tamura, T., Isobaric Spin in Nuclear Physics (Ed. J.D. Fox and D. Robson, 447) 1966; Phys. Lett. 22, 644, 1966.

Tarbutton, R.M., and Davies, K.T.R., Nuc. Phys. A120, 1, 1968.

Thurlow, N., Nuc. Phys. A109, 471, 1968.

Tjin a Djie, H.R.E., Mulder, K., Udo, F., Gronewald, A., Koerts, L.A.C., Hill, A.D., Hodgson, P.E., Nuc. Phys. A106, 85, 1968.

Van Niftrik, G.J.C., Peterson, G:A., and Rawitscher, G.H., Phys. Rev. 177, 1797, 1969.

Van Niftrik, G.J.C., Nuc. Phys. A131, 574, 1969.

Vautherin, D., and Veneroni , M., (Preprint) 1PNO/TH 149, 1969.

Vinh Mau, N., Trieste Preprint 1PNO/TH 154, 1969.

Watson, K.M., Phys. Rev. 89, 575, 1958.

Wesolowski, J.J., Schwarcz, E.H., Roos, P.G., and Ludemann, C.A., Phys. Rev. 169, 878, 1968.

Wilets, L., Rev. Mod. Phys. 30, 542, 1958.

Wilmore, D., and Hodgson, P.E., Nuc. Phys. 55, 673, 1964.

Wong, C., Anderson, J.D., McClure, J., 160, 769, 1967.

Zimanyi, J., and Gyarmati, B., Phys. Rev. 174, 1112, 1968.

LA D.W.B.A. ANTISYMETRISÉE ET L'ÉTUDE DES FONCTIONS D'ONDE MICROSCOPIQUES.

Richard SCHAEFFER

INTRODUCTION

Un modèle microscopique pour la diffusion inélastique de protons à basse et moyenne énergie est intéressant à plusieurs points de vue. La compréhension du mécanisme d'interaction nucléon-noyau est d'une part l'étape indispensable dans la description de réactions plus complexes. D'autre part, une théorie quantitative de la diffusion (pp') est un outil spectroscopique extrêmement puissant qui rend possible l'étude des fonctions d'onde des états excités du noyau à l'aide de cette réaction. Nous nous intéressons plus particulièrement dans ce travail aux niveaux collectifs, caractérisés par le grand nombre de nucléons qui participent à l'excitation. Dans ce cas, les effets de moyenne dans l'amplitude de diffusion réduisent fortement le nombre de paramètres entrant dans le calcul, notamment pour la force nucléon-nucléon dont seules les composantes indépendantes du spin contribuent. Pour cette raison d'ailleurs, le taux de

transition électromagnétique est généralement utilisé pour caractériser ces états et faire la distinction entre les divers modèles nucléaires. Il n'est cependant sensible qu'aux excitations de protons et ne donne une information complète sur la collectivité du niveau considéré que dans le cas d'un état de spin isotopique T = 0 où protons et neutrons jouent le même rôle. L'approximation des phases aléatoires (R.P.A.) s'est ainsi révélée très bonne pour les noyaux à double couche complète (^{12}C, ^{16}O, ^{40}Ca). Lorsque l'une au moins des couches est ouverte, une autre expérience sensible aux neutrons du noyau est nécessaire pour préciser le rôle de ces derniers. La diffusion (pp') à basse et moyenne énergie est, à cet égard, privilégiée car l'interaction nucléon-nucléon est bien plus intense dans le système p-n que dans le système p-p. Celle-ci a d'autre part une forme relativement simple. A plus haute énergie, par contre, il est nécessaire de faire intervenir une interaction effective pour éliminer les effets du coeur dur, avec toutes les complications qu'entraîne une force dépendant de la vitesse des particules.

Le modèle vibrationnel fournit, certes, déjà une interprétation commode des sections efficaces (pp') et permet de caractériser l'intensité de l'excitation par un paramètre de déformation $\beta_{pp'}$.

Il n'y a cependant pas de correspondance directe entre celui-ci et les fonctions d'onde microscopiques, alors que la déformation $\beta_{E.M.}$ obtenue par excitation coulombienne ou par diffusion inélastique d'électrons est très simplement reliée à la valeur moyenne de l'opérateur électro-magnétique entre l'état initial et final du noyau. C'est pourquoi il est sans doute illusoire de vouloir obtenir des renseignements séparément sur les propons et sur les neutrons à l'aide des différences entre les paramètres $\beta_{pp'}$ et $\beta_{E.M.}$.

La simple extension du modèle vibrationnel, en remplaçant le facteur de forme phénoménologique par un facteur de forme calculé dans le cadre du modèle des couches s'est révélé fort décevante. Même dans des cas très somples comme celui de la diffusion sur un noyau avec une particule à l'extérieur d'une double couche complète, les sections efficaces sont bien trop faibles et l'accord pour les distributions angulaires généralement assez pauvre. D'un autre côté, pour des états collectifs qui sont connus pour être bien décrits par la R.P.A., grâce à d'autres expériences, il n'est pas possible d'obtenir un accord satisfaisant avec l'expérience de diffusion (pp'). Nous allons cependant voir que, grâce à l'antisymétrisation[1,2] de la fonction d'onde de toutes les particules, libres et liées, protons et neutrons, une amélioration considérable va pouvoir être apportée à la description du mécanisme de réaction. Moyennant des hypothèses relativement générales, il est possible de montrer [2]

que tenir compte de l'antisymétrisation (et du caractère d'échange de la force nucléon-nucléon) revient à inclure le terme d'échange dans les éléments de matrice de la force à deux corps qui interviennent en D.W.B.A. Ceci permettra d'expliquer les effets les plus importants dans la diffusion (pp') et d'obtenir[1,2] pratiquement en valeur absolue les sections efficaces pour de bonnes fonctions d'onde, sans renormalisation de l'interaction nucléon-nucléon libre.

Dans la première partie, nous exposons le formalisme que nous avons utilisé et mettons en évidence la part de phénoménologie qui reste dans notre théorie et aussi les approximations que nous avons faites. Nous passons ensuite en revue les divers modèles nucléaires qui décrivent les excitations collectives. Le chapitre III est entièrement consacré à des approximations simples que nous n'avons pas utilisées dans le calcul réel, mais qui permettent de dégager les phénomènes physiques essentiels. Enfin, dans la quatrième partie nous confrontons, pour les noyaux d'isospin $T = 0$, notre modèle avec l'expérience, ce qui nous permettra ensuite d'étudier les noyaux à une seule couche fermée et de voir la différence entre les excitations réelles et les descriptions microscopiques qui en ont été données.

LES NOYAUX À DOUBLE COUCHE COMPLÈTE

Maints calculs ont déjà été faits avec le modèle microscopique à l'aide de l'approximation des ondes distordues, mais en négligeant les effets d'échange et en utilisant une force nucléon-nucléon phénoménologique. Le principe de ces calculs était de fixer l'intensité de la force en normalisant la section efficace théorique, pour l'excitation d'un niveau donné, d'après la section efficace expérimentale. Comme nous l'avons vu, c'est surtout la valeur absolue de la section efficace qui est sensible à la description microscopique des niveaux collectifs. Le test des amplitudes spectroscopiques était donc très difficile, d'autant plus que l'intensité de la force obtenue variait avec les noyaux considérés et pour un noyau donné avec les états excités étudiés. Nous avons vu, dans le modèle de rayon fini pour l'échange, que les effets dus à l'antisymétrisation des fonctions d'onde étaient essentiellement variables avec l'énergie: la force effective dépend donc aussi de l'énergie de la particule incidente. De plus, même en adaptant la portée de la force, il est très difficile de reproduire les distributions angulaires expérimentales. Un exemple typique est celui des états 3^- et 5^- les plus bas du ^{40}Ca. La description microscopique (R.P.A.) de ces états[3] est probablement bonne comme cela a été

montré par les calculs de diffusion d'électrons[4] et de protons à 155 MeV[5] où "l'impulse approximation" est réputée valable. Pour la diffusion de protons à 30 MeV par contre, les calculs D.W.B.A. avec une force effective ont donné de piètres résultats. C'est ce qui a amené Satchler à conclure que l'approximation des ondes distordues n'était pas valable dans ce cas[6].

Nous avons donc choisi ces états pour voir quelles améliorations notre description microscopique de la diffusion (pp') allait pouvoir apporter. En plus d'une bonne description des états excités les plus bas, nous disposons en effet d'une gamme assez variée d'expériences, à des énergies suffisamment différentes (55,30 et 20 MeV) pour couvrir une large partie du domaine où l'approximation de Born avec des ondes distordues devrait être valable. Nous avons aussi examiné les autres noyaux à double couche complète où, en général, la R.P.A. décrit bien les états collectifs. Un grand nombre de paramètres entre dans notre calcul, mais nous allons montrer qu'il est possible de les fixer avec précision à l'aide d'autres expériences que celles que nous nous proposons d'expliquer.

A - LES PARAMÈTRES DU CALCUL

Les paramètres du modèle optique[2] sont fixés par la diffusion élastique. Nous avons vérifié, à 55 MeV où il existe deux ensembles de paramètres très différents qui rendent compte de la section efficace expérimentale, que nos résultats dépendent très peu du potentiel optique choisi. En particulier, ils varient beaucoup moins que ceux obtenus en utilisant le modèle vibrationnel où le facteur de forme aussi dépend des paramètres optiques.

Les paramètres relatifs à la description des états liés sont tirés d'expérience très diverses. Les plus importants sont d'une part les énergies de liaison des orbitales du modèle des couches qui sont bien connus par les expériences de transfert d'une particule et d'autre part la force nucléon-nucléon effective employée dans la plupart des calculs phénoménologiques. Celle-ci est déterminée en ajustant les spectres théoriques et expérimentaux des états excités. La section efficace de diffusion (pp') est peu sensible à la forme radiale des fonctions d'onde des orbitales liées en raison de l'utilisation d'une force de portée finie. Nous avons pris les fonctions d'onde de l'oscillateur harmonique qui avait été utilisées dans le calcul des états de la R.P.A.

Nous avons utilisé le potentiel de Blatt-Jackson pour décrire l'interaction nucléon-nucléon. Celui-ci reproduit

les déphasages libres en dessous de 10 MeV. Cette énergie est sans doute un peu faible, mais ce choix nous évite d'introduire les interactions tenseur et $\vec{L}.\vec{S}$. Les éléments de matrice de ce potentiel ont été comparés[7] à ceux de la matrice de réaction calculée avec les potentiels de Kallio-Kolltweit ou de Hamada-Johnston. C.W.Wong et C.Y.Wong ont ainsi montré qu'une interaction simple pouvait, avec une bonne précision, décrire la diffusion nucléon-nucléon à la surface du noyau. Nous avons cependant légèrement modifié la forme radiale de ce potentiel: au lieu de la forme gaussienne (e^{-r^2/λ^2}) testée par Wong, nous prenons[1,2] une forme de Yukawa ($\frac{e^{-r/\mu}}{r/\mu}$).

Nous avons ainsi fixé tous nos paramètres. Le potentiel que nous utilisons donne à peu près les mêmes résultats qu'une force de Serber avec une intensité de 44 MeV et une portée de 1.37 fm. Nous avons inclus l'interaction coulombienne entre protons.

Nous avons utilisé le formalisme de l'"hélicité nucléaire" donné par J. Raynal[8].

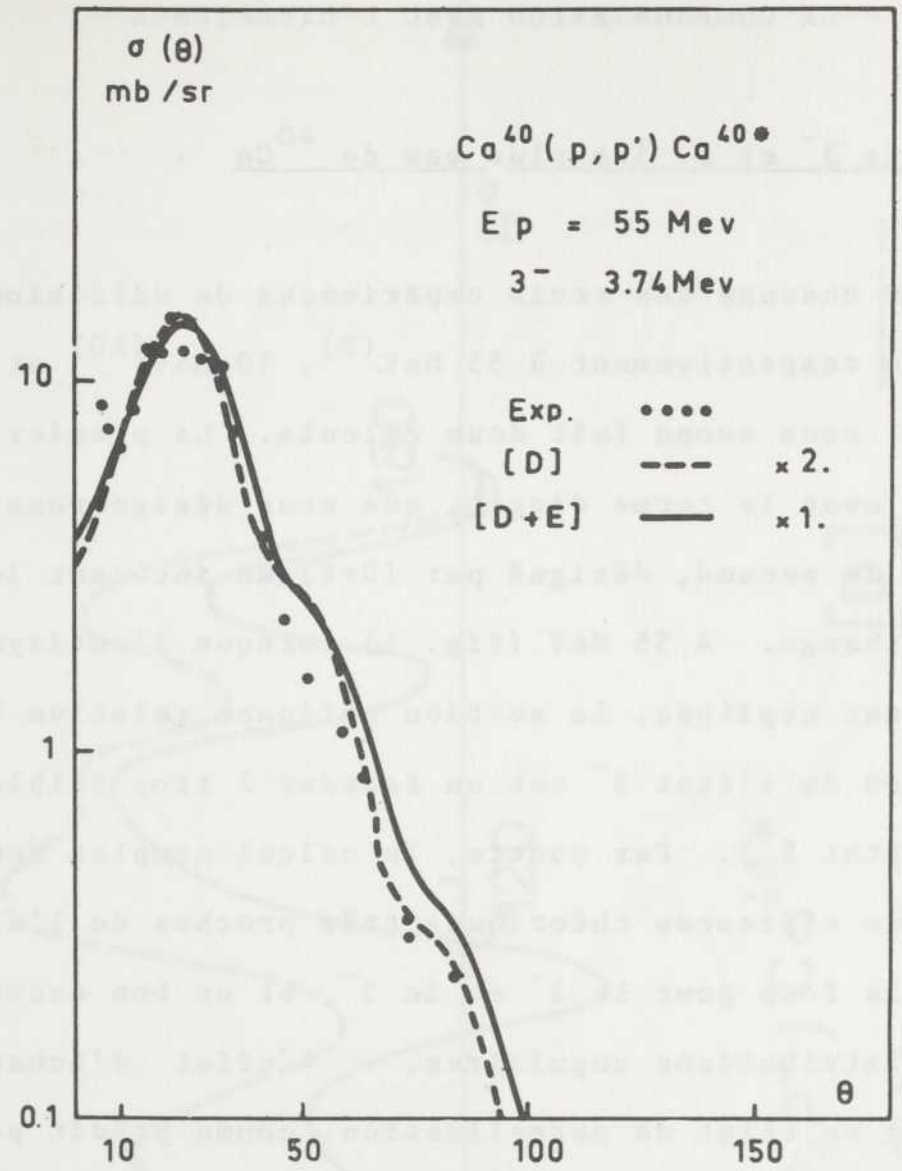

Fig.1 - Section efficace différentielle relative à l'excitation de l'état 3^- à 3,74 MeV du ^{40}Ca. E_p désigne l'énergie du proton incident. Les courbes théoriques sont calculées dans le modèle D.W.B.A. microscopique avec la force nucléon-nucléon libre de Blatt-Jackson (D+E) désigne le calcul fait avec les fonctions d'onde antisymétrisées et (D) le calcul sans la contribution provenant du terme d'échange dans l'amplitude de diffusion. L'état excité est décrit, par le modèle R.P.A. Afin de comparer les distributions angulaires, les sections efficaces ont été multipliées par le facteur de normalisation N indiqué. Ce dernier donne une indication de la qualité de la description microscopique. Pour N = 1, les sections efficaces expérimentales sont obtenues en valeur absolue sans aucun paramètre ajustable pour la diffusion inélastique.

B - LA CONFRONTATION AVEC L'EXPÉRIENCE

I- Les états 3^- et 5^- les plus bas de ^{40}Ca

Pour chacune des trois expériences de diffusion inélastique respectivement à 55 MeV[9], 30 MeV[10] et 20 MeV[11], nous avons fait deux calculs. Le premier, uniquement avec le terme direct, que nous désignerons par (D) et le second, désigné par (D+E) en incluant les termes d'échange. A 55 MeV (fig. 1) lorsque l'antisymétrisation est négligée, la section efficace relative à l'excitation de l'état 3^- est un facteur 2 trop faible (3 pour l'état 5^-). Par contre, le calcul complet donne des sections efficaces théoriques très proches de l'expérience, à la fois pour le 3^- et le 5^-, et un bon accord pour les distributions angulaires. L'effet d'échange est surtout un effet de normalisation, comme prédit par notre modèle de portée nulle[2], mais sur les asymétries calculées avec et sans échange il est possible de voir des différences significatives vers 90° (fig.2).

Les sections efficaces à 30 MeV ont été publiées par Fulling et Satchler, en même temps qu'une analyse microscopique avec une force phénoménologique et sans antisymétriser les fonctions d'onde. Avec une force ajustable la normalisation de la section efficace est arbitraire.

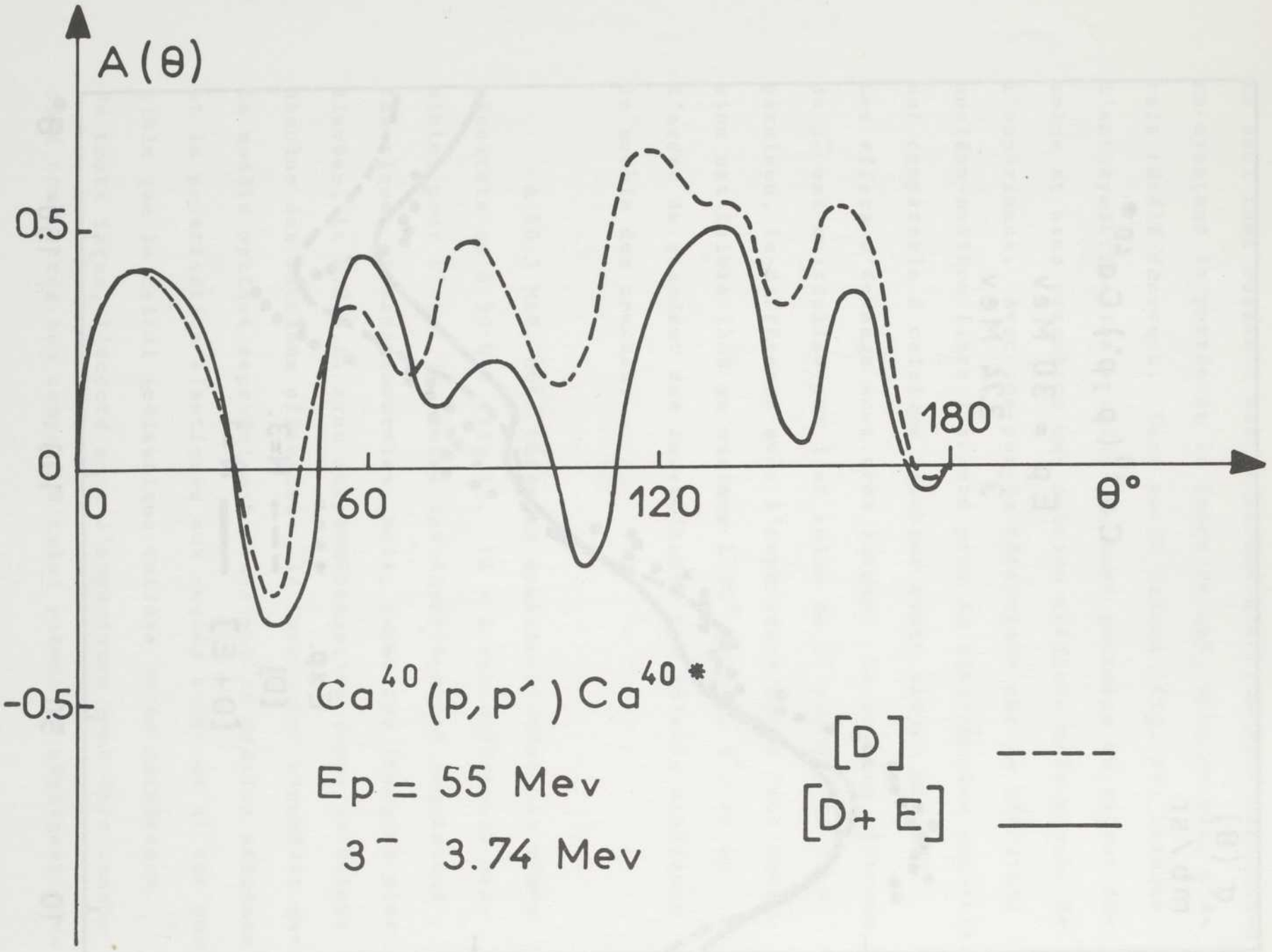

Fig.2 - Asymétrie (pp') à 55 MeV. Etat 3^- à 3,74 MeV du ^{40}Ca. cf fig.1.

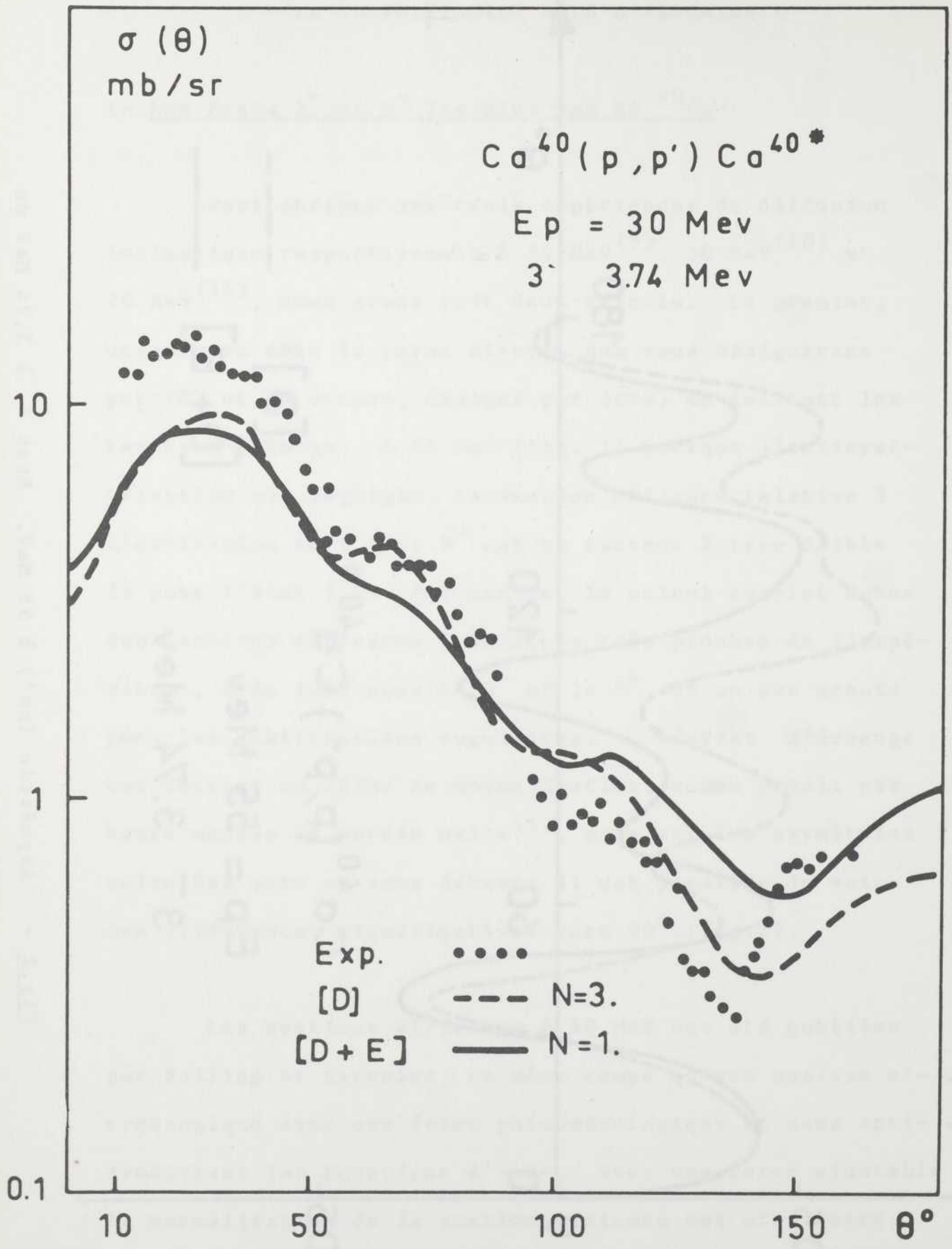

Fig.3 - Section efficace (pp') à 30 MeV. Etat 3^- à 3,74 MeV du ^{40}Ca. cf. fig.1.

Le seul test possible est celui des distributions angulaires en ajustant la portée de la force ce qui, dans ce cas, s'était révélé décevant. Dans notre calcul (fig. 3), lorsque l'antisymétrisation est inclue, nous obtenons en valeur absolue et sans paramètre une section efficace très proche de l'expérience. Avec une portée déterminée par la diffusion nucléon-nucléon libre l'accord pour la distribution angulaire est comparable à celui que Satchler avait obtenu par fit. Les effets d'échange sont très larges: la section efficace du 3^- est multipliée par 3 et celle du 5^- par 8. En comparaison, la différence avec l'expérience après leur inclusion est faible (30% au maximum à 20^o pour le 3^-) et de l'ordre de grandeur des incertitudes des calculs utilisant le modèle des couches.

A 20.3 MeV, nous obtenons qualitativement les mêmes résultats qu'à 30 MeV (fig.4). Il y a une différence sensible, pour l'état 5^-, entre les distributions angulaires théoriques et expérimentales, mais, comme aux énergies plus élevées, la D.W.B.A. avec antisymétrisation donne la valeur absolue des sections efficaces. Il faut noter cependant que le modèle optique reproduisait assez mal la section efficace et la polarisation élastiques aux angles avant et il est possible que le calcul inélastique reflète cette différence. De toute façon, l'accord avec l'expérience peut être considéré comme très bon comparé à celui obtenu en négligeant les

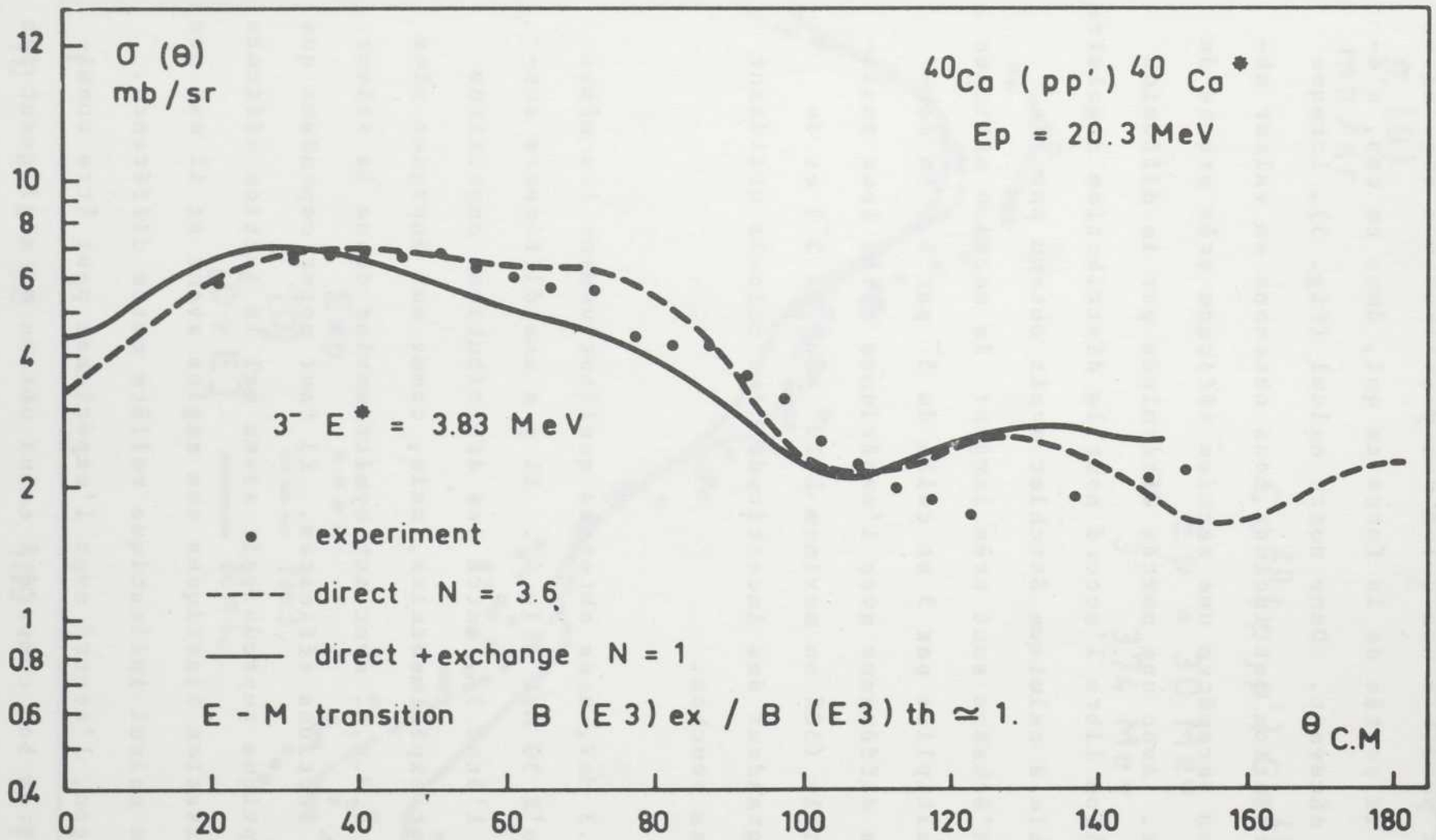

ANTISYMMETRIZED MICROSCOPIC D.W.B.A CALCULATION WITH THE FREE NUCLEON - NUCLEON BLATT - JACKSON POTENTIAL

Fig.4 - Section efficace (pp') à 20,3MeV. Etat 3^- à 3,74 MeV du ^{40}Ca. cf. fig.1.

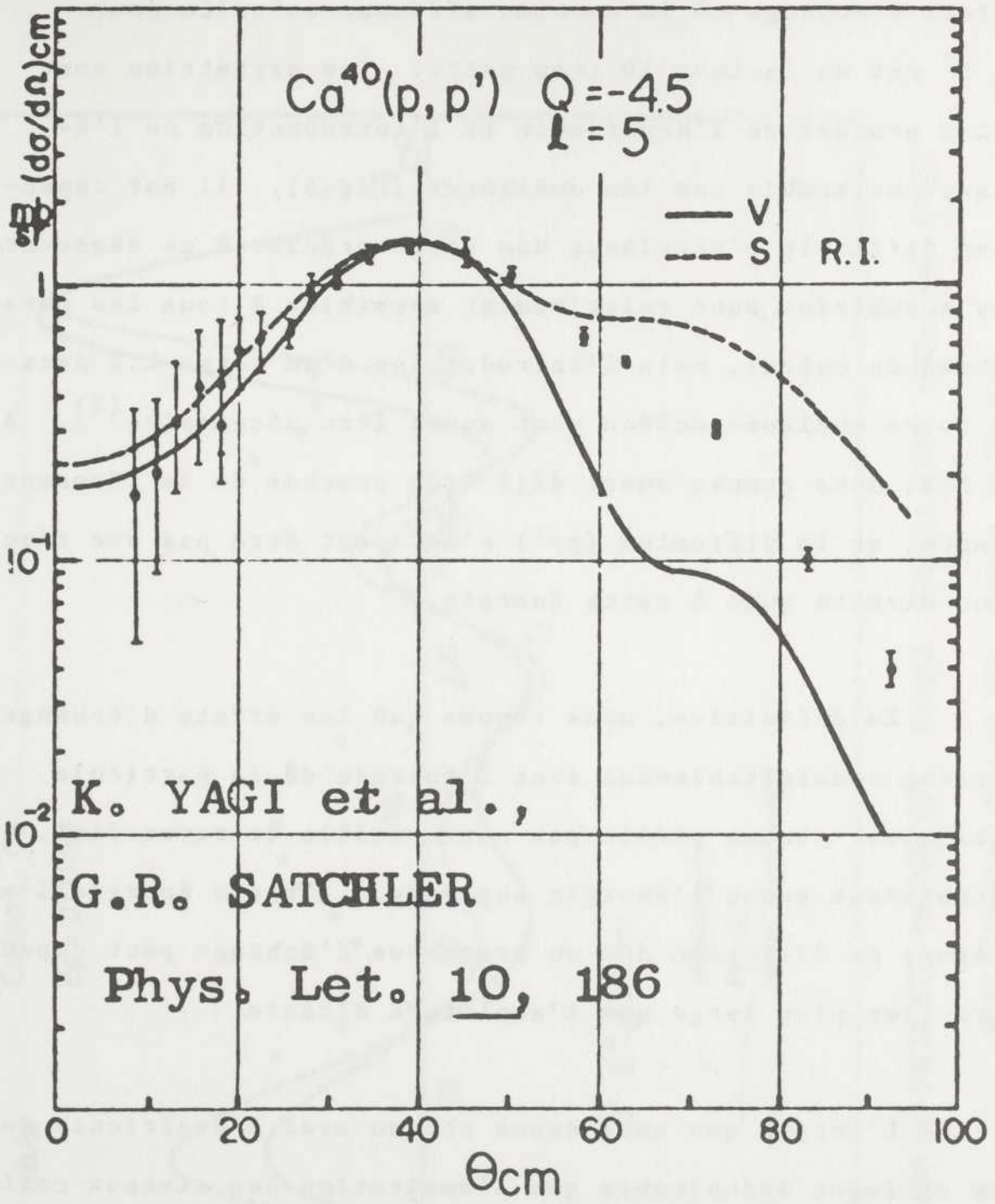

Fig. 4b. An attempt to fit the same data assuming the real interaction. A deformability $\beta_5 = 0.099$ for (V) and $\beta_5 = 0.21$ for (S) are used.

effets d'échange où la section efficace calculée pour le 5^- est un facteur 10 trop petit. Les asymétries sont moins proches de l'expérience et l'introduction de l'échange ne semble pas les améliorer (fig.5). Il est cependant difficile d'attribuer une cause précise à ce désaccord Les asymétries sont relativement sensibles à tous les paramètres du calcul, mais l'introduction d'un terme L.S dans la force nucléon-nucléon peut aussi être nécessaire[2]. A 20 MeV, nous sommes aussi déjà très proches de la résonance géante, et la diffusion (pp') n'est peut être pas une réaction directe pure à cette énergie.

En définitive, nous voyons que les effets d'échange varient considérablement avec l'énergie de la particule incidente. Comme prédit par notre modèle de rayon fini, ils décroissent quand l'énergie augmente. A basse énergie l'amplitude de diffusion due au processus d'échange peut cependant être bien plus large que l'amplitude directe.

L'accord que nous avons obtenu avec l'expérience montre de façon indubitable que l'excitation des niveaux collectifs par fiffusion (pp') se fait de façon importante par l'échange de la particule incidente et de la particule excitée. Calculé pour les protons du noyau seulement, l'effet dû à l'antisymétrisation des fonctions d'onde est plus de deux fois

ASYMMETRY

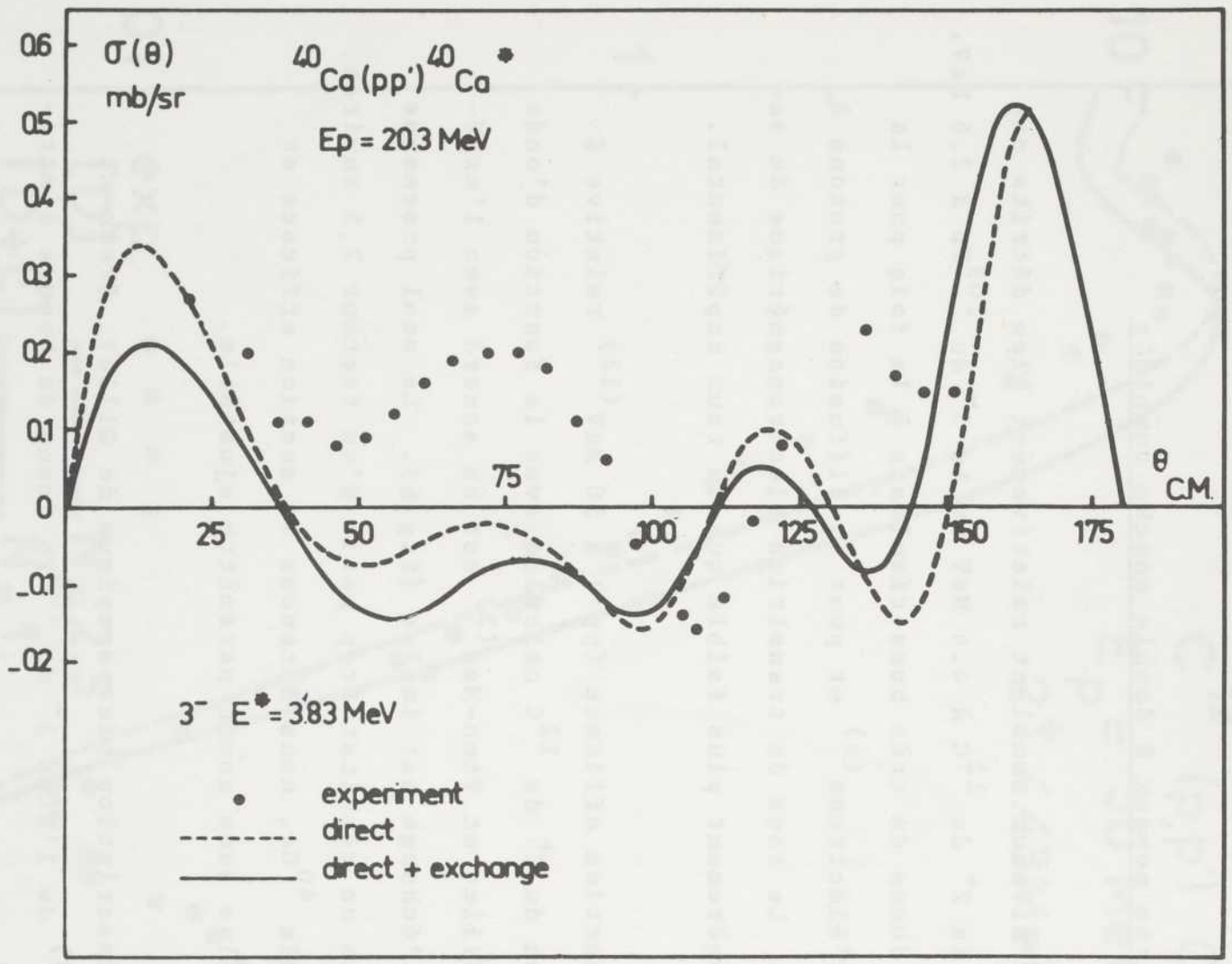

ANTISYMMETRIZED MICROSCOPIC DWBA CALCULATION WITH THE FREE NUCLEON-NUCLEON BLATT-JACKSON POTENTIAL

Fig.5 - Asymétrie (pp') à 20,3 MeV. Etat 3^- à 3,74 MeV du ^{40}Ca. cf. fig.1.

moins important et ne permet pas de rendre compte de la normalisation des sections efficaces expérimentales.

II- Les autres noyaux à double couche complète

Deux niveaux semblent relativement bien décrits par la R.P.A., le 2^+ du ^{12}C à 4.4 MeV et le 3^- du ^{208}Pb à 2.6 MeV. Le premier donne de très bons résultats à la fois pour la diffusion d'électrons[4] et pour la diffusion de protons à 155 MeV[5]. Le taux de transition électromagnétique du second est légèrement plus faible que le taux expérimental.

La section efficace (pp') à 50 MeV[12] relative à l'excitation du 2^+ du ^{12}C calculée avec la fonction d'onde R.P.A. de Gillet et Vinh-Mau[3] est en accord avec l'expérience si l'échange est inclus (fig.6). Le seul processus direct donne un résultat trop petit d'un facteur 2,5 environ. Comme pour le ^{40}Ca, nous obtenons la section efficace en valeur absolue sans aucun paramètre ajustable.

La description microscopique de Gillet, Green et Sanderson[3] de l'état 3^- du ^{208}Pb donne de bonnes distributions angulaires (fig.7) pour la diffusion (pp') à 24.5 MeV[13]. La section efficace théorique est cependant trop petite d'un facteur 3 sans l'échange et d'un facteur 1.5 seulement pour le calcul complet. Ceci peut être considéré comme un très bon résultat, comparable à celui obtenu pour

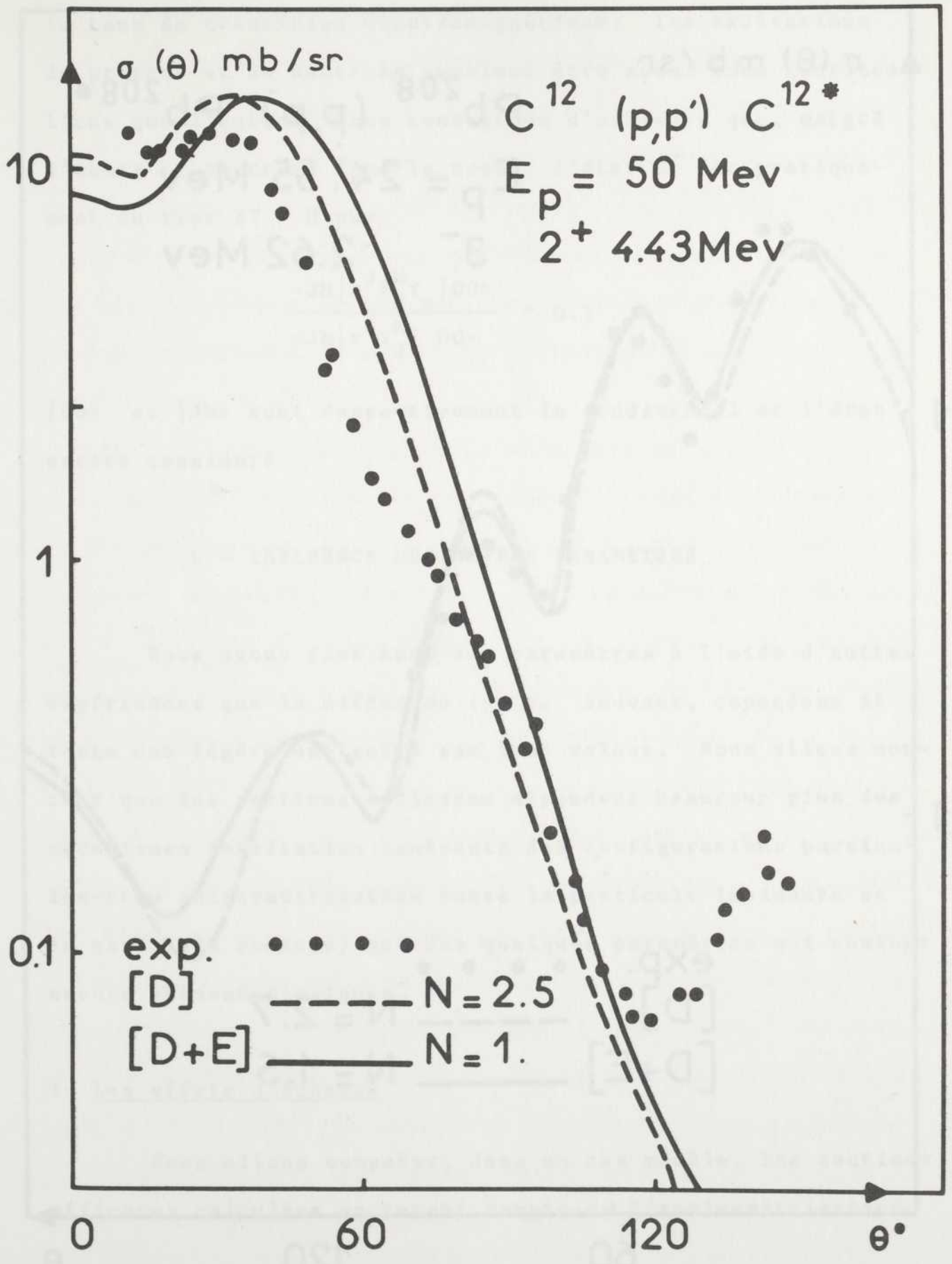

Fig.6 - Section efficace (pp') à 50 MeV. Etat 2^+ à 4,4 MeV du ^{12}C. cf. fig.1.

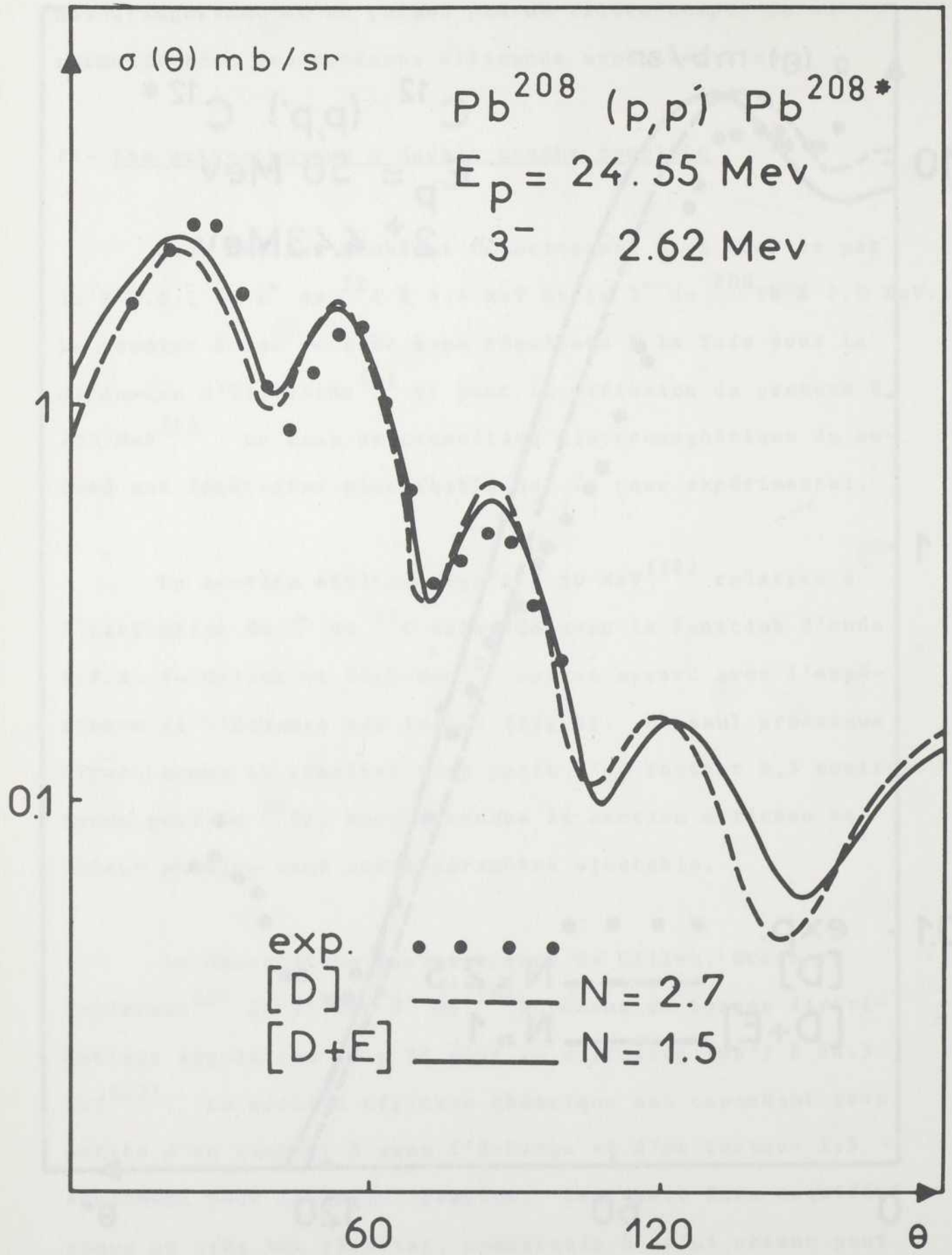

Fig.7 - Section efficace (pp') à 24,5 MeV. Etat 3^- à 2,62 du ^{208}Pb. cf. fig.1.

le taux de transition électromagnétique: les excitations de protons et de neutrons semblent être aussi bien décrites l'une que l'autre. Nous constatons d'ailleurs que, malgré l'excès de neutrons dans le noyau, l'état 3^- est pratiquement du type $\Delta T = 0$ pur

$$\frac{\langle JM|r^J Y_J^M \tau_z|00\rangle}{\langle JM|r^J Y_J^M|00\rangle} \sim 0.1$$

$|00\rangle$ et $|JM\rangle$ sont respectivement le fondamental et l'état excité considéré.

C - INFLUENCE DES DIVERS PARAMETRES

Nous avons fixé tous nos paramètres à l'aide d'autres expériences que la diffusion (pp'). Souvent, cependant il reste une légère ambiguité sur leur valeur. Nous allons montrer que les sections efficaces dépendent beaucoup plus des mécanismes (excitation cohérente des configurations particules-trou antisymétrisation entre la particule incidente et la particule excitée) que des quelques paramètres qui restent encore phénoménologiques.

I- Les effets d'échange

Nous allons comparer, dans un cas modèle, les sections efficaces calculées en tenant compte de l'antisymétrisation

ou en la négligeant. Nous avons choisi un noyau avec deux particules dans l'orbitale $f_{7/2}$, à l'extérieur du coeur formé par le ^{40}Ca et nous étudierons la section efficace de diffusion de l'état $|f_{7/2}\ f_{7/2}|^{J_i=0}$ vers $|f_{7/2}\ f_{7/2}|^{J_f=0 \text{ à } 7}$. Pour $J_f = 0$, celle-ci peut s'interpréter comme la contribution des deux particules à l'extérieur du coeur à la section efficace de diffusion élastique, au premier ordre du potentiel nucléon-nucléon.

Si nous utilisons le mélange de Serber, l'interaction entre le proton incident et les deux nucléons est

$$v(1-P_\sigma P_\tau P_{\vec{r}}) = (-10+10\ \vec{\sigma}_1\cdot\vec{\sigma}_2)(1+P_{\vec{r}}) \quad \text{pour deux protons dans } f_{7/2}$$

$$= -20\ (1 + P_{\vec{r}}) \quad \text{pour deux neutrons}$$

$$= (-15+5\ \vec{\sigma}_1\cdot\vec{\sigma}_2)(1+P_{\vec{r}}) \quad \text{pour un état } T = 0.$$

Dans la limite où la non-localité due à $P_{\vec{r}}$ est faible, d'une part le terme central seul contribue aux excitations de parité naturelle et d'autre part seul le terme en $\vec{\sigma}_1\cdot\vec{\sigma}_2$ contribue aux transitions de parité non naturelle. Les sections efficaces sont calculées dans le cas d'une paire proton-neutron couplée à $T = 0$ (nous utilisons donc une description simplifiée des états du ^{42}Sc).

La diminution de la section efficace vient pour une faible part des coefficients géométriques et pour une part plus importante de la décroissance des multipôles $V_L(r_1,r_2)$ de l'interaction. Pour une force $\delta(\vec{r})$ ceux-ci seraient constants: cette décroissance est donc typiquement un effet de la porté finie de l'interaction nucléon-nucléon qui varie moins brusquement qu'une force δ en fonction de la distance entre les particules et ne peut donc ainsi transférer des moments élevés.

Dans l'amplitude de diffusion du processus d'échange, tous les multipôles V_L interviennent quelque soit le moment angulaire transféré. Celle-ci varie donc bien moins que l'amplitude directe en fonction de ce dernier. Pour les sections efficaces avec antisymétrisation, la différence entre le 0^+ et le 7^+ est réduite d'un facteur 10 environ. L'effet de l'antisymétrisation, que nous allons caractériser par le rapport $\rho = \frac{\sigma(D+E)}{\sigma(D)}$ (fig.8), est donc bien plus grand pour les moments élevés ($\rho \sim 15$ pour le 7^+) que pour les moments faibles ($\rho \sim 2$ pour le 0^+). Pour une force de portée nulle ρ est constant et égal à 4: les effets dus à la portée finie sont donc très importants. A très basse énergie, la particule incidente pénètre peu dans le noyau. A grande énergie, l'antisymétrisation est moins importante car ni la force, ni les fonctions d'onde du modèle des couches ne contiennent des composantes de moments très élevés[2].

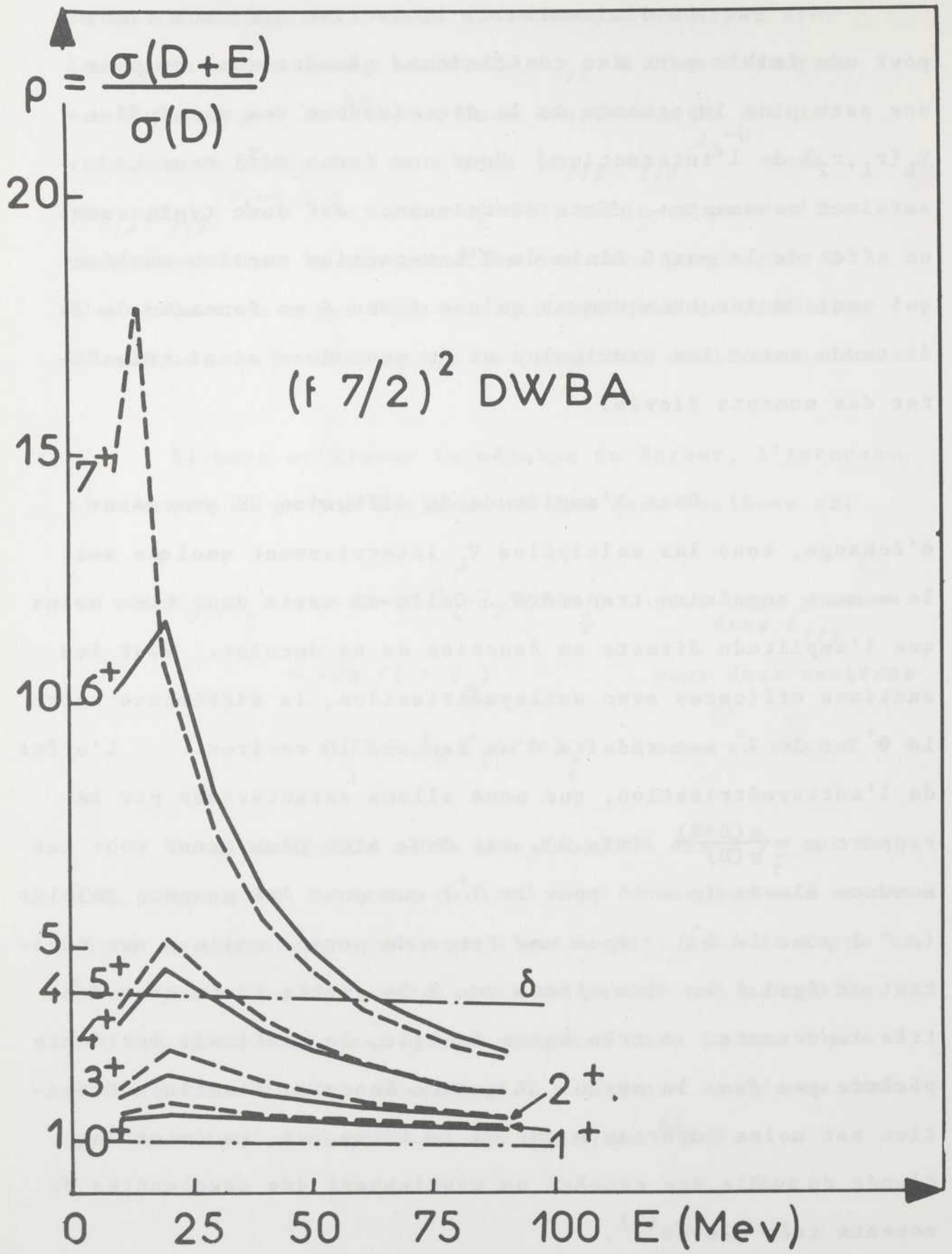

Fig.8 - Rapport entre les sections efficaces totales avec et sans la contribution du terme d'échange dans l'approximation des ondes distordues. Le potentiel optique utilisé est celui (V) du ^{40}Ca à 55 MeV. Les paramètres et les conventions sont ceux de la fig. 14.

II- Le modèle nucléaire

Nous allons comparer les sections efficaces obtenues dans divers modèles nucléaires: une simple excitation particule-trou, l'approximation de Tamm-Dancoff et la R.P.A. A titre d'exemple, nous avons choisi le ^{40}Ca à 55 MeV. Les sections efficaces augmentent régulièrement lorsque l'espace de configuration s'accroît (fig.9). Les distributions angulaires ne sont cependant pas modifiées. Elles ne permettent pas de distinguer entre les divers modèles nucléaires. C'est pourquoi il est nécessaire de décrire la diffusion (pp') sans paramètre de normalisation adaptable.

Les asymétries (fig.10) aussi dépendent peu de la fonction d'onde microscopique utilisée.

III- La force nucléon-nucléon

Dans le cas du ^{40}Ca à 55 MeV, nous donnons (tableau 1) les diverses sections efficaces obtenues avec le mélange de Rosenfeld et la force CAL que Gillet, Green et Sanderson avaient utilisé pour le calcul des états excités. La valeur absolue des sections efficaces dépend considérablement du mélange choisi, alors que les distributions angulaires n'en dépendent absolument pas. Les effets d'échange

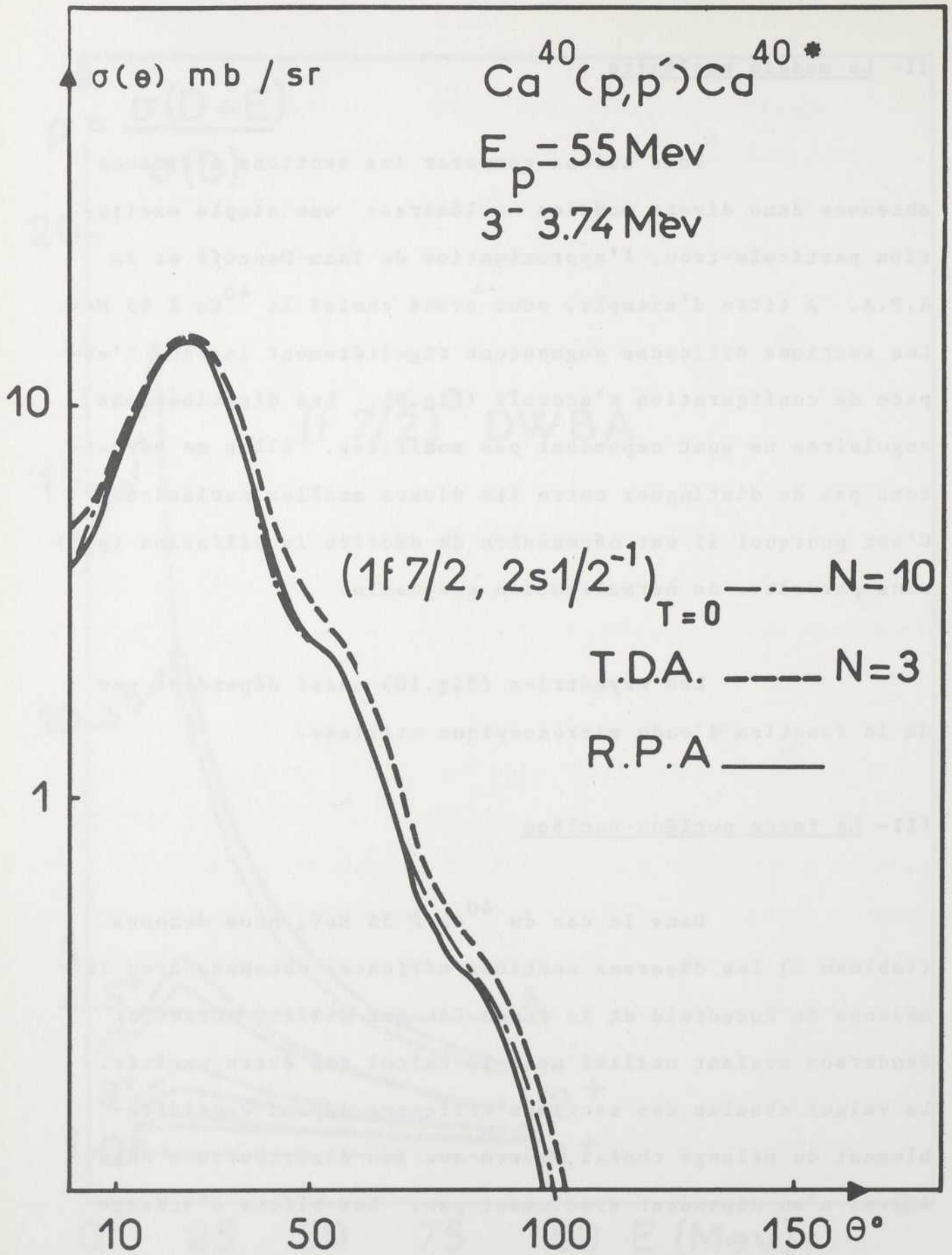

Fig.9 - Comparaison, à 55 MeV des sections efficaces différentielles relatives à l'excitation de l'état 3^- à 3,74 MeV du ^{40}Ca pour divers modèles nucléaires: R.P.A., T.D.A. et une simple excitation particule-trou $(1f_{7/2}\ 2s_{1/2}^{-1})_{T\ 0}$. L'échange est inclus dans les trois calculs. Les sections efficaces T.D.A. et lp-t ont été multipliées par les facteurs N indiqués.

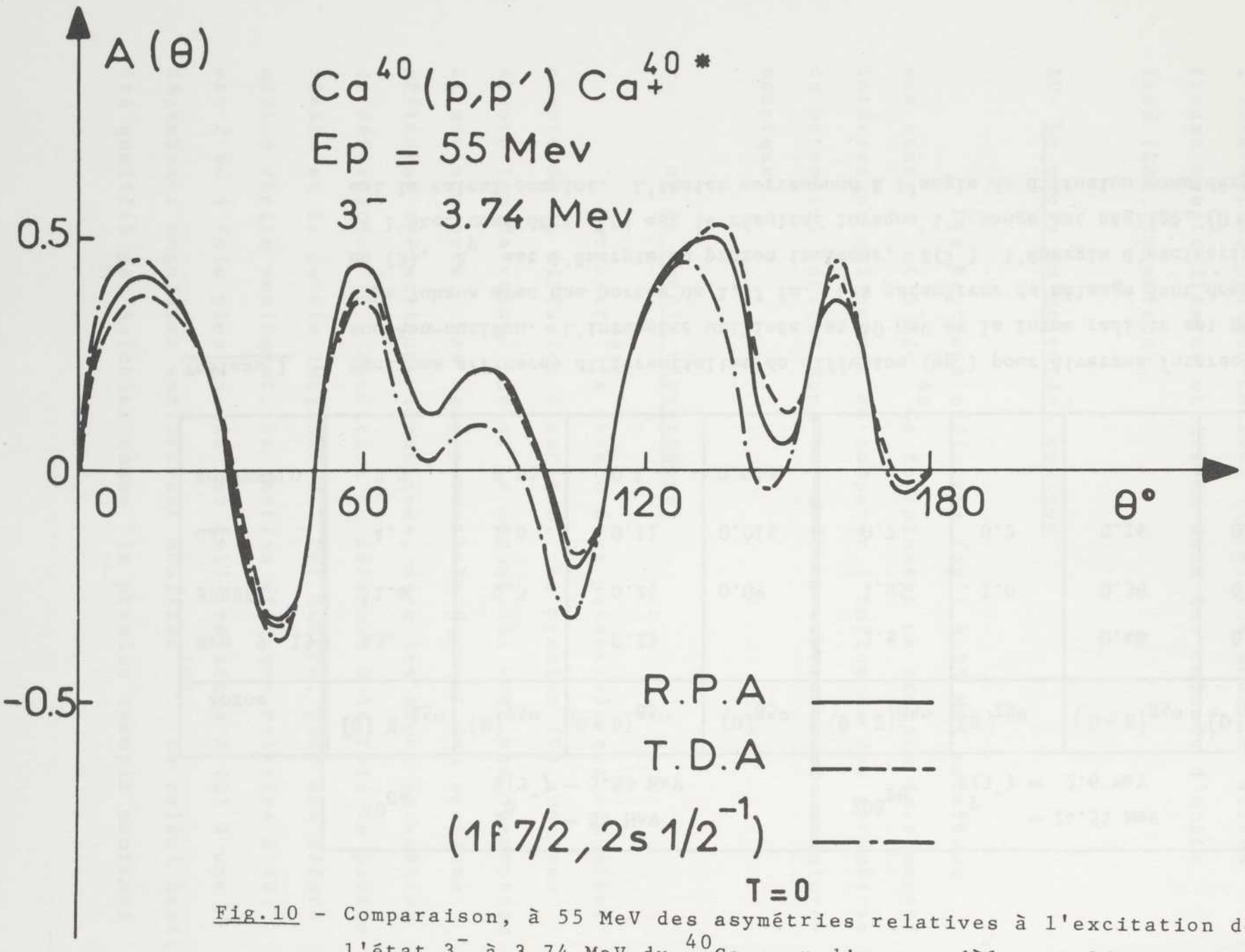

Fig.10 - Comparaison, à 55 MeV des asymétries relatives à l'excitation de l'état 3^- à 3,74 MeV du ^{40}Ca pour divers modèles nucléaires: R.P.A., T.D.A. et une excitation particule-trou $(1f_{7/2}\ 2s_{1/2}^{-1})_{T=0}$. L'échange est inclus dans les trois calculs.

	^{40}Ca $E_p = 55$ MeV $E(3^-) = 3.83$ MeV				^{208}Pb $E_p = 24.55$ MeV $E(3^-) = 2.6$ MeV			
Force	$(D)_{25°}$ E	$(D)_{25°}$	$(D+E)_{85°}$	$(D)_{85°}$	$(D+E)_{85°}$	$(D)_{25°}$	$(D+E)_{85°}$	$(D)_{85°}$
Exp 9, 13	13.		0.25		2.8		0.48	0.22
SERBER	11.6	6.3	0.24	0.09	1.85	1.0	0.38	0.22
CAL	4.	1.0	0.11	0.015	0.7	0.2	0.14	0.05
ROSENFELD	2.2	0.01	0.1	0.0001				

Tableau 1 - Sections efficaces différentielles de diffusion (pp') pour diverses interactions nucléon-nucléon. L'intensité utilisée est 40 MeV et la forme radiale est du type Yukawa avec une portée de 1,37 fm. Les paramètres du mélange sont donnés en (3), E_p est l'énergie du proton incident, $E(3^-)$ l'énergie d'excitation de l'état considéré, (D) est le résultat lorsque l'échange est négligé, $[D+E]$ est le calcul complet. L'indice correspond à l'angle de diffusion considéré.

sont moins importants pour la force de Serber (proche de l'interaction nucléon-nucléon libre) que pour les autres forces habituellement utilisées dans les calculs d'états liés (CAL, Rosenfeld).

IV- Le choix du potentiel optique

Les sections efficaces (pp') à 55 MeV relatives aux états 3^- et 5^- du ^{40}Ca fournissent un exemple extrêmement intéressant qui permet de comparer l'influence des paramètres du potentiel optique dans les modèles vibrationnel et microscopique.

a) Le modèle vibrationnel

Satchler[9] a obtenu deux potentiels qui rendaient compte de la diffusion élastique. Le premier (V) avec une absorption de volume pur et le second (S) avec une absorption de surface pure. Les deux potentiels donnent des sections efficaces inélastiques identiques, avec les mêmes paramètres de déformation[9] à condition de déformer à la fois la partie réelle et la partie imaginaire. Par contre, pour une déformation réelle seulement, la section efficace relative à (V) est 2 ou 4 fois plus grande, et celle relative à (S) à une dépendance angulaire entièrement modifiée[9]. Ce calcul avait été qualifié par Satchler comme "le premier exemple montrant

sans ambiguité qu'un couplage complexe était de toute évidence nécessaire pour décrire la diffusion inélastique de protons".

b) Le modèle microscopique

Dans ce modèle, le facteur de forme (réel, mais non local à cause du terme d'échange) est donné et ne dépend pas des paramètres du modèle optique. Les deux sections efficaces relatives aux potentiels (V) et (S) sont identiques à moins de 10% près (fig. 11). Les asymétries qui, à cette énergie, sont pourtant très sensibles à tous les paramètres du calcul ne présentent pas de variation sensible (fig.12). Ceci montre que, dans le modèle microscopique, il n'est peut-être pas nécessaire d'introduire le couplage complexe que Satchler[6,9] suggère.

CONCLUSION

Les effets liés à l'antisymétrisation de la fonction d'onde du proton incident avec celle du noyau et au caractère d'échange de la force nucléon-nucléon sont donc très importants. Ils augmentent les sections efficaces d'un facteur allant de 2 à 10 et dépendent de l'énergie de la particule incidente ainsi que du spin transféré. La D.W.B.A. avec échange rend compte des sections efficaces expérimentales en valeur absolue, sans

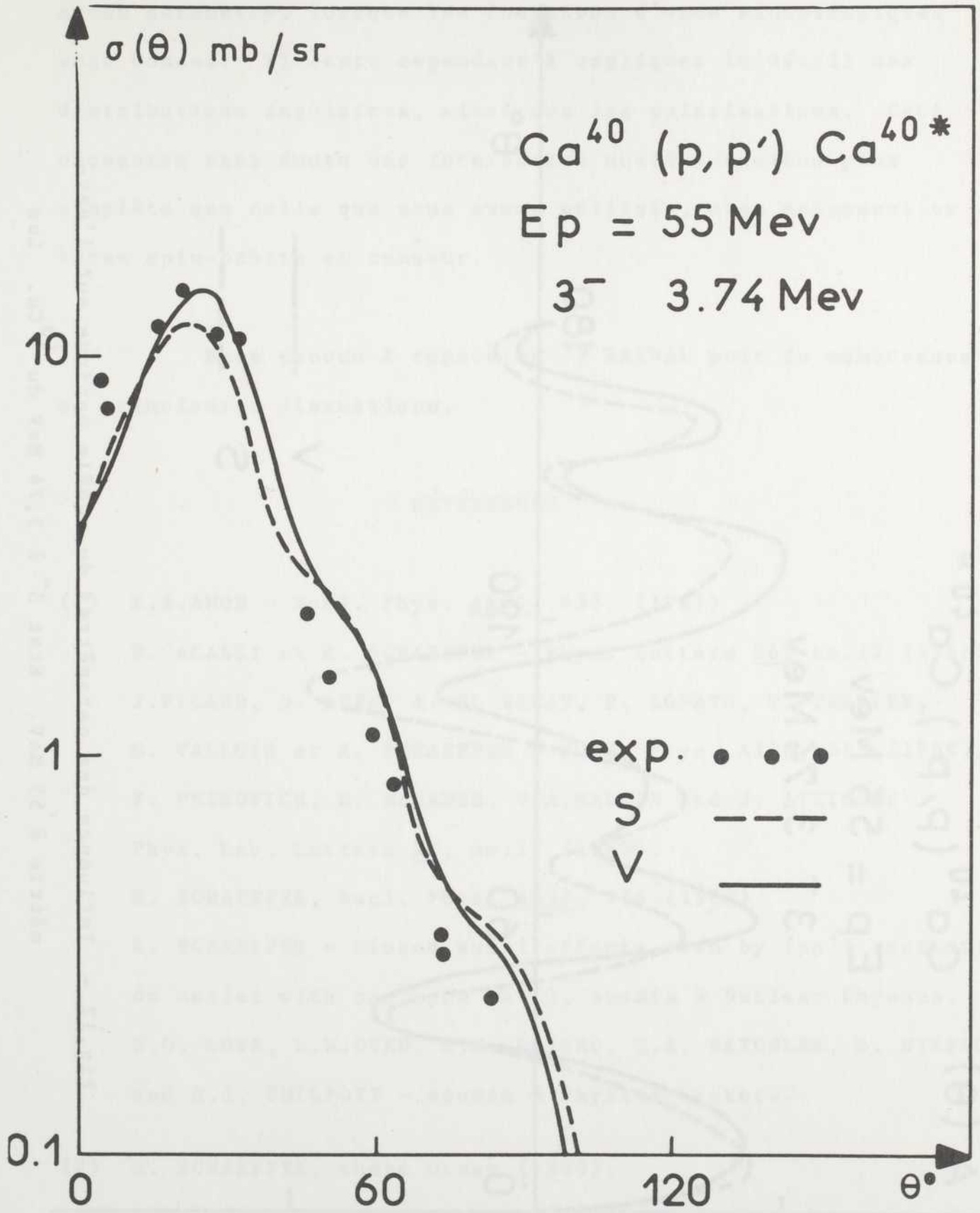

Fig.11 - Influence des paramètres du modèle optique sur la section efficace différentielle à 55 MeV. Etat 3^- à 3,74 MeV du ^{40}Ca. Les potentiels optiques (V) et (S) sont ceux de la ref. 9.

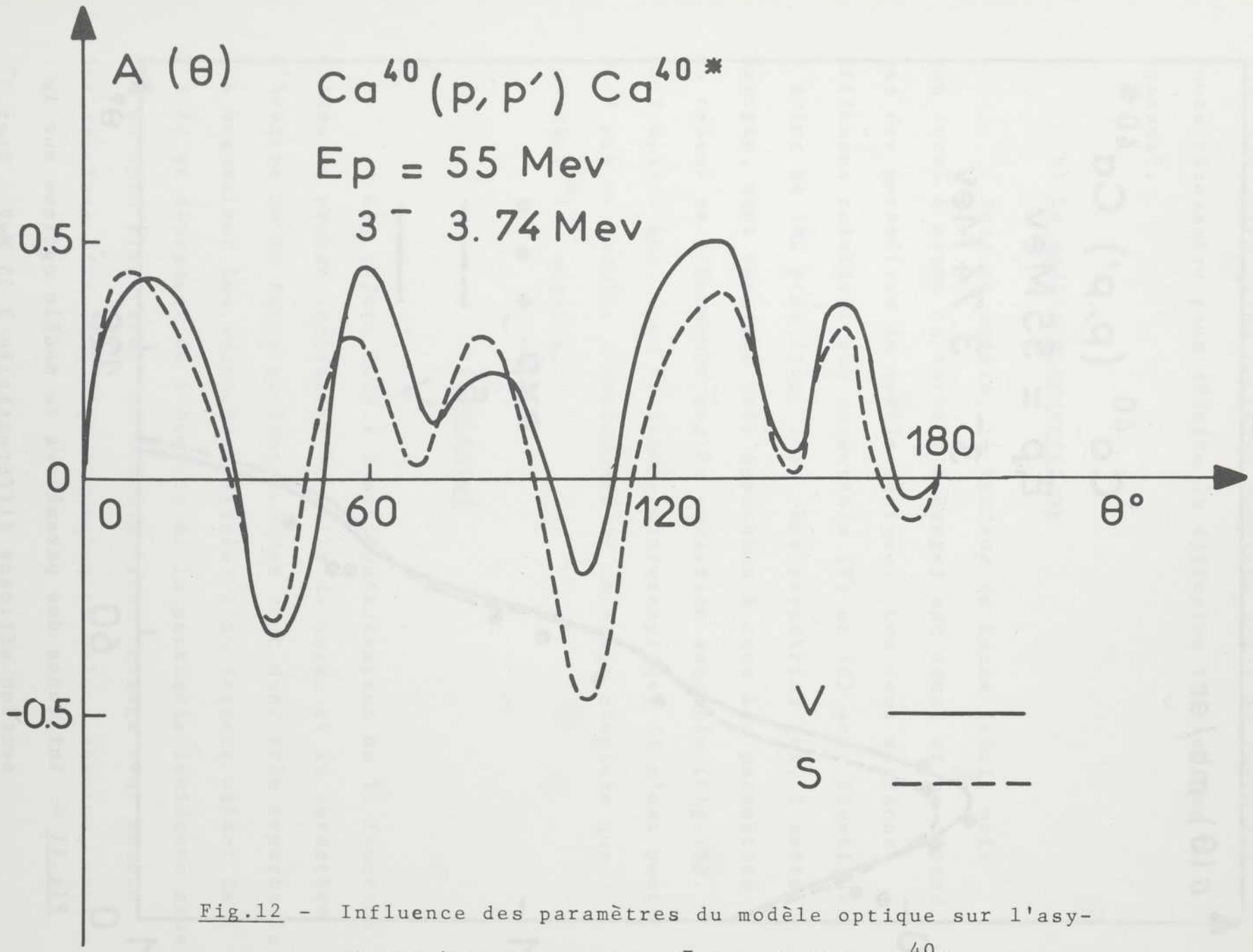

Fig.12 - Influence des paramètres du modèle optique sur l'asymétrie à 55 MeV. Etat 3^- à 3,74 MeV du ^{40}Ca. Les potentiels optiques (V) et (S) sont ceux de la ref.9.

aucun paramètre, lorsque les fonctions d'onde microscopiques sont bonnes. Il reste cependant à expliquer le détail des distributions angulaires, ainsi que les polarisations. Ceci nécessite sans doute une interaction nucléon-nucléon plus complète que celle que nous avons utilisée, avec notamment un terme spin-orbite et tenseur.

Nous tenons à remercier J. RAYNAL pour de nombreuses et stimulantes discussions.

RÉFÉRENCES

(1) K.A.AMOS - Nucl. Phys. A103, 657, (1967)

D. AGASSI et R. SCHAEFFER - Phys. Letters 26B no.12 (1968)

J.PICARD, O. BEER, A. EL BEHAY, P. LOPATO, Y. TERRIEN, G. VALLOIS et R. SCHAEFFER - Nucl. Phys. A128, 481 (1969).

F. PETROVICH, H. McMANUS, V.A.MADSEN and J. ATKINSON Phys. Rev. Letters 22, no.17 (1969).

R. SCHAEFFER, Nucl. Phys. A132, 186 (1969)

R. SCHAEFFER - Closed shell effects seen by (pp') scattering on nuclei with one open shell, soumis à Nuclear Physocs.

W.G. LOVE, L.W.OVEN, R.M. DRISKO, G.R. SATCHLER, R. STAFFORD and R.J. PHILPOTT - soumis à Physics Letters.

(2) R. SCHAEFFER, thèse Orsay (1969).

(3) V. GILLET et N. VINH MAU - Nucl. Phys. 54 321 (1964)

V. GILLET, A. GREEN et E. SANDERSON - Nucl. Phys. 88, 321 (1966)

V. GILLET et E. SANDERSON - Nucl. Phys. 91 292 (1967)

(4) V. GILLET et M.A. MELKANOFF - Phys. Rev. 133, B1190 (1964).

(5) R.M. HAYBRON et H. McMANUS - Phys. Rev. 140, B638(1965).

A. WILLIS - Thèse Orsay (1968).

(6) S.A. FULLING et G.R. SATCHLER - Nucl. Phys. A111, 81(1968).

(7) C.W.WONG et C.Y.WONG - Nucl. Phys. A91, 433 (1967).

(8) J. RAYNAL - Nucl. Phys. A97, 572(1967).

(9) K.YAGI, H.EJIRI, M.RURUKAWA, Y.ISHIZAKI, M.KOIKE, K.MATSUDA, Y. NAKAJIMA, I.NONAKA, Y.SAJI, E.TANAKA et G.R. SATCHLER - Phys. Letters 10, 186 (1964).

(10) B.W.RIDLEY et J.F. TURNER - Publié dans la réf. (6).

(11) C. GLASSHAUSER, R. de SWINIARSKI, J. GOUDERGES, R.M. LOMBARD, B. MAYER et J. THIRION - Communication privée.

(12) J.A. FANNON, E.J. BURGE, D.A. SMITH et N.K. GANGULY, Nucl. Phys. A97, 263 (1967).

(13) J. SAUDINOS, G. VALLOIS, O. BEER, M. GENDROT et P. LOPATO - Phys. Letters 22, 492 (1966).

(14) G.R. SATCHLER - Nucl. Phys. A95, 1 (1967).

Equivalence of Different Optical Model Potentials for the ^{40}Ca /α, α/ Scattering.

A. Budzanowski, K. Grotowski, L. Jarczyk, B. Kamys, K. Olkiewicz and A. Strzałkowski.

Institute of Physics, Jagiellonian University

and

Institute of Nuclear Physics, Cracow, Poland

Ca /α, α/ elastic scattering angular distributions of six different energies of α particles between 23,37 MeV and 28,92 MeV have been analysed using the four parameter optical model with the Saxon Woods form factor. Three discrete sets of the optical model parameters have been found giving similar acceptable fits to the experimental data at the scattering angles form about 20^0 up to 179^0 /CM/. The optical model parameters are presented in table I. An example of obtained fits is shown in fig. 1. It can be seen from the table I that the half-way radius and the mean-square radius of the potential are functions of the depth of the real part of the potential and therefore cannot be regarded as significant nuclear size parameters. However the strong absorption radius /R_{ab}/ corresponding to the classical turning point for the scattered alpha particle with Re η_l =1/2 is similar for different potentials. As can be seen from table II the magnitudes of the potentials at this radius are also very close to each other. According to the suggestion made by Jackson and Morgan [1] the above mentioned property can be used as a criterion for equivalence of optical model potentials.

Table I.

	E_α MeV	U MeV	W MeV	r_o fm	a fm	$\langle R^2 \rangle^{1/2}$ fm	R_{ab} fm
1		186.8	18.1	1.248	0.660	4.16	7.59
2	23.37	241.8	21.1	1.217	0.668	4.08	7.61
3		302.7	23.9	1.185	0.661	3.99	7.63
1		182.3	15.1	1.251	0.675	4.16	7.51
2	24.15	239.8	17.8	1.209	0.665	4.05	7.52
3		305.8	20.8	1.171	0.659	3.95	7.52
1		202.6	17.9	1.172	0.742	4.15	7.53
2	24.7	261.5	20.7	1.146	0.718	4.04	7.53
3		328.6	23.5	1.121	0.702	3.95	7.54
1		227.0	21.8	1.075	0.804	4.14	7.53
2	25.23	291.1	24.4	1.059	0.772	4.01	7.53
3		362.2	27.0	1.042	0.743	3.90	7.51
1		229.0	24.4	1.066	0.791	4.08	7.43
2	26.37	309.8	28.4	1.013	0.778	3.95	7.43
3		389.8	32.0	0.991	0.759	3.85	7.45
1		207.6	23.1	1.150	0.743	4.11	7.40
2	28.92	271.2	25.9	1.118	0.726	4.01	7.43
3		345.4	29.2	1.086	0.718	3.92	7.47

Table II.

E_α MeV	U/R_{ab}/ MeV 1	2	3
23.38	1.39	1.37	1.35
24.15	1.51	1.48	1.46
24.7	1.74	1.70	1.68
25.23	1.87	1.82	1.78
26.37	1.88	1.88	1.84
28.92	1.92	1.86	1.84

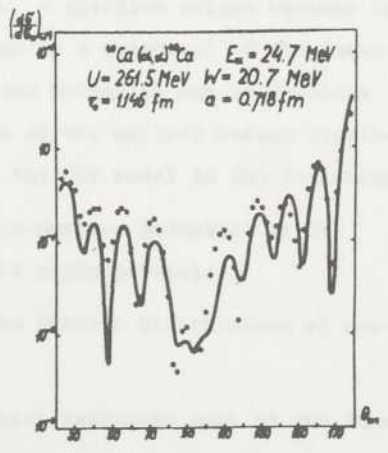

Fig. 1.

Optical model fit to the ^{40}Ca /α, α/ ^{40}Ca angular distribution

[1] D.F. Jackson and C.G. Morgan /preprint /

REFORMULATED OPTICAL MODEL FOR THE INTERACTION OF ALPHA PARTICLES WITH NUCLEI

A. Budzanowski, A. Dudek, K. Grotowski and A. Strzałkowski

Institute of Nuclear Physics, Cracow 23, Poland
and
Institute of Physics, Jagellonian University, Poland

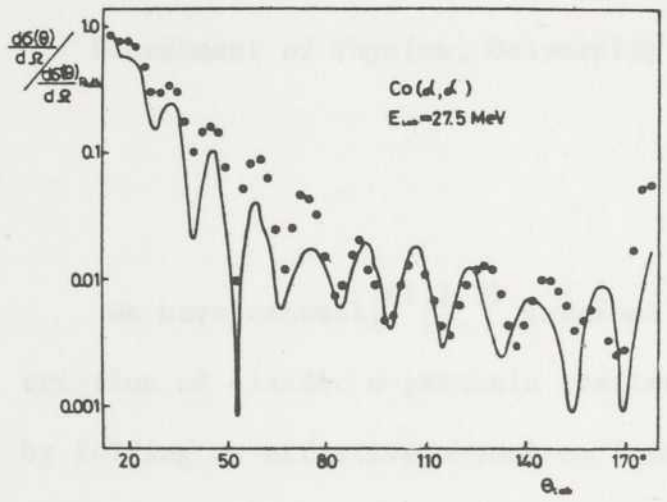

Fig. 1

Co (α, α) angular distribution with an optical model fit. The optical potential was generated with following parameters: Yukawa N-N potential μ = 1.408 fm^{-1}, V_{NN} = 51.15 MeV; Fermi parameters of the nuclear matter distribution $r_{o\alpha}$ = 0.7162 fm a_α = 0.3162 fm /α particle/; r_{oT} = 1.272 fm, a_T = 0.5162 fm /target nucleus/; imaginary potential r_{ow} = 1.300 fm, a_w = 0.7152 fm, W = 20.28 MeV

It was shown recently [1] in an extensive optical model analysis of $^{39}K(\alpha, \alpha)$ data that it is difficult to fit differential cross-sections at large angles and small angles with the same potential of the Saxon-Woods form. The potential which gives the best fit at forward angles has the radius of the real part of about 1 fm larger than that fitting the backward scattering data. A question arises whether the scattering of alpha particles in the whole angular region can be described by a potential of the Saxon-Woods form. Greenlees, Pyle and Tang[2] have shown that the nucleon-nucleus potential can be obtained from an effective nucleon-nucleon interaction and a Fermi parametrisation of the nuclear matter distribution. In order to calculate the α - nucleus potential we have applied the GPT model in the following way:

1/ The nucleon - α potential has been derived by folding the nucleon-nucleon potential of the Yukawa form with the density distribution of nuclear matter in the alpha particle.

2/ The α - nucleon potential obtained in this way was folded with the density distribution of nuclear matter in the target nucleus.

3/ The calculated real potential was supplemented by a phenomenological imaginary part of the Saxon Woods form.

The preliminary fit to the 27.5 MeV $^{59}Co(\alpha, \alpha)$ data is presented in fig. 1. A microscopic description of the α - nucleus interaction was attempted recently by Jackson and Kembhavi[3]. They assumed an Yukawa shape of the α - nucleon potential and used a single step folding procedure. They obtained satisfactory agreement with the 42 MeV Ca (α, α) scattering data only up to the angle 30°.

References

1/ A. Budzanowski, A. Dudek, R. Dymarz, K. Grotowski, L. Jarczyk, H. Niewodniczański and A. Strzałkowski, Nucl. Phys. A126, 369 /1969/

2/ G.W. Greenlees, G.J. Pyle and Y.C. Tang /Preprint/

3/ D.F. Jackson and V.K. Kembhavi /Preprint/.

The microscopic description of α-particle scattering and the investigation of the nuclear matter distribution

Daphne F. Jackson, V. K. Kembhavi, and C. G. Morgan†

Department of Physics, University of Surrey, Guildford, England

We have recently[1,2,3] examined the feasibility of a microscopic description of elastic α-particle scattering using optical potentials derived by folding an effective α-nucleon interaction into the nuclear matter distribution. It has been shown that with a judicious choice of the effective interaction V_{eff} it is possible to construct an optical potential which resembles closely the phenomenological optical potential in the important surface region[2,3] and which yields an equally good fit to the data[3]. One of the advantages of this procedure is that it permits a consistent microscopic description of elastic and inelastic scattering[3] and removes uncertainties due to ambiguities in the optical potential for α-particles. This microscopic approach has since been used by other groups[4] with some success.

The use of the simple folding integral permits the calculation of the real part of the optical potential, and it is usual to assume that the imaginary part of the potential has the same radial behaviour as the real part and to treat the strength as a free parameter. The folding procedure also implies the neglect of terms in the multiple scattering expansion which

proceed through intermediate excited states[1]. However, studies using phenomenological optical potentials show that the data on elastic α-particle scattering at medium energies can be fitted very well using the same parameters for the real and imaginary parts. Further, it may be argued that since the characteristic features of the α-nucleus scattering arise from the interaction in the nuclear surface where the effects of the exclusion principle and the nuclear binding are least important, the effective interaction should approximate to the free interaction and should not vary markedly with the target nucleus. This argument is supported by the fact that there is a difference of only 2% in the values of the strengths of the effective interaction which give the best fit to the data on ^{42}Ca and ^{50}Ti. It has also been observed[5] that folding a gaussian nucleon-nucleon potential interaction into the α-particle density leads to a gaussian α-nucleon interaction whose parameters are very close to those obtained by us.

We may now discuss whether the elastic scattering of α-particles can be used to investigate the nuclear matter distribution. By studying the relation between the calculated potential and the matter distribution we have shown[2] that the potential in the surface region is determined primarily by the matter distribution in the transition region. We have also shown[1] that the change in the nuclear matter distribution through the calcium isotopes probably accounts for the isotopic variation in the strong absorption radius. (This conclusion is based on calculations using a form for V_{eff} which gave rather poor fits to the data, and these calculations are being repeated using the V_{eff} of ref. 3.) Preliminary results for heavier nuclei indicate that if <u>substantial variations in V_{eff} are not permitted</u> it is possible to draw conclusions about the shape of the nuclear matter distribution and in particular about the difference between the proton and neutron distributions.

REFERENCES

(1) D. F. Jackson, and V. K. Kembhavi, Phys. Rev. 178 (1969) 1626.

(2) D. F. Jackson, Nucl. Phys. A123 (1969) 273.

(3) C. G. Morgan, and D. F. Jackson, Phys. Rev., to be published.

(4) A. Budzanowski, A. Dudek, K. Grotowski, and A. Strzalkowski, contribution to this conference.

M. Veneroni, reported at this conference.

(5) A. M. Bernstein, Advances in Nuclear Physics, Vol. 3, to be published.

†Present address: Department of Atmospheric Physics, University of Oxford, Oxford, England.

NUCLEAR POLARIZATION OF $^{12}C^*(4.44)$ NUCLEI EXCITED BY INELASTIC ALPHA PARTICLE SCATTERING

F.H. Schmidt and T.D. Hayward, University of Washington, Seattle 98105

We have studied the coincident de-excitation gamma rays in the $^{12}C(\alpha,\alpha'\gamma)^{12}C^*(4.44)$ reaction. Our measurements include the γ-angular correlation function in the plane of the reaction, and the circular polarization of the γ-rays emitted near the normal to the reaction plane. Taken together, the results yield the polarization of the $^{12}C^*$ nuclei.

The normalized in-plane angular correlation function for a $0^+ \rightarrow 2^+ \rightarrow 0^+$ sequence is

$$W(\phi_{\alpha'},\phi_\gamma) = (5/16\pi)[(a_{+2} - a_{-2})^2 + 4a_{+2}a_{-2} \sin^2 2(\phi_\gamma - \delta/4)],$$

where $a_{\pm 2}$ are the amplitudes for production of the $m = \pm 2$ substates, respectively, and δ is their relative phase. The axis of quantization is normal (Basel Convention) to the reaction plane. Both a_{+2} and a_{-2} can thus be determined, but they cannot be distinguished from one another.

The γ-ray circular polarization, averaged over ϕ_γ, is

$$P_\gamma = [(a_{+2}^2 - a_{-2}^2) \cos\theta_\gamma]/[(a_{+2}^2 + a_{-2}^2)(1 + \cos^2\theta_\gamma) + 6a_0^2 \cos^2\theta_\gamma],$$

where θ_γ is the polar angle of the γ-ray. a_0 is the amplitude for the $m = 0$ substate, and is given by

$$a_0^2 = 1 - (a_{+2}^2 + a_{-2}^2).$$

Alpha particles were accelerated to 22.75 MeV by the University of Washington FN Tandem Van de Graaff. The energy was chosen after a study of the excitation function; the cross-section in the region near 22.75 MeV is reasonably smooth, and 22.75 MeV is consistent with long steady accelerator performance. In-plane correlations were measured at 35 scattering angles. The circular polarization was measured by Compton Scattering from a large magnetized iron polarimeter, the axis of which was placed normal to the reaction plane.

The results show: (1) that each of the three substate partial cross-sections exhibit a different diffraction-like pattern, with the $m = 0$ being the most regular; (2) that the $m = -2$ predominates from $\sim 20°$ to $75°$; and (3) that the $m = +2$ predominates from $75°$ to $170°$. The nuclear polarization

$$P_n = a_{+2}^2 - a_{-2}^2$$

ranges from -0.5 in the forward direction to +0.7 in the backward direction, and shows a diffraction-like structure. The results cannot be explained by existing simple theoretical models. The method can, in principle, be applied to more tractable nuclei, the scattering from which is more readily understood in terms of theoretical models. We chose ^{12}C because of the large cross-section for inelastic scattering, and for the general absence of background radiation.

STRIPPING TO UNBOUND LEVELS

B.J.Cole, R.Huby and J.R.Mines

The University of Liverpool, Liverpool, England

Recent (d, n) and (^{3}He, d) measurements include a number of angular distributions for reactions leading to excited states of the residual nuclei unstable to the decay of the captured proton. Huby and Mines have shown that the appropriate DWBA theory for stripping to these unbound states is closely related to standard DWBA theory for bound states; the main difference is the substitution of a resonant scattering wave-function for the bound state wave-function of the captured proton. However, computations cannot be made in a straightforward manner because of the slow convergence of the radial integrals. It is therefore of interest to try and devise a simple non-rigorous modification of the ordinary DWBA for bound states such that we can deduce the spectroscopic information about the unbound states.

The approach adopted is the following: we construct a quasi-bound wave-function from the resonant scattering wave-function. The well-depth of a Saxon-Woods potential is adjusted to give a resonance (i.e. a nuclear phase shift of $\pi/2$) at the observed energy of the level. The resonant wave-function, which has a large amplitude inside the nucleus, is then modified by cutting it off smoothly in the region of the first node outside the nucleus. The resulting function is normalised to unity and substituted for the bound state wave function in the ordinary DWBA calculation. Calculations made in this way should be accurate for states which are slightly unbound and become progressively more uncertain as the excitation energy increases.

Trial calculations have been made for the ^{15}N(^{3}He, d)^{16}O and ^{20}Ne(d,n)^{21}Na reactions. Good fits to the angular distributions have been obtained for states unbound by as much as $2\frac{1}{2}$ MeV. The sensitivity of the calculated angular distributions to the method of cutting off the resonant wave function has been investigated. This is found to be insignificant for states unbound by up to $\sim$1 MeV but gives rise to uncertainties in the magnitude of the cross section for more highly excited states. In the case of the ^{20}Ne(d,n)^{21}Na reaction we intend to compare our results with those obtained from proton elastic scattering on ^{20}Ne and the mirror ^{20}Ne(d, p)^{21}Ne reaction. (The mirror levels of ^{21}Ne are bound states.)

DWBA ANALYSIS OF THE $Be^9(d,n)B^{10}$ REACTION

T. G. Miller and J. J. Duffy

U.S. Army Missile Command, Redstone Arsenal, Al 35809, U.S.A.

Recent measurements[1] on the polarization of five groups of neutrons from the $Be^9(d,n)B^{10}$ reaction reveal polarization distributions whose shapes do not change appreciably from 1.5 to 2.5 MeV. These data along with the angular distribution data of Siemssen et al[2] have been analyzed using a DWBA formalism.[3] In general, it has been possible to obtain qualitative fits to the polarization data or the cross-section data individually, but not to both simultaneously.

[1] T. G. Miller and J. A. Biggerstaff, Phys. Rev. to be published.

[2] R. M. Siemssen, M. Cosack and R. Feist, Nucl. Phys. 69, 227 (1965).

[3] R. M. Bassel, R. M. Drisko and G. R. Satchler, Oak Ridge National Laboratory Report No. ORNL-3240 (unpublished).

AN IMPROVED METHOD OF CALCULATING FINITE RANGE EFFECTS IN TWO-NUCLEON TRANSFER REACTIONS

N.S. Chant and N.F. Mangelson, Physics Department, University of Washington, Seattle 98105

There have been few estimates of finite range effects in two-nucleon transfer reactions although such effects may be appreciable[1]). An expression for the DWBA matrix element has been given by Bencze and Zimanyi[2]) in which both the finite range of the nucleon-nucleon effective interaction and the finite spatial separation of the transferred nucleon pair are treated approximately (BZ). Using harmonic oscillator wave functions, a more exact description of the relative motion of the transferred nucleons has been given[3,4]) but a zero-range interaction was assumed (ZRI). Fortunately, the zero-range assumption can easily be eliminated and a finite range expression obtained (FRI) which involves fewer approximations than the BZ result.

For the mass 3 or mass 4 nucleide wave function Φ and for the interaction V_{ij} a Gaussian shape is assumed.

$$\Phi = N \exp(-\eta^2 \sum_{ij} r_{ij}) \text{ and } V_{ij} = U_0 \exp(-\beta^2 r_{ij}^2) \qquad (1)$$

If we consider a pick-up reaction A(a,b)B, the following expression is obtained for the DWBA matrix element[5])

$$I_\Lambda^L \sim \int \{\exp(\frac{C_b \nabla_b^2}{4\epsilon^2}) \chi_b^{(-)*}(\underline{r})\} \{\exp(\frac{C_x \nabla_x^2}{4\epsilon^2}) F_x(r) Y_\Lambda^L(\hat{\underline{r}})\} \{\exp(\frac{C_a \nabla_a^2}{4\epsilon^2}) \chi_a^{(+)}(\underline{r})\} d\underline{r} \qquad (2)$$

where the finite range interaction has been included using a Taylor's series expansion. The quantities $\chi_{a,b}$ are distorted waves, $F_x(r)Y_\Lambda^L(\hat{\underline{r}})$ is the zero-range form factor obtained either as in ref. 3) or 4). The constants C_i depend upon the masses of the reacting particles and $\epsilon^2 = \beta^2 + 2a\eta^2$. As in the BZ calculations the exponential operators acting upon the distorted waves are evaluated in local W.K.B. approximation, i.e.

$$\exp(C\nabla^2)\chi(\underline{r}) \sim \exp(\frac{2mC}{\hbar^2}(V(r)-E))\chi(\underline{r}) \qquad (3)$$

However the remaining operator is evaluated more exactly by expanding the exponential and evaluating

$$\nabla_x^2 = \frac{1}{r}\frac{d^2}{dr^2} r - \frac{L(L+1)}{r^2} \qquad (4)$$

by a numerical difference method.

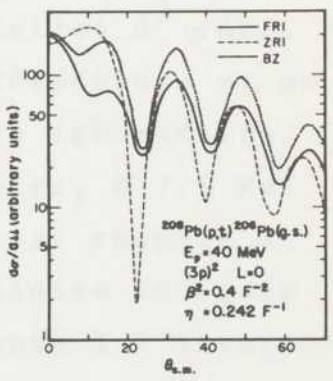

In the figure the FRI method is compared with ZRI and BZ calculations for $^{208}Pb(p,t)^{206}Pb$(g.s.) at 40 MeV. Both neutrons are bound by 7.055 MeV in 3p orbits of a Saxon-Woods well with radius 1.25F and diffuseness 0.65F. The optical parameters used are the volume absorption set of ref. 6). For the ZRI and FRI calculations the form factor $F_x(r)$ was obtained by expanding the Saxon-Woods wave functions in an oscillator basis as in ref. 4). In the FRI calculations the exponential operator evaluated by successive numerical differentiation of $F_x(r)$ converged rapidly yielding excellent accuracy after 7 terms in the expansion. The ZRI calculation was normalized so that, at large radii, the integrand had approximately the same magnitude as in the FRI calculation.

Appreciable differences exist between the FRI and ZRI predictions. In additon the BZ calculation is not a good approximation to the more accurate FRI treatment.

Finally we point out that a correction term can be given arising from the use of approximation (3) in the FRI calculation. This term is similar to an expression given by Smith[7]) for single nucleon transfer. We have not yet included this term in calculations. However it should provide a valuable indication of the accuracy of the FRI treatment itself.

REFERENCES

1) N. Austern et al., Phys. Rev. 133 (1964) B3
2) GY. Bencze and J. Zimanyi, Nucl. Phys. 81 (1966) 76
3) N.K. Glendenning, Phys. Rev. 137 (1965) B102
4) R.M. Drisko and F. Rybicki, Phys. Rev. Letters 16 (1966) 275
5) N.S. Chant and N.F. Mangelson, to be published
6) N.K. Glendenning, Phys. Rev. 156 (1967) 1344
7) W.R. Smith, Nucl. Phys. A94 (1967) 550

DISTRIBUTION ANGULAIRE DE LA REACTION $^3He(^3He,\alpha)2p$ A 7.9 MeV †

M. L. V. L. de Slobodrian, B. Cujec, R. Roy, R. J. Slobodrian

Université Laval, Physique, Québec 10, Canada.

La réaction $^3He(^3He,\alpha)2p$ a été étudiée en utilisant le faisceau de $^3He^{++}$ de l'accélérateur Van de Graaff à Laval. Expériences antérieures[1] à 44 et 53 MeV ont montré que la distribution angulaire du pic correspondant à l'interaction p-p dans l'onde $^1S_0$ a une structure de diffraction très marquée. Le pic est d'ailleurs bien répresenté par l'interaction p-p déduite des expériences de la diffusion élastique de protons sur protons.

A 7.9 MeV on a mesuré les spectres différentielles $d^2\sigma/dEd\Omega$ des particules α (fig. 1) avec un télescope de deux détecteurs et un circuit d'identification ORTEC entre 11^o et 41^o du laboratoire. En comparant avec les spectres à plus hautes énergies, à 7.9 MeV la contribution de l'interaction p-p est réduite par rapport à la contribution p-^{4}He (^{5}Li). La distribution angulaire intégrée par rapport à l'energie sur la région correspondante à l'interaction p-p (fig. 2) indique même à 7.9 MeV une anisotropie très marquée du type des reactions directes de transfert d'un nucléon. Le spectre $d^2\sigma/dEd\Omega$ près de la limite d'energie est consistent avec l'interaction p-p.

On continue avec l'analyse détaillée de la région d'interference entre l'interaction p-p et p-^{4}He, qui doit fournir l'information d'intérêt pour le problème nucléaire à trois corps.

† Recherche appuyée par la Commission de Contrôle de L'Energie Atomique du Canada

1) R. J. Slobodrian, J. S. C. McKee, W. F. Tivol, D. J. Clark and T. A. Tombrello, Physics Letters 25B (1967) 19.

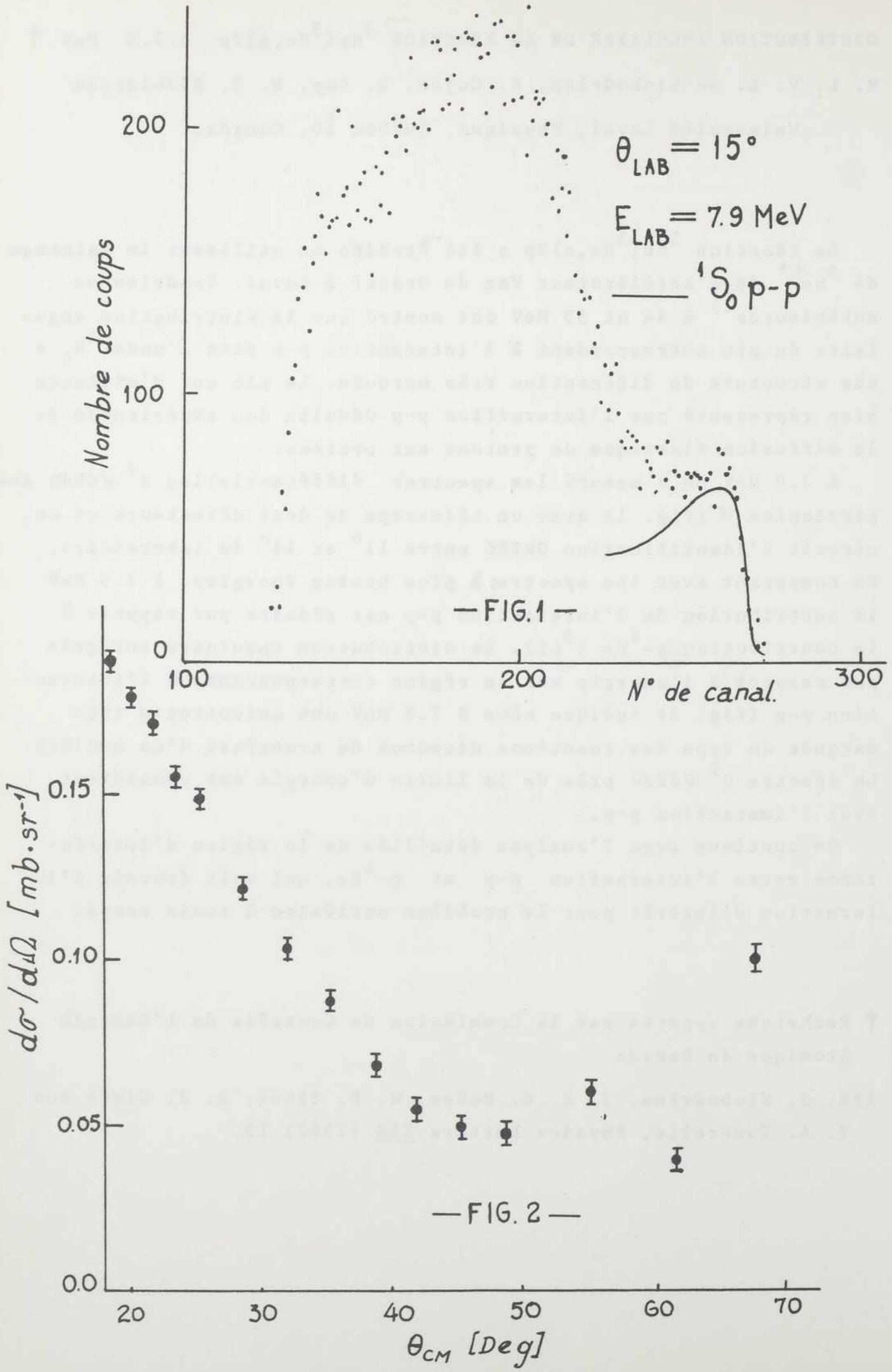
200
100
0
Nombre de coups
100
200
300
N° de canal.
$\theta_{LAB} = 15°$
$E_{LAB} = 7.9$ MeV
$^1S_0$ p-p
0.15
0.10
0.05
0.0
$d\sigma/d\Omega$ [mb.sr^{-1}]
20
30
40
50
60
70
θ_{CM} [Deg]

— FIG. 1 —

— FIG. 2 —

SEANCE
SESSION 3

PRESIDENT CHAIRMAN

D.W. MILLER

REACTIONS WITH POLARIZED DEUTERONS ON LIGHT ELEMENTS

P. Huber

Institute of Physics, University Basel.

1. The reactions of deuterons with light nuclei have been studied very extensively. With the possibility of producing intensive beams of polarized nucleons and nuclei, that is particles with unequally populated magnetic substates, a new dimension has been added to our methods of investigations. With the use of polarized particles and polarized target nuclei, only certain of the otherwise open channels are allowed, so that very detailed investigation can be performed.

To produce a beam of polarized deuterons an atomic deuterium beam is separated according to the electron-spin by the Stern-Gerlach method (Fig.1). As proposed by Abragam and Winter, high frequency transitions between Zeeman-levels of the deuterium atoms are induced to polarize the deuterons. To create various nuclear polarization states, transitions in both strong and weak magnetic fields are used. The ionization of the deuterium atoms then occurs in a longitudinal magnetic field of 1 kilogauss. An electric field extracts the deuterons from the ionization region, after which the beam is focused by an electrostatic lens and traverses a Wien filter (velocity filter). This filter serves two purposes:

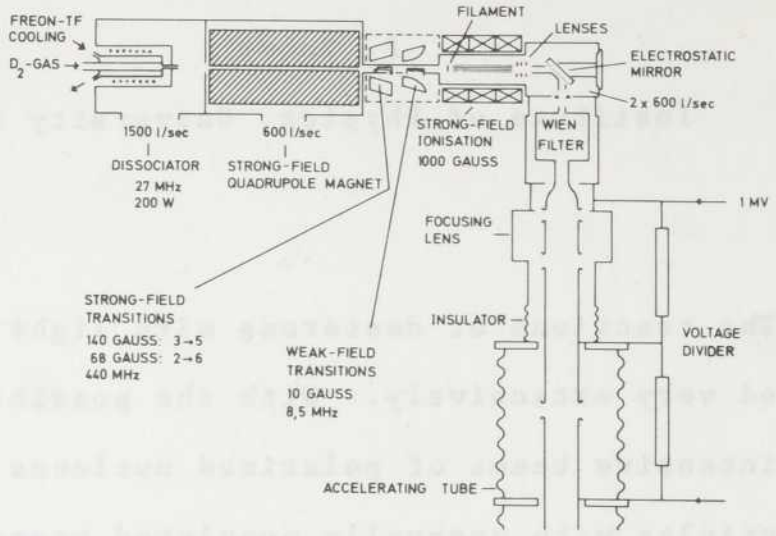

Fig. 1 Source of polarized deuterons.

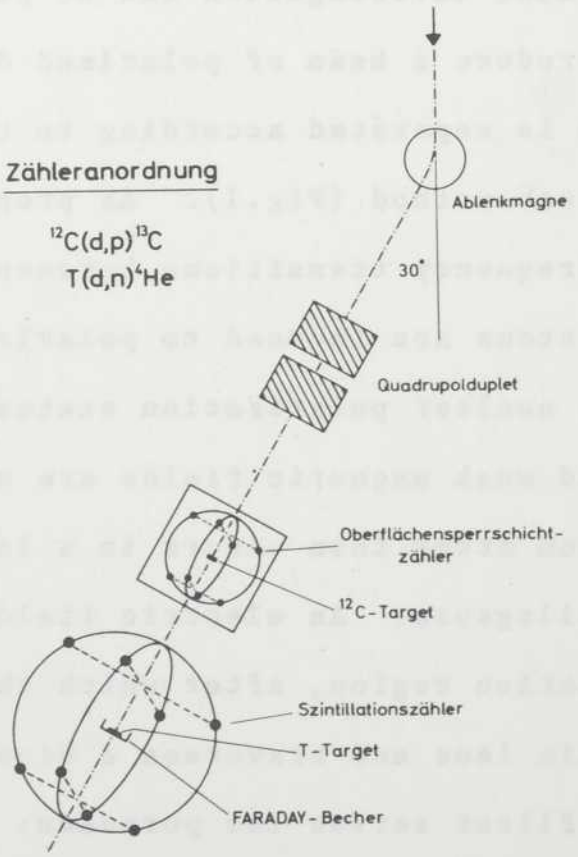

Fig. 2 Counter geometry for measurements using surface-barrier-detectors for charged particles and scintillators for neutrons.

1. The D^+ ions are separated from the D_2^+ and H^+ ions.
2. The symmetry axis of polarization can be rotated by changing the direction of the magnetic field relative to the polarization axis.

Some of the possible beam polarizations are:

P_{33}	P_3	
0,55(+1)	0,17(+1/3)	for the radiative transition 2-6
-0,55(-1)	0	for the radiative transition 3-5
-0,52(-1)	-0,17(-1/3)	for the strong field transition (2-6) and a subsequent weak field transition
+0,52(+1)	0	for the strong field transition (3-5) and a subsequent weak field transition
-0,01(0)	0,44(-2/3)	for weak field transition only (calculated from the transition probability).

The values listed for the vector polarization are calculated from measurements of the tensor polarization and the known transition probabilities. In parantheses are given the maximum possible values for the polarization of a beam produced by an ideal source with 100% transition probability and without contamination of the beam. The following values were obtained for the transition probabilities of our source:

Strong-field transition: $s = 0,76 - 1,0$
(depending on the high frequency power)

Weak field transition: $r = 0,993$

The measurement of the tensor polarization was carried out using the $T(d,n)^4He$ reaction in the vicinity of the 107 KeV resonance.

2. The reactions being investigated at our institute include:

$D(d,p)^3H$

$D(d,n)^3He$

$^6Li(d,p)^7Li$, $^6Li(d,p)^7Li^*$, $^6Li(d,\alpha)^4He$.

$^3He(d,p)^4He$ both with polarized and unpolarized target

$^3H\ (d,n)^4He$.

In addition I would like to present some measurements performed at the Federal Institute of Technology at Zurich of the elastic scattering of vector polarized deuterons from ^4He. Participating in this measurement were W. Grubler, V. Konig, P.A. Schmelzbach and P. Marmier.

The measurements at our institute* involved the determination of the analysing powers of the reactions previously mentioned as a function of scattering angle at energies less than 1 MeV. For the case of a polarized beam the differential cross section can be written as

$$\sigma_{pol}(\theta,\phi) = \sigma_o(\theta) + \sigma_1(\theta,\phi),$$

where σ_o is the differential cross section for unpolarized deuterons, θ the scattering angle and ϕ the azimuthal angle.

---

* Those participating in the measurement included E. Baumgatner H. Bürgisser, R. Benenson, H. Grunder, P. Huber, K. Jeltsch, Ch. Leemann, G. Lietz, G. Michel, G. Morgan, H.P. Naegeli, R.Neff, C. Petitjean, U. Rohrer, H. Rudin, H. Schieck, F. Seiler and H.R. Striebel.

In this relation σ_1 is a function of beam and target polarization. σ_1/σ_o is a sum of the products of the polarization components P_{ik}, the analyzing power D_{ik} and functions of the azimuthal angles ϕ.

In the case of a polarized beam and an unpolarized target the analyzing power of a reaction can be expressed in terms of the three tensor components

$$D_{33}(\theta),\ D_{13}(\theta) \text{ and } D_{11}(\theta) - D_{22}(\theta)$$

and the vector component

$$D_1(\theta).$$

These quantities are functions of the reaction angle θ and can be expressed in terms of the participating reaction matrix elements.

The arrangement of the proton or neutron detectors is shown in Fig.2. For each angle θ four counters placed at azimuthal angles of 0^o, 90^o, 180^o and 270^o were used. This allows a simple calculation of the analyzing power from a combination of the ratios of counting rates with polarized and unpolarized incoming deuterons.

3. Results

a) $D(d,p)^3He$

The four polarization components were measured as a function of θ at four energies between 150 keV and 460 keV.

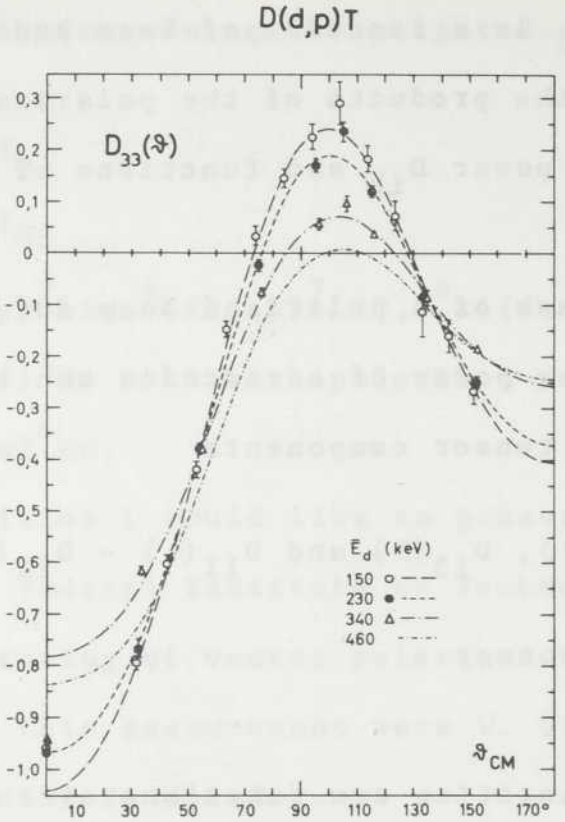

Fig. 3 Analyzing power D_{33} of the D(d,p)T-reaction as a function of c.m. angle for deuteron energies 150, 230, 340 and 460 keV.

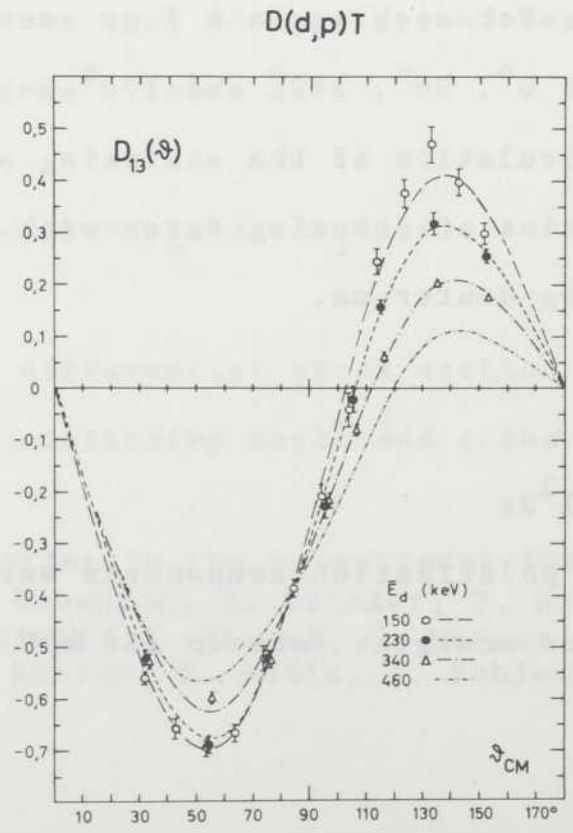

Fig. 4 Analyzing power D_{13} of the D(d,p)T-reaction as a function of c.m. angle for deuteron energies 150, 230, 340 and 460 keV.

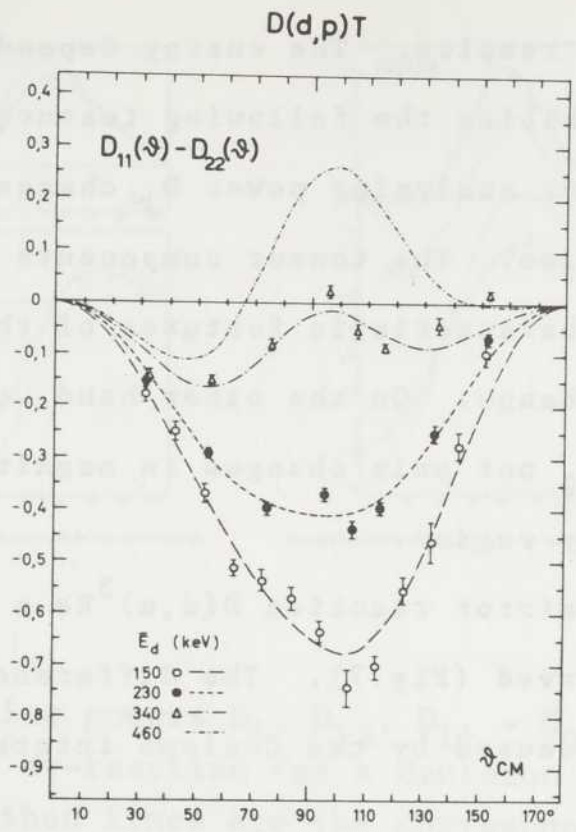

Fig. 5 Analyzing power $D_{11} - D_{22}$ of the D(d,p)T-reaction as a function of c.m. angle for deuteron energies 150, 230 340 and 460 keV.

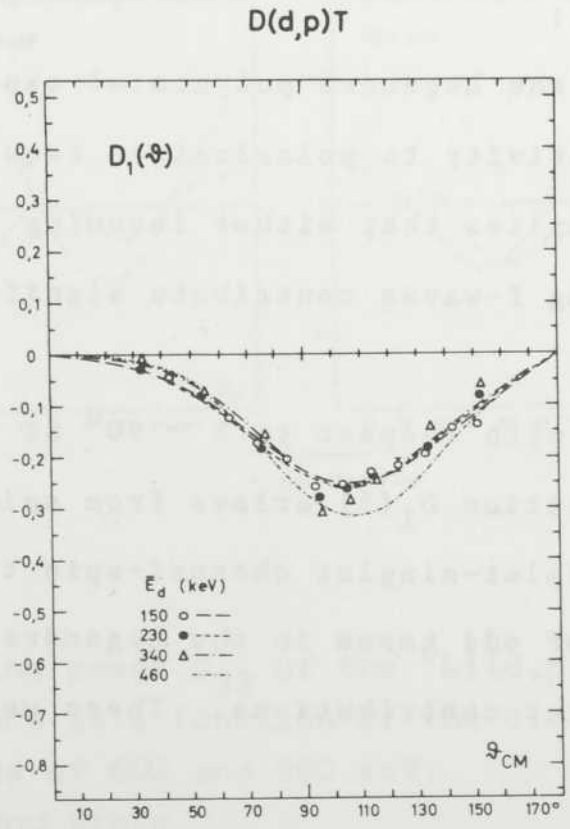

Fig.6 Analyzing power D_1 of the D(d,p)T-reaction as a function of c.m. angle for deuteron energies 150, 230, 340 and 460 KeV.

Fig.3 - 6 show the results. The energy dependence of the analyzing power exhibits the following features:

The vector analyzing power D_1 changes very little in this energy region. The tensor components D_{33} and D_{13} vary smoothly but the characteristic features of the angular distribution do not change. On the other hand, the third tensor component $D_{11} - D_{22}$ not only changes in magnitude but also in sign in this energy region.

For the mirror reaction $D(d,n)^3He$ a similar angular dependence is observed (Fig.7). The differences between the two reactions are caused by the Coulomb interaction in the exit channel.

Our analysis of the measurements show that the assumptions of the present theories are too limiting. There are three areas in which the experiments indicate a need for wider assumptions:

1. The fact that the Legendre polynomial expansions of the measured sensitivity to polarization require fourth order polynomials implies that either incoming d-waves ($\ell = 2$) and/or outgoing f-waves contribute significantly to the reaction.
2. The asymmetry with respect to $\theta = 90^\circ$ of the sensitivity to vector polarization $D_1(\theta)$ arises from spin-flips, i.e. quintet-triplet or triplet-singlet channel-spin transitions are present.
3. The presence of odd terms in the Legendre polynomial expansions requires quintet contributions. These were rejected formerly

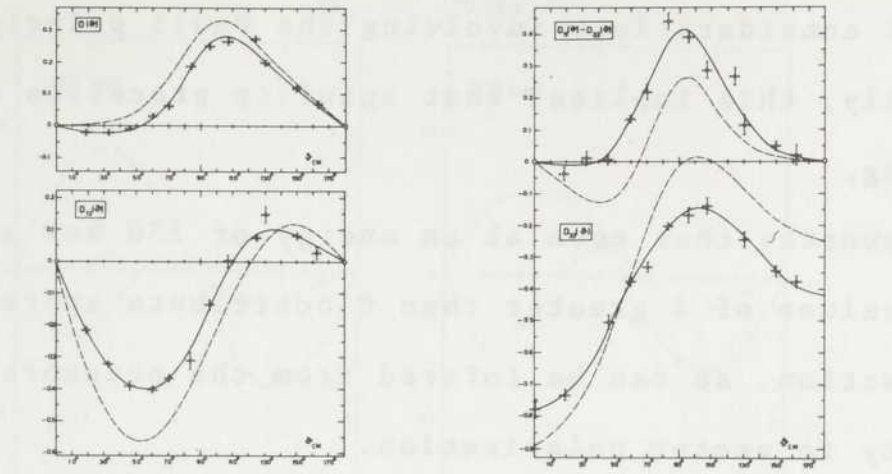

Polarisationsempfindlichkeit $D(\theta)$ und $D_{13}(\theta)$ der $D(d,n)^3He$-Reaktion.

Polarisationsempfindlichkeit $D_{11}(\theta)-D_{22}(\theta)$ und $D_{33}(\theta)$ der $D(d,n)^3He$-Reaktion.

Fig. 7 Analyzing powers D_1, D_{13}, $D_{11} - D_{22}$ and D_{33} of the $D(d,n)^3He$-reaction for a deuteron energy of 430 keV. The dashed lines are the corresponding values for the D(d,p)T-reaction.

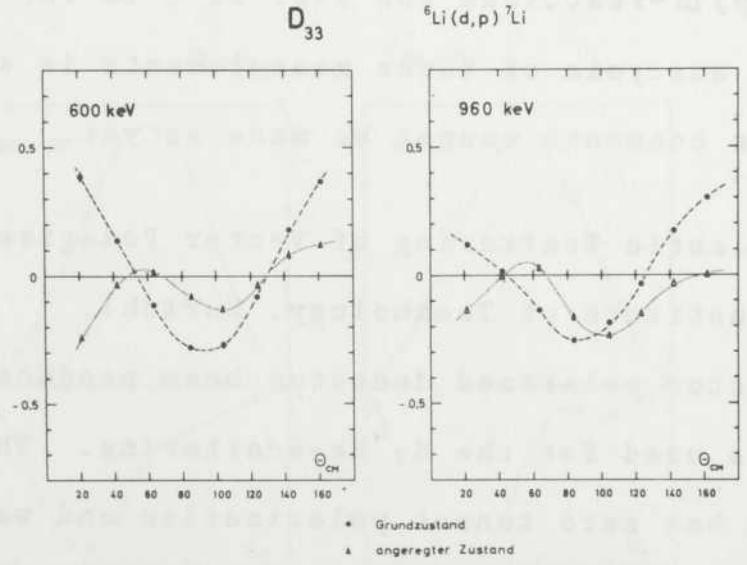

Fig. 8 Analyzing power D_{33} of the $^6Li(d,p)^7Li$- and $^6Li(d,p)^7Li^*$-reactions as a function of the c.m. angle for deuteron energies of 600 and 960 keV.

- ● ground state
- ▲ excited state (478 keV)

because of considerations involving the Pauli principle. Additionally, this implies, that spinflip processes must be occuring.

4. It is noteworthy that even at an energy of 150 keV angular momentum values of ℓ greater than 0 contribute appreciably to the reaction, as can be infered from the presence of the sensitivity to vector polarization.

b) $^{6}Li(d,p)^{7}Li$, $^{6}Li(d,p)^{7}Li^{*}$, $^{6}Li(d,\alpha)^{4}He$.

Polarized deuterons were used to measure the polarization efficiencies for both reactions in the energy region below 1 MeV. In the case of the (d,p) reaction the efficiency was measured for protons leaving the ^{7}Li nucleus in both the ground and the first excited state. Fig.8 - 11 show the result for the $^{6}Li(d,p)^{7}Li$-reactions and Fig. 12 - 15 for the $^{6}Li(d,\alpha)^{4}He$-reaction. The analysis of these measurements is still in progress, so that further comments cannot be made as yet.

c) Elastic Scattering of Vector Polarized Deuterons on ^{4}He (Federal Institute of Technology, Zurich).

A vector polarized deuteron beam produced by a tandem accelerator was used for the d-^{4}He-scattering. The vector polarized beam has zero tensor polarization and was produced by use of weak field transitions. The beam polarization was determined by $^{4}He(d,d)^{4}He$ scattering at $\theta_{Lab} = 45^{\circ}$, an angle for which the analyzing power has been measured by Trier and Haeberli[1)].

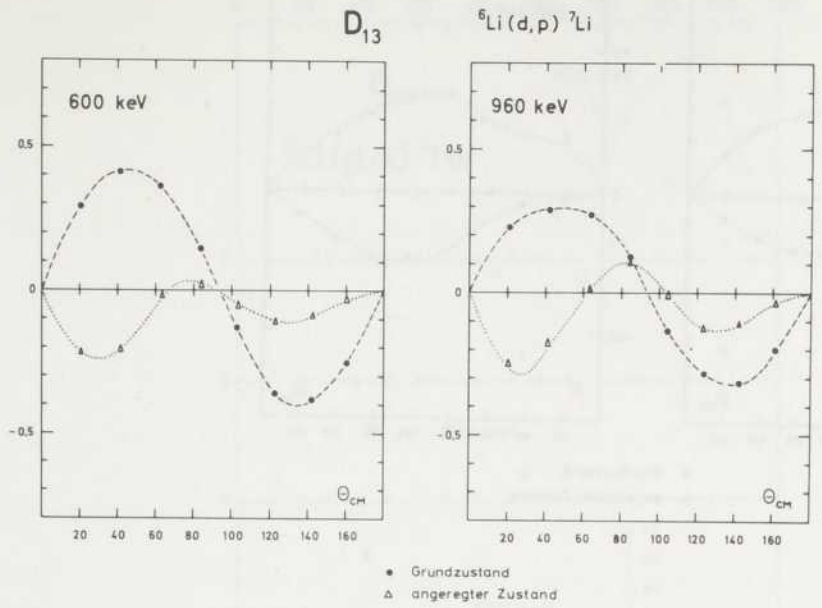

Fig. 9 Analyzing power D_{13} of the $^{6}Li(d,p)^{7}Li$- and $^{6}Li(d,p)^{7}Li^{*}$-reactions as a function of the c.m. angle for deuteron energies of 600 and 960 keV.

- ● ground state
- Δ excited state (478 keV)

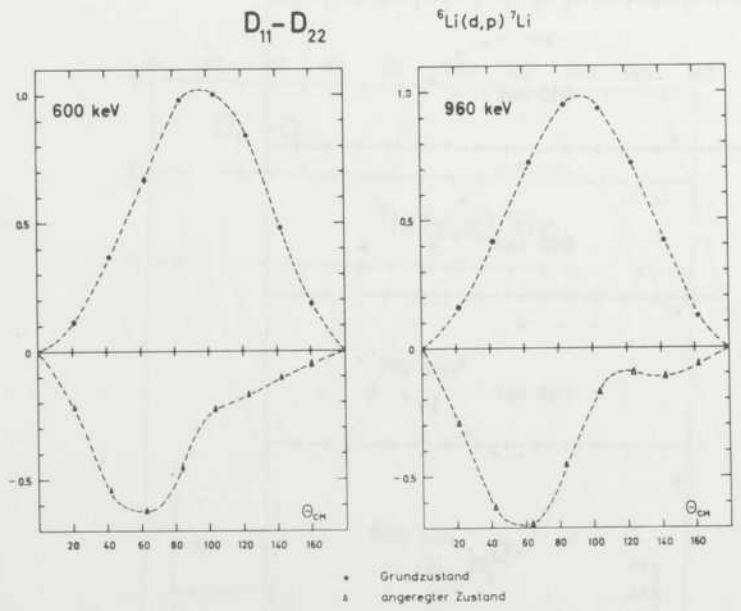

Fig. 10 Analyzing power $D_{11} - D_{22}$ of the $^{6}Li(d,p)^{7}Li$- and $^{6}Li(d,p)^{7}Li^{*}$-reactions as a function of the c.m. angle for deuteron energies of 600 and 960 keV.

- ● ground state
- Δ excited state

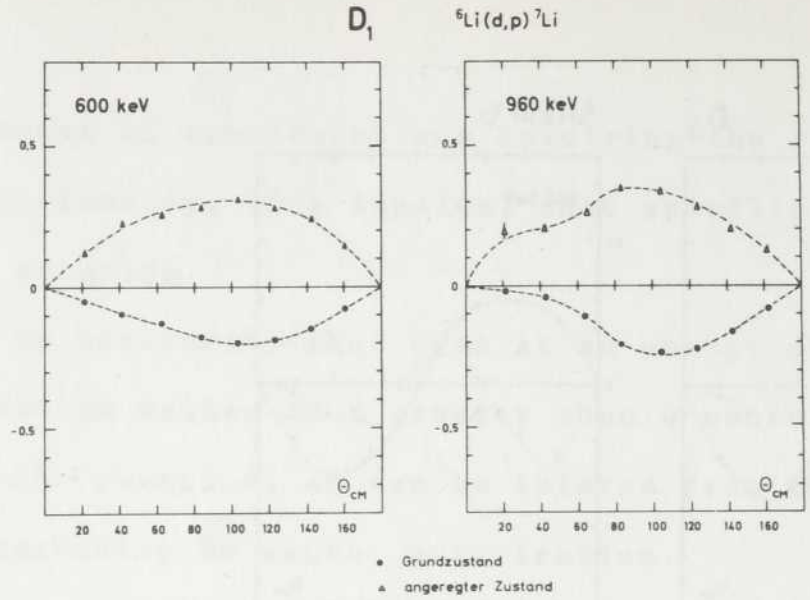

Fig. 11 Analyzing power D_1 of the $^6Li(d,p)^7Li$- and $^6Li(d,p)^7Li^*$-reactions as a function of the c.m. angle for deuteron energies of 600 and 960 keV.
● ground state
△ excited state

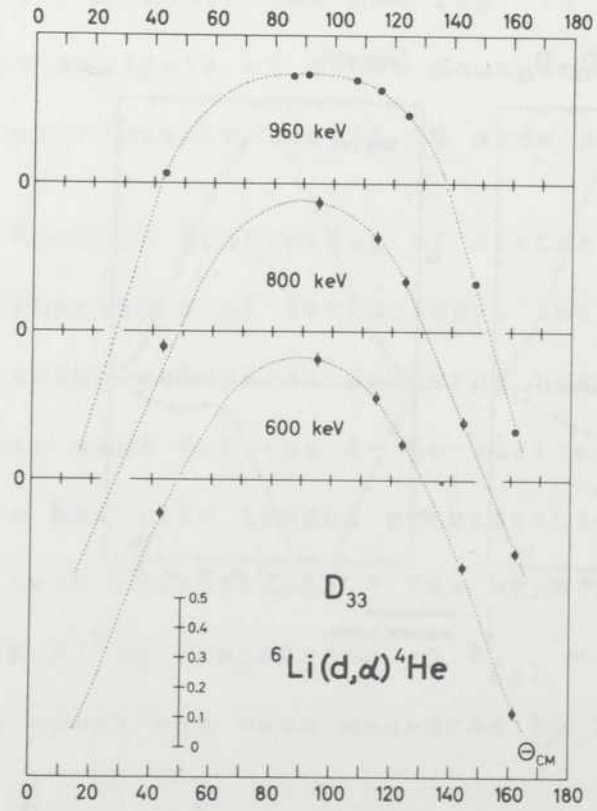

Fig. 12 Analyzing power D_{33} of the $^6Li(d,\alpha)^4He$-reaction as a function of c.m. angle for 600, 800 and 960 keV deuteron energy.

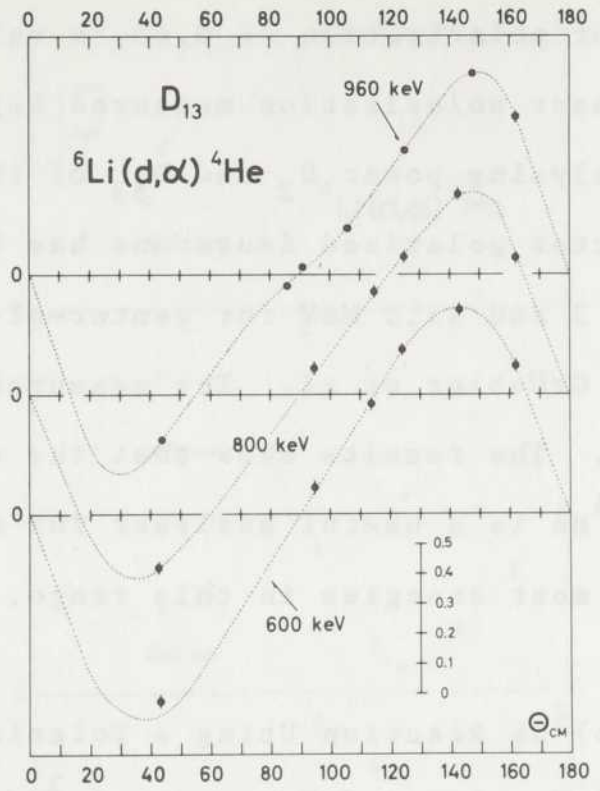

Fig. 13 Analyzing power D_{13} of the $^6Li(d,\alpha)^4He$-reaction as a function of c.m. angle for 600, 800 and 960 keV deuteron energy.

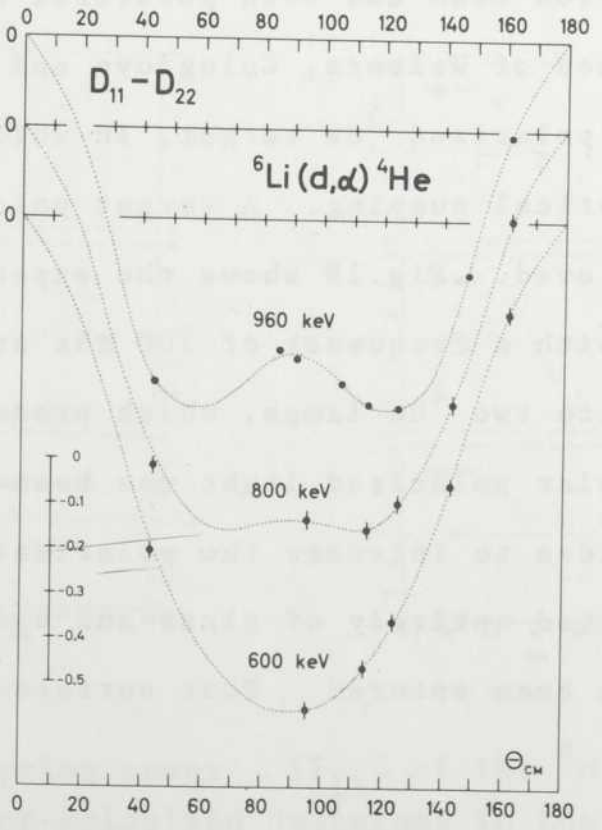

Fig. 14 Analyzing power $D_{11} - D_{22}$ of the $^6Li(d,\alpha)^4He$-reaction as a function of c.m. angle for 600,800 and 960 keV deuteron energy.

This gave a vector polarization of 0.43, a value which agrees well with the tensor polarization measured before acceleration.

The analyzing power D_2 and D_{33} of the $^4He(d,d)^4He$ reaction with vector polarized deuterons has been measured for energies between 3 and 11,5 MeV for center-of-mass angles from 33,6° to 151° by Grüebler et al. The measured values are shown in Fig.16 and 17. The results show that the elastic scattering of deuterons on ^4He is a useful analyser for deuteron vector polarization for most energies in this range.

4. $^3He(d,p)^4He$ Reaction Using a Polarized Deuteron Beam and Polarized and Unpolarized Targets and $^3H(d,n)^4He$ Reaction with Polarized Deuterons.

a) $^3He(d,p)^4He$

The $^3He(d,p)^4He$ reaction was studied at 430 keV with a polarized deuteron beam and both polarized and unpolarized target. The method of Walters, Colegrove and Schearer[2)] was used to obtain a polarized ^3He target, in which the polarization is produced by optical pumping. A target polarization of about 20% could be achieved. Fig.18 shows the experimental arrangement. Two oscillators with a frequency of 100 MHz and a power output of 1 kW each excite two ^4He lamps, which produce the pumping light. The circular polarized light was beamed at the target cell from both sides to increase the polarization. The target cell was constructed entirely of glass and had a thin window through which the beam entered. Four surface-barrier detectors

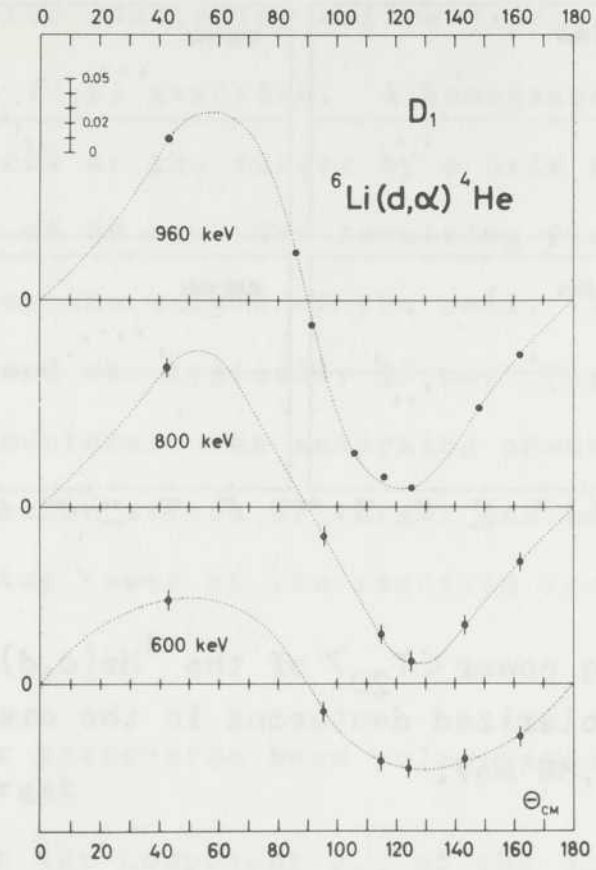

Fig. 15 Analyzing power D_1 of the $^6Li(d,\alpha)^4He$-reaction as a function of c.m. angle for 600, 800 and 960 keV deuteron energy.

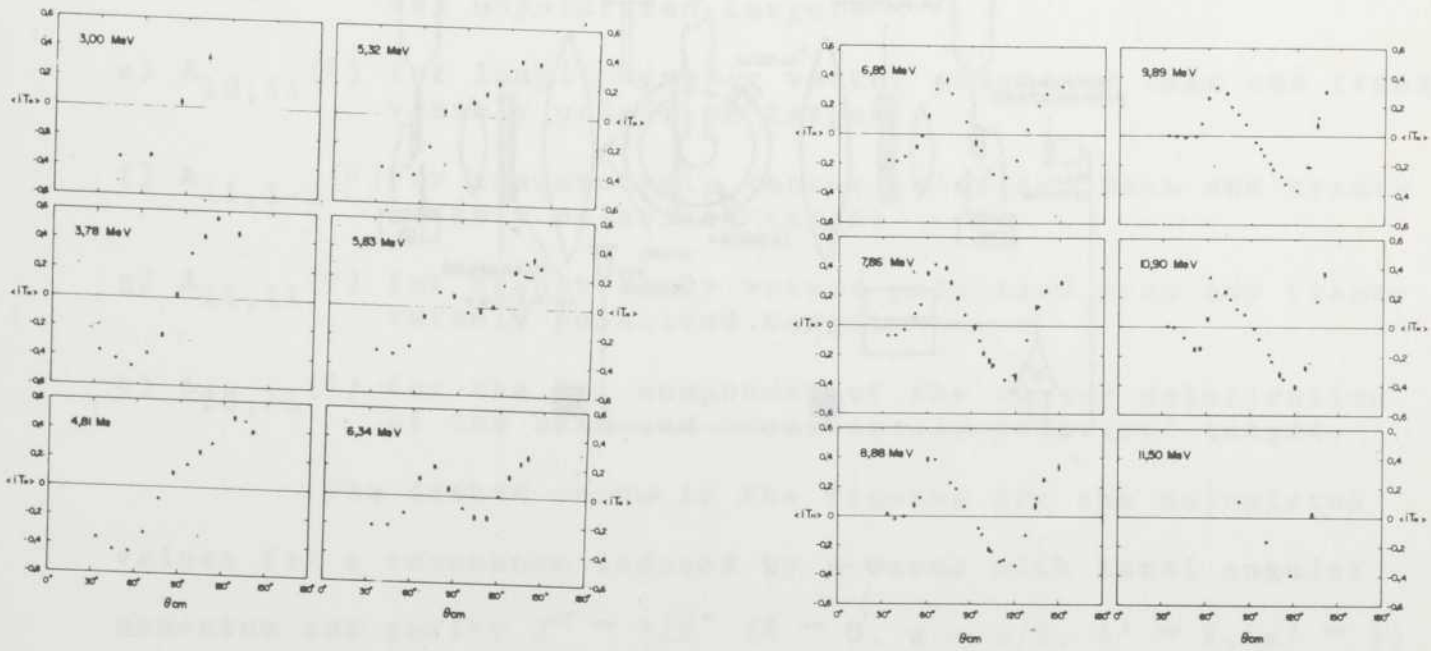

Fig. 16 a & b Analyzing power $\langle iT_{11} \rangle$ of the $^4He(d,d)^4He$-reaction for vector-polarized deuterons in the energy-range 3.00 - 11.50 MeV.

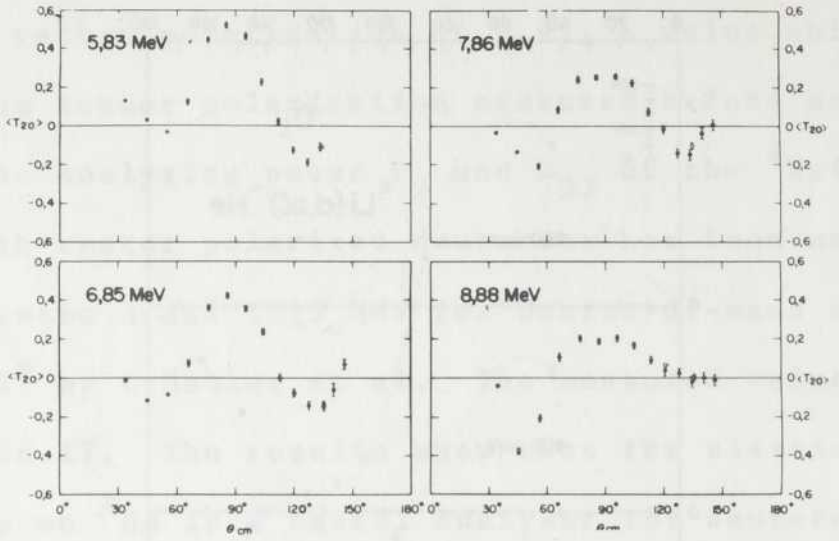

Fig. 17 Analyzing power $\langle T_{20} \rangle$ of the $^4He(d,d)^4He$-reaction for vector-polarized deuterons in the energy range 5.83 - 8.88 MeV.

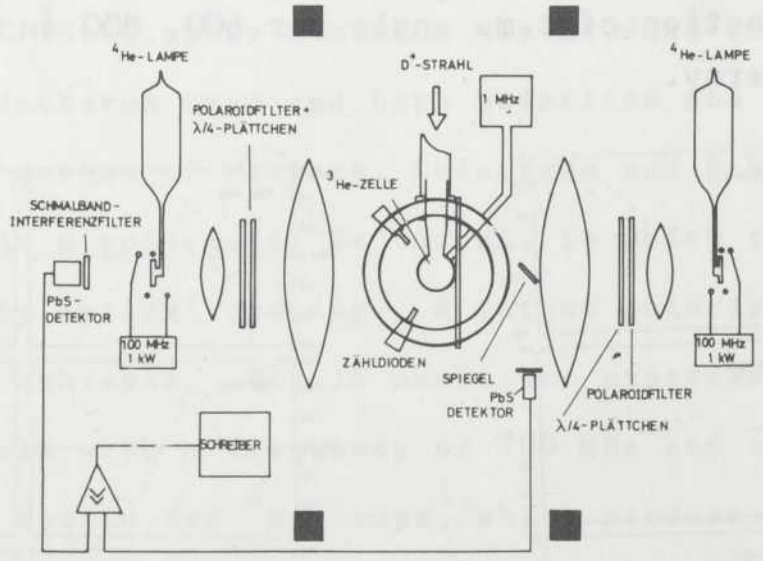

Fig. 18 Scheme of the polarized ^3He-target.

at each of the two scattering angles θ detected the protons produced by the (d,p) reaction. A homogeneous field of 60 Gauss was produced at the target by a pair of Helmholtz coilds with a diameter of 80 cm. The resulting field was constant to withing 0.1% over the volume of the cell. The polarized deuteron beam used was typically 35 nA. Fig.19 shows the ^{3}He-cell with the counters. The analyzing power was measured for various polarization states of target and beam. Fig. 20 - 27 show the analyzing power of the reaction for a set of such combinations

a) $A_{11,00}(\theta)$ for transverse beam polarization and unpolarized target

b) $A_{20,00}(\theta)$ for the component P_{33} of the polarized beam and unpolarized target

c) $A_{21,00}(\theta)$ for the P_{13} component of the tensor polarization of the beam and unpolarized target.

d) $A_{22,00}(\theta)$ for $P_{11}-P_{22}$ tensor polarization of the beam and and unpolarized target.

e) $A_{10,11}(\theta)$ for longitudinally vector polarized beam and transversely polarized target

f) $A_{11,1-1}(\theta)$ for transversely vector polarized beam and transversely polarized target

g) $A_{11,11}(\theta)$ for transversely vector polarized beam and transversely polarized target

h) $A_{20,11}(\theta)$ for the P_{33} component of the tensor polarization of the beam and transversely polarized target.

The dashed curves in the figures are the calculated values for a resonance induced by s-waves with total angular momentum and parity $J^\pi = 3/2^+$ ($\ell = 0$, $s = 3/2$, $\ell' = 2$, $s' = \frac{1}{2}$).

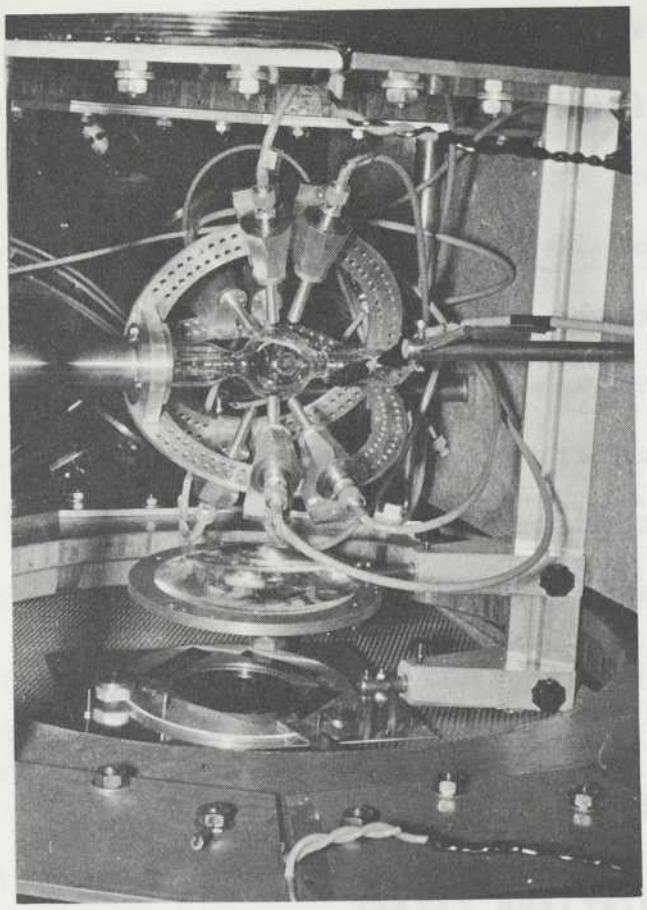

Fig. 19 View of the ^{3}He-target with mounted surface-barrier detectors.

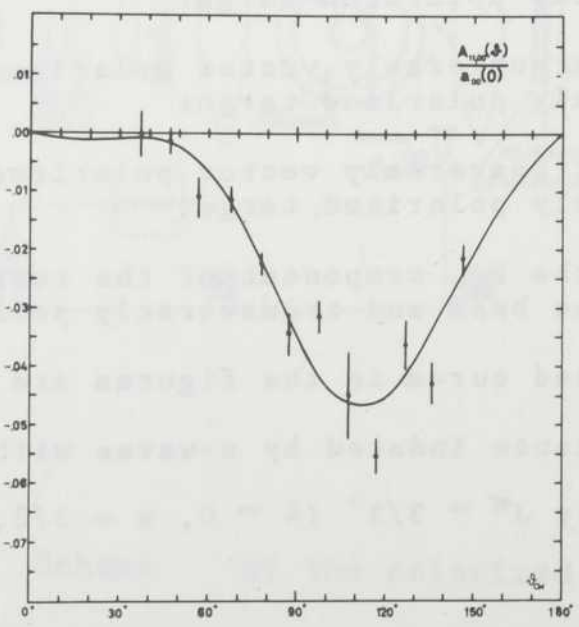

Fig. 20 Analyzing power $A_{11,00}(\vartheta)$ of the ^{3}He(d,p)^{4}He-reaction at 430 keV as a function of the c.m. angle.

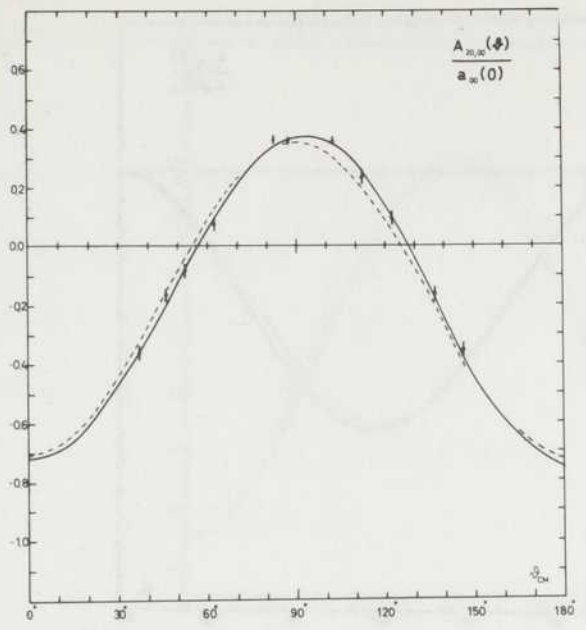

Fig. 21 Analyzing power $A_{20,00}(\vartheta)$ of the $^{3}He(d,p)^{4}He$-reaction at 430 keV as a function of the c.m. angle.

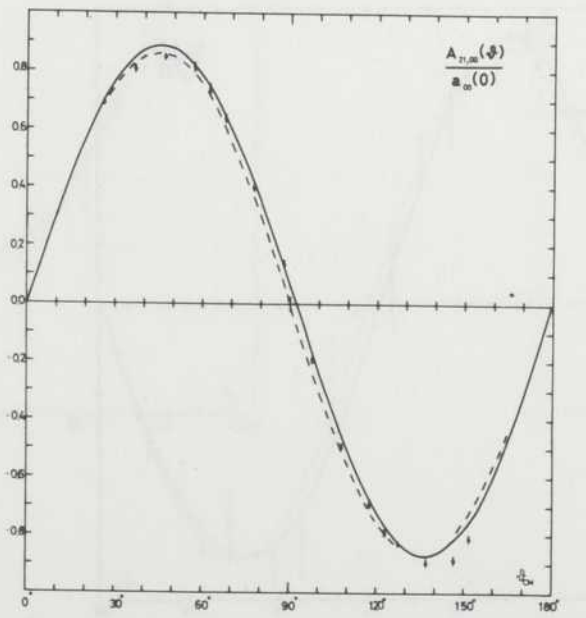

Fig. 22 Analyzing power $A_{21,00}(\vartheta)$ of the $^{3}He(d,p)^{4}He$-reaction at 430 keV as a function of the c.m. angle.

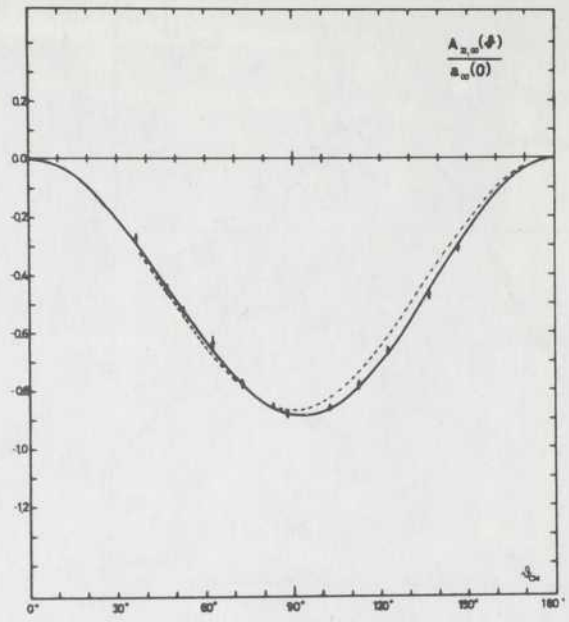

Fig. 23 Analyzing power $A_{22,00}(\vartheta)$ of the $^{3}He(d,p)^{4}He$-reaction at 430 keV as a function of the c.m. angle.

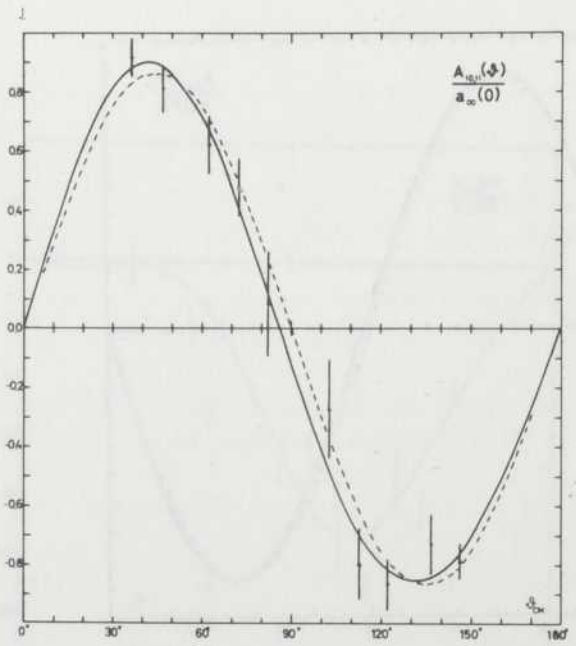

Fig.24 Analyzing power $A_{10,11}(\vartheta)$ of the $^{3}He(d,p)^{4}He$-reaction at 430 keV as a function of the c.m. angle.

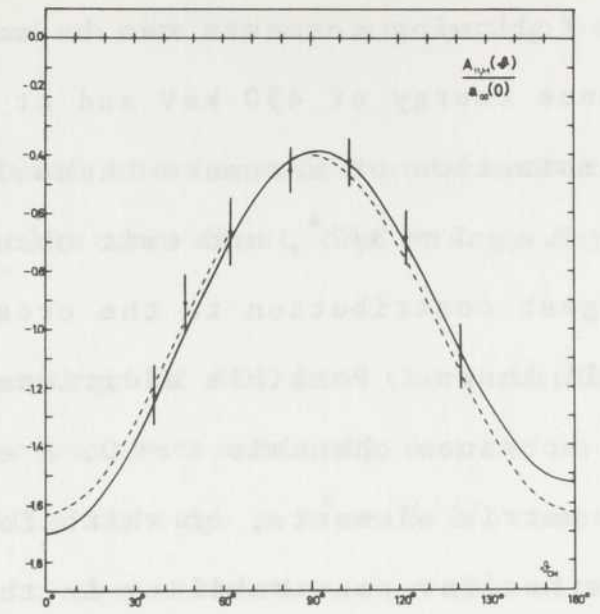

Fig. 25 Analyzing power $A_{11,1-1}(\vartheta)$ of the $^3He(d,p)^4He$-reaction at 430 keV as a function of the c.m. angle.

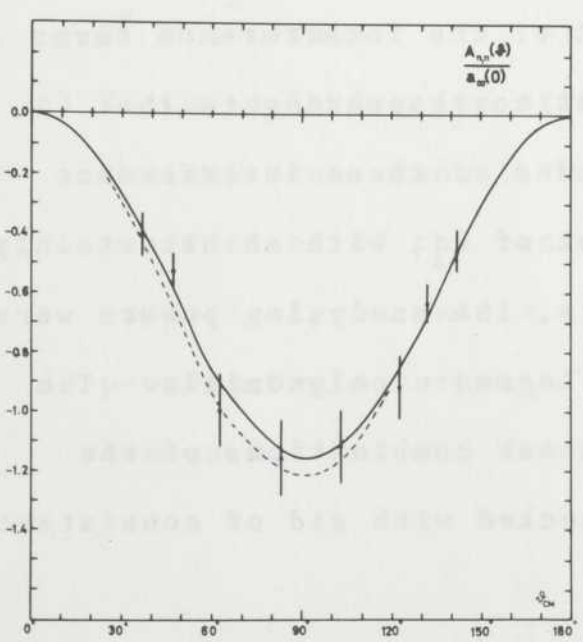

Fig. 26 Analyzing power $A_{11,11}(\vartheta)$ of the $^3He(d,p)^4He$-reaction at 430 keV as a function of the c.m. angle.

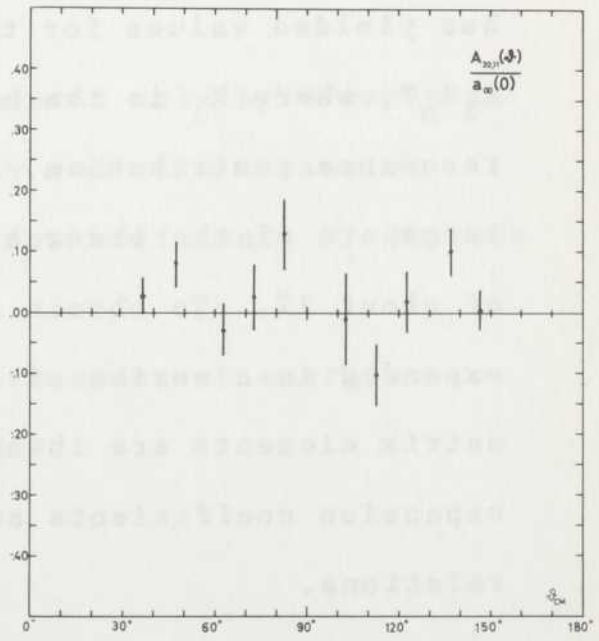

Fig. 27 Analyzing power $A_{20,11}(\vartheta)$ of the $^3He(d,p)^4He$-reaction at 430 keV as a function of the c.m. angle.

The following comments can be made about the results: At the resonance energy of 430 keV and at energies up to about 1 MeV, the combination of entrance channel $\ell = 0$ and channel spin $s = 3/2$, i.e. $J = 3/2^+$, and exit channel $\ell' = 2$ and $s' = \frac{1}{2}$ gives the largest contribution to the cross section. This fact is already well known. Possible additional contribution can come from the entrance channels $\ell = 0$, 1 and 2. There are 13 such reaction matrix elements, of which four can be disregarded because of the nuclear penetrability in the entrance channel, as well as the characteristic of the p-α system in the exit channel, as determined by Weitkamp and Haeberli[3].

Nine matrix elements remain to be determined. The preliminary analysis of the measurements available at present has yielded values for the real part of the interference terms $R_1 R_n^*$, where R_1 is the matrix element corresponding to the resonance contribution. The magnitudes of these interference terms are of the order a few per cent of R_1, with an uncertainty of about 1%. To obtain these results, the analyzing powers were expanded in a series of appropriate Legendre polynomials. The matrix elements are then given by linear combinations of the expansion coefficients and can be checked with aid of consistency relations.

b) $^3H(d,n)^4He$

The analyzing power as a function of scattering angle was also measured for the mirror reaction $^3H(d,n)^4He$ at energies less than 1 MeV.

The measured values of the analysing powers are shown in Fig. 28.

Examination of the Legendre polynomial expansion leads to the following conclusions about the energy dependence of the analyzing power:

a) At the resonance energy of 107 keV the polarization efficiency is to within a few percent entirely due to an s-wave induced resonance proceeding through a $J^{\pi} = 3/2^{+}$ compound nuclear state, analogous to the situation for the mirror reaction.

b) At energies up to 1 MeV the s-wave induced $J^{\pi} = 3/2^{+}$ resonance continues to make the largest contribution to the cross section. The next largest separable contribution stems from real part of the matrix element involving the s-wave induced $J^{\pi} = \frac{1}{2}^{+}$ state.

c) Vector polarization effects are produced only by d-waves in the entrance channel, since the only non-zero expansion coefficient of the vector polarization efficiency D_1 depends exclusively on matrix elements with $\ell = 2$.

d) p-waves begin to contribute to the reaction at energies as low as 0,2 MeV and d-waves at 0,6 MeV.

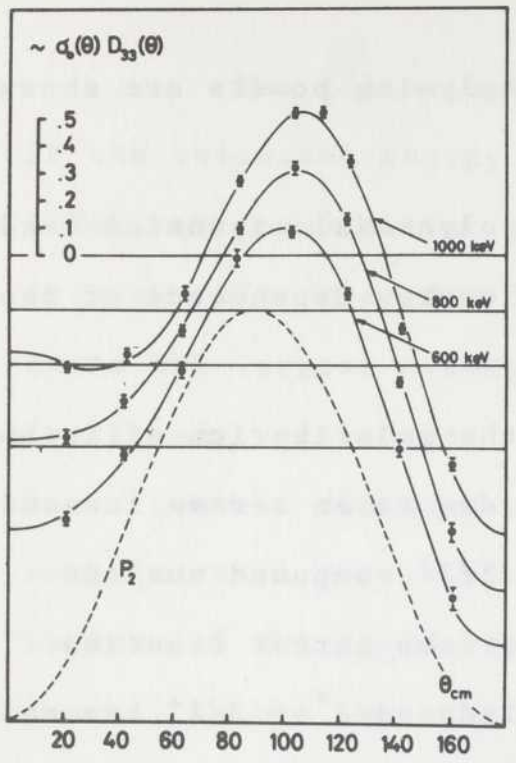

T(d̂,n) ⁴He Empfindlichkeit auf Tensorpolarisation

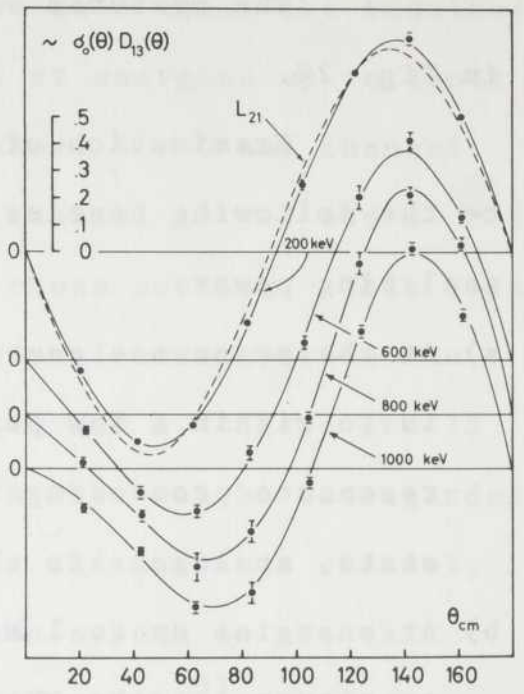

T(d̂,n) ⁴He Empfindlichkeit auf Tensorpolarisation

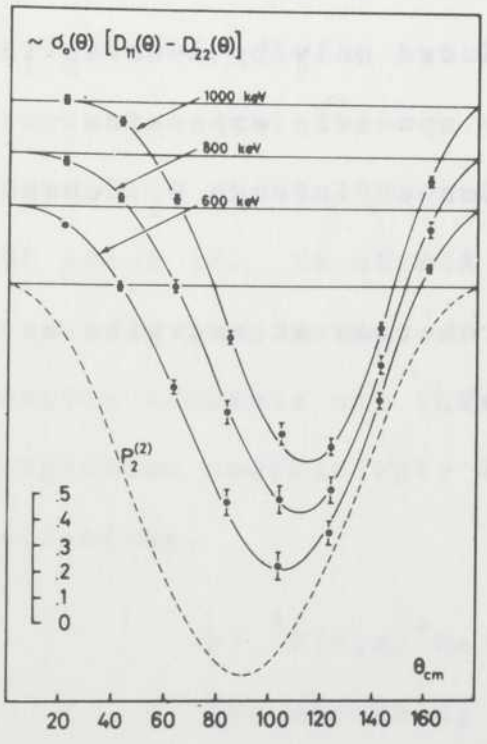

T(d̂,n) ⁴He Empfindlichkeit auf Tensorpolarisation

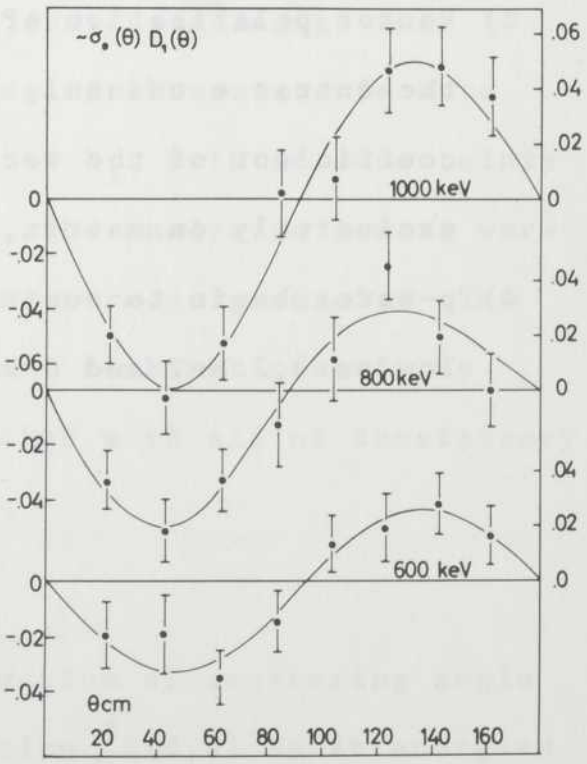

T(d̂,n)⁴ He Empfindlichkeit auf Vektorpolarisation

Fig. 28 a - d Analyzing power $D_{13}(\theta)$ of the $T(d,n)^4He$-reaction as a function of c.m. angle for deuteron energies of 600, 800 and 1000 keV.

REFERENCES

1. Trier and Haeberli, Physical Review Letters 18, 915, 1967

2. Walters, Colegrove and Schearer, Phys. Rev. 132, 2561 (1963).

3. Weitkamp and Haeberli, Nuclear Physics 83, 46, 1966.

EFFETS LIES AU SPIN DANS LA DIFFUSION DE PROTONS ET LES REACTIONS (p-d)

P. CATILLON

Centre d'Etudes Nucléaires de Saclay, France.

I - INTRODUCTION

Le développement des sources d'ions polarisés[1] durant ces dernières années a permis de réaliser un grand nombre d'expériences qui n'étaient pas possibles auparavant.

Les caractéristiques des faisceaux polarisés actuels sont :

- leur grande intensité (20 - 100 nA de faisceau de protons extraits du cyclotron de Saclay[2])
- leur forte polarisation (80 - 90%) et dans le cas des deutons la possibilité d'avoir des polarisations vectorielle ou tensorielle
- la possibilité, grâce aux transitions RF de la source[3] de renverser rapidement la direction de la polarisation sans variation de forme ou d'intensité du faisceau.

L'erreur commise sur la mesure d'une asymétrie est :

$$d\mathcal{A} = \mathcal{A}\frac{dP_i}{P_i} + \frac{1}{P_i}\frac{\sqrt{1-\mathcal{A}^2P_i^2}}{\sqrt{N}} + \varepsilon$$

Le premier terme correspond à l'erreur de mesure de la polarisation du faisceau incident P_i. Il intervient en général comme un facteur de normalisation et il est d'autant plus petit que l'asymétrie mesurée est petite.

Le deuxième terme est l'erreur statistique.

ε, qui correspond à l'erreur géométrique dans le cas d'une asymétrie droite-gauche, correspond, pour une source à transitions RF, à la différence des faisceaux intégrés dans les deux états de spin ; elle peut être facilement inférieure à 10^{-3}.

On peut ainsi avoir des mesures d'asymétrie d'une précision meilleure que les mesures de section efficace, pouvant descendre à 10^{-3} dans des cas favorables[4] (figure 1).

Les améliorations futures dans ce domaine vont dans deux directions :

1) aug mentation d'intensité :

Des ioniseurs basés sur l'échange de charge pourraient donner un gain de l'ordre de 100 permettant ainsi d'avoir des faisceaux polarisés aussi intense que des faisceaux ordinaires[5].

Ce même principe permet d'obtenir des sources de H^- polarisés adaptables aux Van de Graff tandem.

2) adaptation à des synchrotrons de haute énergie :

R. Beurtey[6] a montré qu'il était possible de contrôler la dépolarisation des protons au cours de l'accélération lorsqu'ils traversent une résonance.

D'autre part le nombre beaucoup moins élevé de résonances traversées dans le cas des deutons rend facile l'accélération de ceux-ci jusqu'à des énergies de l'ordre de quelques BeV.

II - DIFFUSION ELASTIQUE

II-1 Asymétrie de la section efficace

Par renversement du sens du temps dans le cas d'une cible avec spin et par rotation seulement dans le cas d'une cible de spin zéro, le paramètre d'asymétrie $A(\theta)$ est égal à la polarisation $P(\theta)$ [7].

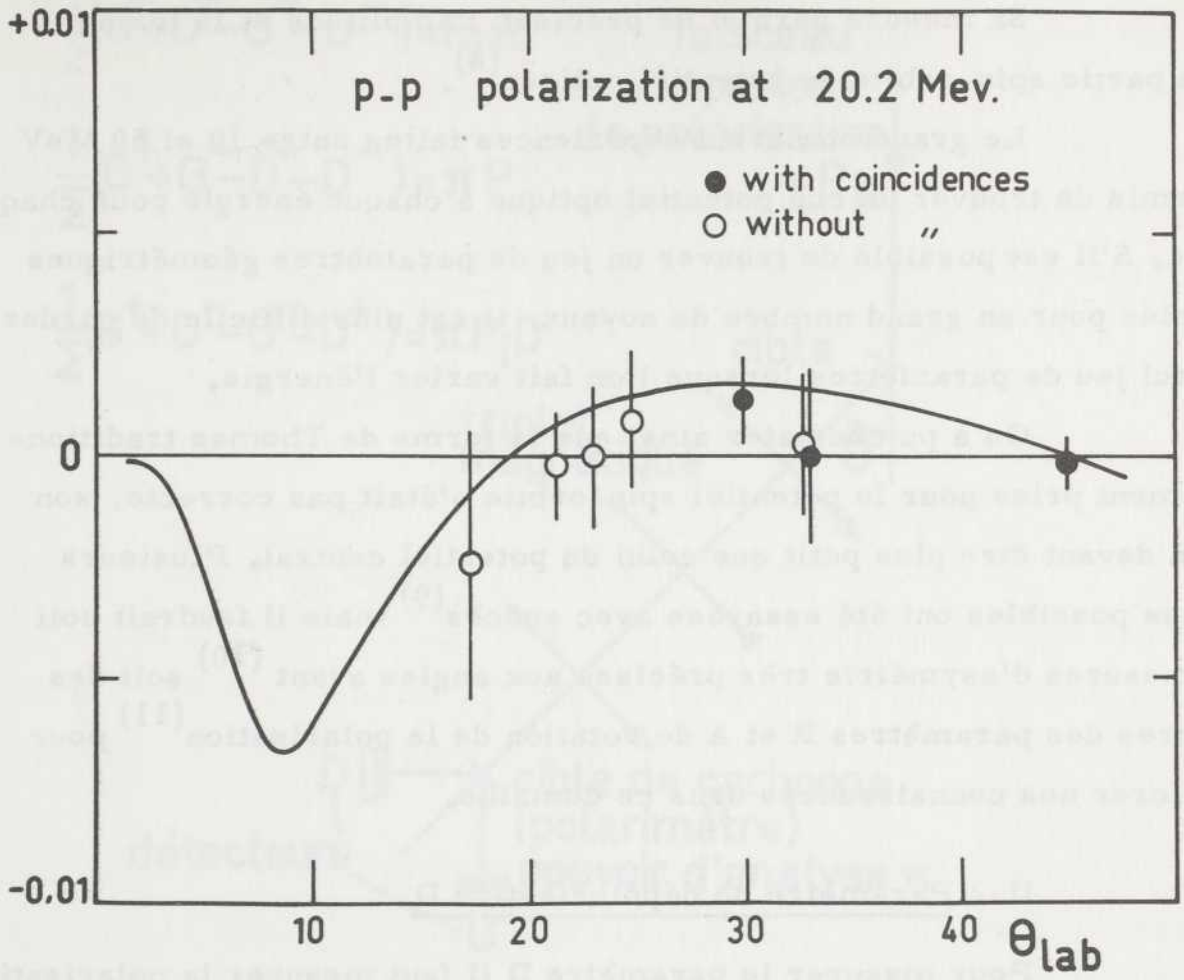

Figure 1 : Asymétrie dans la diffusion p.p à 20.2 MeV (réf. 4)

Sa mesure permet de préciser l'amplitude et la forme de la partie spin-orbite du potentiel optique[8].

Le grand nombre d'expériences faites entre 10 et 50 MeV a permis de trouver un bon potentiel optique à chaque énergie pour chaque noyau. S'il est possible de trouver un jeu de paramètres géométriques valables pour un grand nombre de noyaux, il est plus difficile de garder un seul jeu de paramètres lorsque l'on fait varier l'énergie.

On a pu constater ainsi que la forme de Thomas traditionnellement prise pour le potentiel spin-orbite n'était pas correcte, son rayon devant être plus petit que celui du potentiel central. Plusieurs formes possibles ont été essayées avec succès[9] mais il faudrait soit des mesures d'asymétrie très précises aux angles avant[10] soit des mesures des paramètres R et A de rotation de la polarisation[11] pour améliorer nos connaissances dans ce domaine.

II-2 Paramètre de dépolarisation D

Pour mesurer le paramètre D il faut mesurer la polarisation P_f des protons de polarisation initiale P_i, après diffusion. D est donné par la relation[7]

$$P_f = \frac{P + D P_i}{1 + A P_i}$$

Le montage expérimental correspondant est représenté sur la figure 2.

La différence entre D et 1 donne directement la probabilité de renversement de spin du proton dans la diffusion à l'angle considéré :

$$1-D = 2 \times \frac{\text{section efficace de renversement de spin}}{\text{section efficace}}$$

$$\frac{1}{\Sigma}(G^+ + D^+ - G^- - D^-) = P_i \mathcal{A}$$

$$\frac{1}{\Sigma}(G^+ + G^- - D^+ - D^-) = \pi P$$

$$\frac{1}{\Sigma}(G^+ + D^- - G^- - D^+) = \pi P_i D$$

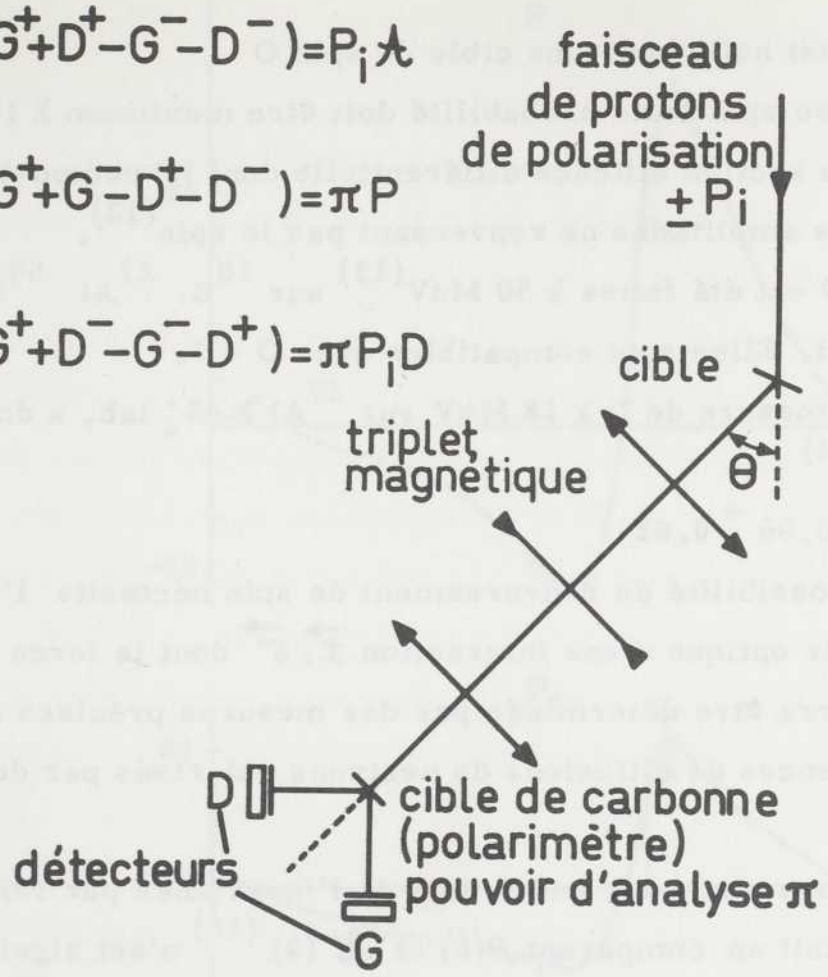

Figure 2 : Montage expérimental de la mesure du paramètre D de dépolarisation

cette probabilité est nulle pour une cible de spin O

Pour une cible avec spin cette probabilité doit être maximum à l'angle du minimum de la section efficace différentielle dont le comportement est dominé par les amplitudes ne renversant pas le spin[12].

Des mesures de D ont été faites à 50 MeV[13] sur ^{10}B, ^{27}Al, ^{59}Co, $^{113\text{-}115}In$ et ^{209}Bi. Elles sont compatibles avec D = 1.

Une mesure de D à 18 MeV sur ^{27}Al à 43° lab. a donné comme résultat[14] :

$$D = 0.96 \pm 0.02$$

La possibilité de renversement de spin nécessite l'introduction dans le modèle optique d'une interaction $\vec{I}.\vec{\sigma}$ dont la force certainement faible pourra être déterminée par des mesures précises de D ou par des expériences de diffusions de neutrons polarisés par des cibles polarisées[15].

Il faut remarquer que le test de l'invariance par renversement du temps fait en comparant P(θ) et $\mathcal{A}(\theta)$[16] n'est significatif que si la probabilité de renversement de spin n'est pas nulle.

II-3 Paramètres de correlation de spin

Ces paramètres A_{xx} et A_{yy}[17] nécessitent la polarisation de la cible.

Ils ont été souvent mesurés dans l'interaction nucléon-nucléon[18] et ces expériences améliorent sensiblement la connaissance que l'on a des déphasages p-p et n-p.

Ils ont été aussi mesurés dans la diffusion p-^{3}He à 19 MeV[19] avec une cible polarisée par pompage optique (figure 3).

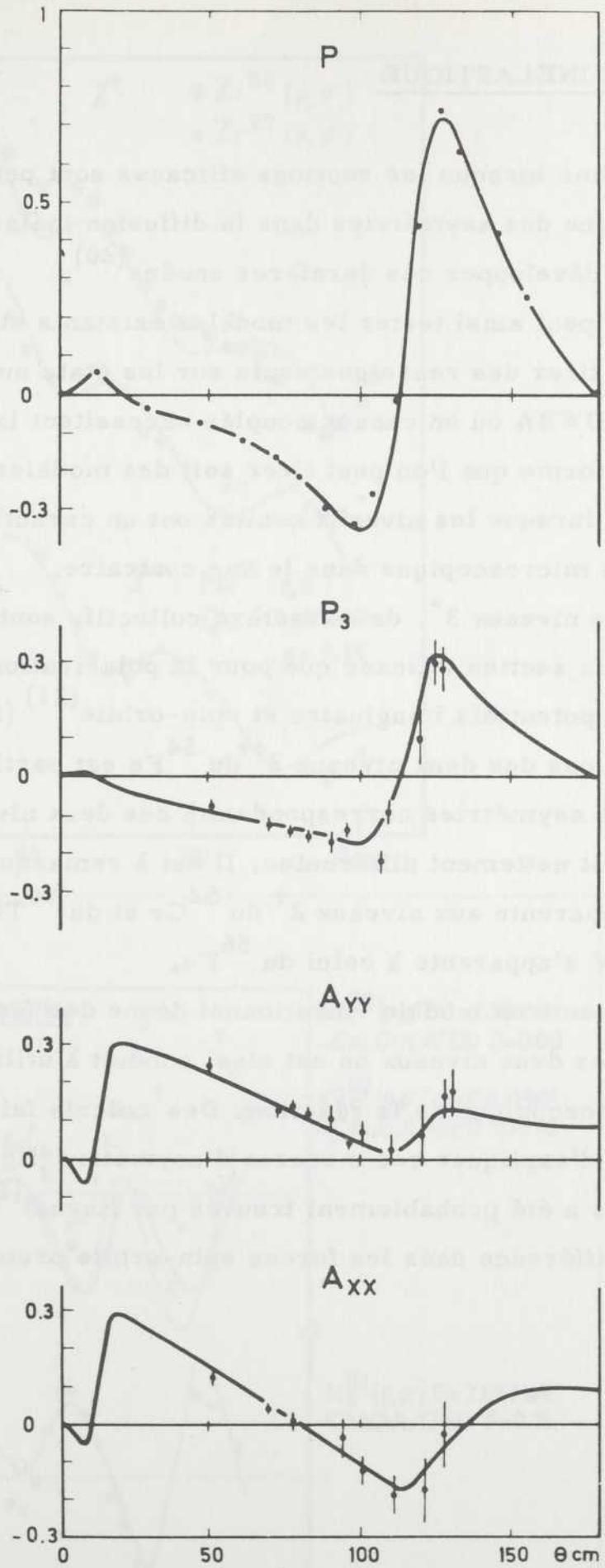

Figure 3 : Paramètres de corrélation de spin dans la diffusion p-^{3}He à 19 MeV avec $(d\sigma/d\omega)_{\text{gauche}} = \left(\frac{d\sigma}{d\omega}\right)_0 \left(1 + \bar{P}P + \bar{P}_3 P_3 + P\bar{P}_3 A_{yy}\right)$

$$\left(d\sigma/d\omega\right)_{ba.} = \left(\frac{d\sigma}{d\omega}\right)_0 \left(1 + \bar{P}\bar{P}_3 A_{xx}\right)$$

$\bar{P}$ et $\bar{P}_3$ étant les polarisations verticales du faisceau et de la cible

III - DIFFUSION INELASTIQUE

Même lorsque les sections efficaces sont petites une étude systématique des asymétries dans la diffusion inélastique de protons a pu se développer ces dernières années[20].

On peut ainsi tester les modèles existants et, s'ils sont satisfaisants, en tirer des renseignements sur les états nucléaires. Les calculs faits en DWBA ou en canaux couplés nécessitent la connaissance des facteurs de forme que l'on peut tirer soit des modèles rotationnel ou vibrationnel, lorsque les niveaux excités ont un caractère collectif, soit d'un modèle microscopique dans le cas contraire.

Les niveaux 3^-, de caractère collectif, sont bien rendus aussi bien pour la section efficace que pour la polarisation à condition de déformer les potentiels imaginaire et spin-orbite[21] (figure 4).

Le cas des deux niveaux 2^+ du ^{54}Fe est particulièrement intéressant. Les asymétries correspondant à ces deux niveaux (1,41 MeV et 2,97 MeV) sont nettement différentes. Il est à remarquer que le niveau à 1,41 MeV s'apparente aux niveaux 2^+ du ^{52}Cr et du ^{50}Ti alors que celui à 2,97 MeV s'apparente à celui du ^{56}Fe.

Comme un modèle vibrationnel donne des facteurs de forme identique pour ces deux niveaux on est ainsi conduit à utiliser une description microscopique de la réaction. Des calculs fait par Satchler[22] sont encore loin d'expliquer ces mesures d'asymétrie (figure 5). L'origine de ces difficultés a été probablement trouvée par Raynal[23] et fait intervenir une différence dans les forces spin-orbite proton-proton et proton-neutron.

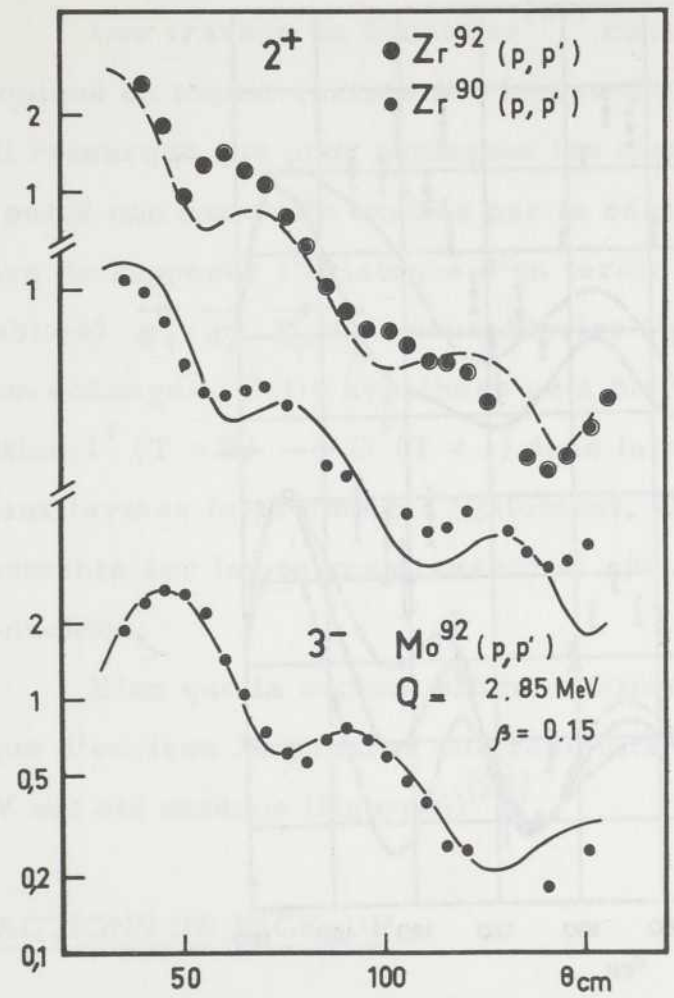

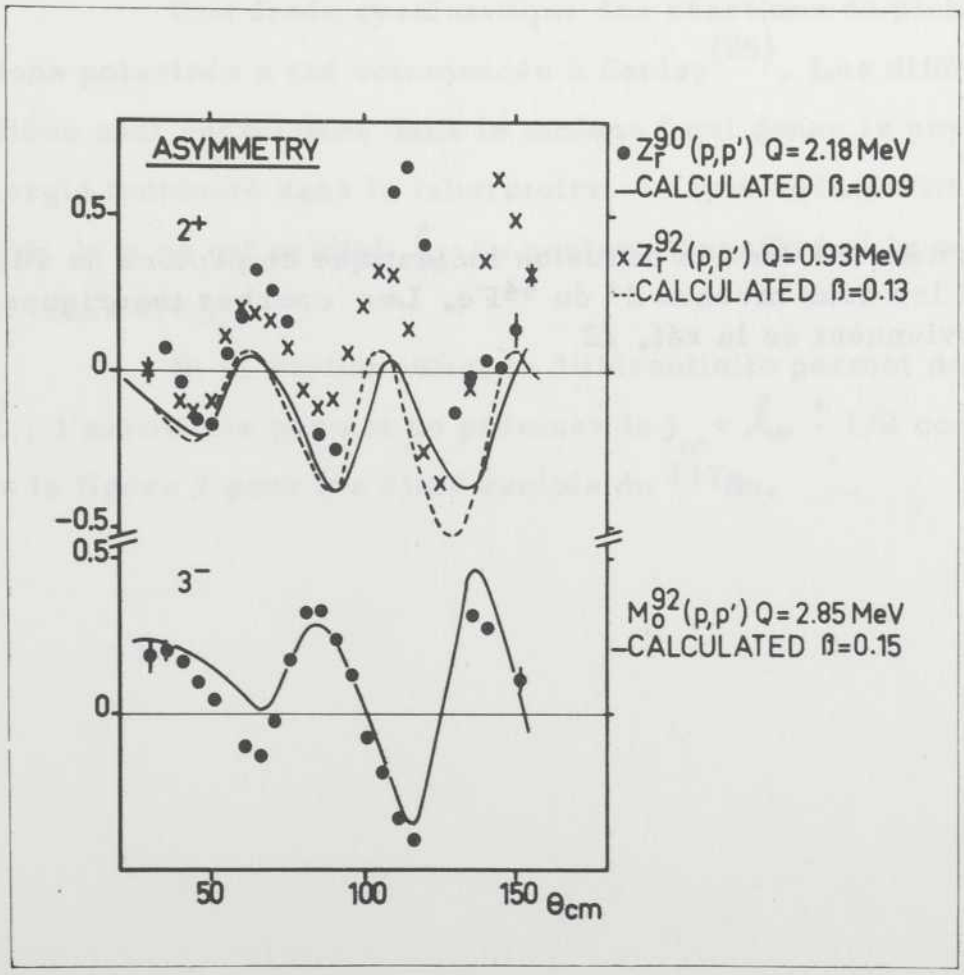

Figure 4 : Analyse au moyen d'équations couplées dans le cadre du modèle vibrationnel (réf. 27) de la diffusion inélastique de protons

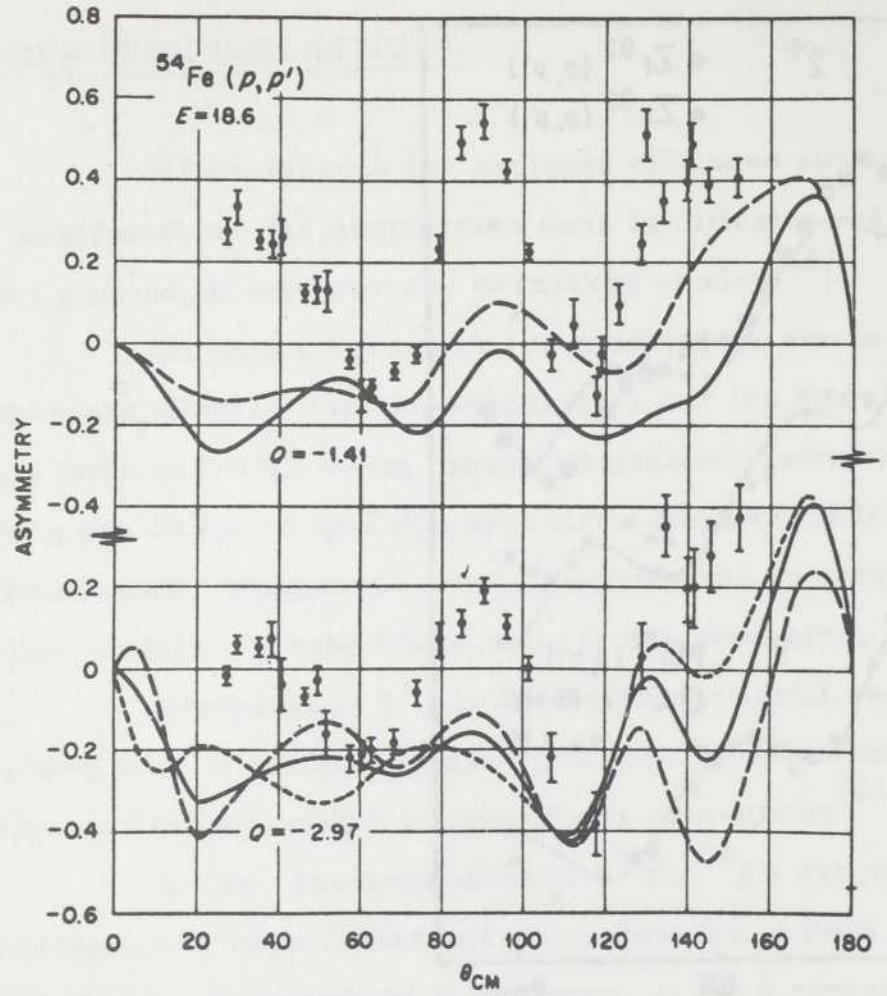

Figure 5 : Asymétries dans la diffusion inélastique de protons de 18.6MeV sur les deux niveaux 2^+ du ^{54}Fe. Les courbes théoriques proviennent de la réf. 22

Les travaux de Schaeffer[24] concernent une description microscopique en tenant compte des forces d'échange ou d'antisymétrisation. Il remarque que pour expliquer les distributions angulaires des états de parité non naturelle excités par la réaction (^{3}He, t) il a été nécessaire de supposer l'existence d'un terme $S_{12}\ \vec{\tau}_1 . \vec{\tau}_2$ en plus du terme habituel $\vec{\sigma}_1 . \vec{\sigma}_2\ \vec{\tau}_1 . \vec{\tau}_2$ pour décrire l'interaction du proton et du neutron échangés. Cette hypothèse peut être vérifiée par l'étude de la transition 1^+ (T = O) $\longrightarrow$ O^+(T = 1) dans la réaction ^{14}N (pp') ^{14}N* où ces deux termes interviennent également. On pourra ainsi avoir des renseignements sur les termes tenseur et spin orbite dans la force nucléon-nucléon.

Bien que la section efficace différentielle sur le O^+ de ^{14}N ne soit que d'environ 30 μbarns des résultats préliminaires d'asymétrie à 24 MeV ont été obtenus (figure 6)[25].

IV - REACTIONS DE PICK-UP

Une étude systématique des réactions de pick-up par protons polarisés a été commencée à Saclay[26]. Les différentes réactions étudiées sont regroupées dans le tableau I qui donne le noyau cible, l'énergie incidente dans le laboratoire, le spin et la parité du niveau excité, le moment orbital l_n du neutron transféré et le moment angulaire total transféré j_n.

Si la section efficace différentielle permet de déterminer le l, l'asymétrie permet de préciser le $j_{n'} = l_n \pm 1/2$ comme on le voit dans la figure 7 pour les états excités du ^{117}Sn.

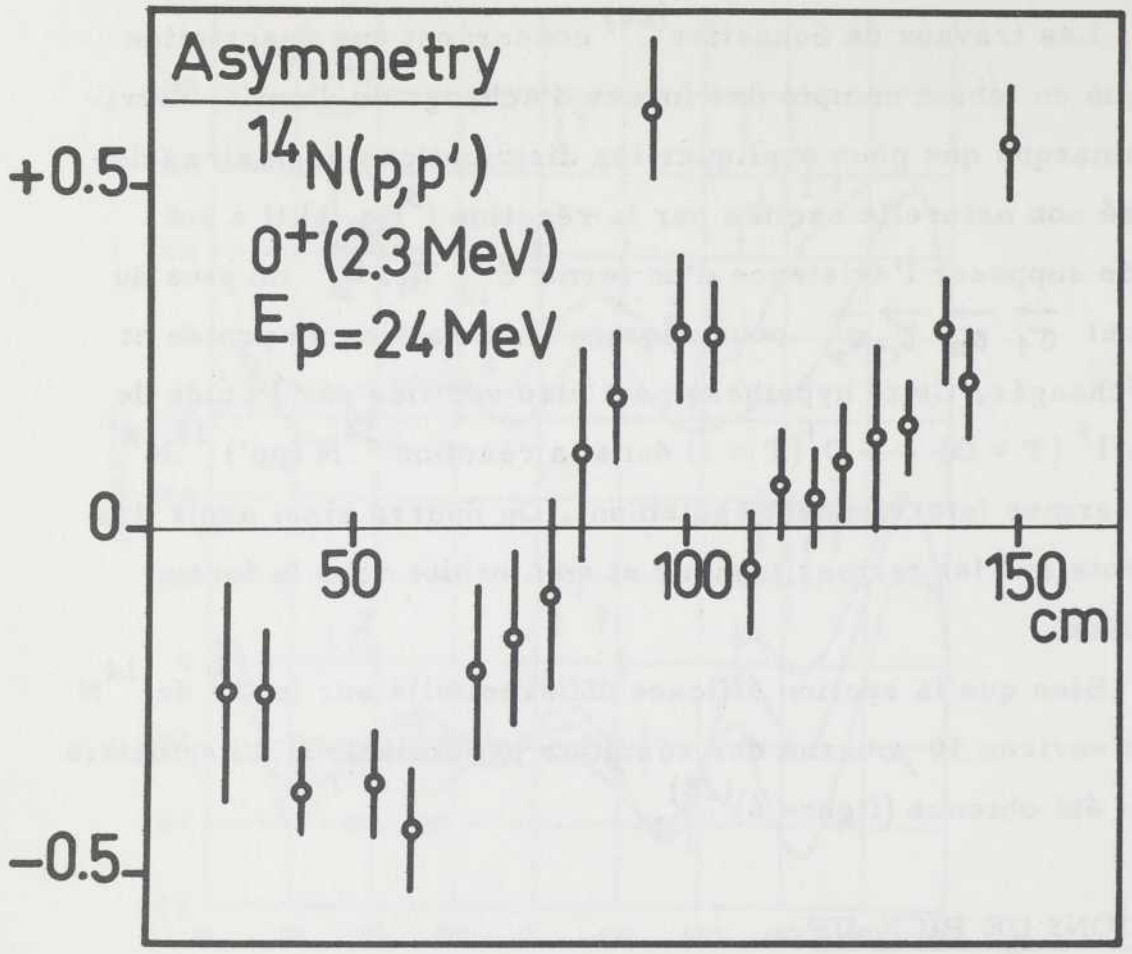

Figure 6 : Résultats préliminaires de la diffusion inélastique de protons de 23,7 MeV sur le niveau O^+ de ^{14}N (réf. 25)

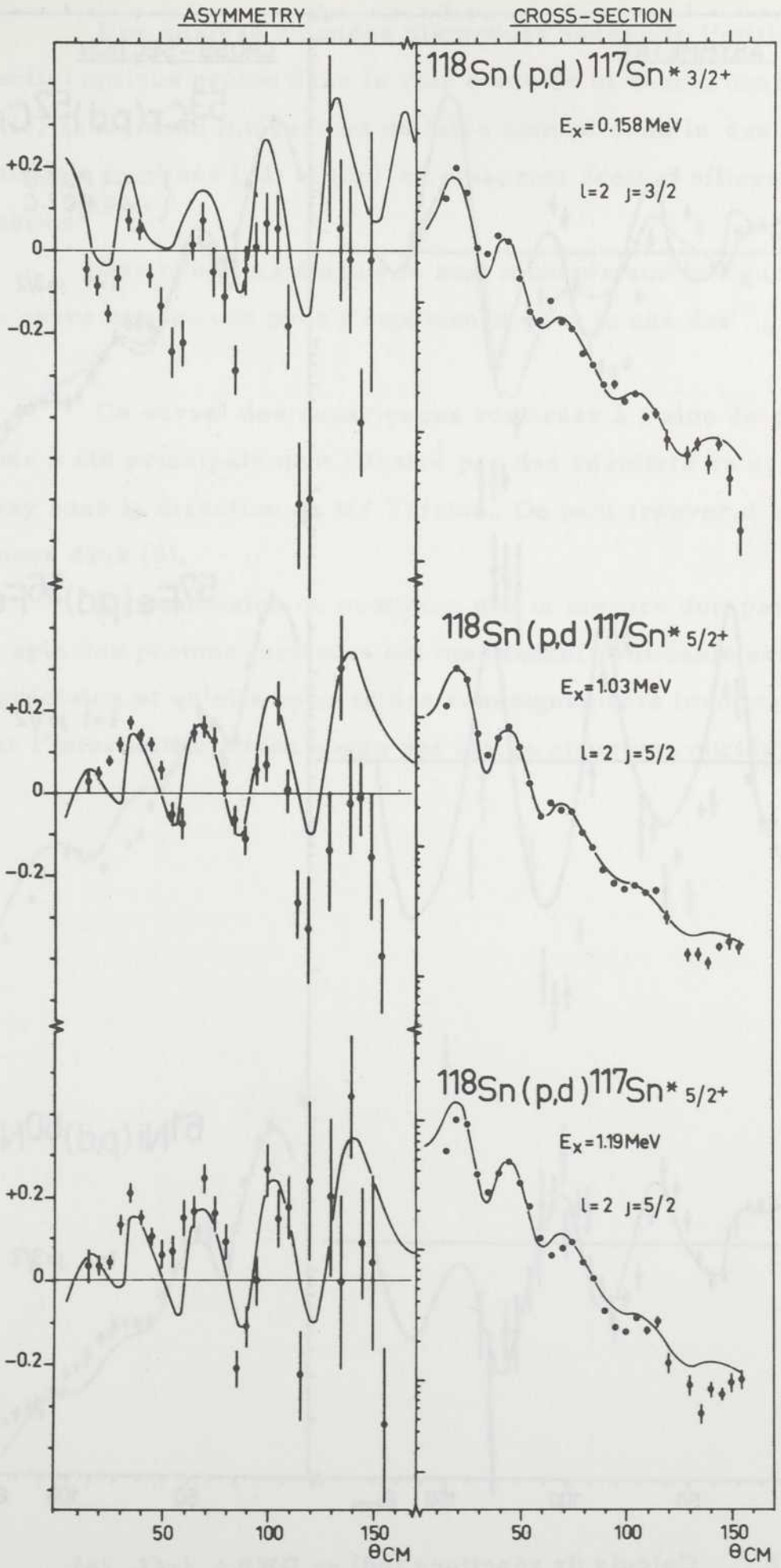

Figure 7 : Asymétries et sections efficaces de la réaction $^{118}Sn(pd)^{117}Sn$ (réf. 26)

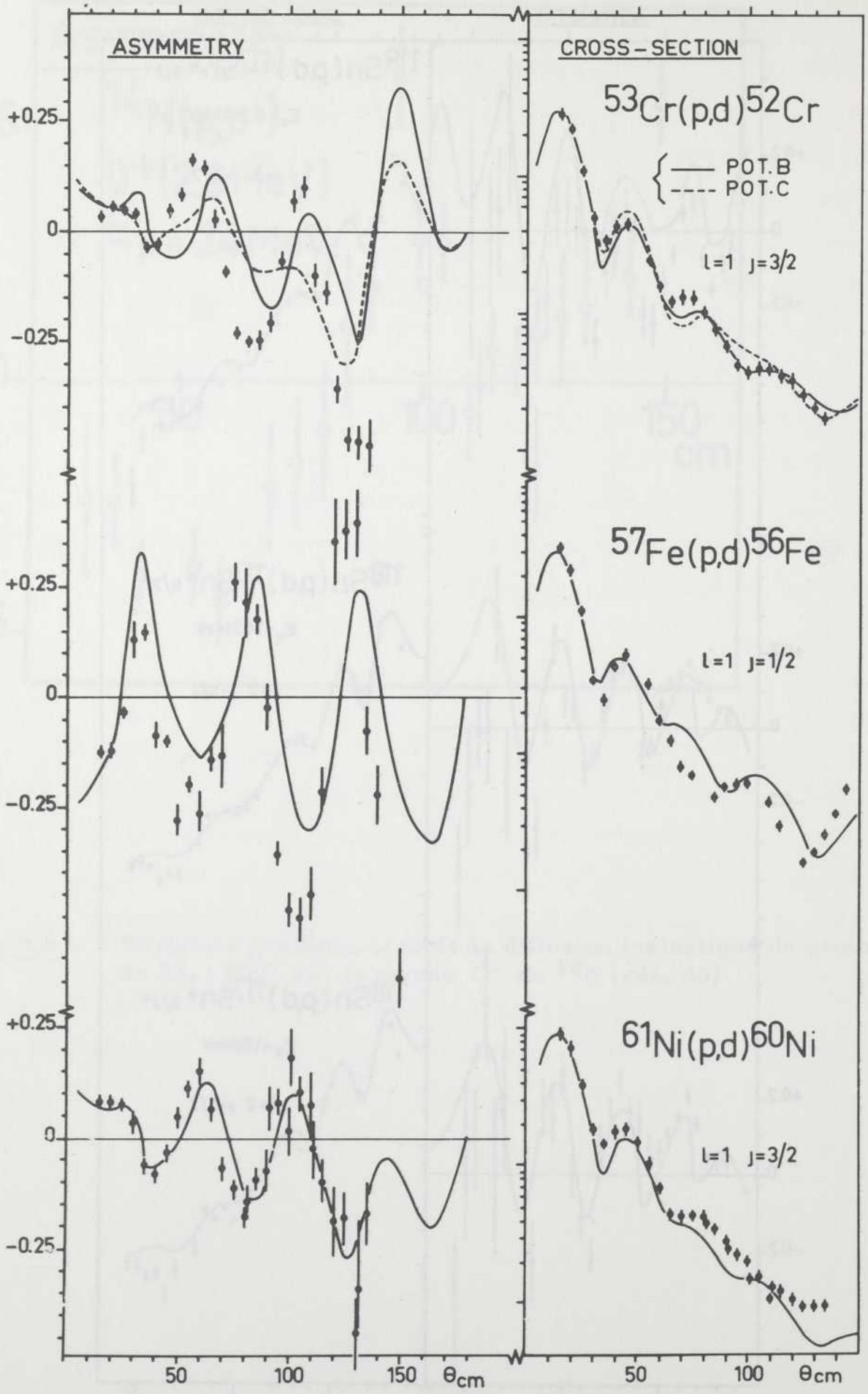

Figure 8 : Calculs de réactions (pd) en DWBA (réf. 26).

Une analyse en ondes distordues nécessite l'utilisation du potentiel optique proton dans la voie d'entrée et deuton dans la voie de sortie. Il est donc intéressant de faire comme dans le cas du chrome les réactions inverses (pd) et (dp) en mesurant section efficace et polarisation[27].

Des résultats d'analyse sont montrés sur la figure 8. Ils sont en assez bon accord avec l'expérience dans le cas des $\ell = 1$.

Ce survol des expériences réalisées à l'aide de protons polarisés a été principalement illustré par des résultats du cyclotron de Saclay sous la direction de Mr Thirion. On peut trouver d'autres références dans (8).

En conclusion on peut dire que la mesure des paramètres liés au spin des protons incidents est maintenant réalisable avec une très bonne précision et qu'elle apporte des renseignements importants aussi bien sur l'interaction proton noyau que sur la structure nucléaire.

TABLE I

	E_i MeV	J^π	E^*	ℓ_n	j_n
^{53}Cr	16.6	0^+ 2^+	0 1.434	1 1.3	3/2 1/2 3/2 5/2 7/2
^{57}Fe	17.3	0^+ 2^+	0 0.847	1 1.3	1/2 3/2 5/2
^{61}Ni	16.6	0^+ 2^+	0 1.333	1 1.3	3/2 1/2 3/2 5/2 7/2
^{90}Zr	22.9	$9/2^+$ $1/2^-$ $3/2^-$	0 0.588 1.094	4 1 1	9/2 1/2 3/2
^{91}Zr	24.5	0^+	0	2	5/2
^{118}Sn	24.5	$1/2^+$ $3/2^+$ $11/2^-$ $7/2^+$ $5/2^+$ $5/2^+$	0 0.158 0.317 0.73 1.03 1.19	0 2 5 4 2 2	1/2 3/2 11/2 7/2 5/2 5/2
^{119}Sn	24.5	0^+ 2^+	0 1.230	0 2	1/2 3/2 5/2

Mesures de l'asymétrie dans les réactions p-d faites à Saclay par B. Mayer et al.

REFERENCES

(1) Polarized targets and ion sources, Saclay 1966
(2) R. Beurtey et J.M. Durand, Nucl. Instr. Methods 1967, 57, 313
(3) R. Beurtey, Symposium Karlsruhe 1965 p. 33
(4) P. Catillon et al, Phys. Rev. Letters 1968, 20, 602
(5) R. Beurtey, Rapport d'activité, Dép. phys. nucléaire, CEA 68-69
(6) R. Beurtey, Rapport CERN NPIP 67-21
(7) L. Wolfenstein, Ann. Rev. Nucl. Sci. 1956, 6, 43
(8) C. Glashausser, J. Thirion, Advances in Nucl. Phys. 1969, 2 79
(9) G.R. Satchler, Nucl. Phys. 1967, A92, 273
P. Kossanyi-Demay et al, J. Phys (à paraître)
G.E. Brown, Proc. Phys. Soc. 1957, 70A, 361
(10) L.J.B. Goldfarb et al, Phys. Rev. 1966, 144, 829
(11) J. Raynal, Thèse CEN/Saclay rapport R-2366
(12) A.P. Stamp, Phys. Rev. 1967, 153, 1052
(13) C.J. Batty, C. Tschalär, communication à cette conférence
(14) R. Beurtey et al, Rapport d'activité, Dép. Phys. Nucléaire CEA 68-69
(15) T.R. Fisher et al, Phys. Rev. 1967, 157, 1149
S. Kobayashi et al, Prog. Theor. Phys. 1968, 40, 1451
(16) A. Zucker et al, Communication à cette conférence
(17) J. Raynal, Nucl. Phys. 1961, 28, 220
P. Catillon et al, Nucl. Phys. 1967, B2, 93
(18) Congrès de Gainesville, Rev. Mod. Phys. 1967, 39, 495
(19) S. Baker et al, Rapport d'activité, Dép. Phys. Nucléaire CEA 68-69
(20) Voir Table II de la référence (8)
(21) J. Raynal, rapport à cette conférence
H. Shérif, J. Blair, Phys. Lett. 1968, 26B, 489
(22) G.R. Satchler, Nucl. Phys. 1967, A95, 1
(23) J. Raynal, communication privée
(24) R. Schaeffer, Thèse et rapport à cette conférence
(25) A. Tarrats, communication privée
(26) J.L. Escudié et al, contribution à la Conf. de Montreal 69, suppl. p.11
Phys. Rev. Lett. (à paraître)
Rapport d'activité, Dép. Phys. Nucléaire CEA 68-69
P.J. Bjorkholm et al, Phys. Rev. Lett. 1969, 22, 955
(27) R. Lombard, B. Mayer, Rapport d'activité, Dép. Phys. Nucléaire CEA 67-68 p. 90.

WORK WITH POLARIZED TRITONS AT LOS ALAMOS†

P. W. Keaton, Jr.

Los Alamos Scientific Laboratory

August, 1969

I. INTRODUCTION

A few years ago an effort[1] to produce a beam of polarized tritons was undertaken at the Los Alamos Scientific Laboratory. As a result, the first triton polarization measurements were reported[2] in June, 1968, by D. D. Armstrong, L. R. Veeser, and me.

I will present some of the basic double-scattering techniques that we have used to measure absolute polarization values. With these techniques, we have obtained over one picoampere of tritons elastically scattered from ^{4}He, with a polarization of 84%. I will also report on our very recent measurements[3] of ^{3}He polarization. We have obtained one-half picoampere of ^{3}He elastically scattered from ^{4}He, with a polarization of 64%.

Several applications with polarized tritons and ^{3}He will be presented. These include a number of few-nucleon problems, a direct reaction involving pickup, and our latest attempt to measure the strength of the triton spin-orbit term in a triton optical potential for intermediate weight nuclei.

II. TECHNIQUES

A. Basic Concepts and Notations

Nucleon standards have existed for over a decade which could be used

†Work performed under the auspices of the U.S. Atomic Energy Commission.

to "calibrate" an analyzer or polarizer. Prior to our work, no such standards existed for polarized tritons or ^{3}He. Therefore, we had to use the techniques which were common in the 1950's.

By choosing three appropriate energies and angles, one can measure three dependent asymmetries, P_1P_2, P_2P_3, and P_1P_3. An alternative is to measure P^2 but that was not practical for us. The sign cannot be determined by double scattering experiments, but we have been able to determine this unambiguously by phase-shift analyses.

A typical pair of measurements would be: $^4\text{He}(t,\vec{t})^4\text{He}$ at the primary target to polarize the tritons, and $^4\text{He}(\vec{t},\hat{t})^4\text{He}$ at the secondary target to analyze the tritons. This introduces the notation which has been very helpful to us in discussing the more complicated problems that are to come. A vector ($\rightarrow$) over a symbol to the left of the comma indicates a polarized beam (and/or target). A vector to the right of the comma indicates a polarization measurement of the designated particle. A caret ($\hat{}$) over a symbol indicates that the left-right asymmetry is measured.

B. Brief History

In 1966, when we started to search for polarized tritons, we were impressed with the fact that large proton polarizations combined with large differential cross sections had been observed in scattering from intermediate weight nuclei. Indeed, Oak Ridge[4] successfully used the elastic scattering of protons from ^{40}Ca to produce 80 picoamperes of 27% polarized protons. We began by double scattering tritons from nickel[5] at various angles and energies. We always got very small asymmetries, consistent with zero. This was an indication, of course, that P_1 is small, that P_2 is small, or that both are small. Consider Fig. 1 showing the results of one of our recent measurements. The polarization of 14.5-MeV protons[6] on ^{60}Ni are compared with our preliminary polari-

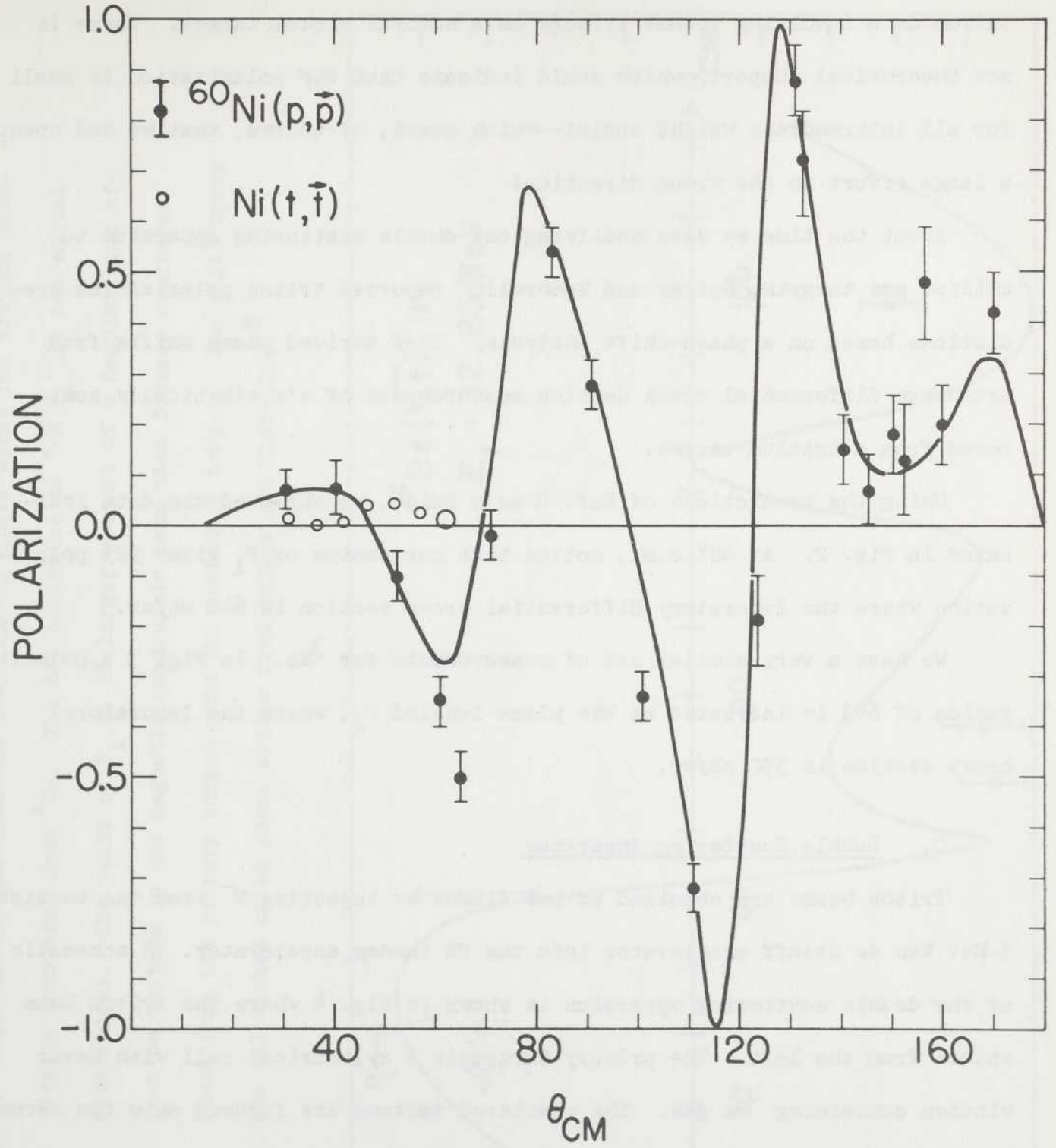

Fig. 1. Proton polarization measurements of Rosen et al.[6] are compared with preliminary triton polarization measurements (this work).

zation data involving 16-MeV tritons on a natural nickel target. There is now theoretical support[7] which would indicate that the polarization is small for all intermediate weight nuclei--which means, of course, that we had spent a large effort in the wrong direction!

About the time we were modifying our double scattering apparatus to utilize gas targets, Spiger and Tombrello[8] reported triton polarization predictions based on a phase-shift analysis. They derived phase shifts from extensive differential cross section measurements of α's elastically scattered from a tritium target.

Using the predictions of Ref. 8 as a guide, we obtained the data indicated in Fig. 2. At 40° c.m., notice that our choice of P_1 gives 92% polarization where the laboratory differential cross section is 640 mb/sr.

We have a very similar set of measurements for ^{3}He. In Fig. 3 a polarization of 64% is indicated at the place labeled P_2, where the laboratory cross section is 530 mb/sr.

C. Double Scattering Apparatus

Triton beams are obtained at Los Alamos by injecting T^- from the vertical 7-MeV Van de Graaff accelerator into the FN tandem accelerator. A schematic of the double scattering apparatus is shown in Fig. 4 where the triton beam enters from the left. The primary target is a cylindrical cell with Havar windows containing ^{4}He gas. The scattered tritons are focused onto the secondary target with a magnetic quadrupole triplet which is attached to a rotating gun mount. Small angle detectors help in the alignment of the secondary chamber, and also monitor alignment while data is being taken. We can have up to eight ΔE-E telescopes in operation at one time. The signals are mixed and routed to the SDS-930 on-line computer for particle identification and energy sorting.[9]

Before I present the applications, I must point out the energy limita-

Fig. 2. Polarization distribution measurements (this work) for tritons elas-

Fig. 2. Polarization distribution measurements (this work) for tritons elastically scattered from ^{4}He. The dot indicated as "$\sqrt{\beta}\ P_1$" is the actual measurement. The value of P_1 is 8% larger because of a depolarizing effect on tritons in the magnetic quadrupole lens that focuses scattered beams from the primary target onto the secondary target. The solid curve was calculated using phase shifts from Spiger and Tombrello.[8]

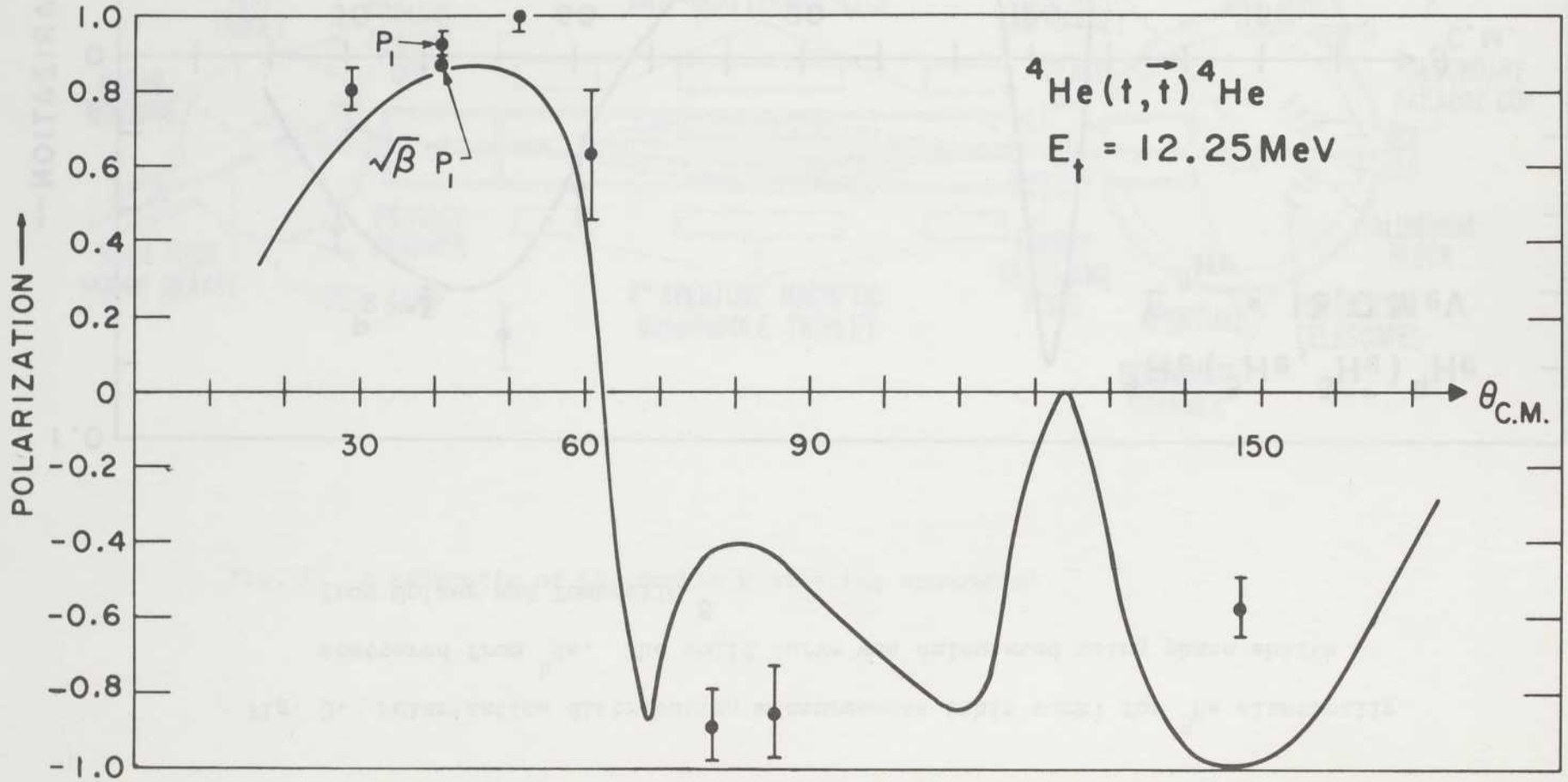

Fig. 3. Polarization distribution measurements (this work) for ^{3}He elastically scattered from ^{4}He. The solid curve was calculated using phase shifts from Spiger and Tombrello.[8]

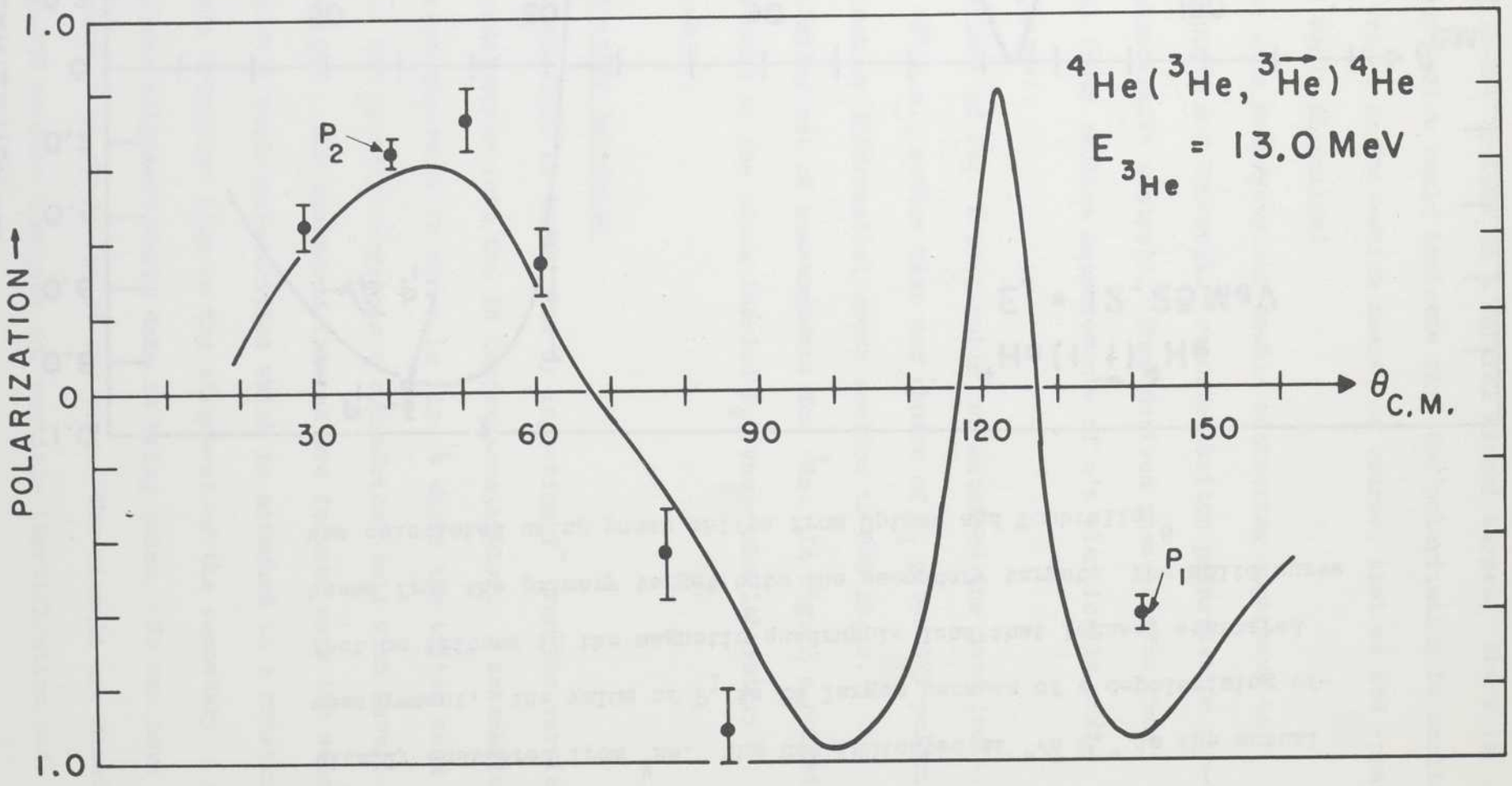

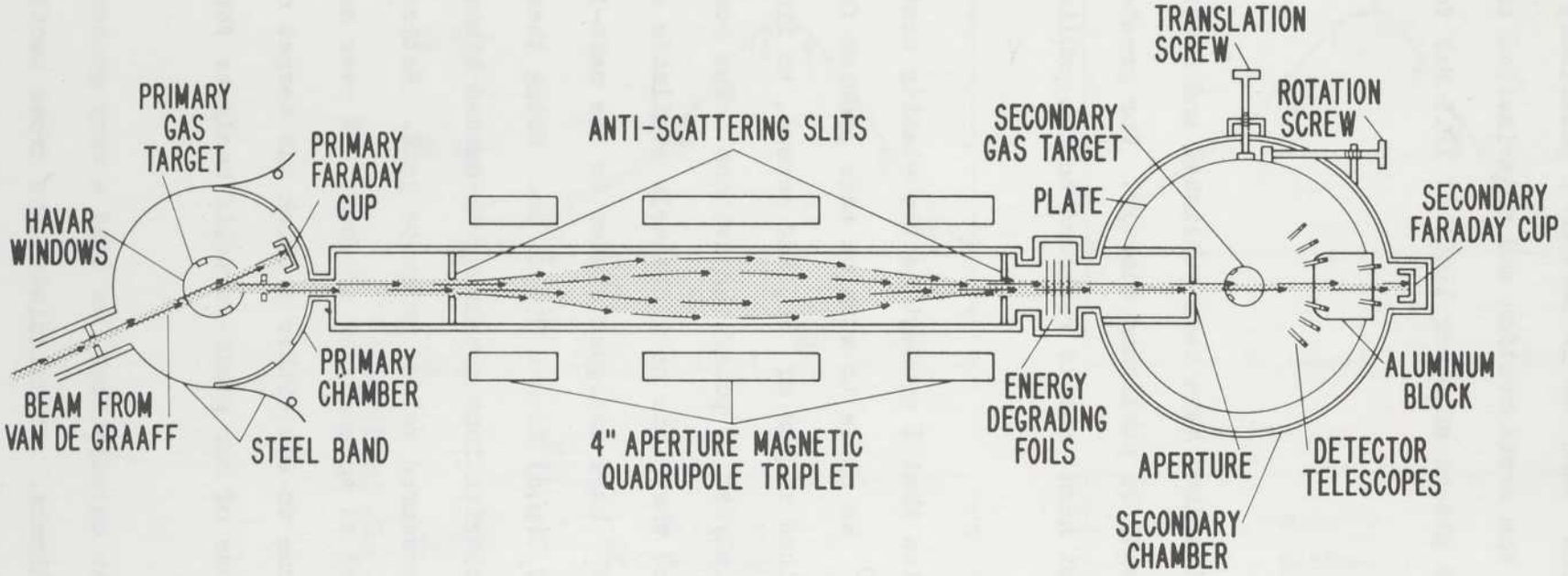

Fig. 4. A schematic of the double scattering apparatus.

tions on these techniques. When ^{4}He is used as a polarizer, we are restricted to energy regions where the cross section and polarization are "reasonably" large. At present, this places an upper limit of 12.5 MeV for tritons and 13.5 MeV for ^{3}He.

III. APPLICATIONS

Some of these applications have been published and others appear here for the first time and will be published shortly. For greater detail than I will have time to present here, one is referred to the publications.

A. $\underline{H(\vec{t},\hat{t})H}$

The first application that I present is the elastic scattering of polarized tritons from hydrogen.[10] We chose to work on this problem for two reasons: first, to study the excited states of ^{4}He, and second, to find an alternative to helium-4 gas as an analyzer of polarized tritons. The bombarding energies range from 6.4 to 9.7 MeV where the only channels available are t+p and ^{3}He+n.

Werntz and Meyerhof[11] have assigned states in the mass-four problem based on measurements of $T(p,n)^3He$ and $T(p,\vec{n})^3He$. Using these levels, we calculated the triton polarizations appearing as dashed lines in Fig. 5. The agreement with our measured values is quite good. Notice that at 110° c.m. hydrogen can be used as an analyzer of about 40% over an energy range of 2 MeV. This allows one to use either a thick gas target or more than 10 mils of polyethylene. One of our goals--a solid analyzer for tritons--has been thus achieved.

In order to make the calculations, we used a very general computer program† by D. C. Dodder of Los Alamos. It calculates the cross sections and polarizations from the reaction matrix using the formulas of Lane and Thomas.[13] I should

---

†A description of this program is to be published as a LASL report.[12]

Fig. 5. Polarization distribution measurements (this work) for tritons elastically scattered from hydrogen. The dashed

Fig. 5. Polarization distribution measurements (this work) for tritons elastically scattered from hydrogen. The dashed curves were calculated with Dodder's program[12] using energy levels of Werntz and Meyerhof.[11]

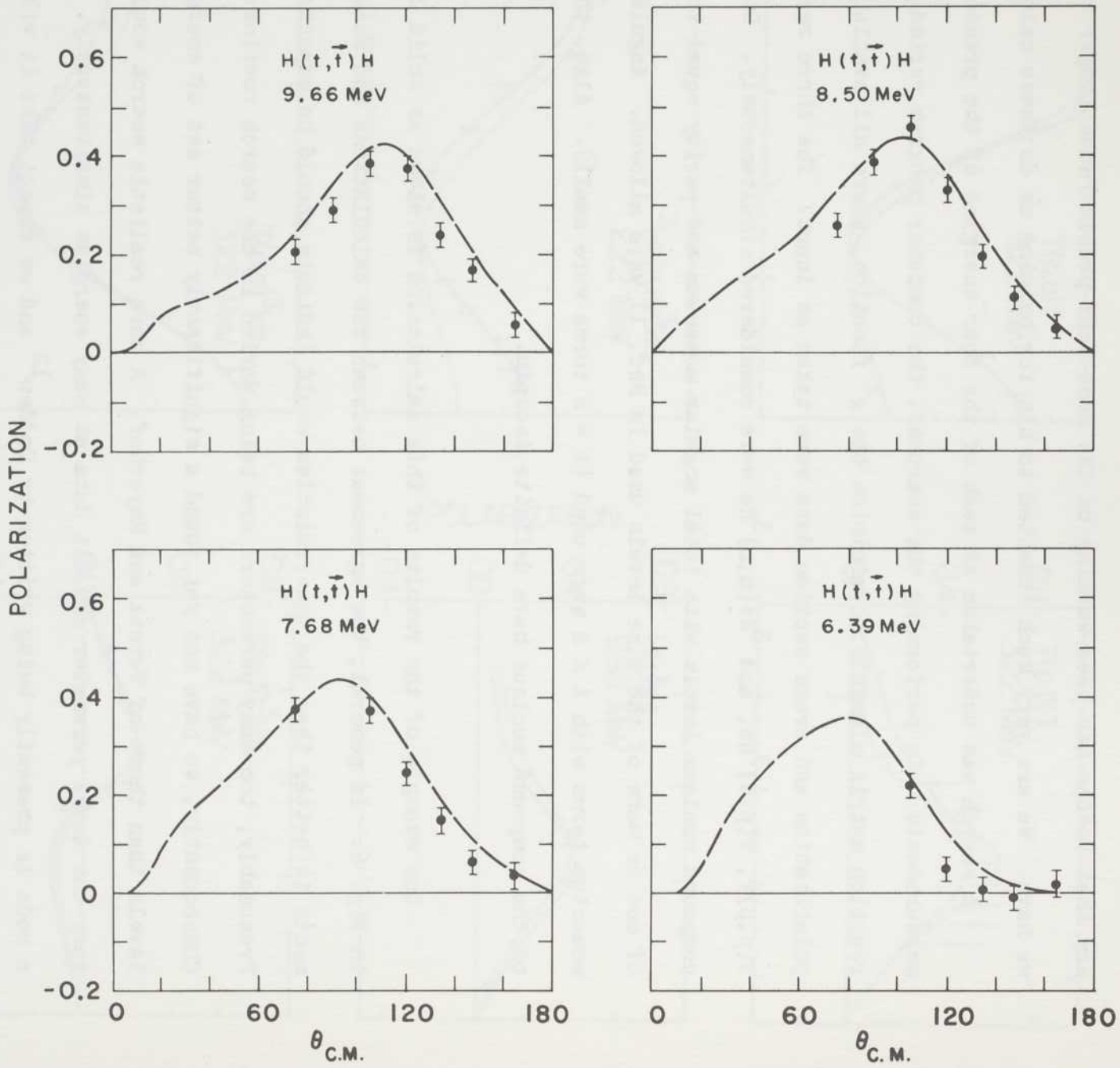

say that Dodder has been working on the mass-four problem much longer than we have. We are very much indebted to him for helping us do these calculations.

A search was undertaken at each of the four energies of the present measurements. In performing the searches, the computer program varied the reaction matrix elements to minimize the χ^2 function, where all available polarization and cross section data were taken as input. The three reactions T(p,p)T, T(p,n)^{3}He, and ^{3}He(n,n)^{3}He were considered simultaneously. Only compound nuclear levels with total angular momentum and parity equal to that of one or more of the nine levels used in Ref. 11 were allowed. Angular momentum terms with $\ell \leq 2$ were used ($\ell = 2$ terms were small). Also, the states of the compound nucleus have definite isospin.

One example of the results of this calculation is shown as solid lines in Fig. 6. In general, the agreement between the calculations and measurements is better than the uncertainties would indicate should be expected. Presumably, too many parameters are being varied in the search routine. Consequently, we have not yet found a significantly better set of energy levels than those of Werntz and Meyerhof. A more realistic search would vary the level parameter and fit data at many energies simultaneously. Such a code is presently being written by Dodder[12] and we expect that it will permit a more meaningful search on the present data.

B. Ni(t,$\vec{t}$)Ni and Fe(t,$\vec{t}$)Fe

Next I wish to discuss the problem that we have worked on for the longest time but it is still unfinished. The exciting question here is, "If one uses an optical potential to describe the elastic scattering of tritons from intermediate weight nuclei, what is the strength of the spin-orbit term?"

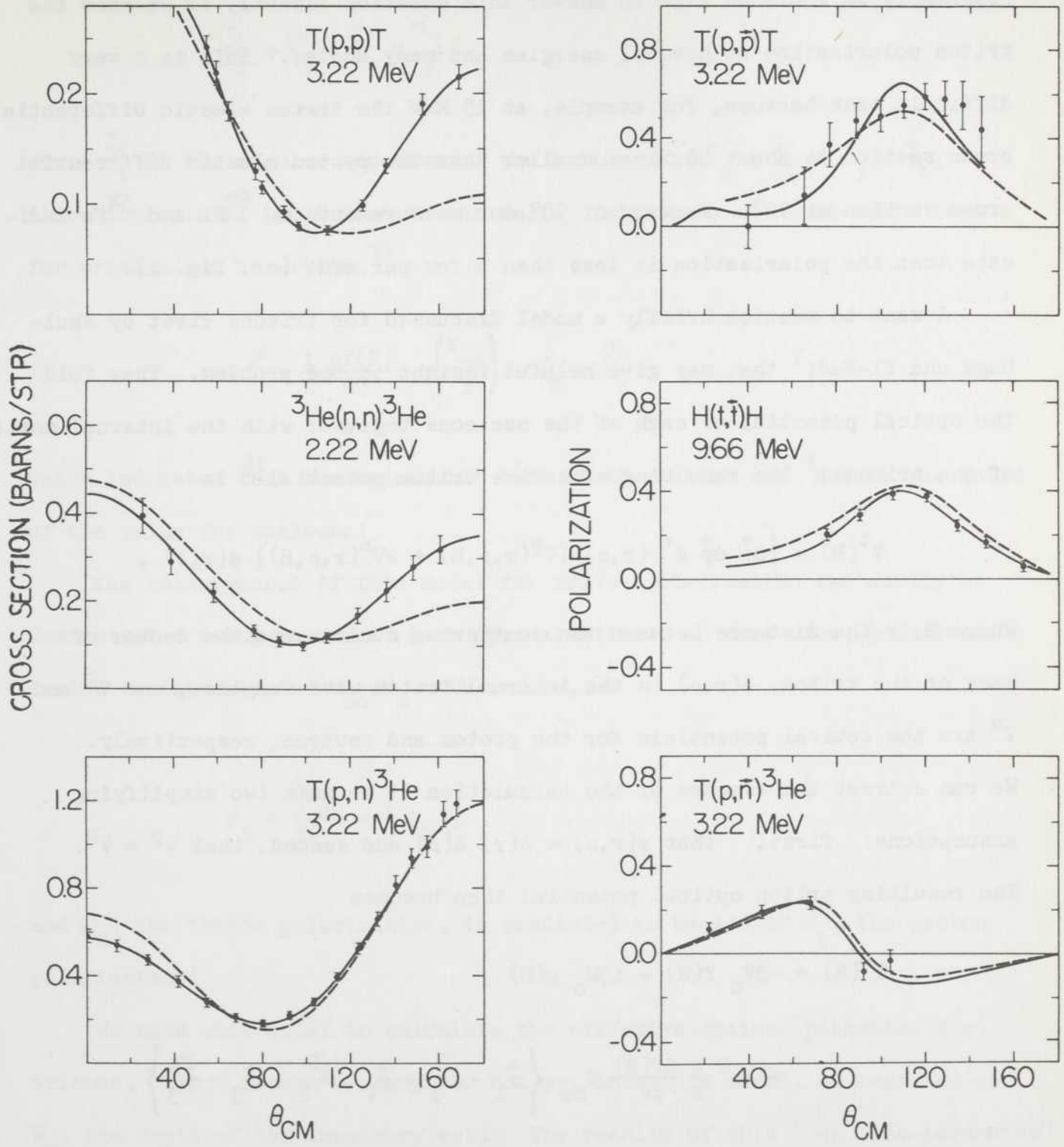

Fig. 6. The dashed curves were calculated with Dodder's program[12] using energy levels of Werntz and Meyerhof.[11] The solid curves are the results of a two-channel search on reaction matrix elements. The input data are referenced by Veeser et al.[10]

Presumably we would be able to answer this question directly if we knew the triton polarization at several energies and many angles. This is a very difficult task because, for example, at 15 MeV the triton elastic differential cross section is about 50 times smaller than the proton elastic differential cross section at 90°. Forward of 90° our measurements on ^{62}Ni and ^{54}Fe indicate that the polarization is less than a few per cent (cf. Fig. 1).

I want to mention briefly a model discussed for tritons first by Abul-Magd and El-Nadi[7] that may give helpful insight to the problem. They fold the optical potential of each of the nucleons together with the internal motion of the tritons. The resulting effective triton potential[14] is

$$V^t(R) = \int d\vec{r}\, d\vec{p}\, \phi^+(r,\rho)\, [V^p(r,\rho,R) + 2V^n(r,\rho,R)]\, \phi(r,\rho) ,$$

Where R is the distance between the scattering nucleus and the center of mass of the triton, $\phi(r,\rho)$ is the internal triton wave function, and V^p and V^n are the optical potentials for the proton and neutron, respectively. We can extract the essence of the calculation if we make two simplifying assumptions: first, that $\phi(r,\rho) = \delta(r)\ \delta(\rho)$ and second, that $V^p = V^n$. The resulting triton optical potential then becomes

$$V^t(R) = -3V_o\, f(R) - i3W_o\, g(R)$$

$$+ \lambda\pi^2 \frac{1}{R} \frac{df(R)}{dR} V_{So} \left\{ \vec{\sigma}_1 \cdot \vec{\mathscr{L}}_1 + \vec{\sigma}_2 \cdot \vec{\mathscr{L}}_2 + \vec{\sigma}_3 \cdot \vec{\mathscr{L}}_3 \right\},$$

where we have substituted a standard[6] optical potential form for the nucleons and where subscripts 1, 2, and 3 refer to each of the nucleons in the triton. Notice that the real and imaginary well depths are three times as deep for tritons as for nucleons. We also find

$$\vec{\mathcal{L}}_1 \equiv \vec{\mathcal{L}}_2 \equiv \vec{\mathcal{L}}_3 \equiv \frac{\vec{\mathcal{L}}_t}{3} ,$$

where $\vec{\mathcal{L}}_t$ is the angular momentum of the triton, and $\vec{\sigma}_1 + \vec{\sigma}_2 + \vec{\sigma}_3 = \vec{\sigma}_t$, since the spin of the triton is one half. Therefore, the spin-orbit term for tritons can be written[15]

$$\lambda\pi^2 \cdot \frac{1}{R} \frac{df(R)}{dR} \cdot \left(\frac{V_{So}}{3}\right) \cdot \vec{\sigma}_t \cdot \vec{\mathcal{L}}_t ,$$

which indicates that the spin-orbit term of the triton (or ^{3}He) is one third of the value for nucleons!

The consequences of this model for triton polarization can easily be demonstrated using the First Born Approximation. In that case, polarization scales as the ratio of V_{So}/V_o. Therefore,

$$P_t \propto \frac{\frac{1}{3}V_{So}}{3V_o} \propto \frac{1}{9} P_p ,$$

and P_t, the triton polarization, is predicted to be 1/9 of P_p, the proton polarization!

We used this model to calculate the effective optical potential for tritons. Since triton breakup was not put into this model, we searched on W_o, the depth of the imaginary well. The results of this "one free-parameter" model looked very promising. However, we found that if the triton Gaussian wave function which we used first is replaced by an Irving-Gunn wave function, the fits are not as good. Also, if we use nucleon parameters of Greenlees et al.[16] instead of Perey,[17] we also have difficulties. Of course, one could always get a fit by allowing several parameters to vary, but this is not satisfactory.

We intend to make a detailed study of this problem after we have completed triton polarization measurements which, hopefully, will be within the year.

C. $\underline{^4\text{He}(t,\vec{t})^4\text{He}}$

Our first use of the $^4\text{He}(t,\vec{t})^4\text{He}$ reaction was as a tool--to polarize tritons. We have recently returned to this reaction to make extensive polarization distribution measurements. Some of the measurements are shown in Fig. 7.

Starting with the phase shifts of Ref. 7, we allowed all seven real phase shifts to vary in a search on cross section and polarization data. From this preliminary search, several points of interest can be made. (1) The phase shifts change very little (less than 15° for the most part). (2) Fits are considerably better to the polarization data but the energy dependence of the phase shifts is not as smooth as those in Ref. 8. (3) In the region where there is no ℓ = 1 or 2 state nearby, the P and D waves exhibit very little splitting, even though they were not restricted. This satisfies our intuition developed for the optical model case that unless tritons are near a resonance they have only a weak spin-orbit term! (4) Poor fits around E_t = 12.25 MeV indicate that the imaginary phase shifts are not correct in Ref. 8.

Clearly, a great deal more analyses must be done with these data.

D. $\underline{D(\vec{t},\hat{\alpha})n \text{ and } D(^3\vec{\text{He}},\hat{\alpha})\text{H}}$

In 1965, theoretical interest was aroused by a very nice experiment at Rice[18] with a polarized ^{3}He target. They accelerated unpolarized deuterons onto a polarized ^{3}He target and measured the left-right asymmetry of protons coming from the $^3\vec{\text{He}}(d,\hat{p})^4\text{He}$ reaction. Assuming time-reversal invariance and a 100% polarized target, this is equivalent to measuring ^{3}He polarization

Fig. 7. Polarization distributions of measurements (this work) for tritons elastically scattered from ^{4}He. The labels "P_i" refer to points taken in dependent asymmetry measurements leading to absolute polarization determination.

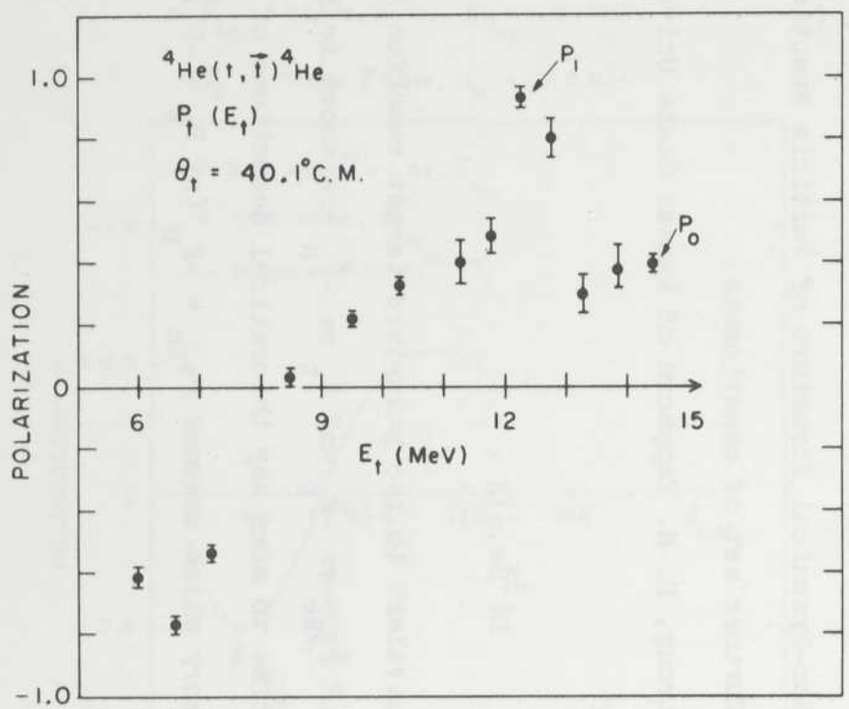

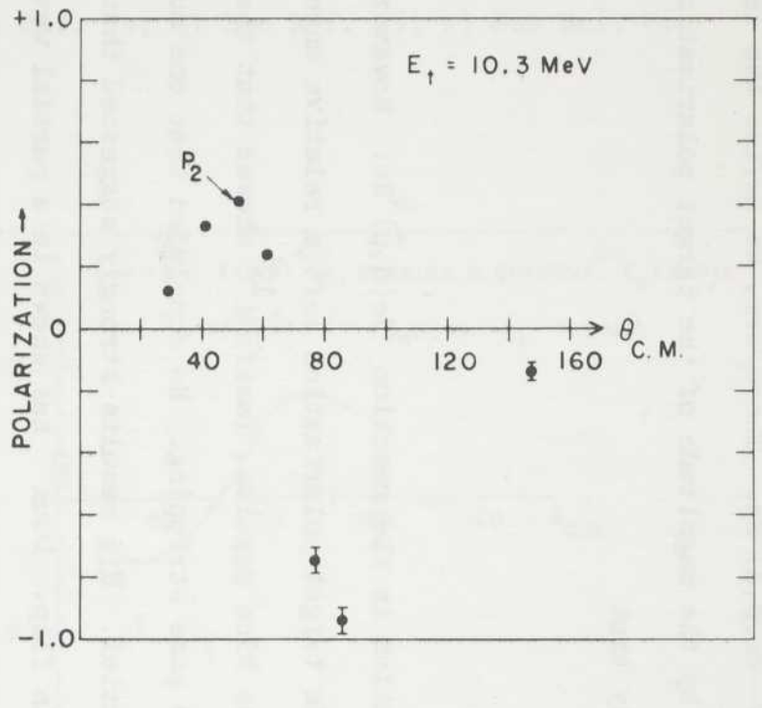

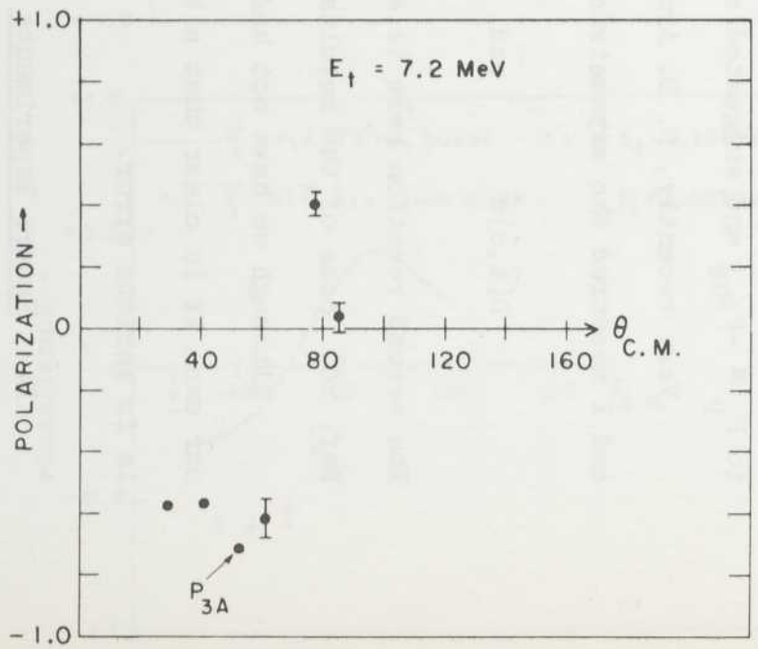

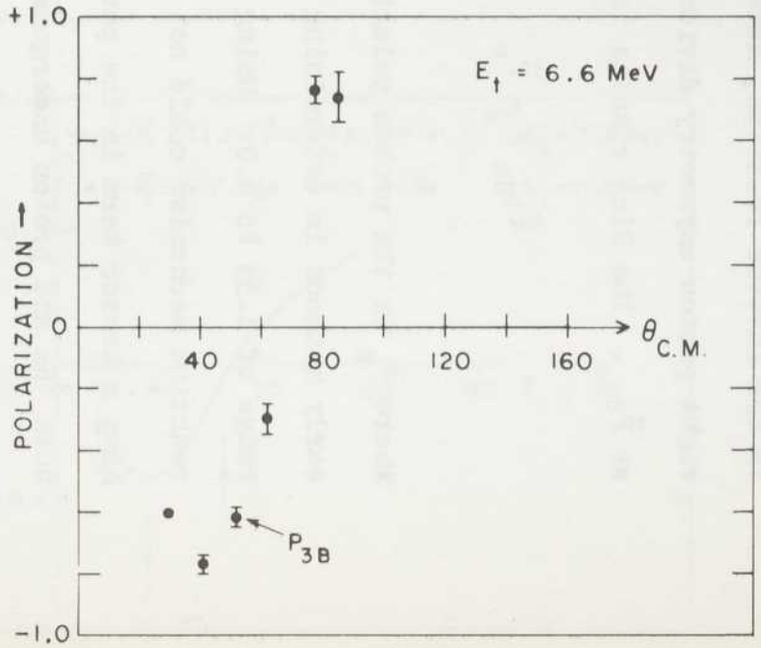

in the inverse reaction, namely $^{4}He(p,d)^{3}\vec{He}$. Therefore, we define the left-right proton asymmetry divided by the magnitude of the target polarization as $\vec{P}_{^3He}$. The Rice results imply that

$$\vec{P}_{^3He} \simeq - \vec{P}_{p} ,$$

where $\vec{P}_{p}$ is the proton polarization in the reaction $^{3}He(d,\vec{p})^{4}He$. However, early methods in determining ^{3}He target polarization left a relative uncertainty range of 1.35 to 1.0. Using the Rice results, Tanifuji[19] showed that the reaction mechanism could not be pure stripping. He concluded that one must have a tensor term in the potential. His results strongly suggested that both ^{3}He and proton undergo spin flip. Duck[20] has shown in a partial wave analysis that only spin-flip amplitudes appear to be important. Csonka et al.[21] have applied the formalism of Non-Dynamical Structure of Particle Reactions to $P_{p} \equiv -P_{^3He}$ and suggested a further set of experiments.

Very recently, D. D. Armstrong, R. M. Tapphorn of Kansas State University, and I measured the asymmetries:

$$D(\vec{t},\hat{\alpha})n \qquad \text{and} \qquad D(\vec{^3He},\hat{\alpha})H .$$

The second reaction here is equivalent to the polarized target reaction in Ref. 18. Some of the results of $\vec{P}_{^3He}$ vs $-\vec{P}_{p}$ and $\vec{P}_{t}$ vs $-\vec{P}_{n}$ are shown in Fig. 8.

Although we have not had time to make any theoretical deductions of our own, it is clear that a theory which assumes $P_{^3He} = -P_{p}$ (or $P_{t} = -P_{n}$) is in serious error.

E. Future Experiments

Lastly, I would like to mention two other experiments that we plan to do.

Fig. 8. Alpha left-right asymmetries resulting from polarized mass-3 projectiles incident on a deuterium target. The solid curves indicate proton or neutron polarization measurements: a) See Ref. 18; b) See Ref. 23; c) See Ref. 24; d) See Ref. 25; e) See Ref. 26.

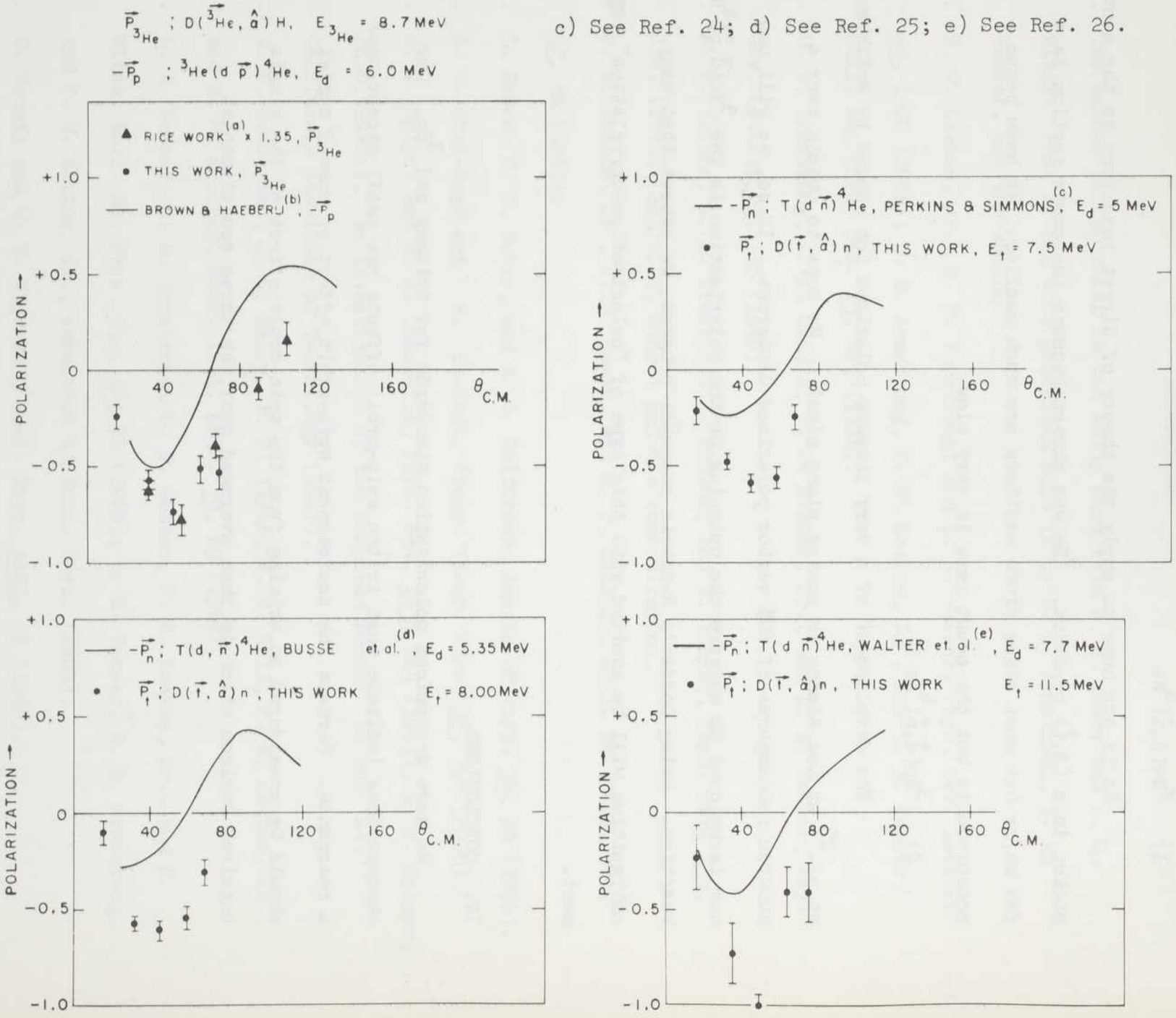

1) $^{9}Be(d,\vec{t})^{8}Be$

It is our hope to apply the theory of direct reactions to the neutron pickup in a $(d,\vec{t})$ reaction. ^{9}Be was chosen because the cross section is a few mb/sr but most other cross sections are much smaller. We have begun measurements but the count rate is very slow.

2) $^{3}He(\vec{d},\vec{p})^{4}He$

The development of a very intense polarized ion source by McKibben et al.[22] at Los Alamos is coming along nicely. We hope to obtain over a hundred nanoamperes of 80% vector polarized deuterons. If so, we will use our techniques to measure the outgoing proton polarization in the $^{3}He(\vec{d},\vec{p})^{4}He$ reaction. Using Dodder's R-matrix computer program, we expect that many ambiguities will be avoided with this type of "polarization-correlation" experiment.

IV. CONCLUSIONS

We have determined polarization standards for tritons and ^{3}He. Our observations indicate that triton spin-orbit effects are small except near a resonance. Perhaps the nonresonant spin-orbit effect of mass-3 nuclei should be considered as arising from the spin-orbit effect of the single unpaired nucleon which is then averaged over the three constituents.

REFERENCES

1. The author collaborated in the early work with J. G. Beery and A. G. Blair. Most of the work presented here is by D. D. Armstrong, L. R. Veeser, and the author.
2. P. W. Keaton, Jr., D. D. Armstrong, and L. R. Veeser, Phys. Rev. Letters 20, 1392 (1968); D. D. Armstrong, P. W. Keaton, Jr., and L. R. Veeser, Bull. Am. Phys. Soc. 13, 873 (1968).
3. D. D. Armstrong, L. L. Catlin, P. W. Keaton, Jr., and L. R. Veeser, Phys. Rev. Letters 23, 135 (1969).
4. M. P. Fricke, E. E. Gross, B. J. Morton, and A. Zucker, Phys. Rev. 156, 1207 (1967); and E. E. Gross, private communication.
5. P. W. Keaton, Jr., J. G. Beery, and M. P. Kellogg, Bull. Am. Phys. Soc. 12, 86 (1967).
6. L. Rosen, J. G. Beery, and A. S. Goldhaber, Annals of Phys. 34, 96 (1965).
7. A. Y. Abul-Magd and M. El-Nadi, Progr. Theor. Phys. 35, 798 (1966).
8. R. J. Spiger and T. A. Tombrello, Phys. Rev. 163, 964 (1967); R. J. Spiger, Ph.D. Thesis, "An Investigation of the Compound Nuclei ^{7}Li and ^{7}Be," California Institute of Technology (1967).
9. D. D. Armstrong, J. G. Beery, E. R. Flynn, W. S. Hall, P. W. Keaton, Jr., and M. P. Kellogg, Nucl. Inst. Meth. 70, 69 (1969).
10. L. R. Veeser, D. D. Armstrong, D. C. Dodder, P. W. Keaton, Jr., and K. Witte, Bull. Am. Phys. Soc. 14, 21 (1969); L. R. Veeser, D. D. Armstrong, and P. W. Keaton, Jr., submitted to Nucl. Phys. (1969).
11. C. Werntz and W. E. Meyerhof, Nucl. Phys. A121, 38 (1968).
12. D. C. Dodder, private communication.
13. A. M. Lane and R. G. Thomas, Rev. Mod. Phys. 30, 257 (1958).

14. L. R. Veeser, D. D. Armstrong, and P. W. Keaton, Jr., Bull. Am. Phys. Soc. 13, 117 (1968).

15. The author gratefully acknowledges helpful discussions with Leonard S. Rodberg which led to this approach.

16. G. W. Greenlees, G. J. Pyle, and Y. C. Tang, Phys. Rev. 171, 1115 (1968).

17. F. G. Perey, Phys. Rev. 131, 745 (1963).

18. S. D. Baker, G. Roy, G. C. Phillips, and G. K. Walters, Phys. Rev. Letters 15, 115 (1965).

19. M. Tanifuji, Phys. Rev. Letters 15, 113 (1965).

20. I. Duck, Nucl. Phys. 80, 617 (1966).

21. P. L. Csonka, M. J. Moravcsik, and M. D. Scadron, Phys. Rev. 143, 775 (1966).

22. J. L. McKibben, G. P. Lawrence, and G. G. Ohlsen, Bull. Am. Phys. Soc. 13, 1443 (1968).

23. R. I. Brown and W. Haeberli, Phys. Rev. 130, 1163 (1963).

24. R. B. Perkins and J. E. Simmons, Phys. Rev. 124, 1153 (1961).

25. W. Busse, J. Christiansen, D. Hilsher, U. Morfeld, and J. A. Scheer, Nucl. Phys. A100, 490 (1967).

26. R. L. Walter, W. Beneson, T. H. May, and C. A. Kelsey, Nucl. Phys. 59, 235 (1964).

STUDY OF STRIPPING REACTIONS INDUCED BY 12 MeV VECTOR POLARIZED DEUTERONS

S. ROMAN

University of Birmingham, England*)

Abstract

Recent work in Birmingham on polarization effects in stripping reactions is described, carried out with the 12.3 MeV vector polarized deuteron beam of the Birmingham University Radial Ridge Cyclotron. Experimental results for a range of target nuclei from ^{9}Be to ^{208}Pb are reported, some in a preliminary form. A comparison is made with predictions of DWBA calculations, considering j-dependent effects and showing that the additional information contained in polarization data ought to make the derivation of spectroscopic factors less ambiguous. The observed angular distribution of the vector analysing power for the reaction ^{208}Pb(d,p)^{209}Pb at 1.57 MeV excitation suggests a Mott-Schwinger type of magnetic interaction which may be dominant near the Coulomb Barrier.

*) Work in collaboration with:

J.A.R. Griffith, M. Irshad, S.W.Oh, O.Karban and A.A.Debenham.

Experimental method

The analysing power of a scattering process or a reaction induced by a pure vector polarized beam can in principle be obtained from asymmetry measurements in the scattering plane, however, "left-right" asymmetry measurements may lead easily to large systematic errors due to misalignements and beam wander. A method involving frequent (10 Hz) "on-off" switching of the beam polarization at the source was chosen[1] to replace the conventional left-right method of asymmetry measurement and more recently the system was used much more efficiently with "up-down" switching at the source instead of the on-off mode. The polarization analysing power of a reaction (scattering investigated at an angle θ can then be obtained from the expression

$$P_d = \frac{2}{\sqrt{3}} \langle iT_{11} \rangle \frac{N_{up}/N_{down} - 1}{\sqrt{3}\,(\langle it_{11} \rangle_{up} + N_{up}/N_{down} \langle it_{11} \rangle_{down})},$$

where N_{up} and N_{down} are numbers of counts recorded over a period of time separately for the spin "up" and "down" mode of the operation of the source and $\langle it_{11} \rangle_{up}$ and $\langle it_{11} \rangle_{down}$ are the corresponding numbers describing the vector polarization of the incident beam for the two modes of operation of the source, which may not be equal. The beam polarization must be monitored simultaneously with all measurements of P_d. This is done using a carbon polarimeter placed downstream with respect to the main scattering chamber. In earlier work[1] the elastic scattering of

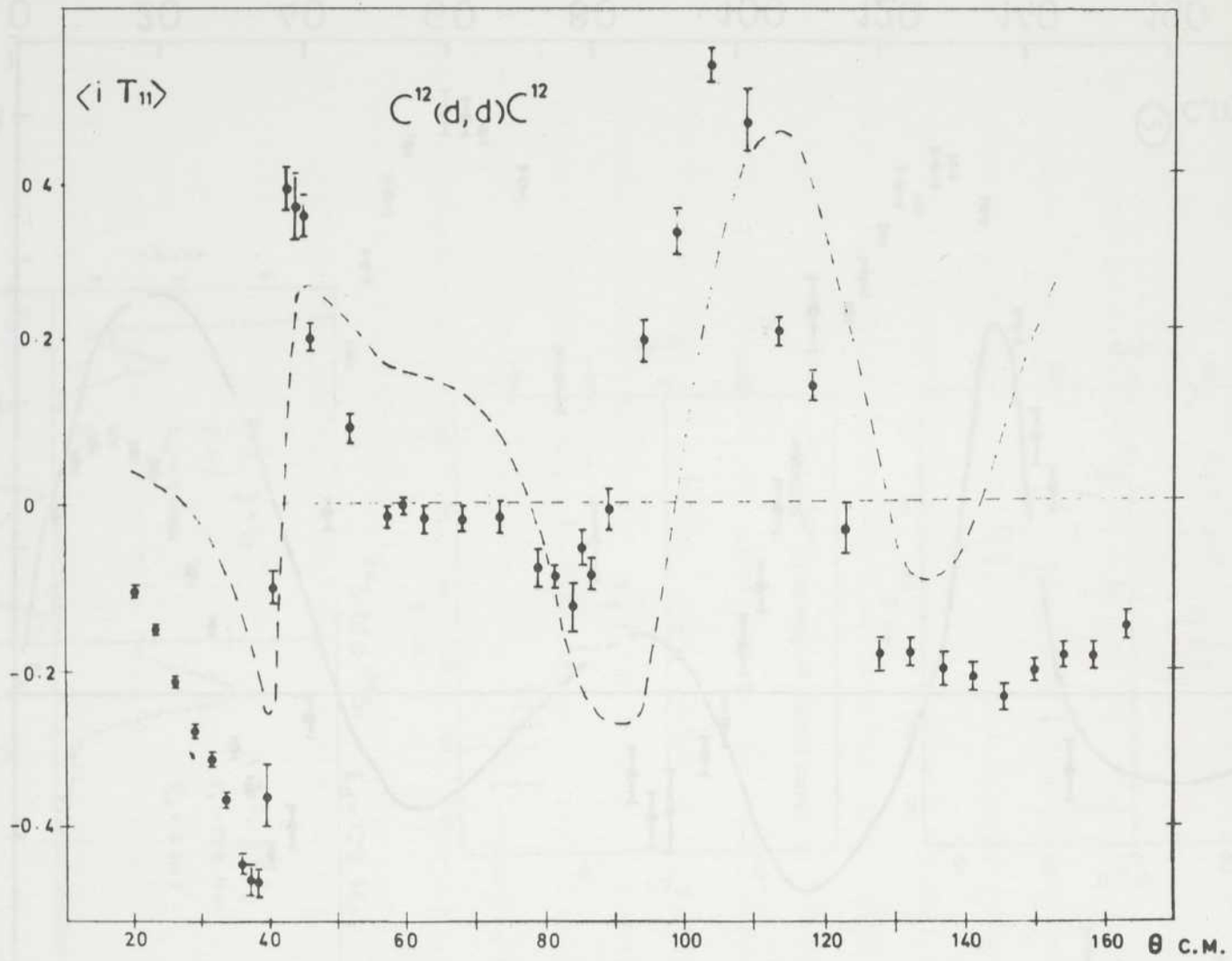

Fig. 1. Vector analysing power for elastic scattering of deuterons by carbon and a comparison with the optical model.

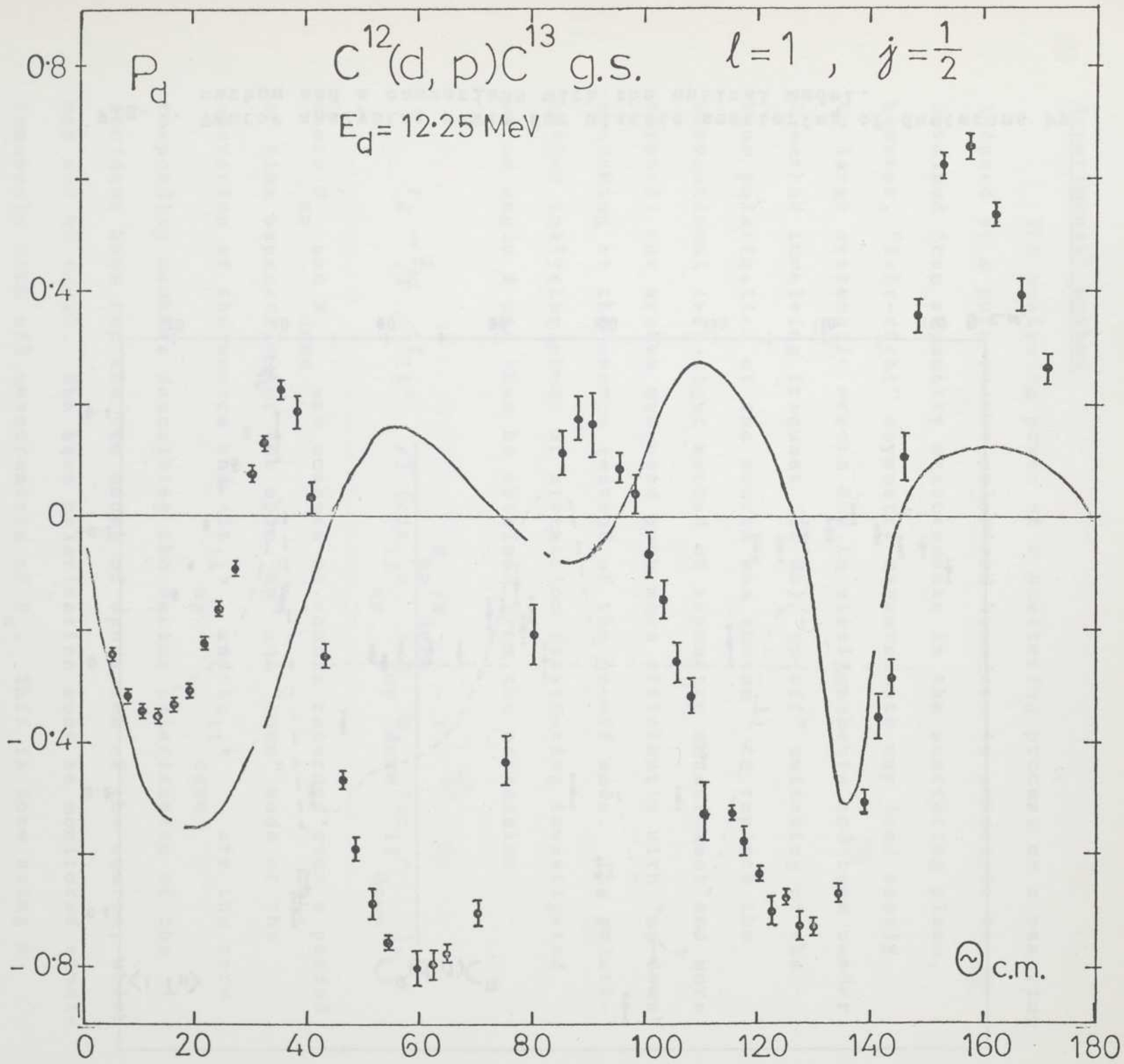

fig. 2. Vector analysing power of the $^{12}C(d,p)^{13}C$ g.s. reactions and a DWBA prediction

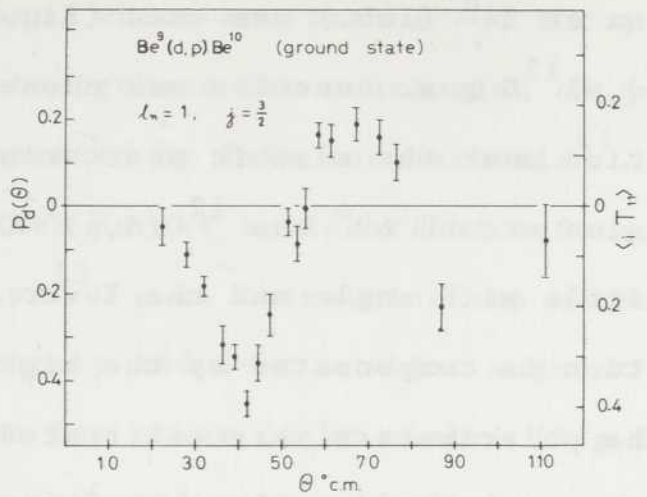

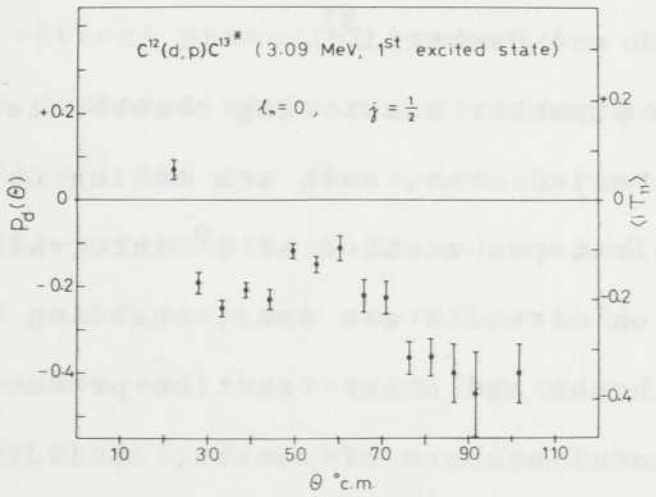

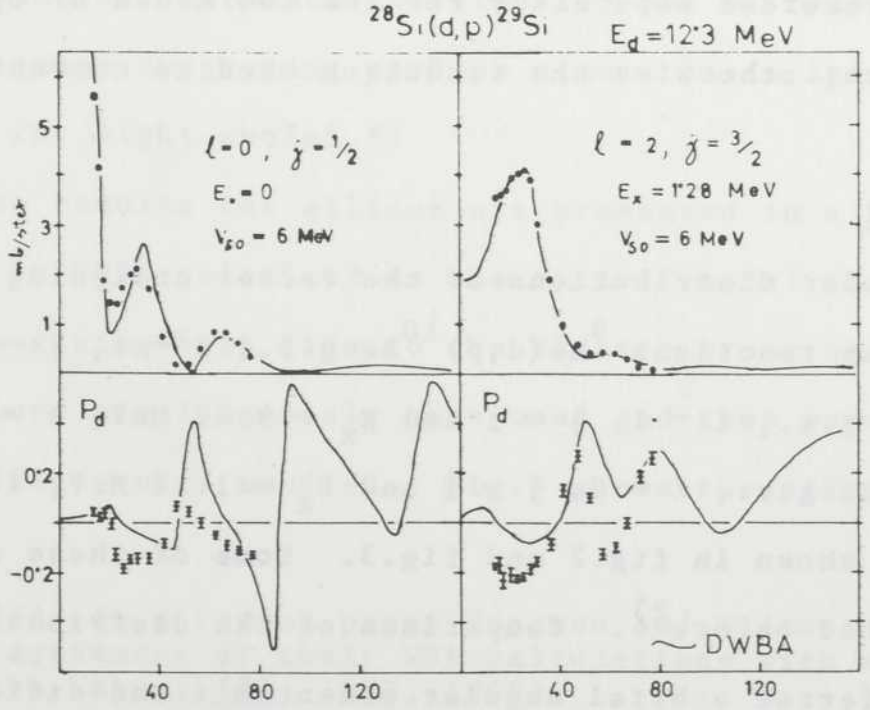

Fig. 3. Vector analysing power for the $^{9}Be(d,p)^{10}Be$ g.s., $^{12}C(d,p)^{13}C$ 3.09 MeV, the g.s. and the 1.28 MeV transitions in $^{28}Si(d,p)^{29}Si$. Continuous line for Si indicate DWBA predictions.

deuterons by carbon at 24^{o} (lab.) was used (fig.1), but more recently the $^{12}C(d,p)^{13}C$ g.s. reaction was chosen. The advantage of the (d,p) reaction over the elastic scattering is in that in the angular region around 60^{o} the $^{12}C(d,p)^{13}C$ reaction cross-section changes little with angle and the lower cross-section value of the reaction is compensated by the higher analysing power (fig.2). The polarimeters were calibrated against the scattering of deuterons by helium whose analysing power is known from work of Trier and Haeberli[3].

A 25 inch diameter scattering chamber is used, having two remotely controlled arms, each arm taking upto 5 E-ΔE solid state detector telescopes mounted at 5^{o} intervals. Analogue mass identification circuits are used, enabling separation of protons from deuterons and other reaction products. Proton spectra and the total numbers of counts, including the polarimeter counts are recorded separately for the two modes of operation of the source; otherwise the technique used is conventional.

Light nuclei

Angular distributions of the vector analysing power for the following reactions $^{9}Be(d,p)^{10}Be$ g.s., $\ell = 1$, $j = 3/2$; $^{12}C(d,p)^{13}C$ g.s., $\ell = 1$, $j = \frac{1}{2}$ and $E_x = 3.09$ MeV, $\ell = 0$, $j = \frac{1}{2}$; $^{28}Si(d,p)^{29}Si$ g.s., $\ell = 0$, $j = \frac{1}{2}$ and $E_x = 1.28$ MeV, $\ell = 2$, $j = 3/2$ are shown in fig.2 and fig.3. Some of these data have been described before[2]. Comparison of the distributions with equal transferred orbital angular momentum ℓ and different values of the total angular momentum j for carbon and beryllium ground

state transitions, which are both $\ell = 1$ but $j = \frac{1}{2}$ and $j = 3/2$ respectively, strengthens the conclusion of j-dependence of polarization reported by Yule and Haeberli[4]. Carbon is used as the polarimeter target as described before, and because of this the $^{12}C(d,p)^{13}C$ g.s. transition was measured to a higher statistical accuracy and over a wider angular range with tighter collimation than for other light nuclei (fig.2). The angular distribution is compared with a prediction of DWBA calculation using deuteron optical potential parameters obtained from an analysis of the deuteron elastic scattering polarization (fig.1) and cross-sections[5] and for the outgoing proton distortion the optical potential parameters of Greenlees and Becchetti[6]. The calculated DWBA curve does not reproduce well the measured angular distribution and the reason for this failure of the Born approximation is open to discussion. It does seem unlikely that compound nucleus resonance contribution can be responsible for the discrepancy suggesting perhaps a more basic inadequacy of the model for light nuclei.*)

The results for silicon are presented in a separate paper[7]. In DWBA calculations the optical-model distorting potentials giving best fits to the elastic cross-sections and polarizations simultaneously were used and they were not adjusted. Various effects were studied. Fig.4 shows the effect of the

---

*)Note added: In a recent paper Pearson and Wilcott obtained an excellent agreement of their WBP calculations with our data for carbon (Phys. Rev., 181, 1477, 1969).

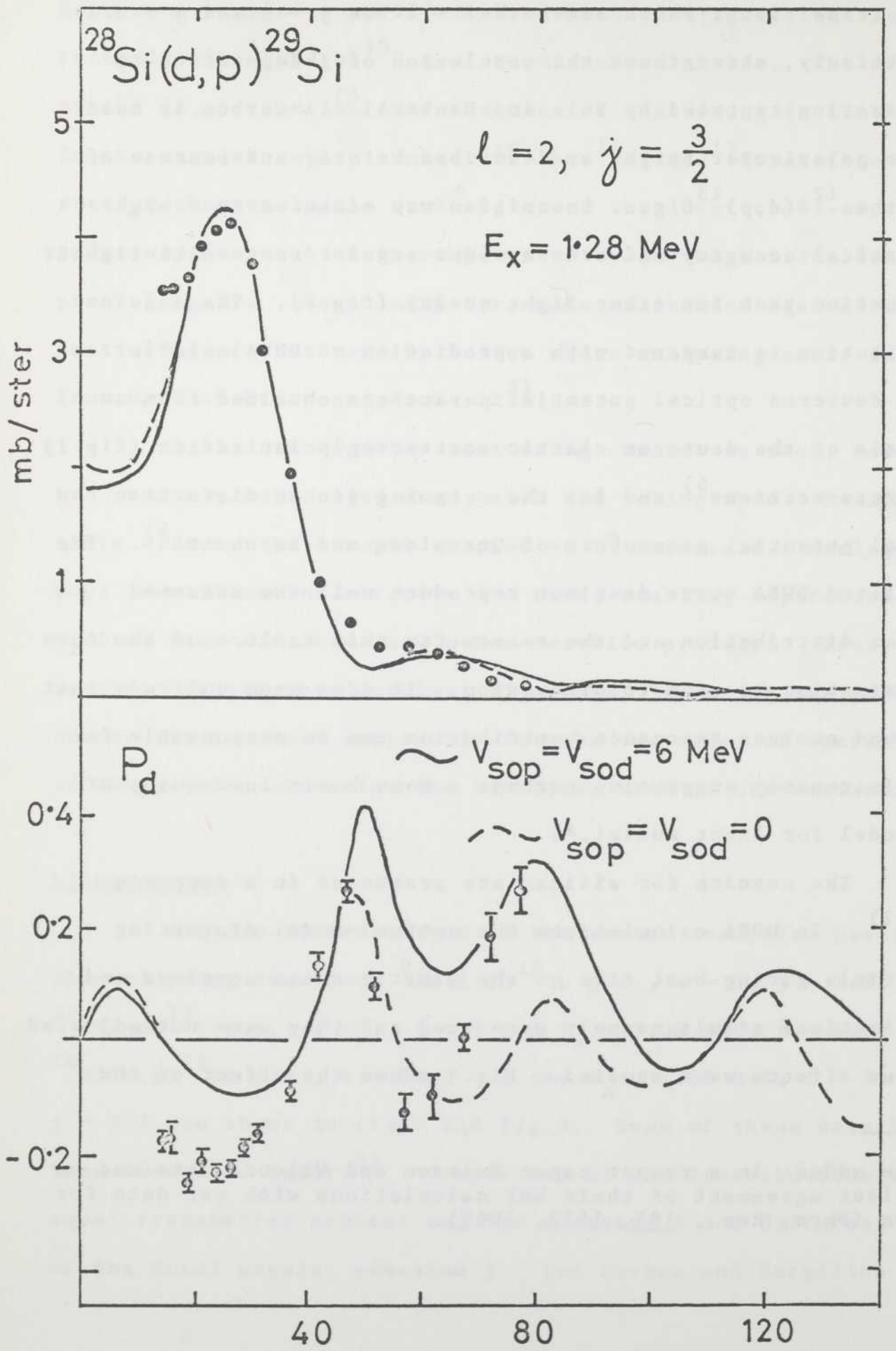

Fig. 4. The effect of the spin-orbit term of the distorting potential in DWBA description of the reaction $^{28}Si(d,p)^{29}Si$ at 1.28 MeV excitation.

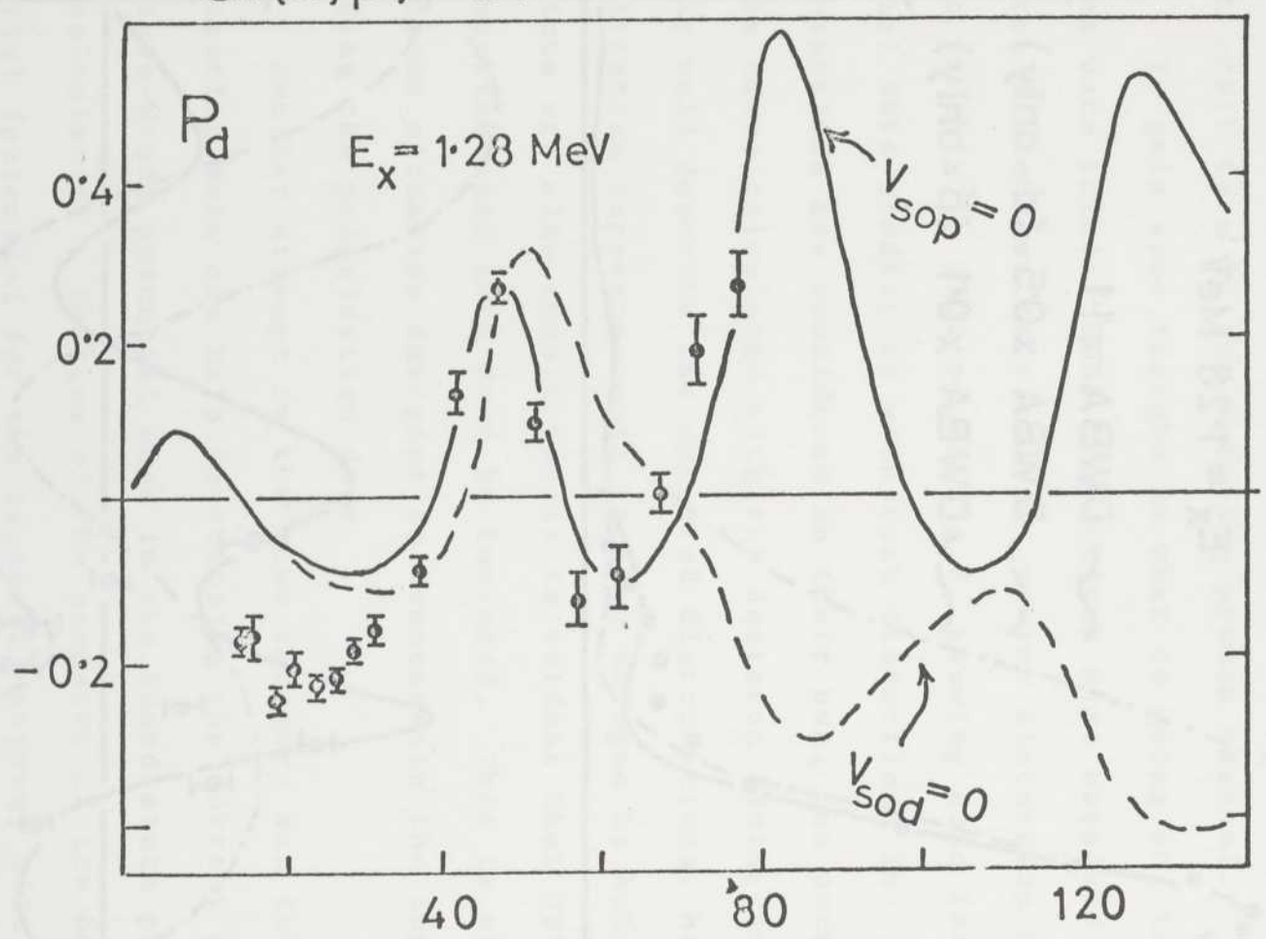

Fig. 5. The effect of the spin-orbit term of the distorting potential for $^{28}Si(d,p)^{29}Si$, $E_x = 1.28$ MeV separately for the incident deuteron and the outgoing proton channels.

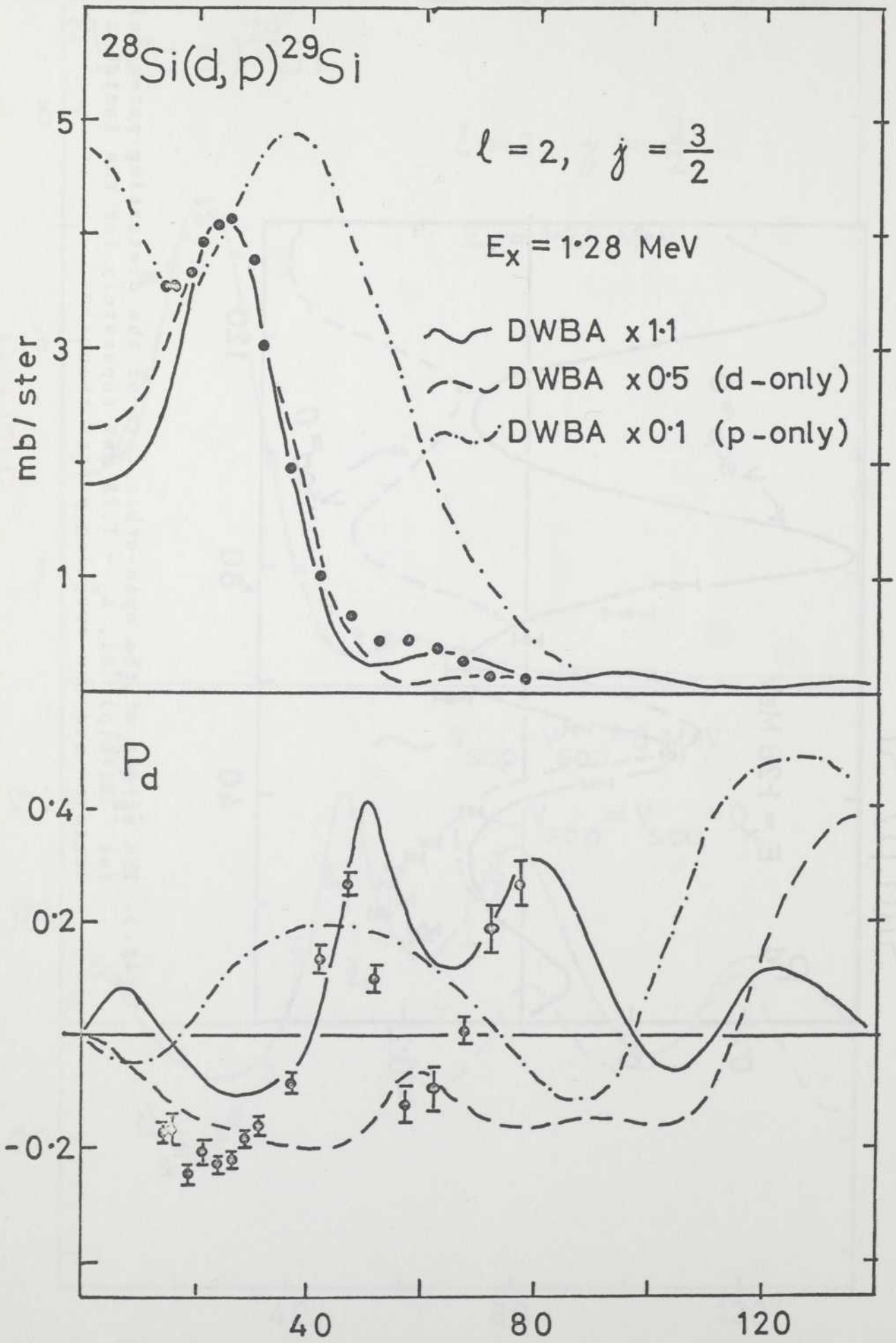

Fig. 6. The effect of separate distorting potentials for DWBA description of the $^{28}Si(d,p)^{29}Si$ reaction at 1.28 MeV excitation.

spin-orbit term upon the polarization for the 1.28 MeV state in ^{29}Si. As expected, the cross-sections can be quite well described without the spin-orbit force but not the polarizations. Fig.5 demonstrate that the presence of the spin-orbit term in the incident deuteron channel is of much more consequence than a spin-orbit term in the outgoing proton channel.

To gain some insight on what is going on, two drastic changes were tried: DWBA predictions were obtained a) for deuteron distortion only, b) for proton distortion only. The result of this is plotted in fig.6, showing also for comparison a normal DWBA prediction with both distortions in. When the cross-sections are considered on their own, the normal prediction and the curve calculated with the deuteron distortion only equally well describe the measured distributions, however, the normalization (spectroscopic factor) changes by 4.5. When polarizations are also considered it is evident that both distortions are important and both must be included. This is of course an extreme situation designed to demonstrate the importance of including the polarization data.

Another attempt in the same category was to see if the polarization data can help in choosing the correct geometry of the Saxon-Woods potential used in the bound state part of the DWBA calculation. Changes of the geometry of the bound state potential (potential for the captured neutron) will obviously

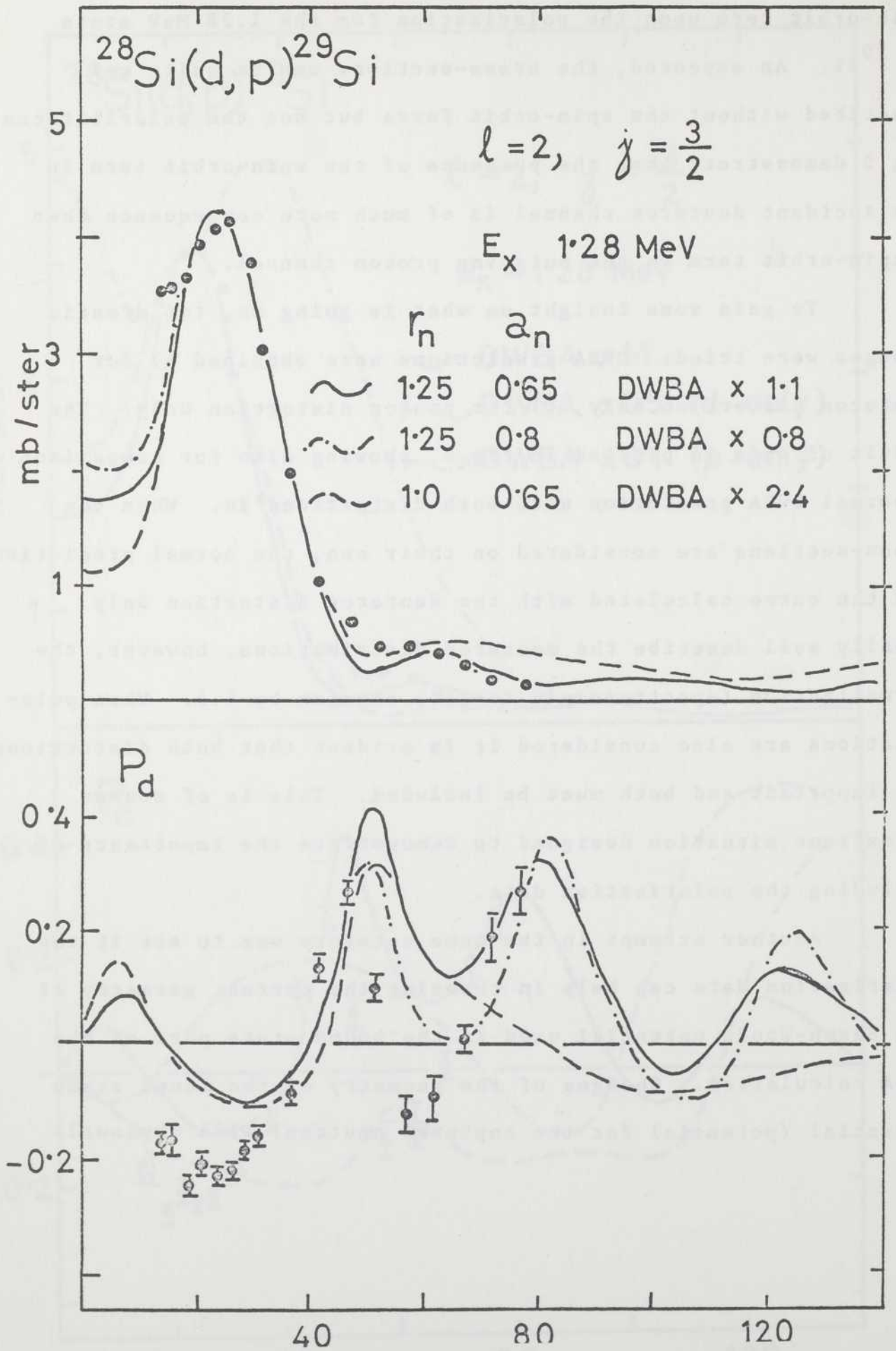

Fig. 7. Effects of changes of the bound state potential geometry on the DWBA description the $^{28}Si(d,p)^{29}Si$ reaction at 1.28 Mev excitation.

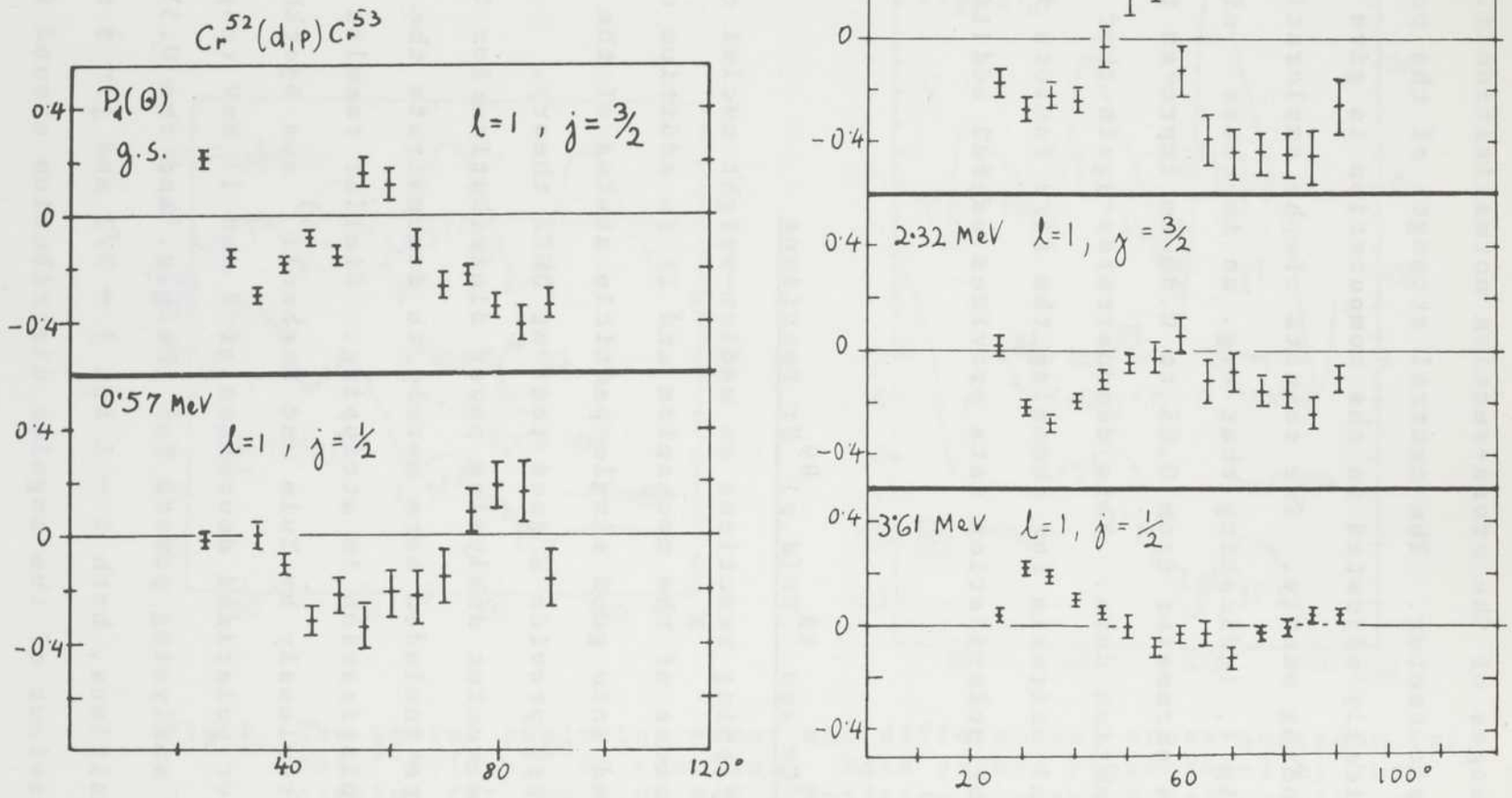

Fig. 8. Vector analysing power for the five transitions observed in the $^{52}Cr(d,p)^{53}Cr$ reaction.

produce changes of the cross-section normalization i.e. spectroscopic factor. The central strength of the potential is automatically adjusted in the computation to give the correct binding energy. The results of the exploration are shown in fig.7, indicating that e.g. an increase of the diffuseness parameter from 0.65 to 0.80 fm improves the agreement for polarization data. This demonstrates again that in addition to the usual criteria for choosing the form factors in DWBA, inclusion of polarization data provides useful additional restriction.

$^{52}Cr(d,p)^{53}Cr$ and $^{88}Sr(d,p)^{89}Sr$ reactions

Stripping reactions on medium-weight nuclei offer a clearer picture of the mechanism and if in addition neutrons are captured into good single-particle states of the residual nucleus, they provide a good test of DWBA theory.

The vector analysing power distributions for Cr shown in fig.7 are included here merely to demonstrate the j-dependence of polarization in stripping. Similar results were reported previously by Yule and Haeberli[4] and Bjorkholm et al[8]. using vector polarized deuterons of 8 and 11 MeV respectively. The vector analysing powers for the g.s. and the 0.57 MeV excited state transitions, both $\ell = 1$ but $j = 3/2$ and $j = \frac{1}{2}$ respectively, show a behaviour of the angular distribution around 60^{o} very

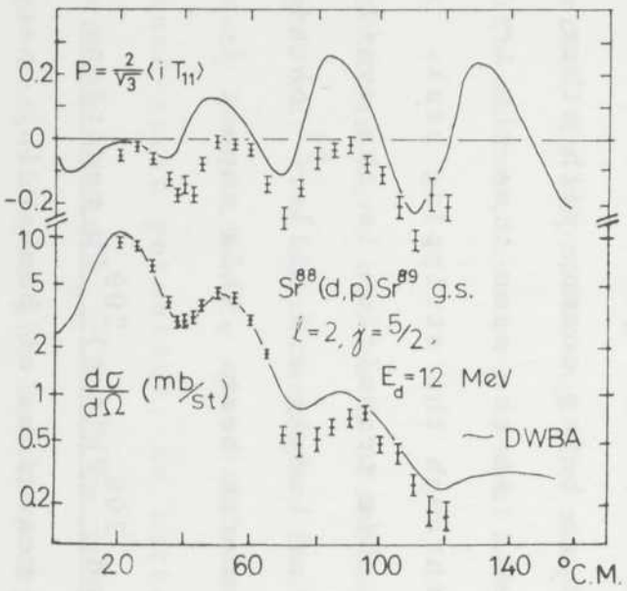

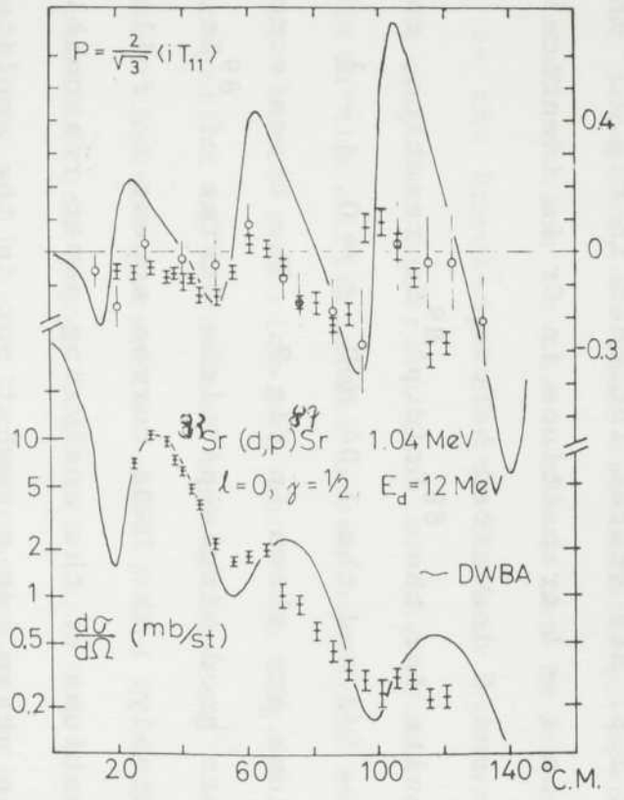

Fig.9. The vector analysing power and differential cross-sections for the ^{88}Sr(d,p)^{89}Sr reaction. Data points represented by open circles for the 1.04 MeV transition are the $P_p(\theta)$ results of Ludwig and Miller [9].

distinctly depending upon the j-value. The same applies again to the 2.32 and 3.61 MeV states included in fig.7. This behaviour for the $\ell = 1$ transitions in Cr is identical to the stripping on Be and C described before.

The results for the $^{88}Sr(d,p)^{89}Sr$ reaction, the ground state $\ell = 2$, $j = 5/2$ and the 1.04 MeV, $\ell = 0$, $j = \frac{1}{2}$ excited state transitions are shown in fig.9. The transferred neutrons are captured into good single-particle states of ^{89}Sr, 2d5/2 and $3s\frac{1}{2}$ respectively. The DWBA curves appear to follow the angular distributions of the analysing power reasonably well, being correct in phase but somewhat out in the amplitude of oscillations, overestimating the polarization data above the zero axis. The description of the $\ell = 0$ transition is less satisfactory; this feature being common with other $\ell = 0$ reactions so far investigated. At the same time the $\ell = 2$ reaction is reproduced right through the stripping peak. An important reason for investigating this transition is the availability of proton polarization data of Ludwig and Miller[9] obtained with an unpolarized incident deuteron beam. This aspect is discussed separately.

$^{207}Pb(d,p)^{208}Pb$ and $^{208}Pb(d,p)^{209}Pb$ reactions

Stripping reactions at bombarding energies near the Coulomb barrier are dominated by Coulomb forces described adequately by DWBA, and the stripping process proceeding away

from the nucleus ought to be quite insensitive to features of the nuclear interior, so that extraction of spectroscopic factors and other information on the nucleus can be expected to be little dependent on the knowledge of the nuclear potential.

The angular distributions of the vector analysing power together with the differential cross-sections for the ^{207}Pb(d,p) ^{208}Pb ground state reaction are shown in fig.10. The proton optical potential of Greenlees and Becchetti[6] was used and for the deuteron channel parameter sets 1 and 2 of Jeans et al[10]. The DWBA predictions shown indicate that the parameters with a deeper imaginary well (set 2) are somewhat better in describing the polarization. The relative importance of the two distorting channels was examined, indicating that the deuteron channel is by far more important in reproducing the shape of the cross-section curve but both distortions are essential to explain the polarization.

The predictions were not much affected by changes of the spin-orbit strength but the spectroscopic factor and the quality of the fits was very sensitive to the diffuseness of the surface of the neutron bound-state potential; an increase from $a_b = 0.65$ to $a_b = 0.85$ fm with a fixed $r_b = 1.25$ fm improved the quality of the predictions and changed the spectroscopic factor by 50% bringing its value close to unity.

The asymmetries observed in the ^{208}Pb(d,p)^{209}Pb reaction were rather large with the exception of the $\ell = 0$, $j = \frac{1}{2}$, 2.03 MeV state in ^{209}Pb shown in fig.11. The angular distribution for the

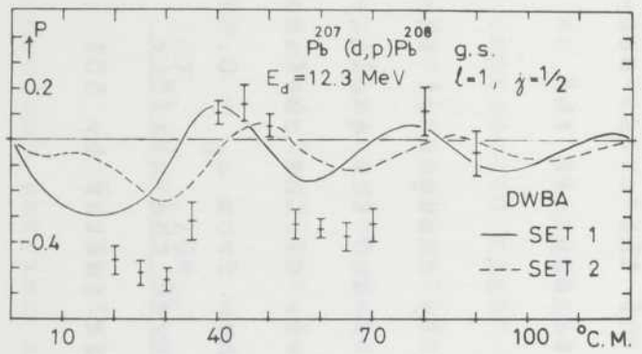

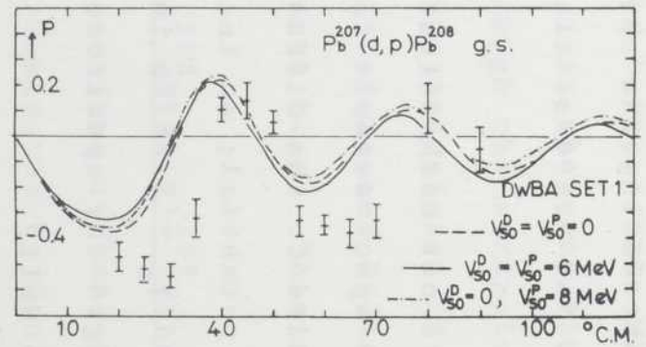

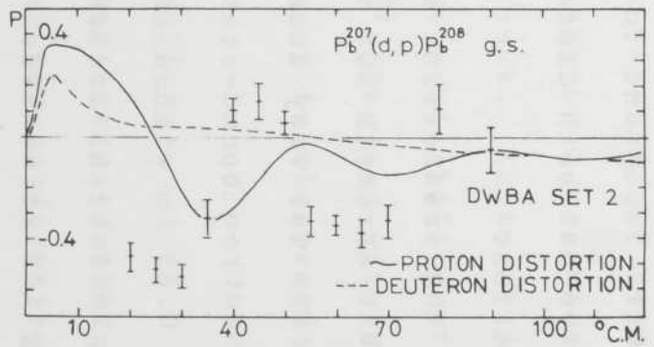

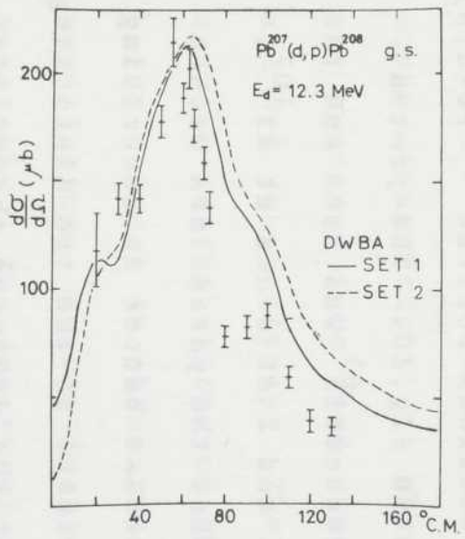

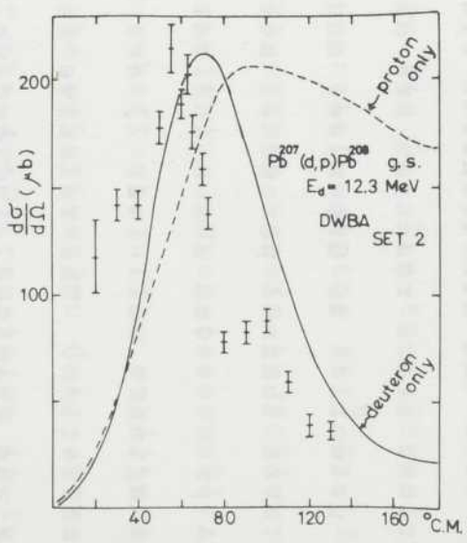

Fig. 10. The vector analysing power and differential cross-sections for the $^{207}Pb(d,p)^{208}Pb$ reactions together with DWBA predictions, showing the effects of the spin-orbit distorting terms and the separate effects of the two distorting channels.

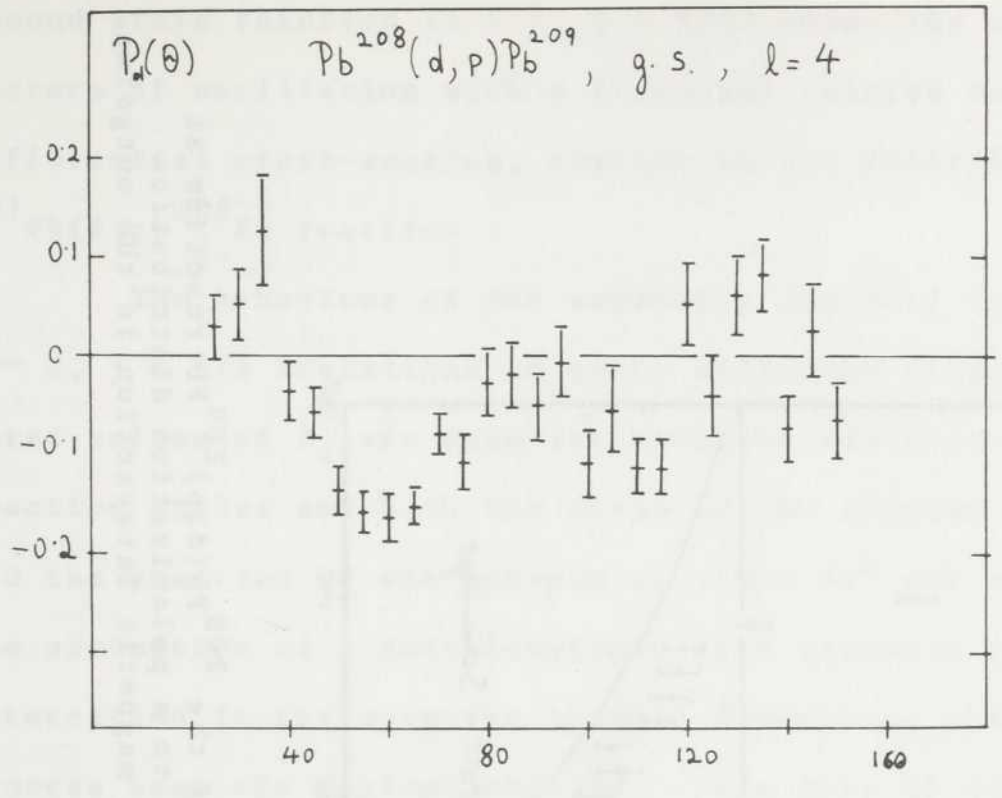

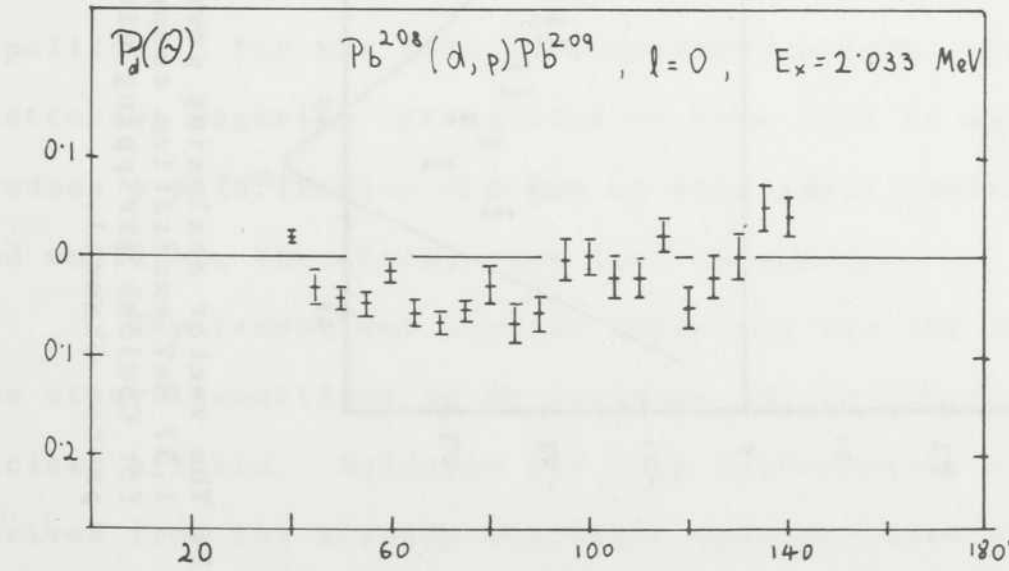

Fig. 11. The vector analysing power for the ^{208}Pb(d,p)^{209}Pb g.s. and E_x = 2.03 MeV reactions.

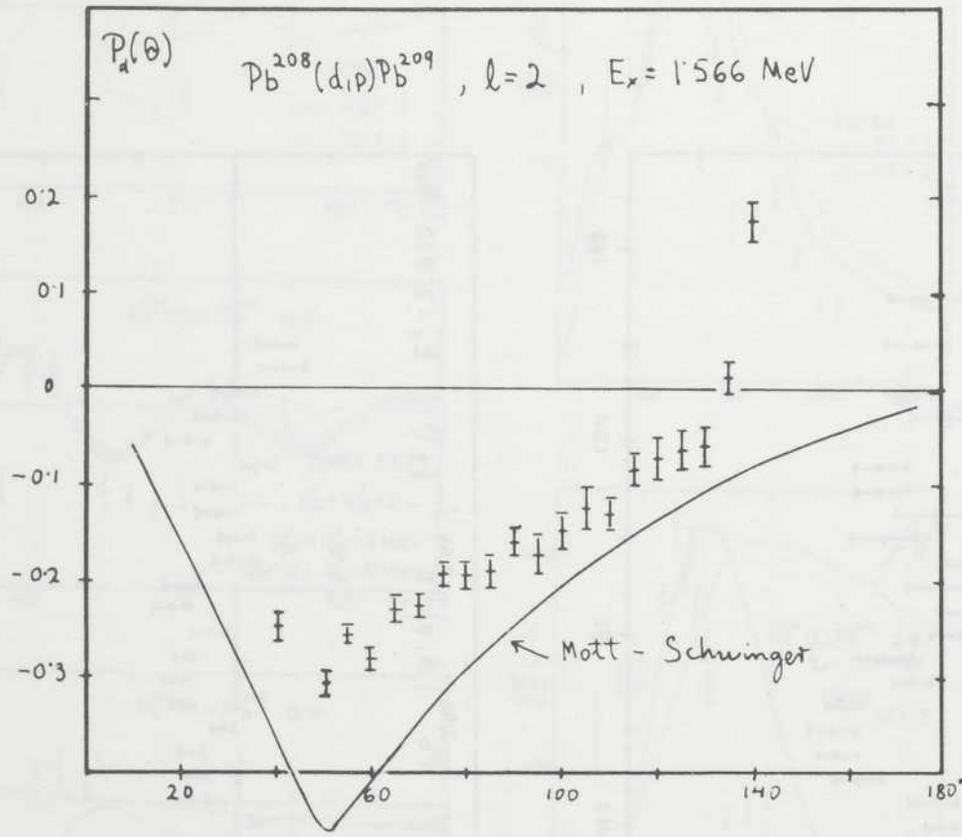

Fig. 12. The vector analysing power of the $^{208}Pb(d,p)^{209}Pb$ reaction at 1.57 MeV excitation compared to a polarization distribution for Coulomb stripping with a magnetic interaction in the outgoing proton channel.

ground state reaction ($\ell = 4$, $j = 9/2$) shows the characteristic pattern of oscillation with a frequency related to that of the differential cross-section, similar to the distribution for the $^{207}Pb(d,p)^{208}Pb$ reaction.

The behaviour of the asymmetry observed for the 1.57 MeV, $\ell = 2$, $j = 5/2$ transition is quite different (fig.12); the measured values of P_d are negative with the exception of very large reaction angles and both the shape of the angular distribution and the position of the minimum at about 45° are consistent with the assumption of a Mott-Schwinger type magnetic spin-orbit interaction in the outgoing channel dominating the stripping process near the Coulomb barrier. This type of polarization in Coulomb stripping has been considered recently by Drukarev and Ippolitov[11] for the case of s-neutron capture. In the elastic scattering magnetic interaction of this type is expected to produce a polarization minimum at very small scattering angles and would be, therefore, very hard to measure.

The reason why similar behaviour was not observed for the other transitions in Pb could be due to interference with nuclear effects. Evidence for such interference can perhaps be derived from the already available results; some of the polarizations observed in stripping by medium and heavy nuclei appear to be "pulled" down at angles in the vicinity of the expected minimum of the magnetic interaction; see for example the polarization distributions for ^{207}Pb and ^{88}Sr (figs.9 and 10).

Comparison between $P_d(\theta)$ and $P_p(\theta)$

The relation between the vector analysing power of a stripping reaction $P_d(\theta)$ and the proton polarization $P_p(\theta)$ produced in the same reaction induced by unpolarized deuteron beam has been considered by Satchler[12], Goldfarb[13], van Rij[14] and Pearson[15]. There is no simple and generally valid relation between these two physically different quantities. For reactions with zero transferred orbital angular momentum ($\ell = 0$) the following limiting relations hold regardless of the deuteron polarization:

a) $P_d(\theta) = P_p(\theta)$ if deuteron spin dependent distortion is dominant;

b) $P_d(\theta) = 2/3\ P_p(\theta)$ if proton spin dependent distortion is dominant.

These are valid in DWBA neglecting second rank terms[14].

For $\ell \neq 0$ the situation is more complicated requiring use of drastic simplifications for the limiting cases. Pearson et al[15] give a limit $P_d(\theta) = 2P_p(\theta)$ for zero proton spin dependent distortion with $P_p(\theta) \leq 1/3$.

Comparison between experimental $P_d(\theta)$ and $P_p(\theta)$ values can provide information on the reaction mechanism and investigation of $\ell = 0$ cases would be preferable at this stage as the process can be better understood. Due to formidable difficulties of double scattering experiments, $P_p(\theta)$ results are rather scarce. Amongst the reactions studied in Birmingham $P_p(\theta)$ data a similar

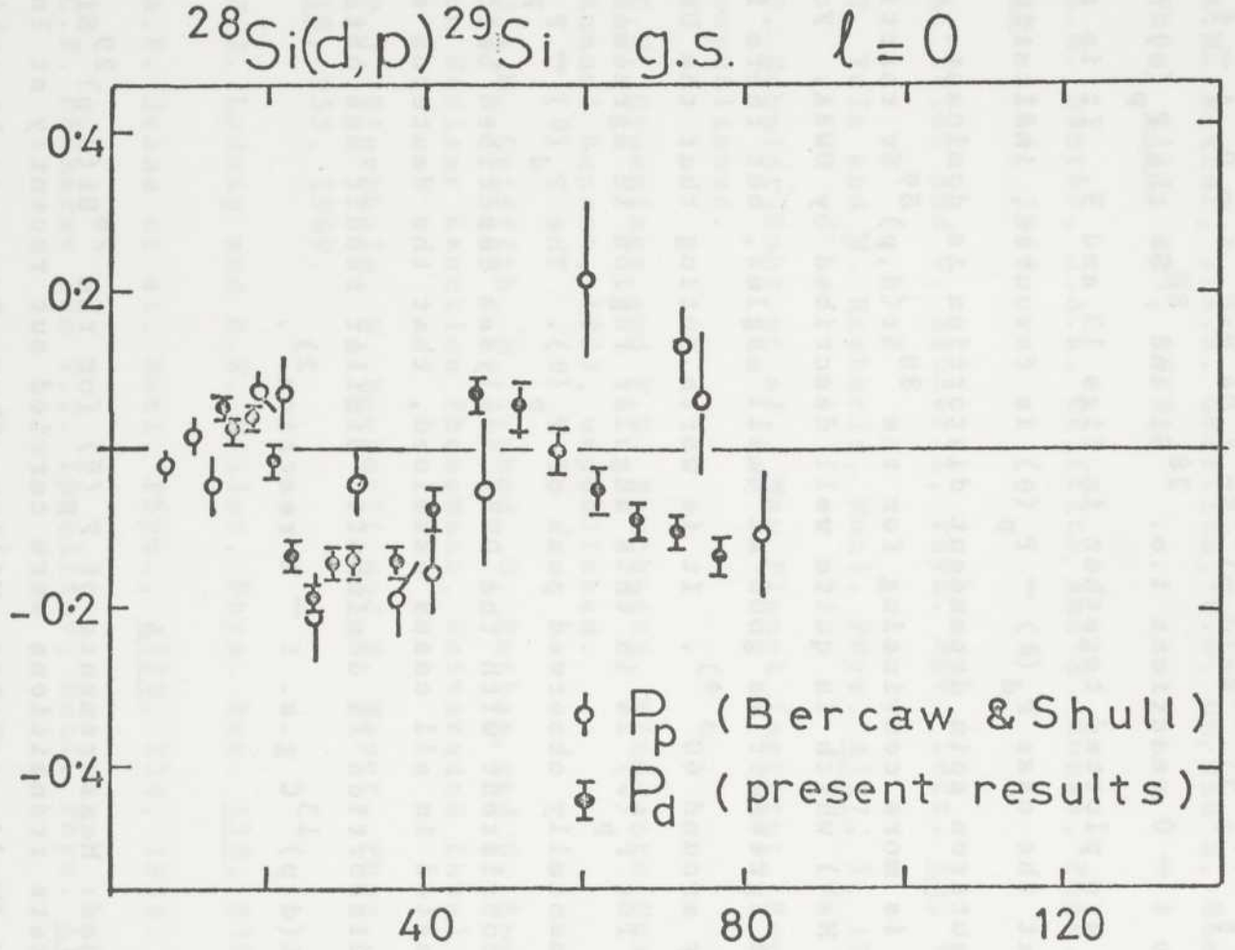

Fig. 13. A comparison between the present $P_d(\theta)$ data and the $P_p(\theta)$ results[17] for Si.

energy are available for the following three reactions: 1) $^{12}C(d,p)^{13}C$ g.s., $\ell = 1$, $j = \frac{1}{2}$ [16]; 2) $^{28}Si(d,p)^{29}Si$ g.s. $\ell = 0$, $j = \frac{1}{2}$ [17]; 3) $^{88}Sr(d,p)^{89}Sr$ 1.04 MeV, $\ell = 0$, $j = \frac{1}{2}$ [9]. For the two $\ell = 0$ reactions i.e. ^{28}Si and ^{88}Sr the $P_p(\theta)$ and $P_d(\theta)$ data are plotted together in figs 13 and 9. It is quite evident that the case $P_d(\theta) = P_p(\theta)$ is favoured, indicating that the deuteron spin dependent distortion is dominant. This conclusion is more convincing for the $^{88}Sr(d,p)^{89}Sr$ reaction ($E_x = 1.04$ MeV) which is quite well described by DWBA. For silicon the agreement is good at small angles, but there is a discrepancy around 60^o *). It is worth noting that the DWBA prediction for $P_p(\theta)$ is in this angular region in agreement with the experimentally observed peak of $P_p(\theta)$. The $P_d(\theta) = P_p(\theta)$ result is consistent with the DWBA analyses described before which suggested in all cases examined, that the deuteron spin dependent distortion is dominant. Similar result was obtained for the $^{12}C(d,p)^{13}C$ g.s. $\ell = 1$ reaction [2].

---

*) Note added: Measurements of $P_p(\theta)$ for the $^{28}Si(d,p)^{29}Si$ g.s. 1.28 MeV state transitions were carried out recently at Indiana at 10.8 MeV (Maddox, Kelly, Miller, Phys. Rev., to be published). The $P_p(\theta)$ data for the 1.28 MeV, $\ell = 2$ transition are similar to our $P_d(\theta)$ data, suggesting that the two quantities are nearly equal in this case. For the g.s., $\ell = 0$ transition the new data are consistent with the results of Bercaw and Shull at 15 MeV, the discrepancy between $P_p(\theta)$ and $P_d(\theta)$ being even more pronounced. I am grateful to Prof. Miller for communicating the results in advance of publication.

REFERENCES

1. A.M. Baxter, J.A.R. Griffith, S.W. Oh, and S. Roman, Nucl. Phys. A112, 209, 1968

2. A.M. Baxter, J.A.R. Griffith, and S. Roman, Phys. Rev. Lett. 20, 1114, 1968.

3. A. Trier and W. Haeberli, Phys. Rev. Lett. 18, 915, 1967

4. T. Yule and W. Haeberli, Nucl. PHys. A117, 1, 1968.

5. U. Schmidt-Rohr et al., Max Planck Institut, Report V13, 1965 unpublished.

6. G.W. Greenlees and F.D. Becchetti, Minnesota University Annual Report, 1967, unpublished.

7. J.A.R. Griffith, M. Irshad, O. Karban, and S. Roman, Symposium on Nuclear Reaction Phenomena, Université Laval Sept. 1-2,1969.

8. P.J. Bjorkholm, W. Haeberli and B. Mayer, Phys. Rev. Lett., 18, 955, 1969.

9. E.J. Ludwig and D.W. Miller, Phys. Rev. 138, B364, 1965.

10. A.F. Jeans et al. Nucl. Phys., A128, 224, 1969.

11. G.F. Drukarev and V.T. Ippolitov, Nucl. Phys. A110, 218, 1968.

12. G.R. Satchler, Nucl. Phys., 55, 1, 1964.

13. L.J.B. Goldfarb, Proc. Karlsruhe Conference, p. 203, Karlsruhe, 1965.

14. W.I. Van Rij., Nucl. Phys. A102, 286, 1967.

15. C.A. Pearson, J.C. Wilcott and L.C. McIntyre, Nucl. Phys. A125, 111, 1969.

16. A. Budzanowski et al., Private communication.

17. R.W. Bercaw and F.B. Shull, Phys. Rev. 133, B632, 1964.

THE DEFORMED SPIN-DEPENDENT OPTICAL POTENTIAL FOR PROTON INELASTIC SCATTERING

H. Sherif
University of Alberta, Edmonton, Canada
and
J. S. Blair
University of Washington, Seattle, U. S. A.

In the analysis of the inelastic scattering of protons exciting low lying collective states in even target nuclei, the extended optical model has been successful in predicting the inelastic angular distributions. In the earlier applications of the model, only the spin-independent parts of the optical potential are deformed. Recent measurements of the asymmetry produced in the inelastic scattering of polarized protons have indicated, beyond doubt, that the spin-dependent (spin-orbit) part of the optical potential must be deformed. The Oak Ridge group proposed the following form for the deformed spin-dependent interaction[1)]

$$\Delta U_{so} = (h/m_\pi c)^2 (V_{so} + i\, W_{so}) \frac{1}{r} \frac{\partial^2}{\partial r \partial R_{so}} f(r, R_{so}, a_{so})$$
$$\times \frac{1}{2} \left[\alpha_{so}(\hat{r})\, \underline{\sigma}.\underline{L} + \underline{\sigma}.\underline{L}\, \alpha_{so}(\hat{r}) \right]. \qquad (1)$$

This lead to improved fits to the observed asymmetries, but in all cases considered the theory failed to reproduce the forward angle asymmetries.

We propose a more appropriate form for the de-

formed spin-dependent interaction, namely the full Thomas form

$$\Delta U_{so} = (h/m_{\pi}c)^2 (V_{so} + i\, W_{so})$$
$$\underline{\sigma}.\left[\underline{\nabla}\{\alpha_{so}(\hat{r})\, \frac{\partial f(r, R_{so}, a_{so})}{\partial R_{so}}\} \times \frac{1}{i}\, \underline{\nabla}\right]. \qquad (2)$$

Inclusion of this term in the DWBA calculations leads to significant improvement in the fits to the observed data:

1. For protons with incident energy in the neighbourhood of 20 MeV, good fits to the asymmetires[2] for the excitation of the lowest octupole states in ^{90}Zr and ^{92}Zr were obtained using the full Thomas form. At forward angles, these fits are superior to those obtained using expression (1). For the lowest quadrupole states, the full Thomas description is so far the best; although the fits are not as good as those for the octupole states mentioned above. They are, however, superior to both those of expression (1) and the fits obtained using a microscopic description. Spin-flip measurements[3] in this energy region also favour the full Thomas form over expression (1). For nuclei with large deformations, the results may be further improved by a coupled channel calculation using the full Thomas form[4].

2. For protons with incident energy of 30-50 MeV, exciting the lowest quadrupole and octupole states in several medium weight nuclei, the observed negative asymmetries at forward scattering angles are reproduced only when the

full Thomas form is used; the simplified form (1) fails to reproduce these forward angle asymmetries. The two expressions give almost the same results for large scattering angles.

The inclusion of the full Thomas form also leads to a substantial improvement in the fit to the observed spin-flip probabilities[5] in this energy region.

3. For protons with incident energy in the neighbourhood of 155 MeV, a good description of the inelastic polarizations[6,7] is obtained with the full Thomas form. When the deformed spin-dependent term is absent or is of the form given by expression (1), the resulting polarizations have little resemblance to those observed. Previous DWIA fits to the polarizations are generally less satisfactory at forward scattering angles than those of the extended optical model with the full Thomas term.

We therefore strongly suggest that any macroscopic description of proton inelastic scattering must include a deformed spin-dependent interaction of the full Thomas form. Moreover, the newly developed microscopic treatment of proton inelastic scattering at lower energies, is not expected to give adequate descriptions of the spin-dependent effects in such processes; unless the two-body spin-orbit term is included in the effective potential.

1) M. P. Fricke et al, Phys. Rev. Lett. 16 (1966) 746

2) C. Glashausser et al, to be published

3) J. Eenmaa et al, Phys. Lett. 28B (1968) 321

4) J. Raynal (invited talk to this symposium)

5) R. O. Ginaven et al, Phys. Rev. Lett. 21 (1968) 552

6) A. Willis et al, Nucl. Phys. A112 (1968) 417

7) H. Sherif and J. S. Blair, to be published.

A Polarization-Asymmetry Test of Time-Reversal Invariance*

E. E. Gross, J. J. Malanify+, A. van der Woude, and A. Zucker

Oak Ridge National Laboratory
Oak Ridge, Tennessee, USA

The polarization-asymmetry equality for the elastic scattering of protons by a non-zero spin target need not be exact if time-reversal invariance is violated.[1] This equality had previously[2] been checked to an accuracy of ± 2.5%. Recent improvements in the experiment have allowed us to reduce the uncertainty to less than ± 1%. We now report P/A = 1.000 ± 0.008 for the ratio of polarization to asymmetry in the elastic scattering of 32.9 MeV protons from ^{13}C at 60° Lab. This result is consistent with no violation of time-reversal invariance. In addition we have measured the absolute polarizing power of ^{12}C for 60° Lab elastic scattering of 32.9 MeV protons to be 0.669 ± 0.004.

---

*Research sponsored by the U. S. Atomic Energy Commission under contract with Union Carbide Corporation.

+Present address: Los Alamos Scientific Laboratory, Los Alamos, New Mexico.

References

1. E. M. Henley and B. A. Jacobsohn, Phys. Rev. 113, 225 (1959).

2. E. E. Gross, J. J. Malanify, A. van der Woude, and A. Zucker, Phys. Rev. Letters 21, 1476 (1968).

Determination of the Scattering Amplitudes from Polarization Measurements.*

Markus Simonius, Carnegie-Mellon University, Pittsburgh, Pennsylvania 15213

With the development of the technique of polarization measurements one seems to have reached the stage where it is possible to determine all spin dependent scattering amplitudes for a given process from such experiments alone without the use of specific models. The question then naturally arises what experimental information is really necessary and which feasible measurements are sufficient for a complete determination of the scattering amplitudes. Rather general solutions to this problem have been obtained recently.[1] We state here the most important results without going into some pathological exceptions (which do not apply in any presently interesting case anyhow). These are treated in the above-mentioned papers. We call a set of measurements complete if it allows to determine the scattering amplitudes uniquely up to a common phase.

We now state the central necessity condition: if the particles in the reaction (incoming and outgoing taken separately) can be divided into two sets such that no polarization correlation is known between a particle from the first and one from the second set, then the measurements are not complete. One thus has to perform measurements in such a way that the polarizations of all particles are "connected". The following sufficiency statements then show that in most cases the simplest sets of the measurements which overcome the above restriction are complete. In the case where only three particles in the reaction have nonzero spin it is sufficient to measure the correlations between a given one of them and each of the two others, unless the first one has spin 1/2 and both other spins are higher. Thus in $He^3(d,p)\alpha$ the correlations (d,He^3) between d and He^3, and (d,p), which are feasible with a polarized d-beam, are complete. In the case of four particles with nonzero spin one can again completely determine the amplitudes from correlations between the beam (or any given particle) and each of the other particles provided that only one or the other particles has higher spin than the beam. Instead of the correlations (1,2), (1,3) and (1,4) mentioned above, one can also use e.g. (1,2), (1,3) and (2,4) provided that the spins j of the particles obey $j_1 \geq j_3$ and $j_2 \geq j_4$. In the case of three particles with $j \neq 0$ the solutions for the amplitudes obtained from these correlations are unique. However, if there are four particles with $j \neq 0$, it is possible that several discrete solutions exist. These can, however, be resolved by relatively crude additional measurements.

Note that for an elastic process, $1 + 2 \rightarrow 3 + 4$, not all the above-mentioned correlations have to be actually measured since e.g. measurement of the correlation (1,2) between the first two particles automatically gives also the result for (3,4) due to timereversal invariance. Similar connections hold also for other correlations and other symmetries.[1]

We finally mention that there exists a fairly simple way to solve special cases on a computer by determining the rank of the Jacobian of the bilinear system of equations connecting the measurables and the amplitudes.[1]

* Work supported by the U. S. Atomic Energy Commission.

1. M. Simonius, Theory of Polarization Measurements I: Formalism and Determination of the Scattering Amplitudes From Measurements (Preprint) and Theory of Polarization Measurements II: Mathematical Tools, Bilinear Equations (Preprint).

2. For an exception see[1] and M. Simonius, Phys. Rev. Letters 19, 279 (1967).

Measurement of the Depolarization parameter for proton-nucleus scattering at 50 MeV

C. J. Batty and C. Tschalär
Rutherford Laboratory, Chilton, Didcot, Berks., England

Using the 50 MeV polarized proton beam from the Rutherford Laboratory proton linear accelerator the triple scattering depolarization parameter D has been measured for a range of nuclei. The purpose of the experiment was to determine the possible existence of a spin-spin interaction in proton-nucleus scattering. Such an interaction would give values of $D < 1$ whereas a value of $D = 1$ is expected when there is no spin-spin interaction as is the case for the scattering from spin zero nuclei.

Polarized protons scattered from the target were magnetically analysed using a $n\frac{1}{2}$ double focussing spectrometer to select those which had been elastically scattered. The polarization of these protons was measured using a high efficiency polarimeter. This polarimeter uses the scattering of protons from a set of carbon vanes. An energy degrader system defines the angular range for acceptance of the scattered particles rather than the conventional guiding vanes or collimators. The total scattering yield is 8×10^{-4} with an analysing power of approximately 48%.

The D-parameter was measured for a series of high-spin nuclei covering a wide range of A values. Two targets of spin-zero nuclei were used to check that the expected value of $D = 1$ was obtained in this case. Measurements were made at angles corresponding to the first minimum in the differential scattering cross-section since calculations for neutrons[1] indicate that it is here that significant effects may be observed. The results are tabulated below.

Nucleus	Spin	Lab. Angle	D
^{10}B	3	49°	0.96 ± .16
^{27}Al	5/2	36°	1.02 ± .06
Si (nat.)	0	36°	1.07 ± .10
^{59}Co	7/2	26°	0.96 ± .05
Ni (nat.)	0	26°	1.04 ± .08
$^{113,115}In$ (nat.)	9/2	21°20'	0.98 ± .14
^{209}Bi	9/2	33°30'	0.93 ± .15

In no case was any significant deviation of D from the value 1 observed indicating that any spin-spin interaction must be relatively small. This result is in agreement with recent measurements[2] using the scattering of polarized neutrons by aligned nuclei.

References: 1) A. P. Stamp, Phys. Rev. 153 (1967) 1052
2) T. R. Fisher et al, Phys. Rev. 157 (1967) 1149
S. Kobayashi et al, Prog. Theor. Phys. 40 (1968) 1451

A COMPARISON OF POLARIZATION ANALYSING POWERS OF TWO NUCLEON TRANSFER REACTIONS LEADING TO MIRROR FINAL STATES.

J.M. Nelson, N.S. Chant*, and P.S. Fisher

Nuclear Physics Laboratory, Oxford.

The comparison of (p,t) and (p,He^3) angular distributions at high incident energies (40 MeV) has been shown to be an effective method of identifying states in the residual nucleus which have isobaric spin one unit greater than that of the target [eg. 1)]. If the interaction responsible for the reaction is charged independent, it can be shown that not only are the angular distributions of the two reactions which lead to such mirror states, identical, but that also the relative magnitudes of the two differential cross sections are simply related by isobaric spin coupling factors and a term depending on the momenta of the triton and He^3. The comparison of two such angular distributions was first made by Cerny and Pehl [2)] for the reactions $O^{16}(p,t)O^{14}$ (g.s.) and $O^{16}(p,He^3)N^{14}$ (2.311 MeV) at 43.7 MeV incident energy. The natural extension of this test is to compare the polarization of the triton and He^3, or, the polarization analysing powers of the two reactions when the incident beam is polarised. In both cases, the chape and magnitude of the polarization angular distribution should be identical.

The results presented here are asymmetry measurements for the (p,t) and (p,He^3) reactions on O^{16} which were obtained with the 49.5 MeV polarized proton beam from the linear

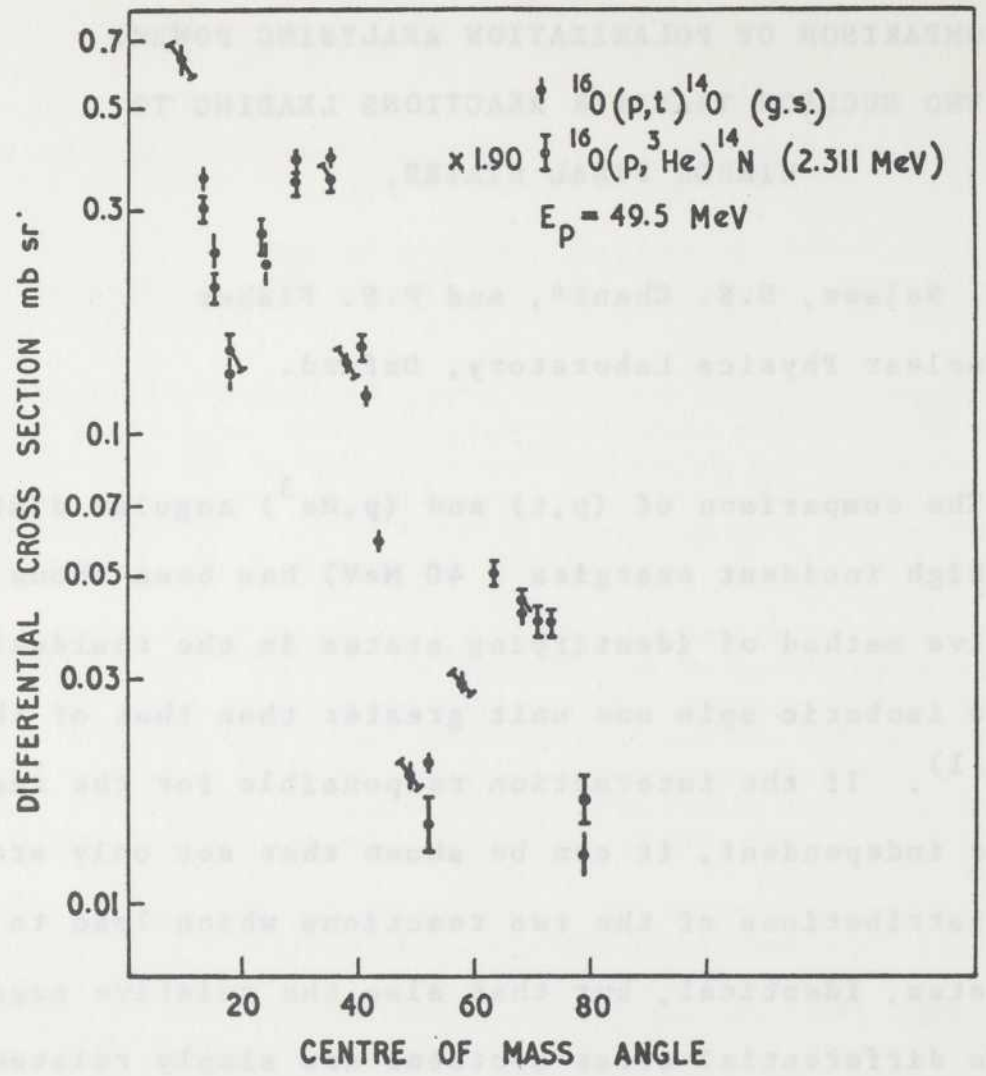
0.7
0.5
0.3
0.1
0.07
0.05
0.03
0.01
DIFFERENTIAL CROSS SECTION mb sr⁻¹
$^{16}O(p,t)^{14}O$ (g.s.)
x 1.90 $^{16}O(p,^3He)^{14}N$ (2.311 MeV)
E_p = 49.5 MeV
20
40
60
80
CENTRE OF MASS ANGLE

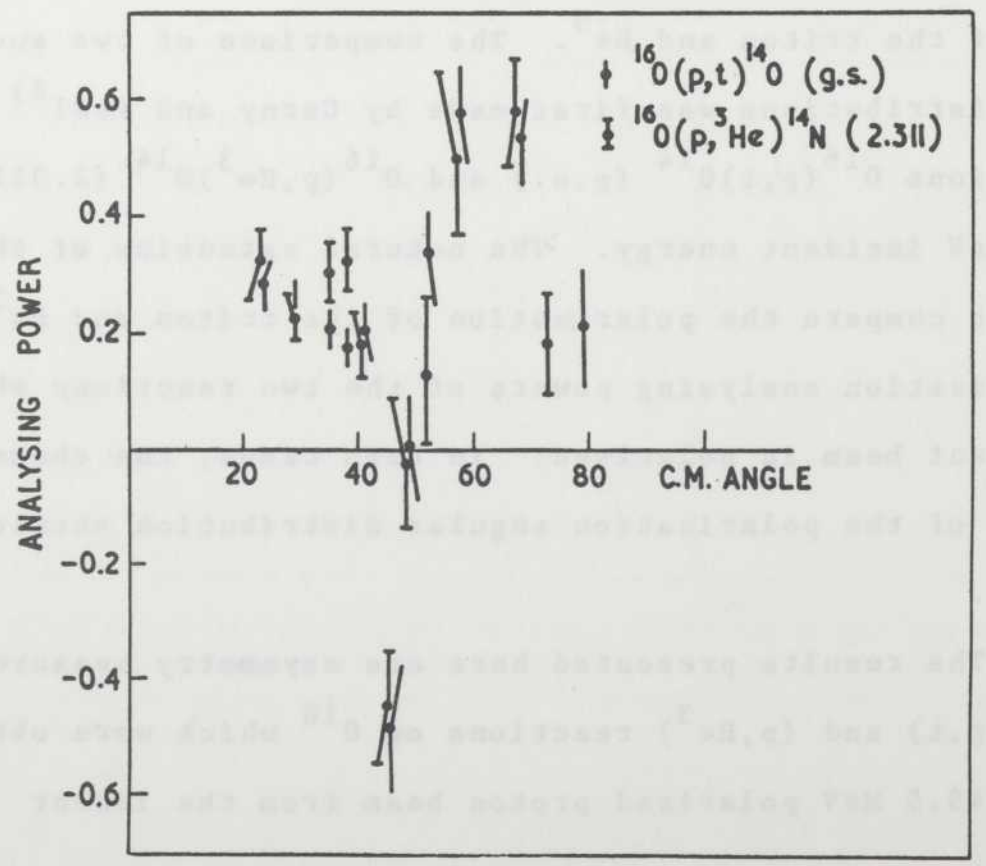
0.6
0.4
0.2
-0.2
-0.4
-0.6
ANALYSING POWER
$^{16}O(p,t)^{14}O$ (g.s.)
$^{16}O(p,^3He)^{14}N$ (2.311)
20
40
60
80
C.M. ANGLE

accelerator at the Rutherford High Energy Laboratory. The reaction products were identified using a system employing silicon semi-conductor counters, and the asymmetries were measured with two telescopes placed symmetrically on either side of the beam. This arrangement, coupled with the ability to reserve the direction of proton polarization at the ion source, eliminates many systematic errors that could otherwise contribute falso asymmetries. The differential cross sections were measured in a separate experiments using the more intense unpolarized beam.

The experimental results are compared in the diagram. The (p,He^3) differential cross section has been multiplied by 1.90. This factor was calculated from isobaric spin coupling factors and the momenta of the outgoing particles. The agreement between the differential cross sections is good thus confirming the findings of Cerny and Pehl. The agreement between the two polarization analysing powers is also good and suggests that the identification of analogue states can be confirmed by polarization measurements. The comparison of these results strongly supports the assumption that the transition amplitudes of the two processes are equal, despite the differences in Coulomb and particle energies in the final channels, and that also the interaction potential is independent of charge.

The observation of such large analysing powers in reactions were the spin of the transferred pair is zero, is

completelely at variance with the predictions of the spin-independent DWBA theory[3]. The data indicate the existence of spin-orbit forces in the entrance and/or exit channels, and emphasize the necessity of using a spin-independent DWBA theory in the analysis. This analysis is proceeding together with the analysis of polarization analysing powers measured in a variety of two nucleon transfer reactions.

REFERENCES

1) G.T. Garvey, J. Cerny and R.H. Pehl; Phys. Rev. Letters 13, (1964) 518.

2) J. Cerny and R.H. Pehl; Phys. Rev. Letters 12, (1964) 619.

3) L.J.B. Goldfarb and R.C. Johnson; Nucl. PHys. 18(1960)353.

POLARIZATION EFFECTS IN THE $^{28}Si(d,p)^{29}Si$ REACTION INDUCED BY POLARIZED DEUTERONS

J.A.R.Griffith, M.Irshad, O.Karban and S.Roman, University of Birmingham, England.

Differential cross-sections for stripping reactions induced by unpolarized beams are well described by the DWBA theory, whereby the values of the transferred orbital momenta and the spectroscopic factors can be determined. Prerequisite of distorted wave calculations is the knowledge of unambiguous values of the distorting potential parameters and the validity of certain assumptions concerning the reaction mechanism. Measurements of polarization in stripping reactions were undertaken to help to resolve some of the ambiguities and test the distorted wave theory.

The vector analysing powers of the $^{28}Si(d,p)^{29}Si$ reaction leading to the ground state ($l=0$, $j=\frac{1}{2}$) and the 1.28 MeV first excited state ($l=2$, $j=\frac{3}{2}$) of ^{29}Si were measured using the 12.3 MeV vector polarized beam of the Birmingham University cyclotron. Surface-barrier silicon detector telescopes were used enabling mass separation of protons from deuterons and other reaction products. The technique used involved frequent switching of the beam polarization at the source and it has been described previously (Baxter et al., Nucl. Phys., A112 209,1968).

The angular distributions of the vector analysing power $P_d = \sqrt{2}\langle iT_{11}\rangle$ obtained are presented in the figure. The corresponding distributions of the differential cross-sections shown above were obtained by adding the numbers of counts for the two spin states of the beam, normalized to the total number of counts in the polarimeter. The experimental cross-section scale is subject to an absolute normalization uncertainty of 20 %.

Distorted wave predictions were calculated using the programme by B.Macefield including spin-orbit terms. The deuteron optical potential parameters were obtained from our previous elastic scattering work (to be published). For the proton channel, parameter sets of Baugh et al. (Nucl.Phys., 65 33,1965) and Greenlees and Becchetti (unpublished) were tried. The contributions of the two distorting potentials, the spin-orbit potentials and the role of the potential chosen for the bound state part of the calculation were examined separately. It was found that the distortion in the deuteron channel had the dominant effect, confirming the conclusion reached for the $^{12}C(d,p)^{13}C$ reaction (Phys.Rev.Lett., 20 1114,1968). Using deuteron distortion only the differential cross-sections could be well reproduced, the spectroscopic facotor, however, changed by 2 when the proton distorting potential was neglected and the polarizations predicted were sensitive to the form and strength of the distorting potentials. A value V_{so} = 6 MeV was found to be about best for both distorting channels, but the predictions were not very sensitive to the spin-orbit stregth.

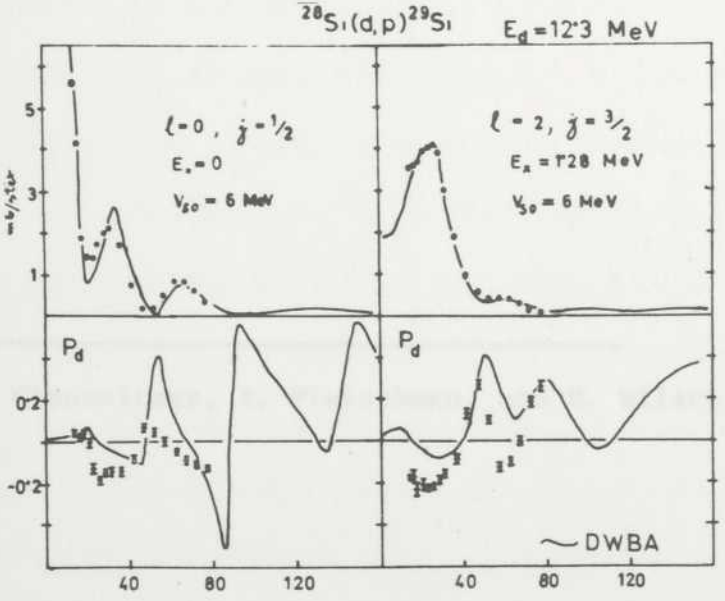

The polarization curve for the g.s. $l=0$, $j=\frac{1}{2}$ transition was similar to the corresponding transition in the $^{12}C(d,p)^{13}C$ reaction and to the reaction $^{24}Mg(d,p)^{25}Mg$ (E_x=0.58; 2.56 MeV, Yule and Haeberli, Nucl.Phys., A117 1,1968). The polarization for the 1.28 MeV group obtained very much resembled the $l=2$, $j=\frac{3}{2}$ polarization at 2.8 MeV in ^{25}Mg (Yule and Haeberli) suggesting j-dependence of polarization in stripping. A comparison of the vector analysing power P_d with the proton polarization P_p measured by Bercaw and Shull (Phys. Rev., 133 B632,1964) for the $l=0$ case indicates that $P_d(\theta) = P_p(\theta)$ is favoured and the deuteron channel ought to be dominant.

Deuteron Double Scattering from Carbon

E.M. Bernstein
Western Michigan University and University of Texas

Azimuthal asymmetries have been measured in d-carbon double scattering at two energies between 7 and 8.5 MeV. The first scattering angle was 45° lab and the second scattering angle was 50° lab. The double scattered deuterons were detected with two semiconductor counter telescopes employing particle identification techniques. The right to left scattering ratios measured were 1.37 ± 0.07 for a first scattering energy of 8.0 MeV and 0.89 ± 0.05 for a first scattering energy of 8.65 MeV. The targets were about 200 keV thick. These results are consistent with the vector polarization measurements of Clausnitzer *et al.*[1] assuming the tensor polarization effects are small.

---

[1] G. Clausnitzer, R. Fleischman, and H. Wilsch, Physics Letters 25B , 466 (1967).

A DETERMINATION OF THE POLARIZATION OF NEUTRONS FROM THE D(d,n)^{3}He REACTION AT 11.3 MeV INCIDENT ENERGY.

J.Birchall, C.O. Blyth, P.B. Dunscombe,
S.Q.G. Mahtaboally, J.S.C. McKee & B.L. Reece.
Dept. of Physics, University of Birmingham, England.

A measurement has been made of the polarisation of Neutrons from the D(d,n)^{3}He reaction, at a laboratory angle of 45^o and an incident deuteron energy of 11.3 MeV, using the method of Schwinger scattering.

Schwinger scattering or electromagnetic polarisation is the name given to the interaction between the magnetic moment of an incident particle and the Coulomb field of a nucleus. It has the form of a spin-orbit interaction and is long range compared with the nuclear force having $1/r^3$ dependence. Schwinger[1] derived expressions for this phenomenon showing that it could produce large polarisations and enhance differential cross-sections at forward angles.

The deuterons were incident on a deuterium gas target[2] and the neutrons produced at 45^o in the lab. were collimated to give a beam divergence of $\pm\frac{1}{2}^o$. After passing through a superconducting solenoid the neutrons were scattered from a lead target through an aperture in a concrete schielding wall and into lead shielded detectors 2 metres away and at an angle of 2.8^o to the incident neutron beam.

Spectra were collected with six field settings of the solenoid from 0 to 46 kg and the background was normalised and subtracted. Fig.I shows the measured asymmetry as a function of solenoid current. This was obtained from the data with a least squares fit to a cosine curve. The theoretically calculated field for 180° precession is 30 kg.

There are several possible corrections appreciable to an experiment of this type one of which is depolarisation in the solenoid due to precession about radial field components. Atkinson and Sherwood[3] have shown that for the solenoid used here the effect will be less than 2%. In addition depolarisation will occur in the lead before scattering takes place but this should be less than 1%.

The effect of the magnetic field of the solenoid on the photomultipliers could have been important in this experiment, but was in fact negligible due to the value of the discriminator setting and the low field at that position. This view is justified by the fact that no change in count rate was found on reversing the field.

To calculate the polarisation of the neutron beam the following form of the Schwinger expression[4] was used for the analysing power of lead

$$P_2(\theta) = \frac{\nu k \sigma_T Z \cot\frac{\theta}{2}}{\sigma(\theta)} \quad \text{where } \nu = \frac{\mu_n}{2} \frac{e^2}{Mc^2}$$

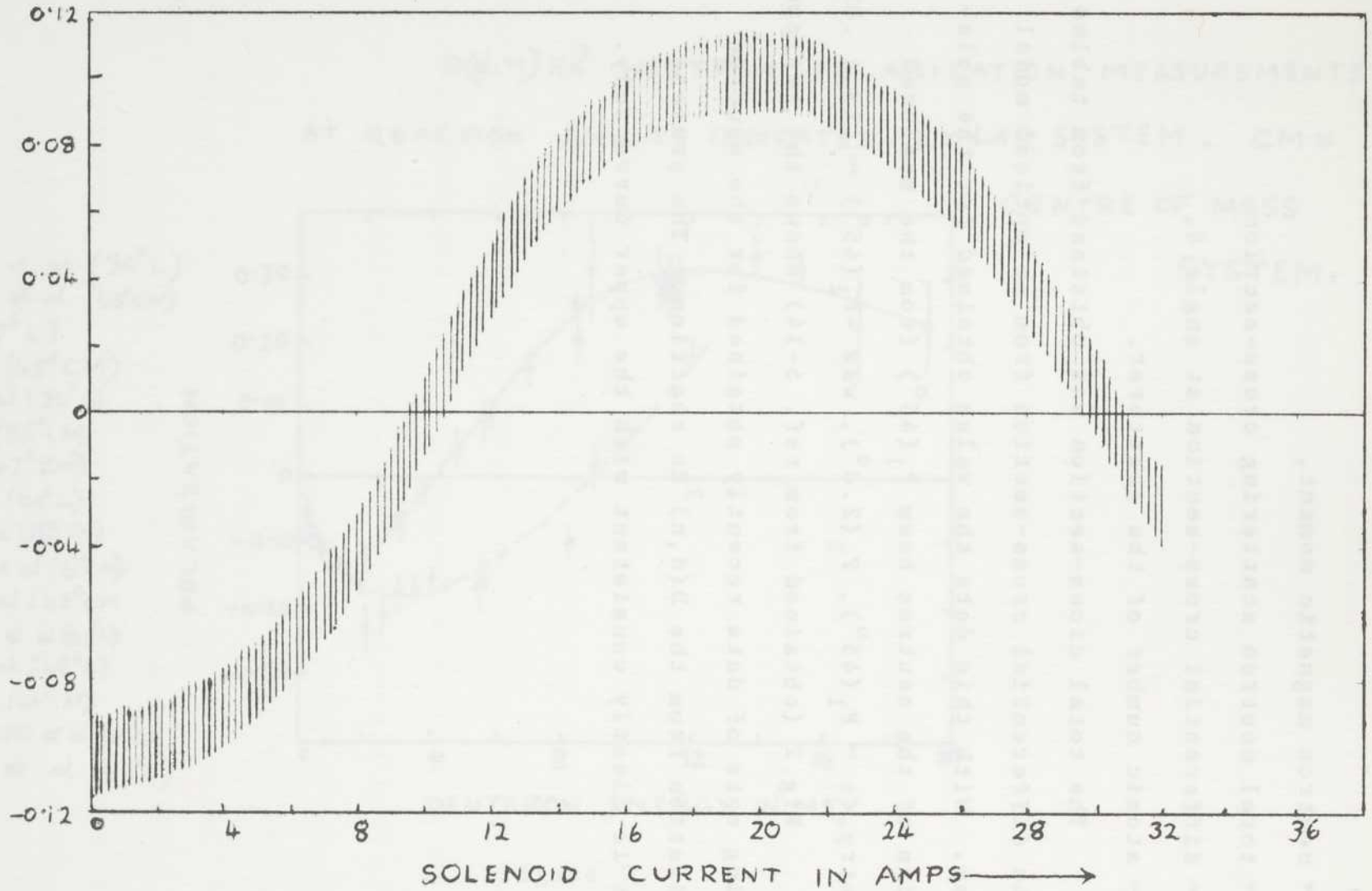
0·12
0·08
0·04
0
-0·04
-0·08
-0·12
ASYMMETRY
0
4
8
12
16
20
24
28
32
36
SOLENOID CURRENT IN AMPS

Figure 1

where,

μ_n = neutron magnetic moment,

σ_T = total neutron scattering cross-section,

$\sigma(\theta)$ = differential cross-section at angle θ,

Z = atomic number of the scatterer.

The total cross-section was obtained from tables and the differential cross-section from an optical model program. With this data the value obtained for the polarisation of the neutron beam $P_1(45^o)$ from the measured asymmetry, $\varepsilon = P_1(45^o)$, $P_2(2.8^o)$, was $-P_1(45^o) = .29 \pm .05$.

Fig.2 (obtained from ref. 5-14) shows the two conflicting sets of data recently obtained for the neutron polarisation from the $D(d,n)^3He$ reaction. The present result is clearly consistant with the upper curve only.

$D(d,n)He^3$ NEUTRON POLARIZATION MEASUREMENTS AT REACTION ANGLES INDICATED. L = LAB SYSTEM. CM = CENTRE OF MASS SYSTEM.

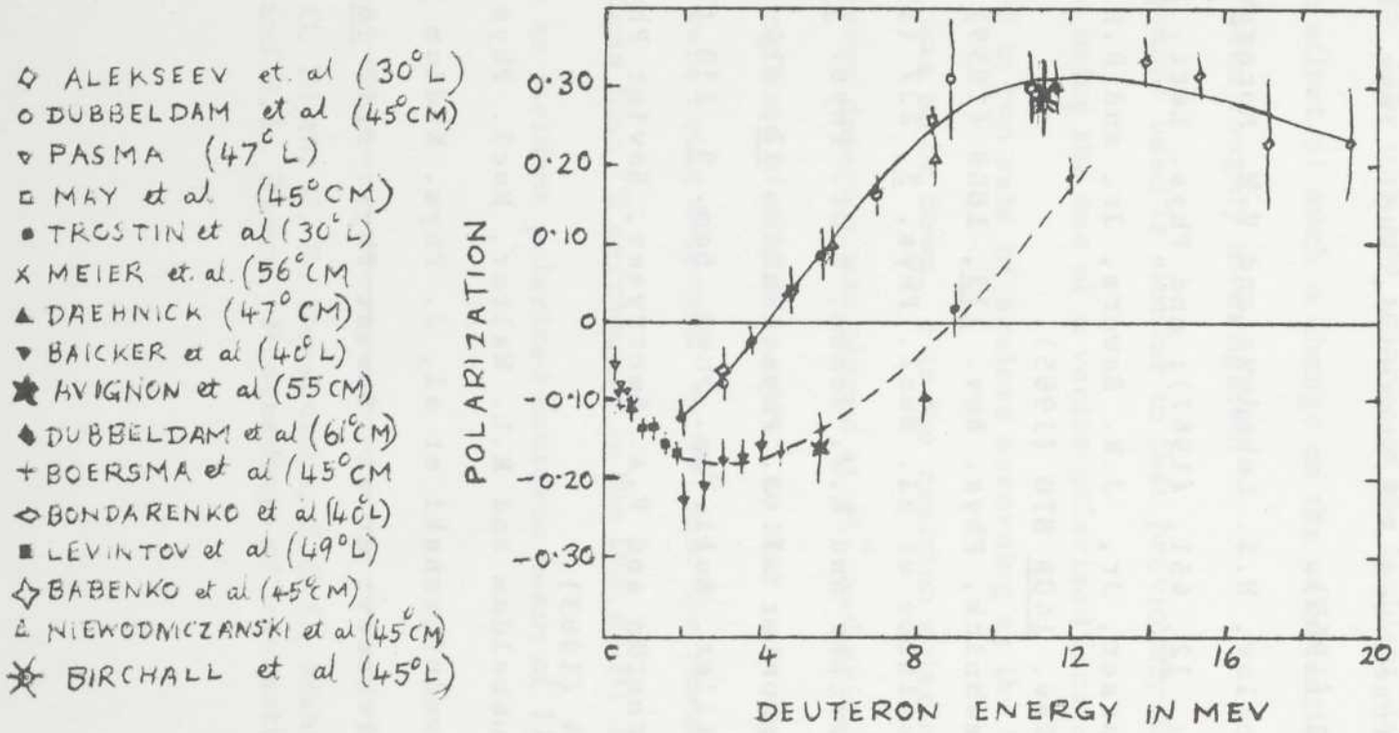

Figure 2

REFERENCES

1. J. Schwinger, Phys. Rev. 73, 407 (1948).
2. J. Birchall, C.O. Blyth, P.B. Dunscombe, S.Q.G. Mahtaboally, J.S.C. McKee, and B.L. Reece; Proceedings of the International Conference on the Three Body Problem. (Birmingham, England) 1969 - North Holland (in press).
3. J. Atkinson and J.E.Sherwood, Nucl. Inst. and Methods. 34, 137 (1965).
4. G.W. Gorlov, N.S. Lebedeva and V.M. Morozov, Soviet Physics Doklady. 12, 451, (1967); and Phys. Lett. 25B,197 (1967).
5. F.O. Purser, Jr, J.R. Sawers, Jr, and R.L. Walter, Phys. Rev. 140B 870 (1965).
6. W.W. Daehnick, Phys. Rev. 115, 1008 (1959).
7. I.I. Levintov et al. Nucl. Phys. 3, 237 (1957).
8. J.A. Baicker and K.W. Jones, Nucl. Phys. 17, 424 (1960).
9. P. Avignon et al. J. Phys. Radium 22, 414 (1961).
10. T.G. Miller, Bull. Am. Phys. Soc. 9, 153 (1964).
11. I.S. Frostin and V.A. Smotryaev, Soviet Physics - JETP 17, 784 (1963).
12. P.S. Dubbeldam and R.L. Walter, Nucl. Phys. 28, 414 (1961).
13. M. Niewodniczanski et al, J. Phys. Radium 24, 871 (1963).
14. N.V. Alekseev, et al, Soviet Phys. JETP 18, 979 (1964).

NEUTRON ASYMMETRY FROM THE D(d,n)^{3}He REACTION USING POLARIZED DEUTERONS

J. Birchall, C. O. Blyth, P. B. Dunscombe, S. Q. G. Mahtaboally, J. S. C. McKee and B. L. Reece.

Department of Physics, University of Birmingham, England.

As part of a programme investigating polarization phenomena in the D(d,n)^{3}He reaction we have measured the effect on the differential cross section at 45° lab. of a 180° change in the incident deuteron vector polarization. The effect of such a change on the polarization of the neutrons has also been roughly investigated.

The equipment used is similar to that previously described[1] the main exception being the use of a vector polarized incident beam. Counts were stored in two sets of scalers according as the incident beam polarization was up or down. For the reaction polarization measurement a conventional neutron detector was placed at 45° and shielding and bias levels adjusted using time of flight spectra, so that only the two body breakup neutrons were being detected. At 45° lab. the result obtained was that there is less than 2% asymmetry in the D(d,n)^{3}He differential cross section, for an incident polarized deuteron beam of 11.3 MeV energy.

---

1) J. Birchall, C.O. Blyth, P. B. Dunscombe, S.Q.G. Mahtaboally, J.S.C. McKee and B.L. Reece. Proceedings of International Conference

Using the analysing power of Schwinger Scattering as discussed previously[2], we further measured the change in neutron polarization with deuteron vector polarization but the count rates are extremely low. To enable more rapid data accumulation a third counter was added to the arrangement so that three counters were used, a left, a right and a monitor counter. From the results obtained in the short time available to us, we estimated that any change with incident deuteron polarization of the outgoing neutron polarization is less than 1/3 of its original value.

---

on the Three Body Problem (Birmingham, England) 1969 - North Holland (in press)

2) J. Birchall, C. O. Blyth, P. B. Dunscombe, S. Q. G. Mahtaboally, J. S. C. McKee and B. L. Reece.

(contribution to this Conference)

The Polarization of Neutrons from the $^{40}Ca(d,n)^{41}Sc(G.S.)$ Reaction at 3.8 MeV*

J. Taylor, Jr.,† G. Spalek, Th. Stammbach, and R. L. Walter

Dept of Physics, Duke University and Triangle Universities Nuclear Laboratory

Abstract: Neutron polarizations from the $^{40}Ca(d,n)^{41}Sc(G.S.)$ at 3.8 MeV are reported and compared to distorted-wave calculations.

The interaction of deuterons with ^{40}Ca has been the subject of many experiments and analyses in the past. Most recently Schwandt and Haeberli[1] have obtained optical model parameters which yield good agreement with the deuteron elastic scattering cross sections and polarization data. Their studies have provided one of the few determinations of the spin-orbit potential for deuteron scattering. Using their potential in DWBA calculations, they also fit the $^{40}Ca(d,p)^{41}Ca(G.S.)$ cross section. However, they reported that little similarity was found between the predictions and the measured proton polarizations produced in this reaction.

---

* Work supported by U. S. Atomic Energy Commission.
† NDEA Predoctoral Fellow.

(1)

We originally intended to study the $^{40}Ca(d,n)^{41}Sc(G.S.)$ polarization and cross section at tandem Van de Graaff energies in order to have more information to test DWBA predictions. The data presented here are the result of an experiment using the 4 MeV accelerator to test the suitability of our techniques for higher energy measurements. This preliminary study showed that an accurate measurement at tandem energies would take prohibitively long with our present techniques.

To analyze the polarization, the neutrons were scattered from helium contained in a gaseous scintillation counter into side detectors placed at 120°. Energy analysis of the coincident helium recoils permitted separation of the $^{40}Ca(d,n)^{41}Sc(G.S.)$ reaction from background neutron groups which originated in (d,n) reactions from O, C, and D contaminants in the target. Table I gives the results of the measurement in the Basel convention for a mean deuteron energy of 3.8 MeV. The polarization results are compared in Figure 1 to non-local, finite-range DWBA calculations performed using the code DWUCK of P. D. Kunz.[2] Also shown are the 6 MeV data of Gedcke et al.[3] and the 4-MeV cross section data of Macefield, Towle and Gilboy.[4]

Table II gives the deuteron optical model parameters for each of the curves in Figure 1. Potential set D1 at 6.0 MeV is from Ref. 1 and the other two sets used at this energy are modifications of the first. At 3.8 MeV, the calculations centered around extrapolated parameters of Ref. 1. In all these calculations the neutron parameters were held fixed. They originated

Table I. Measured neutron polarization at 3.8 MeV for the $^{40}Ca\,(d,n)^{41}Sc\,(G.S.)$ reaction

θ_{lab} (deg)	$\theta_{c.m.}$ (deg)	$P \pm \Delta P$
20.0	20.8	-0.17 ± 0.07
35.0	36.4	- 0.05 ± 0.08
45.0	46.8	0.02 ± 0.04
57.5	59.5	0.01 ± 0.04
65.0	67.2	0.05 ± 0.05
80.0	82.4	-0.01 ±0.06
95.0	97.4	0.02 ± 0.05
110.0	112.3	-0.04 ± 0.06

Fig. 1. The $^{40}Ca(d,n)^{41}Sc(G.S.)$ neutron polarization at 3.8 MeV from the present work. The experimental cross section [4] at 4.0 MeV and polarization and cross section [3] at 6.0 MeV are from earlier reports. The DWBA calculations are for potential sets D 1 (——), D 2 (.-.-.), and D 3 (- - -) at 6.0 MeV and D 4 (——), D 5(- - -), D 6 (...), and D 7 (.-.-.) at 3,8 MeV.

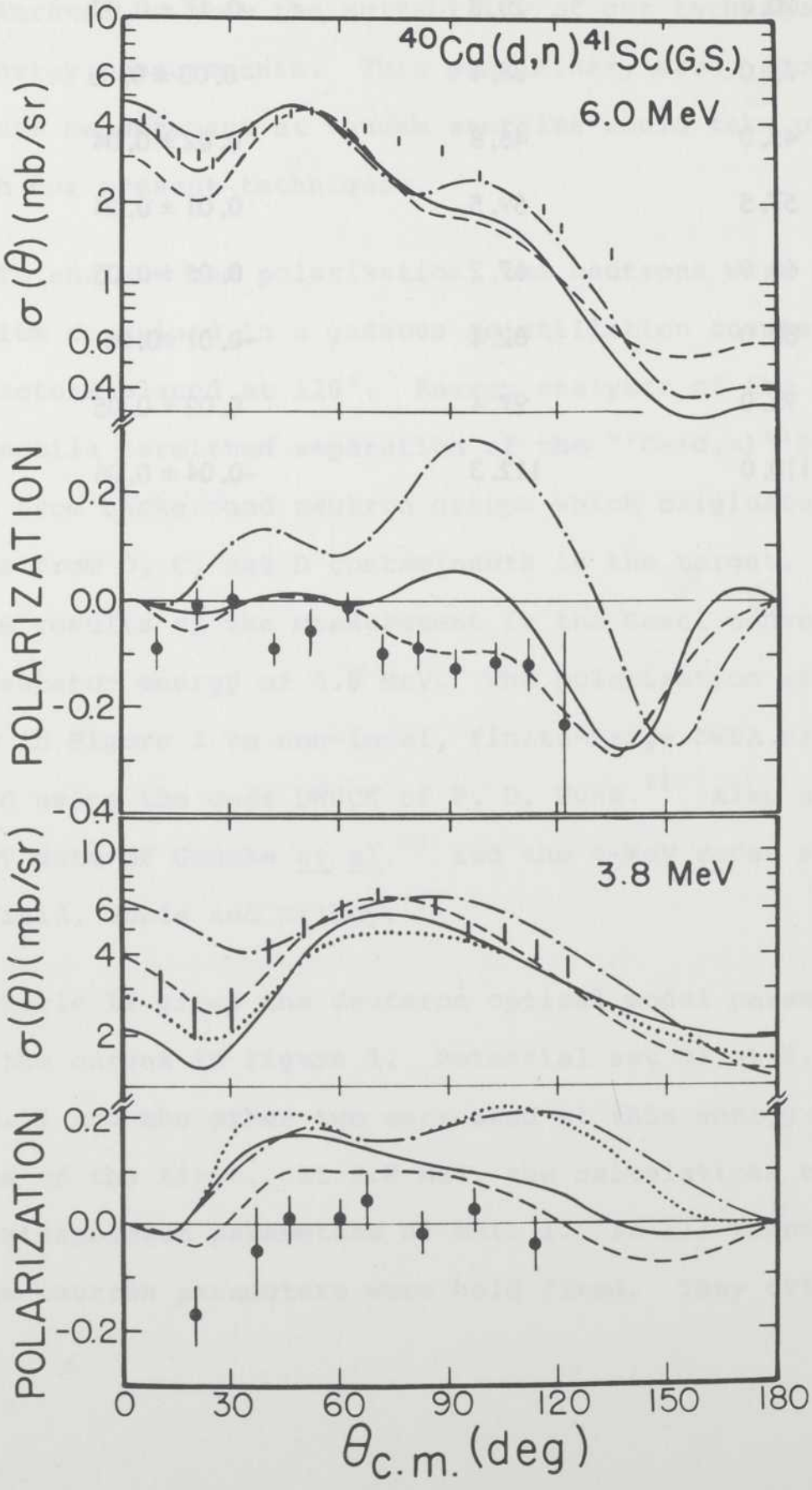

Table II. Deuteron optical model potential sets

Energy (MeV)	Potential	V (MeV)	r (F)	a (F)	W_{surf} (MeV)	r' (F)	a' (F)	V_{so} (MeV)	r_{so} (F)	a_{so} (F)
6.0	D 1	115.5	1.05	0.85	9.5	1.65	0.52	9.0	0.9	0.60
6.0	D 2	115.5	1.05	0.85	9.5	1.65	0.52	0.0	0.9	0.60
6.0	D 3	115.5	1.075	0.85	8.0	1.65	0.52	9.0	0.9	0.60
3.8	D 4	112.0	1.075	0.80	8.5	1.67	0.51	9.0	0.9	0.52
3.8	D 5	112.0	1.075	0.80	9.0	1.67	0.51	8.5	0.9	0.52
3.8	D 6	112.0	1.075	0.80	7.0	1.67	0.51	0.0	0.9	0.52
3.8	D 7	112.0	1.05	0.80	8.5	1.67	0.51	0.0	0.9	0.52

with Perey and Buck and are taken from Ref. 3. The largest sensitivity seen in the DWBA results at 3.8 MeV was when r was increased by several per cent. (Because of the Vr^n ambiguity this corresponds to the effect seen when V is deepened.) This-sensitivity can be seen by comparing the curves for potential D6 to that of potential D7. The sensitivity to changes in W' and V_{so} are also displayed. We have also made calculations at 5 MeV where $^{40}Ca(d,p)$ cross section and polarization data exist and have found that the parameter changes above do not affect the shape of the calculated cross section but do reduce the polarization discrepancy reported by Schwandt and Haeberli. It seems that DWBA may yield suitable fits if appreciable parameter searching were undertaken, but until more is known about the deuteron D-state effects and the effect of coupling in other channels[5] further "trimming" of the parameters has questionable value.

---

[1]Schwandt and Haeberli, Nucl. Phys. A123 (1969) 401.
[2]P. D. Kunz (unpublished).
[3]Gedcke et al., Nucl Phys. A134 (1969) 141.
[4]Macefield, Towle and Gilboy, Proc. Phys. Soc. 77 (1961) 1050.
[5]Rawitscher and Mukerjee, Phys. Rev. 181 (1969) 1518.

The j-dependence of Polarization in the $^{11}B(d,n_o)$ and $^{11}B(d,n_1)$ Reactions*

M. M. Meier, F. O. Purser, Jr., G. L. Morgan, and R. L. Walter

Department of Physics, Duke University and Triangle Universities Nuclear Laboratory

Abstract: Polarization distributions for neutrons from the $^{11}B(d,n_o)$ and $^{11}B(d,n_1)$ reactions have been obtained in the angular range 10° (L) to 135° (L) for energies between 2.8 and 4.0 MeV. The energy dependence is quite weak, indicating the predominance of a direct mechanism in producing the polarization. The sign of the polarization at forward angles is different for the two transitions, indicating the dependence of this quantity on the j-value of the transferred proton.

As part of a program to study polarization produced in (d,n) transitions to states in 1p shell nuclei, we have investigated the $^{11}B(d,n_o)$ $^{12}C(g.s.)$ and $^{11}B(d,n_1)$ $^{12}C(4.43\ MeV)$ reactions. The former reaction must proceed through a $p_{3/2}$ transfer, and the calculations of Cohen and Kurath indicate that the transition to the first excited state is predominately a $p_{1/2}$ transfer. The polarization in the two reactions thus provides a test for the j-dependence of direct reaction theory. Angular distributions were obtained at six energies between 2.8 and 4.0 MeV, the latter being the upper limit of the Duke Van de Graaff. This was done to determine the energy dependence as well as the angular variation of the polarization function. Spin precession and scattering from ^4He were employed in the polarimeter and pulse height analysis of the recoiling alphas was utilized in collecting the data. An automatic search program that fits the alpha recoil spectrum with a sum of gaussians was used to extract the asymmetries of the n_o and n_1 groups which were not completely resolved.

* Work supported by U. S. Atomic Energy Commission.

The results, which were tabulated in Ref. 2, are shown in Figure 1. The smooth curves drawn through the data represent the energy-averaged points at each angle To within statistics, there is negligible deviation from this average, indicating that resonance effects do not contribute significantly to $P(E_d, \theta)$. The j-dependence is quite pronounced for the two groups, further indicating the predominance of a direct mechanism. About ten years ago, Newns proposed that the polarization produced in stripping reactions might be useful in assigning the j-value of the transferred nucleon. At present, though, there is still no general method by which unambiguous assignments can be made. In fact, the empirical evidence[3,4] has indicated that $p_{1/2}$ transfers exhibit appreciably more negative polarization near the stripping peak than is observed in $p_{3/2}$ transfers. Clearly, the $^{11}B(d,n)$ reactions violate this empirical rule. The above-mentioned project has been in the analysis stage for some time and considerable effort has been expended in collaboration with Drisko, Donoghue and Seyler on DWBA calculations with JULIE. Although the main effort has been directed toward an understanding of the $^{14}N(d,n_o)$ reaction, sensitivities to Q-value, A and Z, bombarding energy, non-local and finite-range effects, etc. have been extensively investigated as well. In fact, the sign reversal of the j-dependent polarization is suggested[2] by DWBA to be an effect connected with the large angular momentum mismatch induced by the high Q-values of the reactions (13.73 and 9.30 MeV).

Fig. 1. Polarization distributions for neutrons from the $^{11}B(d,n_o)$ and $^{11}B(d,n_1)$ reactions. The solid curves are the energy averages of the experimental distributions for each transition.

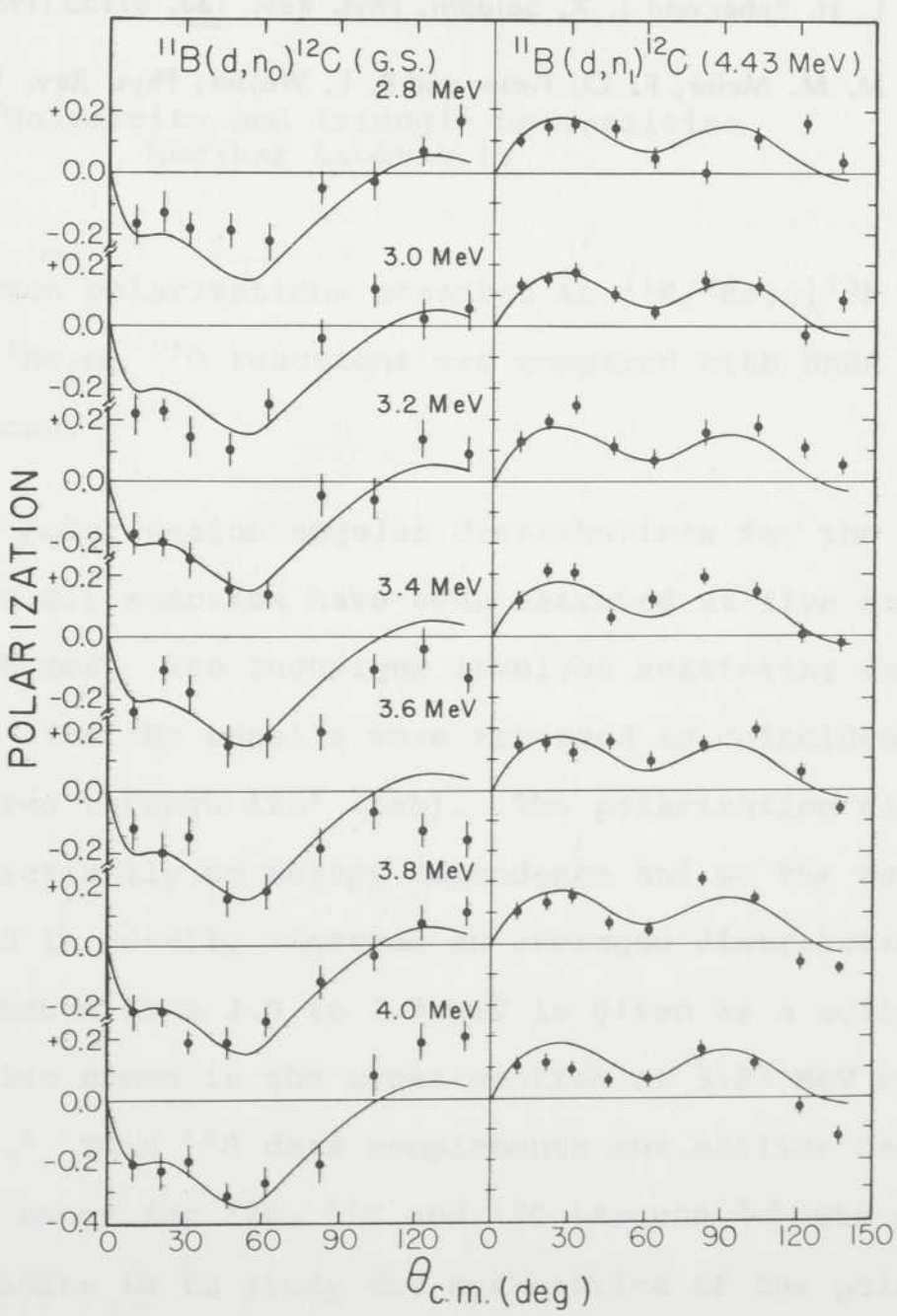

REFERENCES

1) S. Cohen and D. Kurath, Nucl. Phys. A101, 1 (1967).

2) M. M. Meier, "Neutron Polarization for (d,n) Reactions in the 1p Shell", unpublished Ph. D. dissertation, Duke University (1969).

3) L. H. Reber and J. X. Saladin, Phys. Rev. 133, B1155 (1964).

4) M. M. Meier, F. O. Purser and R. L. Walter, Phys. Rev. 163, 1065 (1967).

NEUTRON POLARIZATION IN THE (^{3}He,n) REACTIONS ON ^{11}B and ^{13}C†

R. S. Thomason,* Th. Stammbach, J. Taylor*
and R. L. Walter

Duke University and Triangle Universities
Nuclear Laboratory

Abstract: Neutron polarizations measured in ^{11}B(^{3}He,n)^{13}N and ^{13}C(^{3}He,n) ^{15}O reactions are compared with DWBA calculations.

Neutron polarization angular distributions for the ^{11}B(^{3}He,n) ^{13}N(G.S.) reaction have been measured at five energies from 3.0 to 3.85 MeV. The technique involved scattering from ^{4}He as an analyzer. The ^{4}He recoils were recorded in coincidence with neutrons scattered through 120° (Lab). The polarization distributions showed practically no energy dependence and so the results are not reported in detail. Instead an averaged distribution of all our measurements from 3.0 to 3.9 MeV is given as a solid curve in Figure 1. Also shown is the cross section at 3.83 MeV reported by Din and Weil.[1] This ^{11}B data complements our earlier data over the same energy range for ^{9}Be, ^{12}C and ^{13}C targets.[2,3] The purpose of these experiments is to study the systematics of the polarization in light nuclei. Although the bombarding energy range is

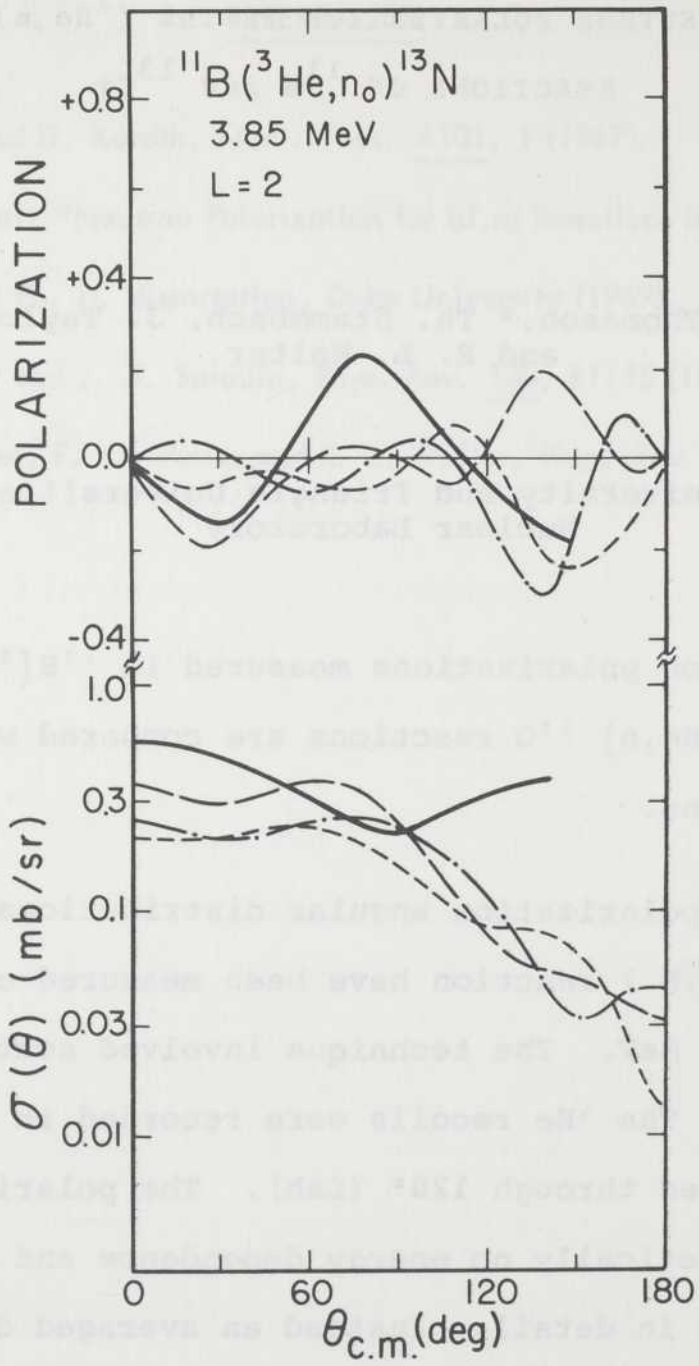

Figure 1. Polarization and cross section for $^{11}B(^{3}He,n)$ compared with DWBA calculations at 3.85 MeV using OM parameters given in Table I. Calculated cross sections are multiplied by an arbitrary factor of 100.

relatively low, it is hoped that some tests for the two-nucleon stripping models might be obtained and also, perhaps, a measure of the spin-orbit interaction for ^{3}He projectiles. In the first reaction studied, $^{12}C(^{3}He,n)$, polarizations exceeded 0.4 near 50° for energies between 3 and 4 MeV, indicating that the polarization for $(^{3}He,n)$ reactions is indeed large.[2] Some similarity was found between DW calculations and the $^{12}C(^{3}He,n)$ data but because of sizeable energy dependence of the data, the conclusions were weak. In this paper we compare the experimental results for $^{11}B(^{3}He,n)$ and $^{13}C(^{3}He,n)$ reactions with DWBA calculations employing the two nucleon transfer form factors from the code of Winner and Drisko.[4]

Our ^{13}C data[3] averaged from 3.4 to 3.9 MeV and the cross sections measured by Din and Weil[5] at 3.83 MeV are represented by the solid curves in Figure 2. The calculations for L = 0 diproton transfer shown in Figure 2 make use of reported optical model (OM) potentials derived from elastic ^{3}He scattering on ^{13}C and ^{12}C by Weller and Van Rinsvelt[6] and Ball and Cerny.[8] The potential reported in Ref. 8 does not include spin-orbit interaction, whose strength is choosen to be 6 MeV. Their radius r is reduced by a factor 0.93. (The plotted DWBA cross sections have been arbitrarily scaled to compare with the measured one. This is necessary because the normalization in our two-nucleon transfer reaction calculations is still an unknown quantity.) The parameters are listed in Table I and refer to a Wood-Saxon potential with either volume (W,r',a') or derivative surface absorption (W',r',a'). Calculations employing the potential of Kellog and

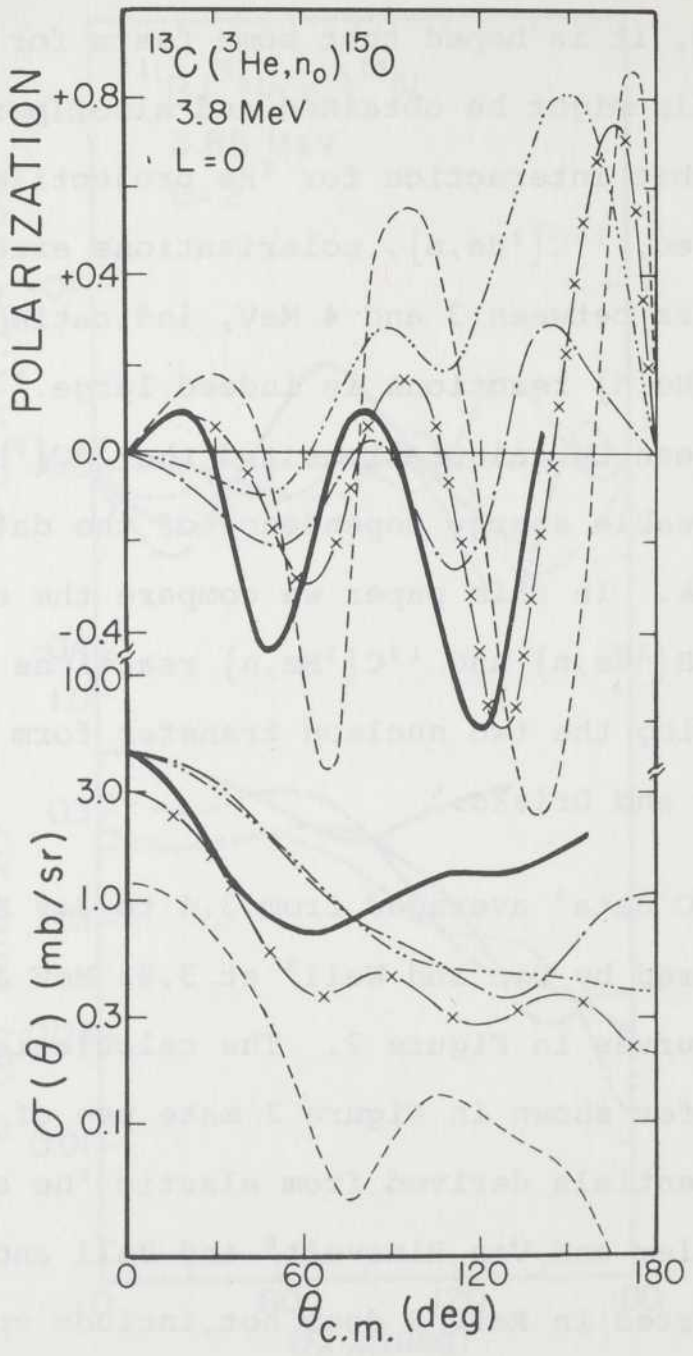

Figure 2. Polarization and cross section for $^{13}C(^{3}He,n)$ compared with DWBA calculations at 3.8 MeV using OM parameters given in Table I. Calculated cross sections are multiplied by an arbitrary factor of 100.

	E (MeV)	V (MeV)	r (F)	a (F)	V_{so} (MeV)	W (MeV)	W′ (MeV)	r′ (F)	a′ (F)	Symbol in Figs. 1 and 2	Ref.
$^{14}N + n$ $^{15}O + n$		46.0	1.32	0.66	9.0	-	8.0	1.26	0.48		9)
$^{11}B + {}^{3}He$	4.0	196.0	1.20	0.67	6.0	-	13.0	1.20	1.07	—— ——	10)
	4.0	202.0	1.20	0.65	6.0	18.0	-	1.20	0.65	——·——	10)
$^{12}C + {}^{3}He$	4.5-6.	137.0	0.93	0.81	6.0	10.6	-	2.17	0.65	——x——	6)
$^{13}C + {}^{3}He$	8.0	161.0	0.93	0.81	6.0	4.73	-	2.56	0.65	——··——	6)
	8.0	161.0	0.93	0.81	3.0	4.73	-	2.56	0.65	——·——	
	15.0	158.0	0.93	0.81	6.0	7.0	-	2.25	0.65	(not shown)	7)
Average set for ^{13}C to ^{15}N	40.0	160.0	1.20	0.57	6.0	12.8	-	1.78	0.82	----------	8)

Table I: Optical model potential parameter.

Zurmühle[7] were also made but are not shown in Figure 2 as they are similar to the result for the ^{13}C potential of Ref. 6. A surprising result in the ^{12}C calculations[2] was that the $(^{3}He,n)$ polarization was insensitive to the ^{3}He spin-orbit depth. In Figure 2 we show that this is not true for ^{13}C where we compare a calculation with a 3 MeV depth (—·—) to a result with 6 MeV (—··—). Good agreement to both, the cross-section and polarization, has not been achieved yet even though numerous other variations of OM parameters have been employed. However, a truly systematic parameter study was not conducted. These calculations will be more meaningful in the future if $^{13}C(^{3}He,^{3}He)$ elastic scattering data becomes available near 4 MeV.

The $^{11}B(^{3}He,n)$ reaction is an L = 2 transfer reaction, assuming the diproton is stripped in its S = 0 state. The small energy dependence of the polarization function and differential cross section indicate a large contribution from direct reaction. DWBA results are shown in Figure 1 for the ^{3}He OM parameters of Park et al.[10] listed in Table I and also those of Ref. 8 used above. Potentials with a different value of V, which Park et al. found also to fit their elastic scattering data, gave similar results in our calculations, too. The agreement in the polarization is reasonably good, especially for the surface absorption case. However, none of the many OM parameter sets tried was able to reproduce the forward peaked cross-section data. This might indicate an admixture of L = 0 transfer with S = 1 for the stripped diproton. The spin-flip admixture could be very small

and yet be visible due to the larger transition probabilities for L = 0 transfers.

It is planned to extend the presented calculations using the code of J. M. Nelson[11] to investigate effects of nonlocality and finite interaction range as well as the sensitivity to the choice of the bound state wave functions for the transferred particles.

---

† Work supported by the U. S. Atomic Energy Commission.
* National Defense Education Act Fellow.

REFERENCES

1) G. U. Din and J. L. Weil, Nucl. Phys. 86, 509 (1966).

2) L. A. Schaller, R. S. Thomason, N. R. Roberson, R. L. Walter, and R. M. Drisko, Phys. Rev. 163, 1034 (1967).

3) Th. Stammbach, R. S. Thomason, J. Taylor, Jr., and R. L. Walter, Phys. Rev. 174, 1119 (1968).

4) D. R. Winner and R. M. Drisko, University of Pittsburgh Technical Report, 1965, (unpublished).

5) G. U. Din and J. L. Weil, Nucl. Phys. 73, 161 (1965).

6) H. R. Weller and H. A. Van Rinsvelt, Nucl. Phys. A129, 68 (1969).

7) E. M. Kellogg and R. W. Zurmühle, Phys. Rev. 152, 890 (1966).

8) G. C. Ball and J. Cerny, Phys. Rev. 177, 1466 (1969).

9) D. Wilmore and P. E. Hodgson, Nucl. Phys. 55, 673 (1964).

10) J. Y. Park, J. L. Duggan, P. D. Miller, M. M. Duncan and R. L. Dangle, Bull. Am. Phys. Soc. 13, 1447 (1968) and Nucl. Phys. A134, 277 (1969).

11) J. M. Nelson, present conference report.

SEANCE
SESSION 4

PRÉSIDENT CHAIRMAN

J.S.C. McKEE

REACTIONS NUCLEAIRES A MOYENNE ENERGIE

N. MARTY

Institut de Physique Nucléaire, Orsay.

Entre la conférence de Montréal, où ont été discutés les problèmes de structure nucléaire étudiés surtout à basse énergie, et la conférence de Columbia, où seront traités les résultats apportés par des expériences faites à énergie élevée, il est intéressant d'essayer de dégager ce qu'apporte l'étude des réactions à moyenne énergie (particules de 100 à 200 MeV). C'est un sujet très vaste et je ne parlerai ici en détails que de la diffusion inélastique p p' et des mesures de polarisation, ainsi que plus rapidement d'expériences récentes de diffusion élastique de particules α faites à Orsay à 160 MeV, ainsi que de réactions de transfert d ^{3}He faites avec des deutons de 80 MeV.

1 - Diffusions inélastiques p p' et polarisation

Pour les diffusions p p' on pensait au départ que pour ces énergies élevées les effets de distorsion étaient faibles, et qu'il suffirait d'un traitement approché de ces effets : approximation d'impulsion en ondes planes ou et tout au plus approximation d'impulsion en ondes distordues (DWIA). On pourrait alors atteindre par diffusion p p' les fonctions d'ondes microscopiques des noyaux. La difficulté ici comme toujours est de disposer pour quelques noyaux de fonction d'ondes microscopiques dont on soit sûr, pour tester le mécanisme de réaction.

Les idées que nous avions sur l'importance des effets de distorsion à ces énergies sont seulement partiellement vraies.

Les effets de distorsion sont loin d'être négligeables : ils ont pour effets de diminuer les sections efficaces différentielles d'un facteur à peu près constant pour un noyau donné - 2.2 pour le ^{12}C, 2.8 à 3 pour le Ca - pour lesquels les fonctions d'onde microscopiques peuvent être considérées comme bien connues, de l'ordre de 16 pour un noyau très lourd comme le

plomb. Par contre, ces effets de distorsion ne changent pas la forme de la distribution angulaire, au moins jusqu'au 1er minimum pour les sections efficaces. Tibell [1] avait montré que pour un noyau donné on obtient une droite si l'on porte le log. de la section efficace différentielle expérimentale multipliée par q^{-2} où q est le moment transféré, en fonction de q^2, comme cela peut-être établi par un calcul simple en ondes planes. On obtient encore des droites, même pour des noyaux assez lourds comme Sn où l'atténuation due à la distorsion est importante.

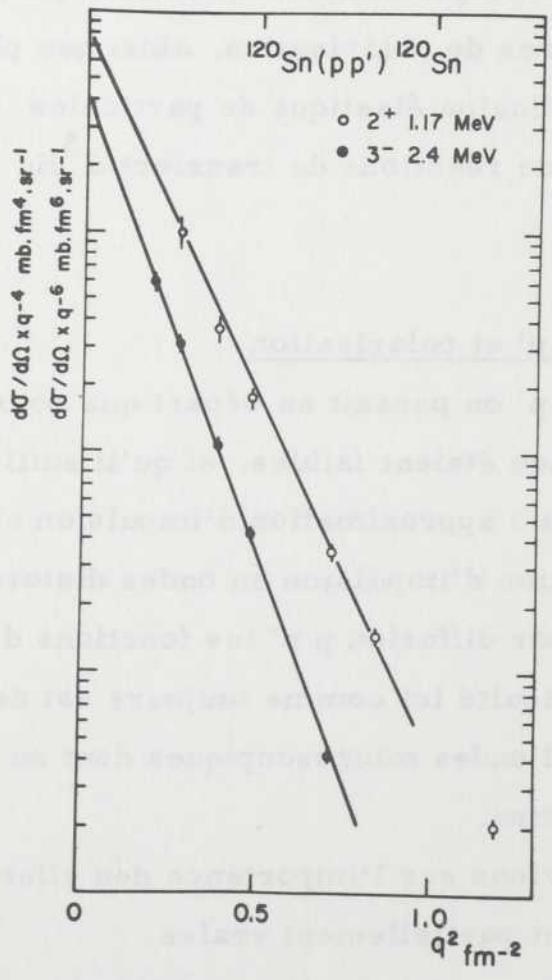

FIG. 1

Comme à énergies plus basses la forme de la distribution angulaire est donc caractéristique du moment orbital transféré - par contre elle ne nous apporte pas de renseignements sur les fonctions d'ondes microscopiques.

Si l'on cherche à donner d'un noyau une description microscopique par un modèle vibrationnel, on obtient à 150 MeV par un calcul en DWBA des paramètres de déformation en très bon accord avec ceux obtenus à plus basse énergie en diffusion ($\alpha\ \alpha'$) ($p\ p'$) ($n\ n'$) ; par exemple, pour le 1er niveau 2^+ de ^{120}Sn, à 1.17 MeV, on obtient un paramètre $\beta_2 = 0.117$ alors que d'autres mesures donnent des valeurs de β_2 comprises entre 0.11 et 0.13. Mais aux énergies intermédiaires la partie imaginaire du potentiel central W_c a une profondeur du même ordre de grandeur que celle de la partie réelle V_{cr} (V_{cr} est de l'ordre de 19 à 22 MeV et W_c de l'ordre de 11 à 17 MeV). On obtient un excellent accord avec la forme de la distribution angulaire jusqu'à des valeurs importantes de moment transféré (fig. 2 et 3) avec des paramètres de déformation identiques pour la partie réelle et la partie imaginaire du potentiel central.

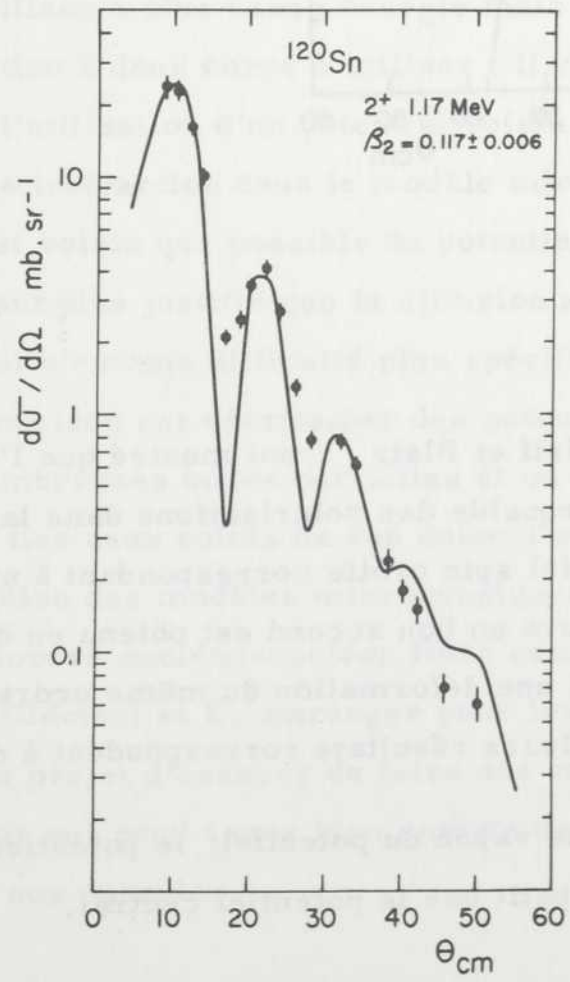

FIG. 2

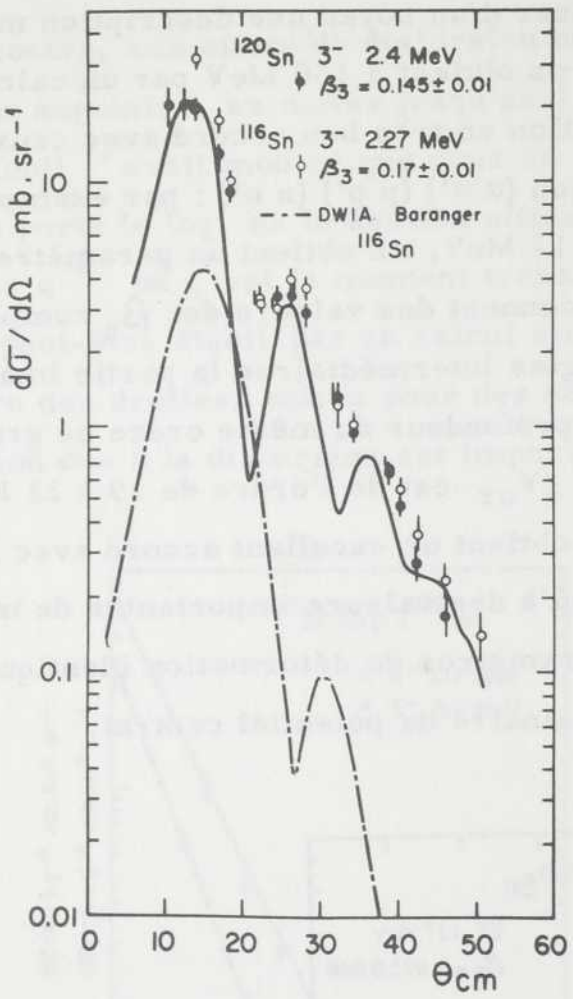

FIG. 3

Enfin, récemment Shérif et Blair [2] ont montré que l'on arrive à rendre compte de façon remarquable des polarisations dans la diffusion inélastique en utilisant un potentiel spin orbite correspondant à une forme de Thomas complète. Là encore un bon accord est obtenu en donnant à la partie spin-orbite du potentiel une déformation du même ordre que celle de la partie centrale; les meilleurs résultats correspondent à des valeurs $(\beta R)_C = (\beta R)_{SO}$ où R est le rayon du potentiel, le potentiel spin orbite ayant toujours un rayon plus petit que le potentiel central.

Les mesures de sections efficaces différentielles et de polarisation faites à énergie intermédiaire ont donc montré qu'on arrive à une description macroscopique satisfaisante des premiers niveaux excités des noyaux en déformant de la même quantité les parties centrales réelle et imaginaire et la partie spin orbite du potentiel optique décrivant l'état fondamental.

Description microscopique

Seules des mesures absolues de sections efficaces différentielles peuvent permettre d'apporter des renseignements sur les fonctions d'ondes microscopiques, les calculs faits avec différents modèles donnant des formes très voisines (jusqu'au 1er minimum) et dans le cas de valeurs absolues, les effets de distorsions sont loin d'être négligeables. On dispose de deux méthodes d'analyse des résultats expérimentaux; la DWBA telle qu'elle est utilisée à plus basse énergie mais la question se pose du potentiel d'intéraction à deux corps à utiliser : il y a là deux écoles, l'une est partisane de l'utilisation d'un potentiel voisin ou identique à celui qui a été utilisé comme intéraction dans le modèle microscopique, l'autre d'un potentiel aussi voisin que possible du potentiel nucléon-nucléon libre. Ceci semble d'autant plus justifié que la diffusion a lieu à plus haute énergie. Par contre, et c'est une difficulté plus spécifique à nos énergies, l'intéraction nucléon nucléon est décrite par des potentiels compliqués. Il faut tenir compte de nombreuses ondes partielles et on ne peut utiliser des potentiels type Serber. Les deux points de vue doivent se rapprocher si l'on arrive à une description des modèles microscopiques qui utilisent des forces très proches des forces nucléon-nucléon libre comme cela a été fait par exemple par Clément et E. Baranger pour les Sn.[3] Pour notre part, nous avons en projet d'essayer de faire des calculs en DWBA avec un potentiel de Tabakin qui rend assez bien compte de la diffusion nucléon nucléon libre jusqu'à nos énergies.

La 2ème méthode d'analyse, la DWIA, a été développée essentiellement par Haybron et Mc Manus. Elle permet de faire des calculs en utilisant la matrice de diffusion nucléon nucléon libre bien connue à 150 MeV (potentiels de Yale ou d'Hamada Johnston) avec l'approximation qu'il n'y a pas de transfert de moment dû aux effets de distorsion, et il reste toujours la difficulté que l'on a affaire à une intéraction nucléon-nucléon hors couche d'énergie.

Pour le ^{40}Ca pour lequel on peut penser que les fonctions d'ondes microscopiques données par les calculs de Gillet et Sanderson sont bonnes ; on obtient un bon accord entre valeurs expérimentales et théoriques calculées en DWIA et un peu moins bon avec le calcul en DWBA utilisant les forces utilisées pour le modèle microscopique.

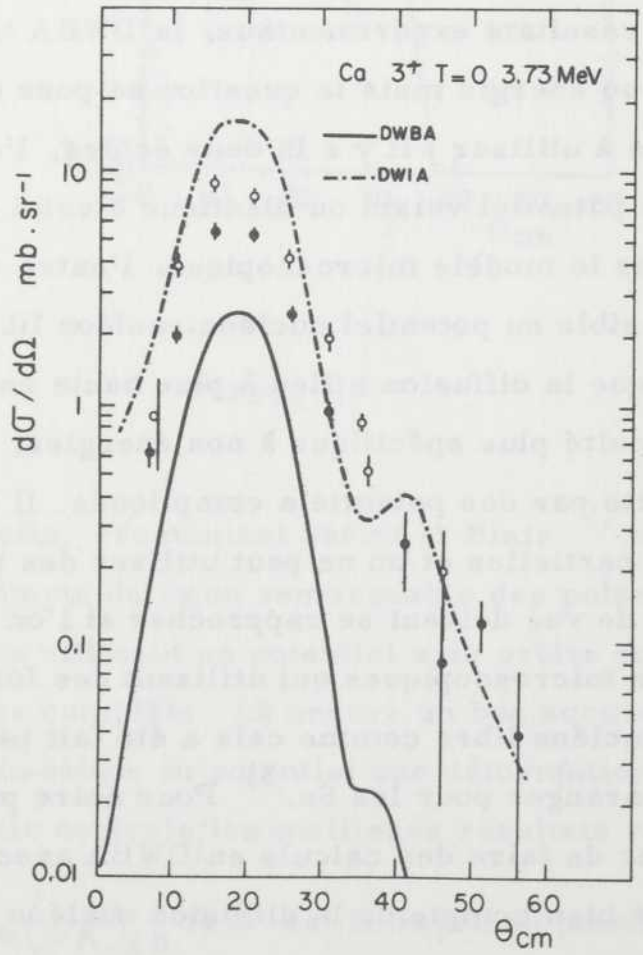

FIG. 4

On obtient ainsi un bon accord entre résultats expérimentaux et valeurs théoriques calculées en DWIA en utilisant le modèle de Gillet pour le niveau 2^+ à 4.43 MeV de ^{12}C

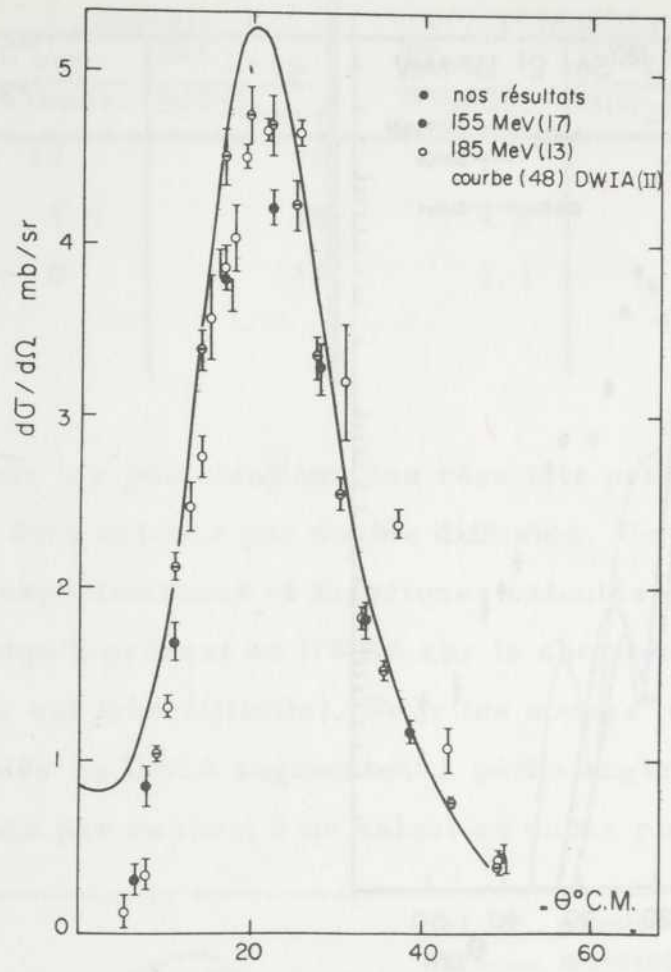

FIG. 5

On peut donc obtenir par diffusion p p' à moyenne énergie des renseignements sur les fonctions d'ondes microscopiques pour des noyaux plus lourds où neutrons et protons occupent des couches différentes et où les mesures par diffusion d'électrons ne permettent pas d'atteindre les configurations de neutrons - un exemple en est le cas des premiers niveaux 2^+ de quelques isotopes pairs de Sn (^{116}Sn, ^{118}Sn, ^{120}Sn) : plusieurs modèles microscopiques ont été proposés pour ces noyaux, les plus récents sont ceux de Gillet (I)[5] et de Clément et Baranger (II)[3]. Les deux modèles diffèrent surtout par le nombre de configurations de protons dont il a été tenu compte, bien plus grand dans le travail [3]. Les mesures de sections efficaces différentielles p p' [6] montrent que le modèle II donne un meilleur accord que le modèle I mais le nombre de configurations qu'il contient est encore insuffisant.

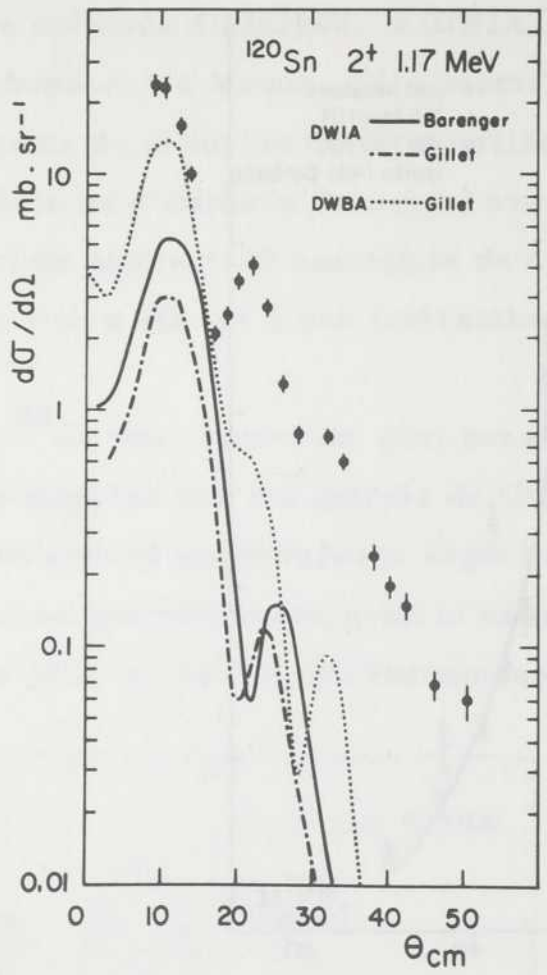

FIG. 6

Le tableau suivant où sont portés les rapports des sections efficaces différentielles (au premier maximum) expérimentales et théoriques ainsi que le rapport correspondant des probabilités de transition électromagnétique $B(E_2)$ pour les modèles I et II et le premier niveau 2^+ dans ^{116}Sn - ^{118}Sn - ^{120}Sn montre que pour les deux modèles les configurations de neutrons sont mieux décrites pour les ^{118}Sn et ^{120}Sn que pour ^{116}Sn

Sn	Modèle I		Modèle II	
	$\frac{\sigma_{exp}}{\sigma_{theor.}}$	$\frac{B(E_2)_{exp}}{B(E_2)_{theor}}$	$\frac{\sigma_{exp}}{\sigma_{theor.}}$	$\frac{B(E_2)_{exp}}{B(E_2)_{theor}}$
116	19	30	8	5.2
118	8.9	28	4.6	
120	8	28	4.4	
124				6.4

Pour les polarisations, des résultats précis peuvent à ces énergies moyennes être obtenus par double diffusion. Un désaccord apparaît entre résultats expérimentaux et théoriques calculés en DWIA (aucun calcul n'a été fait jusqu'à présent en DWBA car le choix du potentiel d'intéraction spin orbite est très difficile). Pour les noyaux légers, les effets de distorsion calculés en DWIA augmentent à petits angles le désaccord avec l'expérience par rapport à un calcul en ondes planes.

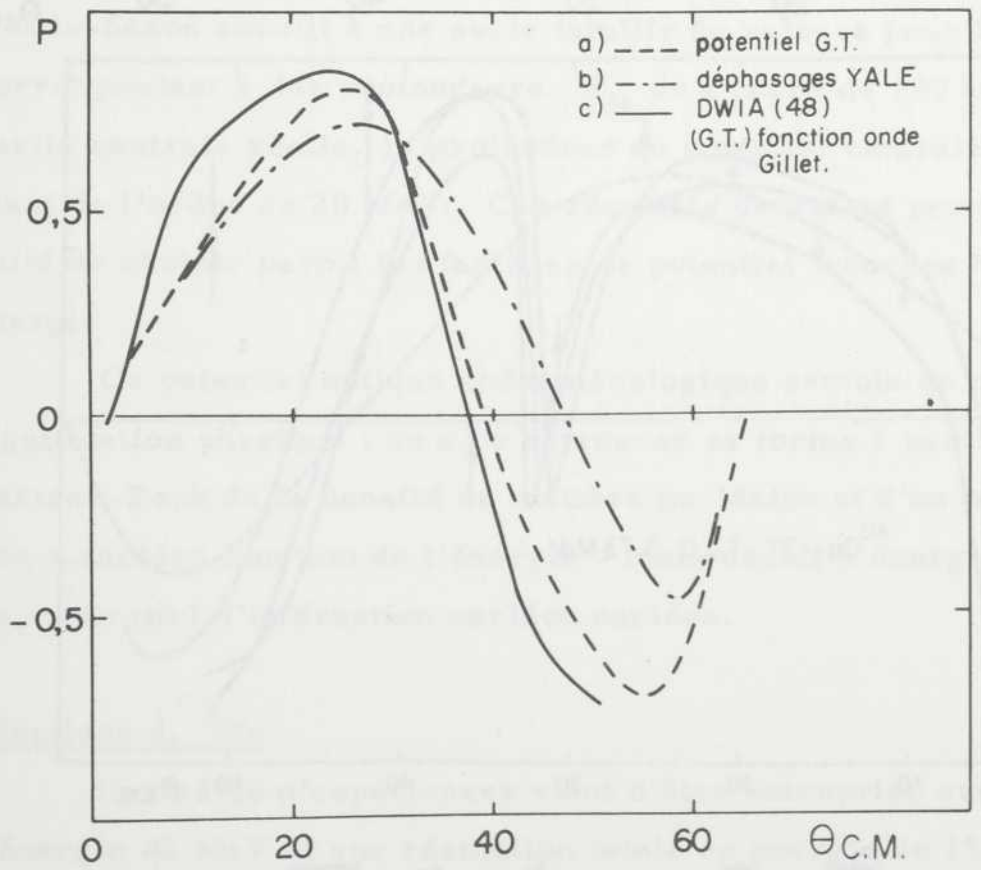

Niveau de 4.43 MeV

FIG. 7

Pour les noyaux plus lourds, les effets de distorsion semblent prédominants pour la forme différentielle des polarisations et ne sont qu'imparfaitement rendus par les calculs.

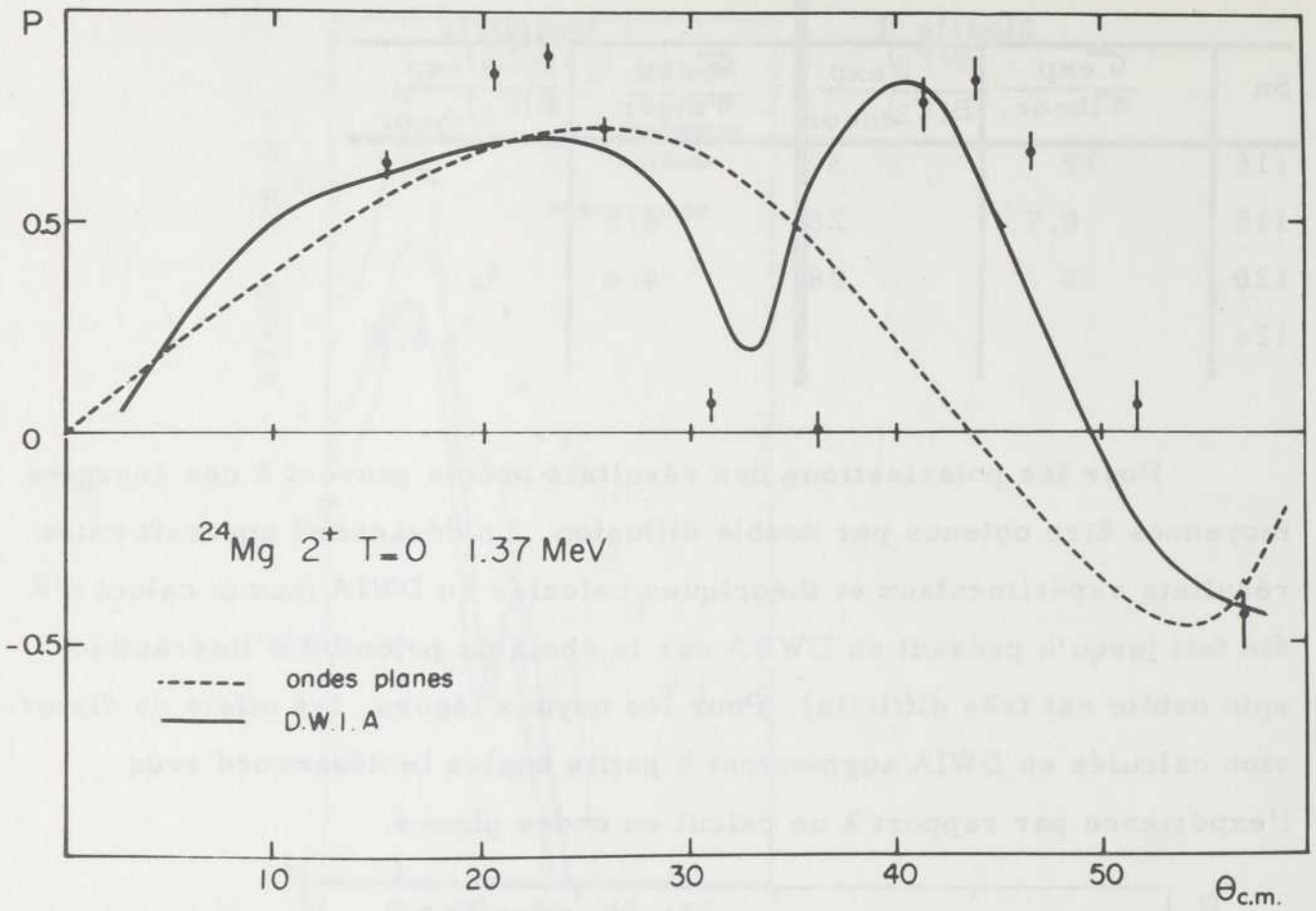

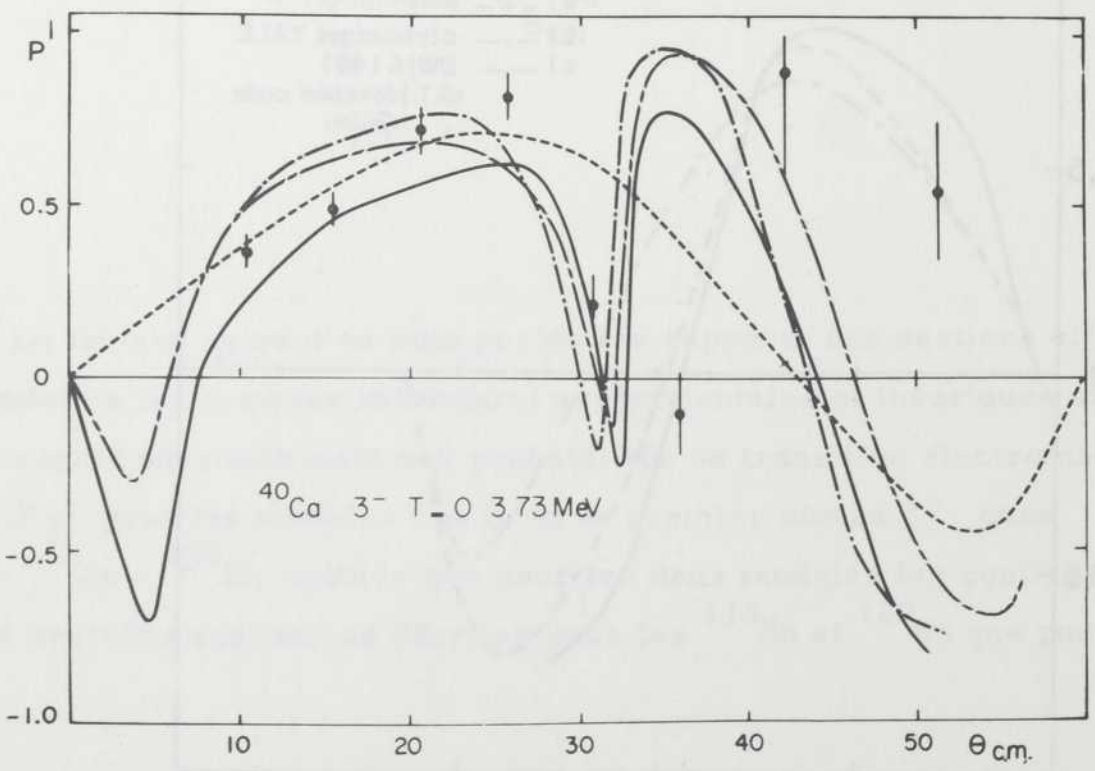

Légende	Calcul	$R_{c.c.}$	$A_{c.c.}$	Interaction
.....	ondes planes			Yale
———	DWIA	$= R_t$	$= A_t$	GT
— — —	DWIA	$\neq R_t$	$\neq A_t$	GT
— - — -	DWIA	$\neq R_t$	$\neq A_t$	Yale

FIG. 8 - 9

Il apparaît donc que les effets de polarisation sont extrêmement sensibles au mécanisme de réaction et que des progrès sont à faire dans ce domaine à ces énergies déjà élevées si l'on veut obtenir à partir des mesures de polarisation des renseignements sur les fonctions d'ondes microscopiques. Par contre, dans ce but les mesures absolues de sections efficaces différentielles apportent dès maintenant des résultats intéressants.

Diffusion élastique d'α de 167 MeV

Jusqu'à présent les études de diffusion élastique de particules α d'énergie inférieure à 100 MeV ne permettaient pas de choisir entre plusieurs familles de paramètres de potentiel optique correspondant à des valeurs très différentes de profondeur du potentiel central - qui rendaient également bien compte des résultats expérimentaux - Des expériences ont été faites tout récemment à 167 MeV à Orsay [7] sur des cibles de C, Si, Sn, Pb. La recherche des paramètres d'un potentiel optique de forme Woods-Saxon aboutit à une seule famille de valeurs pour les quatre cibles correspondant à des profondeurs V_R de l'ordre de 100 à 120 MeV pour la partie centrale réelle, la profondeur du potentiel centrale imaginaire W_I étant de l'ordre de 20 MeV. Ces résultats devraient permettre par continuité de choisir parmi les familles de potentiel trouvées à plus basse énergie.

Ce potentiel optique phénoménologique semble de plus avoir une signification physique : on a pu retrouver sa forme à partir de calculs Hartree-Fock de la densité de matière nucléaire et d'un potentiel d'intéraction α-nucléon fonction de l'énergie - mais déduit à énergie nulle du potentiel d'intéraction nucléon nucléon.

Réactions d, ^{3}He

Une série d'expériences vient d'être entreprise avec des- deutons d'énergie 82 MeV et une résolution totale en énergie de 150 keV, obtenue à l'aide d'un système achromatique [8]. Son but était d'étudier avec une meilleure résolution en énergie que dans les expériences de diffusion quasi

élastique (p, 2p) où la résolution optimum atteinte était de 1.6 MeV, les niveaux de protons des noyaux de la couche 2s 1d, et de comparer les facteurs spectroscopiques obtenus à ceux mesurés dans des réactions identiques faites à plus basse énergie.

Une étude faite sur ^{24}Mg a montré que des niveaux correspondant à la capture de protons de la couche 1p (les distributions angulaires des ^{3}He sont très caractéristiques et en accord avec les calculs faits en DWBA) apparaissent pour des énergies d'excitation du noyau résiduel ^{23}Na aussi basses que certains niveaux dus à la capture de protons des couches 2s, 1d (niveaux à 2.71, 3.68 et 5.94 MeV). Ceci est d'ailleurs en accord avec les résultats obtenus à plus basse énergie à Karlsruhe ; d'autres niveaux correspondant à la capture de protons $\ell = 1$ apparaissent aux environs de 10 MeV d'excitation en accord avec les résultats obtenus, en (p, 2p).

Pour le ^{24}Mg en particulier, la couche 1p apparaît donc comme moins localisée qu'il ne semblait d'après les expériences p 2p.

Les facteurs spectroscopiques extraits à 82 MeV sont très voisins de ceux obtenus à énergie plus basse, 34 ou 52 MeV. Ce sont donc bien des valeurs qui dépendent uniquement de la structure nucléaire des noyaux et non de l'énergie de la réaction.

Dans ces expériences comme dans les expériences de pick-up p d à énergie élevée [9], il semble difficile d'extraire des renseignements sur les nucléons des couches profondes.

TABLEAU III

Comparaisons entre facteurs spectroscopiques extraits de différentes énergies de réaction d, ^{3}He

^{23}Na (d, ^{3}He) ^{22}Ne			^{27}Al (d, ^{3}He) ^{26}Mg			^{28}Si (d, ^{3}He) ^{27}Al		
E_x \ E_d	[a] 34 MeV	[b] 82 MeV	E_x \ E_d	[c] 52 MeV	82 MeV	E_x \ E_d	[d] 34 MeV	82 MeV
0	0.08	0.07	0	0.27	0.26	0.	3.76	3.3
5.14	1.7	1.94	7.86	1.76	1.5	4.05	1.8	1.14
						5.15	1.2	1

REFERENCES

1 - G. Tibell, Phys. Lett. 28B, 1969, p. 638

2 - H. Sheriff, Nucl. Phys.
H. Sheriff, J.S. Blair, à paraître
et symposium sur les mécanismes de réactions nucléaires, Université Laval, 1969

3 - D.M. Clément et E. Baranger, Nucl. Phys. A 120, 1968, p. 25

4 - V. Gillet, E.A. Sanderson, Nucl. Phys. 54, 1964, p. 472

5 - V. Gillet, B. Giraud et M. Rho, Nucl. Phys. A 113, 1967, p. 157
et communication privée.

6 - V. Comparat et al. Conférence internationale sur les propriétés des états nucléaires
Montréal 1969, p. 156

7 - I. Brissaud, M.K. Brussel, M. Sowinski, B. Tatischeff, à paraître

8 - H. Doubre et al. Phys. Lett. 29 B, 1969
M. Arditi, à paraître

9 - D. Bachelier et al., Nucl. Phys. A 126 (1969) p. 60

THE INTERACTION OF INTERMEDIATE ENERGY PROTON WITH LIGHT NUCLEI

E.T. BOSCHITZ
Lewis Research Center
Cleveland, Ohio.

During the past few years there has been an increasing interest in probing the nucleus with high-energy particles. This interest is based on the fact that high-energy particles for which the wavelength is less than the internucleon spacings might provide information about the nuclear structure which is not forthcoming from experiments at lower energies.

When the NASA proton synchrocyclotron became operational in 1966 a program was initiated at the Lewis Research Center to study the interaction of 600 MeV protons with light nuclei. Deuterium, ^{3}He, and ^{4}He were chosen partly for experimental reasons, partly because a systematic study of them might be most suitable for testing multiple scattering theories. The present talk will center around our results, but I also intend to review other experimental work and some theoretical developments in the past two years.

Our experiments were performed in collaboration with members of various universities. In addition to W. K. Roberts, J. S. Vincent and myself from NASA, our team consisted of M. Blecher, K. Gotow, P. C. Gugelot, C. F. Perdrisat and L. W. Swenson from the Virginia Universities and J. R. Priest from Miami University.

Because the object was the study of the details of the elastic cross section and the polarization, it was particularly important to exclude nonelastic events. Figure 1 shows the experimental arrangement. The external proton beam was brought to a focus on the target by the beam transport system. The intensity of the incident beam was monitored by an Argon-filled ion chamber (AIC) and by scattering the particles from aluminum into a pair of range telescopes (M_1 and M_2). The absolute number of incident protons was obtained by carbon activation using the well known $^{12}C(p, pn)^{11}C$ cross section. The beam direction was monitored with two split ion chambers (SIC 1 and SIC 2). The targets consisted of CH_2, CD_2, high-pressure gaseous ^{3}He and liquid ^{4}He. Protons scattered from ^{4}He were detected by multiple counter range telescopes which were mounted on a precision scattering table. Counter 1 and 2 defined the

scattering volume of the helium targets and the solid angle subtended by the range telescopes. The angular resolution was $\Delta\theta = 0.75^{o}$ FWHM at small angles and $\Delta\theta = 2.0^{o}$ at large angles. The overall energy resolution of the range telescope was about 12 MeV which is sufficient for elastic p-^{4}He scattering. The efficiency for detecting elastic events in the range telescope was determined experimentally. It agreed well with a Monte Carlo calculation for the penetration of protons through a copper slab. In the case of p-^{3}He scattering the recoiling ^{3}He particle was detected at the conjugate angle in coincidence with the proton to ensure the elastic $\overset{\text{scattering}}{\wedge}$ of the event. For the p-p and p-d cross section measurements absorbers in the proton telescope were not needed. The detection of the recoiling deuteron or proton in coincidence sufficiently defined the elastic scattering. Background event rates due to the breakup reactions in CD_2 or ^{3}He were determined by placing a sufficient amount of absorber in front of the associate counter telescope to destroy the true p-d or p-^{3}He coincidences. At several conjugate angles the proton or the deuteron telescope was varied about the conjugate angle as a check on the efficiency of the breakup reaction suppression. For the cross section measurements only one set of associate telescopes was used.

The polarization was measured in a conventional double-scattering experiment. The polarized proton beam was produced by an internal carbon target of the synchrocyclotron. This target was placed so that protons scattered at (9±1) degrees would enter the external beam transport system. The polarized proton beam was focused into a 1/2''×2'' spot at the second target with an intensity of 3×10^{7} protons per second. The beam energy determined by range measurements was 544 MeV with a FWHM of about 36 MeV. Two matched telescope systems were positioned at equal angles left and right to record the asymmetries. The telescopes were interchanged several times during a run, to provide a check on some of the possible instrumental asymmetries. The overall accuracy of the beam centroid line was estimated to be ±0.03 degrees, corresponding to a maximum error of ±0.010 in the asymmetry. The beam polarization was determined by measuring the asymmetry in the scattering from carbon at laboratory angles of 6, 8, and 10 degrees and

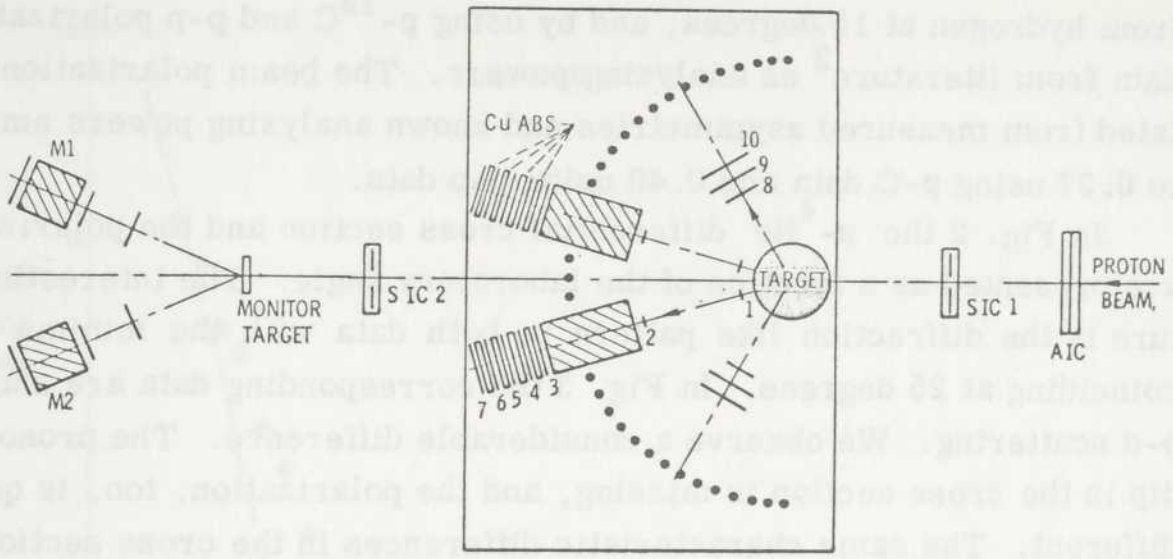

Fig. 1 Schematic diagram of the experimental arrangement.

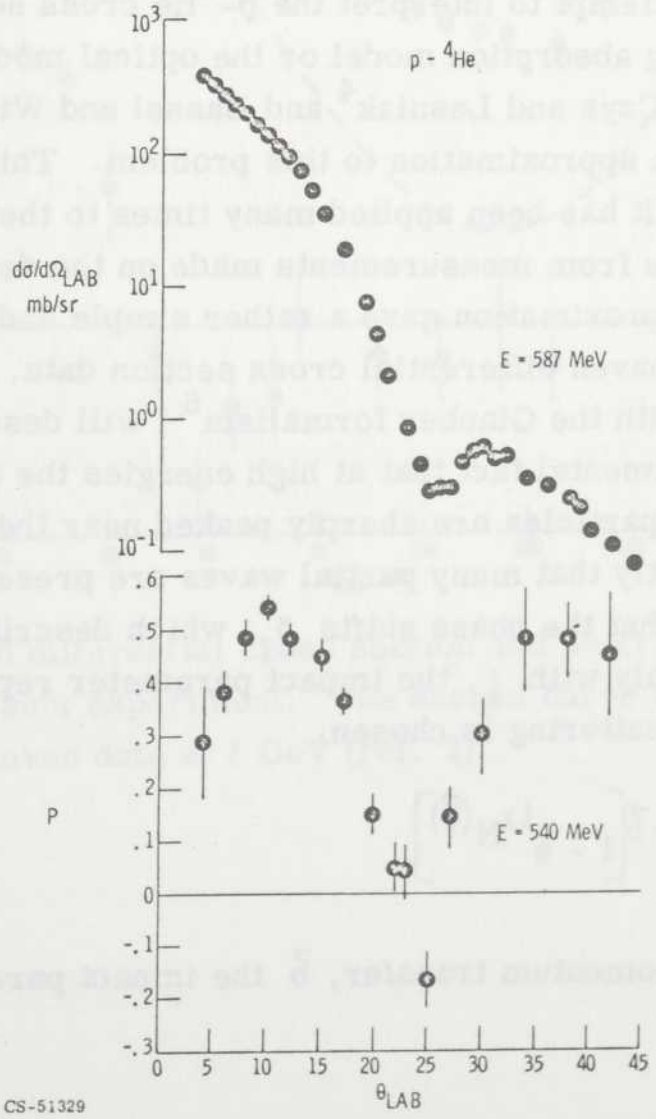

Fig. 2 The p-^{4}He differential cross section and polarization, obtained in the present experiment.

from hydrogen at 15 degrees, and by using p-^{12}C and p-p polarization data from literature[2] as analyzing powers. The beam polarization calculated from measured asymmetries and known analysing powers amounted to 0.37 using p-C data and 0.40 using p-p data.

In Fig. 2 the p-^{4}He differential cross section and the polarization are presented as a function of the laboratory angle. The interesting feature is the diffraction like pattern in both data with the minima coinciding at 25 degrees. In Fig. 3 the corresponding data are shown for p-d scattering. We observe a considerable difference. The pronounced dip in the cross section is missing, and the polarization, too, is quite different. The same characteristic differences in the cross sections have been observed by the Brookhaven group in their data at 1 GeV.[3] How can we understand these results? Instead of giving a quick answer, let me go back a couple of years and describe some of the developments.

After a vain attempt to interpret the p-^{4}He cross section at 1 GeV in terms of the strong absorption model or the optical model using reasonable parameters, Czyz and Lesniak[4] and Bassel and Wilkin[5] applied the Glauber diffraction approximation to this problem. This approximation is not at all new. It has been applied many times to the deduction of neutron cross sections from measurements made on the deuteron. What is new is that this approximation gave a rather simple and transparent explanation of the Brookhaven differential cross section data. For those that are not familiar with the Glauber formalism[6] I will describe it briefly.

It is an experimental fact that at high energies the angular distributions of scattered particles are sharply peaked near the forward direction which shows directly that many partial waves are present in the scattering field. Assuming that the phase shifts δ_l which describe the elastic scattering vary smoothly with l, the impact parameter representation of the nucleon-nucleus scattering is chosen.

$$F = \frac{ik}{2\pi} \int d^2b\, e^{i\vec{q}\cdot\vec{b}} \left[1 - e^{i\chi_N(\vec{b})} \right],$$

where q is the momentum transfer, $\vec{b}$ the impact parameter, $\chi(\vec{b})$ the

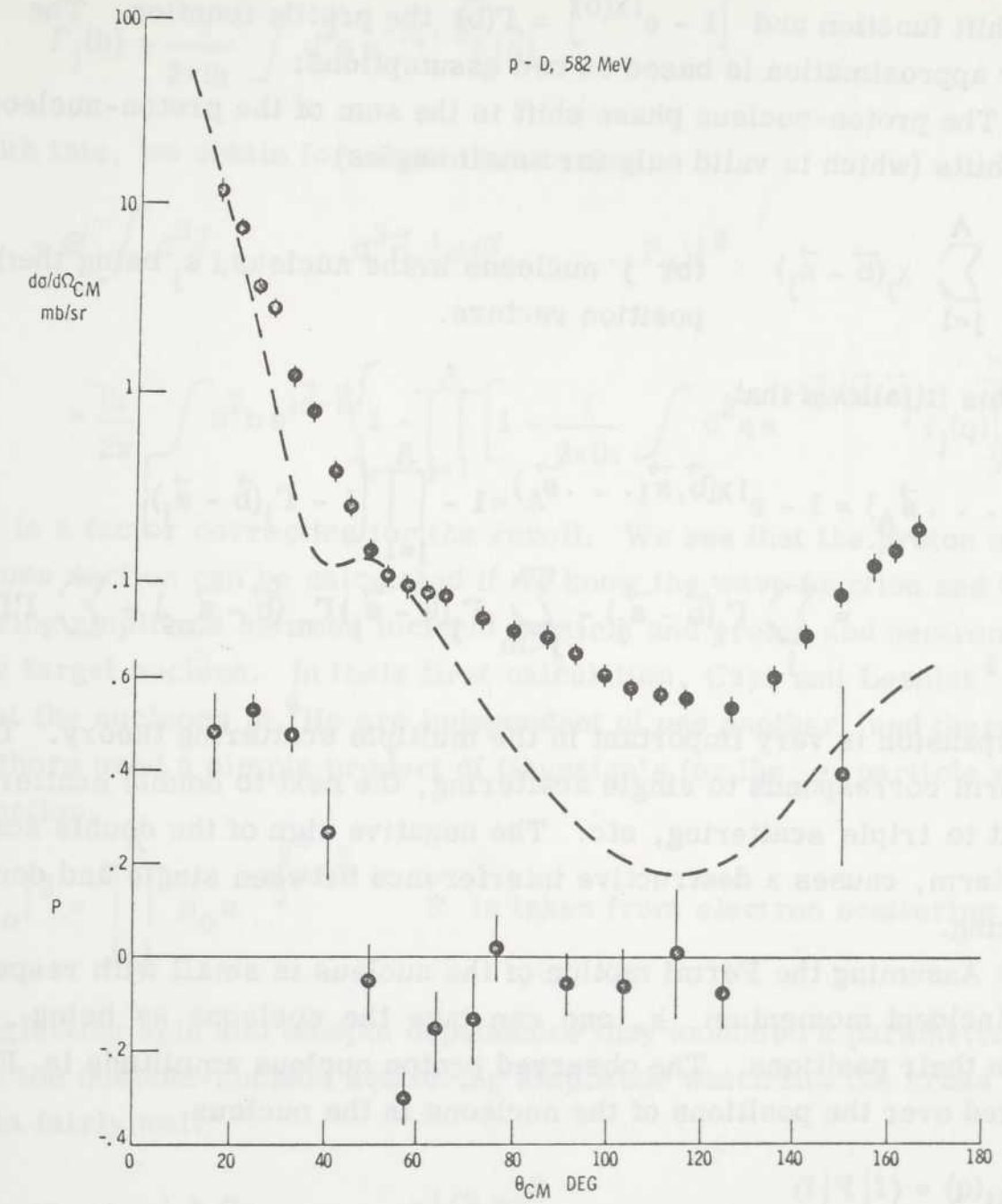

Fig. 3 The p-d differential cross section and polarization, obtained in the present experiment. The dashed curve represents the Brookhaven data at 1 GeV (ref. 3).

phase shift function and $\left[1 - e^{i\chi(\vec{b})}\right] = \Gamma(\vec{b})$ the profile function. The Glauber approximation is based on two assumptions:

(1) The proton-nucleus phase shift is the sum of the proton-nucleon phase shifts (which is valid only for small angles)

$$\chi_N(\vec{b}) = \sum_{j=1}^{A} \chi_j(\vec{b} - \vec{s}_j)$$ for j nucleons in the nucleus, s_j being the position vectors.

From this it follows that

$$\Gamma(\vec{b}, \vec{s}_1 \ldots \vec{s}_A) = 1 - e^{i\chi(\vec{b}, \vec{s}_1 \ldots \vec{s}_A)} = 1 - \prod_{j=1}^{A}\left[1 - \Gamma_j(\vec{b} - \vec{s}_j)\right]$$

$$= \sum_j \Gamma_j(\vec{b} - \vec{s}_j) - \sum_{j<m} \Gamma_j(\vec{b} - \vec{s}_j)\Gamma_m(\vec{b} - \vec{s}_m) + \sum \Gamma\Gamma\Gamma \ldots$$

This expansion is very important in the multiple scattering theory. The first form corresponds to single scattering, the next to double scattering, the next to triple scattering, etc. The negative sign of the double scattering term, causes a destructive interference between single and double scattering.

(2) Assuming the Fermi motion of the nucleus is small with respect to the incident momentum k, one can take the nucleons as being fixed in their positions. The observed proton nucleus amplitude is F averaged over the positions of the nucleons in the nucleus

$$F_{fi}(q) = \langle f | F | i \rangle$$

In order to evaluate this matrix element we need to know the individual profile functions $\Gamma_j(\vec{b} - \vec{s}_j)$. If the incident particle - j^{th} target nucleon scattering amplitude is known,

$$f_j(q) = \frac{ik}{2\pi} \int d^2b\, e^{i\vec{q} \cdot \vec{b}} \Gamma_j(\vec{b})$$

then the profile function can be constructed by the inverse transformation

$$\Gamma_j(b) = \frac{1}{2\pi ik} \int d^2q\, e^{-i\vec{q}\cdot\vec{b}} f_j(\vec{q})$$

with this, we obtain for elastic scattering

$$F_{fi} = \Theta \int d^3\vec{r}_1, \ldots, d^3\vec{r}_A |\psi(\vec{r}_1, \ldots, \vec{r}_A)|^2$$

$$\times \frac{ik}{2\pi} \int d^2b\, e^{i\vec{q}\cdot\vec{b}} \left\{ 1 - \prod_{j=1}^{A} \left[1 - \frac{1}{2\pi ik} \int d^2q\, e^{-i\vec{q}\cdot(\vec{b}-\vec{s}_j)} f_j(q) \right] \right\}$$

Θ is a factor correcting for the recoil. We see that the proton nucleus cross section can be calculated if we know the wave function and the scattering amplitude between incident particle and proton and neutrons of the target nucleus. In their first calculation, Czyz and Lesniak[4] assumed that the nucleons in ^{4}He are independent of one another, and therefore the authors used a simple product of Gaussian's for the α particle wave function.

$$|\psi_o|^2 = \prod_{j=1}^{A} \rho_o e^{-r_j^2/R^2}$$

R is taken from electron scattering data

Neglecting spin and isospin dependence they assumed a parametized form for the nucleon-nucleon scattering amplitude which fits the cross section data fairly well.

$$f(k,q) = \frac{i + \alpha}{4\pi} k \cdot \sigma_T \cdot e^{-1/2\, aq^2}$$

σ_T is the total nucleon-nucleon cross section, α the ratio of real to imaginary part of the nucleon-nucleon scattering amplitude. We have followed Czyz's calculation at our energy for p-^{4}He, p-^{3}He, and p-d scattering. The results are shown in the next three figures.

In Fig. 4 the curves labeled 1, 2, 3, and 4 are the calculated differential cross sections, if only single (1), single and double (2), single, double and triple (3), and finally also 4-fold scattering is included. We find that for small momentum

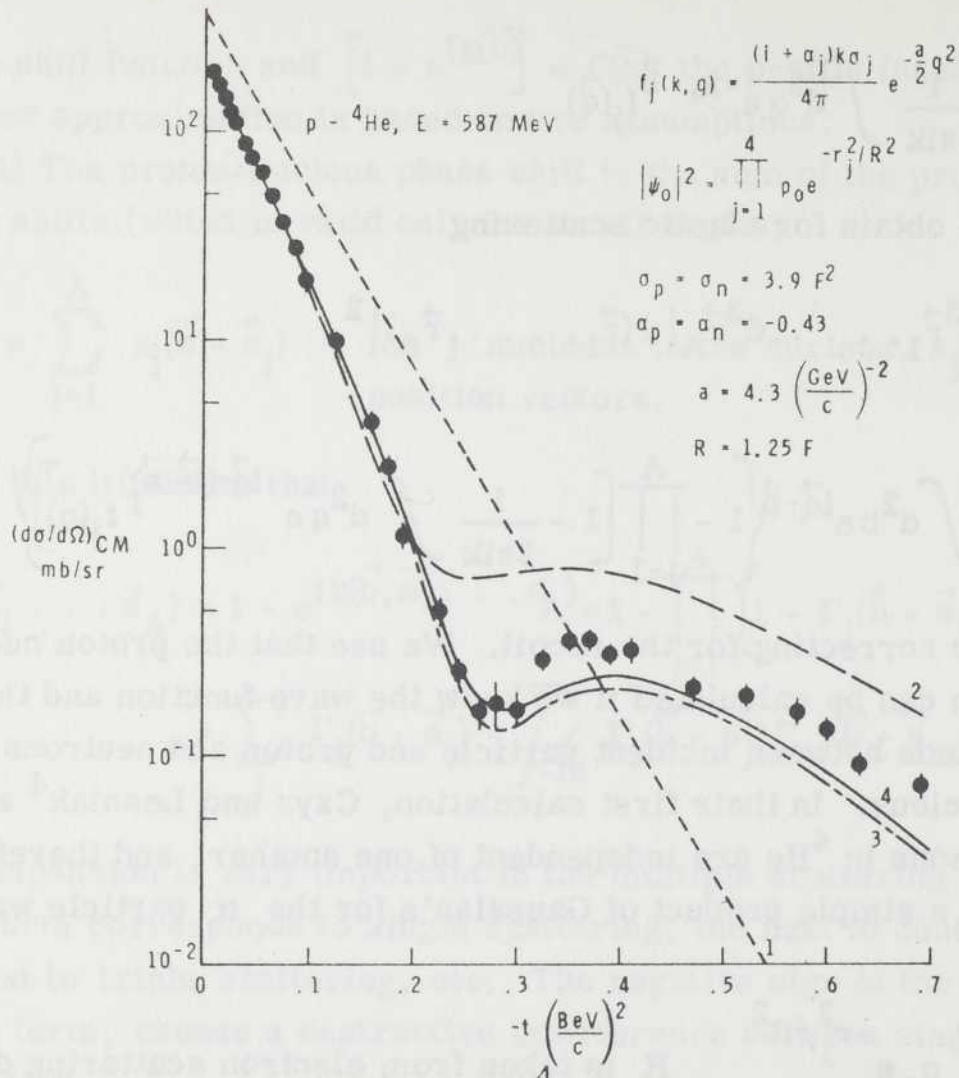

Fig. 4 Comparison of the p-^{4}He data with calculations based on the Glauber approximation. The curves marked 1, 2, 3, and 4 indicate the number of multiple scattering terms included in the calculation.

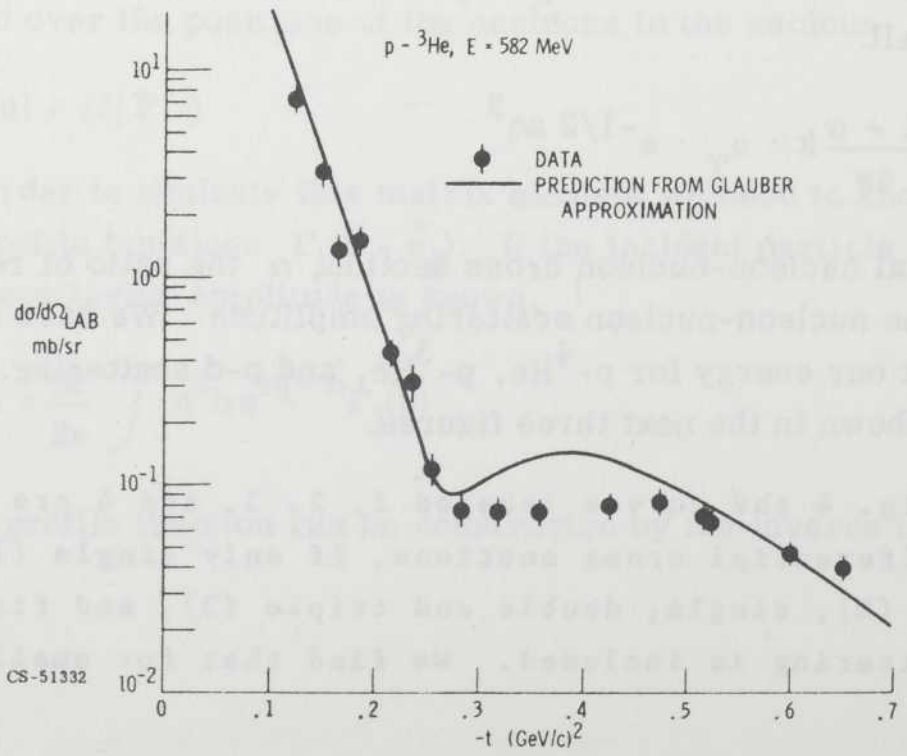

Fig. 5 Comparison of p-^{3}He data with the calculation based on the Glauber approximation.

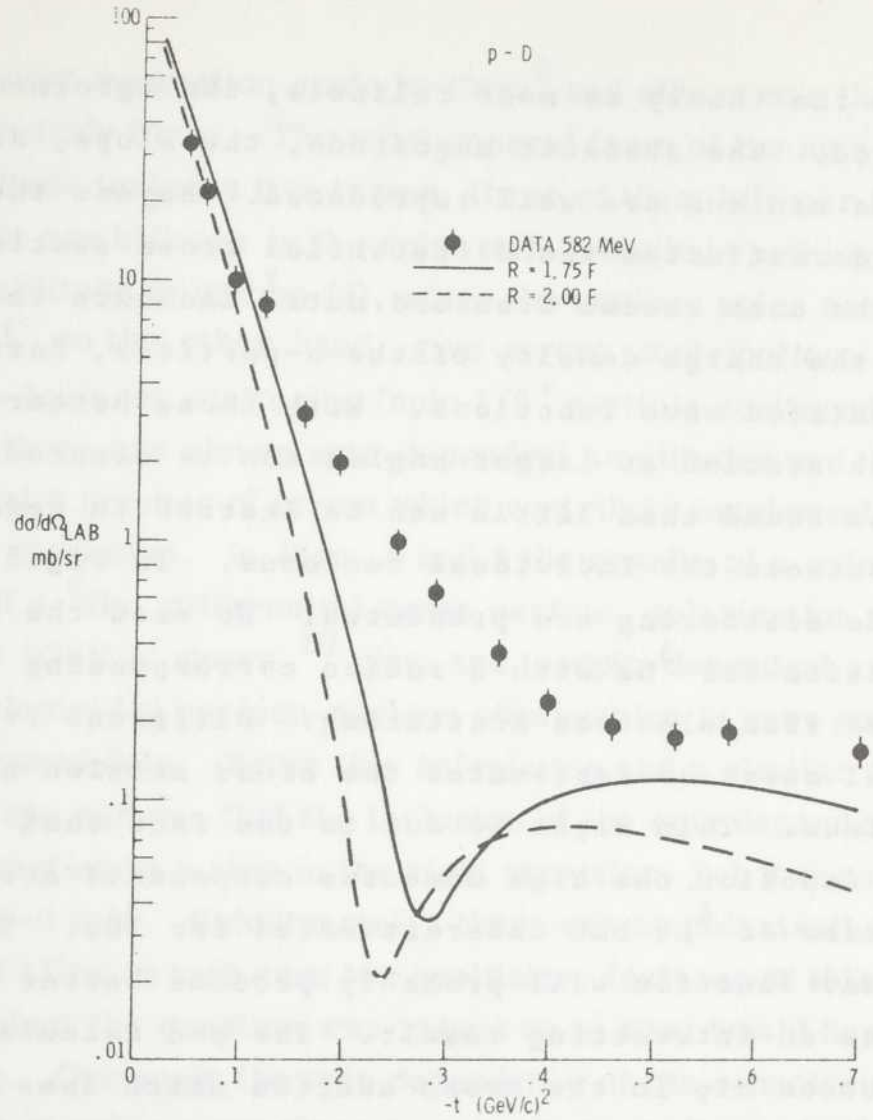

Fig. 6 Comparison of p-d data with calculations based on the Glauber approximation, using two different radii in the Gaussian wave function.

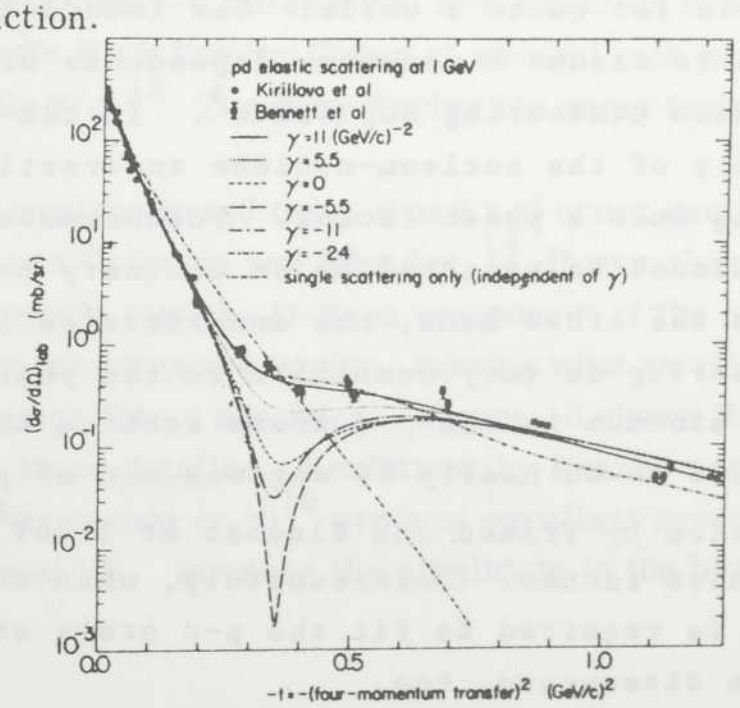

Fig. 7 The p-d elastic scattering at 1 GeV. Data are from ref. 3. Curves are calculations by Franco and Glauber (ref. 8) showing the effects of a momentum dependence of the phase between single and double scattering.

transfer where the theory is most reliable, the agreement with the data is good. The absolute magnitude, the slope, and the location of the minimum are well reproduced. Beyond the minimum the calculation underestimates the differential cross section. Observing that the most recent Stanford data[7] indicate the need of spreading out the charge density of the α-particle, Bassel and Wilkin used modified wave functions. With those better fits to the p-^{4}He cross section at larger angles can be secured. Unfortunately, it was found that little can be learned in regard to the correlations between the individual nucleons. In Fig.5 the results for p-^{3}He scattering are presented. We used the same product wave function for ^{3}He with a radius corresponding to the rms radius obtained from electron scattering. Different from before, the theoretical curve overestimates the cross section at the secondary maximum. This might be due to the fact that, using a Gaussian wave function, the high momentum components are overestimated in the case of ^{4}He but underestimated for ^{3}He. The use of a better ^{3}He wave function will probably produce better agreement. In Fig.6 we see an interesting result. The p-d calculation produces a pronounced dip in the cross section which does not exist in the data.

The absence of a minimum in the p-d angular distribution presented a puzzle for quite a while. The immediate idea that came to mind was to assume a momentum dependence of the phase of the nucleon-nucleon scattering amplitude[3]. In the absence of a fundamental theory of the nucleon-nucleon interaction there is no way of predicting such a phase factor. Furthermore the phase at non zero angle cannot be measured in an ordinary p-p cross section measurement. On the other hand, the interference between single and double scattering is very sensitive to the phase. In order to wipe out the minimum in the p-d cross section, single and double scattering have to be nearly 90 degrees out of phase. Fig. 7 shows a calculation by Franco and Glauber at 1 GeV[8]. γ is the exponent of the phase factor. Unfortunately, when using the phase variation which is required to fit the p-d cross section, the minimum in p-^{4}He dissapears, too.

The next suggestion made by Czyz[9] and others was the spin dependence in the two-body force. The most general form of the spin dependent scattering amplitude includes five terms, three of them bilinear in spin. Those terms that are bilinear in the spins will contribute nothing to the single scattering amplitude in helium (4), since the nucleon spins are paired in helium (4). They will, on the other hand, give strong contributions in the deuteron. In proton-deuteron scattering (spin $1/2^+$ particle scattered from a spin 1^+ particle) there are eleven spin-dependent amplitudes and there is a good chance that a number of terms which contribute incoherently will tend to fill in the minimum. In Figs. 8 and 9 the results of a calculation by Franco of p-d and p-^{4}He, differential cross section, polarization and total cross section at 1GeV is shown.[10] Spin and isospin-dependent amplitudes were used which yielded nucleon-nucleon observables in very good agreement with measured data. From this calculation and a similar one by Kujawski, et al.[11], one can see that the inclusion of the spin dependence in the two-body interaction is a step in the right direction, but it does not fully explain the p-d data. Unfortunately, there are no polarization data at 1 GeV that would allow to test even the qualitative features of this calculation. In this context the question was raised as to what would happen in π-d scattering. Obviously the spin dependence of the π-nucleon amplitude is very much simpler since there is only the term linear in the proton spin and this kind of spin dependence, one hoped, would leave the dip in the cross section. Recently the π-d differential cross section has been measured by the CERN Trieste High Energy Group at several pion energies between 0.9 GeV/c and 15 GeV/c.[12] The data display the same feature as the p-d cross section.

Finally an explanation of the p-d and π-d cross section was given by Harrington[13], and Coleman and Rhoades.[14] It was shown by them and later by other people that the D-wave component of the deuteron is very important in the interference region, turning what would be a definite dip in the cross section into a shoulder. Figure 10 shows Harrington's qualitative results. More detailed calculations by Franco and Glauber (p-d)[15] and Alberi and Bertocchi (π-d)[16] produce excellent agreement with the data (Figs. 11 and 12). Because the amplitude in the break region is

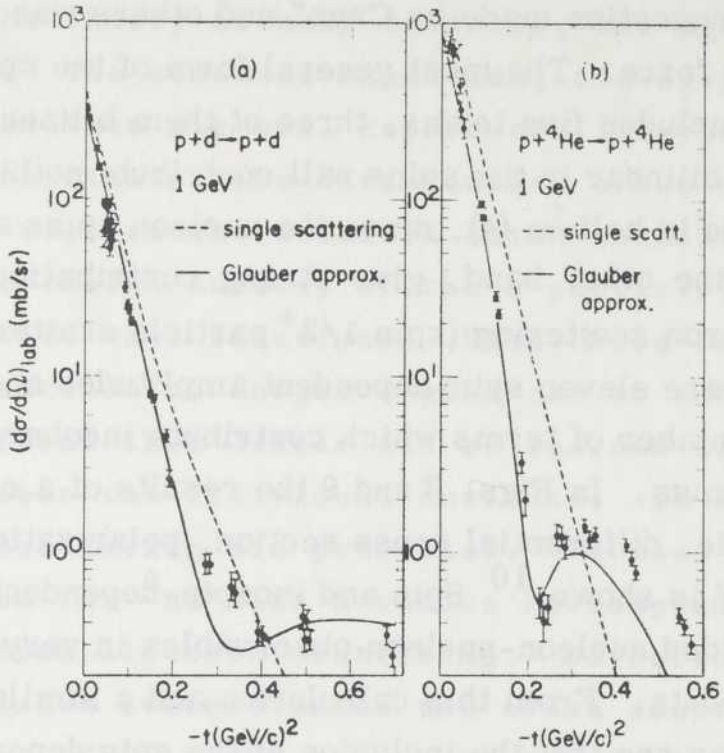

Fig. 8 The p-d and the p-^{4}He elastic scattering at 1 GeV. Data are from refs. 1 and 3. Curves are calculations by Franco (ref. 10) showing the effects of the spin dependence in the nucleon-nucleon scattering amplitude.

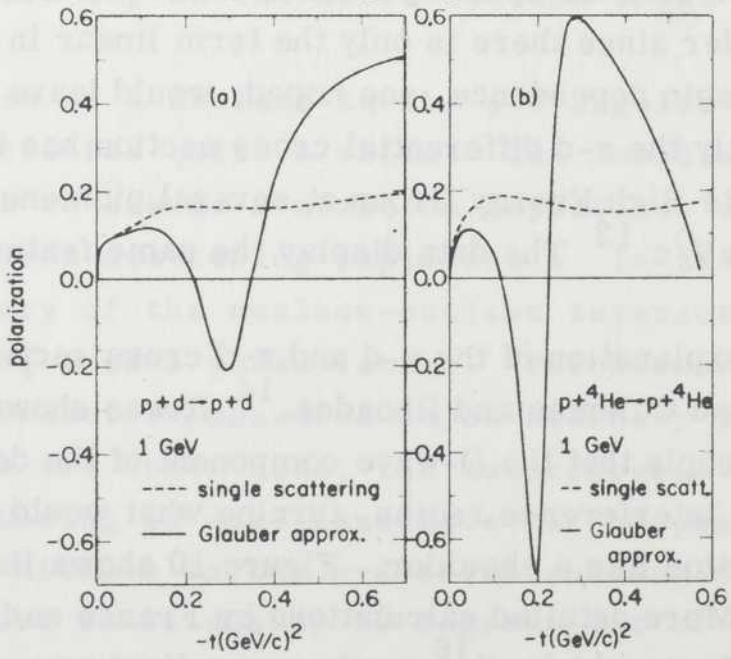

Fig. 9 Predictions of the polarization at 1 GeV by Franco (ref. 10).

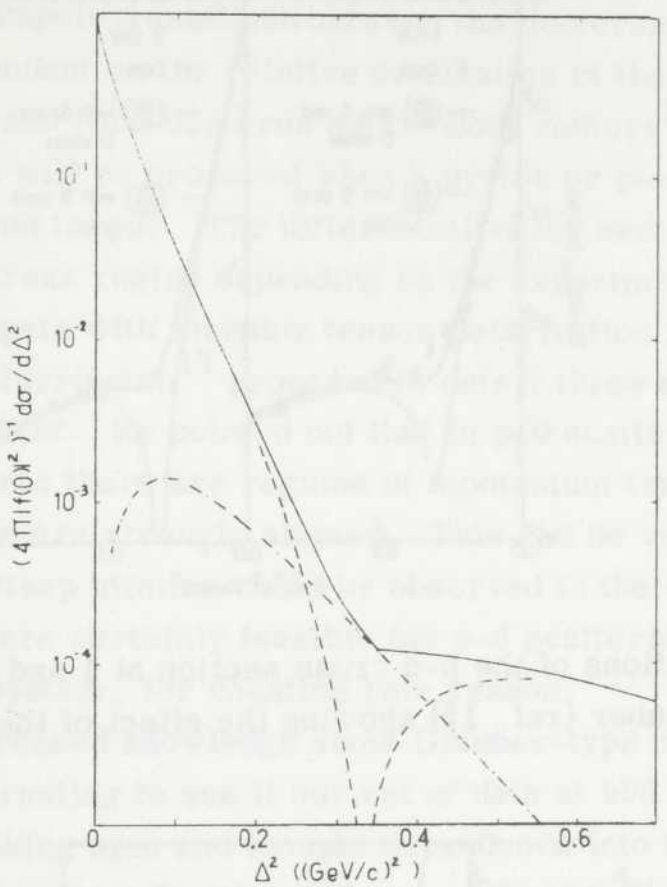

Fig. 10 The p-d differential cross section calculated by Harrington (ref. 13). The dashed curve is the S-wave contribution, the dashed dotted curve is the D-wave contribution. The solid curve is their sum.

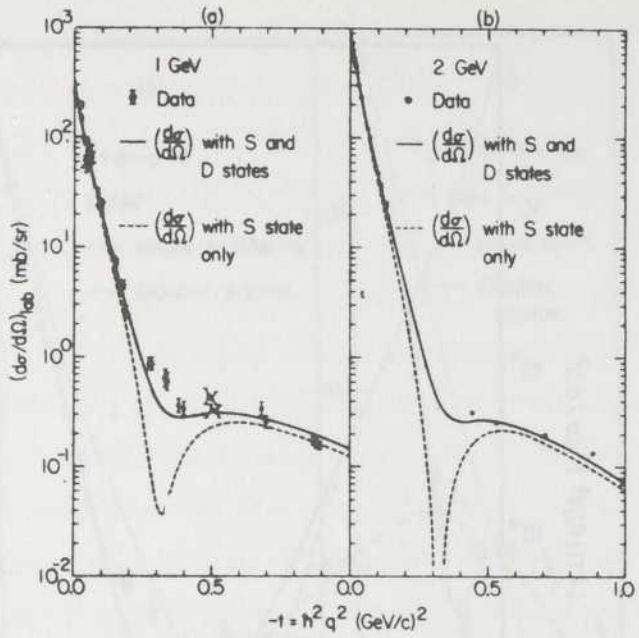

Fig. 11 Calculations of the p-d cross section at 1 and 2 MeV by Franco and Glauber (ref. 15) showing the effect of the D-state.

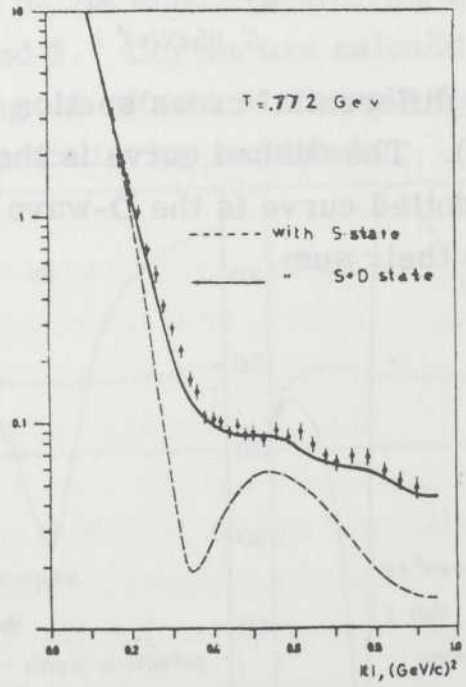

Fig. 12 Calculation of the π-d cross section at 0.772 GeV (ref. 12) by Alberi and Bertocchi (ref. 16) showing the effect of the D-state.

dominated by quadrupole transitions between the deuteron D and S states, it is strongly dependent on the relative orientation of the momentum transfer and the initial and final deuteron spin. Both authors[15,16] show that interesting effects will be produced when a proton or pion is scattered from a polarized deuteron target. The differential cross section can have dips or no dips in the break region depending on the experimental arrangement. Since deuteron targets with sizeable tensor polarization are not yet being made available, Harrington[17] proposed to detect these effects in a double-scattering experiment. He pointed out that in p-d scattering with unpolarized deuteron targets there are regions of momentum transfer where the recoiling deuterons are strongly aligned. This can be verified in a second scattering where steep minima could be observed in the cross section. Such experiments are certainly feasible for p-d scattering but rather difficult for the π-d system, for counting rate reason.

With such increased knowledge about Glauber-type calculations it would be very interesting to see if our set of data at 580 MeV could be correctly predicted taking spin and isospin dependence into account and using the correct wave functions for the deuteron, ^{3}He and ^{4}He; so far, this calculation has not yet been done. However, I will show you some other interesting calculations at our energy. First, some general remarks:

In the past two years the Glauber formalism has proven to be very successful, being applied to many high-energy problems like hadron-hadron scattering, meson production, etc.[18-22]

There has been some concern about the limitations of the Glauber approximation. It is a high-energy, small-angle approximation. Yet the physically most interesting part of the cross section is not located at small angles, but it is in the interference region or even at larger angles. From a study of the dip for instance one might extract information about the phase of the particle-nucleon amplitude at non-zero angles, and the region of larger momentum transfer might reveal interesting details about the nuclear wave function. All this is possible only if we can rely on the basic scattering theory. Recently efforts have been made by Schiff[23] and Ross[24] to modify Glauber's theory to extend its range of validity to larger

dominated by quadrupole transitions between the deuteron D and S states, it is strongly dependent on the relative orientation of the momentum transfer and the initial and final deuteron spin. Both authors[15,16] show that interesting effects will be produced when a proton or pion is scattered from a polarized deuteron target. The differential cross section can have dips or no dips in the break region depending on the experimental arrangement. Since deuteron targets with sizeable tensor polarization are not yet being made available, Harrington[17] proposed to detect these effects in a double-scattering experiment. He pointed out that in p-d scattering with unpolarized deuteron targets there are regions of momentum transfer where the recoiling deuterons are strongly aligned. This can be verified in a second scattering where steep minima could be observed in the cross section. Such experiments are certainly feasible for p-d scattering but rather difficult for the π-d system, for counting rate reason.

With such increased knowledge about Glauber-type calculations it would be very interesting to see if our set of data at 580 MeV could be correctly predicted taking spin and isospin dependence into account and using the correct wave functions for the deuteron, ^{3}He and ^{4}He; so far, this calculation has not yet been done. However, I will show you some other interesting calculations at our energy. First, some general remarks:

In the past two years the Glauber formalism has proven to be very successful, being applied to many high-energy problems like hadron-hadron scattering, meson production, etc.[18-22]

There has been some concern about the limitations of the Glauber approximation. It is a high-energy, small-angle approximation. Yet the physically most interesting part of the cross section is not located at small angles, but it is in the interference region or even at larger angles. From a study of the dip for instance one might extract information about the phase of the particle-nucleon amplitude at non-zero angles, and the region of larger momentum transfer might reveal interesting details about the nuclear wave function. All this is possible only if we can rely on the basic scattering theory. Recently efforts have been made by Schiff[23] and Ross[24] to modify Glauber's theory to extend its range of validity to larger

angles. Since Glauber's theory can be derived from Watson's multiple-scattering theory by suitably approximating the propagator such attempts to incorporate large-angle corrections may be viewed alternately as attempts to approximate the propagator more accurately. Pumplin[25] and Remler[26] have stressed the importance of a careful treatment of the propagator. Studying the behavior of the integrands in the multiple-scattering integrals, Ford and Pentz[27] have proposed a new approximation based on Watson's multiple-scattering formalism. To evaluate the error in the various approximations (Schiff, Glauber, Ford and Pentz) the approximate double-scattering terms are compared with the exact Watson theory results. Ford and Pentz show that their suggested approximation predict the correct phase and magnitude of the double-scattering term within 5 percent for scattering angles between 0 and 80 degrees CM. They also show that the Glauber approximation gives fairly good values for the magnitude of this term, but it fails to predict the proper phase at larger angles.

In Fig. 13 preliminary calculations are shown of the p-^{4}He cross section and polarization at our energy by Ford and Pentz. Watson's multi-scattering expansion is used to second order with an approximation in the double-scattering term. The spin and isospin dependent nucleon-nucleon scattering amplitudes are expressed as Gaussian functions of momentum transfer, chosen by means of a least square fit to the pp and np cross section and polarization as predicted by the most recent Livermore phase shift analysis. For the α particle wave function one of the forms suggested by Bassel and Wilkin[5] was used which would yield a good fit to the single-particle form factor recently measured in Stanford. Since higher-order scatterings are omitted, and the nucleon-nucleon amplitudes are oversimplified, there is no good agreement with the data, but the qualitative features are reproduced.

Remler[28] calculated the differential cross section and the polarization in p-d scattering at our energy. His calculation is a straight forward application of Watson's theory in the impulse approximation and takes single and "direct" double scattering terms into account. The transition operators describing the free nucleon-nucleon scattering were obtained

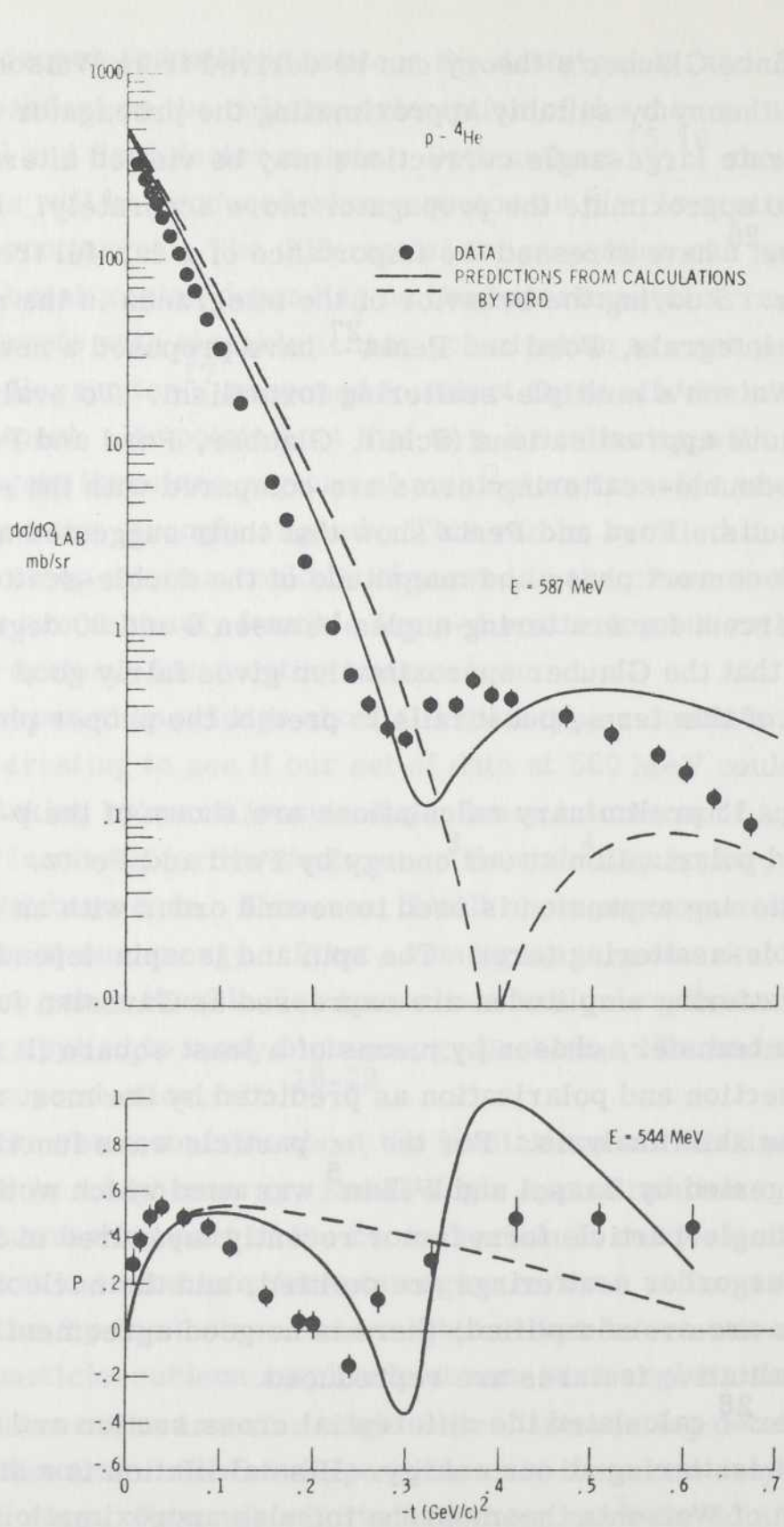

Fig. 13 The p-^{4}He differential cross section and polarization. Data are from the present experiment. Curves are predictions by Ford (ref. 27).

from the Livermore phase shifts.[29] Since the phase shifts at this energy are only imperfectly known a comparison was made between the observables predicted by these phase shifts and the experimental data.[30] A typical agreement is shown in Fig. 14 for the p-p differential cross section and the polarization at our energy. A further ingredient for the calculation is the deuteron wave function. Remler used a rough fit to the Hamada-Johnston S-state wave function[31] as a sum of three Gaussians. The quadrupole form factor was taken from Glendenning and Kramer[32] with a D-state probability altered to about 7 percent. The results are presented in Fig. 15. The three heavy lines correspond to calculations using the S-state wave function just mentioned. The dotted curve is single scattering only. The dashed one single and double scattering without the D-state component. The solid line is the result when the D-state is included. Although the shape of the cross section and polarization angular distribution is reproduced, the magnitude is not. Since in the beginning there were uncertainties about the experimental normalization of the small angle cross section, a fit to the data beyond the break region was attempted by allowing the computer to vary the shape parameters of the deuteron wave function. An excellent fit to the data at larger angles and, after checking the normalization, also at the smaller angles was obtained with a wave function that is peaked at a smaller radius than the Hamada-Johnston wave function (Fig. 16). This may indicate the need for more high momentum particles in the deuteron wave function. Since Remler plans to improve upon his calculation this is a tentative result only. Another interesting result of Remler's calculation is the large effect of the D-state component on the polarization.

Now I would like to talk about our studies of (p, 2p) reactions. We have seen that proton scattering at these energies show evidence for multiple scattering with the individual nucleons. The analysis of such data requires the knowledge of the nuclear wave function, or equivalently Fermi momentum distribution. Although multiple scattering effects will, at these energies, distort the apparent momentum distribution calculated from the measurement of the (p, 2p) differential cross section, the avail-

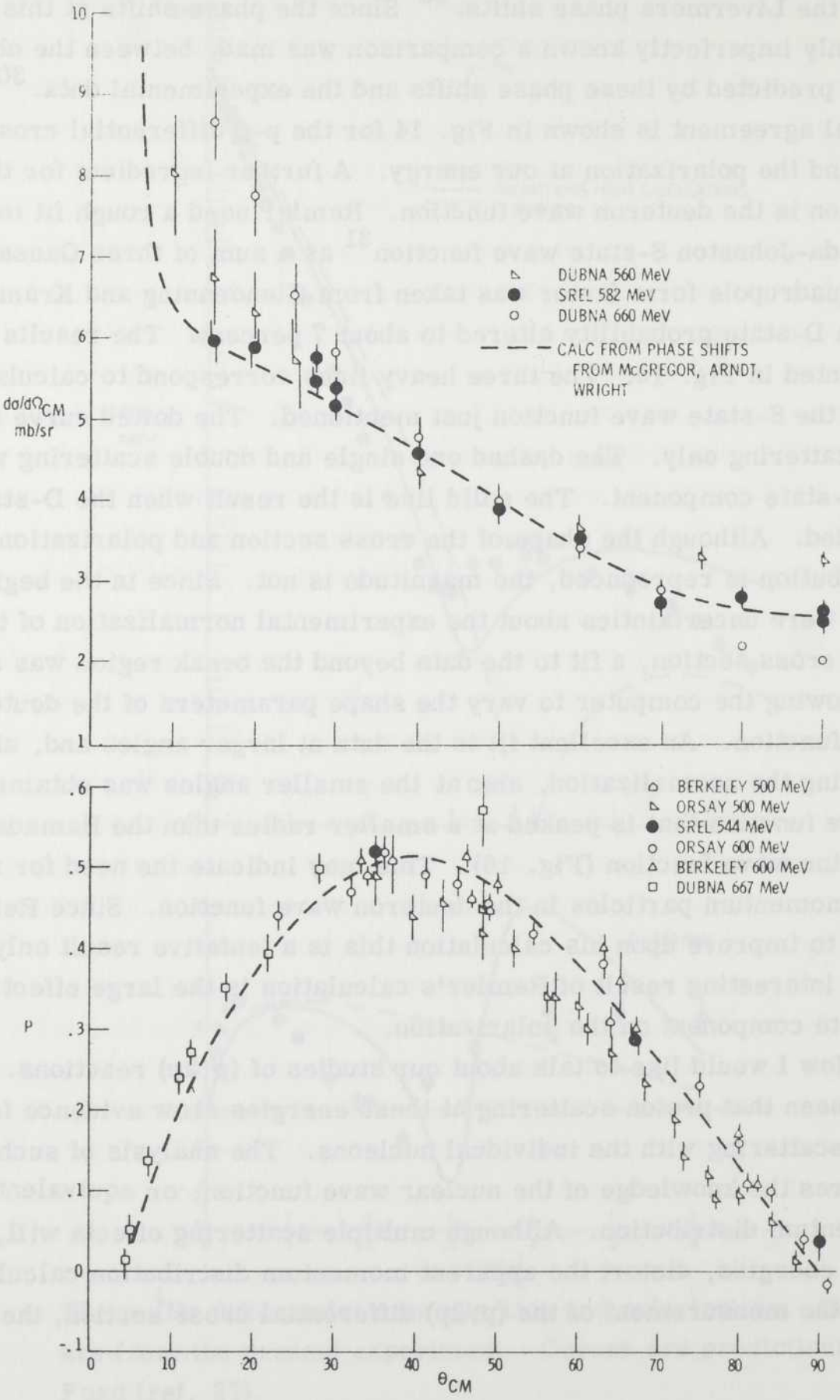

Fig. 14 The p-p differential cross sections and polarizations. Dashed lines are the predictions from the phase shift solution of reference 29, page 1161, Table III for 570 MeV.

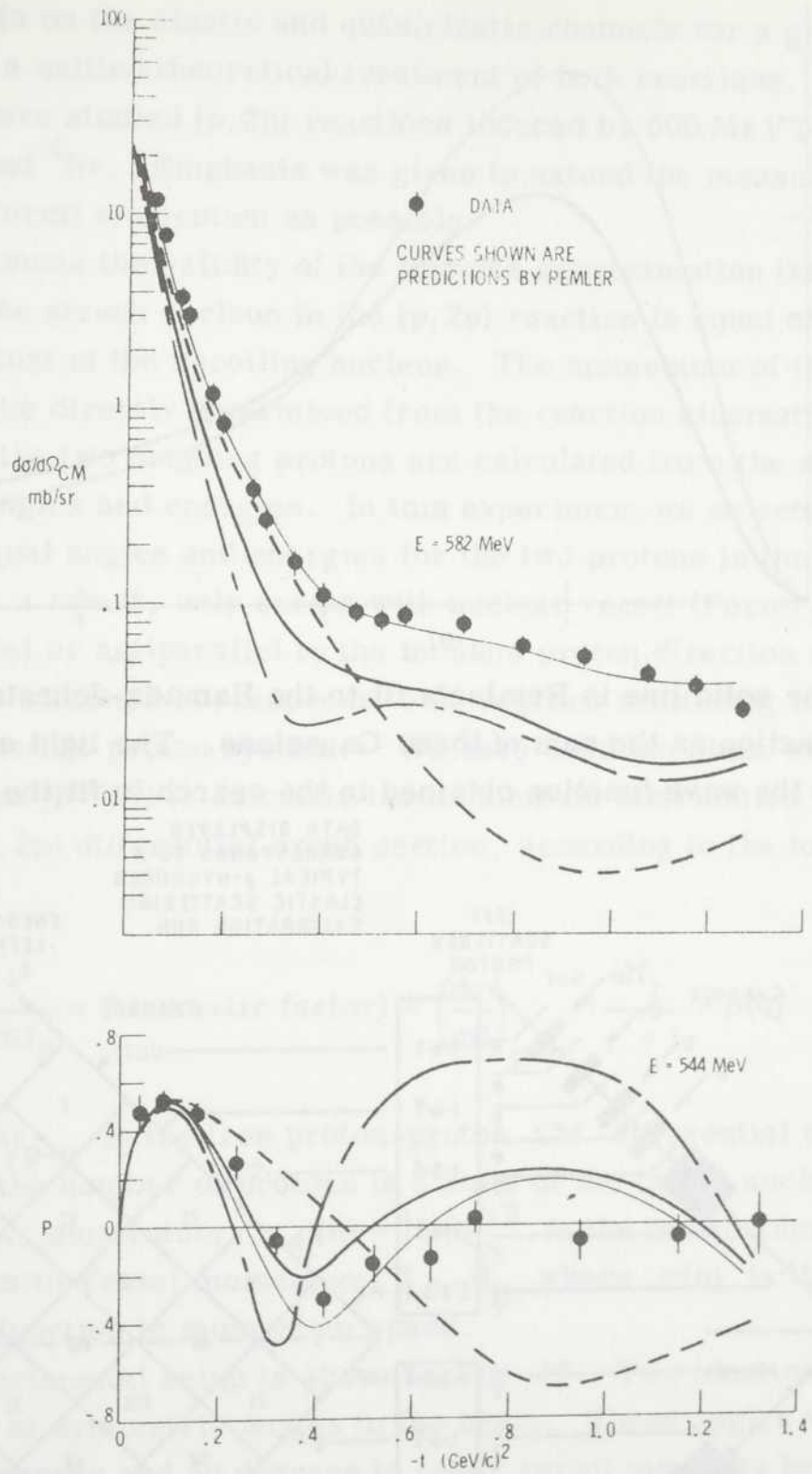

Fig. 15 The p-d differential cross section and polarization. Data are from the present experiment, curves are calculations by Remler. The three heavy lines (dotted, dashed, and solid) were obtained with the Hamada-Johnston wave function (including single scattering only, single and double scattering, and single and double scattering with D-state). The light solid line is the full calculation with a modified radial distribution in the wave function (Fig. 16).

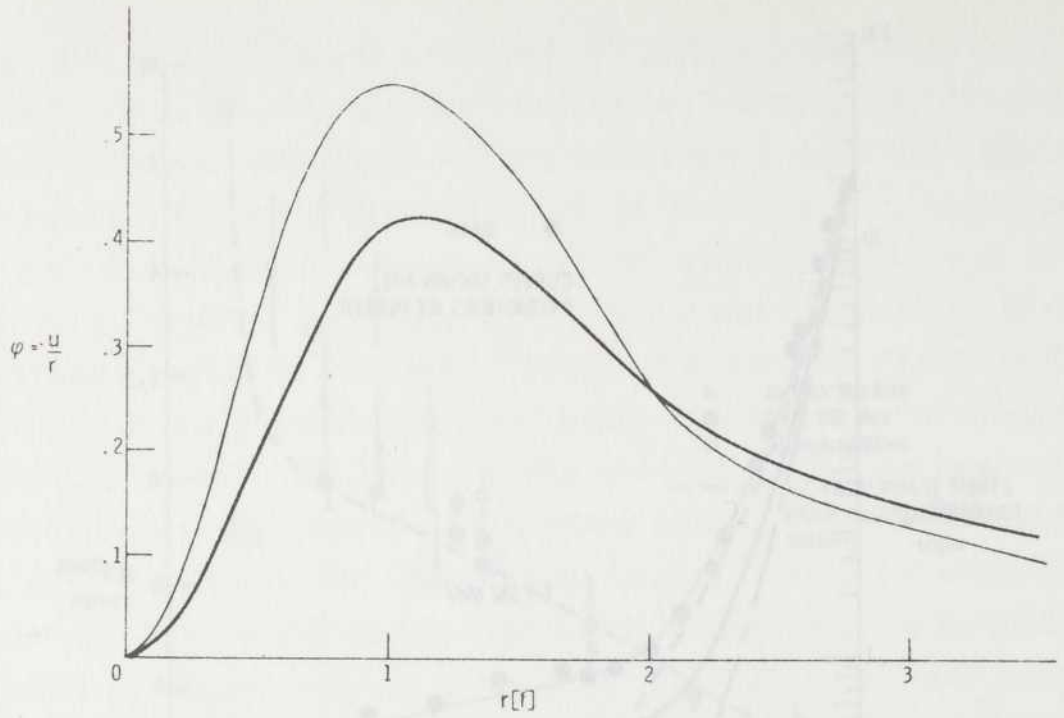

Fig. 16 The solid line is Remler's fit to the Hamada-Johnston wave function as the sum of three Gaussians. The light solid line is the wave function obtained in the search to fit the p-d data.

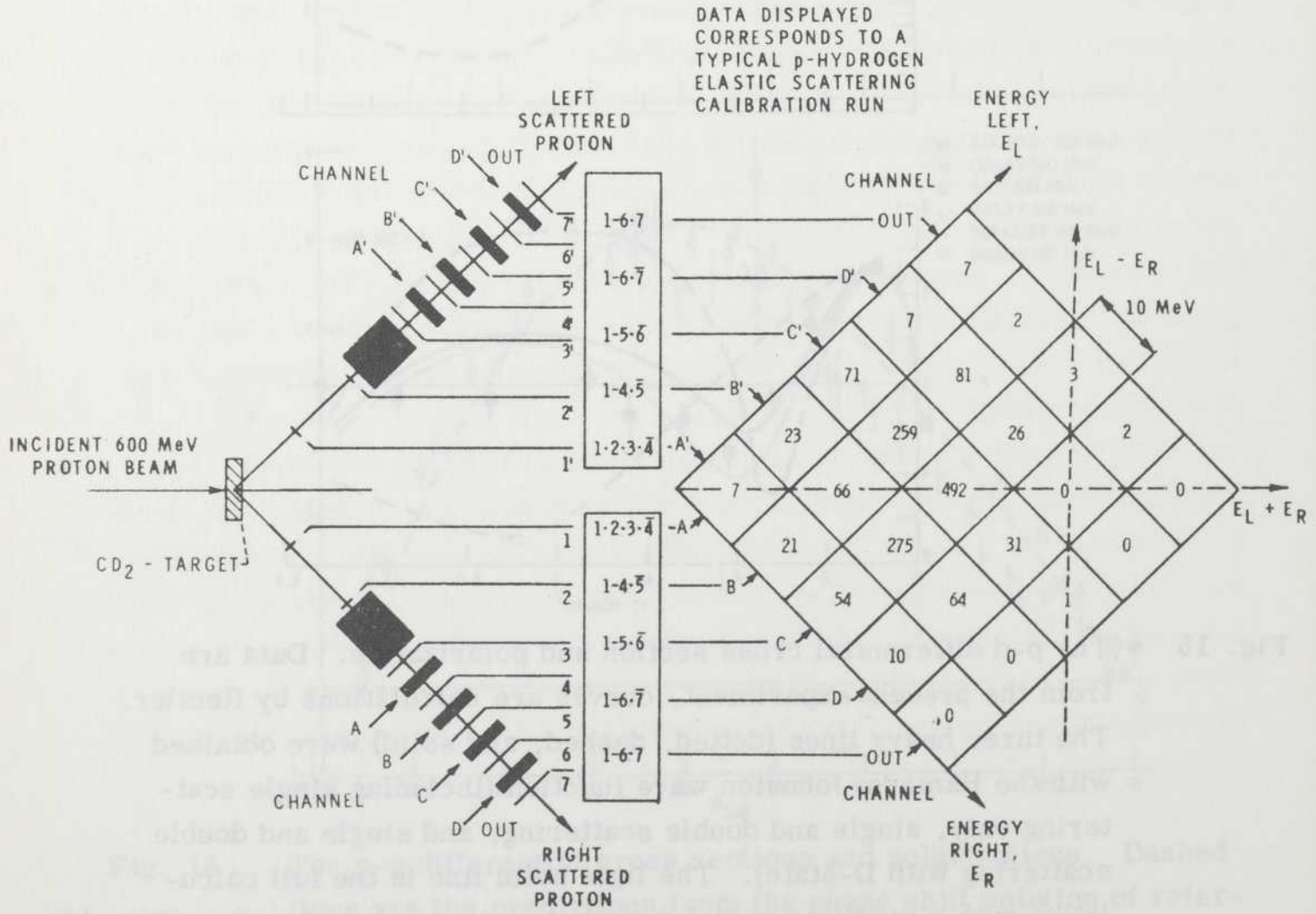

Fig. 17 Experimental arrangement used in the present (p, 2p) experiments.

ability of data on the elastic and quasielastic channels for a given nucleus might allow a unified theoretical treatment of both reactions. For this reason we have studied (p, 2p) reactions induced by 600 MeV protons on deuterium and ^{4}He. Emphasis was given to extend the measurements to as large a Fermi momentum as possible.

If we assume the validity of the impulse approximation then the momentum of the struck nucleon in the (p, 2p) reaction is equal and of opposite sign to that of the recoiling nucleus. The momentum of the recoiling nucleus can be directly determined from the reaction kinematics. The momenta of the two outgoing protons are calculated from the measured laboratory angles and energies. In this experiment we selected reactions with equal angles and energies for the two protons in the exit channel. As a result, only events with nuclear recoil (Fermi momentum) either parallel or antiparallel to the incident proton direction were detected. This situation corresponds to 90 degrees scattering in the center of mass of the two proton system. We have used the plane wave impulse approximation (PWIA) to calculate the momentum distribution from the measured (p, 2p) differential cross section, according to the following relationship:

$$\frac{d\sigma}{dE\, d\Omega_1\, d\Omega_2} = (\text{kinematic factor}) \times \left(\frac{d\sigma}{d\Omega}\right)_{p\text{-}p} \times \frac{N_l}{l+1} \times \rho(q)$$

where $(db/d\Omega)_{p\text{-}p}$ is the free proton-proton CM differential cross section, N_l is the number of protons in a state of the target nucleus with orbital angular momentum l, $\rho(q) = |\varphi(q)|^2$ is the momentum probability for a proton with Fermi momentum $\vec{q} = -\vec{q}_R$ where $\varphi(q)$ is the single proton wave function in momentum space.

The experimental setup is shown in Fig. 17. Two identical telescopes were located at symmetric angles to the beam. These angles were varied between 25 degrees and 50 degrees to cover recoil momenta between -200 MeV/c and +360 MeV/c along the beam direction. The resolution for the recoil momenta was determined by the angular acceptance of the system.

It varied between 16 and 43 MeV/c along the beam, depending on the magnitude of the cross section. The absorbers in the telescopes were matched and adjusted to stop the two outgoing protons in a sandwich of five counters interspaced with 1/8" Cu. The total energy resolution on the sum of the energies of the proton pairs was about 16 MeV. The (p,2p) events were selected electronically by the requirement of a stopped proton in both telescopes. The coincident two proton events were displayed in a 5×5 matrix. The diagonal channels corresponded to events sharing equal energy, the off-diagonal channels corresponded to energy differences between the protons of 10, 20, 30 MeV, respectively. A typical event distribution for p-p scattering is shown in the matrix. The actual (p,2p) data were obtained by adding the events in four intervals centered at the sum of the two proton energies.

The D(p,2p) cross section calculated from each angle is shown in Fig. 18. From these data and the 90^{o} CM p-p cross section taken from literature[30] the momentum distribution $\rho(q)$ was determined. It is presented in Fig. 19. The experimental results are compared with the momentum distributions obtained by Fourier transforming various deuteron wave functions. Curve A corresponds to an S-state Hulthén wave function. Above 150 MeV/c there is a definite discrepancy between our data and the Hulthén S-state momentum distribution. Curve B is a D-state momentum distribution obtained by assuming the radial distribution to have the same shape as the S-state Hulthén wave function and the deuteron to consist of a pure D-state. The D-state normalization is taken to be 7 percent. Although it is evident that at large Fermi momenta, the D-state contributes an important part of the momentum distribution, it will not account for all of the discrepancy. We have furthermore investigated the momentum distributions to be expected from S- and D-state wave functions obtained by Hamada and Johnston. Both the S- and D-state momentum distributions vanish at a momentum corresponding to the radius of the hard core (400 MeV/c).

We conclude that our momentum distribution cannot be explained from known deuteron wave functions within the Plane Wave Impulse Approximation. We note that the large discrepancy observed at Fermi momenta

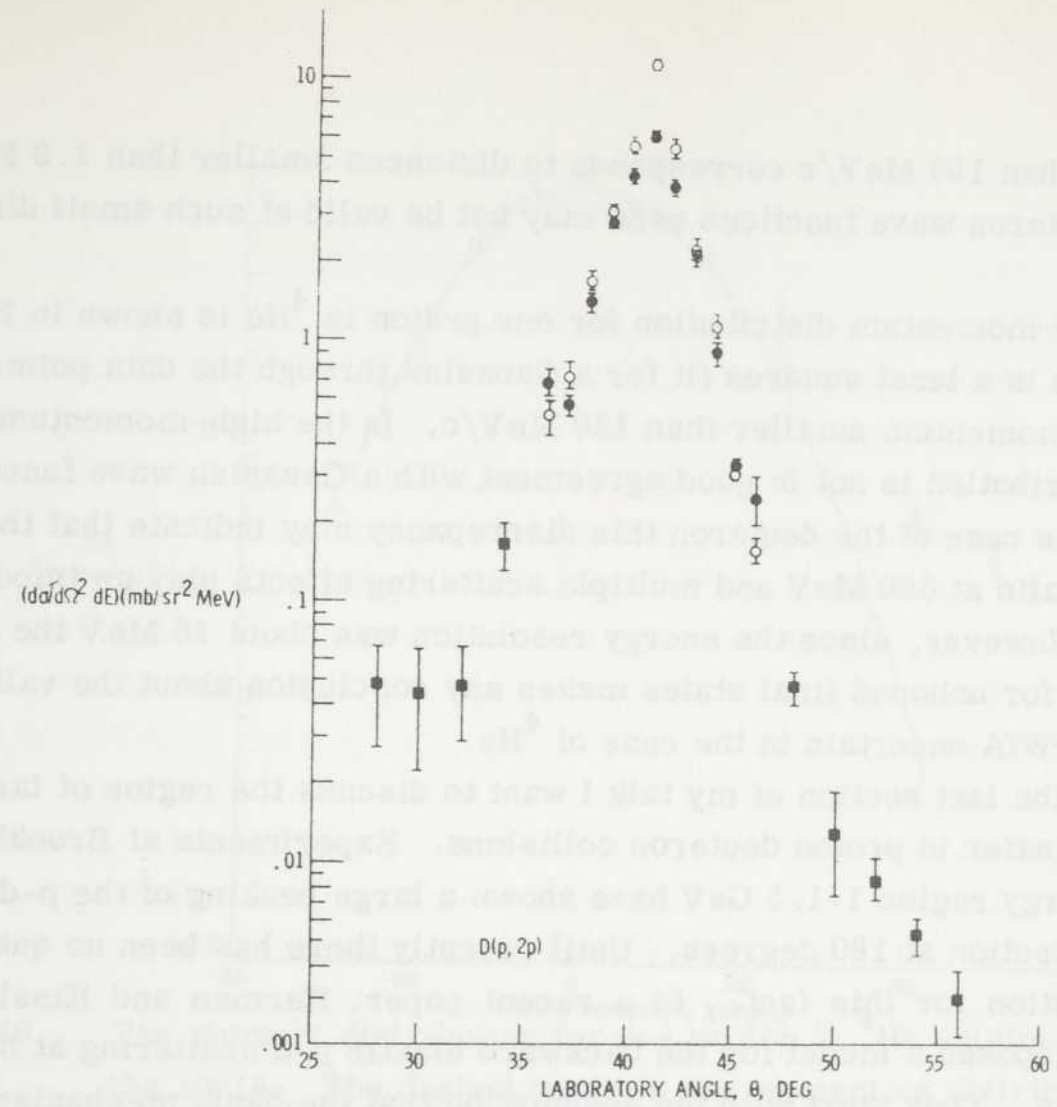

Fig. 18 The D(p, 2p)n cross section is a function of laboratory angle.

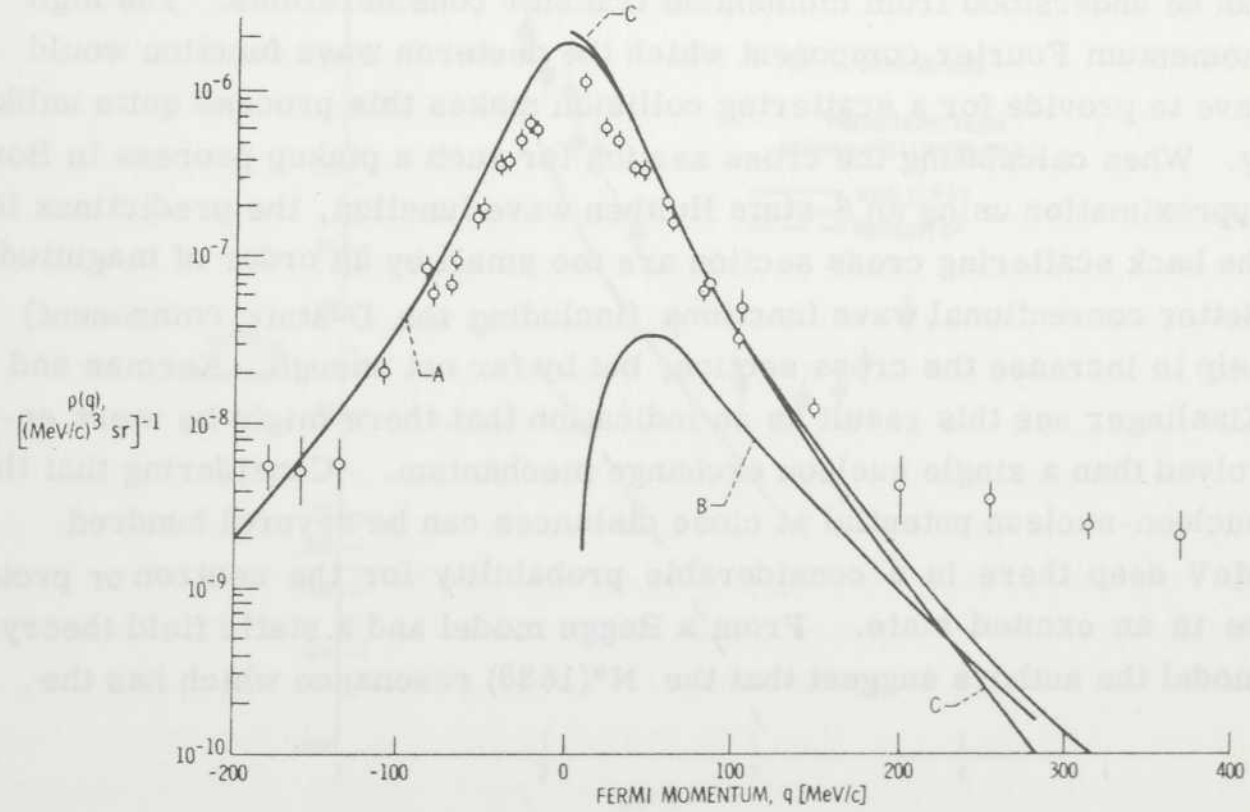

Fig. 19 The momentum distribution for the proton in Deuterium calculated from the (p, 2p) data with the PWIA. The curves A, B, and C are the momentum distributions calculated from A, the S-state Hulthén wave function, B, a pure D-state wavefunction normalized to 0.07, C, the S-state Hamada-Johnston wave function.

larger than 150 MeV/c corresponds to distances smaller than 1.3 F The deuteron wave functions used may not be valid at such small distances.

The momentum distribution for one proton in ^{4}He is shown in Fig. 20. Curve A is a least squares fit for a Gaussian through the data points with Fermi momentum smaller than 120 MeV/c. In the high-momentum region the distribution is not in good agreement with a Gaussian wave function. As in the case of the deuteron this discrepancy may indicate that the PWIA is not valid at 600 MeV and multiple scattering effects play an important role. However, since the energy resolution was about 16 MeV the possibility for unbound final states makes any conclusion about the validity of the PWIA uncertain in the case of ^{4}He.

In the last section of my talk I want to discuss the region of large momentum transfer in proton deuteron collisions. Experiments at Brookhaven in the energy region 1-1.5 GeV have shown a large peaking of the p-d elastic cross section at 180 degrees. Until recently there has been no quantitative explanation for this fact. In a recent paper, Kerman and Kisslinger[33] here proposed a model for the backward elastic p-d scattering at high energies. They start with the assumption that the basic mechanism is not a scattering collision, but a fermion transfer (pickup) process. This can be understood from momentum transfer considerations. The high momentum Fourier component which the deuteron wave function would have to provide for a scattering collision makes this process quite unlikely. When calculating the cross section for such a pickup process in Born approximation using an S-state Hulthén wave function, the predictions for the back scattering cross section are too small by an order of magnitude. Better conventional wave functions (including the D-state component) help to increase the cross section, but by far not enough. Kerman and Kisslinger see this result as an indication that there might be more envolved than a single nucleon exchange mechanism. Considering that the nucleon-nucleon potential at close distances can be several hundred MeV deep there is a considerable probability for the neutron or proton be in an excited state. From a Regge model and a static field theory model the authors suggest that the N*(1688) resonance which has the

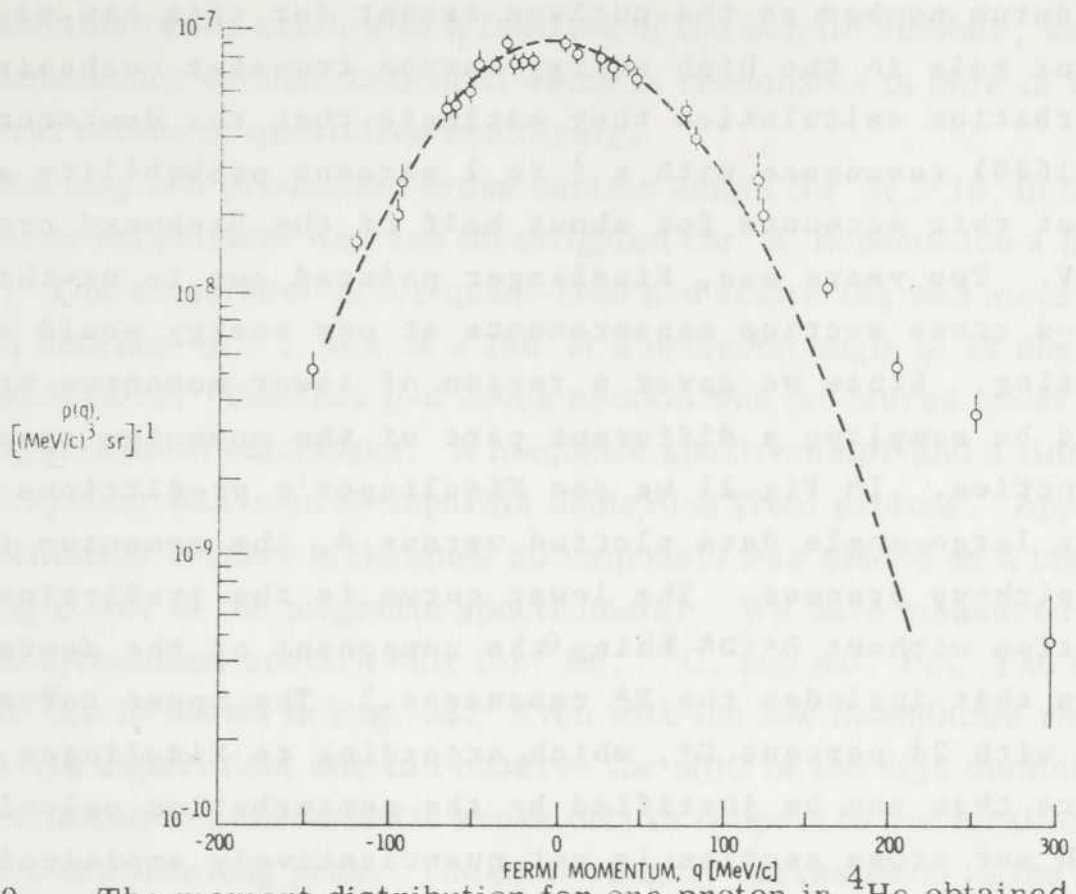

Fig. 20 The moment distribution for one proton in ^{4}He obtained with the PWIA. The dashed curve is the momentum distribution calculated from a Gaussian wave function.

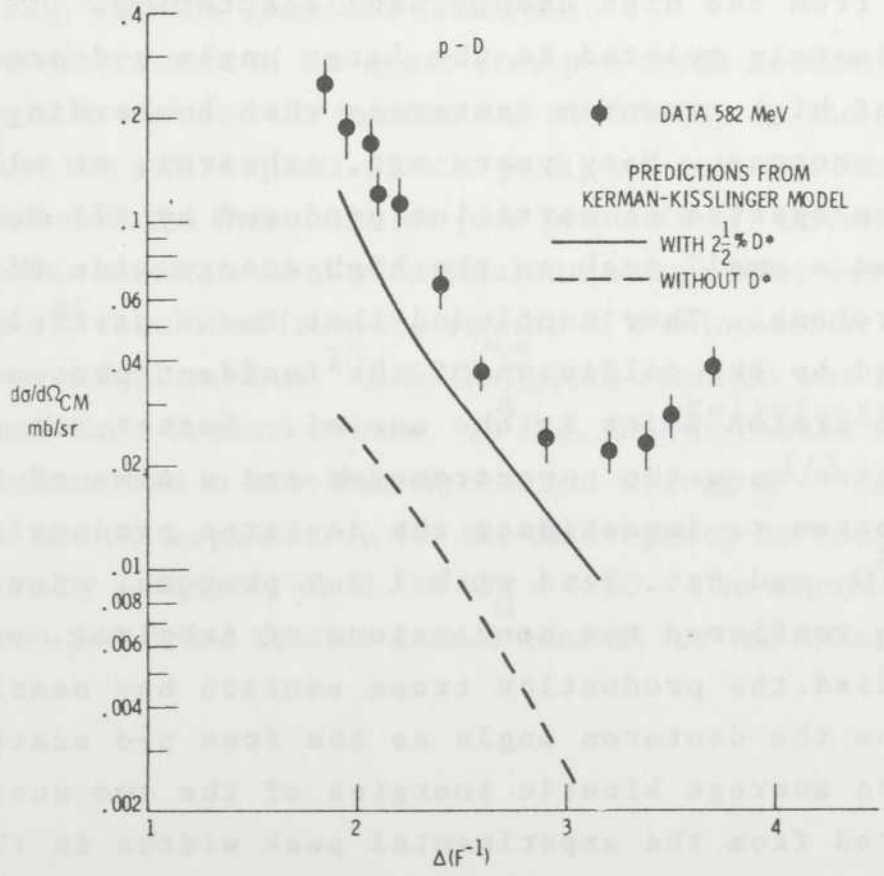

Fig. 21 Large angle p-d cross section from present experiment plotted as a function of Δ, the momentum transfered in a pickup reaction. The solid and dashed curves are the predictions from the Kerman-Kisslinger model (ref. 33).

same quantum numbers as the nucleon, except for spin, may play an important role in the high energy baryon transfer mechanism. From a perturbation calculation they estimate that the deuteron contains the N*(1688) resonance with a $\frac{1}{2}$ to 1 percent probability and they show that this accounts for about half of the backward cross section at 1 GeV. Two years ago, Kisslinger pointed out to us that large angle p-d cross section measurements at our energy would be quite interesting. Since we cover a region of lower momentum transfer, we would be sampling a different part of the momentum space deuteron wave function. In Fig.21 we see Kisslinger's predictions together with our large-angle data plotted versus Δ, the momentum transfered in the pick-up process. The lower curve is the prediction of the calculation without D*(D* being the component of the deuteron wave function that includes the N* resonance.) The upper curve is calculated with $2\frac{1}{2}$ percent D*, which, according to Kisslinger, is probably more than can be justified by the perturbation calculation. Although our cross section is not quantitatively explained, these results for the large-angle scattering are quite encouraging. They show that interesting details about the deuteron wave function may be obtained from the high energy back scattering.

Intimately related to the large angle p-d scattering is the production of high momentum deuterons when bombarding nuclei with high energy protons. Many years ago, Azhgirei, et al[34] studied the high momentum spectra of particles produced by 675 MeV protons, and they observed a small peak on the high energy side of the elastically scattered protons. They concluded that these particles were deuterons produced by the collision of the incident protons with quasi-free neutron-proton pairs in the nuclei. Sutter, et al[35] used the high resolution magnetic spectrometer and a time of flight system of the cosmotron to investigate the deuteron production from ^{4}He ^{6}Li, ^{12}C, ^{16}O, and nat. lead with 1 GeV protons. Several of their observations confirmed the conclusions of Azhgirei, et al: For each nucleus studied, the production cross section has nearly the same dependence on the deuteron angle as the free p-d scattering cross section. The average kinetic energies of the two nucleon clusters were estimated from the experimental peak widths in the observed deuteron spectra and were found to be the correct order of magnitude for explanation by conventional nuclear models[36]. Finally when plotting

the production cross section as a function of the atomic number, an $A^{1/3}$ dependence seemed indicated which is reasonable in view of the peripheral nature of quasi-free scattering.

Since only one production cross section exists for $A > 16$ in the Brookhaven experiment we have investigated the A dependence a little further. The cross section for quasi-free p-d scattering was measured for 9 nuclei between $A = 3$ and $A = 208$ at a deuteron angle of 12 degrees in the laboratory. The free p-d cross section was measured under the same experimental conditions. A magnetic spectrometer and a time of flight system was used to separate deuterons from protons. Applying scintillation counter techniques no emphasis was placed on a high resolving power of the magnetic spectrometer. We have measured the deuteron momentum spectra only for ^{9}Be, ^{12}C, and nat. Pb. The spectrum for ^{9}Be is shown in Fig. 22. Even with the low momentum resolution of this experiment one can observe the shift of the high momentum peak (attributed to quasi-elastic knock out) in respect to the location of the free p-d scattering peak. The shift roughly corresponds to the 16.7 MeV binding energy of the deuteron in Beryllium (9). The broad peak at lower momenta is probably connected with processes that produce pions along with the observed deuterons.

For the measurement of the quasi-free p-d cross section as a function of A we have widened the momentum window Δp of the spectrometer to accept the entire quasi-elastic peak, but rejected deuterons with momenta below the threshold for pion production. Obviously we cannot tell in this measurement what final state the nuclei were left in, but Sutter, et al.[35] concluded from the results of a coincidence experiment that the residual nucleus ^{10}B of the $^{11}C(p, pd)$ reaction was left at or near the ground state in most events. In Fig. 23 our preliminary results are shown. The cross sections are in excellent agreement with an $A^{1/3}$ dependence. At present we have no explanation for the discrepancy between our data and those taken by Azhgirei, et al. at $\Theta_d = 7.60$. The angular dependence of the free p-d cross section cannot account for the difference.

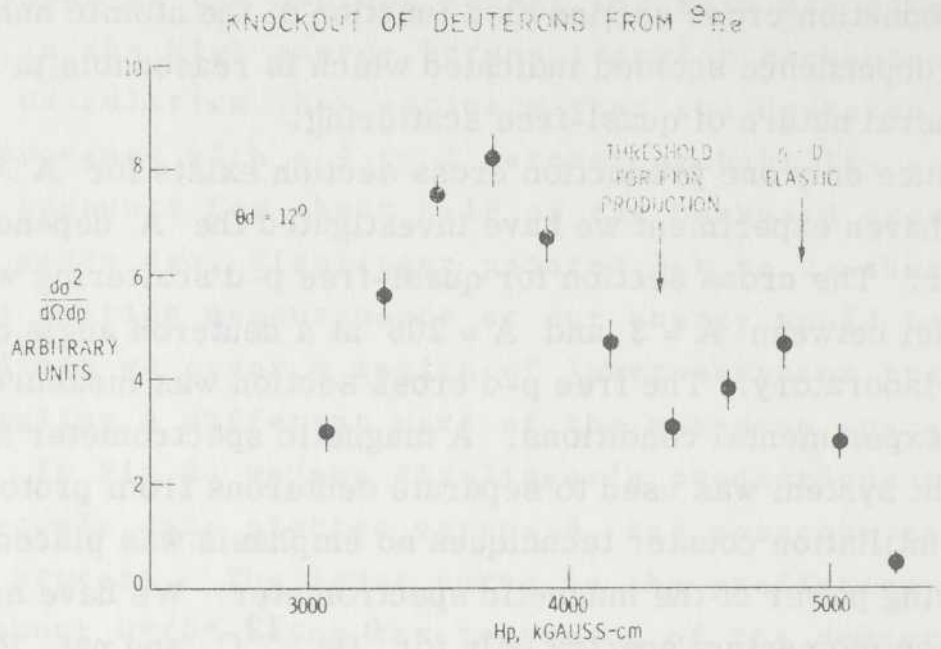

Fig. 22 Momentum distribution of high energy deuterons knocked out of ^{9}Be.

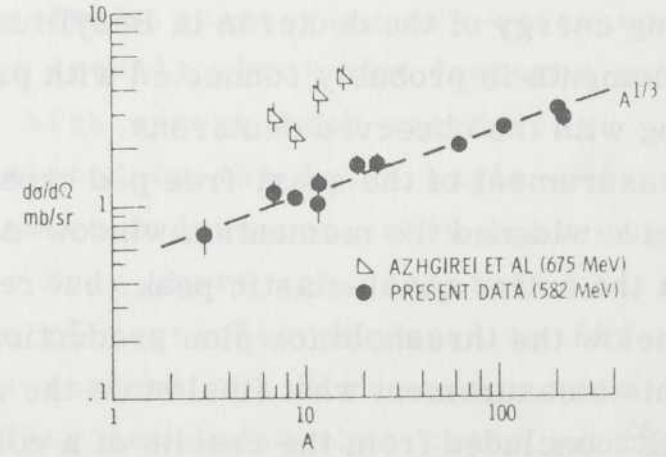

Fig. 23 Cross sections for quasifree p-d scattering in various nuclei. The dashed line indicates the $A^{1/3}$ dependence of the cross sections.

1. H. Palevsky, et al., Phys. Rev. Letters 18, 1200 (1967).
2. D. Cheng, UCRL 11926 (1965).
3. G. W. Bennett, et al., Phys. Rev. Letters 19, 387 (1967).
4. W. Czyż and L. Leśniak, Phys. Letters 24B, 227 (1967).
5. R. H. Bassel and C. Wilkin, Phys. Rev. Letters 18, 871 (1967) and Phys. Rev. 174, 1179 (1968).
6. R. J. Glauber, in Lectures in Theoretical Physics, edited by W. E. Britten, et al. (Interscience Publishers, Inc., New York, 1959), Vol. I, p. 315.
7. R. F. Frosch, et al., Phys. Rev. 160, 874 (1967).
8. R. J. Glauber, in Proceedings of the Symposium on the Use of NIMROD for Nuclear Structure Physics, RHEL/R166.
9. W. Czyz and L. Leśnick, Bull. Pol. Ac. of Science (1967).
10. V. Franco, Phys. Rev. Letters 21, 1360 (1968).
11. E. Kujawski, et al., Phys. Rev. Letters 21, 583 (1968).
12. F. Bradamante, et al., Phys. Letters 28B, 191 (1968) and Lund International Conference on Elementary Particles, June 1969.
13. D. R. Harrington, Phys. Rev. Letters 21, 1496 (1968).
14. E. Coleman and T. G. Rhoades, Effects of D-state in deuterium Scattering, Minnesota preprint, 1968.
15. V. Franco and R. J. Glauber, Phys. Rev. Letters 22, 370 (1969).
16. C. Alberi and L. Bertocchi, Phys. Letters 28B, 186 (1968) and Nuovo Cimento 61, 203 (1968).
17. D. R. Harrington, Phys. Letters 29B, 188 (1969).
18. J. Formánek and J. S. Trefil, Nucl. Phys. B3, 155 (1967) and Nucl. Phys. B4, 165 (1967).
19. J. S. Trefil, Phys. Review (to be published), and references in this paper.
20. V. Franco, Los Alamos Scientific Lab., preprint, LA-DC-9663.
21. L. Durand and R. Lipes, Phys. Rev. Letters 20, 637 (1968).
22. T. T. Chou and C. N. Yang, Phys. Rev. 170, 1591 (1968), 175, 1832, (1968).
23. L. I. Schiff, Phys. Review 176, 1390 (1968).

24. D. K. Ross, Phys. Review 173, 1965 (1968).
25. J. Pumplin, Phys. Review 173, 1651 (1968).
26. E. A. Remler, Phys. Rev. 176, 2108 (1968).
27. W. F. Ford and N. E. Pentz, NASA TM X-52594.
28. E. A. Remler, William and Mary Report (unpublished VM-T6) (1969).
29. M. H. MacGregor, R. A. Arndt, and R. M. Wright, Phys. Rev. 169, 1149 (1968).
30. M. H. MacGregor, R. A. Arndt, and R. M. Wright, UCRL 50426.
31. T. Hamada and I. D. Johnston, Nucl. Phys. 34, 382 (1962).
32. N. K. Glendenning, and G. Kramer, Phys. Rev. 126, 2159 (1962).
33. A. K. Kerman and L. S. Kisslinger, Phys. Review (to be published).
34. L. Azhgirei, et al., Soviet Phys.-JETP 6, 911 (1958).
35. R. J. Sutter, et al., Phys. Rev. Letters 19, 1189 (1967).
36. M. Riou, Rev. Mod. Phys. 37, 375 (1965).

THE STATUS OF THE LOS ALAMOS MESON FACTORY†

L. Rosen

(Presented by P.W. Keaton, Jr)

Los Alamos Scientific Laboratory, University of California

I. INTRODUCTION

Design effort on the Los Alamos Meson Physics Facility (LAMPF) has been underway for more than five years. Although some preparatory site development and a bit of construction was started quite early in this period, substantial funds for LAMPF construction were not released until October, 1968. Since then activities have proceeded at a very good pace. As of this moment, approximately half of the $55 million required for construction have been obligated. Beam date remains July 4, 1972. (The design parameters of LAMPF are shown in Fig. 1.)

II. PURPOSES OF LAMPF

Although the purpose of this talk is to provide a progress report on design and construction of this facility at the Los Alamos Scientific Laboratory (LASL), a few words about the motivation for this rather ambitious undertaking is in order.

First it should be mentioned that LAMPF will be the largest single basic research facility ever to be constructed in the Southwest and Rocky Mountain region of the United States. As such, it is expected to stimulate the development

† Work performed under the auspices of the U.S. Atomic Energy Commission.

DESIGN PARAMETERS FOR THE LOS ALAMOS LINAC (LAMPF)

Ion Source: Duoplasmatron - 30 keV

Preaccelerator: 750 keV Pierce-type short column

Alvarez Accelerator:

Frequency 2.0125×10^8 Hz

Structure - Alvarez, 4 tanks

Tank 1	- 0.75	- 5.0	MeV
2	- 5.0	- 41.2	MeV
3	- 41.2	- 72.3	MeV
4	- 72.3	- 100.3	MeV

Waveguide Accelerator:

Frequency 8.050×10^8 Hz

Structure - side-coupled shaped cavities $\pi/2$-mode standing wave

Number of tanks - 90

Current: Peak - 17 mA
Average - 1 mA

Duty Factor: 6 - 12 %

Overall Length: 850 m

Peak RF power for cavity excitation	38 MW
" " " " beam excitation	14 MW
Total	52 MW
Average RF power (6%)	3 MW

Fig. 1.

of science, education, and technology in that entire region. This is in harmony with U.S. federal policy which attempts to achieve a more uniform geographic distribution of scientific resources throughout the United States.

LAMPF will be the largest medium-energy laboratory and the highest-power meson-producing accelerator in the world, and we feel an obligation to make the facility available to the entire scientific community. We would hope that not only scientists in the U.S., but also scientists from other countries, and especially from Canada, will be able to participate in the use of this novel tool for nuclear science. It is, therefore, planned that fifty percent of the accelerator time will be dedicated to use by non-LASL groups. More than 200 scientists have already indicated their intention to become users of LAMPF.

Why all this interest in medium-energy physics? The reasons are many and diverse. The radiochemists, for example, see LAMPF as a God-given opportunity to make and study new families of proton-rich isotopes which up to now have not been readily producible. The biophysicists and radiologists look to LAMPF for kinds of radiations which have heretofore been in short supply. I refer specifically to the negative pions which can bring to bear large amounts of ionization in a small volume without seriously perturbing the integrity of the host organism. Astrophysicists might be intrigued by the prospect of using the 800-MeV protons to produce spallation products and try thereby to unravel the mystery of how heavy particles originate in the cosmic radiation. The physicists look at LAMPF as a vehicle for advancing their knowledge of nuclear structure, nuclear forces, and even fundamental particles, in most dramatic ways. While the 200-BeV accelerator is producing quarks, LAMPF will produce intense beams of pions that can be used to excite resonances in nucleons and nuclei which then decay by emission of very-high-

energy gamma rays--an exciting prospect indeed! The same pion beams can also be used in precision experiments which measure rare decay modes. The branching ratios of such modes may shed light on fundamental symmetries. The high flux of pions would permit a study of pi-mesons themselves. The charge distribution of the pion is sensitive to experiments such as $\pi^{\pm}$ scattering from ^{4}He.

Pions give rise to muons and it is quite likely that the further pursuit of muonic atoms and the properties of muonium will still be rewarding. For example, the possibility that muonium may convert to anti-muonium makes that subject well worth pursuing. And, too, there is the question of rare decay modes of the muon. Such information may shed light on the existence of an intermediate boson.

The more adventuresome among you might be fascinated by the high-intensity neutrino beams which arise from pion decay. They may well offer a new approach to nuclear structure studies because the absorption of a neutrino by a nucleon probably depends on the influence of other nucleons in the immediate vicinity.

For the more conservative among you, there will be almost-monoenergetic and high-energy neutron beams for experiments in neutron-proton and neutron-neutron scattering. Here, one shall be able to bring into play a polarized beam and also a polarized target.

And, for the ultraconservative among you, there will be a proton area which will house a high-resolution spectrometer capable of providing better than 200-keV energy resolution at 800 MeV. With this facility, it will be possible to do elastic and inelastic scattering on many nuclei and to use this approach to explore nuclear form factors and nucleon correlations within nuclei. The energy will be high enough to substantially enhance the validity of the impulse approximation over that which you are familiar with at lower

energies, and to reduce the complicating refraction of the incoming and outgoing nucleons by the nucleus.

III. STATUS OF LAMPF CONSTRUCTION

Figure 2 is a site plan for the facility. The areas in yellow are part of the $55M construction package. Starting at the west, the Equipment Test Laboratory is complete. In this laboratory we are operating the rf test stands to determine reliability and life span. In addition, we are performing here the complicated and time-consuming hydrogen-atmosphere brazing operation for the main portion of the accelerator.

The Laboratory-Office Building is 40% complete; the Injector Building is complete, including the building which houses the drift-tube accelerator. The entire beam channel is complete. The service aisle, the housing for the rf modules, and the Operations Building are under construction. A contract has just been signed to construct part of the experimental area. The experimental areas will be constructed in phases as funds become available. The 45-MW substation is essentially complete. This is as much power as is presently used by all of Los Alamos, Laboratory and townsite combined.

Figure 3 shows the accelerator layout. It is a three-stage machine comprising a 750-keV Cockcroft-Walton, a 100-MeV drift-tube accelerator, and a new concept in waveguide accelerators. Only the C-W machine power supply is more or less conventional. It was built by Haefely Company in Switzerland and is now erected at LASL (Fig. 4). This supply is regulated to an accuracy of a few hundred volts. We constructed the ion source at LASL. It is designed to provide a peak current of $\approx$50 mA at 12% duty factor and with radial beam emittance $< \pi$ mrad-cm at 750 kV. It must also operate for at least 50 hours without breaking down. It does all of these things. The high-gradient column

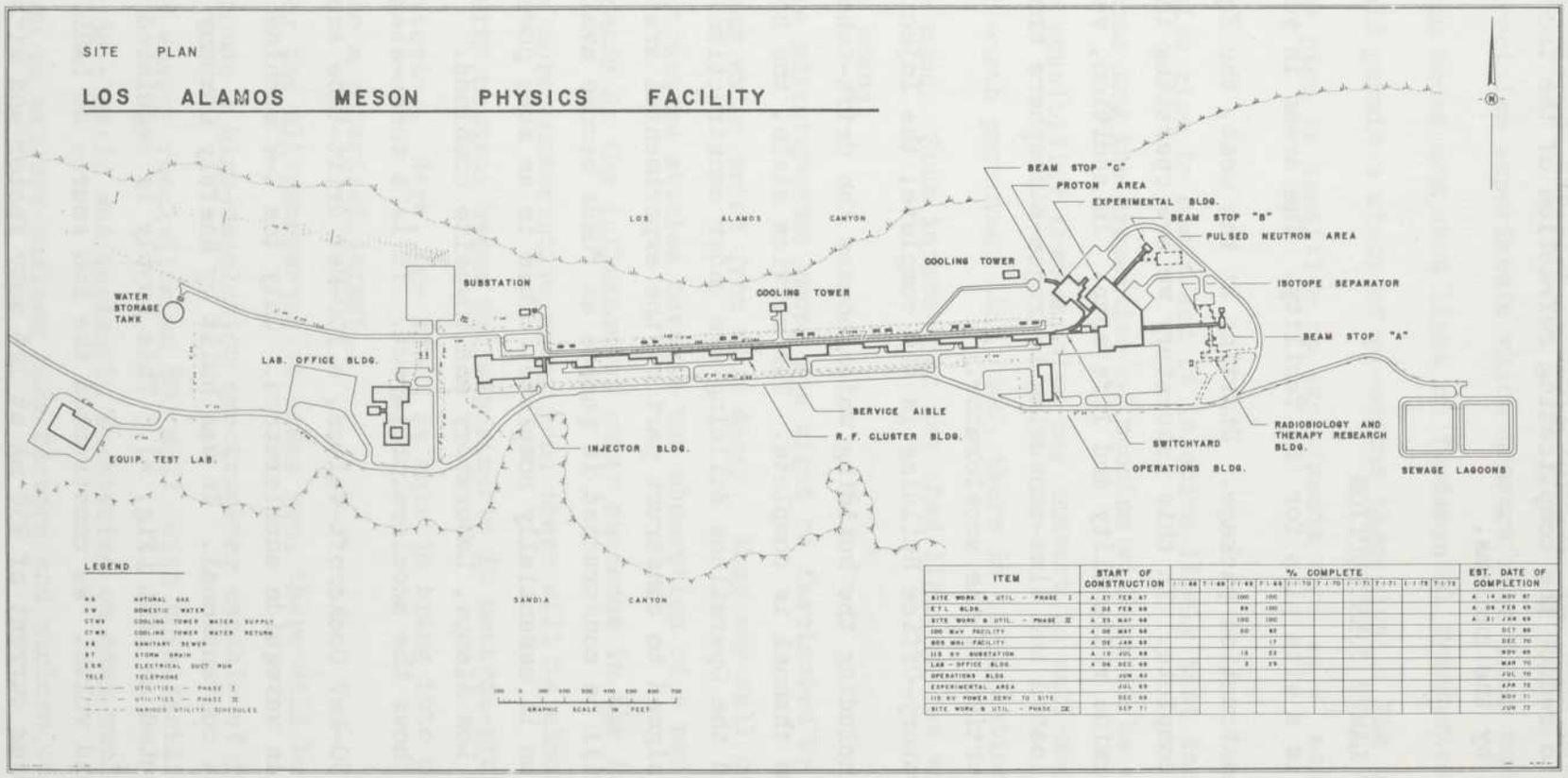

Fig. 2. LAMPF site plan.

Fig. 3. Accelerator layout.

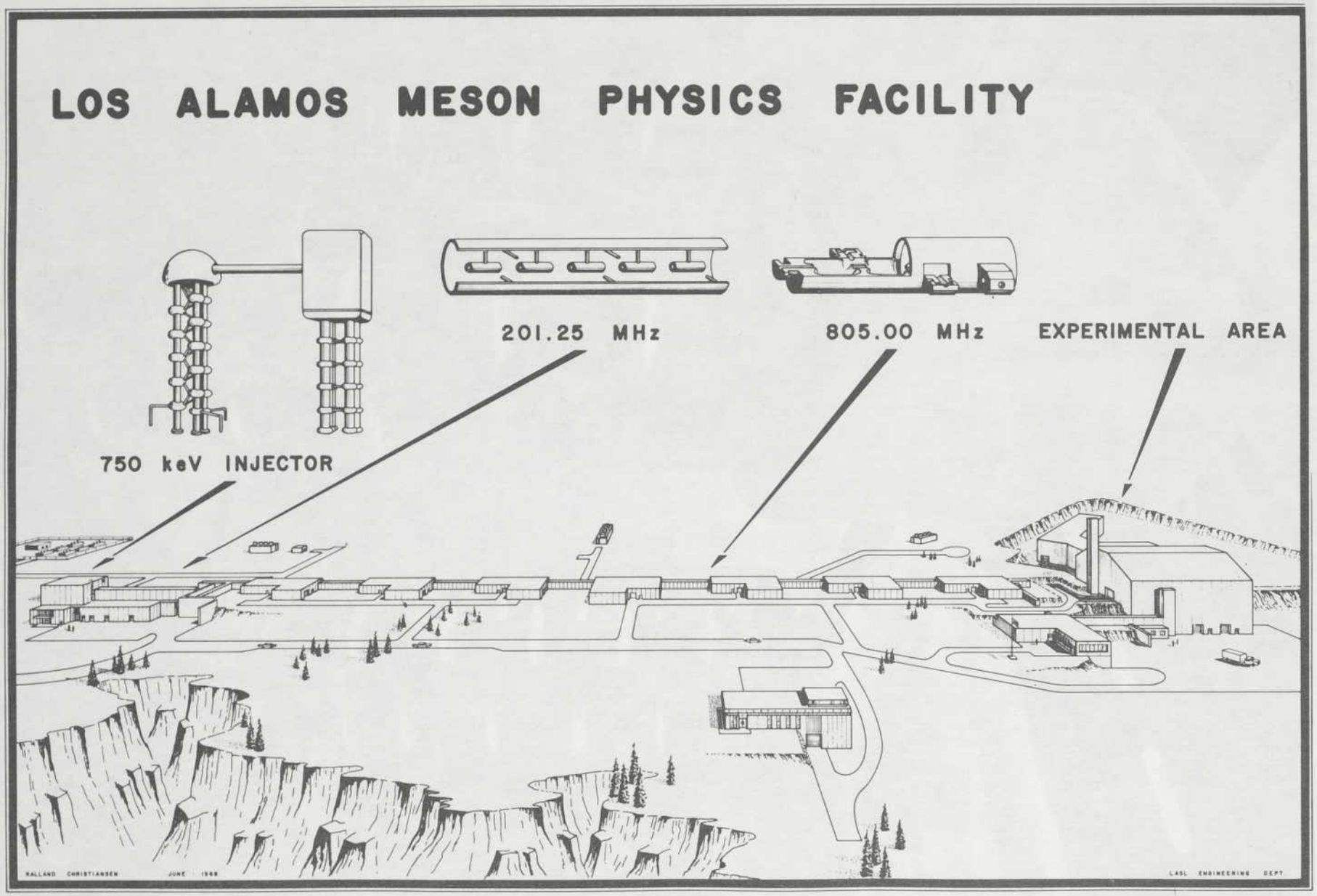

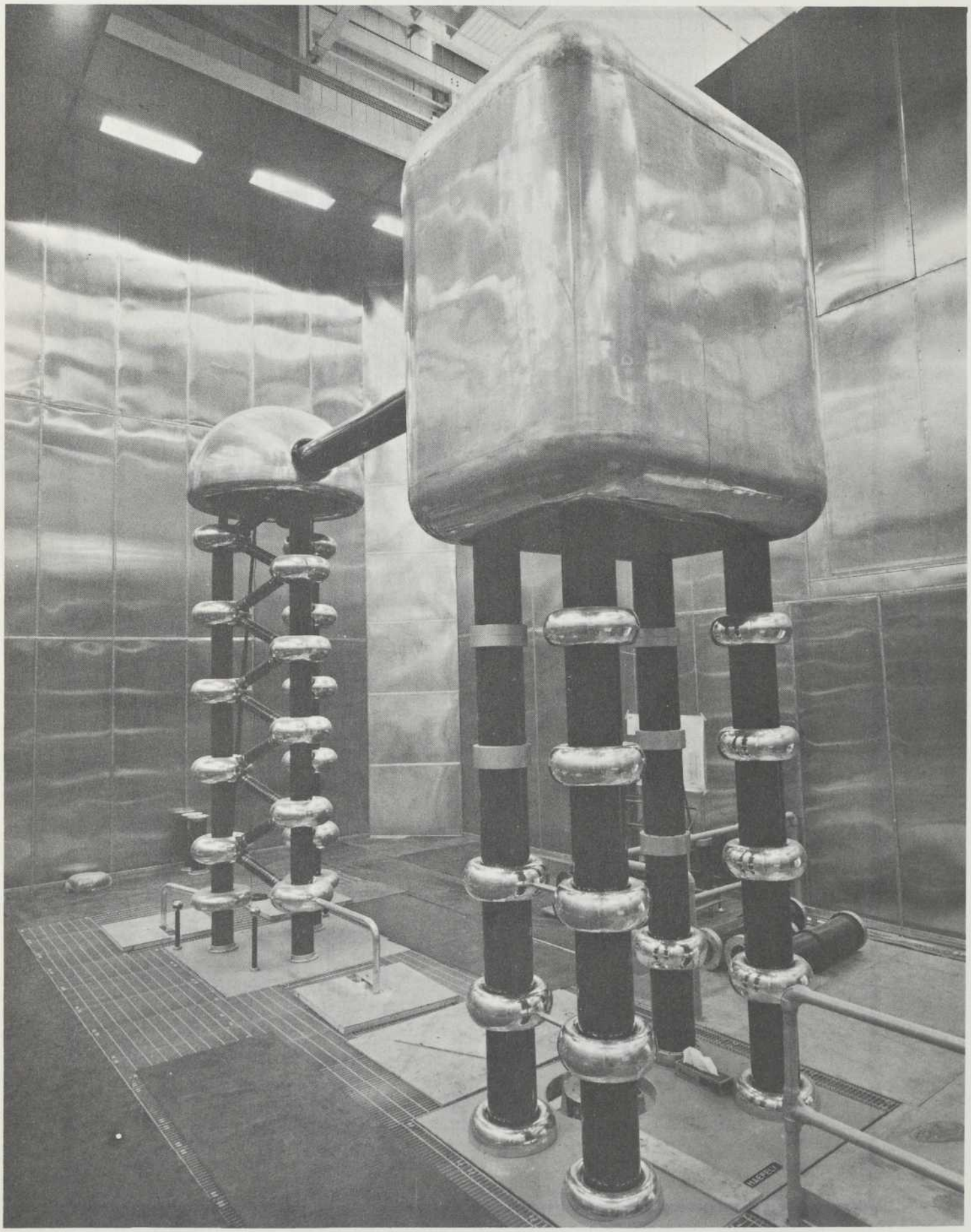

Fig. 4. Cockroft-Walten injector.

has been prototyped and is now being constructed at LASL. Fig. 5 shows a 200-keV section which operates as specified. The electrodes are made of titanium; insulation is of porcelain; it is pressurized to ∿2 psi; the containing vessel is acrylic. The drift-tube accelerator looks like the traditional Alvarez machine from the outside, but not from the inside (Fig. 6). We have found it possible and highly advantageous to use the $\pi/2$ mode of operation rather than the 2π mode. This is accomplished by adding post couplers to the Alvarez structure. This simple change results in an enormous improvement in stability--a factor of 200. As a result, this structure is now very hard to tilt and therefore is extremely tolerant of beam-loading effects. Figure 7 shows how such a tank fills with rf energy, compared to a tank operating in the 2π mode.

However, by far the most crucial success which emerged from the LASL effort during the past half-dozen years is the development of the side-coupled waveguide accelerator. A drift-tube accelerator becomes prohibitively expensive beyond 200 MeV, especially at high-duty factor. An iris-loaded waveguide as used for electron accelerators is also inefficient at high-duty factor and, in addition, requires that the fabrication and alignment errors be extremely small. It was discovered that the $\pi/2$-mode side-coupled cavity system is very tolerant of structural dimensions and beam loading. It is also highly efficient for converting rf power into beam power. At 6% duty factor and 1 mA average current, more than 30% of the rf power is converted to beam power. Figure 8 shows a section of a side-coupled cavity chain. The segments off the beam line are resonant cavities which couple fields between adjacent accelerating cavities. Under normal conditions, when the resonant frequencies in it and adjacent cavities are reasonably the same (within 100 kHz), very little power is dissipated in the coupling cavities (less than 1% of power dissipated in the main cells).

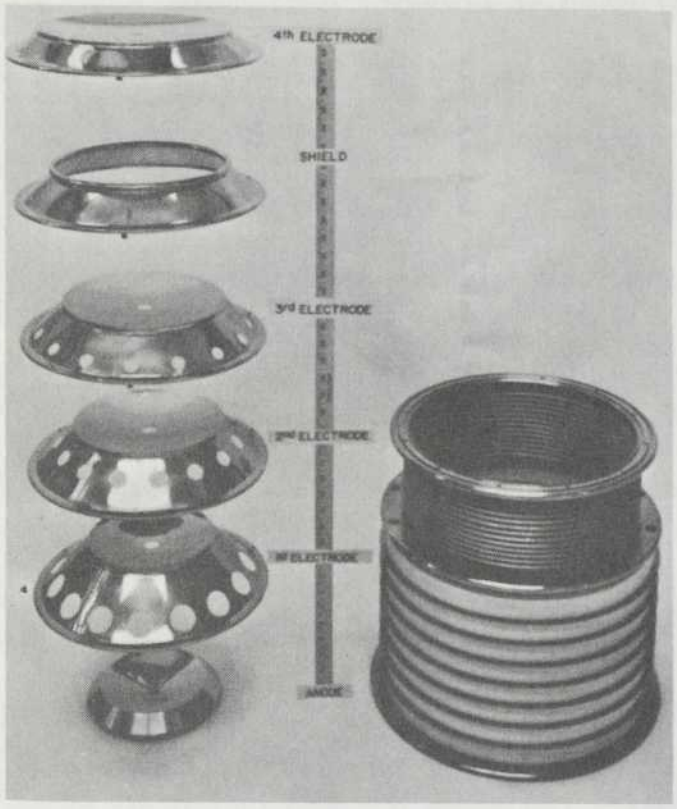

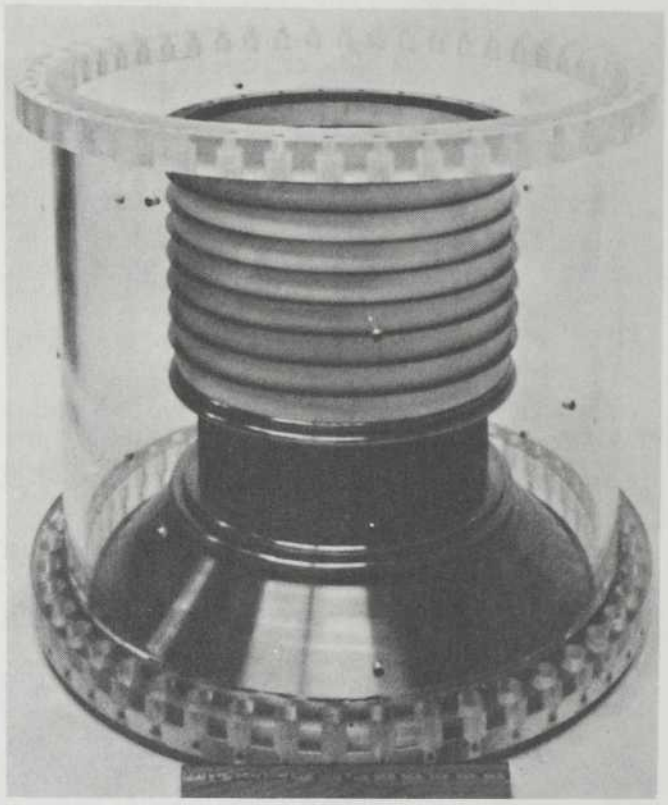

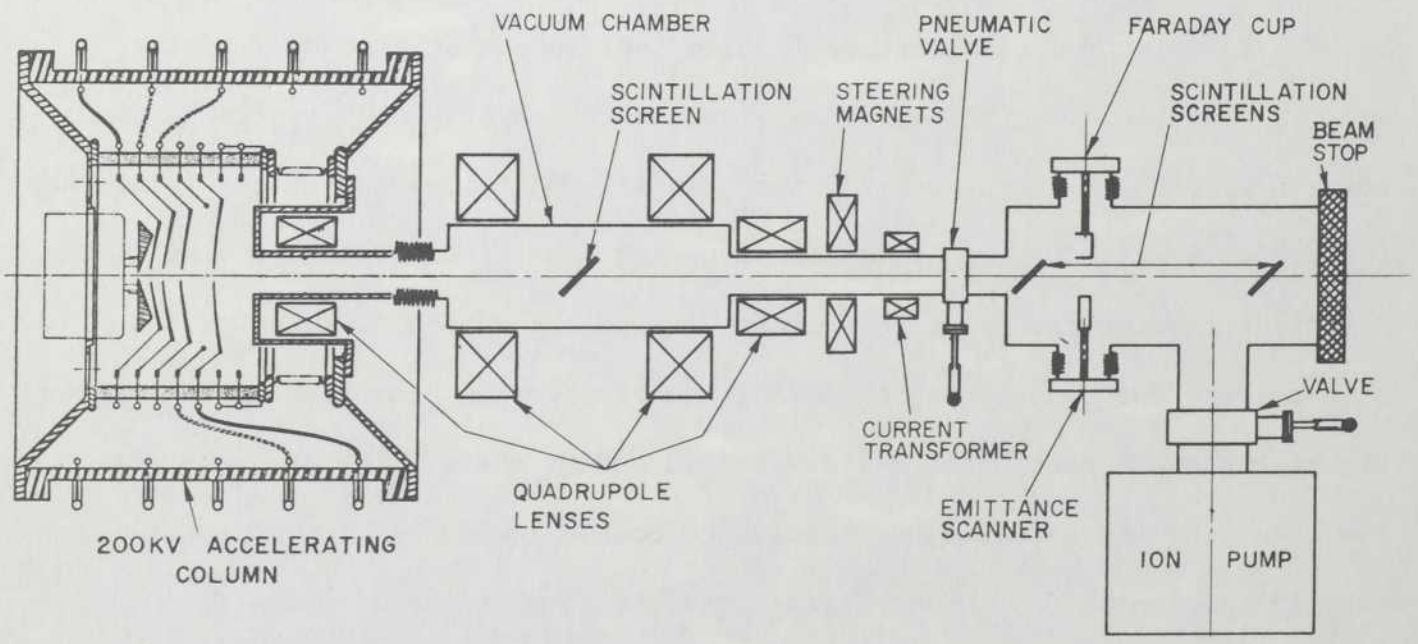

Fig. 5. Accelerating column.

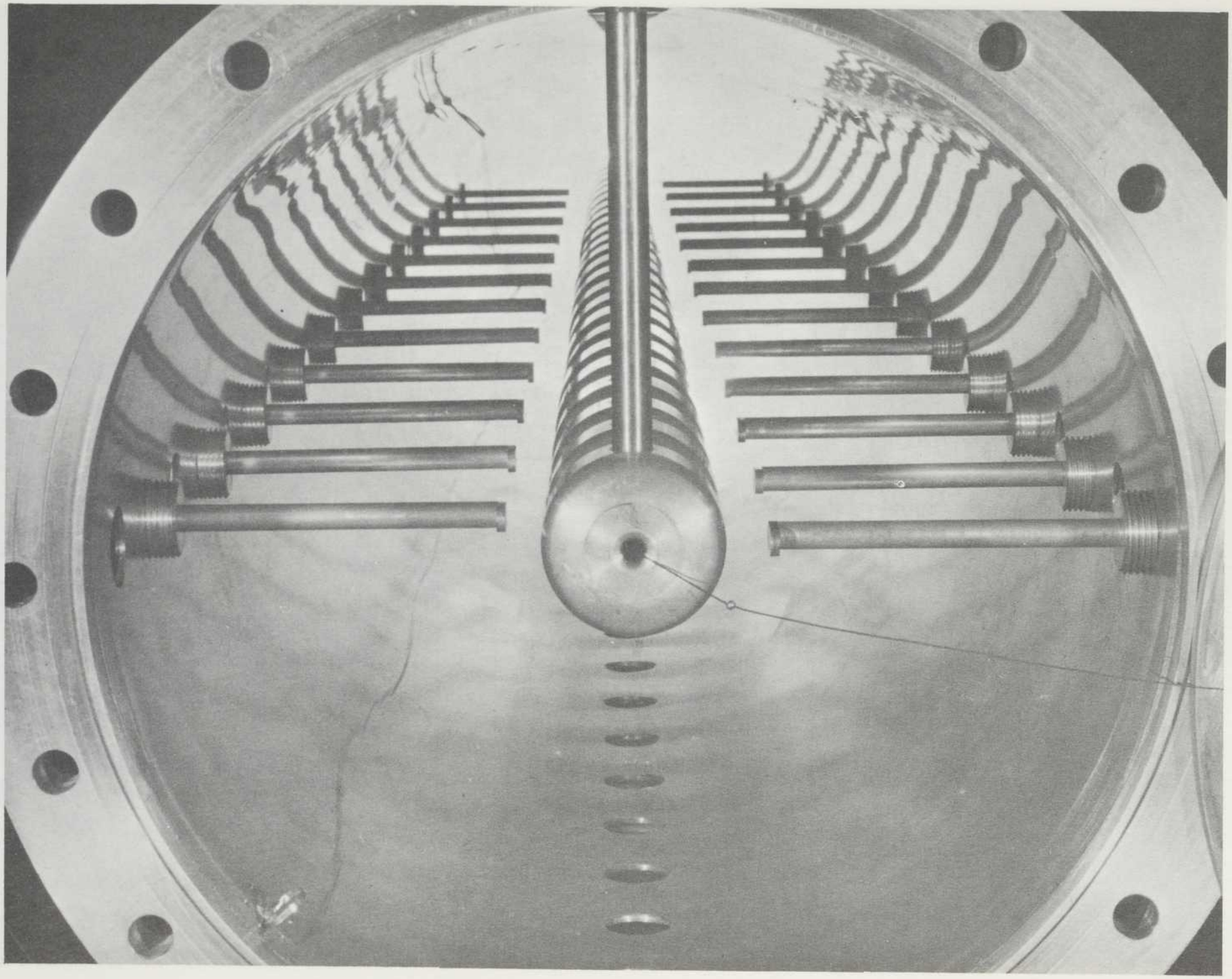

Fig. 6. Drift-tube accelerator.

FILLING CHARACTERISTICS OF DRIFT TUBE LINAC

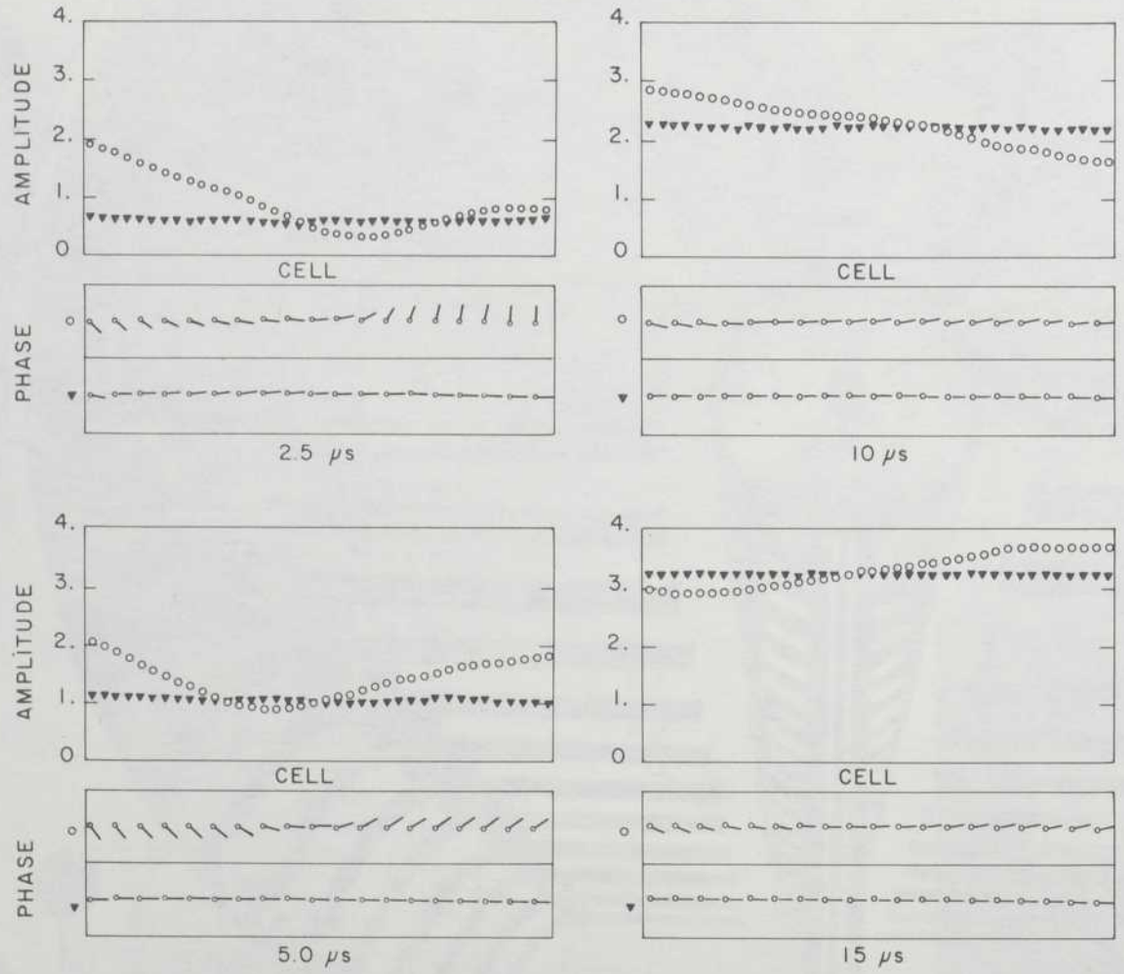

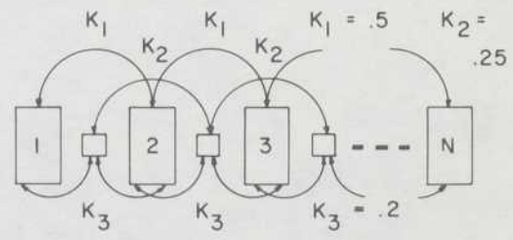

N = 38
AMPLITUDES ARE FRACTIONS OF STEADY STATE VALUE. ONLY PHASES OF EVERY OTHER ACCELERATING CELL SHOWN. UPPER ROW OF VECTORS IS UNSTABILIZED CASE; LOWER ROW, STABILIZED.

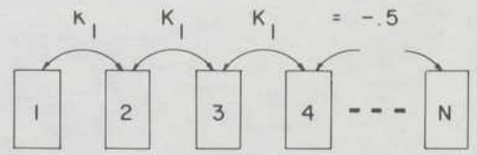

Fig. 7. Filling characteristics

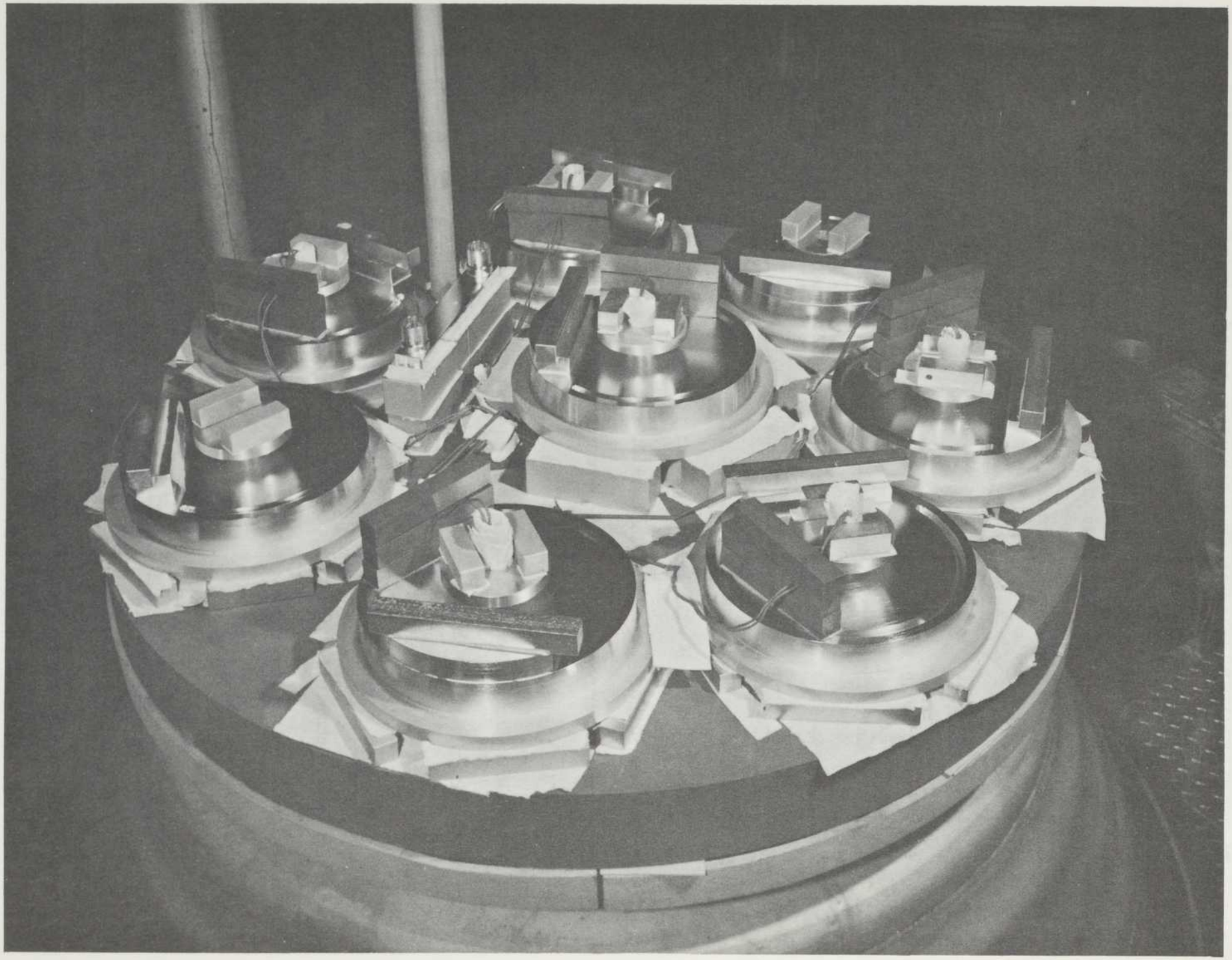

Fig. 10. Main segments prior to brazing.

Figure 9 shows how tolerant this structure is of machining errors in the accelerating cells.

Figure 10 shows a stack of main segments prior to brazing in the hydrogen-atmosphere furnace. Figure 11 shows the retort just after the furnace is removed. Inside are the copper segments, hopefully not melted down.

IV. EXPERIMENTAL AREA

Let's now move to the beam switchyard and the experimental area as shown in Fig. 12. We have found a way to simultaneously accelerate positive and negative hydrogen ions. This almost doubles the usefulness of the facility. The negative ions will be diverted in the switchyard to Area C and/or Area B. The negative ion beam can be split at will by introducing a stripping foil and magnet. Area B will be devoted to neutron experiments, including low-energy time-of-flight work. In Area C, the main instrument will be a high-resolution energy-difference spectrometer (Fig. 13).

Area A is the main experimental area and will house the pion and muon beam channels. Here, the full 1-mA average beam will traverse targets which are housed in a vault. These targets will be serviced by a remote-handling facility comprising manipulators and cranes housed in a 200-ton mobile shielded room. Figure 14 shows the stopped muon beam line. The design of this channel is essentially complete. It will provide $\sim 10^8$ stopped muons/sec at $\Delta R \sim 1$ gm/cm^2 in 10×10 cm, with pion contamination of <1% and typical longitudinal polarizations of $\sim \pm 0.8$.

V. CONTROL OF ACCELERATOR AND EXPERIMENTAL BEAMS

A unique feature of LAMPF will be that complete control and monitoring of the accelerator and experimental beams will be by computer. The control

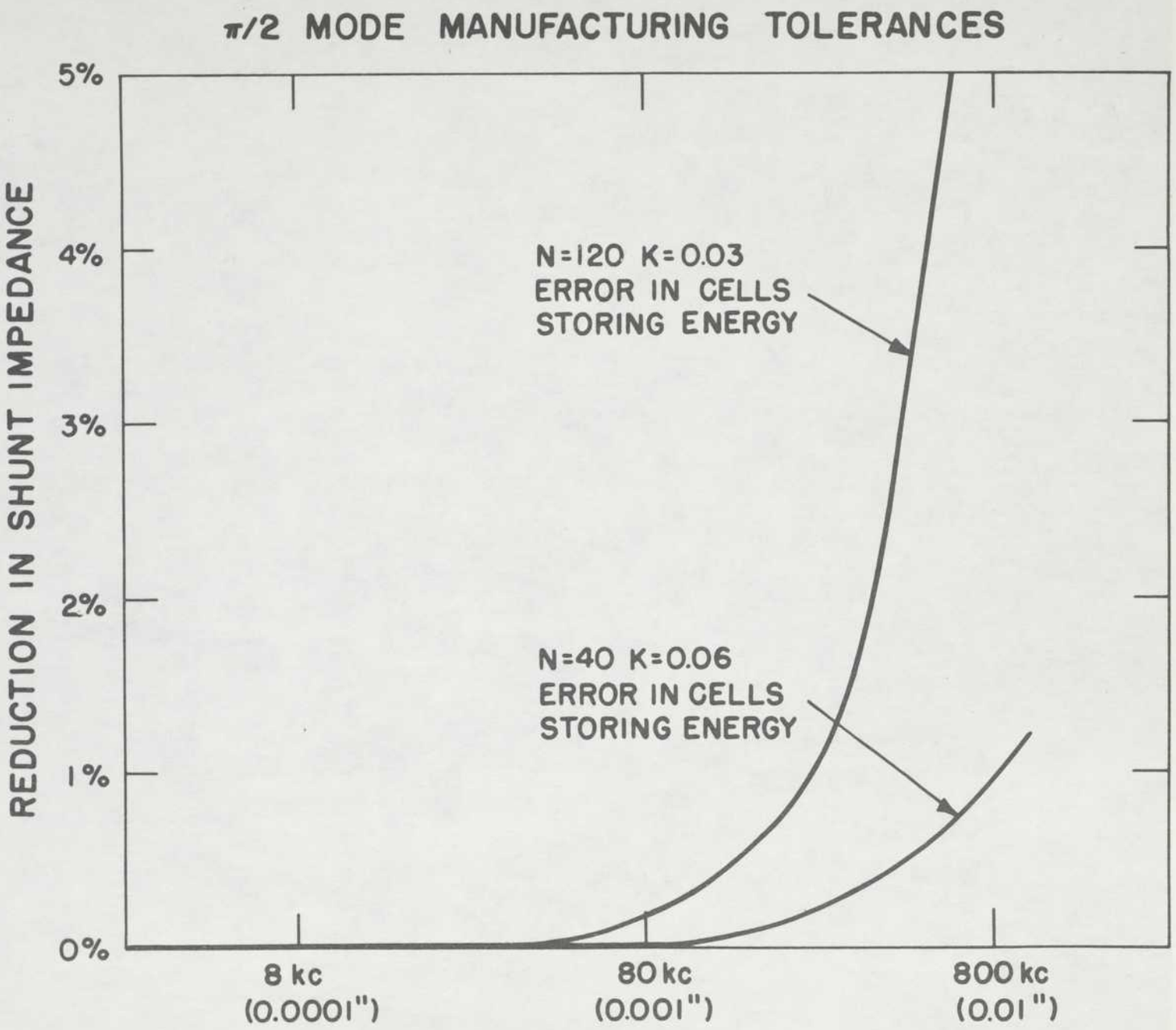
π/2 MODE MANUFACTURING TOLERANCES
REDUCTION IN SHUNT IMPEDANCE
5%
4%
3%
2%
1%
0%
N=120 K=0.03
ERROR IN CELLS
STORING ENERGY
N=40 K=0.06
ERROR IN CELLS
STORING ENERGY
8 kc
(0.0001")
80 kc
(0.001")
800 kc
(0.01")
MAGNITUDE ERROR (±),800 mc CAVITIES

Fig. 9.

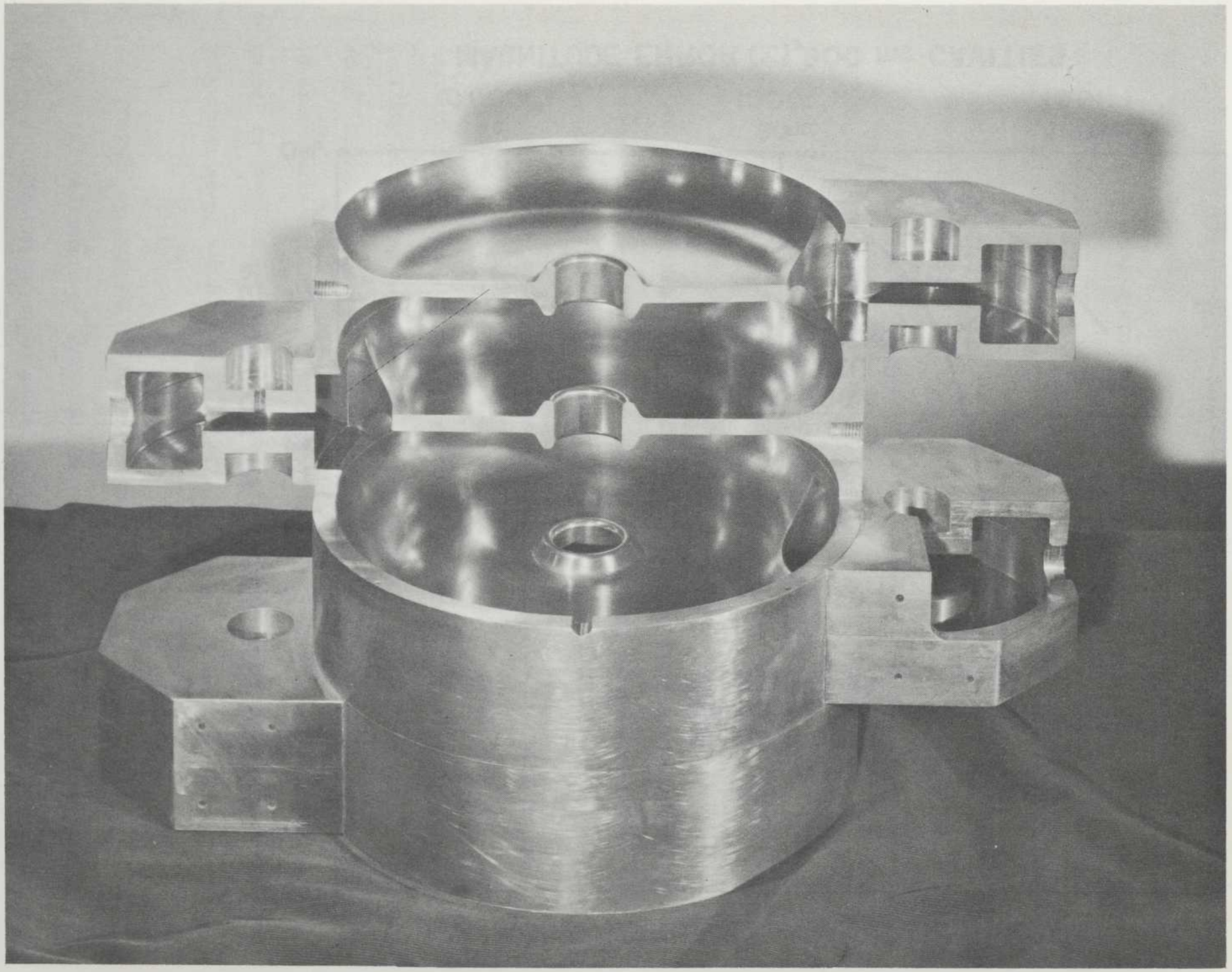

Fig. 8. Side-coupled cavity.

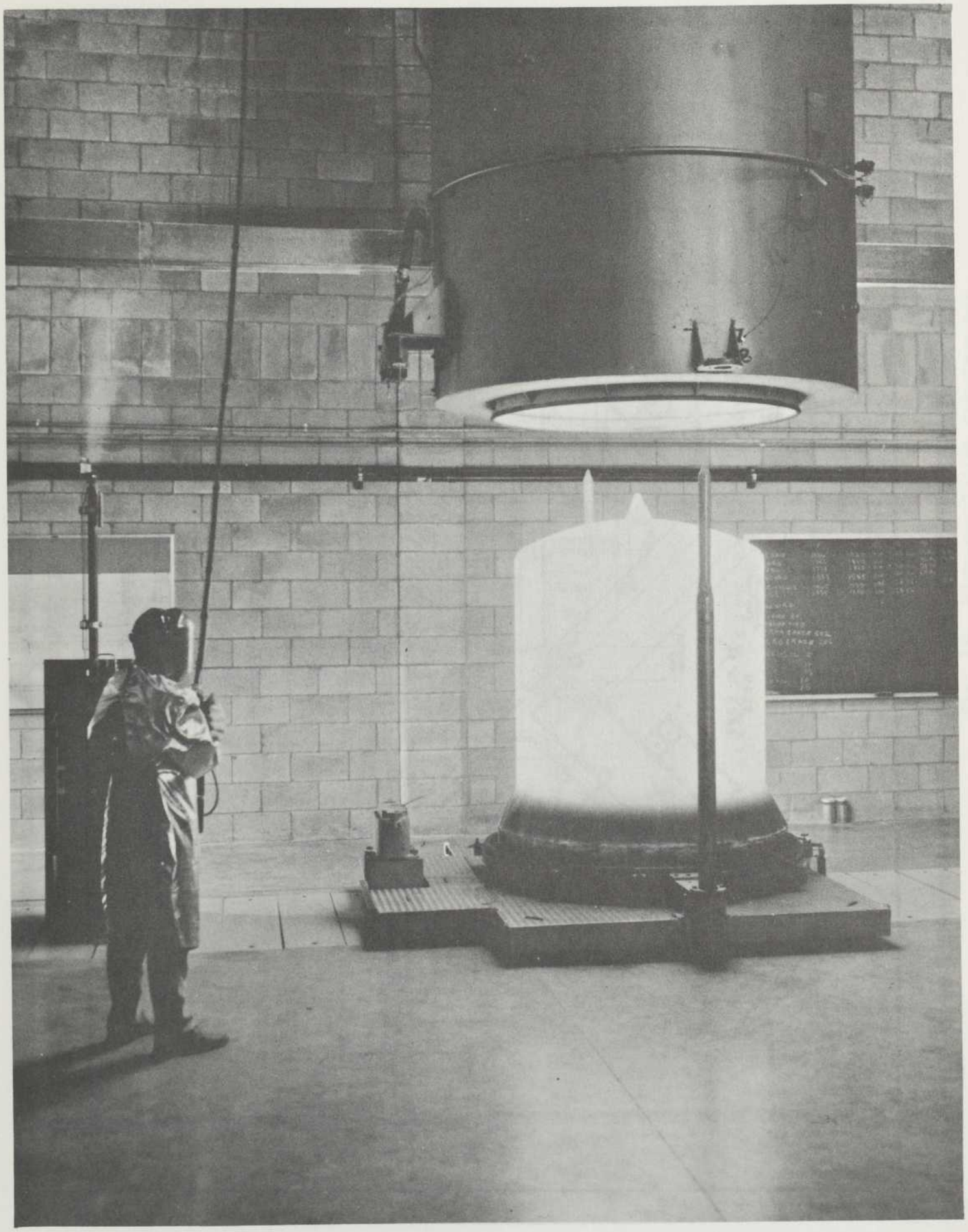

Fig. 11. Retort after furnace is removed.

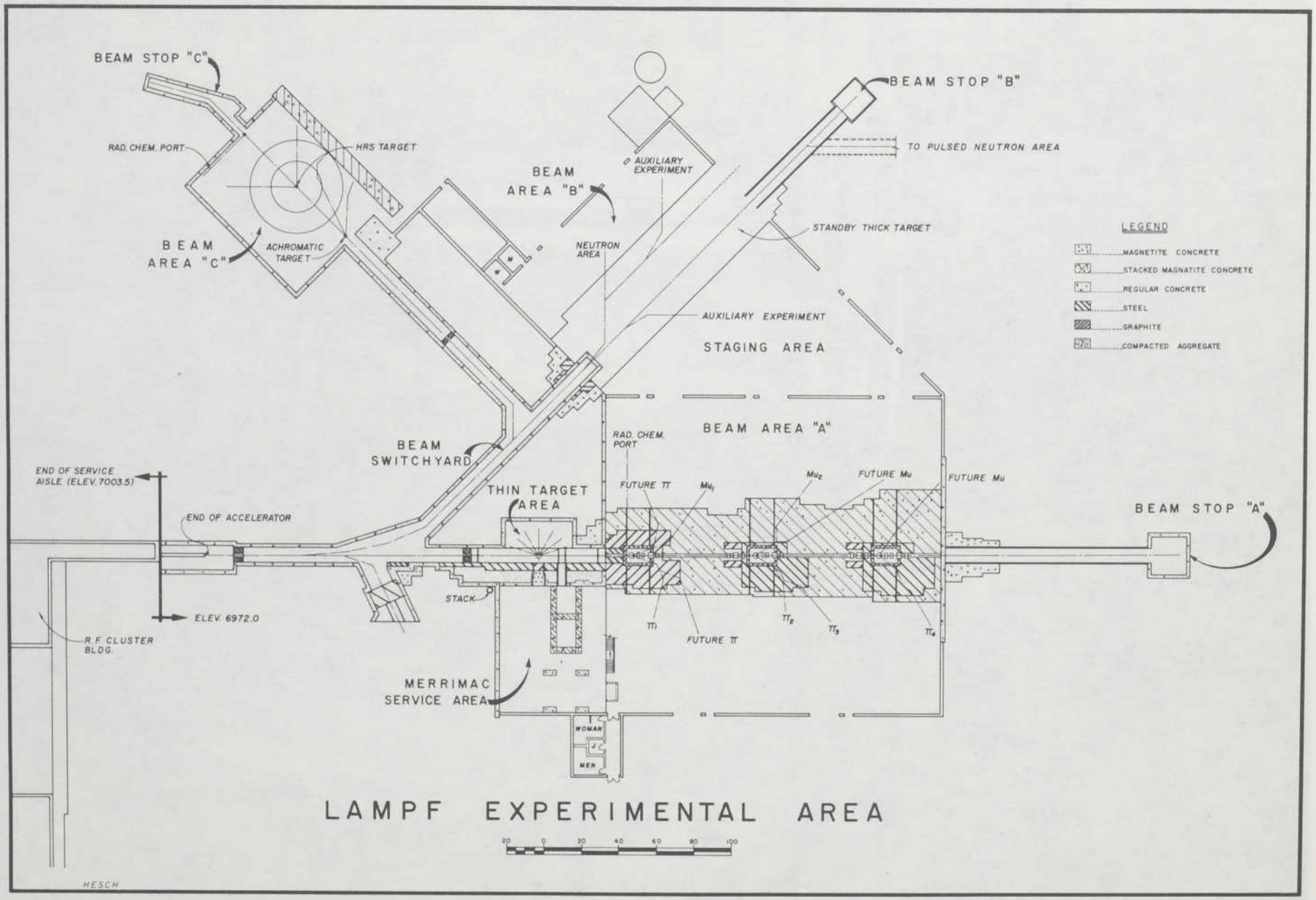
BEAM STOP "C"
RAD. CHEM. PORT
HRS TARGET
BEAM AREA "C"
ACHROMATIC TARGET
BEAM AREA "B"
NEUTRON AREA
AUXILIARY EXPERIMENT
BEAM STOP "B"
TO PULSED NEUTRON AREA
STANDBY THICK TARGET
AUXILIARY EXPERIMENT
STAGING AREA
BEAM AREA "A"
RAD. CHEM. PORT
BEAM SWITCHYARD
END OF SERVICE AISLE (ELEV. 7003.5)
END OF ACCELERATOR
THIN TARGET AREA
FUTURE TT
Mu1
Mu2
FUTURE Mu
FUTURE Mu
BEAM STOP "A"
STACK
ELEV. 6972.0
R.F. CLUSTER BLDG.
TT1
FUTURE TT
TT2
TT3
TT4
MERRIMAC SERVICE AREA
WOMAN
MEN
LEGEND
MAGNETITE CONCRETE
STACKED MAGNATITE CONCRETE
REGULAR CONCRETE
STEEL
GRAPHITE
COMPACTED AGGREGATE
LAMPF EXPERIMENTAL AREA
20 0 20 40 60 80 100
HESCH

Fig. 12.

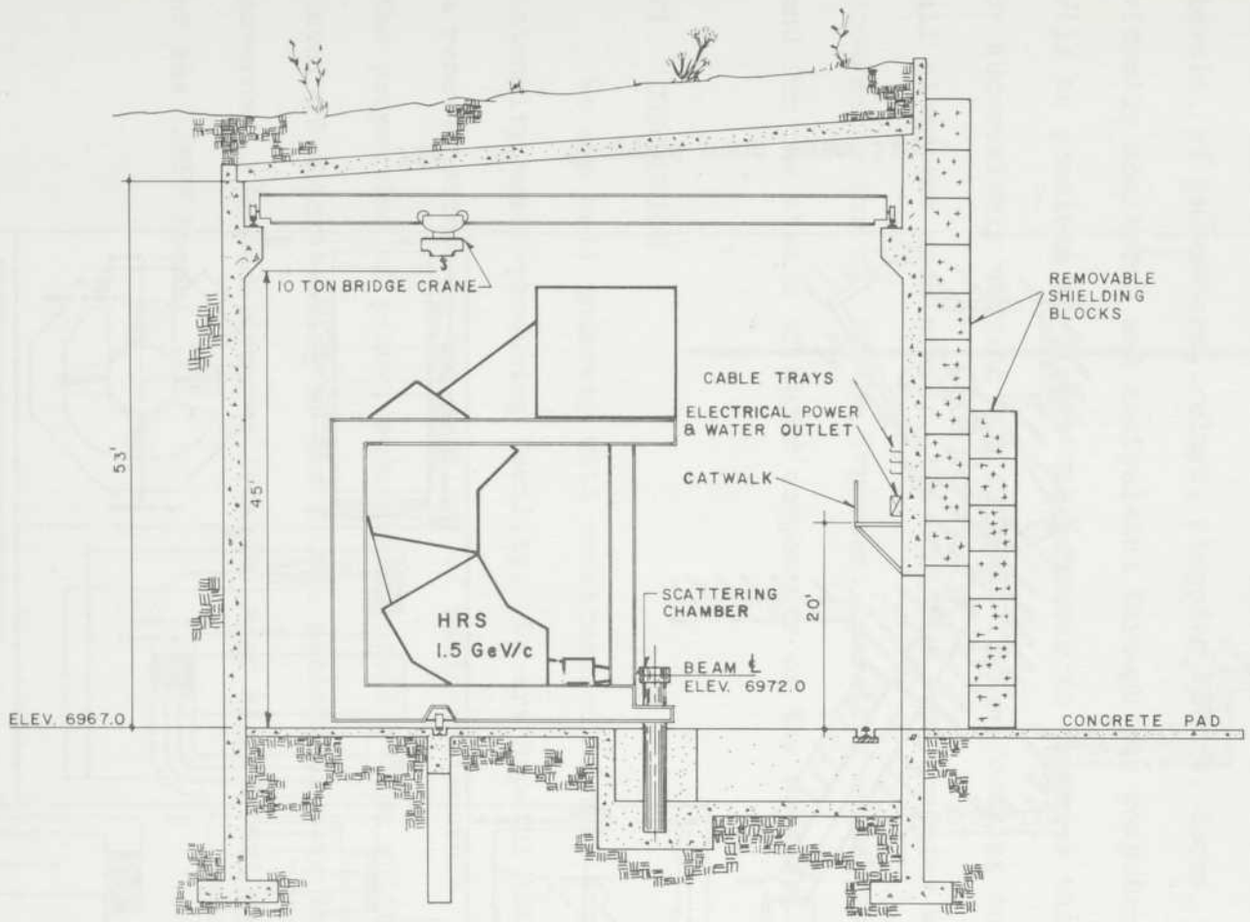

LOS ALAMOS MESON PHYSICS FACILITY

VERTICAL SECTION - AREA "C"

10 0 10 20 30
GRAPHIC SCALE

L'HEUREUX JULY 1969

ENG-IL-50
LASL ENGINEERING DEPT.

Fig. 13. High-resolution spectrometer.

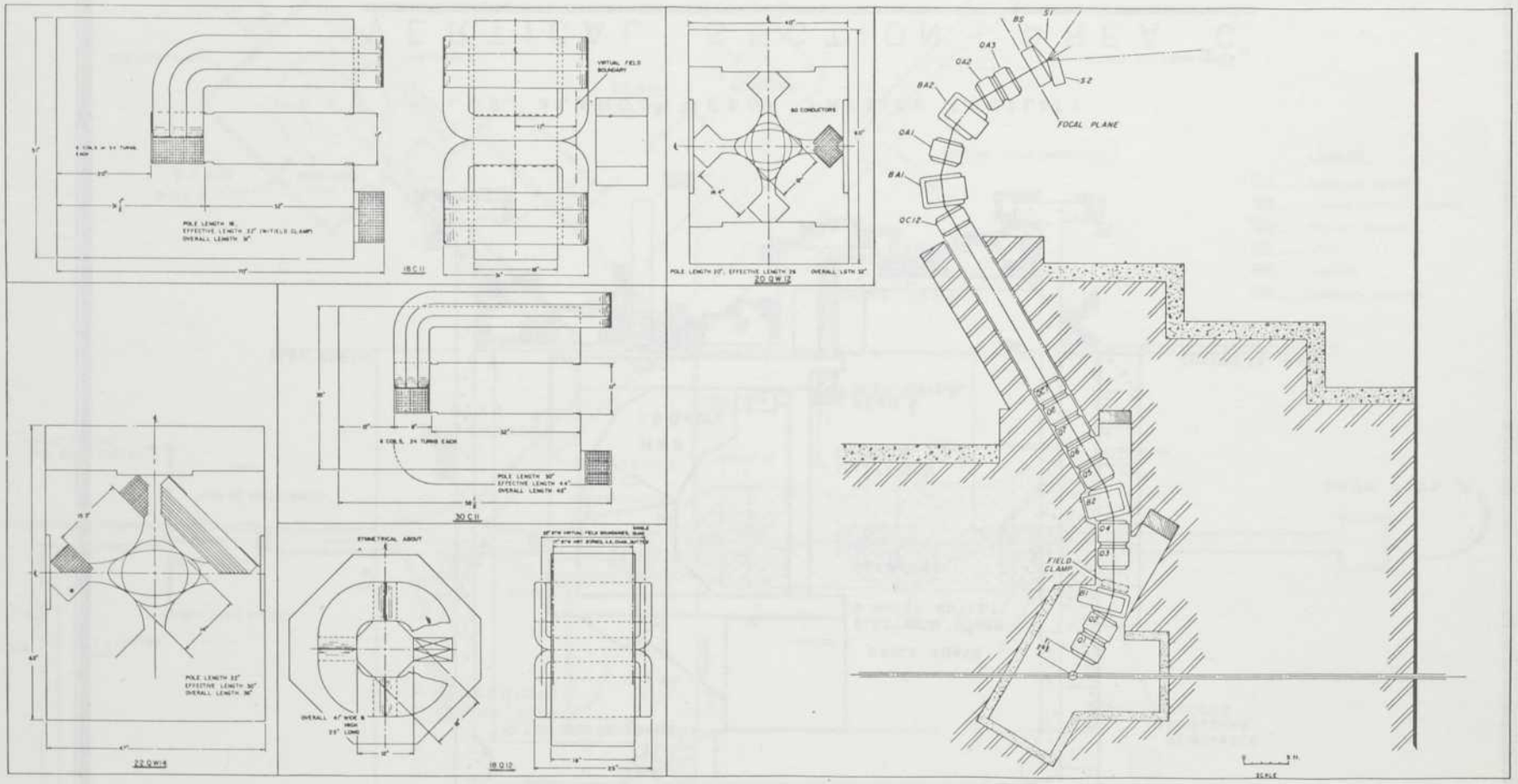

Fig. 14. Stopped muon beam line.

computer is shown in Fig. 15. The operator will interface with the computer by means of one or more display scopes, light-pen and teletype units. The electrical-mechanical circuitry of every major element of the accelerator can be displayed on the scope. Beam profiles, magnet settings, radiation levels, rf parameters, relays, stepping motors, doors, etc. can all be individually monitored and manipulated through the computer. In addition, it will be possible to direct the computer to optimize the beam, for example, by successively varying the currents in the focusing and steering of magnets all along the accelerator. In addition, the computer will serve as a master bookkeeper for all of the important operating sequences for the accelerator and for the status of major components of the machine.

VI. CONCLUSION

We are well underway with construction of this most sophisticated high-intensity meson-producing facility. We are hopeful that it will stimulate a renewed attack on the problems of nuclear structure, nuclear forms and the properties of pions, muons and neutrinos from which will emerge a new level of understanding of the atomic nucleus and the laws by which it is governed. In addition, we look for many significant practical applications of the LAMPF beams.

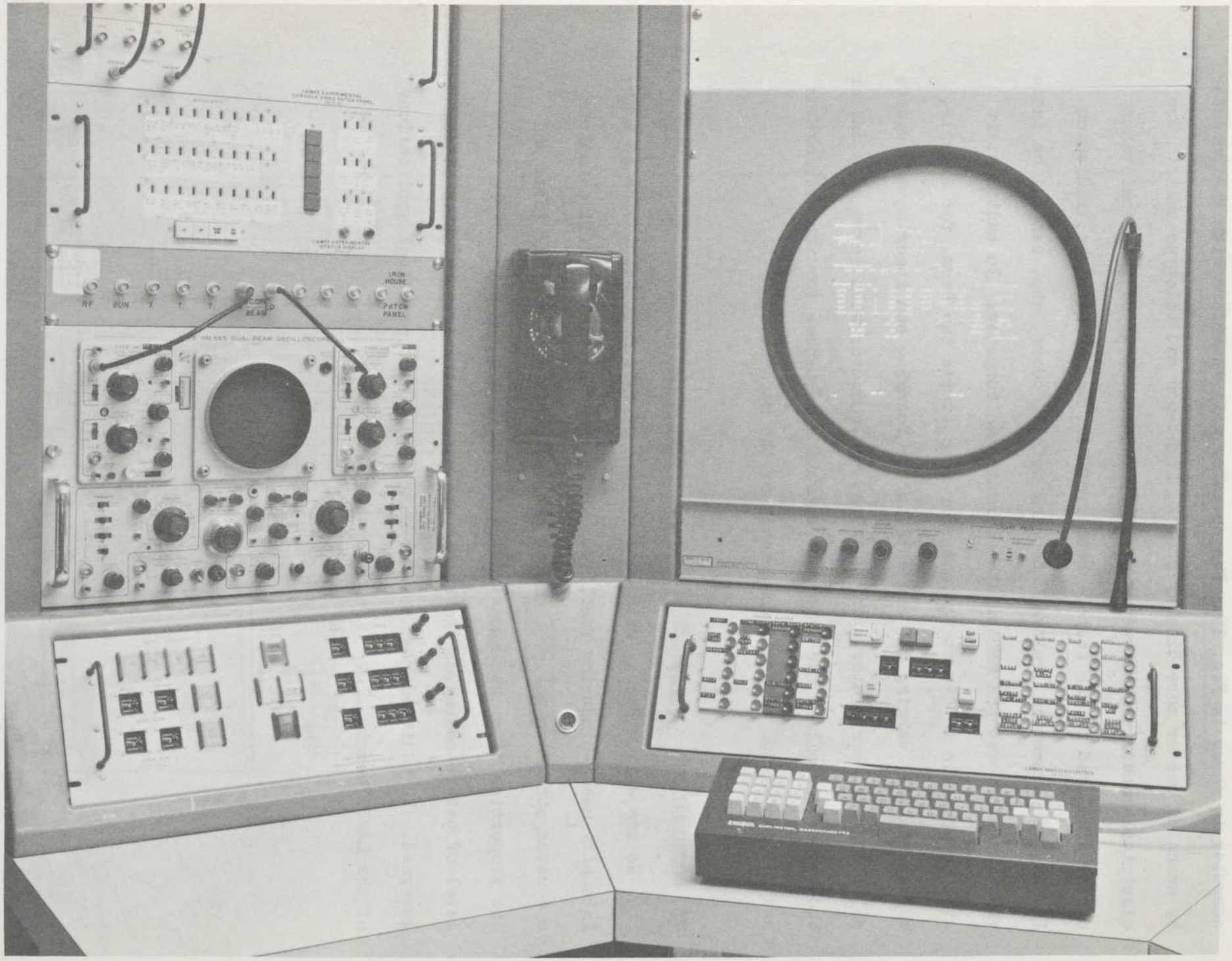

Fig. 15. Control computer for electron prototype accelerator.

REFERENCES

1. L. Rosen, "Meson Factory," Phys. Today 19, 21 (1966).

2. D. E. Nagle, "Linear Accelerator for Protons: New Developments," Science 157, 145 (1967).

3. L. Rosen, "The Los Alamos Meson Factory," Science Journal 5A, 39 (July, 1969).

THE OPTICAL POTENTIAL FOR ^{12}C BETWEEN 100 MEV and 1 GEV.

Daphne F. Jackson and M. B. Shah

Department of Physics, University of Surrey, Guildford, England.

We have analysed the elastic scattering, polarization and reaction cross-sections for proton scattering from ^{12}C at 182, 310, 424, 725, 970 and 1000 MeV, using a Saxon-Woods potential of the form

$$V(r) = V_o\, f(r,R_1,a) + i\, W_o\, f(r,R_2,a) + V_{so}\, \frac{1}{r}\frac{d}{dr}\, f(r,R_1,a)$$

$$+ i\, W_{so}\, \frac{1}{r}\frac{d}{dr}\, f(r,R_2,a) + V_{coulomb} \quad ,$$

where

$$f(r,R,a) = \left\{1 + e^{(r-R)/a}\right\}^{-1}$$

We use a modified form of the non-relativistic Schrödinger equation which takes account of relativistic kinematics and use the semi-classical approximation to obtain the phase shifts which are then inserted into the usual partial wave expansions for the differential cross-section, polarization and reaction cross-section. The object of this work was to examine the energy dependence of the parameters and to make a comparison with the results obtained by Batty[1] who used a semi-classical approximation for the scattering amplitude and an optical potential with the same radial form as the nuclear matter distribution calculated from oscillator wavefunctions.

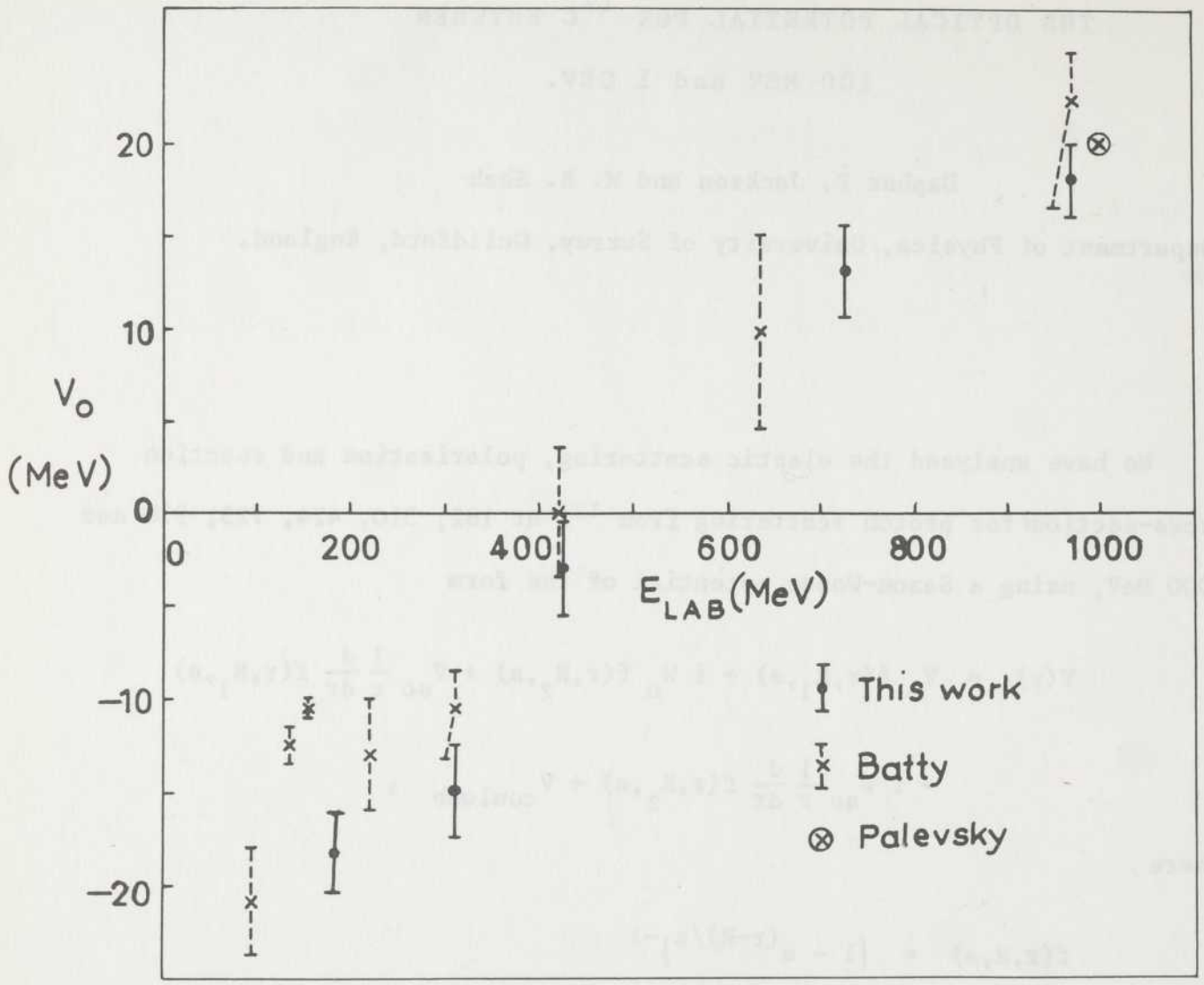

Figure 1.

Satisfactory fits to the data were obtained with a diffuseness a = 0.5 fm at all energies. The parameters obtained are summarised in Figures 1-3 where they are compared with the results of Batty, and of Palevsky et al[2] at 1 GeV. It can be seen that our results confirm the

energy dependence observed by Batty and are in full agreement with his result that the real potential changes sign at about 400 MeV. For energies above 700 MeV we obtain fits to the data with $R_1 = R_2$ but for energies below this we require $R_2 > R_1$. Batty took the same size parameters for the real and imaginary parts of the potential at all energies, and this accounts for the difference between the values of W_o obtained at the lower energies. The volume integrals of the potentials are in reasonable agreement. The magnitudes of the parameters V_o, W_o, found at 1 GeV, are consistent with those calculated using impulse approximation.

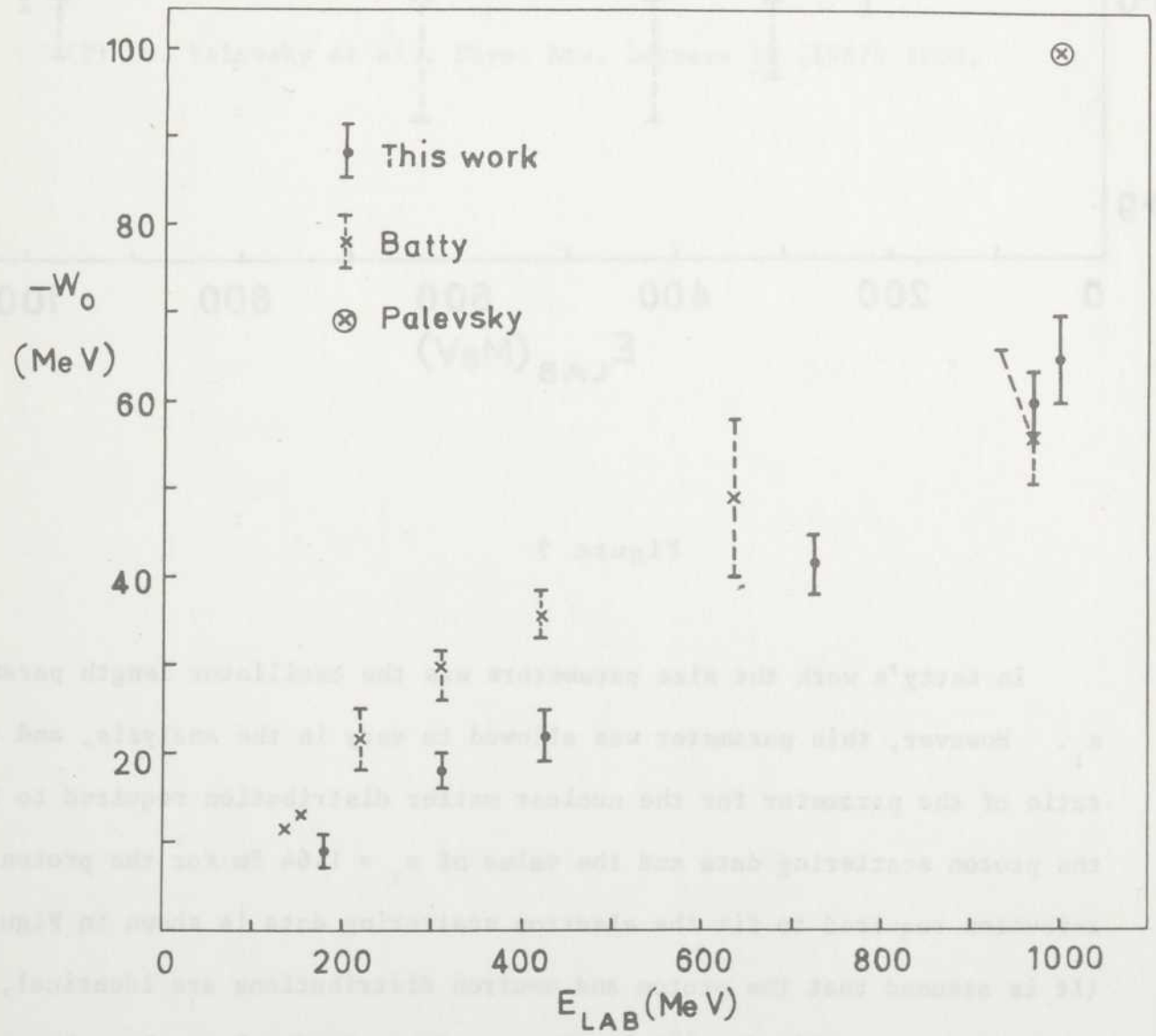

Figure 2.

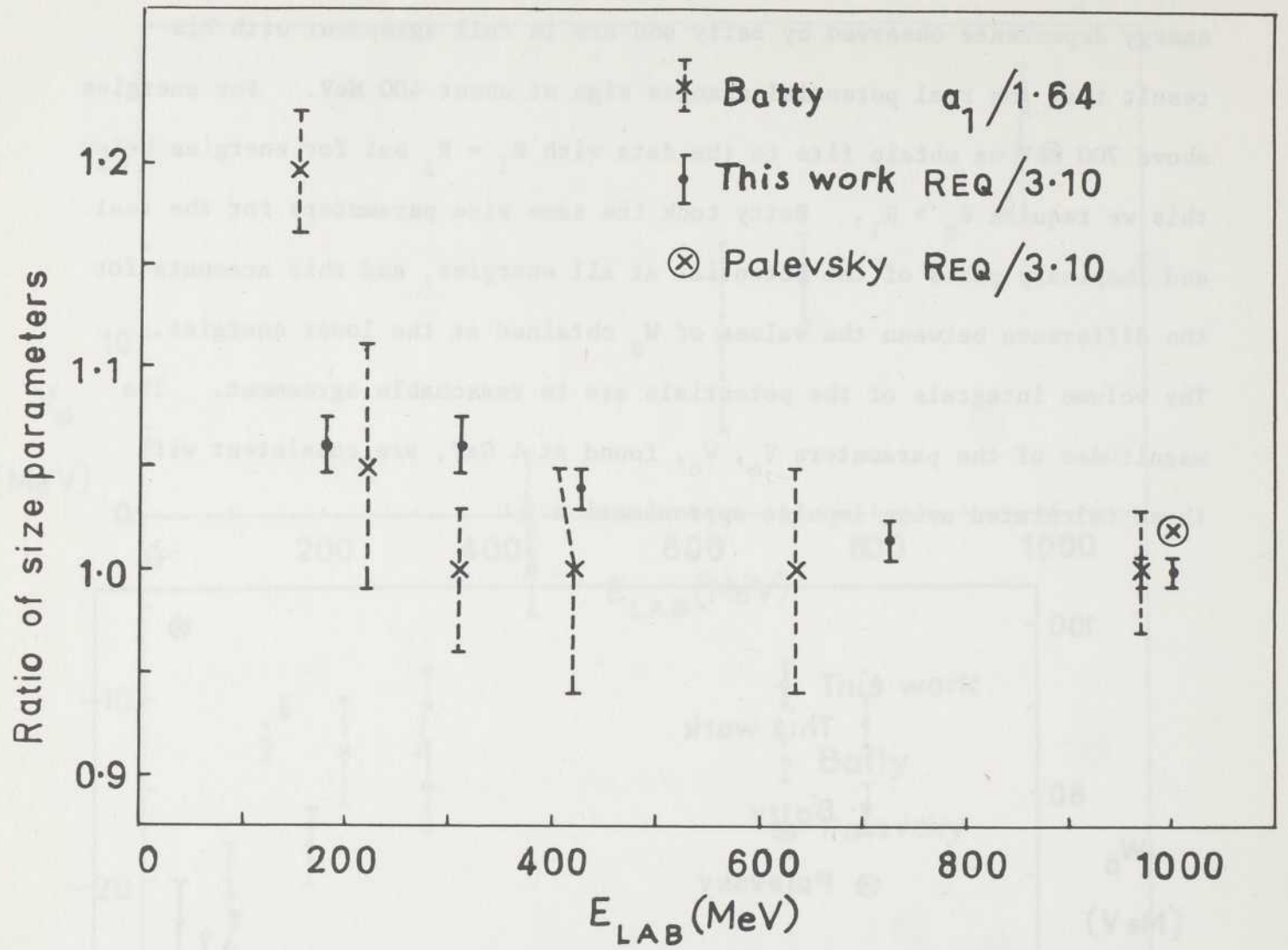

Figure 3

In Batty's work the size parameters was the oscillator length parameter a_1. However, this parameter was allowed to vary in the analysis, and the ratio of the parameter for the nuclear matter distribution required to fit the proton scattering data and the value of $a_1 \simeq 1.64$ fm for the proton distribution required to fit the electron scattering data is shown in Figure 3. (It is assumed that the proton and neutron distributions are identical, which seems very reasonable for ^{12}C.) For our Saxon-Woods shape the relevant size parameter is the equivalent uniform radius R_{EQ} defined by the relation

$$R_{EQ}^2 = R^2 + \frac{7}{3}\pi^2 a^2$$

The value of R_{EQ} for the proton distribution is ~ 3.10 fm. It can be seen from Figure 3 that the values of $a_1/1.64$, $R_{EQ}/3.10$ for the real part of our potential and for the potential of Palevsky et al at 1 GeV, are in satisfactory agreement. These results also suggest that the nuclear matter distribution can be investigated through high energy elastic scattering.

(1) C. J. Batty, Nuclear Physics 23 (1961) 562.

(2) H. Palevsky et al., Phys. Rev. Letters 18 (1967) 1200.

INDEX DES AUTEURS ET DES PARTICIPANTS

LIST OF CONTRIBUTORS AND PARTICIPANTS

ASLANIDES, Elie	C.R.N. Strasbourg	
AUSTIN, Sam M.	Michigan State Univ.	
BATTY, C.J.	Rutherford Laboratory	385
BEAUMEVIEILLE, H.	Institut d'Etudes Nucléaires d'Alger,	
BEAULIEU, René	Université Laval	
BECKER, François	C.R.N. Strasbourg	
BERGERON, J.	Université Laval	
BENN, Joachim E.	Universität Zürich	
BERNSTEIN, E.M.	Western Michigan University	393
BIRCHALL, J.	University of Birmingham	395,401
BLAIR, J.S.	University of Washington	377
BLEULER, K.	Université de Bonn	
BLYTH, C.O.	University of Birmingham	395,401
BOHIGAS, Oriol	Inst. Phys. Nucl. Nucl. Orsay	
BOSCHITZ, E.T.	Nasa-Lewis Research Center	437
BOUCHARD, Chs-A.	Université Laval	69
BRAY, Kevin	University of Manitoba	
BROMLEY, D.A.	Yale University	71
BRUGE, Gaston	C.E.N. Saclay	
BUBB, Ian F.	University of Manitoba	
BUDZANOWSKI, Andrzej	Inst. Nucl. Phys. Krakow	267,269
BURDE, Jacob	Hebrew University, Jerusalem	
BURDET, G.	Université de Lyon	
CAHILL, Thomas A.	University of California, Davis	
CAMPI, Francisco	Inst. Phys. Nucl., Orsay	
CASTEL, B.	Queen's University	
CATILLON, Philippe	CEN/Saclay	313
CHANT, N.S.	University of Washington	281,387
CHARBONNEAU, Royal	Université Laval	
CLEGG, T.	University of North Carolina	
COFFIN, Jean-Pierre	C.R.N. Strasbourg	
COLE, B.J.	University of Liverpool	277
COTE, J.	Université Laval	
CRADDOCK, Michael K,	University of British Columbia	
CUJEC, Bibiana	Université Laval	69,283
DARDEN, S.E.	University of Notre Dame	
DAVIS, R.H.	Florida State University	21
DAYRAS, Roland	Université Laval	
DONOGHUE, Thimothy	Ohio State University	
QUANG-HUE, N.	Université de Sherbrooke	
DUDEK, A.	Inst. Nucl. Phys., Krakow	269
DUFFY, J.J.	U.S. Army Missile Command	279
DUNSCOMBE, P.B.	University of Birmingham	395,401

EDWARDS, V.	King's College, London University	
ELBAZ, Edgar	University de Lyon	
FAIVRE, Jean-Claude	C.E.N. Saclay	
FALK, W.	University of Manitoba	
FALLIEROS, S.	Brown University	3
FISHER, P.S.	Nucl. Phys. Lab. Oxford	387
FOURNIER, R.	University of Ottawa	
FRIEDMAN, E.	Hebrew University, Jerusalem	
GAGNON, Richard	Université Laval	
GALLMANN, André	CRN, Strasbourg	71
GAUVIN, Laurie	Université Laval	
GILL, Gurbax	Université Laval	
GLENDENNING, N.K.	University of California	
GORDON, Earl Mark	McGill University	
GOULARD, Bernard	Université Laval	
GOULARD, Gisèle	Université Laval	62
GRIFFITH, J.A.R.	University of Birmingham	391
GROSS, Edward E.	Oak Ridge National Lab.	381
GROTOWSKI, K.	Inst. Nucl. Phys., Krakow	267,269
HAAS, F.	Université Laval	71
HAEBERLI, W.	University of Wisconsin	
HALLER, P.	Université Laval	
HAMMANN, Théophile	University d'Alger, Algérie	
HARA, K.	University of Sao Paolo	
HAUSMAN, Hershel J.	Ohio State University	
HAYWARD, T.D.	University of Washington	275
HEUSCH, B.	C.R.N. Strasbourg	71
HILSCHER, Dietrich	Hahn-Meitner Inst. Berlin	
HIRD, B.	University of Ottawa	
HODGSON, P.E.	Oxford University	121
HOFMANN, A.	Universität Erlangen	
HO KIM, Quang	Université Laval	
HSU, T.H.	University of Ottawa	
HUBER, P.	Universität Basel	287
HUBY, R.	University of Liverpool	59,277
IRSHAD, M.	University of Birmingham	391
JACKSON, Daphne	University of Surrey	271,493
JAIN, M.	University of Manitoba	
JARCZYK, L.	Inst. Nucl. Phys., Krakow	267
JAYARAMAN, K.S.	University of Manitoba	
JOVANOVICH, J.	University of Manitoba	
JUNDT, Francis C.	C.R.N. Strasbourg	
KAMYS, B.	Inst. Nucl. Phys. Krakow	267

KARBAN, O.	University of Birmingham	391
KAZAKS, Peter A.	Ohio University	
KEATON, P.W.	Los Alamos Scientific Lab.	331
KEMBHAVI, K.	University of Surrey	271
KERMAN, Arthur K.	Massachussets Ins. of Tech.	
KERMODE, Mark W.	Liverpool University	
KINSEY, B.B.	University of Texas	
KOSHEL, Richard D.	Ohio University	
KRAUSHAAR, J.J.	University of Colorado	
KULISIC, P.	University of Manitoba	
LAMONTAGNE, Raymond	Université Laval	69
L'ECUYER, J.	Université de Montréal	
LEDOYEN, Fernand	Université Laval	
LIZEE, Gérald	Université Laval	
LINCK, Isabelle	C.R.N. Strasbourg	
LORAZO, Bernard	Université Laval	
MACDONALD, N.	University of Glasgow	
MANGELSON, N.F.	University of Wasghington	281
MAHTABOALLY, S.Q.G.	University of Birmingham	395,401
MALANEFY, J.J.	University of Los Angeles	381
MARINOV, Amnon	Hebrew University of Ferusalem	
MARTIN, Peter	University of British Columbia	
MARIN, P.W.	University of British Columbia	
MARTY, M.	Inst. Phys. Nucl. Orsay	
MARTY, N.	Inst. Phys. Nucl. Orsay	423
MCKEE, J.S.C.	University of Birmingham	395,401
MEIER, M.M.	Duke University	409
MERCIER, Guy-François	Université Laval	
MICHITOSHI, Soga	Western Michigan University	
MILLER, Dan W.	Indiana University	
MILLER, Thomas G.	Redstone Arsenal, Huntsville	279
MINES, J.R.	University of Liverpool	277
MO, Joe-Nin	Université Laval	
MOLIMARI, Alfredo	Cornell University	
MONSONEGO, Georges	C.R.N. Strasbourg	
MORGAN, C.G.	University of Surrey	271
MORGAN, G.L.	Duke University	409
NELSON, John M.	University of Oxford	387
NGUYEN VAN, Giay	Inst. Phys. Nucl. Orsay	
NOACK, Cornelius	Universität Heidelberg	
OERS, W.T.H. Van	University of Manitoba	
OLIVO, Miguel A.	University of British Columbia	
OLKIEWICZ, K.	Inst. Of Nucl. Phys. Krakow	267
PAPINEAU, Lily	C.E.N. Saclay	
PARKINSON, W.C.	University of Michigan	

PETROVICH, Fred	Michigan State University	
PIANAROSA, P.	Université Laval	
PIRES	Inst. Phys. Nucl. Orsay	
POLLOCK, R.E.	Princeton University	
PURSER, F.O.	Duke University	409
QUANG HOC N.	Université de Sherbrooke	
QUESNE	Université de Mexico	
RAMAVATARAM, Kil	Université Laval	
RAMAVATARAM, S.	Université Laval	63
RAPHAEL, R.	Catholic University Washington	
RAWITSCHER, G.	University of Connecticut	
RAYNAL, J.	Centre d'Etudes Nucl. Saclay	75
REECE, B.L.	University of Birmingham	395,401
ROBBINS, Allen B.	Rutgers University	
ROBERTSON, I.P.	University of Victoria	
ROMAN, S.	University of Birmingham	351,391
RONSIN, G.	Faculté d'Orsay	
ROSEN, L.	Los Alamos Scientific Lab.	469
ROULSTON, K.I.	University of Manitoba	
ROY, Gérald	Université Laval	
ROY, René	Université Laval	283
RUHLA, Charles	Université de Lyon	
SOGA, M.	Western Michigan University	
SALOMON, Martin	University of British Columbia	
SAUDINOS, Jean	C.E.N. Saclay	
SAUMIER, G.	Université de Montréal	
SCHAEFFER, Richard	C.E.N. Saclay	231
SCHAPIRA, J.P.	Institut de Physique Nucléaire, Orsay	
SCHIECK, Hans G.	The Ohio State University	
SCHMIDT, Fred H.	University of Washington	275
SELTZ, Raymond	C.R.N. Strasbourg	
SEULER, Richard	Ohio State University	
SIMONIUS, Markus	Carnegie-Mellon University	383
SINGH, Raj Narain	McGill University	
SHAH, M.B.	University of Surrey	493
SHANLEY, Pau E.	University of Notre Dame, Ind.	61
SHERIF, Helmy S.	University of Manchester	377
SLOBODRIAN, M.L.V.L.	Université Laval	283
SLOBODRIAN, Rodolfo	Université Laval	283
SPALEK, G.	Duke University	403
SPERBER, Daniel	Rensselaer Polytech. Inst.	
STAMMBACH, Th.	Duke University	403,413
STANDING, K.G.	University of Manitoba	
STEWART, K.W.E.	Queen's University	
ST-PIERRE, Claude	Université Laval	
STRZALKOWSKI, A.	Inst. Nucl. Phys. Krakow	267,269
SWAN, Peter	Université Laval	
SWENSON, L. Wayne	Oregon State University	
SZOGHY, Etienne	Université Laval	

TAM, W.G.	Université Laval	
TAYLOR, J.	Duke University	403,413
THOMAS, G.	King's College London University	
THOMASON, R.S.	Duke University	413
THIRION, J.	Centre d'Etudes Nucl. Saclay	
TOULEMONDE, Marcel	Université Laval	
TOWNER, I.S.	University of Oxford	
TSCHALAR, C.	Rutherford Laboratory	385
VAN DER WOUDE, A.	Oak Ridge National Lab.	381
VAUTHERIN, D.	Institut de Physique Nucléaire, Orsay	
VENERONI, M.	Institut de Physique Nucléaire, Orsay	
VERNOTTE, J.	Institut de Physique Nucléaire, Orsay	
VINH MAU, Nicole	Institut de Physique Nucléaire, Orsay	
VITOUX, Dominique	Université Laval	69
WALTER, Richard L.	Duke University	403,409,413
WELLS, D.O.	University of Manitoba	
ZUCKER, A.	Oak Ridge National Lab.	381

LIBRARY OF THE QUEBEC CENTRE

Achevé d'imprimer
le trente avril
mil neuf cent soixante-dix
aux Ateliers de
l'Imprimerie Laflamme Ltée
Québec, Canada.

BNQ
000 222 268